State of the art PVDF-based architectures from RAFT/MADIX polymerization of VDF : synthesis, self-assembly and potential membrane application

Enrique Folgado

THÈSE POUR OBTENIR LE GRADE DE DOCTEUR DE L'UNIVERSITÉ DE MONTPELLIER

En Chimie et Physico-chimie des Matériaux

École doctorale Sciences Chimiques Balard ED 459

Unité de recherche Institut Européen des Membranes (UMR 5635)

State of the art PVDF-based architectures from RAFT/MADIX polymerization of VDF: Synthesis, self-assembly and potential membrane application

Présentée par **Enrique FOLGADO**

Le **04 Nov. 2019**

Sous la direction de Vincent LADMIRAL
et l'encadrement de Mona SEMSARILAR

Devant le jury composé de

Paul TOPHAM, Professor, Aston University, Birmingham, Royaume-Uni	Président
Didier GIGMES , Directeur de Recherche, Aix-Marseille Université, Marseille, France	Rapporteur
Jutta RIEGER, Chargée de Recherche, Sorbonne Université, Paris, France	Rapporteur
Volker ABETZ, Professor, Helmholtz-Zentrum Geesthacht, Geesthacht, Allemagne	Examinateur
Simon HARRISSON, Chargé de Recherche, Université de Toulouse, Toulouse, France	Examinateur
Vincent, LADMIRAL, Chargé de Recherche, ENSCM, Montpellier, France	Directeur de Thèse
Mona, SEMSARILAR, Chargée de Recherche, IEM/Université de Montpellier, France	Invité

UNIVERSITÉ DE MONTPELLIER

AKNOWLEDGEMENTS

I would like to extend thanks to the many people, in many countries, who generously contributed to the work presented in this thesis.

First of all, I would like to express my gratitude to my enthusiastic supervisors Mona and Vincent for choosing me for this project. Thanks for the continuous academic support, for your patience, and incredible opportunities. Your guidance helped me all the time of research and writing of this thesis. I could not have presented this manuscript without your help.

I'd also like to thanks Armelle Ouali, My master's thesis supervisor. Thanks for introducing me to Vincent, for all the knowledge you shared with me and for bringing me the opportunity to start publishing articles.

Besides, I would like to thank Didier Gigmes and Jutta Rieger for reviewing my thesis manuscript. Also thanks to Simon Harrisson, Paul Topham and Volker Abetz for accepting being part of my thesis committee.

I'd like to thank all the permanent people in both ICGM and IEM, especially people from IAM and IP2/M2A, university staff and others who helped me in any way during these three years.

Thanks to Marc Guerre for helping me a lot in the beginnings of this project. Thanks for sharing your immense knowledge. Also thanks to all the people in the 3rd floor office of IAM, the fluorinated polymer guys, especially to Roberto and Maxime and people in the 1st floor, Vincent and many others for their help and support whenever I asked for anything.

I'd like to thanks all the people I've shared office with in IEM and specially to Thomas (amazing colleague that introduce me to everyone the first day, and became a good friend), Antoine, Camille, Arnaud, Aijing (We've shared office 3 years!, it was a pleasure to share a lot of moments and chats with you), Edgar, Tuyen (My TEM mate, thanks for all the chats and discussions), Hana (RAFT-mate, I wish you arrived earlier to our office) Morgan, Cyril (You brought lots of good vibes to our office), Dana (I could nag in Spanish all the time since you came to our office)… for all the chats and discussions, jokes, coffee breaks and all the good times we spent together. Thanks for being you and for your good humor. I could not imagine better people to share my office with.

Also thanks to my lab mates: Mingyuang (thanks for helping me with XRD measurements and for all the chats and discussions), Rui, Marianne, Carmen...

There is also a lot of people I didn't share office or lab with, but we shared long discussions at lunch, coffee-breaks, after-works, birthday parties: Maryline, Loraine, Sara, Syreina, Marleine, Marine, Gabi, Alice, Azariel, Carole, Lucy…

A special mention to Pierre, Dana, Octavio, Habib, Thomas, Antoine, Carlos, Cyril, … because we've shared a lot of good moments together, we've discussed about everything, and shared every lunch and coffee break, but also, ate, drank, travelled, drank, ate, danced, drank, and ate… Did I said ate and drunk? You are now an important part of my life, we might stop being workmates at some point but you will always be my friends.

My sincere thanks also go to Sebastien Perrier for letting me be part of his team at the University of Warwick during two amazing months last year. Also thanks to the lab-mates in Perrier's group: Qiao, Jie, Fannie, Sean, Thomas, Satu, Maria, Julia, Robert, Jane, Clemont, Patrik, Edward, Carlos, Joji, Guillaume, Raoul, Megan for making those months memorable. Special thanks to Qiao who introduce me to peptide synthesis and help me a lot with this project.

To my home-town friends (Jenny, Carmen, Sonia, Yohanna and many others) because they threat stress with party invitations and other good distractions (thanks for that, It was exactly what I needed) to the good friends I did in Valladolid (Edu, Guio, Alba, Julie, por todos las fiestas, los reencuentros y los ratufi's tour, pero sobre todo por el apoyo moral en las largas horas de estudio en el aulario, en San Nicolás…) and to the good friends I made in Pau (Sara, Diego, Marina, Erato, Aggeliki… my Greco-Spanish family, for all the fun, travels and visits, there will be more very soon) and Toulouse (Fran, Sandra, Leti, Dani, Mery, Edu… el tiempo que vivimos en Toulouse no se me olvidará nunca y me alegro que mantengamos el contacto).

I would like to thank my family, especially my parents because it is only thanks to them that I am who I am today, because they taught me what hard work and perseverance mean, and how to achieve my goals. No pain, no gain ("Quien algo quiere algo le cuesta") they used to say. Gracias papá y mamá, porque si he llegado hasta aquí es gracias a vosotros, por vuestro apoyo económico, pero sobre todo moral. Porque nunca me habéis cortado las alas, me disteis libertad para escoger mis estudios, y construir mi fututo a mi manera. Hoy he conseguido lo que quería, y os lo dedico a vosotros.

Last but not the least, to the person that spent a 10 years journey with me, from the University of Valladolid to Oporto, from Oporto to Pau, from Pau to Toulouse, from Toulouse to Montpellier. To Sofia, because only she knows the long long journey and how many times we moved to be where we wanted to be, doing our PhDs, we've celebrated together very good moments, but she's been also there whenever I've passed through any difficulties. Thanks for your support, your patience, your kind words when I was stressed or sad and for taking care of me. It would have not been the same without you.

ABSTRACT

This thesis presents new approaches for the preparation of PVDF-based architectures. The synthesis and characterization of different PVDF-based amphiphilic block copolymers (BCPs) and cyclic peptide-PVDF conjugates are described. RAFT/MADIX polymerization of gaseous VDF monomer and different chemistries were employed for the preparation of the BCPs. PVDF- and P(VDF-*co*-HFP)-containing ABA triblock copolymers were obtained through Thia-Michael addition using a "one-pot" strategy involving both PVDF-Xanthate (or P(VDF-*co*-HFP)-Xanthate) and PEG-diacrylates. PNIPAM-*b*-PVDF diblock copolymers were prepared by RAFT polymerization of VDF using PNIPAM macroCTAs. The synthesis of peptide sequences, cyclic peptide (CP) preparation and the synthesis of PVDF-CP conjugates is also described. The self-assembly in solution of all the novel PVDF-based BCPs and CPs-conjugates was also studied. Finally, PVDF blend membranes were prepared by non-solvent induced phase-separation (NIPS) process using one of the amphiphilic BCPs as an additive. The performance of the membrane and evolution of membrane properties over a period of 9 months was studied.

Key words: PVDF, fluoropolymer, RAFT, MADIX, block copolymer, self-assembly, cyclic peptide, membrane.

RÉSUMÉ

Cette thèse présente de nouvelles approches pour la préparation d'architectures basées sur le PVDF. La synthèse et la caractérisation de différents copolymères amphiphiles à base de PVDF et d'hybrides peptides cycliques-PVDF sont décrites. La polymérisation RAFT/MADIX du monomère VDF gazeux et différentes chimies ont été utilisées pour la préparation des copolymères à bloc. Des copolymères triblock ABA à base de PVDF ou de copolymères P(VDF-*co*-HFP) ont été obtenus par Thia-addition de Michael utilisant une stratégie « one-pot » impliquant à la fois des PVDF-Xanthate (ou P(VDF-*co*-HFP)-Xanthate) et des PEG-diacrylates. Des copolymères diblocs PNIPAM-*b*-PVDF ont également été préparés par polymérisation RAFT du VDF à l'aide de macroCTAs PNIPAM. La synthèse des séquences peptidiques, la préparation des peptides cycliques (PC) et la synthèse des conjugués PVDF-CP sont également décrites. Enfin, des membranes à base de PVDF ont été préparées par un procédé de séparation de phase (NIPS) utilisant un des copolymères a bloc amphiphiles comme additif. La performance de ces membranes et l'évolution de leurs propriétés sur une période de 9 mois ont également été étudiées.

Mots clés: PVDF, fluoropolymère, RAFT, MADIX, copolymère à bloc, auto-assemblage, peptide cyclique, membrane.

TABLE OF CONTENT

ABBREVIATIONS

1D	One dimensional
2D	Two dimensional
ACN	Acetonitrile
AGET	Activator generated by electron transfer
AIBN	2,2'-azobis(iso-butyronitrile)
ATRP	Atom-Transfer Radical Polymerization
Au NPs	Gold Nanoparticles
BCP	Block copolymer
BIBB	2-bromo-2-methylpropionyl bromide
Bpy	2,2'-bipyridine
CA / CAs	Contact Angle/s
CDSA	Crystallization-Driven self-Assembly
CMRP	Cobalt-Mediated Radical Polymerization
CP	Cyclic peptide
CP-$(PVDF)_2$	PVDF difunctional cyclic peptide
CP-$(XA)_2$	Xanthate difunctional cyclic peptide
CTA	Chain Transfer Agent
CTA-XA	*O*-Ethyl-*S*-(1-methoxycarbonyl) ethyldithiocarbonate
CTA-$(XA)_4$	Tetrafunctional Xanthate Chain Transfer Agent
CTFE	Chlorotrifluoroethylene
CTP	4-cyano-4-(phenylcarbonothioylthio)pentanoic acid
CuAAc	Copper-catalyzed azide-alkyne cycloaddition
DCPMA	Dicyclopentyloxyethyl methacrylate
DIPEA	*N*,*N*-diisopropylethylamine
DLS	Dynamic light scattering
DMAc	Dimethylacetamide
DMAP	4-dimethylaminopyridine

DMC	Dimethyl carbonate
DMF	*N*,*N*-dimethylformamide
DMPP	Dimethylphenylphosphine
DMSO	Dimethyl sulfoxide
DMTMM·BF4	4-(4,6-dimethoxy-1,3,5-triazin-2-yl)-4-methylmorpholinium tetrafluoroborate
DOSY	Diffusion-Ordered Spectroscopy
DP	Degree of polymerization
DP_{theo}	Theoretical degree of polymerization
DSC	Differential scanning calorimetry
Đ	Dispersity
EDC	1-ethyl-3-(3- dimethylaminopropyl)carbodiimide
EGDMA	Ethylene glycol dimethacrylate
EHA	2-ethylhexylacrylate
EtOH	Ethanol
EVE	Ethyl vinyl ether
FO	Forward osmosis
GPC	Gel permeation chromatography
HBTU	*O*-(benzotriazole-1-yl)-*N*,*N*,*N*',*N*'-tetramethyluronium hexafluorophosphate
HEA	2-hydroxyethyl acrylate
HFIP	1,1,1,3,3,3-Hexafluoroisopropanol
HFP	Hexafluoropropene
HH	Head-to-head
HHHs	Hexagonally packed hollow hoops
HMDSO	Hexamethyldisiloxane
hPEA	Hyperbranched poly(ether amine)
HPG-NH_2	Amino-terminated hyperbranched polyglycerol
HPLC	High performance liquid chromatography
Hz	Hertz
IPMC	Ionic polymer-metal composite actuator
ITP	Iodine transfer polymerization
l	Length

LAMs	Less-activated monomers
LCMs	Large compound micelles
LCST	Lower critical solution temperature
M	Micellization
MADIX	Macromolecular design via interchange of xanthates
MAMs	More activated monomers
MC	Membrane contactor
MD	Membrane distillation
MEMs	Proton exchange membranes
MeOH	Methanol
MF	Microfiltration
MMA	Methyl methacrylate
N_3-PVDF	Azide functionalized PVDF
N_{agg}	Aggregation number
NaOH	Sodium hydroxide
NEt_3	Triethylamine
NF	Nanofiltration
NHS	N-hydrosuccinimide
NHS-CTA-XA	N-hydrosuccinimide and xanthate functional chain transfer agent
NIPAM	*N*-isopropylacrylamide
NIPS	Non-solvent induced phase separation
NMM	N-methylmorpholine
NMP	*N*-methyl-2-pyrrolidone
NMR	Nuclear magnetic resonance
NP	Nanoprecipitation or nanoparticle
NPs	Nanoparticles
NTs	Nanotubes
NVP	N-vinylpyrrolidone
N_3-CTA-XA	Azide functional Xanthate Chain Transfer Agent
p	Packing parameter
P(VDF-*co*-CTFE)	Poly(vinylidene fluoride-*co*-chlorotrifluoroethylene)

P(VDF-*co*-HFP)	Poly(vinylidene fluoride-*co*-hexafluoropropylene)
P(VDF-*co*-HFP)	Poly(vinylidene fluoride-co-hexafluoropropylene)
P3HT	Poly(3-hexylthiophene)
PAA	Poly(acrylic acid)
pBA	Poly(butyl acrylate)
PCL	Poly(ε-capro-lactone)
PCTFE	Poly(chlorotrifluoroethylene)
PDMAEMA	Poly[2-(dimethylamino)ethyl methacrylate]
PE	Polyethylene
PEBA	Poly(ether-*b*-amide)
PECTFE	Poly(ethylene-*alt*-chlorotrifluoroethylene)
PEG	Polyethylene glycol
PEG_{6000}	Polyethylene glycol M_w = 6000 g mol^{-1}
PEGDA	PEG diacrylate or difunctional PEG acrylate
PEO	Poly(ethylene oxide)
PES	Poly(ether sulfone)
PETFE	Poly(ethylene-*alt*-tetrafluoroethylene
PEVE	Poly(ethyl vinyl ether)
PF8TBT	Poly((9,9-dioctylfluorene)-2,7-diyl-alt-[4,7-bis(3hexylthien-5-yl)-2,1,3-benzothiadiazole]-2′,2″-diyl))
PFB	Pentafluorobutane
PFPE	Perfluoropolyether
PFS	Poly(ferrocenyldimethylsilane)
PFS	Poly(ferrocene-dimethylsilane)
PMMA	Poly(methyl methacrylate)
PNIPAM	Poly(*N*-isopropyl acrylamide)
PP	Polypropylene
PPFMA	Poly(pentafluorophenyl methacrylate)
PS	Polystyrene
PSSA	Poly(styrene sulfonic acid)
PTFE	Poly(tetrafluoroethylene)

PTFE	Poly(tetrafluoroethylene)
PTFE	Polytetrafluoroethylene
PV	Pervaporation
PVA	Poly(vinyl alcohol)
PVDF	Poly(vinylidene fluoride)
PVDF-*g*-PHPGMA	Poly[hyperbranched poly(glycerol methacrylamide)]-*g*-poly(vinylidene fluoride)
PVDF-*g*-PPFMA	Poly(vinylidene fluoride)-graft-Poly(pentafluorophenyl methacrylate
PVF	Poly(vinyl fluoride)
PVP	Polyvinylpyrrolidone
RAFT	Reversible Addition-Fragmentation chain Transfer
RDRP	Reversible Deactivation Radical Polymerization
RO	Reverse Osmosis
SAED	Selected Area Electron Diffraction
SBMA	*N*-(3-sulfopropyl)-*N*-(methacrylox-yethyl)-*N*,*N*-dimethylammonium betaine
SBS	Polystyrene-*b*-polybutadiene-*b*-polystyrene
SEC	Size Exclusion Chromatography
SEM	Scanning Electron Microscopy
SPI	Sulfonated polyimide
T_c	Crystallization temperature
T_d	Decomposition temperature
TEA	Triethylamine
TEM	Transmision Electron Microscopy
tetraPEG-BAH	tetrabenzaacylhydrazide-terminated 4-arm star poly(ethylene glycol)
TFA	Trifluoroacetic acid
TFE	Tetrafluoroethylene
TFE	Trifluoroethanol
T_g	Glass transition temperature
TGA	Thermogravimetric analysis
THF	Tetrahydrofuran
TI-CDSA	Temperature-Induced Crystallization-Driven Self-Assembly

TIPS	Temperature Induced Phase Separation
TIPS	Triisopropylsilane
T_m	Melting temperature
TrFE	trifluoroethylene
UF	Ultrafiltration
v	Volume
VAc	Vinyl acetate
VDF	Vinylidene fluoride
VIPS	Vapor Induced Phase Separation
VTES	Triethoxyvinylsilane
XRD	X-Ray Diffraction
δ	Chemical shift
λ	Wavelength

GENERAL INTRODUCTION

Self-assembly has become one of the holy grails of nanotechnology, and numerous researchers are working on using self-assembled structures as an effective nano-engineering tool. For decades, scientists have studied “supramolecular” chemistry, learning not only how molecules bind to one another but also how large numbers of molecules could team up to form larger ordered structures. The concept of self-assembly largely grew out of chemists' attempts to make molecules that aggregated spontaneously into specific configurations, in the same way, biological molecules form complex structures such as cell membranes for example. The assemblies’ properties, shape, and size are determined by the properties of their constituents. The choice of the material of these constituents is thus decisive.

Thanks to its excellent mechanical properties, chemical inertness, easy processing and high-temperature resistance poly(vinylidene fluoride) (PVDF) is an appealing material for the fabrication of membranes for water filtration. Also, PVDF presents piezoelectricity, ferroelectricity, and pyroelectricity. As a result, they find applications in membranes for energy (such as batteries, energy harvesters, contactors, etc…) and the emerging field of printed electronics.

To date the solution self-assembly of block copolymers (BCPs) where one of the blocks is a fluorinated polymer (such as PVDF) has not been explored much. Only a few references show some attempts to self-assemble amphiphilic fluorinated BCPs.

In the last 7 years our team has developed the MADIX polymerization of VDF. The use of MADIX in combination with efficient coupling chemistries allowed the preparation of a range of novel PVDF-based architectures. However, the studies of the self-assembly of these PVDF-based BCPs architectures are still in their infancy.

PVDF based self-assembled structures could be employed to prepare nanostructured PVDF based membranes where the pore size is determined by the size and shape of the nanoparticles and their packing. Additionally, PVDF-based amphiphilic BCPs can find application as novel additives for PVDF water-filtration membranes.

This works aims to synthesize PVDF-based amphiphilic block copolymers and study their self-assembly behavior to get a better insight in how PVDF properties such as high crystallinity affect the self-assembly mechanisms.

This thesis is divided into 6 Chapters.

Chapter 1 is a literature review, on existing knowledge related and necessary to understand the overall work gathered in this thesis. An introduction to fluoropolymers and more specifically to PVDF homo- and copolymers and their application in membrane science is provided. The introduction also gives some background on the synthesis of PVDF and PVDF-based architectures made my MADIX as well as a general introduction to the preparation of self-assembled structures in solution.

Chapter 2 describes the synthesis, characterization and self-assembly behavior of an ABA amphiphilic PVDF-based block copolymer where A is PVDF and B is poly(ethylene glycol) (PEG).

Chapter 3 describes the synthesis, self-assembly and Crystallization-Driven Self-Assembly (CDSA) behavior of an ABA block copolymer in which block A is a P(VDF-*co*-HFP) copolymer, a less crystalline and more soluble fluoropolymer as compared to PVDF.

In **Chapter 4** the synthesis of PNIPAM-*b*-PVDF based diblock copolymers, their self-assembly, and the application of the aggregates obtained for immobilization and in-situ preparation of gold nanoparticles is described.

Chapter 5 deals with the preparation of cyclic peptide-PVDF conjugates and their self-assembly into hollow tubular structures.

Chapter 6 describes how the triblock copolymer described in chapter 2 can be employed as an additive for the preparation of PVDF porous membranes by phase inversion method. The study of the performance and aging of the resulting membranes for water filtration application is also reported.

Finally, a summary of conclusions of the chapters and future perspectives of this work are given.

INTRODUCTION GÉNÉRALE

L'auto-assemblage est devenu le Saint-Graal de la nanotechnologie. Actuellement les chercheurs dans de nombreux laboratoires travaillent pour le transformer en un outil efficace de nano-ingénierie. Au cours des dernières décennies, les chercheurs ont étudié la chimie «supramoléculaire», en apprenant non seulement comment les molécules se lient les unes aux autres, mais aussi à quel point un grand nombre de molécules peuvent s'associer pour former des structures ordonnées plus grandes. Le concept d'auto-assemblage est en grande partie issu des tentatives des chimistes de fabriquer des molécules capables de s'agréger spontanément dans des configurations spécifiques, de la même manière que les molécules biologiques forment des structures complexes telles que les membranes cellulaires ou les structures tertiaires des protéines et enzymes, par exemple. Les propriétés des nano-objets auto-assemblés, leur forme et leur taille sont déterminées par les propriétés de leurs constituants. Le choix du matériel de ces constituants est donc décisif.

Grâce à ses excellentes propriétés mécaniques, son inertie chimique, et sa résistance aux hautes températures, le poly(fluorure de vinylidène) (PVDF) est très attrayant pour la fabrication de membranes pour la filtration de l'eau. De plus, le PVDF peut également être utilisé dans d'autres applications membranaires (telles que les batteries, les capteurs d'énergie, les contacteurs, etc) et dans le domaine émergent de l'électronique imprimée grâce à ses propriétés électroactives (piézoélectricité, ferroélectricité et pyroélectricité).

L'auto-assemblage en solution de copolymères à blocs dont l'un des blocs est un polymère fluoré (tel que le PVDF) n'a pas été suffisamment exploré à ce jour. Seules quelques références montrent des tentatives d'assemblage de polymères amphiphiles ou l'un des blocs est un polymère fluoré.

Récemment, l'équipe ICGM-IAM a développé la polymérisation MADIX du VDF. L'utilisation de MADIX en combinaison avec des chimies de couplage efficaces a permis la préparation d'une gamme de nouvelles architectures à base de PVDF. Cependant, les études sur l'auto-assemblage de ces architectures basées sur le PVDF en sont encore à leurs balbutiements.

Des assemblages à base de PVDF pourraient aussi être utilisés pour préparer des membranes nanostructurées dans lesquelles la taille des pores serait déterminée par la taille

et la forme des nanoparticules et par leur agencement dans l'espace. De plus, les copolymères à blocs amphiphiles à base de PVDF pouraient trouver des applications en tant que nouveaux additifs pour les membranes de filtration d'eau en PVDF.

L'objectif de ce travail est de synthétiser des copolymères à blocs amphiphiles à base de PVDF et d'étudier leur comportement d'auto-assemblage et de déterminer comment les propriétés du PVDF, telles que la haute cristallinité, affectent ces mécanismes d'auto-assemblage.

Cette thèse est divisée en 6 chapitres.

Le **chapitre 1** est une étude bibliographique présentant les différents aspects nécessaires à la compréhension de la thèse. Une introduction aux polymères fluorés et plus particulièrement des homopolymères PVDF et les copolymères à base de PVDF et leur application dans les sciences eta technologies membranaires. Ce chapitre presente aussi l'état de l'art de la synthèse de PVDF et des architectures à base de PVDF faites par MADIX ainsi qu'une introduction générale à la préparation de structures par l' auto-assemblage de copolymères à blocs en solution.

Le **chapitre 2** décrit la synthèse, la caractérisation et le comportement d'auto-assemblage d'un copolymère à bloc amphiphile ABA à base de PVDF, où A est du PVDF et B est un poly (éthylène glycol) (PEG).

Le **chapitre 3** décrit la synthèse, l'auto-assemblage et l'assemblage dirigé par la cristallisation (CDSA, de l'anglais crystallization-driven self-assembly) d'un copolymère à bloc similaire à celle décrit dans le chapitre 1 dans lequel le bloc PVDF a été remplacé par un copolymère de type P(VDF-*co*-HFP).

Dans le **chapitre 4** la synthèse de copolymères à blocs PNIPAM-*b*-PVDF, leur auto-assemblage, et leur application pour l'immobilisation et la préparation in-situ de nanoparticules d'or est décrite.

Le **chapitre 5** traite la préparation de conjugués peptide cyclique-PVDF et leur auto-assemblage en nanostructures tubulaires creuses.

Le **chapitre 6** décrit comment le copolymère tribloc décrit au chapitre 2 peut être utilisé comme additif pour la préparation de membranes poreuses en PVDF par inversion de phase. L'étude de la performance des membranes résultantes pour l'application de filtration de l'eau est également rapportée.

Finalement, un résumé des conclusions de chaque chapitre et des perspectives futures de ce travail de thèse sont présentées.

Chapter 1

Introduction

1. Membrane technology

Water shortage and energy consumption are global problems even in developed countries. With population and economies growth, problems of water scarcity and energy source rarefaction are expected to worsen in the coming decades.[1] Membrane technology is an important and a promising way to mitigate these two problems. The principal advantages of membrane technologies are the relatively low energy consumption, easy use, low footprint (large specific surface area), environmental friendliness and well-understood process methods.[2–4] With the progress in membrane materials, many processes including reverse osmosis (RO), ultrafiltration (UF), microfiltration (MF), nanofiltration (NF), electrodialysis, pervaporation (PV), etc. have been widely employed in diverse applications.[5–12] Recently, some innovative new processes like forward osmosis (FO), membrane contactors (MC), catalytic membrane reactors, and fuel cell membranes have been widely investigated and have strong potential for application in the process industry.[3,13,14]

New processes often require novel membranes, thus, research dealing with the development of new membrane materials is increasing. For a specific membrane application, polymers need to have specific properties such as good film-forming ability, high mechanical, chemical and thermal stability, and a good balance of permeability and selectivity. Additionally, membranes should also be hydrophilic when used for MF/UF with aqueous solutions, but should be very hydrophobic when they are used for membrane distillation (MD).[15] Membranes must have high gas permeability and selectivity for gas separation applications. When they are used for energy applications such as fuel cells, membranes should have high proton exchange capacity.[16–18] During the past decades, most studies have been focused on making more hydrophilic membranes due to the prosperous research on MF/UF. However, recently, more attention has been paid to new membrane processes, especially MD, which requires more hydrophobic membranes.[15,19,20]

2. Fluoropolymers in Membrane Science

A fluoropolymer or fluorinated polymer is a carbon-based polymer with multiple carbon-fluorine bonds. Although the use of fluorine in organic and inorganic chemistry dates back to the XVIIth century, the development of fluoropolymers (polymers where the fluorine atoms are connected directly to the backbone) is more recent.[21–23] Fluoropolymers have attracted wide attention both in industry and academics, due to their outstanding thermal, physical and chemical stability.[22–24] They often exhibit excellent inertness to chemicals, strong weather resistance, superior oil and water repellence and low flammability. Due to the extraordinary properties of this special class of polymers, fluoroplastics are nowadays applied in the production of paints and coatings,[25] batteries,[26] (fuel cell) membranes,[27] or energy-harvesting devices.[28,29]

2.1. Fluoropolymers for membrane applications

Fluoropolymers, such as poly(vinyl fluoride) (PVF), poly(vinylidene fluoride) (PVDF), poly(chlorotrifluoroethylene) (PCTFE), poly(tetrafluoroethylene) (PTFE), poly(vinylidene fluoride-*co*-chlorotrifluoroethylene) (P(VDF-*co*-CTFE)), poly(vinylidene fluoride-*co*-hexafluoropropylene) (P(VDF-*co*-HFP)), poly(ethylene-*alt*-tetrafluoroethylene) (PETFE), and poly(ethylene-*alt*-chlorotrifluoroethylene) (PECTFE) have been widely studied.[23,30–34] These polymers constitute a unique class of materials endowed with unique combinations of properties that, in the past few decades, have attracted significant attention for very diverse applications. These polymers present high thermal stability, improved chemical resistance, and lower surface tension due to the low polarizability and the strong electronegativity of the fluorine atom, its small van der Waals radius (1.32 Å), and the strong C-F bond (485 kJ mol^{-1}). These outstanding properties, make fluoropolymers excellent candidates for membrane technology (see Table 1).

Table 1. Fluoropolymers for membrane opearations.[3]

	Polymer	Membrane process
Poly(vinylidene fluoride) (PVDF) homopolymer		MF, UF, MD, MCr, ME, PV
PVDF copolymer	Poly(vinylidene fluoride-*co*-tetrafluoroethylene) (P(VDF-*co*-TFE))	MF/UF, MD
	Poly(vinylidene fluoride-*co*-hexafluoropropene) (P(VDF-*co*-HFP))	MF/UF, MD, PV, fuel cell, lithium ion battery
	Poly(vinylidene fluoride-*co*-chlorotrifluoroethylene) P(VDF-*co*-CTFE)	MF/UF, NF, MD, PV, fuel cell
	Poly(vinylidene fluoride)-graft-poly-(styrene sulfonic acid) PVDF-*g*-PSSA	Fuel cell
	Poly(vinylidene fluoride-trifluoroethylene) (P(VDF-TrFE))	Lithium ion battery, tissue regeneration
Poly(tetrafluoroethylene) (PTFE) homopolymer		MD, MC, PV, MGA
PTFE copolymer	Perfluorosulfonic acid (PFSA)	Fuel cell, lithium ion battery, chlor-alkali industry
	Poly(tetrafluoroethylene-*co*-perfluoropropyl vinyl ether) (PFA)	Fuel cell
	Poly(tetrafluoroethylene-*co*-hexafluoropropylene) (FEP)	MD, fuel cell
	Poly(ethylene-*alt*-tetrafluoroethylene) (ETFE)	Fuel cell
Poly(ethylene chlorotrifluoroethylene) (ECTFE)		PV, has potential in MD, MC and MF/UF
Other fluoropolymers	Poly(chlorotrifluoroethylene) (PCTFE)	
	Poly(vinyl fluoride) (PVF)	Fuel cell
	Poly(fluorenyl ether) (PFE)	Fuel cell
	Hyflon® AD, Teflon® AF, Cytop®	Gas separation, have potential in MD, MC

Some fluoropolymers possess desirable properties for a wide range of membrane and thin film applications. The required properties of a fluoropolymer for different membrane processes are listed in Table 2. More details can be found in dedicated reviews.[3,6,15]

Table 2. Representative membrane processes and requirements for membrane materials.[3]

Membrane process	General mechanism	Main properties
MF/UF	Pressure-driven, liquid passes through the membrane pores	Hydrophilic used in aqueous systems, while hydrophobic used in oil systems
MD	Thermally-driven, water vapor passes through the membrane pores	Hydrophobic, high porosity
Membrane crystallization (MCr)	Thermally-driven, vapor passes through the membrane pores	Hydrophobic used for hydrophilic (aqueous) crystallizing solutions, while hydrophilic used for oleophilic solutions
Membrane emulsification (ME)	Pressure-driven, contentious phase passed through the membrane pores	Hydrophobic used for producing O/W emulsions, while hydrophilic used for producing W/O emulsions
Osmotic distillation	Vapor pressure-driven, vapor diffuses through the membranes	Hydrophobic typically
PV	Concentration-driven, vapor passes through the membranes	Hydrophilic for dehydration of organic solvents or organic mixtures; hydrophobic for removal of organic solvents or volatile organic compounds (VOCs) from water;organophilic for organic/organic separation
Proton-exchange membrane (PEM)	Proton transports in membranes	High proton conductivity, mechanical, chemical and thermal stability, good barrier properties for gas and methanol
Membrane separator for Li-ion battery	Transport ionic charge carriers and prevent electric contact between anode and cathode electrodes	High ionic conductivity and good barrier for electron
Gas separation membrane	Pressure-driven	High diffusivity and/or high solubility to permeate gases
Membrane gas absorption (MGA)	Concentration gradient-driven, gas passes through the membrane pores	Hydrophobic

2.2. Preparation of fluoropolymer membranes

Numerous methods have been studied and employed for the preparation of fluoropolymer membranes. These include phase inversion, electro-spinning, sintering, stretching, track

etching, etc. Most commercial fluoropolymer membranes are commonly produced via phase separation methods due to their simplicity and flexible production scales. Phase inversion can be described as a de-mixing process that allows the transformation of a homogeneous polymer solution from liquid to solid state in a controlled manner. Recently, electro-spinning has gained attention as an easier alternative to prepare hydrophobic membranes for MD.[15,35,36] Table 3 summarizes the main preparation methods of fluoropolymer membranes.

Table 3. Preparation methods of fluoropolymer membranes[3]

Preparation method	Mechanism
Phase inversion	
Non-solvent induced phase separation (NIPS)	Phase separation is induced by the exchange of the solvent in polymer solution with the non-solvent from the coagulation bath.
Thermally induced phase separation (TIPS)	Phase separation is induced by the temperature change.
Vapor induced phase separation (VIPS)	Phase separation is induced by penetration of non-solvent vapor into the solution.
Solution-casting	Polymer solution is cast and evaporated.
Casting-freezing	Polymer solution is cast and frozen at a temperature lower than solvent's freezing point.
Electro-spinning	Polymer solution is injected through the nozzle onto the electrode or collector to prepare nano-fibres.
Sintering	Polymer films are sintered.
Stretching	Polymer melts are subject to orientation.
Track etching	Dense polymer films are exposed to radiation to create holes for permeation.

2.3. PVDF

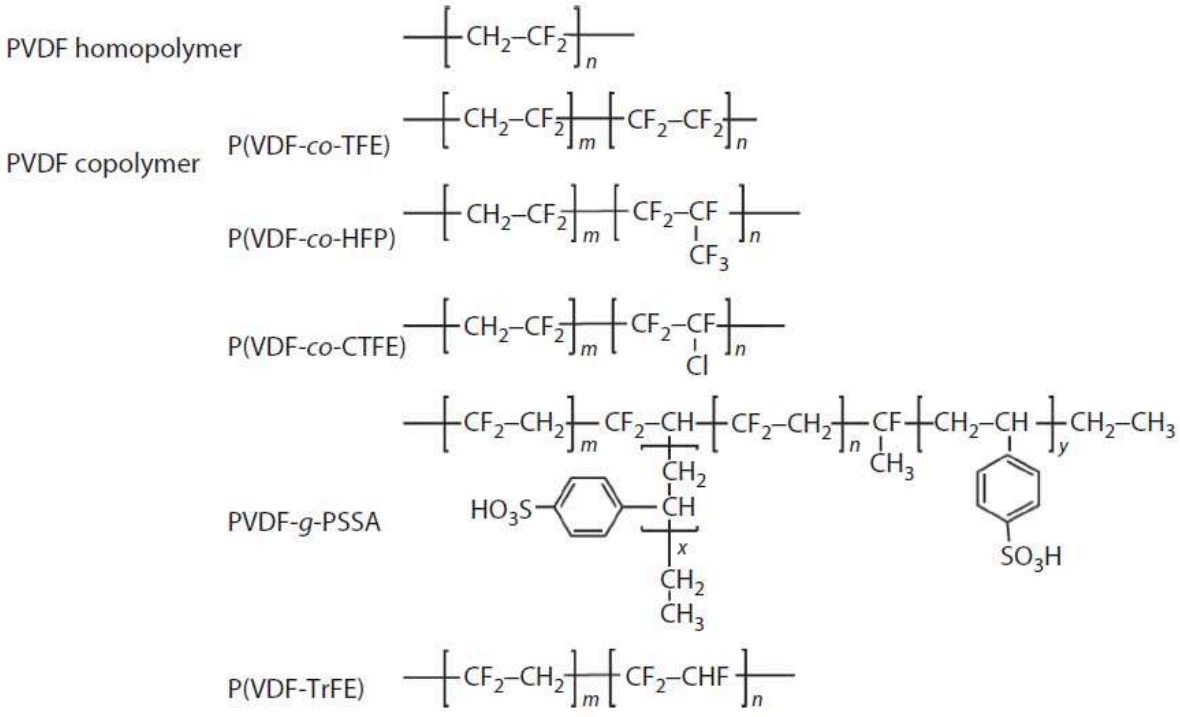

Figure 1. Chemical structures of PVDF homo and copolymers.[3]

Poly(vinylidene fluoride) (PVDF), the second fluoro-plastic in production volume after PTFE,[37] is an exceptional member of the fluoropolymer family. PVDF (chemical structure in Fig. 1.) is an interesting fluoropolymer with remarkable properties such as thermal stability, chemical inertness to solvents, oils and acids (but not to bases), and piezo-, pyro-, and ferroelectric properties.[6,23,32,38–40] However, a high melting temperature together with the poor solubility of PVDF in common organic solvents result in high processing costs. To overcome these issues, various fluorinated copolymers based on VDF have been designed and manufactured in the last decades.[3,32,41] In recent years, well-defined PVDF-containing copolymers like block-, graft- and alternating copolymers received more attention, and their preparation have been discussed in some excellent reviews.[22,42,43]

PVDF homopolymers are semicrystalline.[23,44] Their crystallinity ranges from 35 to 70% depending on the preparation method, thermomechanical history and proportion of chain defects. Molar mass, polydispersity, chain defects, crystallinity and crystalline phase are the major factors affecting the properties of PVDF.[45]

PVDF can crystallize in five crystalline phases called α, β, γ, δ and ε. The crystallized chains in PVDF present 3 different conformations designated as all trans (TTT) planar zigzag for the β-phase, TGTG’ (trans-gauche-trans-gauche) for the α and δ phases and TTTGTTTG’ for γ and ε phases. However, the most common and more investigated ones are α, β and γ-phases (see Figure 2).[31,45]

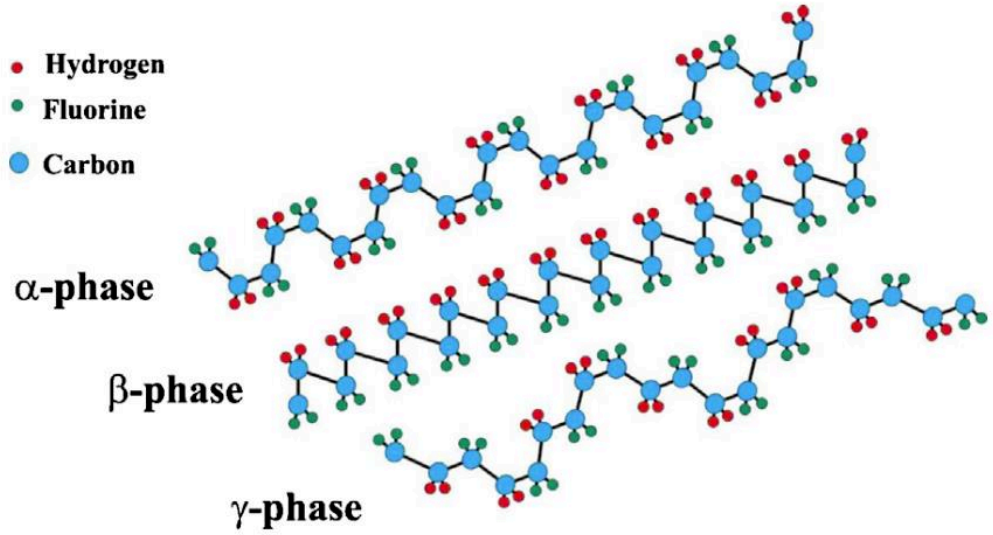

Figure 2. Schematic representation of the chain conformation of the α, β and γ phases of PVDF. [31]

Each phase of PVDF imparts different properties to the polymer but other characteristics such as the molecular weight, molecular weight distribution and extent of irregularities along the polymer chain also play an important role. The glass transition (T_g) and melting temperatures (T_m) of the amorphous and crystalline PVDF regions are in the ranges of −40 to −30 °C and 155 to 192°C, respectively. Amorphous PVDF regions have a density of 1.68 g cm^{-3}, alpha and gamma polymorphs have a density of 1.92 and 1.93 g cm^{-3}, respectively, while that of the beta polymorph is 1.97 g cm^{-3}. Thus, the typical density of commercial products is in the range of 1.75 to 1.78 g cm^{-3}, reflecting a crystallinity degree of around 40%. The melt density of a PVDF homopolymer is ca. 1.45–1.48 g cm^{-3} at 230 °C and 1.0 bar.[23,31] Because of its excellent combination of properties and processability (albeit requiring relatively high T), PVDF is available in a wide range of melt viscosities as powders and pellets to fulfill typical fabrication requirements. All common extrusion and molding techniques can be applied to process PVDF into shapes.[22]

2.3.1. PVDF in membrane applications

PVDF membranes are widely employed in the process industry and have been used in UF/MF, MD, PV and other processes. They have also been adopted in energy applications such as fuel cell membranes and separators in lithium ion batteries. Apart from the

membranes employed for energy applications, PVDF membranes are usually porous membranes.

2.3.1.1. PVDF membrane preparation

Porous membranes are very similar in structure and function to conventional filters. They present a rigid, highly voided structure with randomly distributed, interconnected pores, in the 0.01–10 µm diameter range.[3,46] Separation of solutes by microporous membranes is mainly a function of solute size and membrane pore size distribution.

To date, most of the commercial membranes, including fluoropolymer membranes, are produced via phase inversion[47] (see Scheme 1) mainly because of the simplicity and flexibility to scale up production, resulting in a low cost of production.[3] Post-treatment is a useful method to improve the membrane structure and properties. Stretching is frequently employed to increase the pore size and porosity.[48–50] Commonly, the stretching step also improves the mechanical properties of microporous PVDF membranes. The effects of stretching parameters such as, temperature, ratio and holding time on the membrane properties have been studied.[50]

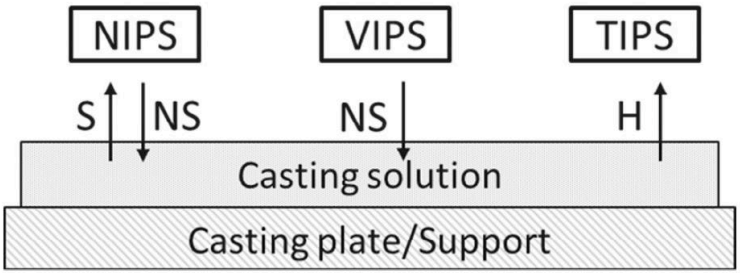

Scheme 1. Schematic of the main phase inversion processes. Non-solvent induced phase separation (NIPS), Vapor induced phase separation (VIPS) and Temperature induced phase separation (TIPS) (S : Solvent, NS : non-solvent, H : Heat).[49]

Phase inversion processes are based on a transition between two phases, induced by a change of polymer solubility. Starting from a homogeneous mixture, i.e. the dope, a change in composition or conditions induces de-mixing of the mixture into a polymer rich and a polymer poor phase.[49] Upon further separation, the solubility of the polymer decreases and

a solid phase with specific morphology is formed. The phase separation and precipitation can be induced in different ways:

Non-solvent induced phase separation (NIPS): In NIPS, the casting solution is immersed in a coagulation bath containing a non-solvent, resulting in solvent-nonsolvent exchange.

Solvent and non-solvent selection: First step is to dissolve or obtain a homogeneous dispersion by choosing an appropriate solvent. NMP, DMF, DMAc and THF are the most common solvents used to prepare PVDF solutions. The effect of solvent on membrane morphology has been discussed in detail by Tao and co-workers.[51] The second step is the selection of the non-solvent. Solvent and non-solvent miscibility is mandatory. In the case of high mutual affinity (or miscibility), a more porous membrane is likely to be obtained due to fast de-mixing. Low mutual affinity is likely to delay de-mixing, resulting in asymmetric membranes presenting a dense non-porous top layer.

Both symmetric and asymmetric membranes can be prepared by NIPS by solvent and non-solvent selection:

- Asymmetric membranes with a dense skin top layer supported by a porous structure.[52]
- Asymmetric membranes made of a thin top layer with a narrow pore size (20–100 nm) supported by a very open porous structure (macrovoids or finger-like structures).[53]
- Symmetric membranes with a relatively well-defined pore size along their entire thickness.[52,54]

The most common non-solvent is water, mainly because it is environmentally friendly and cheap.

Polymer solution composition:

- Polymer concentration and properties: Since the polymer is the component forming the membrane matrix, the polymer concentration, molecular weight (viscosity increase with PVDF molecular weight)[55] of the polymer in the casting

solution can greatly influence the final morphology. Typically, the higher the concentration, the lower the porosity (see Figure 4).[47]

- Additives in the polymer solution: Additives (organic or inorganic components such as hydrophilic polymers, surfactants or nanoparticles) can influence the pore formation and structure of the membrane, but also, enhance the hydrophilicity and performance of the membrane.[56,57]

Film casting conditions:

- Composition of the coagulation bath: The addition of small amounts of solvent or other non-solvents (methanol, isopropanol) in the coagulation bath can greatly influence the formation of the membrane by affecting the rate of mass exchange between the non-solvent and casting solution.[58,59]
- Temperature: The casting temperature can affect the solution viscosity affecting also the exchange rate. The temperature of the coagulation bath can also influence the final morphology (see Figure 3).[47,60]
- Precipitation time: Delayed immersion in the coagulation bath can induce the formation of a denser top-layer due to exposure to air/humidity (as in the case of delayed de-mixing).[54]

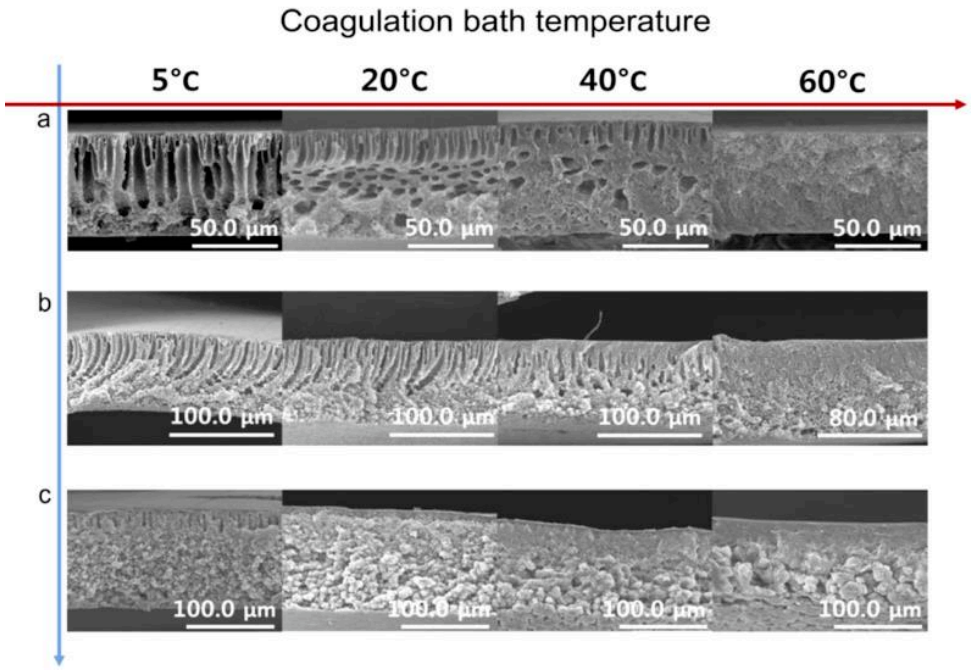

Figure 3. Morphologies of PVDF membranes prepared using an additive (Polarclean®) under different coagulation temperatures and polymer concentrations of (a) 15 wt.%, (b) 20 wt.% and (c) 25 wt.%.[47]

Table 4. Effects of various parameters on PVDF membrane morphology via NIPS.[61]

System		Factor	Membrane Structure
Solvent		weak solvent power stronger solvent power	sponge-like Macrovoids
Non-solvent		weak non-solvent strong non-solvent	Symmetric membrane consists of uniform spherical particles asymmetric structure consists of dense skin layer accompanied by finger-like or/and sponge-like structure
Coagulation bath temperature		high temperature low temperature	finger-like sponge-like structure or/and particles (if crystallization occurs)
Additives	Inorganic salts	low concentration higher concentrations up to a certain value	larger cavities and hence increase of gravimetric porosity and maximum pore size less macrovoids formation
	Polymeric additives	PVP PEG	more large finger-like macrovoids, higher gravimetric porosity and mean pore size higher pure water flux with a relatively lower rejection rate of membranes
	Non-solvent additives	water 1,2-ethanediol	larger pore radius and effective gravimetric porosity larger gravimetric porosity and pore size becomes more uneven

Vapor induced phase separation (VIPS): In VIPS, the casting solution takes up the non-solvent from the vapor phase.

Generally, a polymer solution is placed in an environment containing a non-solvent (usually air containing water vapor). The non-solvent is absorbed by the polymer solution and, as a result, de-mixing occurs and the membrane is formed. More details about PVDF membrane formation by VIPS can be found in some very good reviews.[62,63]

Temperature induced phase separation (TIPS): In TIPS, a decrease in temperature induces the precipitation.

TIPS is a method in which a polymer dope solution is prepared in high boiling point solvent at elevated temperatures (typically above the crystallization temperature (T_c) of the dope solution)[50] and the resulting polymer solution is then casted on the support. Then, the temperature is reduced to induce de-mixing. Notably, to remove the solvent in TIPS, evaporation, extraction, and freeze-drying are used.[34,47,64] The unique advantages of TIPS are as follows: simplicity of the process, high reproducibility, low propensity to generate defects,

high porosity, and narrow pore size distribution. In addition, polymer polymorphism can be induced.[50]

The dope composition and the conditions during preparation will determine the morphology of the membrane.[65]

Only polymers that can be dissolved are suitable for the phase inversion process, which limits the choice of materials. However, this process benefits from the versatility in membrane structures that can be produced by tuning the preparation conditions.

2.3.1.2. PVDF membrane modification

Properties of PVDF membranes can be enhanced or modified applying numerous methods. Surface coating, grafting of polymers on the membrane surface, use of polymer blends or pore-filling have been investigated and employed.[3,15] Some modifications, such as polymer grafting or pore filling, despite offering the possibility to influence the properties of the PVDF membranes vastly, are modifications that could be not very efficient. With the grafting method often a good grafting density is not obtained, leading to modest improvements. In the case of pore filling, since the additives are not bound to the pore surface they gradually leak during the filtration process, hence the conferred properties do not last long. Blending is a simpler approach which does not always leads to prompt loss of enhanced membrane properties (if there is affinity between PVDF and the other components of the blend, the latter are less prone to leaching during the filtration process). It is thus the most commercially advantageous approach compared to other methods.

2.3.1.2.1. Surface modification

Surface modification can be useful for improving the surface properties of PVDF membranes. Most studies are directed towards changing or enhancing hydrophilicity, hydrophobicity or oleophobicity of PVDF membrane surfaces.[66] Surface modification includes chemical modification methods, plasma technology[67] or surface-modifying macromolecules (particles or polymers).[12,68–71] Jeong *et al.* improved hydrophobicity in PVDF membranes for a MD application by applying plasma treatment with different gases and plasma polymerization (O_2 or CF_4).[67] O_2 plasma treatment led to increased hydrophobicity while CF_4 treatment led to increased hydrophilicity. However, posterior hydrophobic coating

with plasma polymerization of hexamethyldisiloxane (HMDSO) conferred much higher hydrophobicity to the CF_4 treated membrane (see Figure 4).

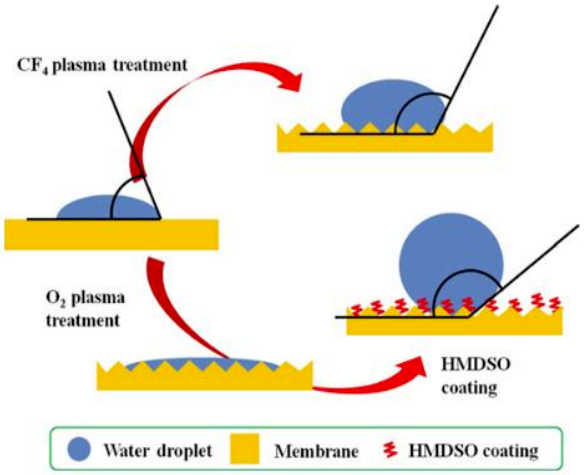

Figure 4. Representation of the modification of a PVDF membrane by O_2 plasma treatment and a hydrophobic coating or modified by CF_4 plasma.[67]

2.3.1.2.2. Pore-filling

The pore-filling method is a simple way to modify PVDF membranes by filling PVDF membrane pores with polymers, inorganic particles,[72] or carbon nanotubes.[7] Adjustable size[73] or enhanced hydrophilicity[74] of membrane pores are some of the improvements that can be obtained by this method. Wan *et al.* functionalized porous PVDF membranes by directly polymerizing poly(acrylic acid) (PAA) inside the membrane pores and studied the viability of the system for the *in situ* preparation and regeneration of Fe/Pd nanoparticles for an application in remediation of organic compounds (see Figure 5).

Figure 5. Example of pore functionalized PVDF membranes via pore-filling. Poly(acrylic acid) (PAA) directly synthesized inside the pores and in-situ preparation of Fe/Pd NPs for remediation of chlorinated organic compounds.[72]

2.3.1.2.3. Blending

Blending is a simple and recurrent method to modify the properties of fluoropolymer membranes. Blending of polymers and/or inorganic particles have been used to improve membranes hydrophilicity/hydrophobicity, proton conductivity, or ionic strength.[26,35,63,75–80] Interestingly, amphiphilic copolymers can bring hydrophilicity to a PVDF membrane in a single step process.[81,82] Generally, the synthesis of amphiphilic copolymers can be achieved by free radical polymerization,[83] graft copolymerization, cationic and anionic polymerization,[84] and reversible-deactivation radical polymerization techniques (RDRP) such as RAFT or ATRP for example.[6,85–87] Filtration membrane properties have been improved by blending PVDF with different polymers or NPs. Thermoresponsive membranes with enhanced wettability by using a PNIPAM/PVDF blend,[35] *N*-vinyl-2-pyrrolidone (NVP), triethoxyvinylsilane (VTES) copolymers were used to immobilize PVP segments in PVDF membrane via *in situ* cross-linking (after hydrolysis treatment) to obtain membranes with persistent hydrophilicity.[79] Blends with polyether block amide (PEBA) allowed the preparation of pervaporation (PV) membranes with better performance for the removal of isopropyl alcohol from aqueous solutions.[88] Blends with poly(vinyl alcohol) (PVA) modified SiO_2 NPs led to improved antifouling property membranes.[89] Also blends of TiO_2 embedded PVDF with polymethyl methacrylate (PMMA) have been studied for the preparation of photocatalytic membranes with enhanced hydrophilicity and mechanical properties.[78]

An interesting approach is to use polymers or polymer blocks compatible with PVDF to avoid leaking during the coagulation bath or filtration process. A hyperbranched poly(ether amine) (hPEA) hydrogel (first functionalized with fluorocarbon chains to enhance compatibility with PVDF and photosensitive moieties to have cross-linking functionality) was synthesized and blended with PVDF. The hPEA@PVDF membranes (see Figure 6) prepared by NIPS could adsorb dyes via molecular filtration and presented, good adsorption rates and capacity.[90]

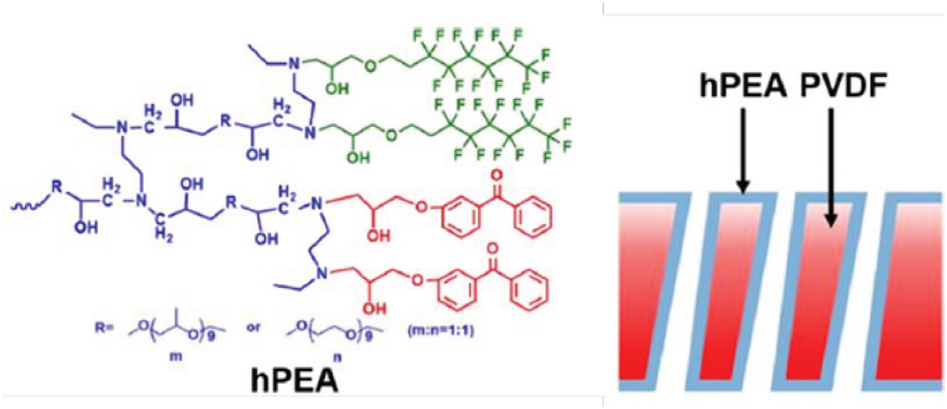

Figure 6. Chemical structure of hPEA and proposed model of the hPEA@PVDF membrane.[90]

Regarding energy applications, sulfonated polyimide (SPI)/PVDF blends were employed to prepare proton exchange membranes (MEMs) with higher swelling ratio and higher proton conductivity than commercial Nafion.[91]

2.3.1.2.4. Graft copolymers

This includes the use modification of PVDF-based membranes by grafting copolymers to confer certain properties, such increased hydrophilicity. Poly(vinylidene fluoride)-graft-Poly(pentafluorophenyl methacrylate (PVDF-*g*-PPFMA) was synthesized by RAFT graft copolymerization of poly(pentafluorophenyl methacrylate) (PPFMA) from the ozone-preactivated PVDF. Poly[hyperbranched poly(glycerol methacrylamide)]-*g*-poly(vinylidene fluoride) (PVDF-*g*-PHPGMA) was obtained by ulterior modification of PPFMA chains with amino-terminated hyperbranched polyglycerol (HPG-NH_2). MF membranes were prepared by NIPS with this branched copolymer (PVDF-*g*-PHPGMA). After membrane formation ATRP initiation sites were introduced on the membrane via postmodification of the diol moitiess with 2-bromo-2-methylpropionyl bromide (BIBB) present on the PHPGMA. PVDF-*g*-PHPGMA-GPSBMA membrane was prepared via surface-initiated atom transfer radical polymerization (SI-ATRP) of the zwitterionic monomer, *N*-(3-sulfopropyl)-*N*-(methacrylox-yethyl)-*N*,*N*-dimethylammonium betaine (SBMA) to obtain a final hierarchical membrane with improved antibiofouling property (see Figure 7).[92]

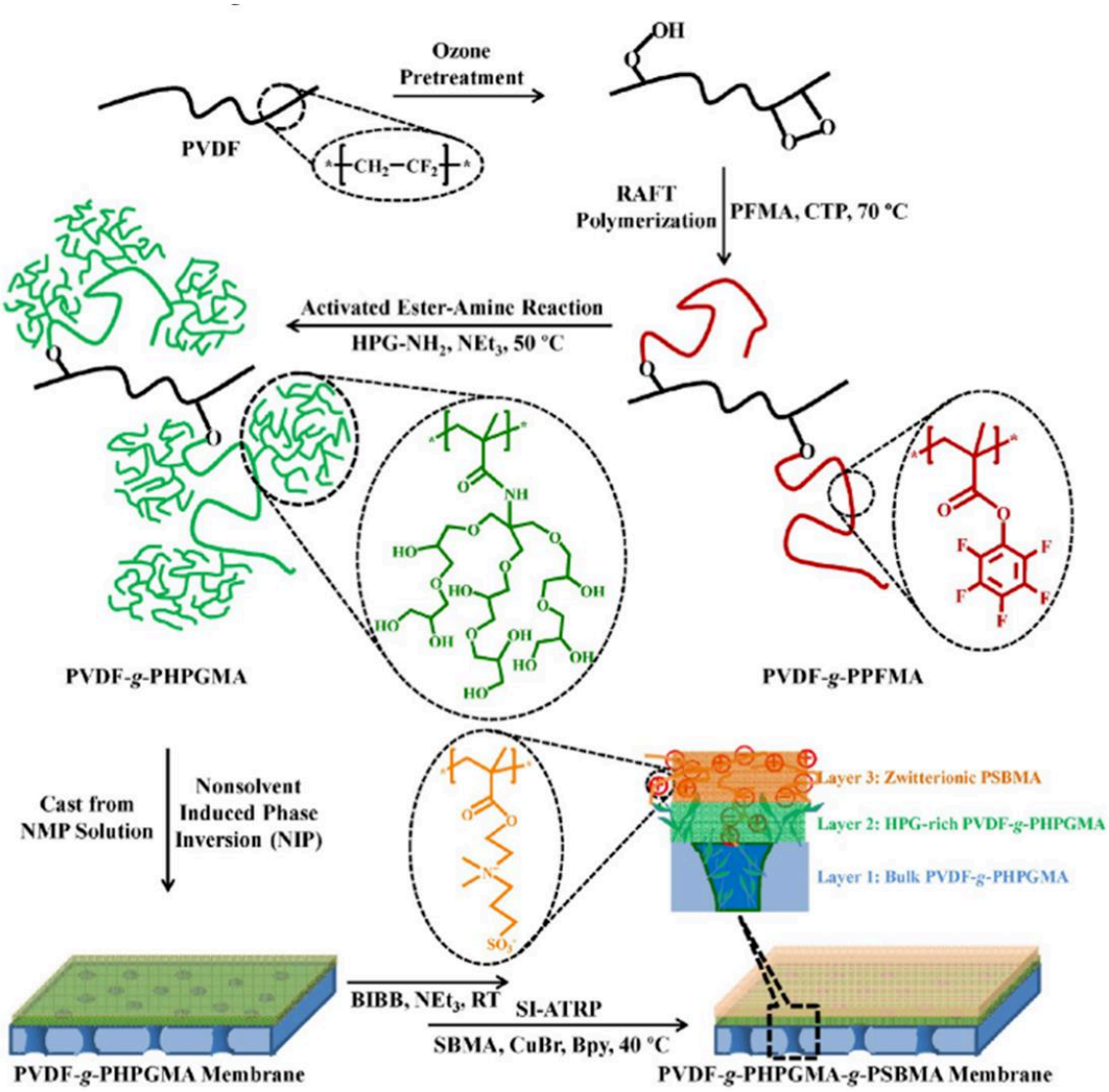

Figure 7. Schematic illustration of the processes of ozone pretreatment and RAFT graft copolymerization of PVDF with PFMA, Activated ester-amine reaction, preparation of PVDF-*g*-PHPGMA-*g*-PSBMA membrane via SI-ATRP of SBMA from the PVDF-g-PHPGMA Membrane. PFPMA (pentafluorophenyl methacrylate), CTP (4-cyano-4-(phenylcarbonothioylthio)pentanoic acid, HPG-NH_2 (amino-terminated hyperbranched polyglycerol), NEt_3 (trimethylamine), NMP (1-methyl-2-pyrrolidone), NIP (Non-solvent induced phase separation, also referred as NIPS), BIBB (2-bromo-2-methylpropionyl bromide), SBMA (N-(3-sulfopropyl)-N-(methacryloxyethyl)-N,N-dimethylammonium betaine), CuBr (Copper bromide), Bpy (2,2'-bipyridine) [92]

Regarding membranes for energy application, a research group recently described the synthesis of SiO_2–PVDF nanocomposite fibers that were prepared from KOH treated PVDF powder blended with SiO_2 NPs. Then those nanocomposite fibers were placed in a solution containing ethylene glycol dimethacrylate (EGDMA), 2,2'-azobis(iso-butyronitrile) (AIBN) initiator, and methyl methacrylate (MMA) and heated to produce SiO_2–PVDF-*g*-PMMA

membranes able to retain electrolytes within the fibrous membranes in lithium-ion batteries.[93]

2.3.2.PVDF copolymers in membrane science

Although PVDF has been widely employed in membrane processes, the use of copolymers of VDF allow to access specific properties to match the new requirements emerged in membrane processes. Properties such as higher or lower crystallinity, melting point, glass transition temperature, stability, elasticity, permeability, and chemical reactivity can be changed as a result of copolymerization of VDF with other fluorinated monomers such as TFE, HFP, CTFE or TrFE (chemical structures are listed in Fig.2).

2.3.2.1. Poly(vinylidene fluoride-*co*-tetrafluoroethylene) (P(VDF-*co*-TFE))

In P(VDF-*co*-TFE) the increase in fluorine content results in more hydrophobic material compared to PVDF. It can be dissolved in common organic solvents and used for the fabrication of microporous membranes through the phase inversion process. The hydrophobicity of this copolymer leads to membrane that can be used in MD process. In addition, it also found applications in gas separation.[3] Amira *et al.*[94] prepared an asymmetric P(VDF-*co*-TFE)/Deep Eutectic Solvent supported membrane by phase inversion for CO_2/N_2 separation. They prepared a PVDF-co-PTFE solution in DMAc solvent with PEG as additive and obtain the porous membrane by NIPS technique in a water/ethanol coagulation bath. The obtained membrane was immersed in a deep eutectic solvent (chloromethylene:ethylene glycol 1:3) and vacuum was applied to ensure filling of membrane pores. The membrane showed an improvement in both CO_2 permeance and CO_2/N_2 selectivity compared to empty P(VDF-*co*-TFE) membrane.

Due to its ferroelectric properties, this copolymer also find application as thin-films in organic ferroelectric-gate (FETs), organic ferroelectrics and semiconductors.[95]

2.3.2.2. Poly(vinylidene fluoride-*co*-hexafluoropropene) (P(VDF-*co*-HFP))

The first VDF/HFP copolymer was produced by E.I du Pont de Nemours & Co., under the Viton® trademark in 1957.[33] This copolymer can be either a thermoplastic or an elastomer by varying the HFP content.[33]

P(VDF-*co*-HFP) copolymers have broad applications because the incorporation of HFP not only affects the crystallinity and thus the solubility of the resulting copolymer but also increases the fluorine content.[33] A fluorine content increase makes the copolymer more hydrophobic and very appealing for microporous membranes intended for use as membrane contactors for pervaporation[96] and membrane distillation.[73,97,98] These copolymers also find applications in methanol fuel cell membranes,[27,75,99] lithium batteries[100,101], or actuators,[102] among others.[103–105]

2.3.2.3. Poly(vinylidene fluoride-*co*-chlorotrifluoroethylene) (P(VDF-*co*-CTFE))

In P(VDF-*co*-CTFE) copolymers, the content of CTFE is a crucial factor for the final properties of the copolymers. Small VDF content leads to semicrystalline polymers while those containing 25-70 mol.% of VDF are amorphous. VDF content above 70 % leads to a thermoplastic copolymer with a monoclinic crystalline structure. These copolymers are usually called flexible PVDF.[3]

Flat-sheet microporous membranes for MD have been prepared from P(VDF-co-CTFE) using phase inversion.[106–110] Factors affecting the final membrane morphology, such as the addition of LiCl additive, the polymer concentration, or post-modification by second bath immersion in ethanol and sodium hydroxide (NaOH) have been evaluated for their application in desalination by MD.[106] However, NaOH post-treatment led to some dehydrochlorination and dehydrofluorination leading to a decrease in crystallinity, melting temperature and hydrophobicity of the membrane surface. The effect of LiCl in PVDF crystalline polymorphism among other properties was also investigated.[107] The addition of PEG or PEG/LiCl mixed additives to prepare MD membranes has also been studied.[108,109] The addition of LiCl in PEG containing casting solutions benefited the crystallization process during phase inversion leading to increased hydrophobicity, porosity and pore interconnectivity affecting MD performance.[107] It was found that LiCl have both thermodynamic and kinetic effect on phase inversion. An interesting feature is that the content of β-phase PVDF increased due to the crystallization process in the presence of LiCl, resulting in membranes with increased thermo-resistance.[109]

2.3.2.4. Poly(vinylidene fluoride)-*graft*-poly(styrene sulfonic acid) (PVDF-*g*-PSSA)

The presence of sulfonic acid promotes water uptake, enabling PSSA-containing membranes to be good protonic conductors. Protons become mobile when dissociated from the sulfonic acid groups in an aqueous environment.[111] As a result, membranes prepared from PVDF-*g*-PSSA found applications as proton conducting membranes for fuel cells.[112–115] Incorporating inorganic nanoparticles, such as $BaTiO_3$, in such membranes was found to be a way to improve the proton conductivity.[115] PVDF-*g*-PSSA membranes have also been investigated for oil-water separation,[116] and actuators.[117]

Yu *et al.* described the preparation of a PVDF membrane modified with styrene and acetyl sulfate by solution bulk graft polymerization, and a PSSA grafted membrane was prepared. The modified membrane pure water flux was increased compared to PVDF membrane, and rejection rate of oil (diesel fuel) was very high (99.8 %). The prepared membranes showed enhanced stability, antifouling properties and high rejection proving the potential of such modification for the petrochemical wastewater treatment.[116]

PSSA was radiation grafted on PVDF at different graft levels to fabricate a high performance ionic polymer-metal composite actuator (IPMC) thanks to the proton conductivity of PSSA. The highest graft level membrane showed good performance and could be a candidate to replace commercial Nafion®.[117]

2.3.2.5. Poly(vinylidene fluoride-*co*-trifluoroethylene) P(VDF-*co*-TrFE)

TrFE can be copolymerized with VDF in all proportions, leading to semicrystalline thermoplastic copolymers. PVDF has to be stretched and poled to induce a net dipole in the materials (β-phase) (see Figure 8) and the ferroelectric behavior, but in the case of P(VDF-*co*-TrFE) copolymers these treatments are not necessary. Thus, these copolymers are appealing for applications requiring electroactive properties.

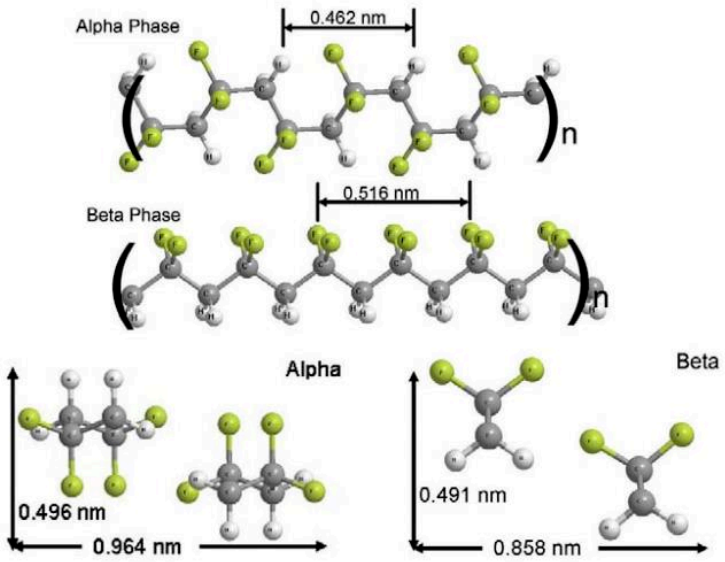

Figure 8. α and β phases in PVDF, looking along the chains (top) and perpendicular to the chains (bottom). A transition from a nonpolar α to a polar β phase is induced in P(VDF-*co*-TrFE). This also results in dimensional changes.[45]

This copolymer, in the form of nanofibers, has been employed for the preparation of an endovascular pressure sensor[118] or an hybrid nano-generator thanks to its piezoelectricity.[119] Chaharsoughi *et al.* reported the preparation of a device that transformed plasmonic heating of gold nano-disks by solar light into energy thanks to the use of a pyroelectric P(VDF-*co*-TrFE) film (see Figure 9).[120]

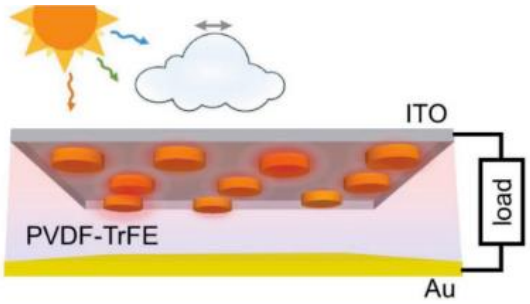

Figure 9. Schematic illustration of the hybrid device (upside down and substrate omitted).[120]

3. Synthesis of PVDF

Homopolymers of vinylidene fluoride (VDF), like most polyfluoroolefins, can be obtained by free radical polymerization. Since VDF is a gaseous monomer, having a melting and boiling temperature of -144 °C and -84 °C respectively, the radical polymerization is usually carried out in a high pressure vessel. (Figure 10).

Figure 10. Pictures of a high pressure reactor set-up typically used for the radical polymerization of gaseous fluoromonomers like vinylidene fluoride.

Industrial synthesis is performed in aqueous emulsion or suspension, involving pressures of 10-300 bar and temperatures between 10 and 130 °C. The emulsion process requires fluorinated surfactants. Alternatively, radical polymerization in solution using initiators such as persulfates, organic peroxides or percarbonates have also been investigated.[121,122]

In an alternating chain, head ($-CF_2-$) to tail ($-CH_2$) addition dominates. However, in the case of some monomers (i.e. VDF or VAc) occasional reversed head-to-head and tail-to-tail additions in the order of 3 - 7 % are not unusual,[32] resulting in chain defects, the extent of which depends on the polymerization conditions.

The ratio between normal $–CH_2CF_2–CH_2CF_2–$ (head-to-tail) and reverse $–CH_2CF_2– CF_2CH_2–$ (head-to-head) or $–CF_2CH_2–CH_2CF_2–$ (tail-to-tail) structures, assessed in great detail by high resolution ^{19}F and ^{1}H NMR techniques,[123,124] is influenced by the polymerization conditions (particularly temperature). For instance, emulsion polymerization gives rise to higher contents of chain defects compared to suspension polymerization probably due to the higher temperature involved in the emulsion process.[125] The melting behavior and crystallinity of PVDF is strongly influenced by the extent of head-to-head and tail-to-tail structures.[126] Consequently, such defects affect many properties of PVDF such as the mechanical strength or electroactive properties, for example.[127]

The controlled radical polymerization of fluoroolefins, and of VDF in particular, is very challenging, and only few studies have been reported so far.

Iodine Transfer Polymerization (ITP)[38,128] and RAFT/MADIX[40,129] polymerization have emerged as the most efficient techniques to control the polymerization of VDF and to prepare well-defined fluoropolymer architectures.[25,130–132]

Daikin company opened the route to ITP, by using fluorinated iodo compounds in a controlled process based on degenerative transfer.[133] Later, ITP of vinylidene fluoride in the presence of $C_6F_{13}I$ allowed the synthesis of PVDF with low polydispersity.[38,134] Interestingly, a $Mn_2(CO)_{10}$ photomediated polymerization of vinylidene fluoride was later discovered, allowing ITP at mild temperatures in glass tubes.[132] Addition of $Mn_2(CO)_{10}$ to the photoinitiated ITP of VDF offers also the possibility to reactivate the less reactive $-CF_2CH_2-I$ PVDF chain-ends. Indeed, the *in situ* formed $Mn(CO)_5^{\bullet}$ radicals are able to reactivate all iodine-terminated chains, consequently, the synthesis of relatively pure block copolymers is possible (i.e., block copolymers without contamination from the PVDF first block). However, the second block is synthesized under free radical conditions, and broad distributions are obtained. Recently, MADIX, another degenerative chain transfer process involving xanthates has been developed for the preparation of well-defined PVDF.[39,40,86,129] Detailed information of MADIX/RAFT polymerization of other monomers can be found in the literature.[135,136]

3.1. Synthesis of PVDF by MADIX/RAFT

After the first reported use of macromolecular design via interchange of xanthates (MADIX) for the polymerization of VDF,[86] copolymerization of VDF with 3,3,3-trifluoropropene[129] or *tert*-butyl-2-trifluoromethyl acrylate were achieved.[137] These articles suggested that MADIX could be employed for the preparation of fluoropolymers and, to some extent, fluorinated block copolymers and amphiphilic block copolymers. However, the polymerization conditions were not optimized. The polymerization conditions described could indeed be detrimental to the control of the polymerization. High chain transfer agent to initiator molar ratios ($[I]_0/[CTA]_0$ = 1) combined with high radical flux (i.e., high reaction temperature, at which the decomposition half-life time of the initiator is close to 1 h). The polymerization of VDF under MADIX conditions using relatively low initiator to CTA ratios (0.1−0.2) and a polymerization temperature at which the initiator decomposition half-life is about 10 h.[40]

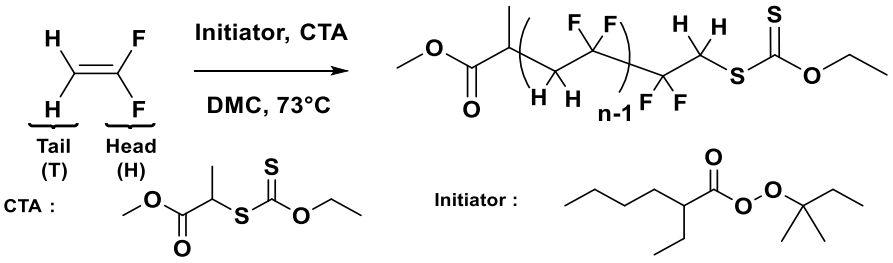

Figure 11. Schematic representation of the RAFT Polymerization of VDF in DMC.[40]

The detailed investigations of the RAFT polymerization of VDF showed that xanthate chain transfer agents (CTA) were indeed very efficient for preparing PVDF with narrow molar mass distributions (Đ < 1.5).[40] Solvents such as dimethyl carbonate (DMC), 1,1,1,3,3-pentafluorobutane (PFB) and acetonitrile (ACN) were shown to be adequate solvents for the polymerization of VDF. DMC was shown to be the solvent of choice.

Asandei and co-workers reported that the iodine transfer polymerization (ITP) of VDF in DMC proceeded much faster than in other solvents and with high yields.[132] The authors also stated that while radicals arising from transfer to acetonitrile were not able to reinitiate the polymerization of VDF, those arising from transfer to DMC were more reactive and could reinitiate the polymerization of VDF.[132]

However, the radical polymerization of VDF is accompanied by a non-negligible amount of chain inversions, head-to-head (HH) VDF additions. These reverse additions are detrimental to the preparation of well-controlled PVDF chains using ITP or RAFT (Scheme 2).[40,132] It has indeed been proven that chain-ends terminated by an inversely added VDF unit accumulate in the reaction medium relatively rapidly (see Figure 12).[40,132,138]

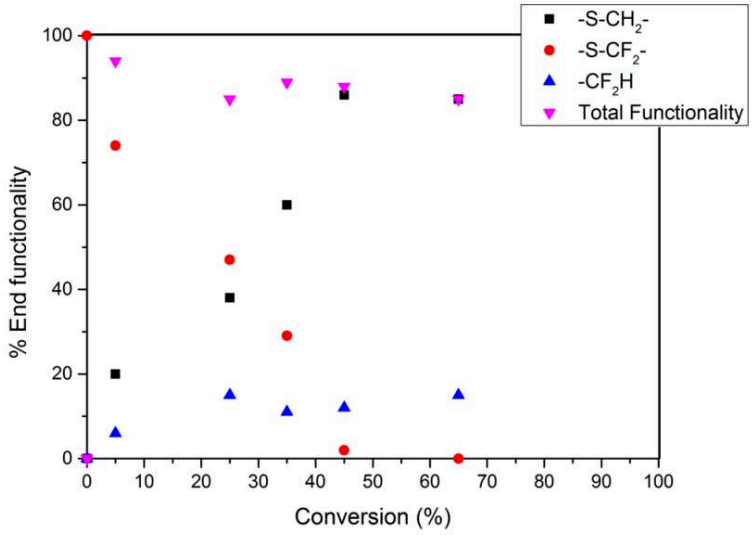

Figure 12. Evolution of chain-end functionality during VDF MADIX polymerization versus conversion.[40]

These PVDF chains were also believed not to be able to participate into further degenerative transfer. In addition, polymerization of VDF in hydrogenated solvents is also affected by undesirable transfer-to-solvent reactions (see Scheme 2, Eqn 7). This H-abstraction results in loss of CTA and chain-end functionality, and in some cases in the generation of undesired additional polymer chains.[40]

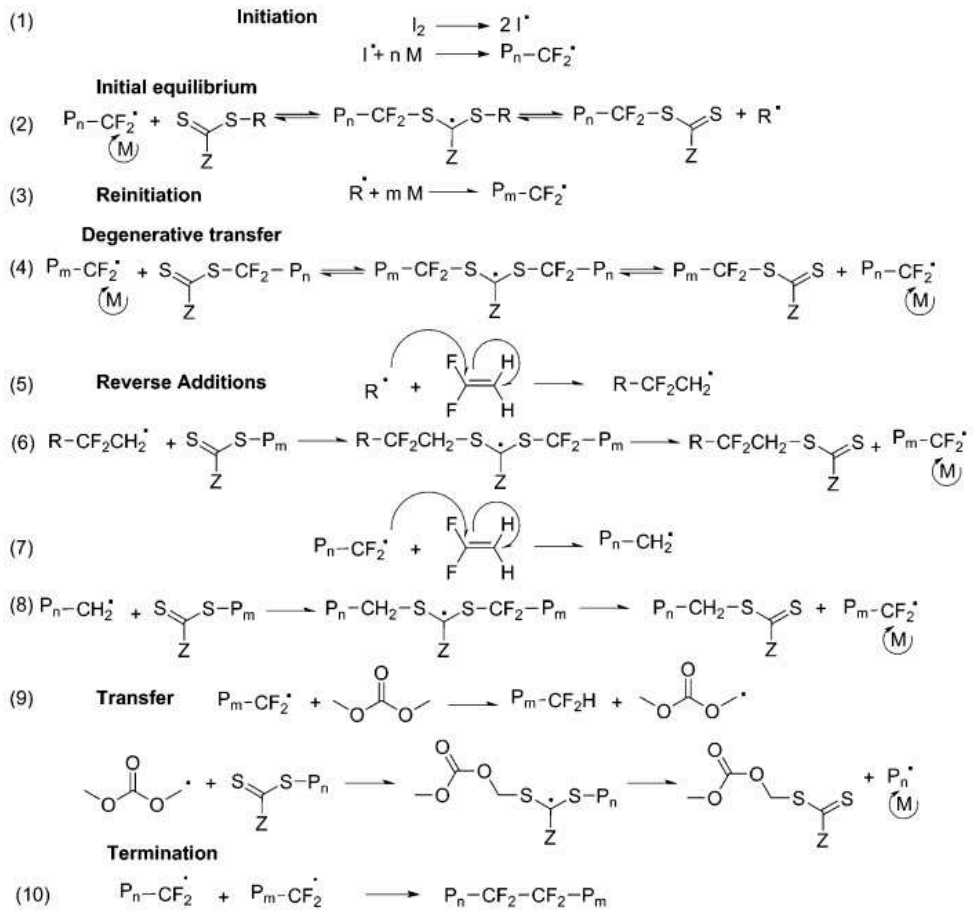

[a] I_2 and P_n (or P_m) represent the initiator and a PDVF chain of DP = n (or m), respectively.

Scheme 2. Mechanism of Reversible Addition-Fragmentation Chain-Transfer Polymerization (RAFT)/Macromolecular Design via the Interchange of Xanthates (MADIX) of VDF.[40]

Since the reverse additions cannot be avoided, the limits of the RAFT polymerization of VDF were established.[39] Combined experimental observations and DFT calculations, showed that the reputedly inactive chains were not "dead", but that they could only engage in degenerative chain transfer process with the minority tail-terminated PVDF radicals.

These investigations also showed that high molecular weight PVDF with high chain-end fidelity could only be prepared at relatively low conversions (< ca. 30 %) (see Figure 13).

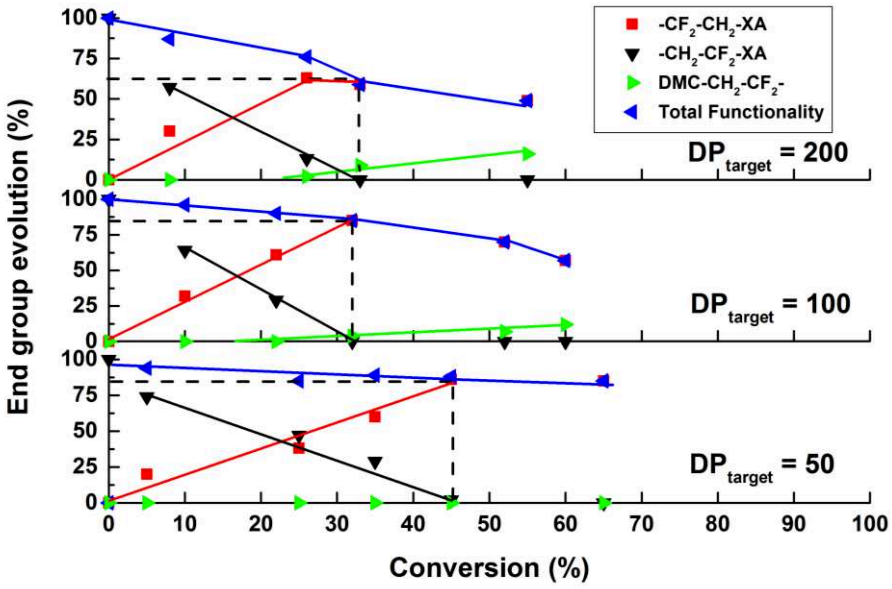

Figure 13. Evolution of the PVDF chains end-group functionality (-CH_2-CF_2-XA ($PVDF_H$-XA), -CF_2-CH_2-XA, ($PVDF_T$-XA)) and of the proportion of DMC-initiated PVDF chains *vs* time for RAFT polymerizations of VDF targeting different DP: DP_{target} = 50 (bottom), DP_{target} = 100 (middle), DP_{target} = 200 (top).[39]

3.2. PVDF-based block copolymers and other architectures made by RAFT.

In recent years, the controlled synthesis of PVDF-based architectures employing RAFT/MADIX polymerization has gained momentum. The more significant results are described in this section and summarized in Figure 14 (The idea of this figure originates from literature).[139]

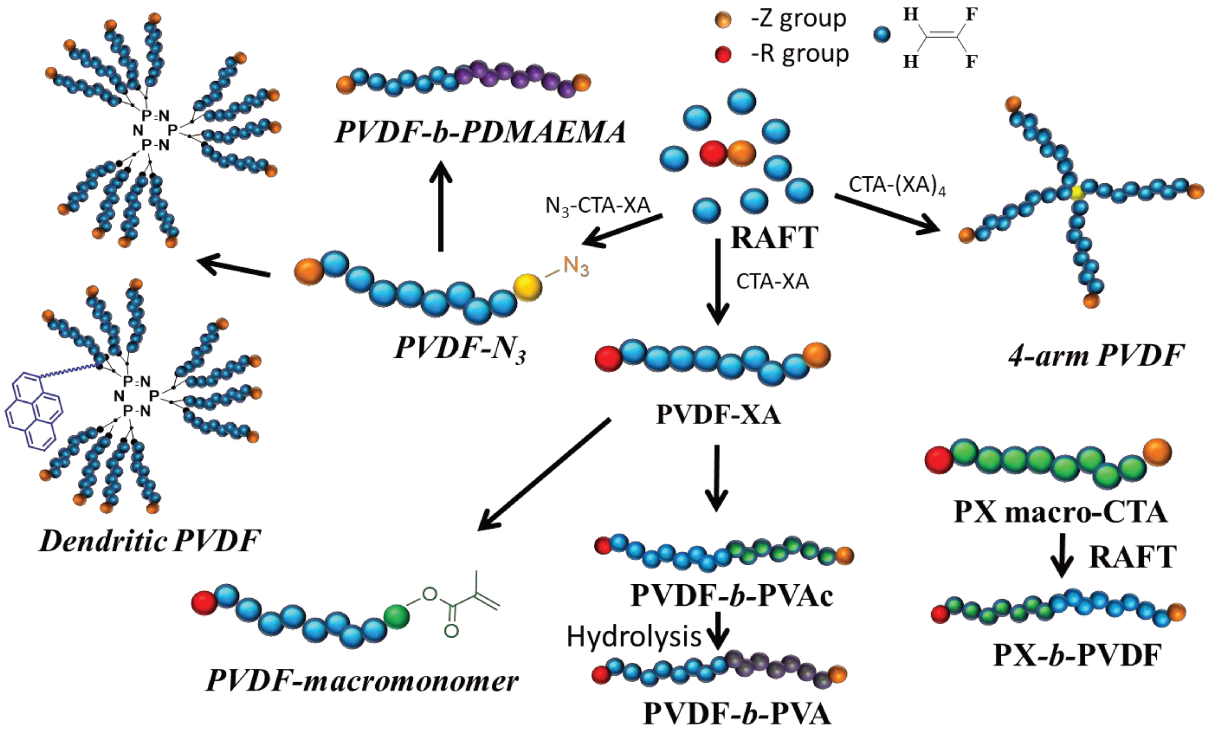

Figure 14. Diblock copolymers,[140–144] dendrimers,[130,145] macromonomers[138] and 4-arm PVDF-based architectures.[25,85]

The radical polymerization of VDF in the presence of azide-functionalized xanthate resulted in N_3-PVDF-XA with narrow distribution allowing the preparation of PVDF-*b*-PDMAEMA diblock copolymers after reaction with an alkyne-functional PDMAEMA.[141] A similar approach allowed the preparation of dendritic PVDF and asymmetric dendritic PVDF bearing a pyrene moiety. CuAAc "Click" chemistry provided the efficient grafting of the polymer onto the alkyne-functionalized dendrimers.[130,145] PVDF macromonomers were also synthesized via regio-selective thia-Michael addition in a "one-pot" reaction.[138] The xanthate end-groups of PVDF were transformed into thiols which immediately added onto the acrylate moiety of an acrylate-methacrylate compound to form PVDF-methacrylate macromonomers.[138] A four-arm PVDF was synthesized from a tetraxanthate chain transfer agent. These star PVDF were modified to obtain photo crosslinkable 4-arm PVDF methacrylates by the same "one-pot" strategy used to prepare macromonomers.[25] Tetra PVDF-OH have also been synthesized via this "one-pot" aminolysis / Thia-Michael addition using a 4-arm star PVDF-XA and 2-hydroxyethyl acrylate (HEA). Esterification of the terminal hydroxyl end-groups using 4-formylbenzoic acid followed by reaction with tetrabenzaacylhydrazide-terminated 4-arm

star poly(ethylene glycol) (tetraPEG-BAH) in the presence of different concentrations of glacial acetic acid produced amphiphilic polymer co-networks.[85] PVDF based block copolymers made by RAFT have also been prepared. Interestingly, it was shown that among all the vinyl monomers studied for the chain extension of PVDF-XA macro-CTAs only vinyl acetate (VAc) radicals were able to reactivate PVDF-CF_2-CH_2-XA chains. Thus, only well-defined PVDF-*b*-PVAc diblock copolymers have been successfully prepared from PVDF macro-CTA.[131] The reverse synthesis, i.e. radical polymerization of VDF in the presence of PVAc-XA macro-CTA, was also achieved.[144] Basic hydrolysis of the PVAc segments led to amphiphilic PVDF-*b*-PVA block copolymers with the ability to self-assemble in aqueous solutions into spherical aggregates.[143] Original PEVE-*b*-PVDF (EVE = ethyl vinyl ether) diblock copolymers were prepared by combining cationic and radical RAFT polymerizations. Fist, the efficient control of carbamates as CTAs for the preparation of PVDF by RAFT was confirmed. PEVE-carbamate macro-CTA was then synthesized by cationic RAFT polymerization. Finally, this macroCTA was employed for the radical RAFT polymerization of VDF, allowing the preparation of well-defined PEVE-*b*-PVDF diblock copolymers.[140]

Detailed information about other methods and polymerization techniques to obtain PVDF-based structures and block copolymers have been reviewed in 2014.[42]

4. Self-assembly of block-copolymers in solution

Molecular self-assembly is a process by which molecules spontaneously form ordered aggregates without guidance or management from an outside source. The self-assembly of small amphiphilic molecules has been studied for many decades, and various morphologies have been observed in bulk and in aqueous solutions. Under appropriate conditions, self-assembling polymers form different types of aggregates such as spherical or cylindrical micelles.

4.1. Accessible morphologies

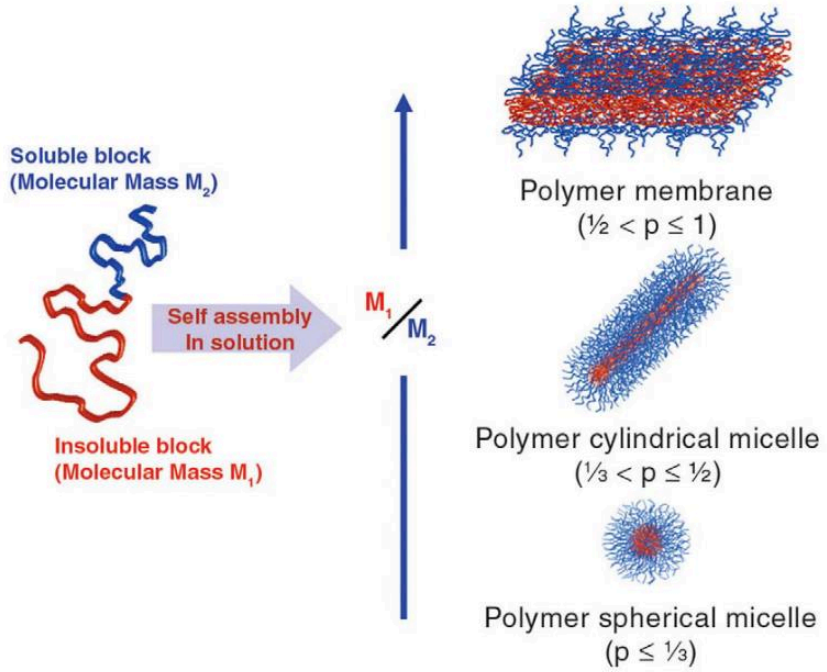

Figure 15. Different geometries formed by diblock copolymer in selective solvent estimated by chain packing parameter (p). $p = v/a_o l$; where v is the hydrophobic block volume, a_o is the equilibrium area per molecule at the aggregate surface and l is the solvophobic block length.[146]

Typical Morphologies obtained by self-assembly of diblock copolymers in selective solvents include spherical micelles (spheres), cylindrical micelles (cylinders), and vesicles, among others. The balance between solvophobic and solvophilic interactions gives rise to an optimal surface area of the solvophobic block at the interface between the solvophobic and solvophilic blocks (a_0). This, together with the length and the volume of the non-soluble domain, contributes to the packing parameter, defined as:

$p = v/a_o l$,

Where v is the volume and *l* is the length of the solvophobic block.[146] When $p < 1/3$, spheres are generally formed; when $1/3 < p < 1/2$, cylinders; when $1/2 < p < 1$, flexible lamellae or vesicles (see Fig. 15); finally, when $p = 1$, planar lamellae are obtained. If $p > 1$, inverted structures can be observed.[146,147]

However, more complex structures have also been reported. For example, PS-*b*-PAA with different block lengths and under different conditions, lead to a wide range of morphologies ranging from spheres, rods, bi-continuous rods, bilayers (lamellae and vesicles), to inverse

rods (hexagonally packed hollow hoops : HHHs) and large spheres (large compound micelles : LCMs), as shown in Figure 16.[147]

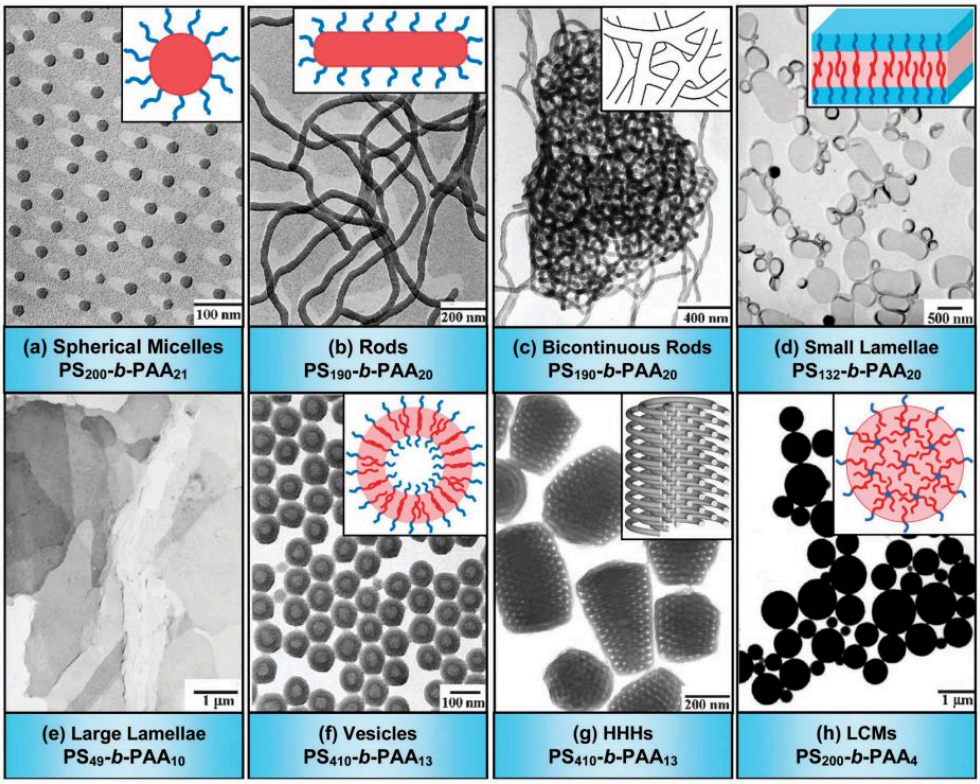

Figure 16. Transmission electron microscopy (TEM) micrographs and corresponding schematic diagrams of various morphologies formed from amphiphilic PS_m-*b*-PAA_n copolymers. In the schematic diagrams, red represents hydrophobic PS parts, while blue denotes hydrophilic PAA segments. HHHs: hexagonally packed hollow hoops; LCMs: large compound micelles, in which inverse micelles consist of a PAA core surrounded by PS coronal chains. Generally, the hydrophilic segments (e.g. coronas) of the crew-cut aggregates cannot be seen in TEM images if they are not stained.[147]

The complexity of the self-assembly and of the resulting aggregates is also increased if more complex polymer architectures, such as, triblocks (ABA,[148] ABC,[149] etc.), or non-linear BCPs (brush-like,[150] star,[151] miktoarm[152,153]) are used (see Figure 17).

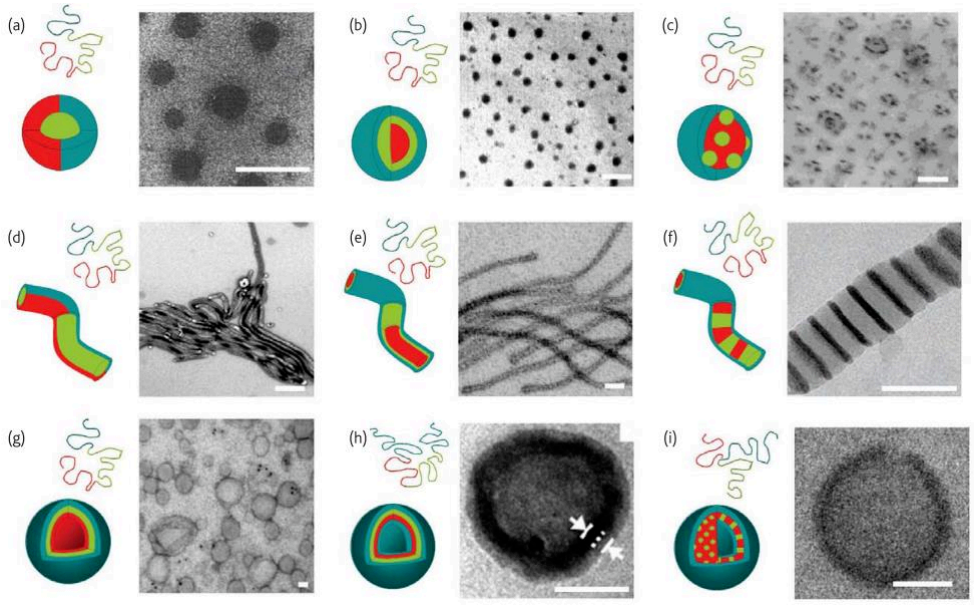

Figure 17. Assemblies formed in selective solvent conditions by multiblock copolymers: (a) Janus spheres (PS-*b*-PB-*b*-PMMA),[154] (b) core-shell spheres (PEO-*b*-DMA-*b*-MEMA)[155] , (c) raspberry-like spheres (PS-*b*-PB-*b*-PMMA)[156], (d) Janus cylinders (PS-*b*-PB-*b*-PMMA),[157] (e) core-shell cylinders (PI-*b*-PCEMA-*b*-PtBA),[158] (f) segmented cylinders (PAA-*b*-PMA-*b*-PS),[159] (g) asymmetric (Janus) membrane vesicles (PEO-*b*-PDMS-*b*-PMOXA),[160] (h) double-layer membrane vesicles, and (i) vesicles with hexagonally packed cylinders (3 arm miktoarm with PEO, PE and poly(perfluoropropylene oxide) arms).[161] Scale bar 50nm.[146]

4.2. Major factors affecting the morphology of self-assembled amphiphilic polymers

The stretching of the core-forming blocks, the interfacial tension between the core and the solvent, and the repulsive interactions among corona-forming block chains are the three factors affecting the formation of thermodynamically stable BCP aggregates. Different morphologies can thus be accessed by varying any of the three above mentioned parameters.[147] Copolymer composition and structure (see Figures 16 and 17), polymer concentration, common and selective-solvent ratio, nature of the common solvent, addition of additives or homopolymers[162] can affect the self-assembly (see Figure 18).[147,163]

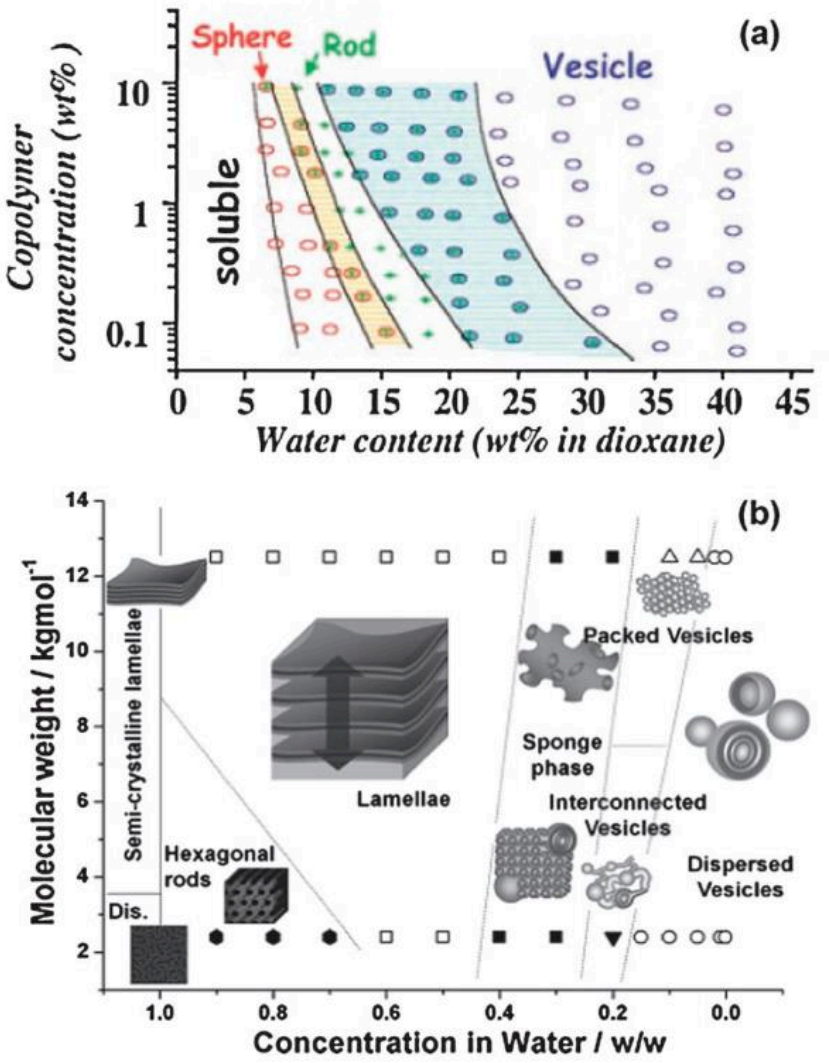

Figure 18. (a) Phase diagram of PS_{310}-*b*-PAA_{52} in dioxane:water mixtures. Morphology dependence on copolymer concentration and water content. Colored regions between phases correspond to coexistence regions. (b) Phase diagram of PBO-*b*-PEO in water. Morphology dependance on copolymer molar mass and concentration.[147]

4.3. Preparation techniques

Block copolymer self-assembly is generally produced by one of the following procedures:

- Solvent switch or micellization: The copolymer is molecularly dissolved in a common solvent (i.e. that is 'good' for both blocks) and then a selective solvent for one of the blocks is added at a fixed rate. This step is eventually followed by removal of the common solvent. An alternative that is often employed is the dialysis technique by which the common solvent is gradually replaced by the selective solvent.[163]

- Nanoprecipitation: The copolymer is dissolved in a common solvent and then the solution of BCP is precipitated in a selective solvent under agitation.[164] The de-mixing time (speed at which the common solvent dissolves in the selective solvent) is much faster than in the micellization protocol, making this method more likely to lead to the formation of kinetically trapped structures.
- Direct solubilization or thin-film rehydration: a solid sample (or thin film, prepared by solvent evaporation of a sample dissolved in a common solvent) of the copolymer is directly dissolved in a selective solvent for one of the blocks. The resulting micellar solution is left to anneal by standing and/or by thermal treatment (sometimes under ultrasonication).[163]

Nevertheless, depending on the block copolymer used, equilibrium is not always reached, especially if the core-forming block has a high glass transition temperature (T_g). In such cases, 'frozen micelles' are obtained.[163]

4.4. Self-assembly of coil-crystalline polymers in solution

Crystallization from solution, a method applicable to BCPs where one of the blocks presents crystallinity, has gained lots of attention in the past years.[165–173] Crystallization have been more studied in the case of homopolymers from bulk. However the self-assembly of coil-crystalline BCPs has been studied by Vilgis *et al.* years ago.[174]

The self-assembly is more complex when one block of the BCP is able to crystallize. In coil-coil BCPs both the core and corona are in an amorphous state in the assembled structures. In the case of coil-crystalline BCPs as crystallization takes place in the micellar core, the initial self-assembled morphology is either preserved or a morphological transformation into a novel structure is triggered. Also, in semicrystalline BCP aggregates, the crystallization of the micellar core compete with the stretching of the corona block resulting in unique often interesting structures.[175]

An interesting feature of core crystallization is the folding of the crystalline block chains.

Fold length is a strong function of the DP (degree of polymerization) in both blocks.[174] This allows tuning and controlling the core crystalline thickness by varying any of the blocks. This can also impact the size and the morphology of the coil-crystalline BCP assembles.

Factors affecting the crystallization and methods described in the literature to control the morphologies obtained by self-assembly of crystalline-coil BCPs are detailed in the following section.

4.4.1. Crystallization-driven self-assembly (CDSA).

Crystallization-Driven self-Assembly (CDSA) has emerged as a powerful method for block copolymer architecture manipulation. Experimentally, different approaches have been employed for coil-crystalline diblock copolymers to obtain semicrystalline micelles and aggregates as summarized in Figure 20. A variety of morphologies have been prepared by adjusting parameters such as the crystallization conditions, the micelle concentration or the volume ratio between insoluble and soluble blocks, the extra addition of crystalline reservoirs (seeds or crystalline homopolymers), and the solvent selectivity.

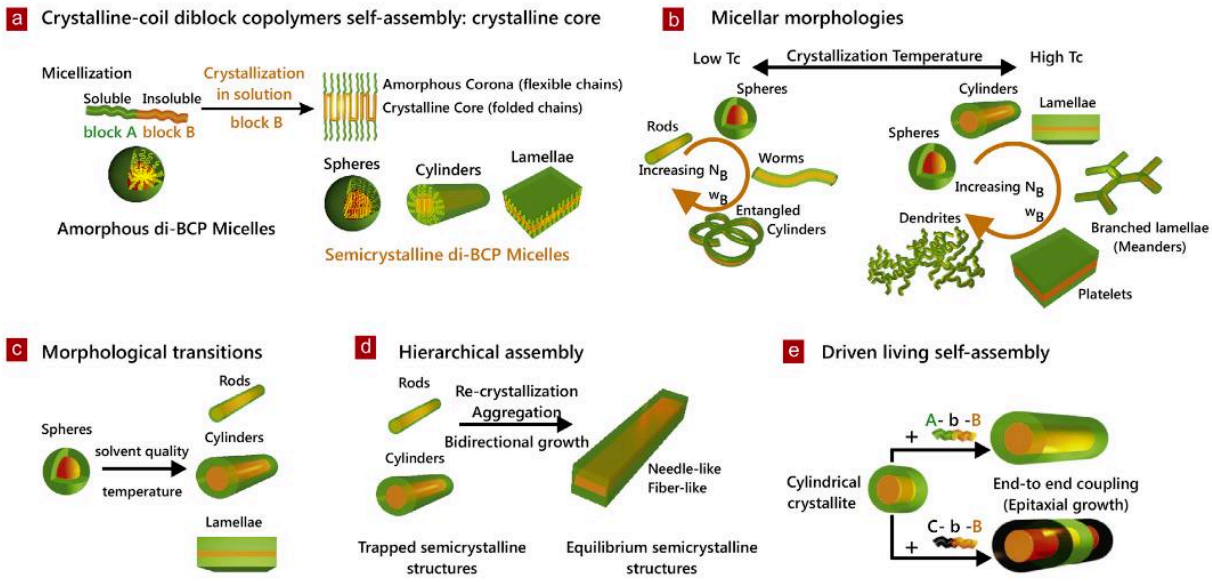

Figure 19. Different self-assembly protocols to prepare micelles from coil-crystallineBCPs: a) Schematic representation of the preparation of semicrystalline BCP micelles from amorphous micelles in solution where the core-forming block undergoes crystallization leading to a folded-chain structure. Typical structures of coil-crystalline BCPs micelles are spheres, cylinders and lamellae. b) Morphologies formed from PB-*b*-PEO in *n*-heptane by varying degree of polymerization and crystallization temperature. c) By changing the solubility of the corona-forming block in the solvent (with addition of another solvent, or changing the temperature), the resulting micellar morphology can be further tuned. d) Kinetically trapped semi-crystalline micelles can lead to the formation of equilibrium structures through re-crystallization and/or aggregation of intermediate structures. e) Epitaxial crystallization process by adding crystallizable BCP-unimers (same or different BCP) can lead to a living extension of the micellar structure.[175]

Key processes in the framework of coil-crystalline BCP micelle formation have been described in the literature (see Fig. 19):

4.4.1.1. Thermally controlled crystallization

Regulation of the temperature, allow some control over the crystallization process. The heating, temperature and duration,[176] crystallization temperature (T_c), the choice of the quench depth (i.e, crystallization temperature selection),[177] rate (speed of cooling), or aging time allowed the preparation of a large variety of equilibrium structures.[178] Heating above the melting temperature T_m of the crystalline block morphologies can evolve (due to the melting of the core and subsequent recrystallization).

- Slow crystallization process at high T_c and a small quench depth/slow quench rate can lead to the formation of different features.
- The crystallization of the core block can take place within confinement, i.e., in a "frozen micelle" when the initial structure is maintained (fast crystallization at low T_c or due to fast quenching).

Boott, *et al.* studied the growth kinetics in the formation of 1D PFS_{63}-*b*-$PDMS_{513}$. They studied the effect of temperature on the controlled growth of 1D cylindrical micelles as well as, the effect of initial concentration, the solvent and the DP of the core forming block. Surprisingly, temperature not only affected the growth rate but also the final length of the cylinders.[168]

4.4.1.2. Morphological transitions

Morphology of the assembled structures is influenced by the competition between stretching of the soluble block chains and the crystallization of the crystalline core forming block. Even if crystallization takes place in the micellar core (and plays the major role in determining the micellar morphology), by modifying the solvent affinity of the corona, morphological transitions could be favored.

Yusoff *et al.* observed that PFS_{74}-*b*-$P2VP_{74}$ BCP in different THF/mixtures evolved into different morphologies due to the different affinity of the blocks in the solvent mixture (the rate of crystallization of the PFS crystalline block seemed to be influenced), leading to

spheres, platelets or mixtures of both structures. Other self-assembly methods and different block polymerization degrees were explored allowing the morphological transitions from spheres-to-rods or sphere-to-platelets.[179]

4.4.1.3. Hierarchical assembly

Equilibrium structures can be accessed from the recrystallization of kinetically trapped metastable structures. In this kind of micelle (generated at an earlier stage of the core crystallization) an aggregation process, such as fusion or coalescence, and subsequent secondary crystallization can take place. This can lead to the development of much larger structures. Low crystallinity of the initial crystalline micelles is believed to be the main factor for such rearrangements and recrystallization.

Gädt *et al.* described the formation of cylinder-cylinder, platelet-cylinder connected structures trough coalescence of PI-*b*-PFS BCPs with different degrees of polymerization. PI_{76}-b-PFS_{76} BCP formed platelets and PI_{342}-*b*-PFS_{57} formed cylinders leading to scarf-like structures.

4.4.1.4. Living crystallization

In contrast to the previous methods, the living character of the CDSA proceeds via an epitaxial growth process. Here, the ends or edges of pre-crystallized seed micelles remain active to the addition of further polymer unimers, and controlled elongation is possible. This process proved to be a very efficient way for the preparing well-defined structures with an additional control over the micellar length and morphology.

Arno *et al.* recently reported the preparation of 1D morphologies from PCL-b-PDMA. Polydisperse cylinders were first prepared in ethanol after cooling to room temperature a solution of the BCP that was heated at 70°C for 3h. In order to control the length of the cylindrical aggregates, they first “cut” them by sonication. Uniform crystalline seeds of 50 nm were obtained and a living CDSA process was observed upon addition of PCL-*b*-PDMA BCP unimers dissolved in THF to the solution. Same approach allowed the preparation of PCL-*b*-PMMA-*b*-PDMA monodisperse cylinders in aqueous solutions. Hudson *et al.* reported the preparation of 2D architectures including platelets and block co-micelles (micelles formed by two different BCPs with a similar core forming block but different corona blocks)

using a similar approach. Addition of platelet-forming, unimers (PFS_x-*b*-$PDMS_y$, PFS_x-*b*-PI_y, PFS_x-*b*-$PMVS_y$) to samples of well-defined, PFS-*b*-PDMS crystalline seeds, allowed the preparation of different 2D structures such as platelet co-micelles and double-headed spear-like micelles.

5. Conclusion

Fluoropolymers have found numerous membrane applications, but also in other fields. Due to the new property requirements, the development of new fluoropolymers and new membrane preparation methods are also receiving lots of attention. However, most common membrane modification and preparation methods are still investigated, leading to new improvements and better understanding of formation mechanisms. The use of additives and blends of polymers is still one of the most employed approaches for the preparation of membranes with more adequate properties for a specific application. The access to improved hydrophilicity by just blending PVDF with hydrophilic or amphiphilic copolymers in a one step process seems a very attractive and easy scalable membrane modification that can be used at industrial scale.

Fluoropolymer synthesis is however not accessible to everyone due to synthesis restrictions (monomer are gases, high pressure autoclaves needed…), this could explain the reduced number of studies dealing with the preparation of fluorinated block copolymers.

Novel applications of fluoropolymers are appearing. Still, only a few references describe the self-assembly of block copolymers where at least one block is a fluorinated block. General aspects of self-assembly such as methods and factors affecting the self-assembly conditions have been presented. In particular crystallization-driven self-assembly is attracting lots of attention in the polymer community. The self-assembly behavior of block copolymers where one block is a fluoropolymer such as PVDF (high crystalline) could be explained and controlled thanks to CDSA. Polymer nanostructures made up of fluorinated polymers could be new promising materials in emergent applications due to their remarkable properties.

6. References

1. Bohn, P. W. *et al.* Science and technology for water purification in the coming decades. *Nanosci. Technol. A Collect. Rev. from Nat. Journals* **452**, 337–346 (2009).

2. Le, N. L. & Nunes, S. P. Materials and membrane technologies for water and energy sustainability. *SUSMAT* **7**, 1–28 (2016).

3. Cui, Z., Drioli, E. & Lee, Y. M. Recent progress in fluoropolymers for membranes. *Prog. Polym. Sci.* **39**, 164–198 (2014).

4. Castel, C. & Favre, E. Membrane separations and energy efficiency. *J. Memb. Sci.* **548**, 345–357 (2018).

5. Kaner, P., Rubakh, E., Kim, D. H. & Asatekin, A. Zwitterion-containing polymer additives for fouling resistant ultra fi ltration membranes. *J. Memb. Sci.* **533**, 141–159 (2017).

6. Cai, T., Neoh, K. G. & Kang, E. T. Functionalized and Functionalizable Fluoropolymer Membranes. *Handb. Fluoropolymer Sci. Technol.* 149–181 (2014). doi:10.1002/9781118850220.ch8

7. Wasim, M., Sagar, S., Sabir, A., Shafiq, M. & Jamil, T. Decoration of open pore network in Polyvinylidene fluoride/MWCNTs with chitosan for the removal of reactive orange 16 dye. *Carbohydr. Polym.* **174**, 474–483 (2017).

8. Li, X. *et al.* Highly stable PDMS-PTFPMS/PVDF OSN membranes for hexane recovery during vegetable oil production. *RSC Adv.* **7**, 11381–11388 (2017).

9. Quist-Jensen, C. A., Macedonio, F. & Drioli, E. Membrane crystallization for salts recovery from brine—an experimental and theoretical analysis. *Desalin. Water Treat.* **57**, 7593–7603 (2016).

10. Sawada, S. ichi *et al.* Effect of citrate-based non-toxic solvents on poly(vinylidene fluoride) membrane preparation via thermally induced phase separation. *J. Memb. Sci.* **493**, 232–242 (2015).

11. Wang, X., Chen, C., Liu, H. & Ma, J. Preparation and characterization of PAA/PVDF membrane-immobilized Pd/Fe nanoparticles for dechlorination of trichloroacetic acid. *Water Res.* **42**, 4656–4664 (2008).

12. Gil, V. V. *et al.* Impact of heterogeneous cation-exchange membrane surface modification on chronopotentiometric and current–voltage characteristics in NaCl, CaCl 2 and MgCl 2 solutions. *Electrochim. Acta* **281**, 472–485 (2018).

13. Kang, G. dong & Cao, Y. ming. Application and modification of poly(vinylidene fluoride) (PVDF) membranes - A review. *J. Memb. Sci.* **463**, 145–165 (2014).

14. Xu, S., Jiang, R. & Gao, Y. Proton and Metal Cage-Based Anion-Conductive

Fluoropolymers for AMFCs. *ECS Trans.* **69**, 391–402 (2015).

15. Drioli, E., Ali, A. & Macedonio, F. Membrane distillation: Recent developments and perspectives. *Desalination* **356**, 56–84 (2015).

16. Kim, D. J., Lee, H. J. & Nam, S. Y. Sulfonated poly(arylene ether sulfone) membranes blended with hydrophobic polymers for direct methanol fuel cell applications. *Int. J. Hydrogen Energy* **39**, 17524–17532 (2014).

17. Sproll, V. *et al.* Radiation Grafted Ion-Conducting Membranes: The Influence of Variations in Base Film Nanostructure. *Macromolecules* **49**, 4253–4264 (2016).

18. Lin, C. X. *et al.* Crosslinked side-chain-type anion exchange membranes with enhanced conductivity and dimensional stability. *J. Memb. Sci.* **539**, 24–33 (2017).

19. Id, I. A., Bamaga, O. A., Id, L. G. & Bassyouni, M. Assessment of Blend PVDF Membranes , and the Effect of Polymer Concentration and Blend Composition. (2018). doi:10.3390/membranes8010013

20. Hassankiadeh, N. T. *et al.* PVDF hollow fiber membranes prepared from green diluent via thermally induced phase separation: Effect of PVDF molecular weight. *J. Memb. Sci.* **471**, 237–246 (2014).

21. Boutevin, B., Kostov, G. & Ame, B. Fluoroelastomers : synthesis , properties and applications. *Prog. Polym. Sci.* **26**, 105–187 (2001).

22. Hansen, N. M. L., Jankova, K. & Hvilsted, S. Fluoropolymer materials and architectures prepared by controlled radical polymerizations. *Eur. Polym. J.* **43**, 255–293 (2007).

23. Soulestin, T., Ladmiral, V., Domingues, F., Santos, D. & Améduri, B. Progress in Polymer Science Vinylidene fluoride- and trifluoroethylene-containing fluorinated electroactive copolymers . How does chemistry impact properties ? *Prog. Polym. Sci.* **72**, 16–60 (2017).

24. Henry, B. J. *et al.* A critical review of the application of polymer of low concern and regulatory criteria to fluoropolymers. *Integr. Environ. Assess. Manag.* **14**, 316–334 (2018).

25. Lopez, G., Guerre, M., Améduri, B., Habas, J. P. & Ladmiral, V. Photocrosslinked PVDF-based star polymer coatings: An all-in-one alternative to PVDF/PMMA blends for outdoor applications. *Polym. Chem.* **8**, 3045–3049 (2017).

26. Barbosa, J. C., Dias, J. P., Lanceros-Méndez, S. & Costa, C. M. Recent advances in poly(Vinylidene fluoride) and its copolymers for lithium-ion battery separators. *Membranes (Basel).* **8**, (2018).

27. Yang, J., Wang, Y., Yang, G. & Zhan, S. New anhydrous proton exchange membranes based on fluoropolymers blend imidazolium poly (aromatic ether ketone)s for high temperature polymer electrolyte fuel cells. *Int. J. Hydrogen Energy* **43**, 8464–8473 (2018).

28. Wu, Y., Qu, J., Daoud, W. A., Wang, L. & Qi, T. Flexible composite-nanofiber based

piezo-triboelectric nanogenerators for wearable electronics. *J. Mater. Chem. A* **7**, 13347–13355 (2019).

29. Yu, Y. *et al.* Biocompatibility and in vivo operation of implantable mesoporous PVDF-based nanogenerators. *Nano Energy* **27**, 275–281 (2016).

30. Alaaeddin, M. H., Sapuan, S. M., Zuhri, M. Y. M., Zainudin, E. S. & Al-Oqla, F. M. Polyvinyl fluoride (PVF); Its Properties, Applications, and Manufacturing Prospects. *IOP Conf. Ser. Mater. Sci. Eng.* **538**, (2019).

31. Martins, P., Lopes, A. C. & Lanceros-Mendez, S. Electroactive phases of poly(vinylidene fluoride): Determination, processing and applications. *Prog. Polym. Sci.* **39**, 683–706 (2014).

32. Ameduri, B. From vinylidene fluoride (VDF) to the applications of VDF-Containing polymers and copolymers: Recent developments and future trends. *Chem. Rev.* **109**, 6632–6686 (2009).

33. Twum, E. B., McCord, E. F., Fox, P. A., Lyons, D. F. & Rinaldi, P. L. Characterization of backbone structures in poly(vinylidene fluoride- co -hexafluoropropylene) copolymers by multidimensional 19F NMR spectroscopy. *Macromolecules* **46**, 4892–4908 (2013).

34. Jung, J. T. *et al.* Tailoring nonsolvent-thermally induced phase separation (N-TIPS) effect using triple spinneret to fabricate high performance PVDF hollow fiber membranes. *J. Memb. Sci.* **559**, 117–126 (2018).

35. Ranganath, A. S., Ganesh, V. A., Sopiha, K., Sahay, R. & Baji, A. Thermoresponsive electrospun membrane with enhanced wettability. *RSC Adv.* **7**, 19982–19989 (2017).

36. Zhang, Y. *et al.* Electrospun porous poly(tetrafluoroethylene-: Co -hexafluoropropylene- co -vinylidene fluoride) membranes for membrane distillation. *RSC Adv.* **7**, 56183–56193 (2017).

37. Markit. *Chemical Economics Handbook*. *Fluoropolymers* (2019).

38. Boyer, C., Valade, D., Sauguet, L., Ameduri, B. & Boutevin, B. Iodine Transfer Polymerization (ITP) of Vinylidene Fluoride (VDF). influence of the defect of VDF chaining on the control of ITP. *Macromolecules* **38**, 10353–10362 (2005).

39. Guerre, M. *et al.* Limits of Vinylidene Fluoride RAFT Polymerization. *Macromolecules* **49**, 5386–5396 (2016).

40. Guerre, M. *et al.* Deeper Insight into the MADIX Polymerization of Vinylidene Fluoride. *Macromolecules* **48**, 7810–7822 (2015).

41. Soulestin, T., Ladmiral, V., Domingues, F., Santos, D. & Améduri, B. Progress in Polymer Science Vinylidene fluoride- and trifluoroethylene-containing fluorinated electroactive copolymers . How does chemistry impact properties ? *Prog. Polym. Sci.* **72**, 16–60 (2017).

42. Voet, V. S. D., Ten Brinke, G. & Loos, K. Well-defined copolymers based on poly(vinylidene fluoride): From preparation and phase separation to application. *J.*

Polym. Sci. Part A Polym. Chem. **52**, 2861–2877 (2014).

43. Shi, Z. & Holdcroft, S. Synthesis of block copolymers possessing fluoropolymer and non-fluoropolymer segments by radical polymerization. *Macromolecules* **37**, 2084–2089 (2004).

44. Harrison, J. & Ounaies, Z. Piezoelectric polymers. *Encycl. Polym. Sci. …* **3**, 474 (2002).

45. Mirfakhrai, T., Madden, J. D. W. & Baughman, R. H. Polymer artificial muscles. *Mater. Today* **10**, 30–38 (2007).

46. Liu, F., Hashim, N. A., Liu, Y., Abed, M. R. M. & Li, K. Progress in the production and modification of PVDF membranes. *J. Memb. Sci.* **375**, 1–27 (2011).

47. Jung, J. T. *et al.* Understanding the non-solvent induced phase separation (NIPS) effect during the fabrication of microporous PVDF membranes via thermally induced phase separation (TIPS). *J. Memb. Sci.* **514**, 250–263 (2016).

48. Chen, K. *et al.* Study on vacuum membrane distillation (VMD) using FEP hollow fiber membrane. *Desalination* **375**, 24–32 (2015).

49. Eykens, L., De Sitter, K., Dotremont, C., Pinoy, L. & Van der Bruggen, B. Membrane synthesis for membrane distillation: A review. *Sep. Purif. Technol.* **182**, 36–51 (2017).

50. Kim, J. F. *et al.* Microporous PVDF membranes via thermally induced phase separation (TIPS) and stretching methods. *J. Memb. Sci.* **509**, 94–104 (2016).

51. Tao, M. mi, Liu, F., Ma, B. rong & Xue, L. xin. Effect of solvent power on PVDF membrane polymorphism during phase inversion. *Desalination* **316**, 137–145 (2013).

52. Zhu, Y. & Zhang, Z. PVDF hollow fiber formation via modified NIPS method: Evolution elucidation of phase separation mechanism, structure and properties of membrane with coagulation strength varied. *Macromol. Res.* **22**, 1275–1281 (2014).

53. Venault, A. *et al.* Low-biofouling membranes prepared by liquid-induced phase separation of the PVDF/polystyrene-b-poly (ethylene glycol) methacrylate blend. *J. Memb. Sci.* **450**, 340–350 (2014).

54. Smolders, C. A., Reuvers, A. J., Boom, R. M. & Wienk, I. M. Microstructures in phase-inversion membranes. Part 1. Formation of macrovoids. *J. Memb. Sci.* **73**, 259–275 (1992).

55. Haponska, M. *et al.* PVDF membrane morphology - Influence of polymer molecularweight and preparation temperature. *Polymers (Basel).* **9**, 1–14 (2017).

56. Chen, L., Wu, Y., Li, Y., Zhang, X. & Qian, J. pH-responsive poly(vinylidene fluoride) membranes containing a novel poly(vinylidene fluoride)-poly(acrylic acid) block copolymer blending material. *Mater. Lett.* **210**, 124–127 (2018).

57. Ngang, H. P., Ahmad, A. L., Low, S. C. & Ooi, B. S. Preparation of thermoresponsive PVDF/SiO 2 -PNIPAM mixed matrix membrane for saline oil emulsion separation and its cleaning efficiency. *Desalination* **408**, 1–12 (2017).

58. Han, M. J. & Bhattacharyya, D. Morphology and transport study of phase inversion polysulfone membranes. *Chem. Eng. Commun.* **128**, 197–209 (1994).

59. Hołda, A. K., De Roeck, M., Hendrix, K. & Vankelecom, I. F. J. The influence of polymer purity and molecular weight on the synthesis of integrally skinned polysulfone membranes. *J. Memb. Sci.* (2013). doi:10.1016/j.memsci.2013.06.023

60. Tsai, H. A., Ruaan, R. C., Wang, D. M. & Lai, J. Y. Effect of temperature and span series surfactant on the structure of polysulfone membranes. *J. Appl. Polym. Sci.* **86**, 166–173 (2002).

61. Tan, X. & Rodrigue, D. A Review on Porous Polymeric Membrane Preparation. Part I: Production Techniques with Polysulfone and Poly (Vinlylidene Fluoride). *Polymers (Basel).* **11**, 1–39 (2019).

62. Venault, A., Chang, Y., Wang, D.-M. & Bouyer, D. A Review on Polymeric Membranes and Hydrogels Prepared by Vapor-Induced Phase Separation Process. *Polym. Rev.* **53**, 568–626 (2013).

63. Marino, T., Russo, F., Figoli, A. & May, H. The Formation of Polyvinylidene Fluoride Membranes with Tailored Properties via Vapour / Non-Solvent Induced Phase Separation. 1–17 (2018). doi:10.3390/membranes8030071

64. Zhao, J., Yi, J., Shi, L. & Wang, R. Explorations of combined nonsolvent and thermally induced phase separation (N-TIPS) method for fabricating novel PVDF hollow fi ber membranes using mixed diluents. *J. Memb. Sci.* **572**, 210–222 (2019).

65. Tan & Rodrigue. A Review on Porous Polymeric Membrane Preparation. Part II: Production Techniques with Polyethylene, Polydimethylsiloxane, Polypropylene, Polyimide, and Polytetrafluoroethylene. *Polymers (Basel).* **11**, 1310 (2019).

66. Kriwet, B. & Kissel, T. pharmaceutics international Interactions between bioadhesive poly (acrylic acid) and calcium ions. *Int. J. Pharm.* **127**, 135–145 (1996).

67. Jeong, S. *et al.* Nanostructured PVDF membrane for MD application by an O2 and CF4 plasma treatment. *Desalination* **399**, 178–184 (2016).

68. Li, J. H. *et al.* Engineering a self-driven PVDF/PDA hybrid membranes based on membrane micro-reactor effect to achieve super-hydrophilicity, excellent antifouling properties and hemocompatibility. *Appl. Surf. Sci.* **444**, 672–690 (2018).

69. Lee, E. J. *et al.* Engineering the Re-Entrant Hierarchy and Surface Energy of PDMS-PVDF Membrane for Membrane Distillation Using a Facile and Benign Microsphere Coating. *Environ. Sci. Technol.* **51**, 10117–10126 (2017).

70. Zhang, S. *et al.* Hydrophilic modification of PVDF porous membrane: Via a simple dip-coating method in plant tannin solution. *RSC Adv.* **6**, 71287–71294 (2016).

71. Song, S., Cao, M., Shan, H., Du, C. & Li, B. Polyhedral oligomeric silsesquioxane functionalized carbon nanotubes for high thermal conductive poly(vinylidene fluoride) composite membrane. *Mater. Des.* **156**, 242–251 (2018).

72. Wan, H., Briot, N. J., Saad, A., Ormsbee, L. & Bhattacharyya, D. Pore functionalized PVDF membranes with in-situ synthesized metal nanoparticles: Material characterization, and toxic organic degradation. *J. Memb. Sci.* **530**, 147–157 (2017).

73. Shaulsky, E. *et al.* Post-fabrication modification of electrospun nanofiber mats with polymer coating for membrane distillation applications. *J. Memb. Sci.* **530**, 158–165 (2017).

74. Xiao, L., Davenport, D. M., Ormsbee, L. & Bhattacharyya, D. Polymerization and functionalization of membrane pores for water related applications. *Ind. Eng. Chem. Res.* **54**, 4174–4182 (2015).

75. Uma Devi, A., Divya, K., Rana, D., Sri Abirami Saraswathi, M. & Nagendran, A. Highly selective and methanol resistant polypyrrole laminated SPVdF-co-HFP/PWA proton exchange membranes for DMFC applications. *Mater. Chem. Phys.* **212**, 533–542 (2018).

76. Zhang, H. *et al.* Study of the dual role mechanism of water-soluble additive in low temperature thermally-induced phase separation. *J. Memb. Sci.* **543**, 1–9 (2017).

77. Ayyaru, S. & Ahn, Y. H. Application of sulfonic acid group functionalized graphene oxide to improve hydrophilicity, permeability, and antifouling of PVDF nanocomposite ultrafiltration membranes. *J. Memb. Sci.* **525**, 210–219 (2017).

78. Benhabiles, O., Galiano, F., Marino, T. & Mahmoudi, H. Preparation and characterization of TiO 2 - PVDF / PMMA blend membranes using an alternative non-toxic solvent for UF / MF and photocatalytic application. 1–20 (2018).

79. Tao, M., Liu, F. & Xue, L. Persistently hydrophilic microporous membranes based on in situ cross-linking. *J. Memb. Sci.* **474**, 224–232 (2015).

80. Fontananova, E. *et al.* Polyvinylidenefluoride/carbon nanotubes mixed matrix membranes with tailored properties. *AIP Conf. Proc.* **1736**, (2016).

81. Venault, A. *et al.* Low-biofouling membranes prepared by liquid-induced phase separation of the PVDF/polystyrene-b-poly (ethylene glycol) methacrylate blend. *J. Memb. Sci.* **450**, 340–350 (2014).

82. Ma, W. *et al.* Effect of type of poly(ethylene glycol) (PEG) based amphiphilic copolymer on antifouling properties of copolymer/poly(vinylidene fluoride) (PVDF) blend membranes. *J. Memb. Sci.* **514**, 429–439 (2016).

83. Jiang, S., Deng, J. & Yang, W. Block copolymers prepared by free radical polymerization using α-methylstyrene-containing precopolymer as macroinitiator. *Polymer Journal* **40**, 543–548 (2008).

84. Le, D., N. T. Phan, T., Autissier, L., Charles, L. & Gigmes, D. A well-defined block copolymer synthesis via living cationic polymerization and nitroxide- mediated polymerization using carboxylic acid-based alkoxyamines as a dual initiator. *Polym. Chem.* **7**, 1659–1667 (2016).

85. Apostolides, D. E. *et al.* Near-Model Amphiphilic Polymer Conetworks Based on Four-Arm Stars of Poly(vinylidene fluoride) and Poly(ethylene glycol): Synthesis and Characterization. *Macromolecules* **51**, 2476–2488 (2018).

86. Girard, E., Marty, J. D., Ameduri, B. & Destarac, M. Direct synthesis of vinylidene fluoride-based amphiphilic diblock copolymers by RAFT/MADIX polymerization. *ACS Macro Lett.* **1**, 270–274 (2012).

87. Zhao, Y. *et al.* Proton exchange membranes prepared via atom transfer radical polymerization for proton exchange membrane fuel cell: Recent advances and perspectives. *Int. J. Hydrogen Energy* **42**, 30013–30028 (2017).

88. Soloukipour, S., Saljoughi, E., Mousavi, S. M. & Pourafshari Chenar, M. PEBA/PVDF blend pervaporation membranes: preparation and performance. *Polym. Adv. Technol.* **28**, 113–123 (2017).

89. Sun, D., Yue, D., Li, B., Zheng, Z. & Meng, X. Preparation and Performance of the Novel PVDF Ultra fi ltration Membranes Blending With PVA Modi fi ed SiO 2 Hydrophilic Nanoparticles. (2019). doi:10.1002/pen.25002

90. Ji, K., Xu, H., Ma, X., Yin, J. & Jiang, X. Hyperbranched poly(ether amine)@poly(vinylidene fluoride) (hPEA@PVDF) porous membranes for selective adsorption and molecular filtration of hydrophilic dyes. 10470–10479 (2017). doi:10.1039/c7ta02176c

91. Yuan, Q., Liu, P. & Baker, G. L. Sulfonated polyimide and PVDF based blend proton exchange membranes for fuel cell applications. *J. Mater. Chem. A* **3**, 3847–3853 (2015).

92. Li, X., Hu, X. & Cai, T. Construction of Hierarchical Fouling Resistance Surfaces onto Poly(vinylidene fluoride) Membranes for Combating Membrane Biofouling. *Langmuir* **33**, 4477–4489 (2017).

93. Yang, C. L. *et al.* Batwing-like polymer membrane consisting of PMMA-grafted electrospun PVdF-SiO 2 nanocomposite fibers for lithium-ion batteries. *J. Memb. Sci.* **495**, 341–350 (2015).

94. Amira, M. N., Irfan Hatim, M. D., Jullok, N., Syahmie Rasidi, M. & Alamery, H. R. Synthesis and Preparation of Asymmetric PVDF-co-PTFE/DES Supported Membrane for CO 2 /N 2 Separation. *IOP Conf. Ser. Mater. Sci. Eng.* **429**, (2018).

95. Kanashima, T. & Okuyama, M. Chapter 9 P (VDF-TeFE)/ Organic Semiconductor Structure Ferroelectric-Gate FETs. doi:10.1007/978-94-024-0841-6

96. Chen, J., Huang, H., Zhang, L. & Zhang, H. A novel high-flux asymmetric p(VDF-HFP) membrane with a dense skin for ethanol pervaporation. *RSC Adv.* **4**, 24126–24130 (2014).

97. Su, C. *et al.* Fabrication and post-treatment of nanofibers-covered hollow fiber membranes for membrane distillation. *J. Memb. Sci.* **562**, 38–46 (2018).

98. Su, C. *et al.* Fabrication of a novel nanofibers-covered hollow fiber membrane via continuous electrospinning with non-rotational collectors. *Mater. Lett.* **204**, 8–11 (2017).

99. Wang, S. H. & Lin, H. L. Poly (vinylidene fluoride-co-hexafluoropropylene)/polybenzimidazole blend nanofiber supported Nafion membranes for direct methanol fuel cells. *J. Power Sources* **257**, 254–263 (2014).

100. Padmaraj, O., Venkateswarlu, M. & Satyanarayana, N. Characterization and Electrochemical Properties of P(VdF-co-HFP) Based Electrospun Nanocomposite Fibrous Polymer Electrolyte Membrane for Lithium Battery Applications. *Electroanalysis* **26**, 2373–2379 (2014).

101. Osińska-Broniarz, M., Pokora, M., Walkowiak, M. & Martyła, A. Composite polymer electrolytes with modified mesoporous silica filler for Li-ion batteries. *Compos. Theory Pract.* **R. 15**, **nr**, 124–129 (2015).

102. Terasawa, N. High-performance ionic and non-ionic fluoropolymer/ionic liquid gel hybrid actuators based on single-walled carbon nanotubes. *RSC Adv.* **7**, 2443–2449 (2017).

103. Khdary, N. H. & Abdelsalam, M. E. Polymer-silica nanocomposite membranes for CO2 capturing. *Arab. J. Chem.* (2017). doi:10.1016/j.arabjc.2017.06.001

104. Mondal, P. & Purkait, M. K. Green synthesized iron nanoparticle-embedded pH-responsive PVDF-co-HFP membranes: Optimization study for NPs preparation and nitrobenzene reduction. *Sep. Sci. Technol.* **52**, 2338–2355 (2017).

105. Nunes-Pereira, J. *et al.* Highly efficient removal of fluoride from aqueous media through polymer composite membranes. *Sep. Purif. Technol.* **205**, 1–10 (2018).

106. Zheng, L. *et al.* Preparation, evaluation and modification of PVDF-CTFE hydrophobic membrane for MD desalination application. *Desalination* **402**, 162–172 (2017).

107. Zheng, L., Wang, J., Yu, D., Zhang, Y. & Wei, Y. Preparation of PVDF-CTFE hydrophobic membrane by non-solvent induced phase inversion: Relation between polymorphism and phase inversion. *J. Memb. Sci.* **550**, 480–491 (2018).

108. Zheng, L. *et al.* Interconnected PVDF-CTFE hydrophobic membranes for MD desalination: Effect of PEGs on phase inversion process. *RSC Adv.* **6**, 20926–20937 (2016).

109. Zheng, L. *et al.* Preparation of PVDF-CTFE hydrophobic membranes for MD application: Effect of LiCl-based mixed additives. *J. Memb. Sci.* **506**, 71–85 (2016).

110. Wang, J., Zheng, L., Wu, Z., Zhang, Y. & Zhang, X. Fabrication of hydrophobic flat sheet and hollow fiber membranes from PVDF and PVDF-CTFE for membrane distillation. *J. Memb. Sci.* **497**, 183–193 (2016).

111. Abdel-Hady, E. E., Abdel-Hamed, M. O., Awad, S. & Hmamm, M. F. M. Characterization and evaluation of commercial poly (vinylidene fluoride)-g-sulfonatedPolystyrene as

proton exchange membrane. *Polym. Adv. Technol.* **29**, 130–142 (2018).

112. Xu, Q. *et al.* Study on improvement of the proton conductivity and anti-fouling of proton exchange membrane by doping SGO@SiO2 in microbial fuel cell applications. *Int. J. Hydrogen Energy* **44**, 15322–15332 (2019).

113. Li, C. *et al.* Fabrication of a SGO/PVDF-g-PSSA composite proton-exchange membrane and its enhanced performance in microbial fuel cells. *J. Chem. Technol. Biotechnol.* **94**, 398–408 (2019).

114. Sadeghi, S., Işıkel Şanlı, L., Güler, E. & Alkan Gürsel, S. Enhancing proton conductivity via sub-micron structures in proton conducting membranes originating from sulfonated PVDF powder by radiation-induced grafting. *Solid State Ionics* **314**, 66–73 (2018).

115. Zhou, Y. *et al.* BaTiO<inf>3</inf>/PVDF-g-PSSA composite proton exchange membranes for vanadium redox flow battery. *Ceram. Int.* **41**, S758–S762 (2015).

116. Yu, X. *et al.* Hydrophilic modification of PVDF membrane with solution bulk polymerization graft and separation performance of oil–water. *Desalin. Water Treat.* **126**, 48–59 (2018).

117. Mehraeen, S., Sadeghi, S., Cebeci, F. Ç., Papila, M. & Alkan Gürsel, S. Polyvinylidene fluoride grafted poly(styrene sulfonic acid) as ionic polymer-metal composite actuator. *Sensors Actuators, A Phys.* **279**, 157–167 (2018).

118. Sharma, T., Naik, S., Langevine, J., Gill, B. & Zhang, J. X. J. Aligned PVDF-TrFE nanofibers with high-density PVDF nanofibers and PVDF core-shell structures for endovascular pressure sensing. *IEEE Trans. Biomed. Eng.* **62**, 188–195 (2015).

119. Chen, X. *et al.* A wave-shaped hybrid piezoelectric and triboelectric nanogenerator based on P(VDF-TrFE) nanofibers. *Nanoscale* **9**, 1263–1270 (2017).

120. Shiran Chaharsoughi, M. *et al.* Hybrid Plasmonic and Pyroelectric Harvesting of Light Fluctuations. *Adv. Opt. Mater.* **6**, 1–7 (2018).

121. Boschet, F. & Ameduri, B. Copolymers of chlorotrifluoroethylene: Synthesis, properties, and applications. *Chem. Rev.* **114**, 927–980 (2014).

122. Guiot, J., Ameduri, B. & Boutevin, B. Radical homopolymerization of vinylidene fluoride initiated by tert-butyl peroxypivalate. Investigation of the microstructure by 19F and 1H NMR spectroscopies and mechanisms. *Macromolecules* **35**, 8694–8707 (2002).

123. Wormald, P., Ameduri, B., Harris, R. K. & Hazendonk, P. High-resolution 19F and 1H NMR of a vinylidenefluoride telomer. *Polymer (Guildf).* **49**, 3629–3638 (2008).

124. Guerre, M. *et al.* A Journey into the Microstructure of PVDF Made by RAFT. *Macromol. Chem. Phys.* **217**, 2275–2285 (2016).

125. Ferguson, R. C. & Brame, E. G. High resolution nuclear magn n etic resonance of fluoro polymers. 2. Fluorine-19 spectra and chain structure of poly(vinylidene fluoride). *J.*

Phys. Chem. **83**, 1397–1401 (1979).

126. Nandi, A. K. & Mandelkern, L. The influence of chain structure on the equilibrium melting temperature of poly(vinylidene fluoride). *J. Polym. Sci. Part B Polym. Phys.* **29**, 1287–1297 (1991).

127. Gadinski, M. R. UNDERSTANDING THE EFFECTS OF DEFECT MODIFICATION ON THE STRUCTURE AND PROPERTIES OF FLUORINATED POLYMERS AND IMPLICATIONS FOR CAPACITIVE ENERGY STORAGE TECHNOLOGIES. (Pennsylvania State University, 2015).

128. David, G. *et al.* Use of iodocompounds in radical polymerization. *Chem. Rev.* **106**, 3936–3962 (2006).

129. Kostov, G. *et al.* First amphiphilic poly(vinylidene fluoride-co-3,3,3-trifluoropropene)-b- oligo(vinyl alcohol) block copolymers as potential nonpersistent fluorosurfactants from radical polymerization controlled by xanthate. *Macromolecules* **44**, 1841–1855 (2011).

130. Folgado, E. *et al.* Well-defined poly(vinylidene fluoride) (PVDF) based-dendrimers synthesized by click chemistry: Enhanced crystallinity of PVDF and increased hydrophobicity of PVDF films. *Polym. Chem.* **7**, 5625–5629 (2016).

131. Guerre, M., Ameduri, B. & Ladmiral, V. RAFT synthesis of well-defined PVDF-b-PVAc block copolymers. *Polym. Chem.* **7**, 441–450 (2016).

132. Asandei, A. D., Adebolu, O. I. & Simpson, C. P. Mild-temperature Mn 2(CO) 10-photomediated controlled radical polymerization of vinylidene fluoride and synthesis of well-defined poly(vinylidene fluoride) block copolymers. *J. Am. Chem. Soc.* **134**, 6080–6083 (2012).

133. M, T. No Title. *Int. Polym. Sci. Technol.* **12**, 85–98 (1985).

134. Valade, D., Boyer, C., Ameduri, B. & Boutevin, B. Poly (vinylidene fluoride) - b -poly (styrene) Block Copolymers by Iodine Transfer Polymerization (ITP): Synthesis , Characterization , and Kinetics of ITP. *Macromolecules* **39**, 8639–8651 (2006).

135. Taton, D., Destarac, M. & Z. Zard, S. Macromolecular Design by Interchange of Xanthates: Background, Design, Scope and Applications. in *Handbook of RAFT Polymerization* (ed. Professor Christopher Barner-Kowollik) 337–421 (2008). doi:10.1192/bjp.112.483.211-a

136. Perrier, S. & Takolpuckdee, P. Macromolecular design via reversible addition-fragmentation chain transfer (RAFT)/xanthates (MADIX) polymerization. *J. Polym. Sci. Part A Polym. Chem.* **43**, 5347–5393 (2005).

137. Patil, Y. & Ameduri, B. First RAFT/MADIX radical copolymerization of tert-butyl 2-trifluoromethacrylate with vinylidene fluoride controlled by xanthate. *Polym. Chem.* **4**, 2783–2799 (2013).

138. Guerre, M., Ameduri, B. & Ladmiral, V. One-pot synthesis of poly(vinylidene fluoride) methacrylate macromonomers via thia-Michael addition. *Polym. Chem.* **7**, 441–450

(2016).

139. Ameduri, B. Fluoropolymers: The Right Material for the Right Applications. *Chem. - A Eur. J.* **24**, 18830–18841 (2018).

140. Guerre, M. *et al.* Combination of Cationic and Radical RAFT Polymerizations: A Versatile Route to Well-Defined Poly(ethyl vinyl ether)-block-poly(vinylidene fluoride) Block Copolymers. *ACS Macro Lett.* **6**, 393–398 (2017).

141. Guerre, M. *et al.* Self-assembly of poly(vinylidene fluoride)-block-poly(2-(dimethylamino)ethylmethacrylate) block copolymers prepared by CuAAC click coupling. *Polym. Chem.* 5203–5211 (2017). doi:10.1039/C7PY00346C

142. Guerre, M., Wahidur Rahaman, S. M., Améduri, B., Poli, R. & Ladmiral, V. RAFT synthesis of well-defined PVDF-: B -PVAc block copolymers. *Polym. Chem.* **7**, 6918–6933 (2016).

143. Guerre, M., Schmidt, J., Talmon, Y., Améduri, B. & Ladmiral, V. An amphiphilic poly(vinylidene fluoride)-: B -poly(vinyl alcohol) block copolymer: Synthesis and self-assembly in water. *Polym. Chem.* **8**, 1125–1128 (2017).

144. Guerre, M., Semsarilar, M., Godiard, F., Améduri, B. & Ladmiral, V. Polymerization-induced self-assembly of PVAc-b-PVDF block copolymers via RAFT dispersion polymerization of vinylidene fluoride in dimethyl carbonate. *Polym. Chem.* **8**, 1477–1487 (2017).

145. Folgado, E., Guerre, M., Mimouni, N. & Collière, V. π -Stacking Interactions of Graphene-Coated Cobalt Magnetic Nanoparticles with Pyrene-Tagged Dendritic Poly (Vinylidene Fluoride). *Chempluschem* **84**, 78–84 (2019).

146. Smart, T. *et al.* Block copolymer nanostructures. *Nano Today* **3**, 38–46 (2008).

147. Mai, Y. & Eisenberg, A. Self-assembly of block copolymers. *Chem Soc Rev* **41**, 5969–5985 (2012).

148. Kong, W., Li, B., Jin, Q., Ding, D. & Shi, A. C. Complex micelles from self-assembly of ABA triblock copolymers in B-selective solvents. *Langmuir* **26**, 4226–4232 (2010).

149. Oliver, A. M., Spontak, R. J. & Manners, I. Solution self-assembly of ABC triblock terpolymers with a central crystallizable poly(ferrocenyldimethylsilane) core-forming segment. *Polym. Chem.* **10**, 2559–2569 (2019).

150. Martinez, A. P., Cui, Z., Hire, C., Seery, T. A. P. & Adamson, D. H. Synthesis and Self-Assembly of Toothbrush-like Block Copolymers. *Macromolecules* **48**, 4250–4255 (2015).

151. Cao, M., Nie, H., Hou, Y., Han, G. & Zhang, W. Synthesis of star thermoresponsive amphiphilic block copolymer nano-assemblies and the effect of topology on their thermoresponse. *Polym. Chem.* **10**, 403–411 (2019).

152. Gadwal, I., Wadgaonkar, P. P., Ichake, A. B. & Mane, S. R. A New Approach for the Synthesis of Miktoarm Star Polymers Through a Combination of Thiol – Epoxy " Click "

Chemistry and ATRP / Ring-Opening Polymerization Techniques. *Polym. Chem.* **57**, 146–156 (2019).

153. Patil, Y. *et al.* A Novel Poly(vinylidene fluoride)-Based 4-Miktoarm Star Terpolymer: Synthesis and Self-Assembly. *Mol. Pharm.* **15**, 3005–3009 (2018).

154. Erhardt, R. *et al.* Amphiphilic Janus micelles with polystyrene and poly(methacrylic acid) hemispheres. *J. Am. Chem. Soc.* **125**, 3260–3267 (2003).

155. Bütün, V. *et al.* Synthesis of shell cross-linked micelles at high solids in aqueous media. *Macromolecules* **33**, 1–3 (2000).

156. Ritzenthaler, S., Court, F., Girard-Reydet, E., Leibler, L. & Pascault, J. P. ABC triblock copolymers/epoxy-diamine blends. 2. Parameters controlling the morphologies and properties. *Macromolecules* **36**, 118–126 (2003).

157. Liu, Y., Abetz, V. & Müller, A. H. E. Janus Cylinders. *Macromolecules* **36**, 7894–7898 (2003).

158. Stewart, S. & Liu, G. Block copolymer nanotubes. *Angew. Chemie - Int. Ed.* **39**, 340–344 (2000).

159. Cui, H., Chen, Z., Zhong, S., Wooley, K. L. & Pochan, D. J. Block copolymer assembly via kinetic control. *Science (80-.).* **317**, 647–650 (2007).

160. Stoenescu, R., Graff, A. & Meier, W. Asymmetric ABC-triblock copolymer membranes induce a directed insertion of membrane proteins. *Macromol. Biosci.* **4**, 930–935 (2004).

161. Li, Z., Hillmyer, M. A. & Lodge, T. P. Laterally nanostructured vesicles, polygonal bilayer sheets, and segmented wormlike micelles. *Nano Lett.* **6**, 1245–1253 (2006).

162. Zhang, Q. *et al.* Low length dispersity fiber-like micelles from an A–B–A triblock copolymer with terminal crystallizable poly(ferrocenyldimethylsilane) segments via living crystallization-driven self-assembly . *Polym. Chem.* (2019). doi:10.1039/c9py00401g

163. Riess, G. Micellization of block copolymers. *Prog. Polym. Sci.* **28**, 1107–1170 (2003).

164. Wang, Y., Li, P., Tran, T. T. D., Zhang, J. & Kong, L. Manufacturing techniques and surface engineering of polymer based nanoparticles for targeted drug delivery to cancer. *Nanomaterials* **6**, (2016).

165. Tritschler, U. *et al.* Toward Uniform Nanofibers with a π-Conjugated Core: Optimizing the “living” Crystallization-Driven Self-Assembly of Diblock Copolymers with a Poly(3-octylthiophene) Core-Forming Block. *Macromolecules* **51**, 5101–5113 (2018).

166. Sha, Y. *et al.* Ring-Closing Metathesis and Ring-Opening Metathesis Polymerization toward Main-Chain Ferrocene-Containing Polymers. *Macromolecules* **51**, 9131–9139 (2018).

167. Ganda, S. *et al.* Two-Dimensional Self-Assembled Structures of Highly Ordered

Bioactive Crystalline-Based Block Copolymers. *Macromolecules* **50**, 8544–8553 (2017).

168. Boott, C. E. *et al.* Probing the Growth Kinetics for the Formation of Uniform 1D Block Copolymer Nanoparticles by Living Crystallization-Driven Self-Assembly. *ACS Nano* **12**, 8920–8933 (2018).

169. Finnegan, J. R. *et al.* Extending the Scope of "living" Crystallization-Driven Self-Assembly: Well-Defined 1D Micelles and Block Comicelles from Crystallizable Polycarbonate Block Copolymers. *J. Am. Chem. Soc.* **140**, 17127–17140 (2018).

170. Li, Z. *et al.* Glyco-Platelets with Controlled Morphologies via Crystallization-Driven Self-Assembly and Their Shape-Dependent Interplay with Macrophages. *ACS Macro Lett.* 596–602 (2019). doi:10.1021/acsmacrolett.9b00221

171. Tao, D. *et al.* Monodisperse Fiber-like Micelles of Controlled Length and Composition with an Oligo(p-phenylenevinylene) Core via "Living" Crystallization-Driven Self-Assembly. *J. Am. Chem. Soc.* **139**, 7136–7139 (2017).

172. Schöbel, J. *et al.* Patchy Wormlike Micelles with Tailored Functionality by Crystallization-Driven Self-Assembly: A Versatile Platform for Mesostructured Hybrid Materials. *Macromolecules* **49**, 2761–2771 (2016).

173. Yu, W., Inam, M., Jones, J. R., Dove, A. P. & O'Reilly, R. K. Understanding the CDSA of poly(lactide) containing triblock copolymers. *Polym. Chem.* **8**, 5504–5512 (2017).

174. Vilgis, T. & Halperin, A. Aggregation of Coil-Crystalline Block Copolymers: Equilibrium Crystallization. *Macromolecules* **24**, 2090–2095 (1991).

175. Crassous, J. J., Schurtenberger, P., Ballauff, M. & Mihut, A. M. Design of block copolymer micelles via crystallization. *Polymer (Guildf).* **62**, A1–A13 (2015).

176. Inam, M. *et al.* 1D: Vs. 2D shape selectivity in the crystallization-driven self-assembly of polylactide block copolymers. *Chem. Sci.* **8**, 4223–4230 (2017).

177. Chen, L., Lee, H. S. & Lee, S. Close-packed block copolymer micelles induced by temperature quenching. *Proc. Natl. Acad. Sci. U. S. A.* **115**, 7218–7223 (2018).

178. Zhou, H., Lu, Y., Yu, Q., Manners, I. & Winnik, M. A. Monitoring Collapse of Uniform Cylindrical Brushes with a Thermoresponsive Corona in Water. *ACS Macro Lett.* **7**, 166–171 (2018).

179. Yusoff, S. F. M., Hsiao, M. S., Schacher, F. H., Winnik, M. A. & Manners, I. Formation of lenticular platelet micelles via the interplay of crystallization and chain stretching: Solution self-assembly of poly(ferrocenyldimethylsilane)- Block -poly(2-vinylpyridine) with a crystallizable core-forming metalloblock. *Macromolecules* **45**, 3883–3891 (2012).

Chapter 2

"One-Pot" Aminolysis/Thia-Michael Addition preparation of well-defined amphiphilic PVDF-*b*-PEG-*b*-PVDF triblock copolymers: Self-assembly behavior in mixed solvents

The first objective of this research work was to synthesize PVDF-based amphiphilic block copolymers made by RAFT. Since MADIX allows the preparation of PVDF polymers bearing a xanthate end-group, accessing thiol allows the preparation of ABA triblock copolymers where the A blocks are PVDF and B block is PEG. Aminolysis of the xanthate end-group allows the access to a thiol allowing the preparation of block copolymers through a thia-Michael reaction between the thiol and an acrylate difunctional PEG. The self-assembly of the obtained triblock copolymer was studied employing different protocols and solvents.

"One-Pot" Aminolysis/Thia-Michael Addition preparation of well-defined amphiphilic PVDF-*b*-PEG-*b*-PVDF triblock copolymers: Self-assembly behaviour in mixed solvents

Enrique Folgado,[a,b] Marc Guerre,[a†] Antonio Da Costa,[c] Anthony Ferri[c], Ahmed Addad,[d] Vincent Ladmiral,[a]* and Mona Semsarilar[b]*

[a]Institut Charles Gerhardt Montpellier, ICGM UMR5253, Univ Montpellier, CNRS, ENSCM, Montpellier, France.

[b]Institut Européen des Membranes, IEM, UMR5635, Univ Montpellier, CNRS, ENSCM, Montpellier, France.

[c]Université Artois, CNRS, Centrale Lille, ENSCL, Université Lille, UMR 8181, Unité de Catalyse et Chimie du Solide (UCCS), F-62300 Lens, France.

[d]Université Lille, Sciences et Technologies, CNRS, Unité Matériaux Et Transformations (UMET), F-59000 Lille, France

†Current address : Department of Organic and Macromolecular Chemistry, Centre of Macromolecular Chemistry, Polymer Chemistry Research Group and Laboratory for Organic Synthesis, Ghent University, Krijgslaan 281 S4-bis , B-9000, Ghent, Belgium.

1. Abstract

Polyvinylidene fluoride- (PVDF) containing block copolymers are scarce and difficult to prepare. Amphiphilic block copolymers containing PVDF have been rarely reported. In consequence, few studies of the self-assembly of PVDF-based block copolymers exist. Here a new synthetic route to prepare poly(vinylidene fluoride)-*b*-poly(ethylene glycol)-*b*-poly(vinylidene fluoride) (PVDF-*b*-PEG-*b*-PVDF) ABA triblock copolymer is presented. The synthesis relies on the efficient coupling of a PVDF prepared by RAFT and a PEG diacrylate in one pot via aminolysis of the xanthate moiety and subsequent thia Michael-addition. The novel amphiphilic triblock copolymer was fully characterized by ^{1}H and ^{19}F NMR spectroscopies, GPC, TGA, DSC and XRD; and its self-assembly in water and ethanol was studied. Micellization (addition of a selective solvent for PVDF to a solution of the triblock) and nanoprecipitation (addition of a solution of the triblock into a non-solvent for PVDF) protocols led to the formation of micelles and vesicles. Surprisingly, under nanoprecipitation conditions (in THF/ ethanol), well-defined crystalline micrometric structures were obtained.

2. Introduction

ABA triblock copolymers are important materials which have found high added value applications. SBS (polystyrene-*b*-polybutadiene-*b*-polystyrene) is a crucial thermoplastic elastomer for the tyre industry for example, and Pluronics® are used in numerous fields as dispersants, emulsifiers, thickeners, antifoaming or wetting agent.[1,2]

Amphiphilic ABA triblock copolymers are indeed very interesting polymer architectures. When the A and B blocks are incompatible, these triblock copolymers readily self-assemble from the melt into well-ordered nanostructures.[3–6] In selective solvents, the self-assembly of such ABA triblock copolymers can generate a variety of morphologies, such as spherical micelles,[7] wormlike micelles,[8] vesicles[9] or more complex structures such as toroids.[10] In aqueous media, and when the B block is hydrophilic, these triblocks readily form self-assembled micelles comprising a hydrophobic core constituted of the A segments, and a stabilizing hydrophilic corona made of the hydrophilic B blocks.[9,11,12] These micelles, sometimes named flower-like micelles,[4,7] may connect to each other via intermicellar bridges. The formation of these bridges depends on several factors such as micelle concentration, size and nature of A and B blocks and interchain interactions for example.[13,14]

The formation of such bridges is favoured when the hydrophobic core-forming block is smaller than the stabilizing corona segments.[15,16] If the hydrophilic block is too short, the conformational energy will not be favourable to the formation of loops. There must be a compromise between inter-chain interactions, increasing with the length of the hydrophilic block, and the formation of loops, also favored by longer chains. Finally, if the system is too diluted, the intremicellar interactions will be too rare for bridges to form.[17]

In industry most ABA triblock copolymers are prepared by anionic polymerization.[12,18] However, progress in Reversible Deactivation Radical Polymerization (RDRP) techniques, such as RAFT (Reversible Addition-Fragmentation chain Transfer),[19,20] ATRP (Atom-Transfer Radical Polymerization)[21,22] or CMRP (Cobalt-Mediated Radical Polymerization)[23] for example, have enabled the facile synthesis of ABA triblock copolymers. Numerous acrylates-,

methacrylates- or styrenics-based ABA triblock copolymers have been described and reported by academic research groups. Singha et al. reported the use of ATRP for the preparation of an ABA PDCPMA-*b*-PHEA-*b*-PDCPMA (DCPMA = dicyclopentyloxyethyl methacrylate, EHA = 2-ethylhexylacrylate) triblock copolymer using a Br-PEHA-Br difunctional macroinitiator.[24] Xie et al. synthesised via activator generated by electron transfer (AGET) ATRP, a poly(n-butylacrylate) homopolymer and a polystyrene-*b*-poly(n-butylacrylate)-*b*-polystyrene (PS-PnBA-PS) triblock copolymer from ethylene bis(2-bromoisobutyrate).[25] Following a similar approach and using a difunctional trithiocarbonate RAFT agent, Semsarilar et al. synthesised a polystyrene-*b*-poly(sodium 4-styrenesulfonate)-*b*-polystyrene (PS-*b*-PNaSS-*b*-PS) ABA triblock.[9] Shipp et al. employed a difunctional polydimethylsiloxane xanthate macro RAFT agents to polymerize *N*-vinylpyrrolidone (NVP) and prepare a PVP-*b*-PDMS-*b*-PVP ABA triblock copolymer.[26] CMRP is particularly well-adapted to prepare ABA triblock copolymers from LAMs (less-activated monomers) such as vinyl acetate for example.[27] It is arguably the most efficient method to control the polymerization of LAMs and to prepare well-defined copolymers from these type of monomers.[27] ABA triblock copolymers are also very easily synthesized by CMRP from diblock copolymers using a very efficient radical coupling cobalt-catalyzed chemistry.[23,28–31]

Fluorinated polymers bearing fluorine atoms on the main chain such as PTFE (polytetrafluoroethylene) or PVDF (poly(vinylidene fluoride)) are valuable specialty polymers endowed with remarkable properties. PVDF in particular displays high resistance to weathering and chemical aggressions as well as unusual electroactivity. Copolymers of VDF, trifluoroethylene and chlorotrifluoroethylene for example are outstanding relaxor ferroelectrics. [32–34] Copolymers of VDF and TrFE possess high sensitivity and wide frequency responses to electric fields, are relatively flexible, and easy to produce. These copolymers have a great potential for emerging applications such as haptics, sensors, artificial muscles, etc.[35]

Only few references describe the self-assembly of PVDF block copolymers in solution, probably because well-defined PVDF-containing block copolymers are difficult to synthesize.[36–38] Qian *et al.* studied the self-assembly of PVDF-*b*-PS block copolymers in DMF-

containing mixtures of solvents. The presence of DMF was necessary to give sufficient mobility to the PVDF segments and gain access to non-spherical self-assembled structures.[39] Rodionov *et al.* prepared interesting 4-miktoarm star copolymers containing 2 PVDF-*b*-PS arms and 2 PEG arms via the combination of ATRP, Iodine Transfer Polymerization (ITP) and copper-catalyzed azide-alkyne cycloaddition (CuAAC); and studied their self-assembly in organic solvents and water.[40] Over the last two years we developed the RAFT polymerization of VDF,[41] and prepared some PVDF-containing block copolymers,[42] which self-assembled in water and organic solvents. PVDF-*b*-PVA (PVA = poly(vinyl alcohol)) formed spherical particles in water,[43] PVDF-*b*-PDMAEMA (PDMAEMA = poly (2-dimethylaminoethyl methacrylate) in water displayed spherical aggregates and rigid rods which are thought to be generated via crystallisation-driven self-assembly;[44] and PVAc-*b*-PVDF (PVAc = poly(vinyl acetate)) readily self-assembled in dimethyl carbonate under polymerization-induced self-assembly conditions into highly crystalline micrometric structures.[45] The synthesis of PVDF-based BCPs by RAFT (or ITP) and sequential addition of monomers is difficult due to the fast accumulation of much less reactive inversely-terminated PVDF chains (-CH_2-xanthate-terminated chains). For example, in spite of what was recently wrongly reported,[46] well-defined PVDF-*b*-PNVP (PNVP = poly *N*-vinyl pyrrolidone)) cannot be synthesized by polymerization of NVP starting from a PVDF macroRAFT agent since only -CF_2-xanthate-terminated chains (which disappear entirely from the reaction medium quickly) can be reinitiated with PNVP radicals.[37] Synthesis strategies based on the coupling of two or more homopolymers may afford better-defined block copolymers provided the coupling reaction is efficient enough, although complete removal of the residual homopolymers is often difficult or requires tedious purification steps. Huck et al., for example, purified a PF8TBT-*b*-P3HT diblock copolymer (P3HT = poly(3-hexylthiophene) and PF8TBT = poly((9,9-dioctylfluorene)-2,7-diyl-alt-[4,7-bis(3hexylthien-5-yl)-2,1,3-benzothiadiazole]-2′,2″-diyl)) via preparative GPC to remove the excess of P3HT homopolymer.[47] This strategy has been successfully implemented with the copper-catalyzed coupling of azides and alkynes (CuAAC) to prepare PVDF-block copolymers[45] and PEG-*b*-PFPE-*b*-PEG (PEG = polyethylene glycol, PFPE = perfluoropolyether) ABA triblock copolymers.[7] CuAAC is a powerful click chemistry technique, but the removal of copper is often tedious. In contrast, the thia Michael addition

does not use copper, and is very well-suited to polymers made by RAFT.[48,49] It does not require functional RAFT agents and can be conducted in one pot.[50,51]

In this chapter, we report the synthesis using RAFT polymerization and a one-pot thia Michael addition procedure, the characterization of a novel amphiphilic PVDF-based ABA triblock copolymer ($PVDF_{50}$-*b*-PEG_{136}-*b*-$PVDF_{50}$), its self-assembly in NMP/water, THF/ethanol and THF/water mixtures and the characterization of the obtained structures using TEM and AFM.

3. Experimental section

3.1. Materials

All reagents were used as received unless otherwise stated. 1,1-Difluoroethylene (vinylidene fluoride, VDF) was supplied by Arkema (Pierre-Bénite, France). *O*-Ethyl-*S*-(1-methoxycarbonyl) ethyldithiocarbonate was synthesized according to the method described by Liu et al.[52] *tert*-Amyl peroxy-2-ethylhexanoate (Trigonox 121, purity 95%) was purchased from AkzoNobel (Chalons-sur-Marne, France). PEG_{6000}, acetonitrile (ACN), ethanol (EtOH), dimethyl carbonate (DMC), hexylamine, *N*-methyl-2-pyrrolidone (NMP), tetrahydrofuran (THF), triethylamine (NEt_3) and laboratory reagent grade hexane (purity >95%) were purchased from Sigma-Aldrich.

3.2. Measurements

Nuclear Magnetic Resonance (NMR).

The NMR spectra were recorded on a Bruker AV III HD Spectrometer (400 MHz for 1H and 376 MHz for 19F). Coupling constants and chemical shifts are given in hertz (Hz) and parts per million (ppm), respectively. The experimental conditions for recording 1H and 19F NMR spectra were as follows: flip angle, 90° (or 30°); acquisition time, 4.5 s (or 2 s); pulse delay, 2

s; number of scans, 32 (or 64); and pulse widths of 12.5 and 11.4 μs for 1H and 19F NMR respectively.

2D DOSY (Diffusion-Ordered Spectroscopy) NMR spectra were recorded at 60 °C on a Bruker Avance 300 MHz spectrometer using deuterated DMSO. All experiments were recorded in static mode (spinning off) with a Bruker Dual z-gradient probe producing gradients in the z direction with strength 55 G cm^{-1}. DOSY proton spectra were acquired with pulsed-gradient stimulated echo (LED-PFGSTE) sequence, using a bipolar gradient. All spectra were recorded with 8 Ko time domain data points in the F2 Frequency axis and 32 experiments (F1). The gradient strength was logarithmically incremented in 32 steps from 2% up to 95% of the maximum gradient strength. All measurements were performed with a diffusion delay (D) of 50 ms in order to keep the relaxation contribution to the signal attenuation constant for all samples. The gradient pulse length (δ) was 3.5 ms in order to ensure full signal attenuation. The diffusion dimension of the 2D DOSY spectra was processed according to the TopSpin standard conditions (version 2.1).

Size-Exclusion Chromatography (SEC).

SEC measurements were recorded using a triple-detection GPC from Agilent Technologies with its corresponding Agilent software, dedicated to multidetector GPC calculation. The system used two PL1113-6300 ResiPore 300 × 7.5 mm columns with THF the eluent with a flow rate of 0.8 mL·min–1 and toluene as the flow rate marker. The detector suite was composed of a PL0390-0605390 LC light scattering detector with two diffusion angles (15° and 90°), a PL0390-06034 capillary viscometer, and a 390-LC PL0390-0601 refractive index detector. The entire SEC-HPLC system was thermostated at 35 °C. PMMA standards were used for calibration. Typical sample concentration was 10 mg/mL.

Differential Scanning Calorimetry (DSC).

DSC measurements were performed on 2–3 mg samples on a TA Instruments DSC Q20 equipped with an RCS90 cooling system. For all measurements, the following heating / cooling cycle was employed: cooling from room temperature (ca. 20 °C) to −73 °C at 20

°C/min, isotherm plateau at −50 °C for 5 min, first heating ramp from −73 °C to 250 °C at 10 °C/min, cooling stage from 250 °C to −73 °C at 10 °C/min, isotherm plateau at −73 °C for 3 min, second heating ramp from −73 °C to 250 °C at 10 °C/min, and last cooling stage from 250 °C to room temperature (ca. 20 °C). Calibration of the instrument was performed with noble metals and checked before analysis with an indium sample. Melting points were determined at the maximum of the enthalpy peaks.

Thermogravimetric analysis (TGA).

TGA analyses were carried out with a TA Instruments TGA G500 from 20 °C to 1000 °C. A heating rate of 10 °C min^{-1} was used under an air atmosphere with a flow rate of 60 mL min^{-1}. A dry sample weighing about 3 mg was used.

Dynamic light scattering (DLS).

DLS measurements of polymer solutions in NMP and THF were carried out in a Malvern ZEN1600 using a quartz cuvette.

Transmission electron microscopy (TEM).

TEM studies were conducted using a JEOL 1200 EXII instrument equipped with a numerical camera, operating with a 120 kV acceleration voltage at 25 °C. To prepare TEM samples, a drop (7.0 µL) of a dilute micellar solution was placed onto a carbon-coated copper grid for 50 s, blotted with filter paper and dried under ambient conditions.

Atomic force microscopy (AFM).

AFM images were obtained with a Pico SPM II provided by Molecular Imaging. The imagery was controlled by the PicoView 1.10 software. The experiments were all carried out in tapping mode. The types of tips used were PPS-FMR purchased from Nanosensors with a frequency resonance between 45 and 115 kHz and a force constant between 0.5 and 9.5 N/m. Gwyddion 2.25 software was used to treat the images.

X-Ray diffraction (XRD).

XRD powder patterns were carried out on a Philips X'pert Pro MPD diffractometer by using Ni-filtered CuKα1 radiation (λ=1.5406 Å) in Bragg–Brentano scanning mode with a 2θ angle range from 5–60°, and a time per step of 50 s.

3.3. Synthesis

Autoclave.

The polymerization of VDF was performed in a 100 mL Hastelloy Parr autoclave system (HC 276) equipped with a mechanical Hastelloy stirring system, a rupture disk (3000 PSI), inlet and outlet valves, and a Parr electronic controller to regulate the stirring speed and heating.

$PVDF_{50}$-XA synthesis.

A solution of Trigonox 121 (158 mg, 6.87 10^{-4} mol) and *O*-Ethyl-*S*-(1-methoxycarbonyl) ethyldithiocarbonate (1.30 g, 6.25 10^{-3} mol) in DMC (60 mL), was degassed by N_2 bubbling during 30 min. Prior to the reaction, the autoclave was pressurized with 30 bar of nitrogen to check for leaks. The autoclave was then put under vacuum (20 10^{-3} mbar) for 30 min to remove any trace of oxygen. The homogenous DMC solution was introduced into the autoclave using a funnel, VDF gas (19.0 g, 2.97 10^{-1} mol) was transferred in the autoclave at low temperature, and the reactor was gradually heated to 73 °C. The reaction was stopped after 18 h. The autoclave was cooled down to room temperature (ca. 20 °C), purged from the residual monomers, and DMC was removed under vacuum. The crude product was dissolved in 30 mL of warm THF (ca. 40 °C), and left under vigorous stirring for 30 minutes. This polymer solution was then precipitated from 400 mL of chilled hexane. The precipitated polymer (white powder) was filtered through a filter funnel and dried under vacuum ($15 \cdot 10^{-3}$ mbar) for two hours at 50°C. The polymerization yield (65%) was determined gravimetrically (mass of dried precipitated polymers / mass of monomer introduced in the pressure reactor).

^{1}H NMR (400 MHz $(CD_3)_2CO$, δ (ppm), Figure S1): 1.09 (d, -CH(C**H$_3$**)(C=O)-, $^{3}J_{HH}$ = 7.1 Hz), 1.31 (t, -S(C=S)O-CH_2-C**H$_3$**, $^{3}J_{HH}$ = 7.1 Hz), 2.13-2.31 (m,-CF_2-C**H$_2$**-C**H$_2$**-CF_2-, VDF-VDF TT reverse addition), 2.66-3.01 (t, -CF_2-C**H$_2$**-CF_2-, VDF-VDF HT regular addition), 3.48–3.57 (s, -(C=O)-O-C**H$_3$**), 3.97 (t, -CF_2-C**H$_2$**-S(C=S)OEt, $^{3}J_{HF}$ = 17.7 Hz), 4.59 (q, (-S(C=S)OC**H$_2$**-CH_3, $^{3}J_{HH}$ = 7.0 Hz), 6.05-6.45 (tt, $^{2}J_{HF}$ = 55 Hz , $^{3}J_{HH}$ = 4.6 Hz -CH_2-CF_2-**H**).

^{19}F NMR (376 MHz $(CD_3)_2CO$, δ (ppm), Figure S2): -115.64 (-CH_2-CF_2-C**F$_2$**-CH_2-CH_2-, VDF-VDF HH reverse addition), -114.29 ($^{2}J_{HF}$ = 55 Hz, -CH_2-C**F$_2$**-H), -113.35 (-CH_2-C**F$_2$**-CF_2-CH_2-CH_2-, HH reverse addition), -113.09 (CH_2-CF_2-**CF$_2$**-CH_2-S-), -112.69 (-CH_2-**CF$_2$**-CF_2-CH_2-S-), -94.79 (-CH_2-CH_2-C**F$_2$**-CH_2-, TT reverse addition), -93.50 (-CH_2-C**F$_2$**-CH_2-CH(CH_3)(C=O)-), -92.12 (-CH_2-C**F$_2$**-CH_2-CF_2H), -91.43 (-CH_2-CH_2-CF_2-CH_2-**CF$_2$**-CH_2-CF_2-, regular VDF-VDF HT addition), -91.00 (-CH_2-C**F$_2$**-CH_2-, regular VDF-VDF HT addition).

The degree of polymerization (DP) and number average molar mass of PVDF were calculated from the ^{1}H NMR spectrum using the following equations:

$$DP = \frac{\int_{2.66}^{3.01} CH_2(HT) + \int_{2.13}^{2.31} CH_2(TT) + \int_{3.89}^{4.06} CH_2(End-group)}{2/3 \times \int_{1.03}^{1.14} CH_3\ (R-CTA_{XA})}$$

$$M_{n,NMR}(R) = M_{n,CTA} + (DP \times M_{n,VDF})$$

Where $M_{n\ CTA}$ = 208.3 g.mol^{-1} and $M_{n\ VDF}$ = 64.04 g.mol^{-1}

According to these equations, DP = 50, and $M_{n,NMR}$ = 3400 g.mol^{-1}

PEGDA$_{136}$ synthesis.

PEG diacrylates were obtained from commercial PEG_{6000} as follows: polyethylene glycol (PEG_{6000}; 7 g; 1.17 mmol; 1 eq.) and acryloyl chloride (0.95 mL; 11.7 mmol; 10 eq.) were

dissolved in dichloromethane (DCM, 48 mL) in a round bottom flask under magnetic stirring at room temperature (25°C). After 10 min, triethylamine (TEA, 0.47 g, 4.68 mmol, 4 eq) was added dropwise The reaction was monitored by ^{1}H NMR. After 60h, the precipitate was filtered off on Celite, and the target polymer was precipitated in cold diethyl ether and then dried under vacuum.

^{1}H NMR (400 MHz, $(CD_3)_2SO$) δ (ppm), Figure S4): 6.43 (d, *J*=17.3 Hz, 2H, -CH=C**H$_2$**), 6.16 (dd, *J*=17.4 Hz and 10.4 Hz, 2H, -C=C**H**-C=O), 5.85 (d, *J*= 10.4 Hz, 2H, -CH=C**H$_2$**), 4.23 (m, 2H, -(C=O)-O-C**H$_2$**-CH_2-O-) 3.4-3.8 (m, -C**H$_2$**-C**H$_2$**-O).

PVDF-b-PEG-b-PVDF triblock synthesis.

$PVDF_{50}$-XA (5.000 g, 1.47 mmol) and $PEGDA_{136}$ (4.410 g, 0.735 mmol) were dissolved in DMF (115 mL). The mixture was degassed with N_2 (10 min). A degassed mixture of hexylamine (0.612 g, 6.05 mmol) and triethylamine (TEA, 2.15 mmol) in DMF was injected into the reaction mixture. N_2 was bubbled for another 10 min. The mixture was stirred 16 h until the reaction was complete and no unreacted acrylate could be detected by ^{1}H NMR. The product was then precipitated twice in cold diethyl ether.

^{1}H NMR (400 MHz $(CD_3)_2SO$, δ (ppm), Figure S5) : 1.15-1,20 -CH(C**H$_3$**)(C=O)-, 2.16-2.38 (m, -CF_2-C**H$_2$**-C**H$_2$**-CF_2-, VDF-VDF TT reverse addition), 2.62-2.71 (m, -S-CH_2-C**H$_2$**(C=O)), 2.71-3.05 (t, -CF_2-C**H$_2$**-CF_2-, VDF-VDF HT regular addition), 3.07-3.14 (m, CF_2-CF_2-C**H$_2$**-S), 3.42-3.60 (m, -(O-(C**H$_2$**-C**H$_2$**)), 3.60-3.69 (s, -(C=O)-O-C**H$_3$**), 3.72-3.81 (m, -C(C=O)-O-CH_2-C**H$_2$**) 4.13-4.23 (-C(C=O)-O-CH_2-C**H$_2$**).

^{19}F NMR (377 MHz, $(CD_3)_2SO$ δ (ppm), Figure S6): -115.16 (-CH_2-CF_2-C**F$_2$**-CH_2-CH_2-), -113.77(-CH_2-C**F$_2$**-CF_2-CH_2-CH_2-), -112.87 (-CH-CF_2-C**F$_2$**-CH_2-S-), -112.25 (-CH_2-C**F$_2$**-CF_2-CH_2-S-), -93.75 (-CH_2-CH_2-C**F$_2$**-CH_2-CF_2-), -92.76 (CH_3-O-(C=O)-(CH_3)C_H-CH_2-C**F$_2$**-), -91.82 (-CH_2-C**F$_2$**-CH_2-CF_2-H), -91.46 (-CH_2-CH_2-CF_2-CH_2-C**F$_2$**-CH_2-CF_2), -91.00 (-CH_2-C**F$_2$**-CH_2-, regular VDF-VDF HT addition).

3.4. Self-assembly

Preparation of the solution.

A 5 % w/w triblock copolymer solution in NMP (60 mg of triblock copolymer in 1.2 mL of solvent) and another solution in THF at 1% w/w (24 mg of triblock copolymer in 2.4 mL of solvent) were prepared in glass vials and heated to 70 °C in the case of NMP and to 60 °C in the case of THF for at least 24h.

Micellization protocol.

To different glass vials placed on a stirring plate and equipped with magnetic bars were added 0.2 mL of triblock solution (5 wt% in NMP or 1 wt% in THF). To each vial a non-solvent for PVDF was added dropwise to reach different solvent/non-solvent ratios (i.e. 0.4 mL for 1:2 ratio; 0.8 mL for 1:4 ratio; 1.2 mL for 1:6 ratio). Only water was used as non-solvent in the case of NMP triblock copolymer solutions.

Nanoprecipitation protocol.

To different glass vials placed on a stirring plate and equipped with magnetic bars was added 1.2 mL of non-solvent. To each vial an adequate triblock solution volume (5 % w/w in NMP or 1 % w/w in THF) was added dropwise to reach different solvent/non-solvent ratios (i.e. 0.6 mL for the 1:2 ratio; 0.3 mL for the 1:4 ratio; 0.15 mL for the 1:6 ratio).

In all micellization and nanoprecipitation samples cloudy solutions were obtained. At the end 18 vials containing micellar solutions were obtained. Three of each protocol in the case of NMP samples and six of each protocol in the case of THF samples (three using water as non-solvent and three using ethanol).

Preparation of AFM samples.

Thin films were prepared from a solution of triblock copolymer micellar solutions in THF/ethanol (or NMP/water). The solution was spin-coated (SPS Spin 150 spin coater) onto a

clean silicon wafer at 1000 rpm for 120 s (or 300 s) with a speed ramp of 100 rpm s^{-1}. The AFM analyses were performed directly on the silicon wafer.

4. Results and discussion

The amphiphilic ABA triblock copolymer was prepared by a one pot aminolysis/thia Michael addition involving a *mono*-functional PVDF-Xanthate (PVDF-XA) and a difunctional PEG acrylate (PEGDA) (Scheme 1).

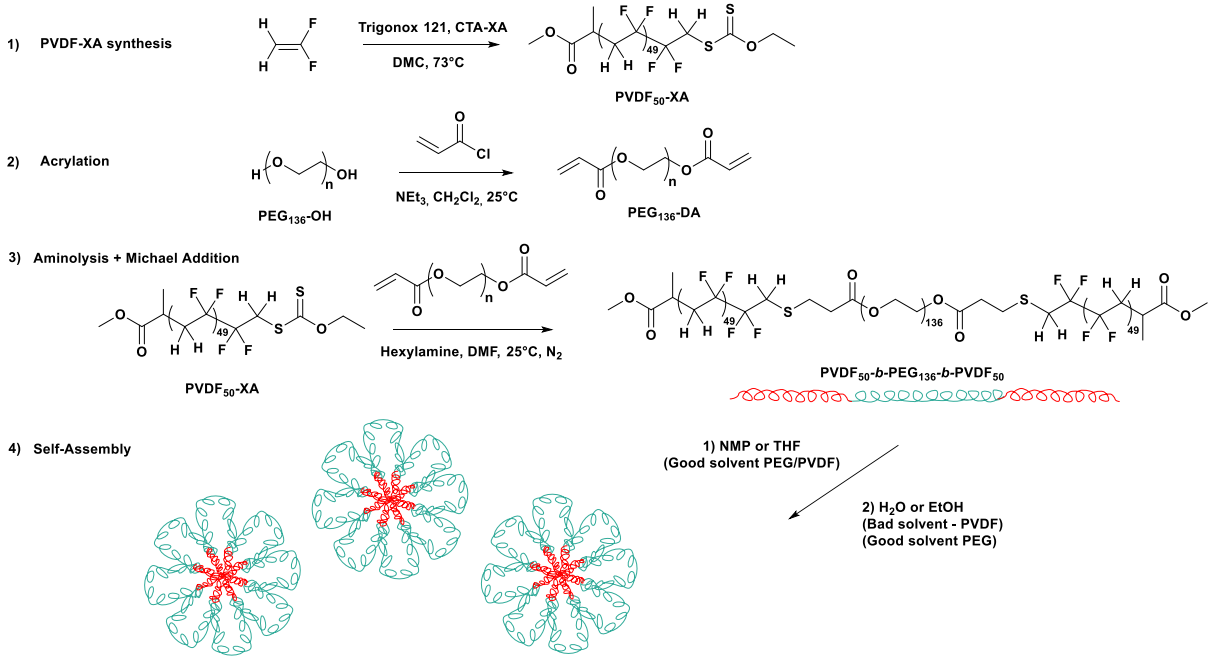

Scheme 1. Synthesis and self-assembly of the amphiphilic PVDF-b-PEG-b-PVDF ABA triblock copolymer. 1) Synthesis of PVDF-XA by RAFT. 2) PEG diacrylate (PEGDA) synthesis in dichloromethane using acryloyl chloride. 3) One-pot synthesis of the triblock copolymer by aminolysis of the xanthate groups and thia-Michael addition of the resulting PVDF-SH to PEGDA. 4) Self-assembly into expected flower-like micelles of the ABA triblock copolymer (nanoprecipitation or micellization).

The $PVDF_{50}$-XA was synthesized by RAFT polymerization following an already established protocol.[41] The PEG diacrylate (PEGDA) was prepared by simple acrylation of a commercial dihydroxylated PEG (Figure S3). The acrylation reaction resulted in quantitative

functionalization of the commercial PEG (Figure S4). Then, the targeted $PVDF_{50}$-*b*-PEG_{136}-*b*-$PVDF_{50}$ ABA triblock copolymer was synthesized in relatively high yield (86 %) by coupling reaction using relative stoichiometric equivalents of PVDF and PEG. The conversion of the coupling reaction was followed by ^{1}H NMR and was evidenced by the disappearance of both signals of the xanthate groups at δ = 1.40-1.46 ppm and δ = 4.67-4.77 ppm (conversion of the xanthate end-groups into thiol via aminolysis), and signals of the acrylate groups at δ = 5.85, 6.16 and 6.43 ppm (thio-Michael addition) (Figure S5). The success of the Thia-Michael addition was also confirmed by ^{19}F NMR spectroscopy with an upflied shift of the fluorine signals of the $–CF_2$ unit directly bonded to the xanthate moiety from δ = -113.09 to δ = -113.77 ppm (Figure S6). The formation of the triblock copolymers was further confirmed by SEC-HPLC. Figure 1 shows the SEC chromatograms of the two homopolymer precursors and of the resulting ABA triblock. These chromatograms confirm the successful coupling reaction with a clear shift of the triblock copolymer trace towards shorter retention time (higher molar masses). However, a small shoulder at lower retention time reveals the presence of small amounts of residual PVDF precursors that were not removed by precipitation. This residual PVDF is likely the non-functional PVDF-H chains (10 mol %) formed by transfer reactions (estimation made from ^{1}H NMR data (Figure 1), PVDF-H signals at 6.05 – 6.45 ppm). Indeed, the starting PVDF was composed of 90 mol % of chains terminated by a head-to-head addition (-$CH_2CF_2CF_2CH_2$-XA) and 10 mol % of chains terminated by an hydrogen (-CF_2H et -CH_3) atom resulting transfer reaction. ^{1}H Diffusion-ordered spectroscopy (DOSY) NMR experiments were also carried out to further characterize the ABA triblock copolymer. These DOSY experiments provide 2D correlation maps showing chemical shifts and diffusion coefficients on the horizontal and vertical axes, respectively. The ^{1}H DOSY map of the $PVDF_{50}$-*b*-PEG_{136}-*b*-$PVDF_{50}$ triblock copolymer (Figure 2. And S7) shows that all ^{1}H NMR signals correlate with a single diffusion coefficient (2.8 10−5 m2 s−1). In comparison DOSY experiments carried out on PVDF-XA and PEGDA provided diffusion coefficients of 9.1 10^{-5} m^2 s^{-1} and 7.5 10^{-5} m^2 s^{-1} respectively.

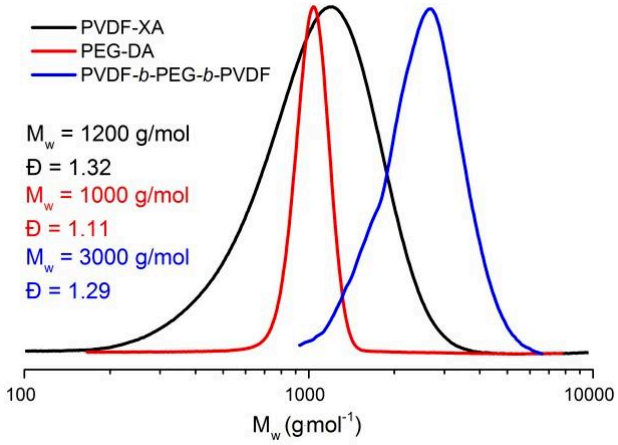

Figure 1. Normalized SEC chromatograms (viscometric detector) of: PVDF-XA (black trace), PEGDA (red trace), PVDF-*b*-PEG-*b*-PVDF (blue trace).

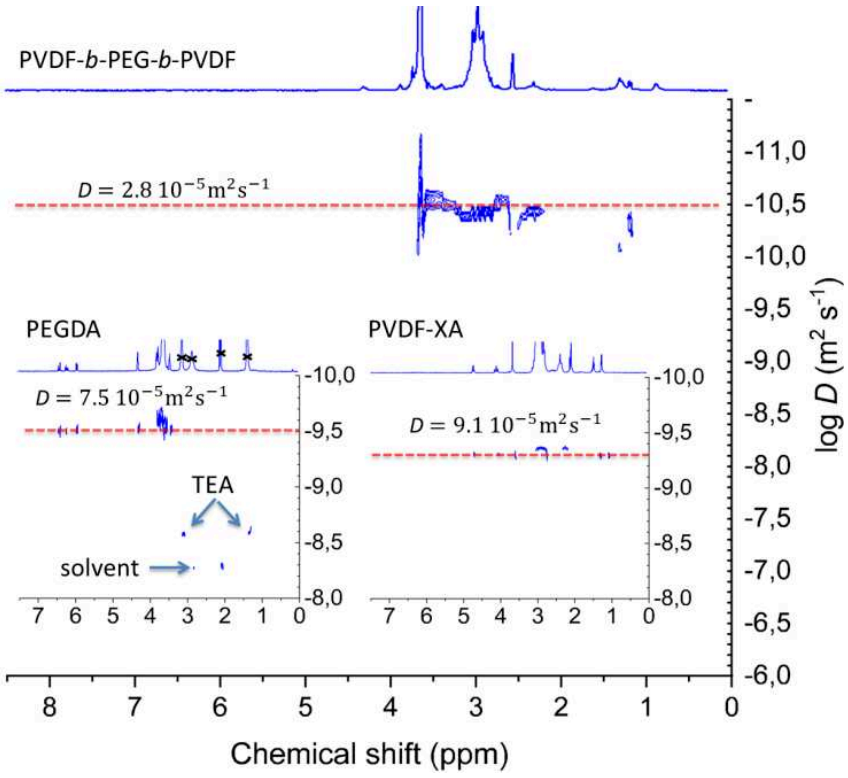

Figure 2. ^{1}H DOSY-NMR spectra of the PVDF-*b*-PEG-*b*-PVDF triblock copolymer (main spectrum), PEGDA (left inset), and PVDF-XA (right inset) recorded in $(CD_3)_2SO$ at 60 °C. D = diffusion coefficient.

These results suggest quantitative coupling reactions without contamination of residual homopolymers. The discrepancy between the SEC and ^{1}H DOSY NMR results are likely due to the higher lower detection limit of ^{1}H DOSY NMR compared to SEC.

Nevertheless these analyses indicate that the protocol used here led to a relatively well defined PVDF-*b*-PEG-*b*-PVDF triblock copolymer (Đ< 1.3).

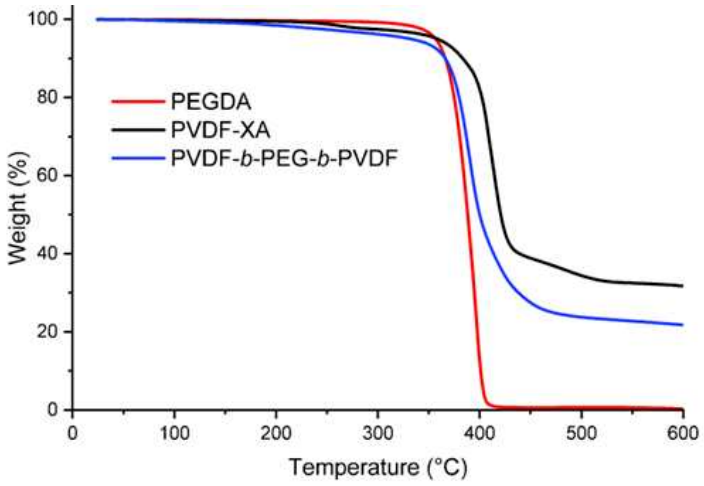

Figure 3. Overlay of the TGA traces the PVDF-xanthate (black trace) and PEG-diacrylate (red trace) precursors, and of the $PVDF_{50}$-*b*-PEG_{136}-*b*-$PVDF_{50}$ triblock copolymer (blue trace).

Thermogravimetric analyses (under air) (Figure 3) revealed that the $PVDF_{50}$-*b*-PEG_{136}-*b*-$PVDF_{50}$ triblock copolymer displayed a thermal behaviour relatively similar to those of its precursors. No significant weight loss was observed before 348 °C ($Td_{5\%}$ of the triblock) close to the degradation temperature of the PEGDA ($Td_{5\%}$ = 360 °C) , while PVDF-XA started to degrade at marginally higher T ($Td_{5\%}$ = 365 °C, $Td_{10\%}$ = 389 °C). Differential scanning calorimetry (DSC) of the $PVDF_{50}$-*b*-PEG_{136}-*b*-$PVDF_{50}$ triblock copolymer revealed the characteristic exothermic and endothermic peaks corresponding to the crystallization and melting transitions at 40.3 and 56 °C for PEG and at 139.5 and 178.3 °C for PVDF, respectively (Figure S13, and Figure 4). These values are in good agreement with those obtained for PEGDA (T_c = 42 °C and T_m = 58 °C) (Figure S12) and PVDF-XA homopolymers (T_c = 140 °C and T_m = 168.7 °C) (Figure. S11). In addition, the DSC thermogram of the triblock

(Figure 4 and figure S13) displayed two distinct glass transition temperatures corresponding to VDF (-34 °C) and PEG (-10 °C), confirming the bulk incompatibility of these two polymers. The DSC thermograms were also used to quantify the degree of crystallinity of the PVDF (47.1%) and of the PEG (53.8%) in the triblock copolymer (See S14 for details on these calculations).

The self-assembly in solution of the new PVDF-based amphiphilic triblock copolymer was then studied.

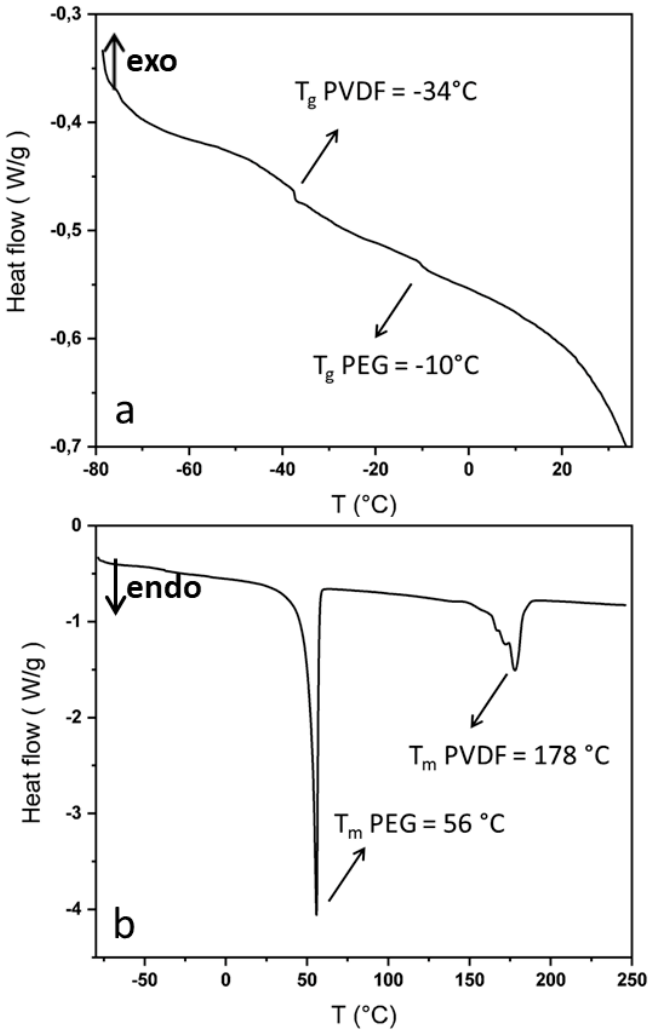

Figure 4. DSC Thermograms of $PVDF_{50}$-*b*-PEG_{136}-*b*-$PVDF_{50}$ triblock copolymer. a) Area highlighting the glass transitions of PVDF and PEG. b) Area presenting the two endothermic signals corresponding to the melting points of PEG and PVDF.

Among the various methods used to promote the self-assembly of amphiphilic block copolymer in solution, we selected the two most common techniques used so far: (i) Direct dissolution of the polymer in a selective solvent for one of the blocks, and (ii) Dissolution of the block copolymer in a good solvent for both blocks, followed by slow addition of a selective solvent for one of the blocks.[53]

The first method, often called nanoprecipitation, is an easy and direct way to provoke self-assembly and is well-suited for block copolymers with relatively low molar masses and relatively short insoluble block.[53] Given the high hydrophobicity and crystallinity of PVDF, the second method (called here micellization), although more time-consuming, is probably more suitable to the present PVDF-*b*-PEG-*b*-PVDF triblock copolymer. Indeed, under nanoprecipitation conditions, self-assembly occurs very fast and generally leads to frozen morphologies. A slower self-assembling process such as the micellization method, is more likely to deliver thermodynamically more stable self-assembled structures. Note that due to the non-ergodicity of amphiphilic block copolymer systems, both methods likely lead to kinetically trapped structures.[54]

Two solutions of the triblock copolymers were prepared: One solution in NMP at 5 wt %, and one solution in THF at 1 wt %. Complete dissolution of the triblock copolymers was achieved only after heating for prolonged time (24 h at 60 °C for THF and at 70 °C for NMP). The molecular dissolution of the triblock was confirmed by DLS. Only 1 wt% solution could be prepared in THF due to the poor solubility of PVDF in THF. The solutions in NMP at 5 wt % and in THF at 1 wt % were then used to investigate the self-assembly of the triblock copolymer via nanoprecipitation and micellization.

Transmission electron microscopy and atomic force microscopy revealed that the nanoprecipitation protocol led to the formation of small roughly spherical aggregates for the 1:6 NMP: water systems (Figure 5, and S15). These small aggregates with size ranging from 20 to 75 nm displayed relatively rough surfaces and were not perfectly spherical. This is likely caused by the high crystallinity of PVDF and the fast solvent de-mixing times, not leading the BCP to reach kinetically stable morphologies.[44]

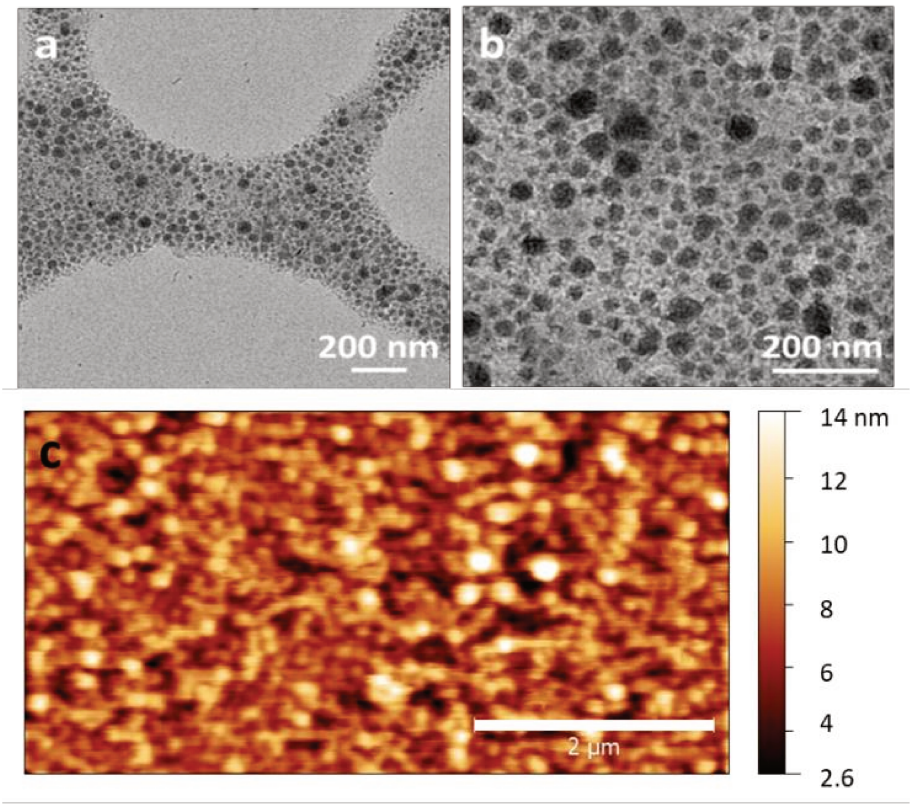

Figure 5. a) and b) TEM images of $PVDF_{50}$-*b*-PEG_{136}-*b*-$PVDF_{50}$ aggregates obtained from a 5 wt% solution in NMP by nanoprecipitation (NMP:water (1:6)). c) AFM topographic image of these aggregates deposited by spin-coating on a silicon wafer.

When micellar solutions at 1:2 and 1:4 NMP: water ratios were analysed by TEM, only large micrometric aggregates were observed (Figure S15). The concentration of non-solvent was probably not enough at these stages, and the observed non-defined aggregates are due to non-self-assembled BCP.

In the case of the THF: water solvent: non-solvent system, both self-assembly protocols produced vesicles of around 300 nm (Figure 6a, 6b and S15). Higher THF: water ratios led to larger aggregates (Figure S15). As above, better defined particles were obtained at lower solvent: non-solvent ratios. In the nanoprecipitation experiments, higher solvent/ non solvent ratios, likely lead to instability of the vesicles and thus, big aggregates of non-assembled polymer are also observed.

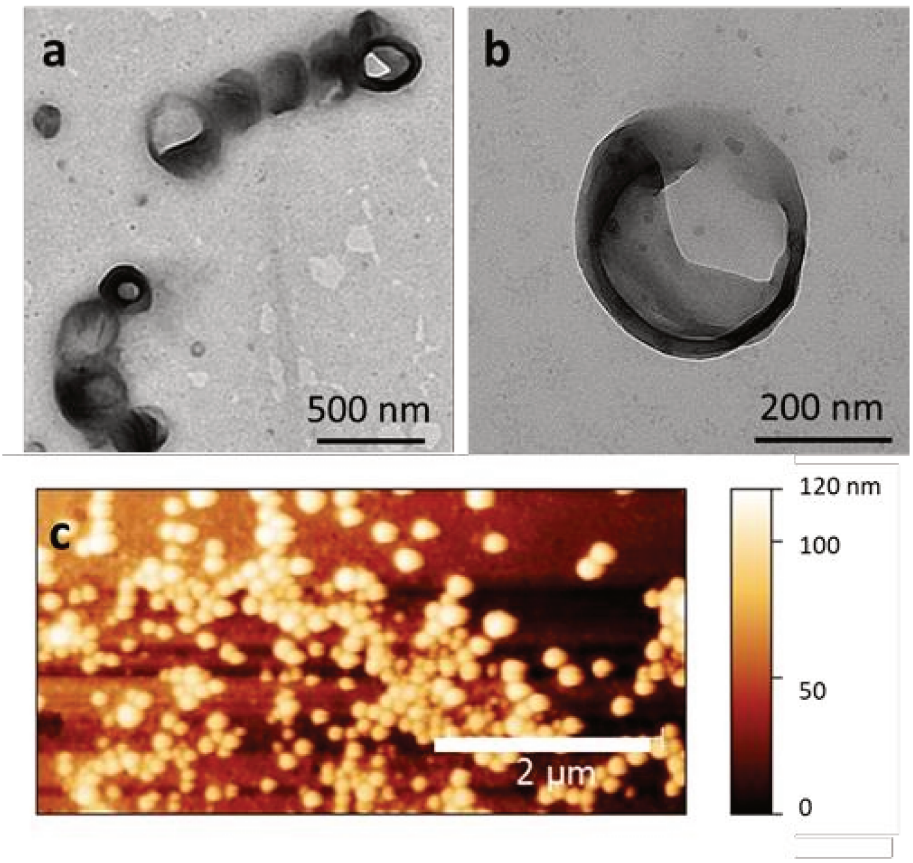

Figure 6. TEM images of $PVDF_{50}$-*b*-PEG_{136}-*b*-$PVDF_{50}$ aggregates obtained from: a) and b) 1 wt% solution in THF by micellization (THF: ethanol (1:6)). c) AFM topographic image of these aggregates deposited by spin-coating on a silicon wafer.

In contrast, nanoprecipitation of the THF solution in ethanol using 1:6 (Figure 7b, and S15) lead to the formation of crystalline structures with ovoidal shape and using 1:4 THF: ethanol ratio a mixture of ovoidal, crystalline shard like structures and spheres of various size were observed (Figure 7a, 7c), and S15). Ovoidal crystalline structures have already been reported in our group from PVAc-*b*-PVDF diblock copolymers.[45] In the latter case the corona forming block was not crystalline so the objects observed by TEM should not differ from the ones in solution (i. e. the corona-forming block does not crystallize when the solvent evaporates). Similar structures have been also described by Wang Y.-Z. et al. for self- assembled PEG-*b*-PPDO, by Wang J. et al. in the case of a (MPEG)(PCL)(PPE) 3-miktoarm star terpolymer, by Chen Y. et al. for PCL-*b*-PDMAEMA and PCL-*b*-PAA block copolymers and by Rizis G. for PEG-

b-PCL. These structures are thought to be formed by crystallisation-driven self-assembly (CDSA).[55–59]

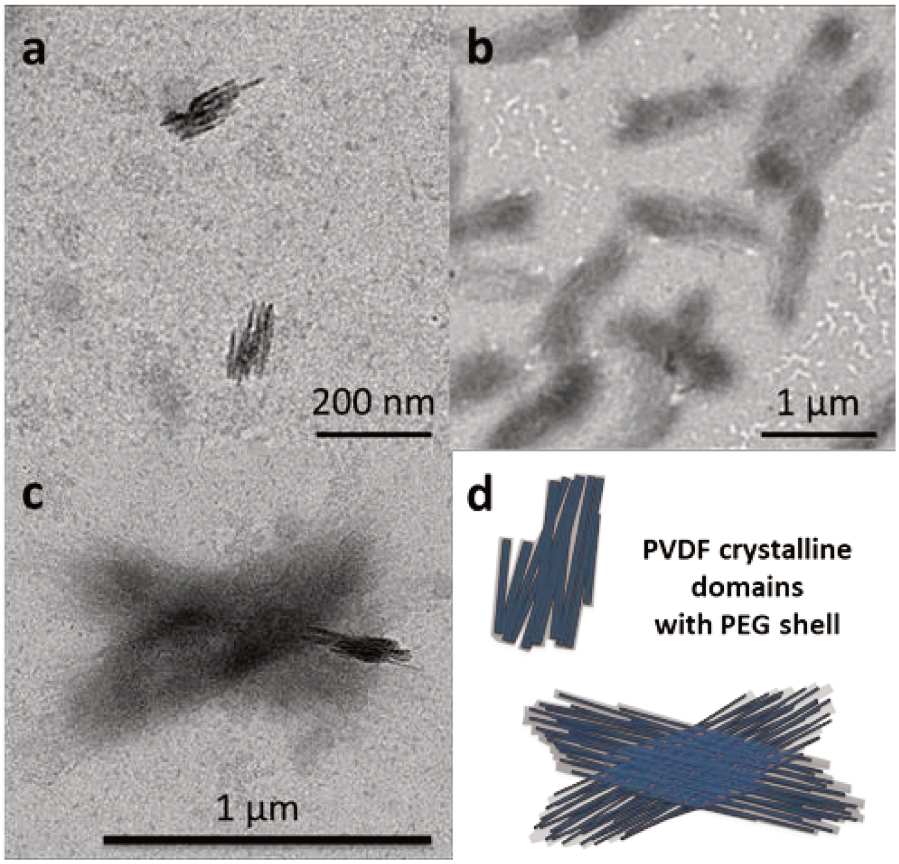

Figure 7. TEM images of $PVDF_{50}$-*b*-PEG_{138}-*b*-$PVDF_{50}$ crystalline nanostructures obtained by nanoprecipitation in ethanol of a 1 wt% THF solution in THF; a) and c): THF: ethanol = 1:4; b): THF: ethanol = 1:6. d) schematic representation of the objects observed in a) and c).

The crystallinity of those structures was highlighted by the analysis of the SAED patterns recorded during TEM analysis and compared to the XRD diffraction pattern (Figure 8). From XRD measurement, the two diffraction peaks observed at 2θ = 19.8 and 26.5° are found to be characteristic of the PVDF phase. In addition, the specific peak at 26.5° unambiguously evidences the α-crystal phase (no existence of the β- and γ-crystal phases).[60] The XRD pattern also shows two peak at 2 θ = 19.2 and 23.4° attributed to the crystalline structure of the PEG (see S17).[61]

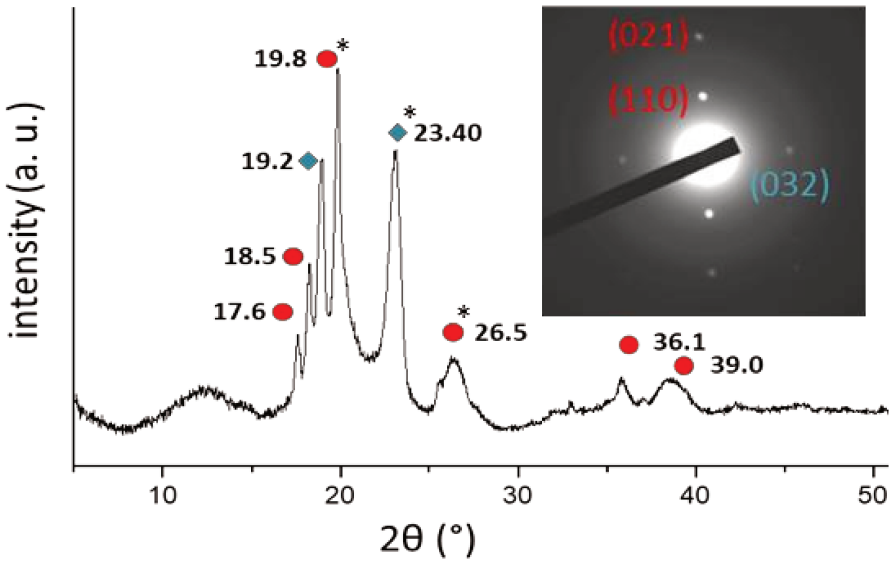

Figure 8. XRD pattern of $PVDF_{50}$-*b*-PEG_{136}-*b*-$PVDF_{50}$ recorded at room temperature. Red dots and blue rhombus are PVDF and PEG characteristic diffractions. The inset is the SAED pattern of the objects observed in Figure 7b and 7c obtained during TEM analysis (* correspond to the Bragg spots observed). Note: Attempts to record SAED patterns on the other self-assembled morphologies presented in this paper failed due to the rapid amorphisation of the structures under the electron beam.

Moreover, the symmetrical Bragg spots of $(110)_{PVDF}$ and $(021)_{PVDF}$ can be clearly observed from the SAED pattern, indicating that the ovoidal structures may be considered to be single crystals of PVDF (the entire object analysed was inside the selected area). In addition, the symmetrical spots of $(032)_{PEG}$ indicate that the PEG is crystalline too. According to previous reports preparation of single-crystals is complicated and time-consuming (self-seeding method) and it has never been reported for PVDF-based block copolymers.[59]

5. Conclusions

An ABA PVDF-*b*-PEG-*b*-PVDF amphiphilic triblock copolymer was synthesized using an efficient one-pot aminolysis / thia-Michael addition of a PVDF prepared by RAFT and PEG

diacrylate. This novel PVDF-based ABA triblock copolymer was thoroughly characterised by ^{1}H, ^{1}H DOSY and ^{19}F-NMR spectroscopies, GPC as well as TGA, DSC and XRD. These characterizations proved the coupling strategy efficient and revealed a relatively well-defined (low Đ) triblock copolymer. As expected, the triblock copolymer had thermal resistance close to that of PEG and inferior to that of PVDF and both blocks present the inherent crystallinity of these materials. The self-assembly of this amphiphilic triblock copolymer was performed using nanoprecipitation and micellization protocols using NMP or THF as good solvents and water or ethanol as the block selective solvents. In most cases, the self-assembly experiments led to roughly spherical aggregates with size ranging from 20 to 75 nm and vesicles up to 300 nm. However, when THF solutions were used under nanoprecipitation protocols in ethanol, micrometric crystalline oval morphologies were obtained. The crystallinity of both α-PVDF and PEG in those structures was confirmed by SAED patterns recorded during TEM analysis and identified by XRD measurement. These original triblock copolymers and self-assembled morphologies may offer new opportunities to design electroactive structures at the nano- and micrometric scales.

Conflicts of interest

There are no conflicts to declare.

Acknowledgements

The authors thank Arkema for providing VDF, and the Institut Carnot Chimie Balard Cirimat, the LabEx CheMISyst (ANR-10-LABX-05-01), IEM and ICGM for funding the PhD of EF and the ANR NanoPIC (ANR-16-CE08-0025).

6. References

1. Genix, A.-C., Baeza, G. P. & Oberdisse, J. Recent advances in structural and dynamical propertiesof simplified industrial nanocomposites. *Eur. Polym. J.* **85**, 605–619 (2016).

2. Herzberger, J. *et al.* Polymerization of Ethylene Oxide, Propylene Oxide, and Other Alkylene Oxides: Synthesis, Novel Polymer Architectures, and Bioconjugation. *Chem. Rev.* **116**, 2170–2243 (2016).

3. Abetz, V., Polymerforschung, I. & Gmbh, G. G. Phase Behaviour and Morphologies of Block Copolymers. *Adv. Polym. Sci.* **189**, 125–212 (2005).

4. Mai, S. *et al.* Microphase-Separation Behavior of Triblock Copolymer Melts . Comparison with Diblock Copolymer Melts. *Macromolecules* **33**, 5124–5130 (2000).

5. Matsen, M. W. Effect of Architecture on the Phase Behavior of AB-Type Block Copolymer Melts. *Macromolecules* 2161–2165 (2012). doi:10.1021/ma202782s

6. Mayes, A. M. *et al.* Microphase separation in multiblock copolymer melts Microphase separation in multiblock copolymer melts. *J. Chem. Phys.* **91**, 7228–7235 (1989).

7. Lopez, G. *et al.* An amphiphilic PEG-b-PFPE-b-PEG triblock copolymer: synthesis by CuAAC click chemistry and self-assembly in water. *Polym. Chem.* **7**, 402–409 (2016).

8. Ding, A., Lu, G., Guo, H. & Huang, X. ATRP synthesis of polyallene-based amphiphilic triblock copolymer. *Polym. Chem.* **8**, 6997–7008 (2017).

9. Nehache, S. *et al.* Self-assembly of PS-PNaSS-PS triblock copolymers from solution to the solid state. *Polym. Chem.* **8**, 3357–3363 (2017).

10. He, P., Li, X., Deng, M. & Liang, H. Complex micelles from the self-assembly of coil-rod-coil amphiphilic triblock copolymers in selective solvents. *Soft Matter* **6**, 1539–1546 (2010).

11. Riess, G. Micellization of block copolymers. *Prog. Polym. Sci.* **28**, 1107–1170 (2003).

12. Zinn, T., Willner, L., Knudsen, K. D. & Lund, R. Self-Assembly of Mixtures of Telechelic and Monofunctional Amphiphilic Polymers in Water: From Clusters to Flowerlike Micelles. *Macromolecules* **50**, 7321–7332 (2017).

13. Jain, S. & Bates, F. S. Consequences of Nonergodicity in Aqueous Binary PEO-PB Micellar Dispersions. *Macromolecules* **37**, 1511–1523 (2004).

14. Bhargava, P. *et al.* Self-assembled polystyrene-block-poly(ethylene oxide) micelle morphologies in solution. *Macromolecules* **39**, 4880–4888 (2006).

15. Annable, T., Buscall, R., Ettelaie, R. & Whittlestone, D. The rheology of solutions of associating polymers: Comparison of experimental behavior with transient network

theory. *J. Rheol.* **37**, 695–726 (1993).

16. Villar-Alvarez, E. *et al.* Reverse poly(butylene oxide)–poly(ethylene oxide)–poly(butylene oxide) block copolymers with lengthy hydrophilic blocks as efficient single and dual drug-loaded nanocarriers with synergistic toxic effects on cancer cells. *RSC Adv.* **5**, 52105–52120 (2015).

17. Cambon, A. *et al.* Micellar self-assembly, bridging and gelling behaviour of two reverse triblock poly(butylene oxide)–poly(ethylene oxide)–poly(butylene oxide) copolymers with lengthy hydrophilic blocks. *RSC Adv.* **4**, 60484–60496 (2014).

18. Park, I. *et al.* Effect of Block Copolymer Chain Architecture on Chromatographic Retention. *Macromolecules* **36**, 8539–8543 (2003).

19. Keddie, D. J. A guide to the synthesis of block copolymers using reversible-addition fragmentation chain transfer (RAFT) polymerization. *Chem. Soc. Rev.* **43**, 496–505 (2014).

20. Jennings, J. *et al.* Advantages of block copolymer synthesis by RAFT-controlled dispersion polymerization in supercritical carbon dioxide. *Macromolecules* **46**, 6843–6851 (2013).

21. Matyjaszewski, K. Atom Transfer Radical Polymerization (ATRP): Current status and future perspectives. *Macromolecules* **45**, 4015–4039 (2012).

22. Tsarevsky, N. V., McCarthy, P., Jakubowski, W., Spanswick, J. & Matyjaszewski, K. Atom transfer radical polymerization (ATRP) as a tool for the synthesis of well-defined functional polymeric materials. *Tech. Proc. 2008 NSTI Nanotechnol. Conf. Trade Show, NSTI-Nanotech, Nanotechnol. 2008* **2**, 665–668 (2008).

23. Peng, C.-H., Yang, T.-Y., Zhao, Y. & Fu, X. Reversible deactivation radical polymerization mediated by cobalt complexes: recent progress and perspectives. *Org. Biomol. Chem.* **12**, 8580–8587 (2014).

24. Mandal, P., Choudhury, S. & Singha, N. K. Acrylic ABA triblock copolymer bearing pendant reactive bicycloalkenyl functionality via ATRP and tuning its properties using thiol-ene chemistry. *Polym. (United Kingdom)* **55**, 5576–5583 (2014).

25. Xue, Z., Wang, Z., He, D., Zhou, X. & Xie, X. Synthesis of poly(n-butyl acrylate) homopolymer and poly(styrene-b-n-butyl acrylate-b-styrene) triblock copolymer via AGET emulsion ATRP using a cationic surfactant. *J. Polym. Sci. Part A Polym. Chem.* **54**, 611–620 (2016).

26. Shipp, D. A., Lou, Q., Linhardt, J. G. & Jay, F. K. Poly (N -vinylpyrrolidone)–Polydimethylsiloxane Amphiphilic ABA Triblock Copolymers. *Polym. Chem.* **55**, 3387–3394 (2017).

27. Riga, B. A. *et al.* Synthesis of cobalt(II)-α-diimines complexes and their activity as

mediators in organometallic mediated radical polymerization of vinyl acetate. *Inorganica Chim. Acta* **471**, 620–629 (2018).

28. Demarteau, J. *et al.* Controlled Synthesis of Fluorinated Copolymers via Cobalt-Mediated Radical Copolymerization of Perfluorohexylethylene and Vinyl Acetate. *Macromolecules* **50**, 3750–3760 (2017).

29. Kermagoret, A. *et al.* Cobalt-Mediated Radical Polymerization of Vinyl Acetate and Acrylonitrile in Supercritical Carbon Dioxide. *Macromol. Rapid Commun.* **37**, 539–544 (2016).

30. Fuhrer, R., Herrmann, I. K., Athanassiou, E. K., Grass, R. N. & Stark, W. J. Immobilized β-cyclodextrin on surface-modified carbon-coated cobalt nanomagnets: reversible organic contaminant adsorption and enrichment from water. *Langmuir* **27**, 1924–9 (2011).

31. Ameduri, B. M. *et al.* Organometallic Mediated Radical Polymerization of Vinylidene Fluoride. *Angew. Chemie Int. Ed.* **57**, 2934–2937 (2018).

32. Li, Y. *et al.* Stretching-Induced Relaxor Ferroelectric Behavior in a Poly(vinylidene fluoride-co-trifluoroethylene-co-hexafluoropropylene) Random Terpolymer. *Macromolecules* **50**, 7646–7656 (2017).

33. Soulestin, T. *et al.* Ferroelectric fluorinated copolymers with improved adhesion properties. *Polym. Chem.* **8**, 1017–1027 (2017).

34. Soulestin, T., Ladmiral, V., Domingues, F., Santos, D. & Améduri, B. Progress in Polymer Science Vinylidene fluoride- and trifluoroethylene-containing fluorinated electroactive copolymers . How does chemistry impact properties ? *Prog. Polym. Sci.* **72**, 16–60 (2017).

35. Soulestin, T., Ladmiral, V., Domingues, F., Santos, D. & Améduri, B. Progress in Polymer Science Vinylidene fluoride- and trifluoroethylene-containing fluorinated electroactive copolymers . How does chemistry impact properties ? *Prog. Polym. Sci.* **72**, 16–60 (2017).

36. Guerre, M. *et al.* Limits of Vinylidene Fluoride RAFT Polymerization. *Macromolecules* **49**, 5386–5396 (2016).

37. Guerre, Marc; Wahidur Rahaman, S. M.; Améduri, Bruno; Poli, R. & Ladmiral, V. RAFT synthesis of well-defined PVDF-b-PVAc block copolymers. *Polym. Chem.* **7**, 6918–6933 (2016).

38. Guerre, M. *et al.* Combination of Cationic and Radical RAFT Polymerizations: A Versatile Route to Well-Defined Poly(ethyl vinyl ether)-block-poly(vinylidene fluoride) Block Copolymers. *ACS Macro Lett.* **6**, 393–398 (2017).

39. Wu, Y. *et al.* Self-assembly of poly(vinylidene fluoride)–polystyrene block copolymers

in solution: Effects of the length of polystyrene block and solvent compositions Effects of the length of polystyrene block and solvent compositions. *J. Saudi Chem. Soc.* **21**, 713–719 (2017).

40. Patil, Y. *et al.* A Novel Poly(vinylidene fluoride)-Based 4-Miktoarm Star Terpolymer: Synthesis and Self-Assembly. *Mol. Pharm.* **15**, 3005–3009 (2018).

41. Guerre, M. *et al.* Deeper Insight into the MADIX Polymerization of Vinylidene Fluoride. *Macromolecules* **48**, 7810–7822 (2015).

42. Guerre, M., Rahaman, M, W., Ameduri, B., Poli, R. & Ladmiral, V. RAFT synthesis of well-defined PVDF-b-PVAc block copolymers. *Polym. Chem.* **7**, 6918–6933 (2016).

43. Guerre, M., Schmidt, J., Talmon, Y., Améduri, B. & Ladmiral, V. An amphiphilic poly(vinylidene fluoride)-b-poly(vinyl alcohol) block copolymer: synthesis and self-assembly in water. *Polym. Chem.* **8**, 1125–1128 (2017).

44. Guerre, M., Semsarilar, M., Totée, C. & Silly, G. Polymer Chemistry copolymers prepared by CuAAC click coupling †. *Polym. Chem.* **8**, 5203–5211 (2017).

45. Guerre, M., Semsarilar, M., Godiard, F., Améduri, B. & Ladmiral, V. Polymerization-induced self-assembly of PVAc-b-PVDF block copolymers via RAFT dispersion polymerization of vinylidene fluoride in dimethyl carbonate. *Polym. Chem.* **8**, 1477–1487 (2017).

46. Li, L., Li, J. & Zheng, S. Poly (vinylidene fl uoride) - block -poly (N -vinylpyrrolidone) diblock copolymers : Synthesis via sequential RAFT / MADIX polymerization and self-assembly behavior. *Polymer.* **142**, 61–71 (2018).

47. Sommer, M. *et al.* Synthesis, Puri fi cation, and Characterization of Well-De fi ned All-Conjugated Diblock Copolymers PF8TBT- b -P3HT. *Macromolecules* 4142–4151 (2012).

48. Ladmiral, V., Semsarilar, M., Canton, I. & Armes, S. P. Polymerization-Induced Self-Assembly of Galactose-Functionalized Biocompatible Diblock Copolymers for Intracellular Delivery. *J. Am. Chem. Soc.* **135**, 13574–13581 (2013).

49. Ladmiral, V., Charlot, A., Semsarilar, M. & Armes, S. P. Synthesis and characterization of poly(amino acid methacrylate)-stabilized diblock copolymer nano-objects. *Polym. Chem.* **6**, 1805–1816 (2015).

50. Guerre, M., Ameduri, B. & Ladmiral, V. One-pot synthesis of poly(vinylidene fluoride) methacrylate macromonomers via thia-Michael addition. *Polym. Chem.* **7**, 441–450 (2016).

51. Mckee, J. R., Ladmiral, V., Niskanen, J., Tenhu, H. & Armes, S. P. Synthesis of Sterically-Stabilized Polystyrene Latexes Using Well-Defined Thermoresponsive Poly (N -isopropylacrylamide) Macromonomers. *Macromolecules* **44**, 7692–7703 (2011).

52. Liu, X. *et al.* Enhanced Solubility of Polyvinyl Esters in scCO 2 by Means of Vinyl Tri fl uorobutyrate Monomer. *ACS Macro Lett.* **4**, 89–93 (2015).

53. Karayianni, M. & Pispas, S. *Self-Assembly of Amphiphilic Block Copolymers in Selective Solvents*. (2016).

54. Hayward, R. C. & Pochan, D. J. Tailored Assemblies of Block Copolymers in Solution : It Is All about the Process. *Macromolecules* **43**, 3577–3584 (2010).

55. Wang, H. *et al.* Temperature dependent morphological evolution and the formation mechanism of anisotropic nano-aggregates from a crystalline-coil block copolymer of poly(p-dioxanone) and poly(ethylene glycol). *Soft Matter* **9**, 8712–8722 (2013).

56. Yuan, Y. & Wang, J. Colloids and Surfaces B : Biointerfaces Temperature-induced morphological change of ABC 3-miktoarm star terpolymer assemblies in aqueous solution. *Colloids Surfaces B Biointerfaces* **85**, 81–85 (2011).

57. Wang, J., Zhu, W., Peng, B. & Chen, Y. A facile way to prepare crystalline platelets of block copolymers by. *Polymer (Guildf).* **54**, 6760–6767 (2013).

58. Wang, J., Lu, Y. & Chen, Y. Fabrication of 2D surface-functional polymer platelets via crystallization- driven self-assembly of poly (ε -caprolactone) -contained block copolymers. *Polymer (Guildf).* **160**, 196–203 (2019).

59. Rizis, G., Van De Ven, T. G. M. & Eisenberg, A. “Raft” Formation By Two-Dimensional Self-Assembly of Block Copolymer Rod Micelles in Aqueous Solution. *Angew. Chemie - Int. Ed.* **53**, 9000–9003 (2014).

60. Martins, P., Lopes, A. C. & Lanceros-Mendez, S. Electroactive phases of poly(vinylidene fluoride): Determination, processing and applications. *Prog. Polym. Sci.* **39**, 683–706 (2014).

61. Mahmood, W. A. K., Azarian, M. H., Wan Fathilah, W. F. bt & Kwok, E. Nanoencapsulation of montmorillonite clay within poly(ethylene glycol) nanobeads by electrospraying. *J. Appl. Polym. Sci.* **134**, 1–9 (2017).

7. Supporting information

Figure S1. PVDF-XA homopolymer ^{1}H NMR (400 MHz $(CD_3)_2CO$).

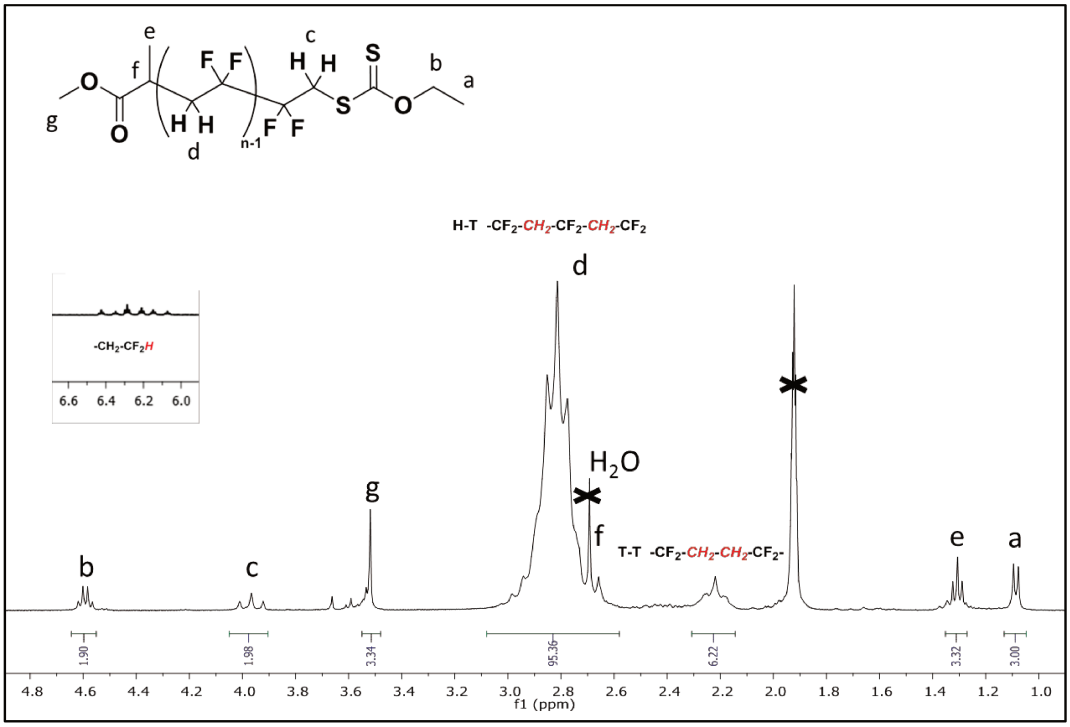

Figure S2. PVDF-XA homopolymer ^{19}F NMR (376 MHz, $(CD_3)_2CO$).

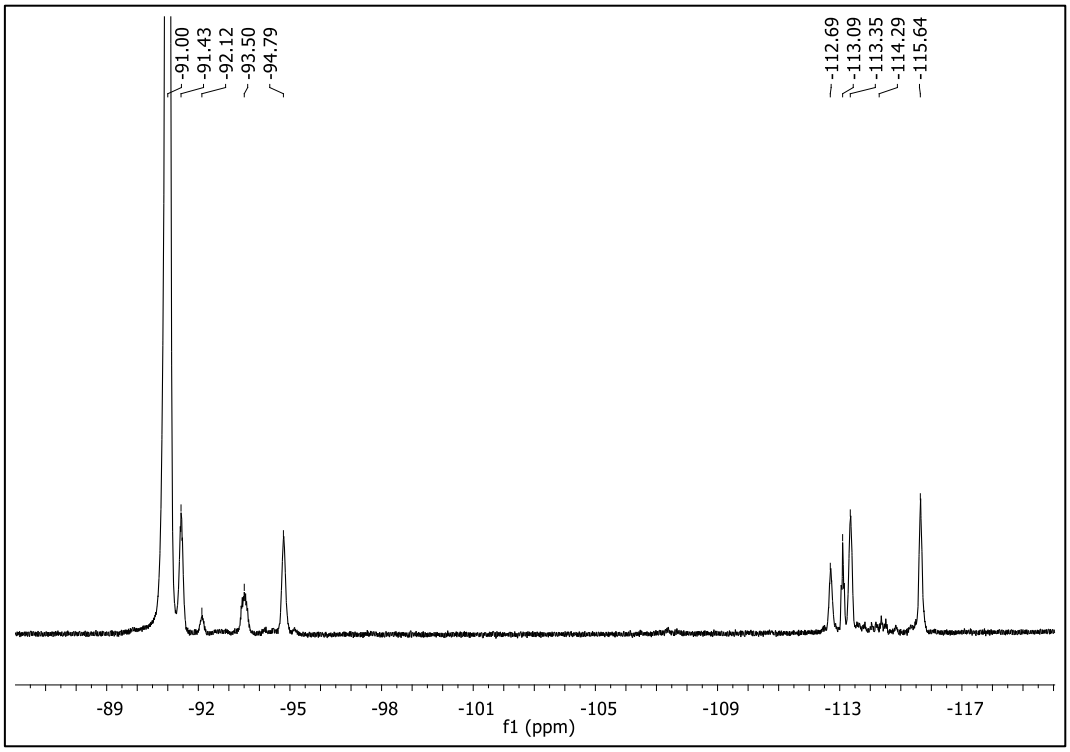

Figure S3. PEG_{6000} commercial polymer ^{1}H NMR (400 MHz, $CDCl_3$).

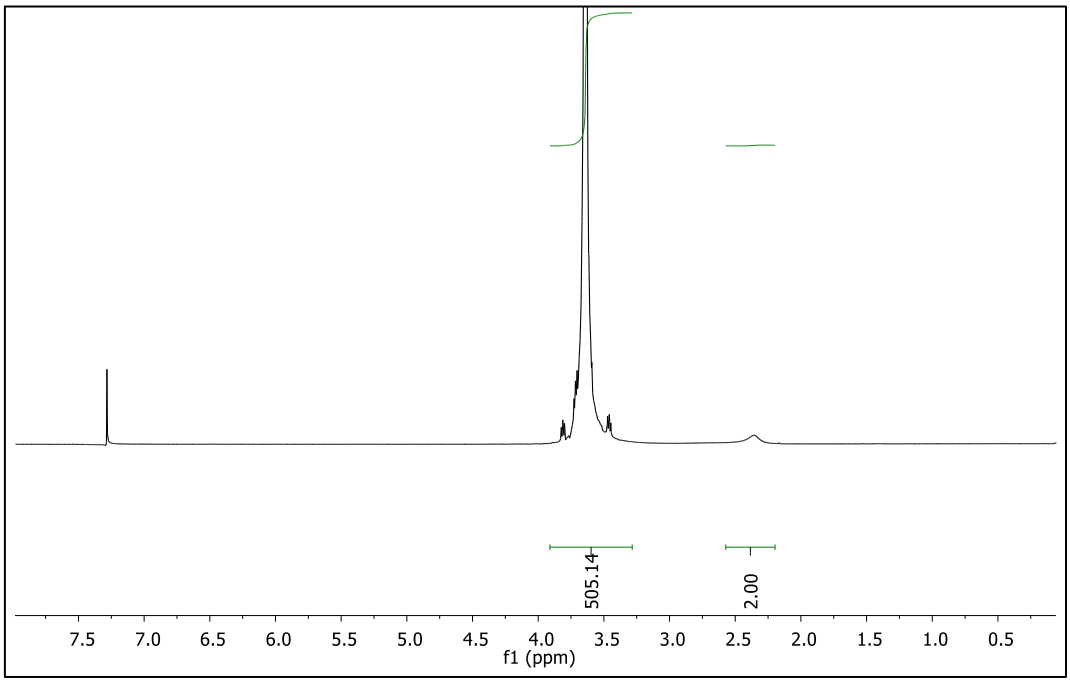

Figure S4. PEG diacrylate homopolymer ^{1}H NMR (400 MHz, $(CD_3)_2SO$).

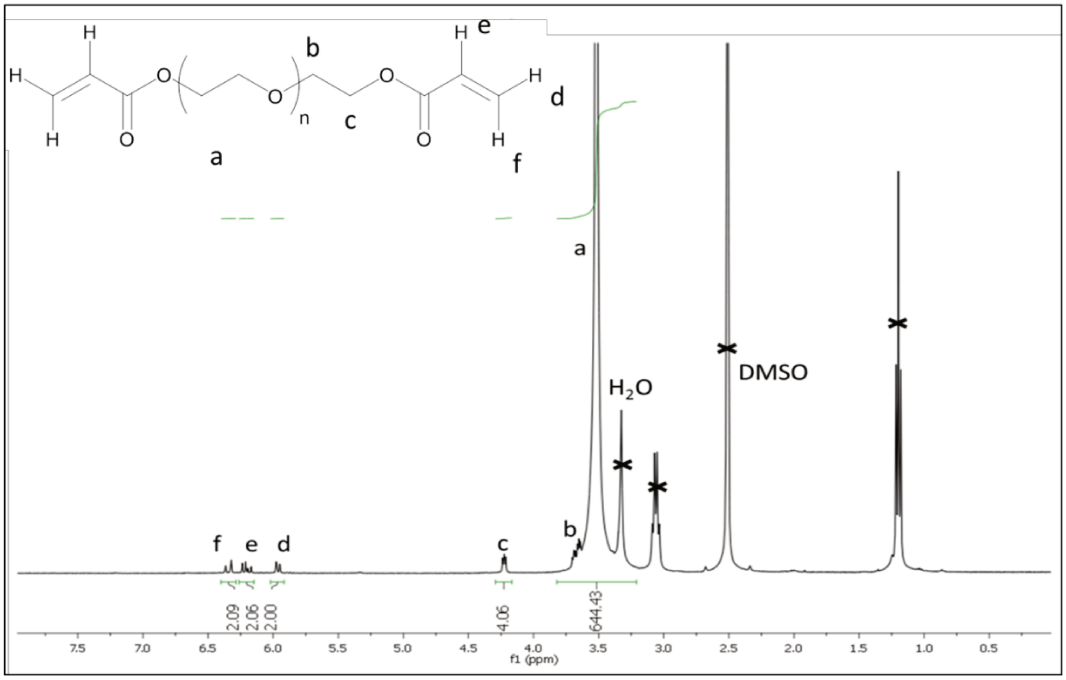

Note: **the peaks at 1.20 and 3.07 ppm are assigned to residual triethylammonium chloride.**

Figure S5. PVDF-*b*-PEG-*b*-PVDF ^{1}H NMR (400 MHz, $(CD_3)_2SO$), recorded at 60 °C).

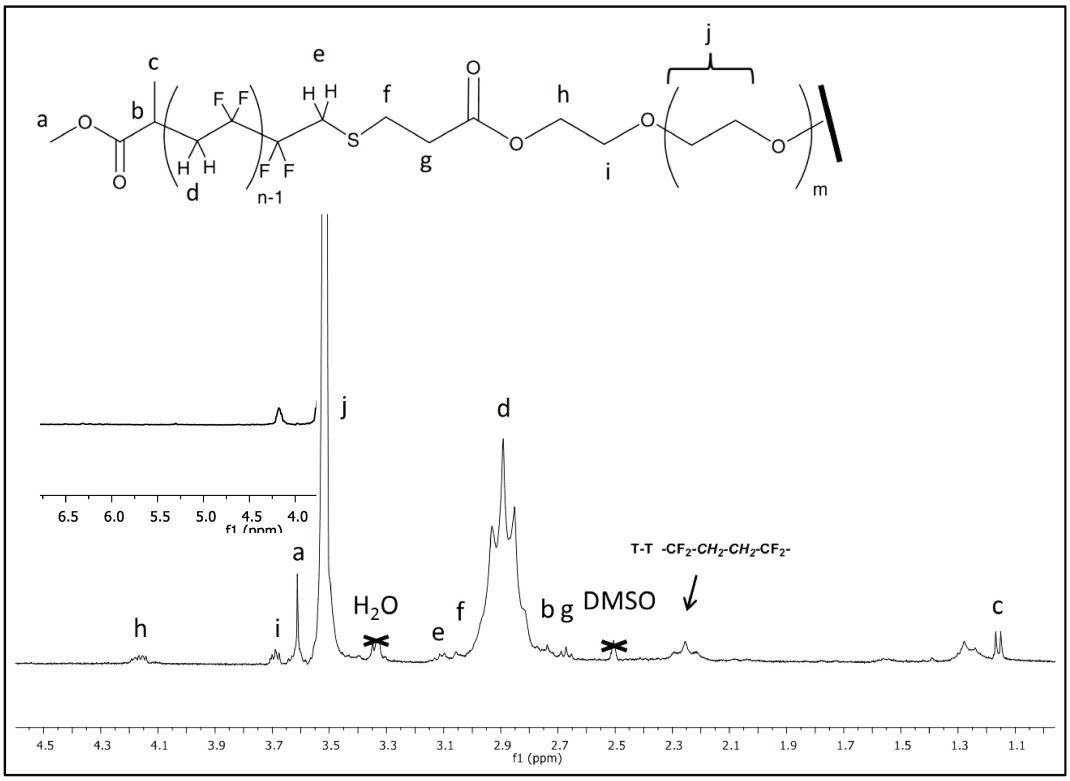

Figure S6. PVDF-*b*-PEG-*b*-PVDF ^{19}F NMR (376 MHz, $(CD_3)_2SO$).

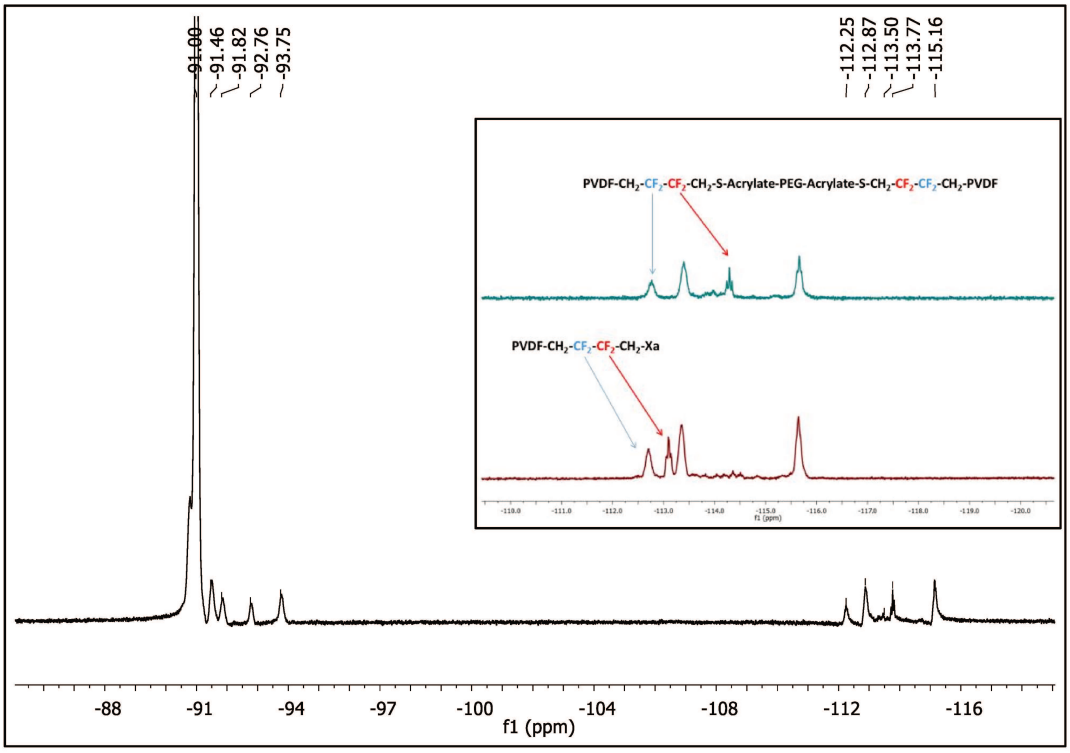

Figure S7. ^{1}H DOSY-NMR experiments recorded in $(CD_3)_2SO$) at 60 °C of PVDF-XA homopolymer.

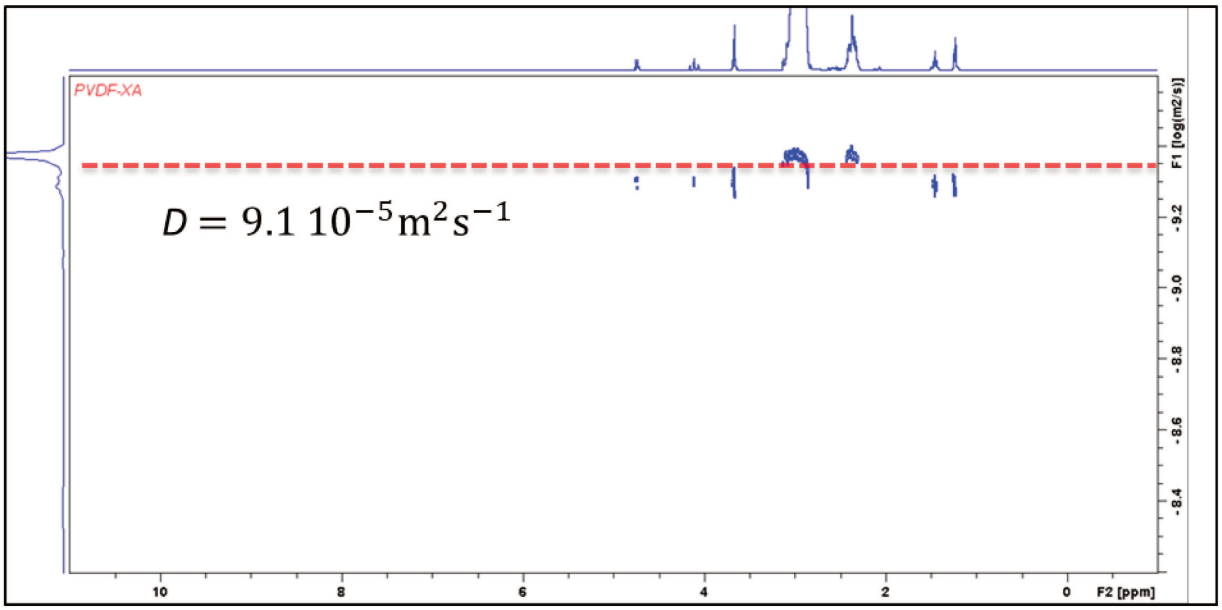

Figure S8. ^{1}H DOSY-NMR experiments recorded in $(CD_3)_2SO$) at 60 °C of PEGDA homopolymer.

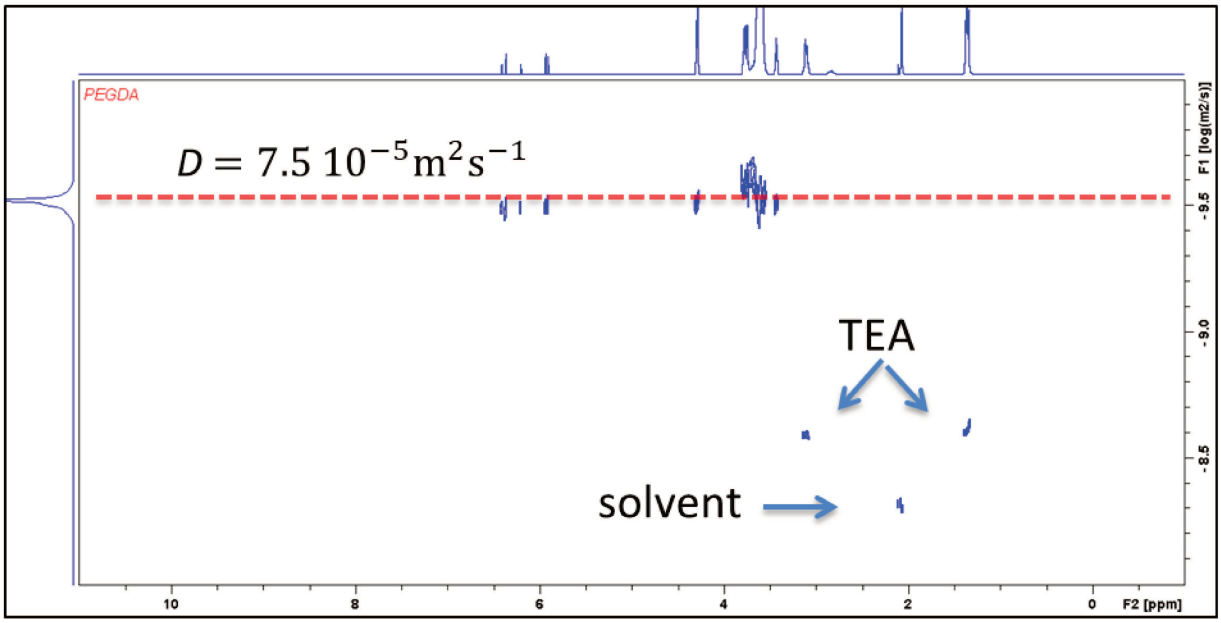

Figure S9. ^{1}H DOSY-NMR experiments recorded in $(CD_3)_2SO$) at 60 °C of PVDF-*b*-PEG-*b*-PVDF triblock copolymer.

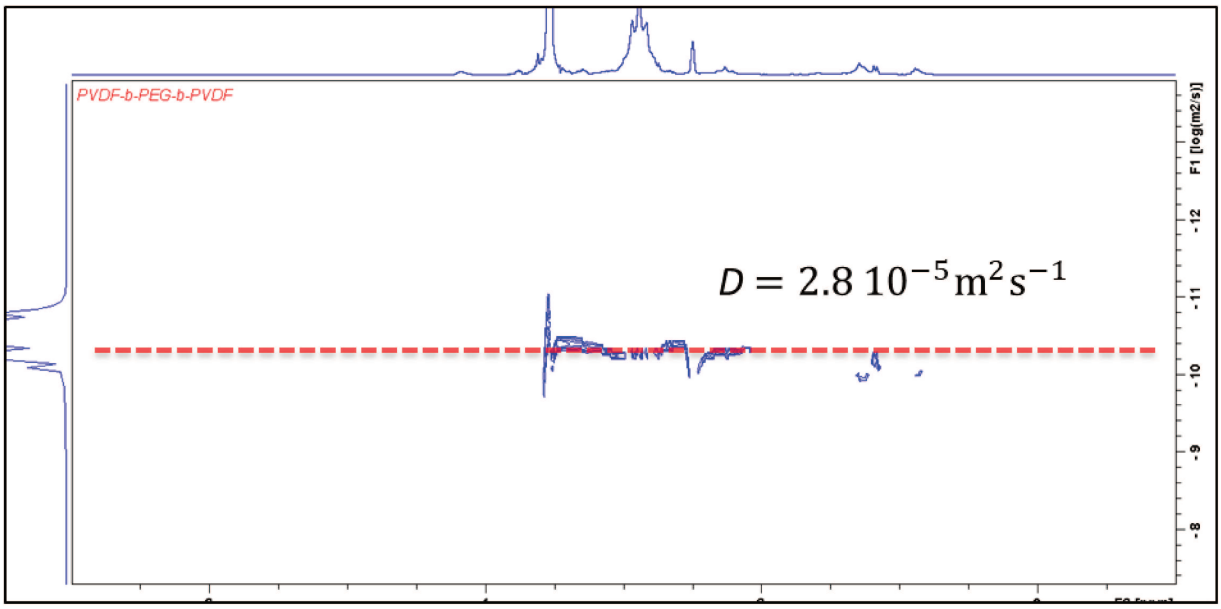

Figure S10. Thermogravimetric analysis (TGA). Weight derivative traces of the PVDF-XA and PEGDA homopolymers and of the $PVDF_{50}$-*b*-PEG_{138}-*b*-$PVDF_{50}$ triblock copolymer.

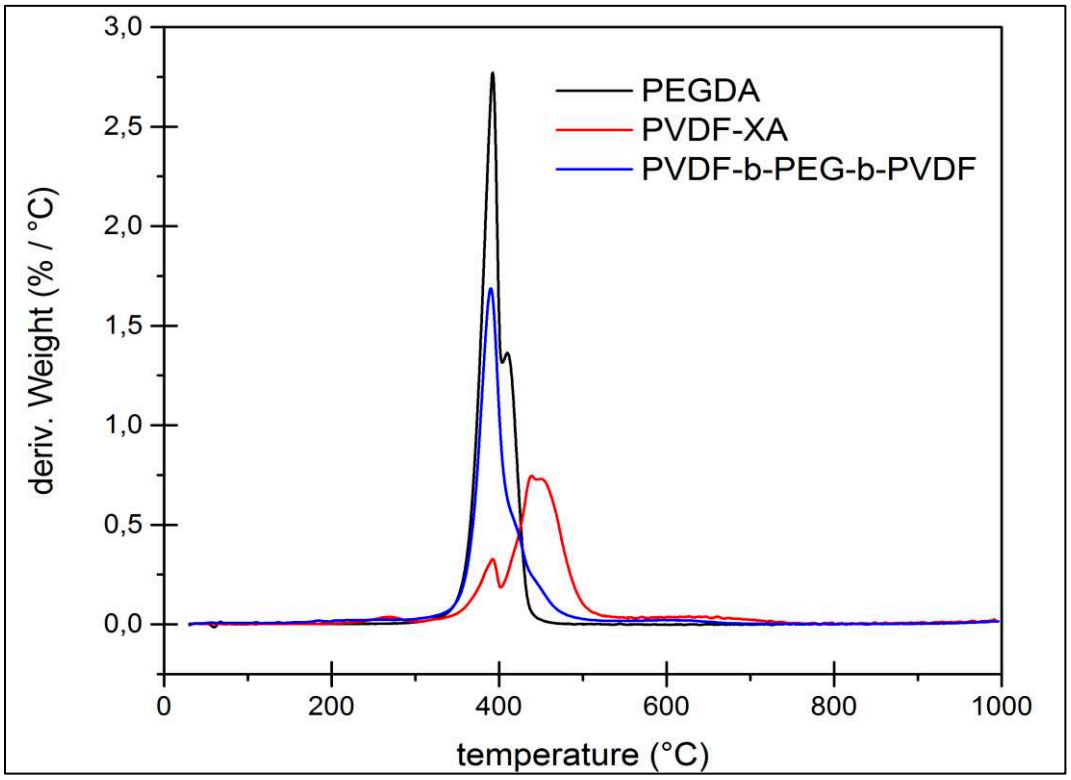

Figure S11. Differential scanning calorimetry (DSC) thermogram of PVDF-XA homopolymer.

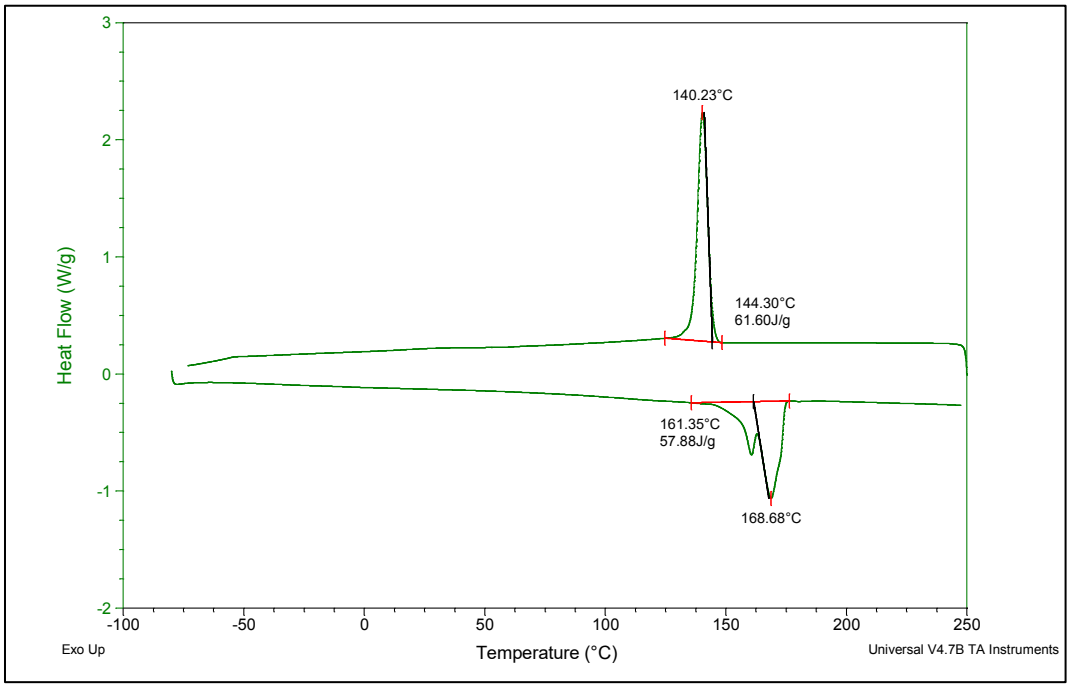

Figure S12. Differential scanning calorimetry (DSC) thermogram of PEGDA homopolymer.

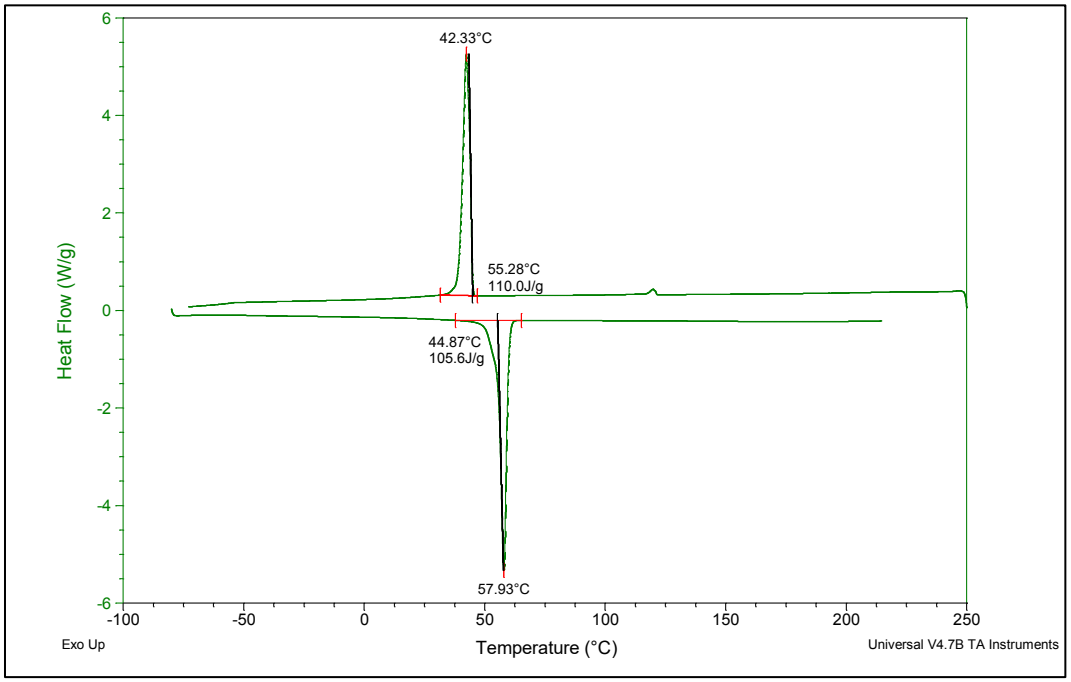

Figure S13. Differential scanning calorimetry (DSC) thermogram of PVDF-*b*-PEG-*b*-PVDF triblock copolymer.

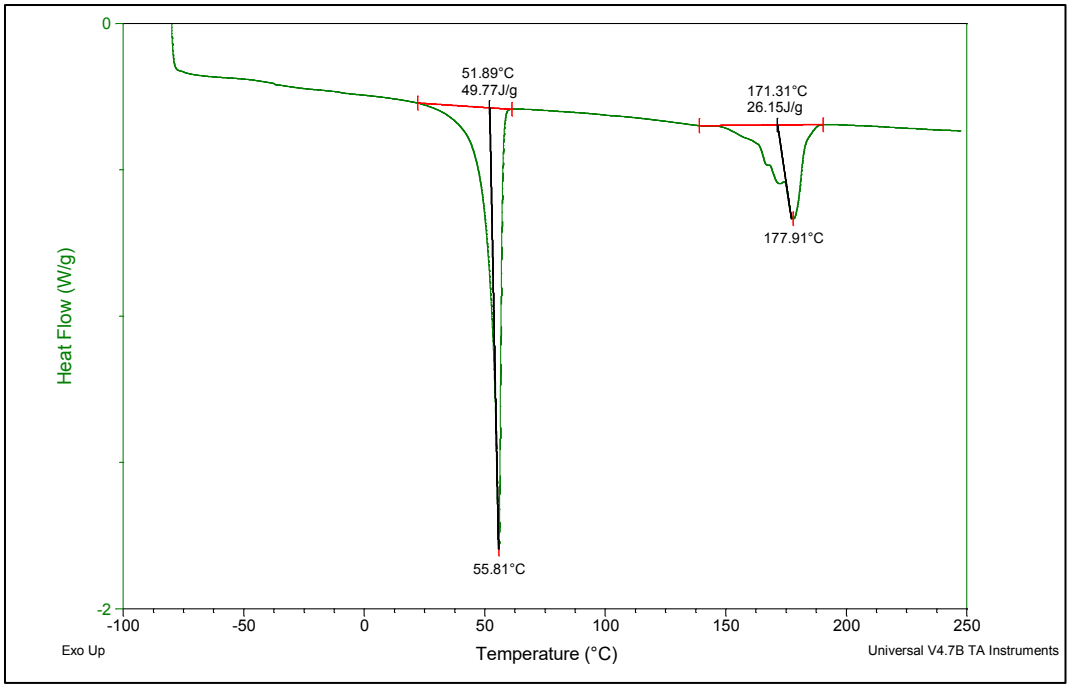

S14. Calculation of the degrees of crystallinity

$$\chi_c(\%) = \frac{\Delta H_f}{\Delta H_{f^\circ}\, \phi_m} \times 100$$

Where ΔH_f is heat of melting (extracted from the DSC trace) and ΔH_{f° is a reference value and represents the heat of melting if the polymer were 100% crystalline (both in J/g). ϕ_m is the weight fraction of the different polymer forming the triblock copolymer.

ΔH_{f° of PVDF and PEG were extracted from the literature as 104.7 $J \cdot g^{-1}$ and 196.8 $J \cdot g^{-1}$ respectively.[62,63]

The molar mass of the triblock copolymer (deduced from NMR) is 12800 $g \cdot mol^{-1}$ and the Weight fraction of the PVDF and PEG blocks (ϕ_m) are 0.53 and 0.47 respectively.

χ_c PVDF = (26.15/(104.7·0.53))x100= 47.1%

χ_c PEG = (49.77/(196.8·0.47))x100=53.8%

62. Hietala, S. *et al.* Structural investigation of radiation grafted and sulfonated poly (vinylidene fluoride), PVDF , membranes. *J. Mater. Chem.* **7**, 721–726 (1997).

63. Pielichowska, K., Bieda, J. & Szatkowski, P. Polyurethane / graphite nano-platelet composites for thermal energy storage. *Renew. Energy* **91**, 456–465 (2016).

Figure S15. TEM images of the self-assembly experiments.

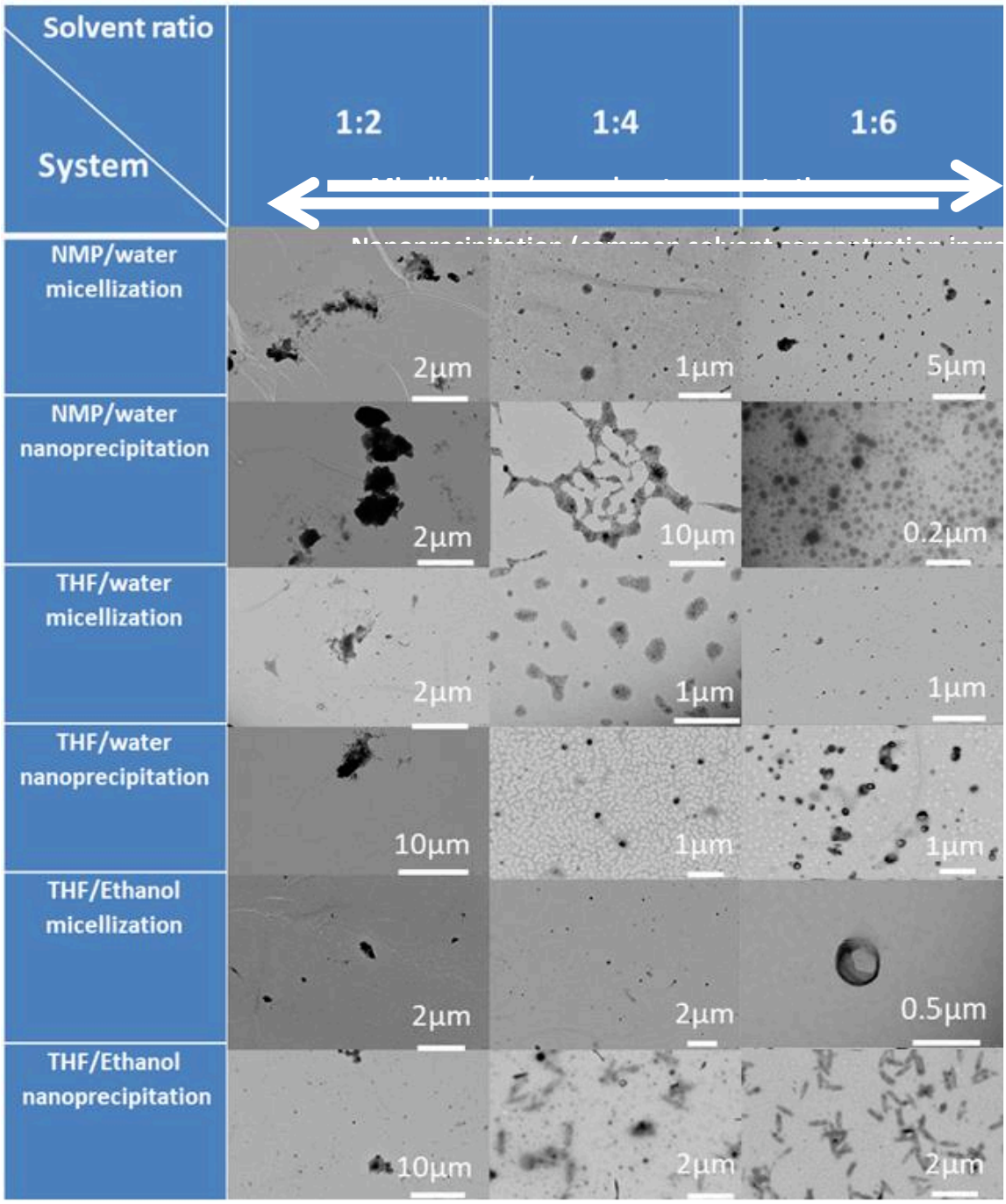

- The micellization protocol leads to the formation of micelles and vesicles when solvent:non-solvent ratios of at least 1:4 are reached (THF/ethanol).

- The nanoprecipitation protocol allowed the rapid formation of micelles, vesicles and crystalline aggregates at 1:6 solvent: non-solvent ratios employing NMP/water, THF/water and THF/ethanol respectively. Addition of more common solvent (containing BCP) leads to destabilization of the BCP assemblies and ill-defined or mixtures of structures were observed by TEM analysis.

Figure S16. AFM topographic images and height profiles of micelles (a) and vesicles (b)

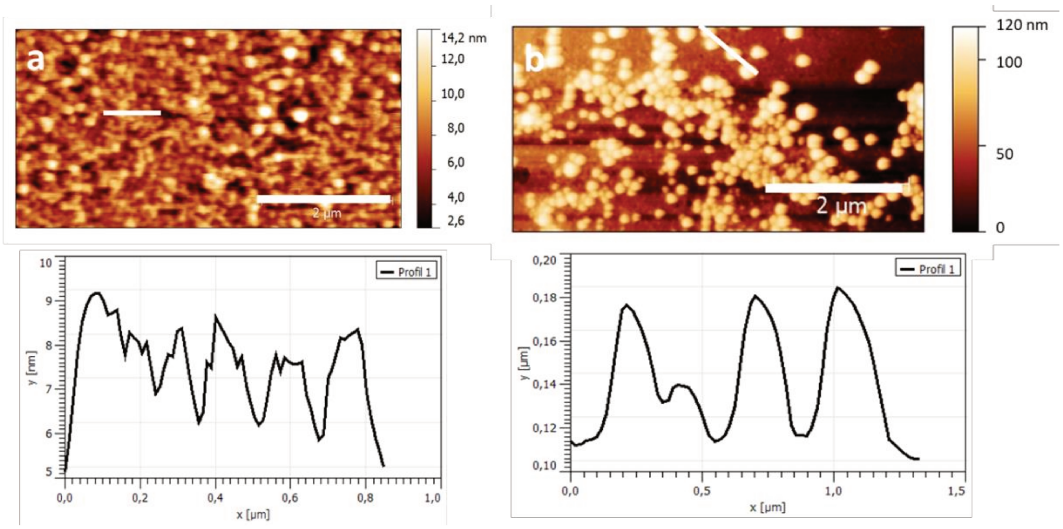

Figure S17. XRD pattern of PEG_{6000}.

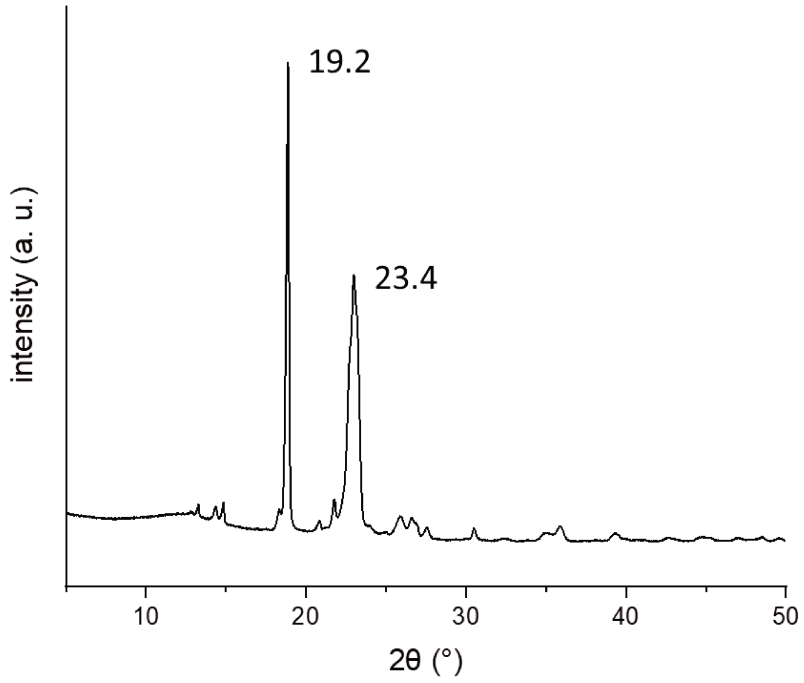

Chapter 3

Amphiphilic P(VDF-*co*-HFP)-*b*-PEG-*b*-P(VDF-*co*-HFP) triblock copolymer. Temperature-Induced Crystallization-driven Self-Assembly (TI-CDSA)

The PVDF based triblock copolymer presented in chapter two, had limited solubility in common solvents due to the high crystallinity of the PVDF blocks. The crystallinity of the PVDF block was reduced by copolymerization of VDF and HFP. A low HFP content was enough to reduce the crystallinity of the fluorinated block and to increase the solubility of the triblock synthesized using the same approach presented in chapter two. This new triblock copolymer was much soluble in THF but also in DMF and acetone. Self-assembly of this triblock copolymer was studied in different mixture of solvents and applying different protocols in order to access a wide range of morphologies. Also, a thermally-induced crystallization-induced self-assembly approach was explored to determine if better control over the morphology shape and size could be obtained.

Amphiphilic P(VDF-*co*-HFP)-*b*-PEG-*b*-P(VDF-*co*-HFP) triblock copolymer. Temperature-Induced Crystallization-driven Self-Assembly (TI-CDSA) behavior

Enrique Folgado,[a,b] Matthias Mayor,[b] Vincent Ladmiral,[a]* and Mona Semsarilar[b]*

[a]Institut Charles Gerhardt Montpellier, ICGM UMR 5253, Univ Montpellier, CNRS, ENSCM, Montpellier, France.
[b]Institut Européen des Membranes, IEM, UMR 5635, Univ Montpellier, CNRS, ENSCM, Montpellier, France.

1. Abstract

To date, amphiphilic block copolymers (BCPs) containing poly(vinylidene fluoride-*co*-hexafluoropropylene) (P(VDF-*co*-HFP)) copolymers are rare. This semi-crystalline fluorinated copolymer can crystallize in solution making such BCPs appealing for the preparation of self-assembled block copolymer morphologies through crystallization-driven self-assembly (CDSA) in selective solvents. Here the synthesis, characterization by ^{1}H and ^{19}F NMR spectroscopies, GPC, TGA, DSC and XRD; and the self-assembly behavior of a P(VDF-*co*-HFP)-*b*-PEG-*b*-P(VDF-*co*-HFP) triblock copolymer was studied. The resulting well-defined ABA amphiphilic fluorinated triblock copolymer was self-assembled in selective solvents using a variety of methods. Thin-film hydration, micellization, nanoprecipitation, and temperature-induced crystallization-driven self-assembly (TI-CDSA) protocols were investigated. A large range of morphologies such as spherical, square, rectangular, fiber-like and platelets structures with sizes ranging from a few nanometres to micrometers were obtained depending on the self-assembly protocols and solvents systems used.

2. Introduction

The ability of block copolymers (BCPs) to spontaneously organize into different morphologies has attracted a great deal of attention due to their potential use in the development of nanomaterials with controlled structures and tunable properties.[1,2] The self-assembly of non-crystalline (coil-coil) BCPs in solution is well-established.[3] Selective solvation gives rise to the formation of structures with a core consisting of the insoluble block surrounded by a corona formed by the soluble block.[4] The resulting morphologies will depend on the intrinsic molecular parameters of the BCP such as the solvent affinity of the blocks, the relative volume fraction and the length of the blocks.[3] However, the complexity of the self-assembly process increases when one block of the BCP is able to crystallize.

The formation of semi-crystalline BCP micelles can be viewed as a two-step self-assembly process. Micelles will form first by minimizing their contact with the solvent, and then start to crystallize in a second step, giving rise to the final micellar structure. As crystallization takes place in the insoluble micellar core, the initial morphology is either preserved or a morphological transformation into a novel structure is triggered.[4]

In 1966, Lotz *et al.* first found that poly(ethylene glycol)-*b*-polystyrene (PEO-*b*-PS) block copolymer (BCP) can form square-shaped platelets through crystallization from ethyl benzene solutions.[5] Since then, the preparation of micelles from crystalline-coil BCPs by crystallization-driven self-assembly (CDSA) has been gaining momentum.[4,6–13]

Cylinders and lamellar architectures are the most commonly observed morphologies.[8,14–16] However, by manipulating the interactions between the two blocks and the solvent, and the interplay between the crystallization of the core-forming block and the corona chain stretching, the micellar morphology is no longer restricted to common geometries and more complex structures that may incorporate desired properties become accessible.[13,17–19] In solvents able to solubilize both blocks the BCP remains as unimers undergoing a slower crystallization process and can form larger defect free crystals (platelets for example).[13,20,21]

Diverse polymeric architectures have been obtained by a crystallization-driven self-assembly (CDSA) approach. Arno *et al.* reported recently the preparation of PCL-*b*-PMMA-*b*-PDMA biocompatible and biodegradable 1D cylindrical and 2D platelet micelles via CDSA. Interestingly, they were able to control the dimensions and dispersity of the self-assembled nanostructures.[6] Li *et al.* have reported a poly(L-lactide)-based diblock glycopolymer that assembles into 1D cylinders and 2D diamond-shaped platelets.[13] Qiu and Gao *et al.* have reported the preparation of rectangular and hollow structures from polymer blends.[19]

The most common crystalline blocks in these assembled structures are poly(ethylene oxide) (PEO),[22] poly(ε-caprolactone) (PCL),[6,17] polyethylene (PE),[23] and poly(ferrocenyldimethylsilane) (PFS).[6,14,15,24,25]

Fluoropolymers are an interesting family of polymers with remarkable chemical and physical properties. Poly(vinylidene fluoride) (PVDF) is a highly crystalline fluoropolymer that have found numerous applications.[26–28] Only few studies describe the self-assembly in solution of BCPs containing a fluoropolymer block.[29–32] Our team has been developing the RAFT polymerization of VDF over the last years[33–35] including BCPs.[29,30,36–39] However, there are not many studies on CDSA behavior of these fluoropolymer-containing BCPs. Guerre *et al.* reported the formation of crystalline structures, thought to be formed by CDSA of PVAc-*b*-PVDF diblock copolymers solutions in DMC, a solvent in which PVDF is soluble at elevated temperatures.[36] To date, this is the only study analyzing the CDSA behavior of BCPs where the semi-crystalline block is a fluoropolymer.

An interesting variation of the CDSA is the thermally controlled crystallization-induced self-assembly, a method in which the crystallization condition can be tuned. The self-assembly procedure starts by dissolving the BCP in a selective solvent for the coil block at a temperature above the T_m of the semi-crystalline block. When the polymer solutions are cooled down, below the T_c, crystallization occurs. This method allows for a chance to control the micellar crystal development.[4]

The CDSA approach in pure alcoholic solvents or water is not easily performed on PVDF-based BCPs due to the poor solubility of PVDF in these solvents, even at high temperatures. Also, due to the high melting temperature of PVDF (T_m ~ 177°C) the thermally controlled CDSA approach is limited by the solvents in which this can be performed.

Copolymers of VDF and HFP present reduced crystallinity compared to PVDF and thus, they have higher solubility and lower T_m. Indeed, the crystallinity of P(VDF-*co*-HFP) copolymer is largely affected by the molar fraction of HFP.[40,41] P(VDF-*co*-HFP) crystallinity can be tuned by controlling the monomer composition. Copolymers with HFP content higher than 19 mol % are amorphous and have elastomeric behavior.[40,41]

P(VDF-*co*-HFP) based block copolymers made by RAFT have not been reported to date. In this work we report the preparation of an amphiphilic ABA P(VDF-*co*-HFP)-*b*-PEG-*b*-P(VDF-*co*-HFP) block copolymer. The P(VDF-*co*-HFP) copolymer with high end-group fidelity was synthesized by RAFT copolymerization of VDF and the triblock copolymer was prepared using an efficient coupling method: a one-pot thia-Michael addition. The characterization of the novel triblock BCP was performed using 1H and 19F NMR spectroscopies, GPC, TGA, DSC and XRD. The self-assembly in diverse solvents as well as the CDSA behavior of this BCP in different solvent mixtures was studied by TEM.

3. Experimental section

3.1. Materials

All reagents were used as received unless otherwise stated. 1,1-Difluoroethylene (vinylidene fluoride, VDF) and hexafluoropropylene (HFP) were supplied by Arkema (Pierre-Bénite, France). *O*-Ethyl-*S*-(1-methoxycarbonyl) ethyldithiocarbonate (CTA_{XA}) was prepared according to the method described by Liu *et al.*[42] *tert*-Amyl peroxy-2-ethylhexanoate (Trigonox 121, purity 95%) was purchased from AkzoNobel (Chalons-sur-Marne, France). PEG_{6000}, Ethanol (EtOH), 1-octanol, acetone, *N*,*N*-

dimethylformamide (DMF) tetrahydrofuran (THF), dimethyl carbonate (DMC), and pentane, were purchased from Sigma Aldrich. Deuterated solvents were purchased from Eurisotop.

3.2. Measurements

Nuclear Magnetic Resonance (NMR).

The NMR spectra were recorded on a Bruker AV III HD Spectrometer (300 or 400 MHz for ^{1}H and 282 or 376 MHz for ^{19}F).

Coupling constants and chemical shifts are given in hertz (Hz) and parts per million (ppm), respectively. The experimental conditions for recording ^{1}H and ^{19}F NMR spectra were as follows: flip angle, 30°; acquisition time, 4s ; pulse delay, 1 s; number of scans, 16 (or 32 for ^{19}F); and pulse widths of 9.25 (P[1] from Pulse) and 11.4 µs for ^{1}H and ^{19}F NMR respectively.

Size-Exclusion Chromatography (SEC).

Size exclusion chromatograms were recorded using a Triple detection GPC from Agilent Technologies with its corresponding Agilent software, dedicated to multi-detector GPC calculation. The system used two PL1113-6300 ResiPore 3µm 300 x 7.5 mm columns with DMF as the eluent with a flow rate of 1 mL/min and toluene as flow rate marker. The detector suite comprised a PL0390-06034 capillary viscometer, and a 390-LC PL0390-0601 refractive index detector. The entire SEC-HPLC system was thermostated at 35°C. Low dispersity PMMA standards were used for the calibration. Typical sample concentration was 10 mg/mL.

Differential Scanning Calorimetry (DSC).

DSC measurements were performed on 2–3 mg samples on a TA Instruments DSC Q20 equipped with an RCS90 cooling system. For all measurements, the following heating / cooling cycle was employed: cooling from 40 °C to −73°C, isotherm at - 73 °C for 5 min, first heating ramp from −73 °C to 250 °C at 10 °C/min, isotherm at 250 °C for 5 min, cooling stage from 250 °C to −73 °C at 10 °C/min, isotherm plateau at −73 °C for 1 min, second heating ramp from −73 °C to 250 °C at 10 °C/min, isotherm at

250 °C for 1 min, and last cooling stage from 250 °C to 40 °C. Calibration of the instrument was performed with noble metals and checked before analysis with an indium sample. Melting points were determined at the maximum of the enthalpy peaks.

Thermogravimetric analysis (TGA).

TGA analyses were carried out with a TA Instruments TGA G500 from 20 °C to 800 °C. A heating rate of 10 °C min^{-1} was used under an air atmosphere with a flow rate of 60 mL min^{-1}. Dry samples weighing approximately 3 mg were used.

Transmission electron microscopy (TEM).

TEM studies were conducted using a JEOL 1400+ instrument equipped with a numerical camera, operating with a 120 kV acceleration voltage at 25 °C. To prepare TEM samples, a drop (10.0 µL) of micellar solution was placed onto a Formvar/Carbon coated copper grid for 60 s, blotted with filter paper and dried under ambient conditions. All TEM grids were prepared from self-assembly experiment solutions without further dilution.

X-Ray diffraction (XRD).

XRD powder patterns were carried out on a Philips X'pert Pro MPD diffractometer by using Ni-filtered CuKα1 radiation (λ=1.5406 Å) in Bragg–Brentano scanning mode with a 2θ angle range from 5–60°, and a time per step of 50 s.

3.3. Synthesis

Autoclave.

The copolymerization of VDF and HFP was performed in a 100 mL Hastelloy Parr autoclave system (HC 276) equipped with a mechanical Hastelloy stirring system, a rupture disk (3000 PSI), inlet and outlet valves, and a Parr electronic controller to regulate the stirring speed and heating.

P(VDF$_{51}$-*co*-HFP$_4$)-XA synthesis.

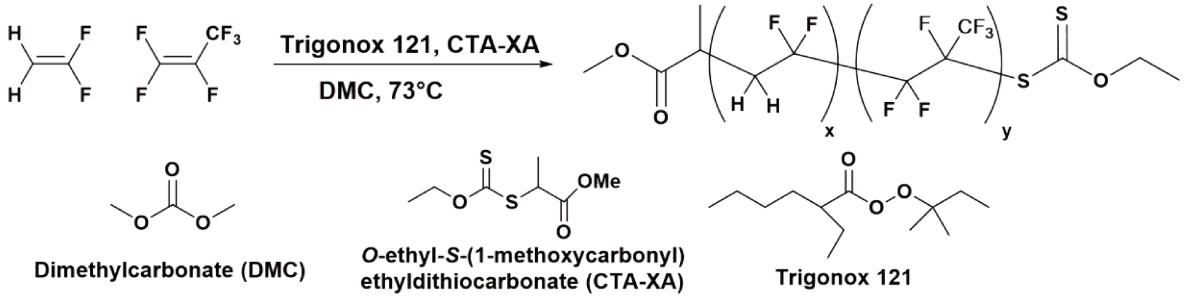

Scheme 1. Synthesis of P(VDF-*co*-HFP) copolymer by RAFT/MADIX.

A solution of Trigonox 121 (158 mg, $6.87 \cdot 10^{-4}$ mol) and CTA-XA (1.30 g, $6.25 \cdot 10^{-3}$ mol) in DMC (60 mL), was degassed by N_2 bubbling during 30 min. Prior to the reaction, the autoclave was pressurized with 30 bar of nitrogen to check for leaks. The autoclave was then put under vacuum ($20 \cdot 10^{-3}$ mbar) for 30 min to remove any trace of oxygen. The homogeneous DMC solution was introduced into the autoclave using a funnel, VDF gas (19.0 g, $2.97 \cdot 10^{-1}$ mol) was transferred in the autoclave at low temperature then HFP gas (8.0 g, $0.53 \cdot 10^{-1}$ mol) was transferred following the same procedure and the reactor was gradually heated to 73 °C. The reaction was stopped after 20 h. The autoclave was cooled down to room temperature (ca. 20 °C), purged from the residual monomers, and DMC was removed under vacuum. The crude product was dissolved in 30 mL of warm acetone (ca. 40 °C), and left under vigorous stirring for 30 minutes. This polymer solution was then precipitated from 400 mL of chilled pentane. The precipitated polymer (white powder) was filtered through a filter funnel and dried under vacuum ($15 \cdot 10^{-3}$ mbar) for two hours at 50°C. The polymerization yield (55%) was determined gravimetrically (mass of dried precipitated polymers / mass of monomer introduced in the pressure reactor).

^{1}H NMR (300 MHz $(CD_3)_2CO$, δ (ppm), Figure S1): 1.24 (d, -CH(C**H$_3$**)(C=O)-, $^3J_{HH}$ = 7.1 Hz, 2.31H). 1.32 (d, -CH(C**H$_3$**)(C=O)-, $^3J_{HH}$ = 7.2 Hz, 0.67H), 1.46 (t, -S(C=S)O-CH$_2$-C**H$_3$**, $^3J_{HH}$ = 7.1 Hz, 3H), 2.37 (m, -CF$_2$-C**H$_2$**-C**H$_2$**-CF$_2$-, VDF-VDF TT reverse addition, 3.2H), 2.81 (s, -C**H**(CH$_3$)(C=O)-, 1H), 2.84-3.50 (m, -CF$_2$-C**H$_2$**-CF$_2$-, VDF-VDF HT and VDF-HFP regular addition, 95.92H), 3.67-

3.70 (s, -(C=O)-O-C**H$_3$**), 3H), 4.12 (t, -CF$_2$-C**H$_2$**-S(C=S)OEt, $^3J_{HF}$ = 17.7 Hz, 2H), 4.74 (q, (-S(C=S)OC**H$_2$**-CH$_3$, $^3J_{HH}$ = 7.1 Hz, 2H), 6.06 – 6.53 (m, -CH$_2$-CF$_2$-**H** and –CF(CF$_3$)H).

^{19}F NMR (282 MHz (CD$_3$)$_2$CO, δ (ppm), Figure S2): -183.65 - -183.75 (-CF$_2$C**F**(CF$_3$)-), -118.13 (-C**F$_2$**CF(CF$_3$)-), -115.65 (-CH$_2$-CF$_2$-C**F$_2$**-CH$_2$-CH$_2$-, VDF-VDF HH reverse addition), -115.00 - -114.00 (CH$_2$-C**F$_2$**-H), -113.36 (-CF$_2$-CH$_2$-C**F$_2$**-CF$_2$-CH$_2$-CH$_2$-, VDF-VDF HH reverse addition), -113.09 (CH$_2$-CF$_2$-**CF$_2$**-CH$_2$-S-), -112.67 (-CH$_2$-**CF$_2$**-CF$_2$-CH$_2$-S-), -109.92 (-CH$_2$-C**F$_2$**-CF$_2$CF(CF$_3$)-VDF-HFP regular addition), -103.01 (-C**F$_2$**-CH$_3$), -94.77 (-CH$_2$-CH$_2$-C**F$_2$**-CH$_2$-, TT reverse addition), -93.50 (-CH$_2$-C**F$_2$**-CH$_2$-CH(CH$_3$)(C=O)-), -91.92 (-CH$_2$-C**F$_2$**-CH$_2$-CF$_2$H), -91.43 (-CH$_2$-CH$_2$-CF$_2$-CH$_2$-**CF$_2$**-CH$_2$-CF$_2$-, regular VDF-VDF HT addition), -91.00 (-CH$_2$-C**F$_2$**-CH$_2$-, regular VDF-VDF HT addition), -74.55 (-CH$_2$-CF$_2$-CF(C**F$_3$**)-CF$_2$-CH$_2$-CF$_2$-), -70.02 (-CH$_2$-CF$_2$-CF$_2$-CF(C**F$_3$**)-CH$_2$-CF$_2$-CH$_2$-).

PEG$_{136}$-DA synthesis.

Polyethylene glycol diacrylate (PEG-DA) synthesis was prepared following the protocol described elsewhere.[43] 1eq. of PEG$_{6000}$ and an excess of 10 eq. of acryloyl chloride were dissolved in DCM in a round bottom flask at room temperature. Then, trimethylamine (4eq.) was added dropwise and the reaction was stirred. The reaction was complete in 60h and the product was filtered off on Celite, precipitated in cold diethyl ether and dried under vacuum.

^{1}H NMR (400 MHz, (CD$_3$)$_2$SO) δ (ppm)): 6.43 (d, $^3J_{HH}$ =17.3 Hz, 2H, -CH=C**H$_2$**), 6.16 (dd, $^3J_{HH}$ =17.4 Hz and 10.4 Hz, 2H, -C=C**H**-C=O), 5.85 (d, $^3J_{HH}$ = 10.4 Hz, 2H, -CH=C**H$_2$**), 4.23 (m, 2H, -(C=O)-O-C**H$_2$**-CH$_2$-O-) 3.4-3.8 (m, -C**H$_2$**-C**H$_2$**-O).

P(VDF-*co*-HFP)-*b*-PEG-*b*-P(VDF-*co*-HFP) synthesis.

The aminolysis and subsequent Michael addition were conducted using a one-pot protocol described by Guerre et al.[44] P(VDF$_{51}$-*co*-HFP$_4$)-XA (5.000 g, 1.35 mmol) and PEGDA$_{136}$ (4.05 g, 0.67 mmol) were dissolved in DMF (115 mL). The mixture was degassed with N$_2$ for 10 min. A degassed mixture of hexylamine (0.546 g, 5.40 mmol), triethylamine (0.205 g, 2.15 mmol) and dimethylphenylphosphine (DMPP) (0.01 mL, 6.75 10^{-2} mmol) in 2 mL of DMF was injected into the reaction mixture. N$_2$ was bubbled into the reaction mixture for another 10 min. The mixture was stirred 16 h at

25 °C until the reaction was complete and no unreacted acrylate could be detected by ^{1}H NMR. The product was then precipitated twice in cold diethyl ether and dried under high vacuum at 70 °C until constant weight to remove traces of DMF.

^{1}H NMR (400 MHz $(CD_3)_2SO$, δ (ppm), Figure S6) : 1.13-1,18 -CH(C**H$_3$**)(C=O)-, 2.17-2.33 (m, -CF_2-C**H$_2$**-C**H$_2$**-CF_2-, VDF-VDF TT reverse addition), 2.64-2.71 (m, -S-CH_2-C**H$_2$**(C=O)), 2.71-3.26 (t, -CF_2-C**H$_2$**-CF_2-, VDF-VDF HT regular addition), 3.40-3.65 (m, -O-C**H$_2$**-C**H$_2$**-), 3.61 (s, -(C=O)-O-C**H$_3$**), 3.66-3.72 (m, -C(C=O)-O-CH_2-C**H$_2$**) 4.08-4.19 (-C(C=O)-O-C**H$_2$**-CH_2).

^{19}F NMR (376 MHz $(CD_3)_2CO$, δ (ppm), Figure S7): -183.38 (-CF_2C**F**(CF_3)-), -117.61 (-C**F$_2$**CF(CF_3)-), -115.15 (-CH_2-CF_2-C**F$_2$**-CH_2-CH_2-, VDF-VDF HH reverse addition), -113.78 (CH_2-CF_2-**CF$_2$**-CH_2-S-), -112.87 (-CH_2-C**F$_2$**-CF_2-CH_2-CH_2-, VDF-VDF HH reverse addition), -112.25 (-CH_2-**CF$_2$**-CF_2-CH_2-S-), -109.34 (-CH_2-C**F$_2$**-CF_2CF(CF_3)- VDF-HFP regular addition),-102.49 (-C**F$_2$**-CH_3), -93.82 (-CH_2-CH_2-C**F$_2$**-CH_2-, TT reverse addition), -92.77 (-CH_2-C**F$_2$**-CH_2-CH(CH_3)(C=O)-), -91.85 (-CH_2-C**F$_2$**-CH_2-CF_2H), -91.51 (-CH_2-CH_2-CF_2-CH_2-**CF$_2$**-CH_2-CF_2-, regular VDF-VDF HT addition), -91.00 (-CH_2-C**F$_2$**-CH_2-, regular VDF-VDF HT addition), -73.63 (-CH_2-CF_2-CF(C**F$_3$**)-CF_2-CH_2-CF_2-), -69.23 (-CH_2-CF_2-CF_2-CF(C**F$_3$**)-CH_2-CF_2-CH_2-).

3.4. Self-assembly

Preparation of block copolymer solutions.

Stock solutions of 1 mg mL^{-1} of block copolymer were prepared in DMF, acetone or THF, and heated at 70°C for 1h under magnetic stirring to complete polymer dissolution.

Nanoprecipitation.

Glass vials containing 2 mL of non-solvent (water, ethanol or octanol) and magnetic bars were placed on stirring plates. To each vial 0.1 mL of block copolymer solution (1 mg mL^{-1}) (in DMF, acetone or THF) were added dropwise under vigorous stirring (maximum speed of the stirring plate). After 1h of stirring TEM grids were prepared.

Micellization.

Vials containing 0.5 mL of the stock solutions (1 mg mL^{-1}) in different solvents (DMF, acetone and THF) were placed on a stirring plate. Non-solvent (water, ethanol or octanol; 2, 3 or 4 mL) was added dropwise using a syringe pump at a fixed rate of 4 mL h^{-1} under gentle stirring. 10 µL were taken to prepare TEM samples at 1:4, 1:6 and 1:8 solvent / non-solvent ratios.

Thin Film Hydration.

A thin film of BCP was formed in a 25 mL round bottom flask by rotary evaporation of a 5 mg mL^{-1} BCP acetone solution. After the solvent was completely removed, water (5 mL) was added to the round bottom flask and the thin film detached and broke into smaller pieces by handshaking. The stirring was pursued on a stirrer plate (set at maximum stirring speed). TEM samples were prepared after 1 day, and 1 week.

Temperature-Induced Crystallization-Driven Self-Assembly (TI-CDSA).

Micellar samples obtained by micellization in DMF: ethanol (1:6), DMF: water (1:6) and acetone: water (1:6) and by nanoprecipitation in THF:octanol (1:20) were heated (at 70°C for ethanol and water samples and at 180°C for octanol) for 1h. The samples were then sonicated for 10 min to help solubilisation of the BCP in the solvents mixtures. The vials were then slowly cooled down at 5°C / h and aged 12h before preparing TEM grids.

4. Results and Discussion

Polymers synthesis and characterizations

A P(VDF_{51}-*co*-HFP_4)-XA (where XA designates the ethyl xanthate moiety) copolymer was synthesized by RAFT. The molar fraction of HFP (7.4 %) as well as the degree of polymerization of both VDF (51) and HFP (4) was estimated using NMR data (see Figures S3-S5 for details of these calculations). The triblock copolymer was synthesized via a one-pot aminolysis-thia Michael addition using 2 equivalents of P(VDF_{51}-*co*-HFP_4)-XA and 1 equivalent of PEG_{136} diacrylate (synthesized from commercial PEG), in the presence of excess hexylamine (to effect the aminolysis of the xanthate end-groups into thiols) and

dimethylphenylphosphine in catalytic amount (for the nucleophilic catalysis of the thia-Michael addition). The disappearance of the acrylate signals and xanthate end-group in ^{1}H NMR as well as the shifts in ^{19}F NMR (–C**F$_2$**-CH$_2$-XA at -113.09 ppm to –C**F$_2$**-CH$_2$-S-CH$_2$-CH$_2$-PEG at -113.78 ppm; see Figure S7) confirmed the success of the coupling reaction.

After purification by precipitation in chilled pentane, the successful synthesis and purity of P(VDF$_{51}$-*co*-HFP$_4$)-*b*-PEG$_{136}$-*b*-P(VDF$_{51}$-*co*-HFP$_4$) ABA amphiphilic triblock copolymer was confirmed by SEC. Despite the proportion of H-terminated dead chains in the P(VDF-*co*-HFP)-XA copolymer estimated to be 15 mol % (see S8 for details of the calculations), the GPC chromatogram of the triblock copolymer (Figure 1) appears as a monomodal symmetrical peak devoid of shoulders or tailing.

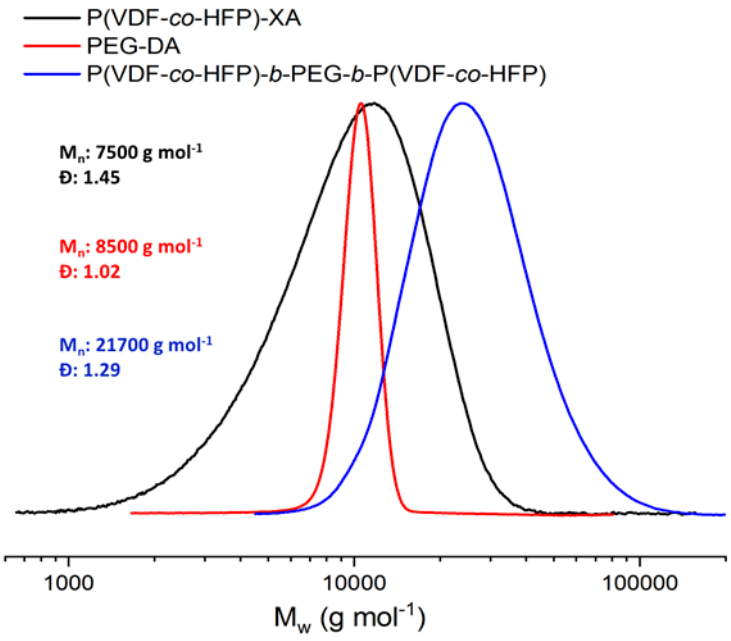

Figure 1. Normalized SEC chromatograms (viscometric detector) of: P(VDF-*co*-HFP)-XA (black trace), PEGDA (red trace), P(VDF-*co*-HFP)-*b*-PEG-*b*-P(VDF-*co*-HFP) (blue trace).

Differential scanning calorimetry (DSC) of the BCP and of its homopolymer precursors revealed an exothermic peak corresponding to the crystallization of P(VDF-*co*-HFP) at 119.2 °C (Figures S9 and S10). As expected, the melting and crystallization temperatures of the P(VDF-*co*-HFP) block are lower than those of a PVDF homopolymer (103.1 °C and 133.5 °C, respectively).[43] P(VDF-*co*-HFP) copolymers are less crystalline than PVDF, but remain semi-crystalline and behave as thermoplastic up to 19 mol % of HFP. At higher content of HFP, these copolymers become elastomers.[40]

The presence of HFP also induces decreases of the melting and crystallization temperatures. Here, relatively low HFP content was chosen to slightly reduce the polymer crystallinity, and thus improve its solubility in organic solvents. The resulting triblock copolymer was highly soluble in DMF, DMSO, acetone and THF whereas a similar PVDF-based triblock copolymer was much less soluble in acetone and barely soluble in THF.[43]

The DSC thermograms were also used to quantify the degree of crystallinity of the P(VDF-*co*-HFP) (10.2%) and of the PEG (88.1%) segments in the triblock copolymer (see figure S11 for details on these calculations). These results are in agreement with the signals observed by XRD (Figure S12a), where the PEG appears to be much more crystalline than the P(VDF-*co*-HFP) segments.

In our previous work, we showed that the morphology adopted by a PVDF-*b*-PEG-*b*-PVDF is highly path- and solvent-dependent due to the non-ergodicity of such systems. Thus, in the present work we focused the investigation on the study of the different morphologies that can be accessed by different self-assembly protocols or by adjusting parameters such as solvent/non-solvent selectivity and ratio, and crystallization conditions (i.e. annealing temperature).

Self-Assembly

Thin-film rehydration

Film rehydration method is established as the formation of a thin layer of an amphiphile copolymer on a surface by solvent evaporation followed by redispersion in pure water. External forces such as stirring or sonication are required to enhance the film hydration of amphiphilic block copolymers. Here, a thin film of P(VDF-*co*-HFP)-*b*-PEG-*b*-P(VDF-*co*-HFP) was prepared in a round bottom flask, then hydrated with pure water and stirred for 1 week. The structures formed are shown in Figure 2.

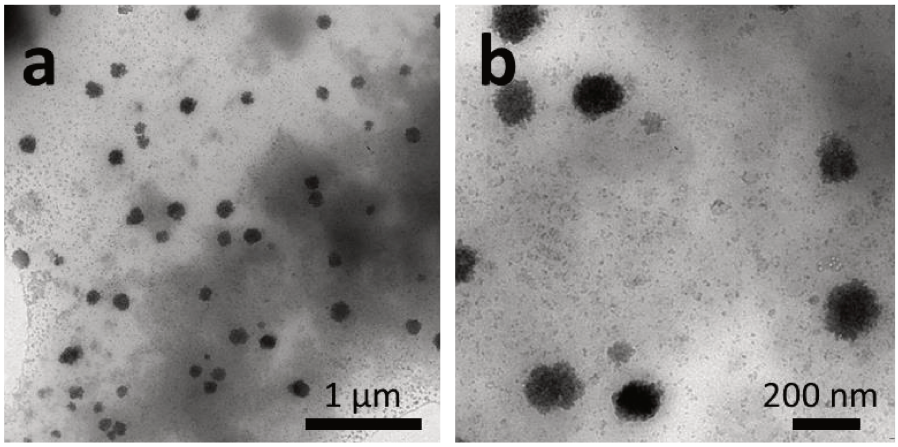

Figure 2. TEM images of BCP aggregates formed by thin-film rehydration with water after 1 week in pure water.

The roughly spherical aggregates of diameter ranging from 100 to 180 nm observed were also accompanied by very small aggregates or BCP film debris. This approach, commonly used for the preparation of vesicles and liposomes from BCP, does not seem suitable to the formation of higher order morphologies in the case of this triblock copolymer (whose core forming block is the semi crystalline P(VDF-*co*-HFP) copolymer) under the conditions the film rehydration process was performed.

Micellization

Micellization, dissolution of the block copolymer in a good solvent for both blocks, followed by slow addition of a selective solvent for one of the blocks, is likely to deliver thermodynamically more stable self-assembled structures due to the slower self-assembly process. However, BCP containing a semi-crystalline block such as P(VDF-*co*-HFP) are non-ergodic. Below their fusion temperature, their crystalline structure prevents the equilibrium between self-assembled and dissolved polymer chains as well as their exchanges between self-assembled morphologies. In consequence, the self-assembly of the P(VDF-*co*-HFP)-*b*-PEG-*b*-P(VDF-*co*-HFP) triblock copolymer will likely lead to kinetically trapped structures. Three common solvents (DMF, acetone and THF) and two PEG selective solvents (ethanol and water) were chosen to study the self-assembly behavior of this BCP. The obtained structures are shown in Figure 3.

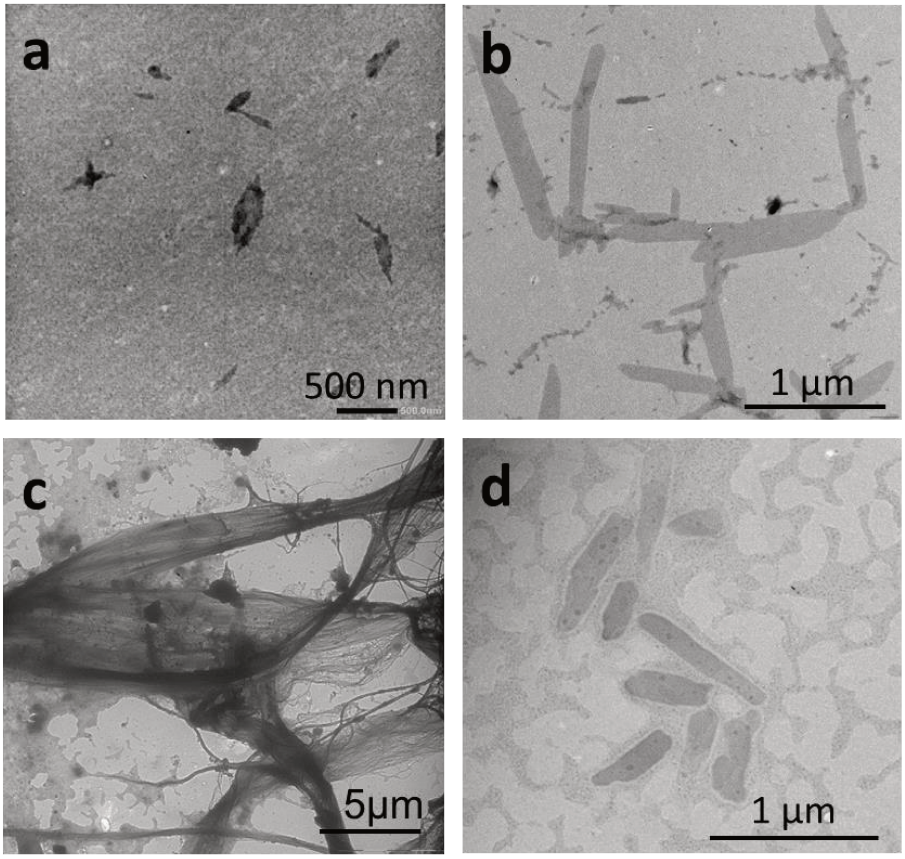

Figure 3. TEM images of self-assembled structures obtained by micellization of 1 mg mL^{-1} solutions of the P(VDF-*co*-HFP)-*b*-PEG-*b*-P(VDF-*co*-HFP) triblock copolymer in: (a) DMF, (b) acetone, employing ethanol as selective solvent for PEG; and (c) DMF, (d) acetone, employing water as the selective solvent for PEG. Final concentration of all samples = 0.14 mg mL^{-1}, solvent: selective solvent final ratio = 1:6.

The self-assembly protocol using DMF as good solvent and ethanol as the PEG selective solvent led to the formation of thin sharp-edge objects, most of them ovoidal with size ranging from 200 nm to 500 nm (Figure 3a). In contrast, when water was used as the selective solvent for PEG, the triblock copolymers formed long fibers (several tens of µm in length) which aggregated into bundles (Figure 3c). When acetone was used as the common solvent, the triblock copolymer self-assembled into micrometer-long 2D strips both when ethanol (Figure 3b) or water (Figure 3d) were used as the PEG selective solvent.

Experiments carried out with THF/ethanol or THF/water solvent systems did not lead to the formation of organized structures (Figure S13).

Nanoprecipitation

Nanoprecipitation (NP) is an easy and direct way to provoke self-assembly and is well-suited for block copolymers with relatively low molar masses and relatively short insoluble block. The use of this technique was recently reported for the preparation of polymeric aggregates from a PVDF-*b*-PEG-*b*-PVDF BCP with similar block lengths.[43] Despite the very crystalline PVDF hydrophobic block, it was shown that NP allowed the preparation of well-defined ovoidal crystalline structures. The structures obtained by the NP approach using different solvents (DMF, acetone and THF) and PEG selective solvents (ethanol and water) are shown in Figure 4.

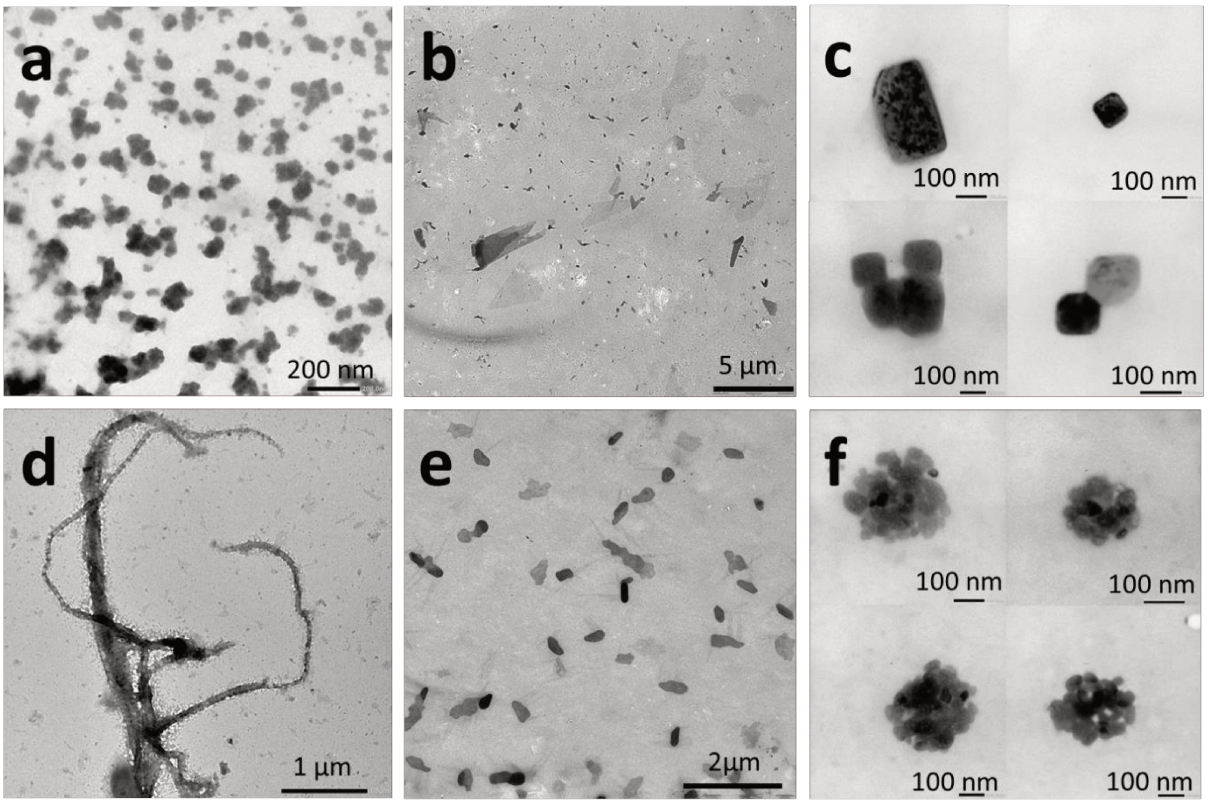

Figure 4. TEM images of self-assembled structures obtained by nanoprecipitation of 1 mg mL^{-1} solutions of the P(VDF-*co*-HFP)-*b*-PEG-*b*-P(VDF-*co*-HFP) triblock copolymer in: (a) DMF, (b) acetone, (c) THF, employing ethanol as selective solvent for PEG and (d) DMF, (e) acetone, (f) THF, employing water as the selective solvent for PEG. Final concentration of all samples = 0.09 mg mL^{-1}. Solvent: selective-solvent final ratio = 1:10.

Nanoprecipitation of DMF solutions in ethanol led to the formation of relatively ill-defined roughly spherical aggregates with size ranging from 20 to 200 nm (Figure 4a). NP of the

triblock copolymer from an acetone solution using the same selective solvent produced micrometric (up to 5 µm) sheet-like structures (Figure 4b). The THF: ethanol system however induced the formation of well-defined square and rectangular aggregates with size comprised between 120 and 300 nm.

When water was employed as the selective solvent for PEG, the BCP self-assembled morphologies obtained using the NP protocol were micrometer-long fibers with diameter of about 60-250 nm (Figure 4d). In comparison, fibers (micron size), micrometric flat pebble-shaped aggregates, and clusters of spherical and ovoidal aggregates (up to 300 nm in size) (Figure 4f) were formed when DMF, acetone and THF were used as the good solvents respectively.

The self-assembly results of the micellization and nanoprecipitation protocols reveal the following trends: 1) the DMF: water system favors the formation of fiber-like structures, 2) the acetone system (both with ethanol and water as selective solvent for PEG) produce sheet-like morphologies. The THF system only leads to defined aggregates when the NP approach was employed. None of these systems and self-assembly protocols afforded any control over the size, length or shape of the self-assembled aggregates.

Temperature-induced crystallization-driven self-assembly (TI-CDSA).

Temperature-induced crystallization driven self-assembly appears to be interesting to gain some control on the preparation of aggregates from crystalline-coil BCPs.[18,19] Samples leading to poorly defined structures (from the micellization and nanoprecipitation approaches) were thus selected to study the influence of a heating and ultrasound treatment followed by controlled slow cooling on their size and shape.

Closed vials containing sharp-edge ovoids (Figure 3a), fibers (Figure 3c) or platelets (Figure 3d) were placed in oil baths and heated at 70°C for 1h under stirring then placed in an ultrasound bath at the same temperature for 10 min. The solutions were slowly cooled down to room temperature at 5°C h^{-1} and aged 12h before the preparation of TEM grids.

The higher temperature increases the solubility of the aggregates in the mixed solvent media (note that all the samples were in 1:6 solvent: selective solvent mixtures). The

sonication should help to solubilize the remaining aggregates (if there were any). The slow cooling step should induce the formation of BCP aggregates. The structures observed by TEM are shown in Figure 5.

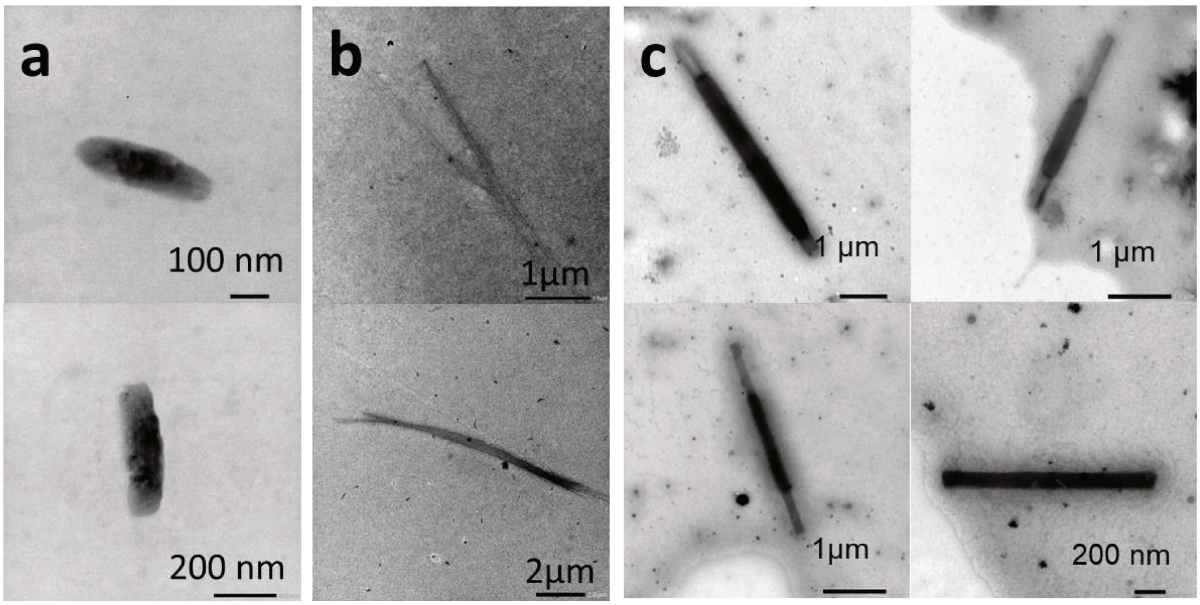

Figure 5. TEM images of the self-assembled structures obtained after micellization and thermal annealing :Images a, b and c correspond to samples 3a, 3c and 3d respectively.

The thermal annealing had significant effect on the self-assembled structures. The sharp-edge ovoids turned into smoother round edge rod-like aggregates. The crystallinity of these aggregates was confirmed by SAED measurements carried out during TEM analysis (Figure S12b). However the crystallinity of the fluoropolymer core could not be confirmed as the signals of the PEG crystals formed during the TEM grid preparation mask those of the P(VDF-*co*-HFP) copolymer (as mentioned earlier the crystallinity of PEG is much higher than that of P(VDF-*co*-HFP)). The fibers initially formed by micellization in the DMF: water system got shorter (10 µm) and isolated after the annealing process. The platelets formed in the acetone: water mixture were changed into rectangular flat rod-like structures with lengths up to 5 µm and widths between 180 and 500 nm after annealing. SAED measurement did not detect any crystallinity in this case, probably because of fast amorphisation under the microscope electron beam.

A second temperature treatment, above the melting temperature of both blocks was also investigated. The melting of the core-forming block followed by slow cooling, should also

modify the self-assembled structures and may provide some control. Octanol and THF were chosen as the selective solvent for PEG and common solvent, respectively. The nanoprecipitation protocol using this THF: octanol system led to the formation of well-defined small (10 - 25 nm) square aggregates (Figure 6a).

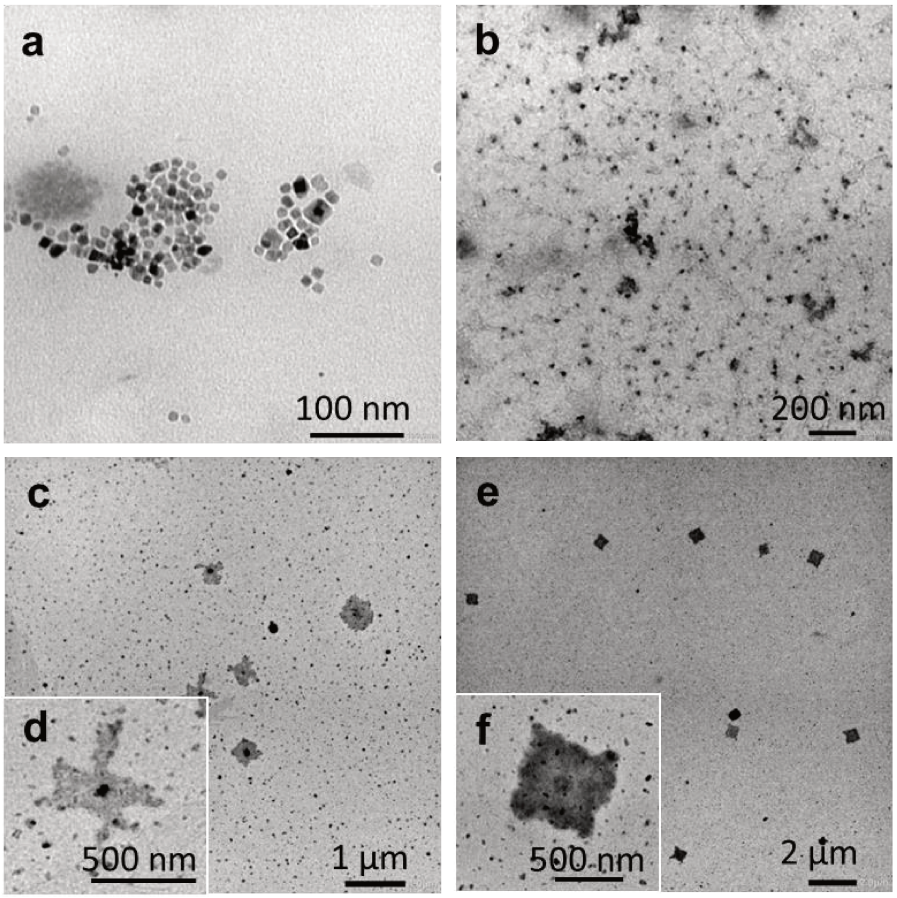

Figure 6 . TEM images of self-assembled P(VDF-*co*-HFP)-*b*-PEG-*b*-P(VDF-*co*-HFP) triblock copolymer using nanoprecipitation in octanol from a 1 mg mL^{-1} THF solution: (a) Final concentration 0.1 mg mL^{-1}. Solution heated to 180°C for 1h and slowly cooled down to room temperature. Structures observed after: (b) 0h, (c, d) 12h and (e, f) 1 week.

This suspension was then heated to 180 °C for 20 min and sonicated for 10 min to ensure the melting of the P(VDF-*co*-HFP) core forming block. The BCP suspension was then examined by TEM which revealed the presence of small ill-defined aggregates (Figure 6b), likely formed during the TEM grids preparation (due to temperature drop and drying). Then the BCP suspension was cooled down to ambient temperature at 5°C h^{-1} and TEM samples were prepared and observed after an aging period of 12h (Figure 6c and 6d) and 1 week (Figure 6e and 6f). These TEM images showed that larger square-shaped aggregates started to form after 12h and well-defined square morphologies were formed after one week of

aging. The analysis of 50 of these square morphologies allowed the determination of their average diagonal size: 764 ± 133 nm. Moreover, the TEM images suggest that these square structures potentially grew from a square seed located at the center of the final structure. During self-assembly, the larger square like crystalline structure is grown from the initial seed (the seed seen in the centre of the final morphology see Fig. 6f) and the final morphology keeps this shape (square) in good agreement with the hypothesis that the unit cell (initial seed) dictates the shape of the crystalline aggregates as described by Han and co-workers.[45] However, since the SAED patterns (Figure S12c) of these aggregates only showed signals from the PEG segments, the determination of the unit cell dimensions was not possible.

Understanding the CDSA process

Unlike other self-assembly processes, which mainly rely on the solvent affinity for the core-forming block, the formation of these nanostructures appears to be governed by the interplay between the crystallization of the P(VDF-*co*-HFP) core after annealing and the solubility of the BCP in the solvent mixtures at the annealing temperatures. Our hypothesis to understand these CDSA results is that: when good solubility is achieved, during the slow cooling step, the block copolymers present as unimers dissolved in the solvent (1-octanol or water: acetone (1:6)) crystallize slowly, thus reducing crystal defects and ultimately forming well-defined structures as in cases of Figures 5c, 6e and 6f. In contrast, when complete solubility is not attained (due to poor solubility or inefficient thermal annealing) such as in DMF/ethanol or DMF/water mixtures, the block copolymer forms bigger aggregates that eventually play the role of a seed for crystal growth (Fig. 5a and 5b). These less defined ovoidal aggregates (Figure 5a) or fibers (Figure 5b) look similar to the structures obtained before the thermal annealing (Fig. 3a and 3c respectively). In the literature, such crystal growth from a well-defined initial seed is described as epitaxial growth where a unimer exchange process takes place akin to the well-established CDSA principle.[16]

5. Conclusion

An ABA P(VDF_{51}-*co*-HFP_4)-*b*-PEG_{136}-*b*-P(VDF_{51}-*co*-HFP_4) amphiphilic triblock copolymer was synthesized using an efficient one-pot aminolysis / thia-Michael addition of a P(VDF_{51}-

co-HFP_4) prepared by RAFT and PEG diacrylate. This BCP was characterized by ^{1}H and, ^{19}F-NMR spectroscopies, GPC as well as TGA, DSC and XRD. These characterizations proved that the coupling strategy was efficient to produce a relatively well-defined (low Đ) triblock copolymer. The self-assembly behavior of this ABA triblock copolymer was studied by TEM. This study demonstrated the strong impact of the self-assembly conditions on the BCP self-assembled morphologies obtained. It is suggested that the Temperature-Induced Crystallization-Driven Self-Assembly conditions allowed the preparation of defined morphologies when the thermal annealing allowed the complete dissolution of the aggregates and the slow crystallization of the semi-crystalline core-forming block.

6. References

1. Kim, J. K., Yang, S. Y., Lee, Y. & Kim, Y. Functional nanomaterials based on block copolymer self-assembly. *Prog. Polym. Sci.* **35**, 1325–1349 (2010).

2. Smart, T. *et al.* Block copolymer nanostructures One of the most important classes of synthetic systems for creating. *Nanotoday* **3**, 38–46 (2008).

3. Mai, Y. & Eisenberg, A. Self-assembly of block copolymers. *Chem Soc Rev* **41**, 5969–5985 (2012).

4. Crassous, J. J., Schurtenberger, P., Ballauff, M. & Mihut, A. M. Design of block copolymer micelles via crystallization. *Polymer.* **62**, A1–A13 (2015).

5. Lotz, B., Kovacs, A. J., Bassett, G. A. & Keller, A. Properties of copolymers composed of one poly-ethylene-oxide and one polystyrene block. *Kolloid-Zeitschrift und Zeitschrift für Polym.* **209**, 115–128 (1966).

6. Arno, M. C. *et al.* Precision Epitaxy for Aqueous 1D and 2D Poly(ϵ -caprolactone) Assemblies. *J. Am. Chem. Soc.* **139**, 16980–16985 (2017).

7. Tao, D. *et al.* Monodisperse Fiber-like Micelles of Controlled Length and Composition with an Oligo(p-phenylenevinylene) Core via “Living” Crystallization-Driven Self-Assembly. *J. Am. Chem. Soc.* **139**, 7136–7139 (2017).

8. Yu, W., Inam, M., Jones, J. R., Dove, A. P. & O'Reilly, R. K. Understanding the CDSA of poly(lactide) containing triblock copolymers. *Polym. Chem.* **8**, 5504–5512 (2017).

9. Finnegan, J. R. *et al.* Extending the Scope of "living" Crystallization-Driven Self-Assembly: Well-Defined 1D Micelles and Block Comicelles from Crystallizable Polycarbonate Block Copolymers. *J. Am. Chem. Soc.* **140**, 17127–17140 (2018).

10. Shi, Z., Wei, Y., Zhu, C., Sun, J. & Li, Z. Crystallization-Driven Two-Dimensional Nanosheet from Hierarchical Self-Assembly of Polypeptoid-Based Diblock Copolymers. *Macromolecules* **51**, 6344–6351 (2018).

11. Shin, S. *et al.* Living Light-Induced Crystallization-Driven Self-Assembly for Rapid Preparation of Semiconducting Nanofibers. *J. Am. Chem. Soc.* **140**, 6088–6094 (2018).

12. Cha, Y. *et al.* Crystallization-Driven Self-Assembly of Metallo-Polyelectrolyte Block Copolymers with a Polycaprolactone Core-Forming Segment. *ACS Macro Lett.* 835–840 (2019).

13. Li, Z. *et al.* Glyco-Platelets with Controlled Morphologies via Crystallization-Driven Self-Assembly and Their Shape-Dependent Interplay with Macrophages. *ACS Macro Lett.* **8**, 596–602 (2019).

14. Zhang, Q. *et al.* Low length dispersity fiber-like micelles from an A–B–A triblock copolymer with terminal crystallizable poly(ferrocenyldimethylsilane) segments via living crystallization-driven self-assembly. *Polym. Chem.* (2019).

15. Guerin, G. *et al.* Lateral Growth of 1D Core-Crystalline Micelles upon Annealing in Solution. *Macromolecules* **49**, 7004–7014 (2016).

16. Inam, M. *et al.* 1D: Vs. 2D shape selectivity in the crystallization-driven self-assembly of polylactide block copolymers. *Chem. Sci.* **8**, 4223–4230 (2017).

17. Qi, H., Zhou, T., Mei, S., Chen, X. & Li, C. Y. Responsive Shape Change of Sub-5 nm Thin, Janus Polymer Nanoplates. *ACS Macro Lett.* **5**, 651–655 (2016).

18. He, X. *et al.* Complex and Hierarchical 2D Assemblies via Crystallization-Driven Self-Assembly of Poly(l -lactide) Homopolymers with Charged Termini. *J. Am. Chem. Soc.*

139, 9221–9228 (2017).

19. Qiu, H. *et al.* Uniform patchy and hollow rectangular platelet micelles from crystallizable polymer blends. *Science* **352**, 697–702 (2016).

20. Wang, J., Lu, Y. & Chen, Y. Fabrication of 2D surface-functional polymer platelets via crystallization- driven self-assembly of poly (ε -caprolactone) -contained block copolymers. *Polymer.* **160**, 196–203 (2019).

21. Ganda, S. *et al.* Two-Dimensional Self-Assembled Structures of Highly Ordered Bioactive Crystalline-Based Block Copolymers. *Macromolecules* **50**, 8544–8553 (2017).

22. Hsiao, M. S. *et al.* Crystal orientation change and its origin in one-dimensional nanoconfinement constructed by polystyrene-block-poly(ethylene oxide) single crystal mats. *Macromolecules* **41**, 8114–8123 (2008).

23. Yin, L. & Hillmyer, M. A. Disklike micelles in water from polyethylene-containing diblock copolymers. *Macromolecules* **44**, 3021–3028 (2011).

24. Yusoff, S. F. M., Hsiao, M. S., Schacher, F. H., Winnik, M. A. & Manners, I. Formation of lenticular platelet micelles via the interplay of crystallization and chain stretching: Solution self-assembly of poly(ferrocenyldimethylsilane)- Block -poly(2-vinylpyridine) with a crystallizable core-forming metalloblock. *Macromolecules* **45**, 3883–3891 (2012).

25. Zhou, H., Lu, Y., Yu, Q., Manners, I. & Winnik, M. A. Monitoring Collapse of Uniform Cylindrical Brushes with a Thermoresponsive Corona in Water. *ACS Macro Lett.* **7**, 166–171 (2018).

26. Barbosa, J. C., Dias, J. P., Lanceros-Méndez, S. & Costa, C. M. Recent advances in poly(Vinylidene fluoride) and its copolymers for lithium-ion battery separators. *Membranes.* **8**, (2018).

27. Ribeiro, C. *et al.* Electroactive poly(vinylidene fluoride)-based structures for advanced applications. *Nat. Protoc.* **13**, 681–704 (2018).

28. Yu, Y. *et al.* Biocompatibility and in vivo operation of implantable mesoporous PVDF-

based nanogenerators. *Nano Energy* **27**, 275–281 (2016).

29. Guerre, M., Schmidt, J., Talmon, Y., Améduri, B. & Ladmiral, V. An amphiphilic poly(vinylidene fluoride)-b-poly(vinyl alcohol) block copolymer: synthesis and self-assembly in water. *Polym. Chem.* **8**, 1125–1128 (2017).

30. Guerre, M. *et al.* Self-assembly of poly(vinylidene fluoride)-block-poly(2-(dimethylamino)ethylmethacrylate) block copolymers prepared by CuAAC click coupling. *Polym. Chem.* 5203–5211 (2017).

31. Lopez, G. *et al.* An amphiphilic PEG-b-PFPE-b-PEG triblock copolymer: synthesis by CuAAC click chemistry and self-assembly in water. *Polym. Chem.* **7**, 402–409 (2016).

32. Wu, Y. *et al.* Self-assembly of poly(vinylidene fluoride)–polystyrene block copolymers in solution: Effects of the length of polystyrene block and solvent compositions Effects of the length of polystyrene block and solvent compositions. *J. Saudi Chem. Soc.* **21**, 713–719 (2017).

33. Guerre, M. *et al.* Deeper Insight into the MADIX Polymerization of Vinylidene Fluoride. *Macromolecules* **48**, 7810–7822 (2015).

34. Guerre, M. *et al.* A Journey into the Microstructure of PVDF Made by RAFT. *Macromol. Chem. Phys.* **217**, 2275–2285 (2016).

35. Guerre, M. *et al.* Limits of Vinylidene Fluoride RAFT Polymerization. *Macromolecules* **49**, 5386–5396 (2016).

36. Guerre, M., Semsarilar, M., Godiard, F., Améduri, B. & Ladmiral, V. Polymerization-induced self-assembly of PVAc-b-PVDF block copolymers via RAFT dispersion polymerization of vinylidene fluoride in dimethyl carbonate. *Polym. Chem.* **8**, 1477–1487 (2017).

37. Guerre, M. *et al.* Combination of Cationic and Radical RAFT Polymerizations: A Versatile Route to Well-Defined Poly(ethyl vinyl ether)-block-poly(vinylidene fluoride) Block Copolymers. *ACS Macro Lett.* **6**, 393–398 (2017).

38. Guerre, M., Ameduri, B. & Ladmiral, V. RAFT synthesis of well-defined PVDF-b-PVAc

block copolymers. *Polym. Chem.* **7**, 441–450 (2016).

39. Apostolides, D. E. *et al.* Near-Model Amphiphilic Polymer Conetworks Based on Four-Arm Stars of Poly(vinylidene fluoride) and Poly(ethylene glycol): Synthesis and Characterization. *Macromolecules* **51**, 2476–2488 (2018).

40. Twum, E. B., McCord, E. F., Fox, P. A., Lyons, D. F. & Rinaldi, P. L. Characterization of backbone structures in poly(vinylidene fluoride- co -hexafluoropropylene) copolymers by multidimensional 19F NMR spectroscopy. *Macromolecules* **46**, 4892–4908 (2013).

41. Ameduri, B. From vinylidene fluoride (VDF) to the applications of VDF-Containing polymers and copolymers: Recent developments and future trends. *Chem. Rev.* **109**, 6632–6686 (2009).

42. Liu, X. *et al.* Enhanced Solubility of Polyvinyl Esters in scCO 2 by Means of Vinyl Tri fl uorobutyrate Monomer. *ACS Macro Lett.* **4**, 89–93 (2015).

43. Folgado, E. *et al.* "One-Pot" Aminolysis/Thiol-ene preparation of well-defined amphiphilic PVDF-b-PEG-b-PVDF triblock copolymers: Self-assembly behaviour in mixed solvents. *Polym. Chem.* (2019).

44. Guerre, M., Ameduri, B. & Ladmiral, V. One-pot synthesis of poly(vinylidene fluoride) methacrylate macromonomers via thia-Michael addition. *Polym. Chem.* **7**, 441–450 (2016).

45. Han, L. *et al.* Uniform two-dimensional square assemblies from conjugated block copolymers driven by π-π Interactions with controllable sizes. *Nat. Commun.* **9**, 1–12 (2018).

7. Supporting information.

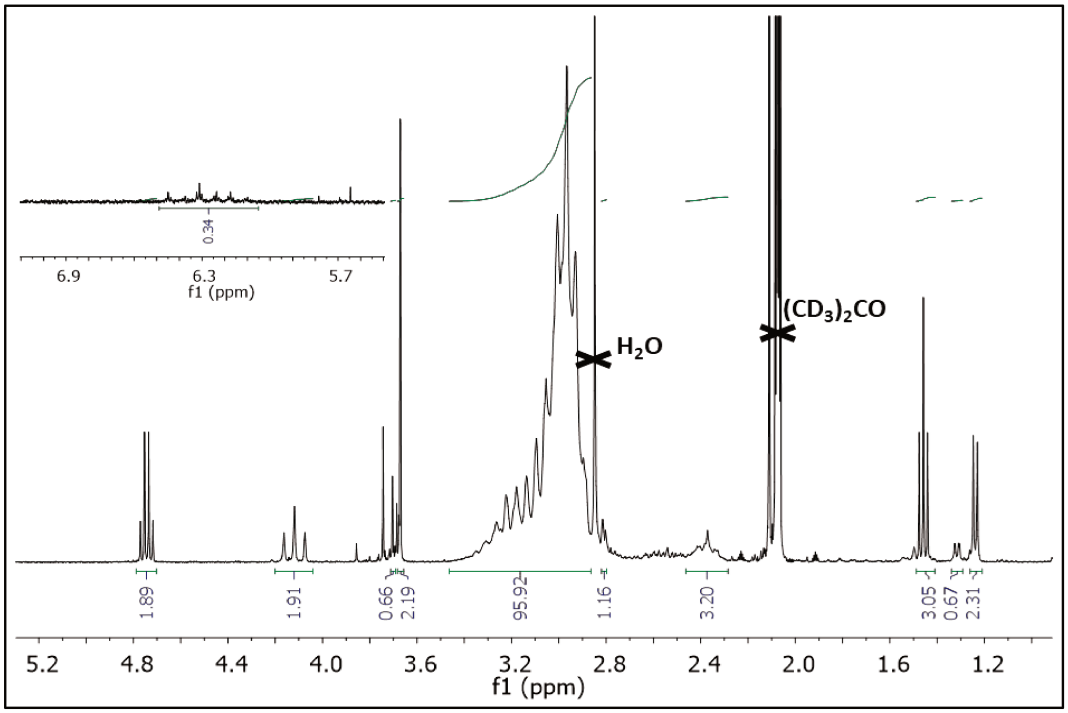

Figure S1. ^{1}H NMR spectrum ($(CD_3)_2CO$, 300 MHz) of P(VDF_{51}-*co*-HFP_4)-XA

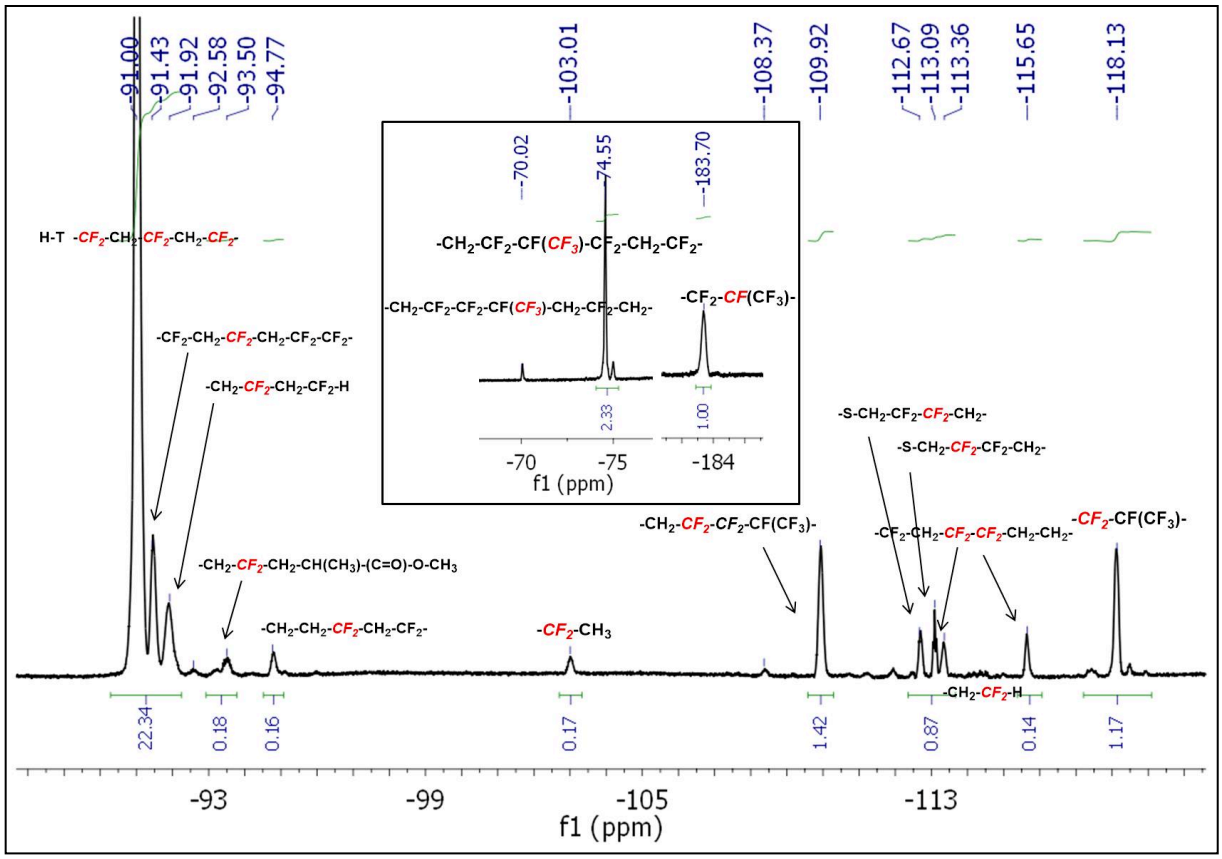

Figure S2. ^{19}F NMR spectrum ($(CD_3)_2CO$, 282 MHz) of P(VDF_{51}-*co*-HFP_4)-XA

S3. VDF and HFP %mol determination from ^{19}F NMR

*(values extracted from Fig. S2)

$$\%\, mol\ VDF = \frac{\sum \int CF_2/_2}{\sum \int CF_2/_2 + \int CF} \times 100 \quad (1)$$

With:

$$\sum \int CF_2 = \int_{-90.3}^{-91.7} CF_2\,(HT) + \int_{-91.7}^{-92.3} CF_2H + \int_{-92.9}^{-93.8} CF_2\,(R\ end\ group) + \int_{-94.6}^{-95.0} CF_2\,(HT) + \int_{-112.4}^{-113.7} CF_2(Z\ end\ group + HH) + \int_{-115.5}^{-115.9} CF_2\,(HH) \quad (2)$$

$$\%\, mol\, VDF = \frac{\frac{22.34 + 0.18 + 0.16 + 1.42 + 0.87 + 0.14}{2}}{\frac{22.34 + 0.18 + 0.16 + 1.42 + 0.87 + 0.14}{2} + 1.00} = \mathbf{92.6} \quad (3)$$

$$\%\, mol\, HFP = 100 - 92.6 = \mathbf{7.4} \quad (4)$$

S4. DP of VDF and DP of HFP determination from ^{1}H NMR data.

*(values extracted from Figure S1)

$$DP_{VDF} = \frac{\int_{2.70}^{3.19} \mathrm{CH_2\,(HT)} + \int_{2.28}^{2.43} \mathrm{CH_2(TT)} \int_{4.02}^{4.17} + \mathrm{CH_2(End\ Group)}}{\frac{2}{3} \times \int_{1.19}^{1.24} \mathrm{CH_3\,(R-CTA)}} =$$

$$DP_{VDF} = \frac{95.92 + 3.20 + 1.91}{\frac{2}{3} \times 3} = \mathbf{50.5}$$

$$DP_{HFP} = \frac{DP_{VDF} \times \%mol_{HFP}}{\%mol_{VDF}} = \mathbf{4.0}$$

S5. P(VDF-*co*-HFP) M_n Determination from NMR data

$$M_{n\,NMR} = M_n CTA + (DP_{VDF} \times M_n\, VDF) + DP_{HFP} \times M_n\, HFP$$

$$M_{nNMR} = 208.3 + 50.5 \times 64.03 + 4.0 \times 150.02 = \mathbf{4041.90\ g/mol}$$

With M_nCTA = 208.3 g/mol, M_n VDF = 64.03 g/mol and, M_n HFP = 150.02 g/mol.

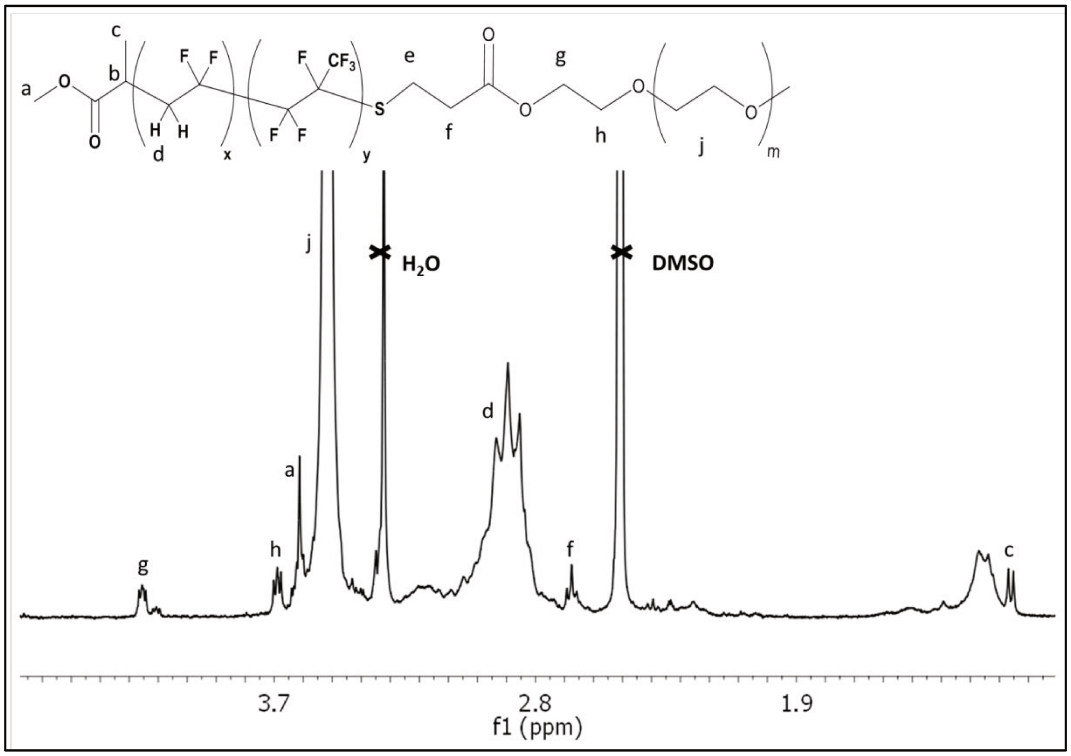

Figure S6. ^{1}H NMR spectrum ($(CD_3)_2SO$, 400 MHz) of P(VDF_{51}-*co*-HFP_4)-*b*-PEG_{136}-*b*- P(VDF_{51}-*co*-HFP_4).

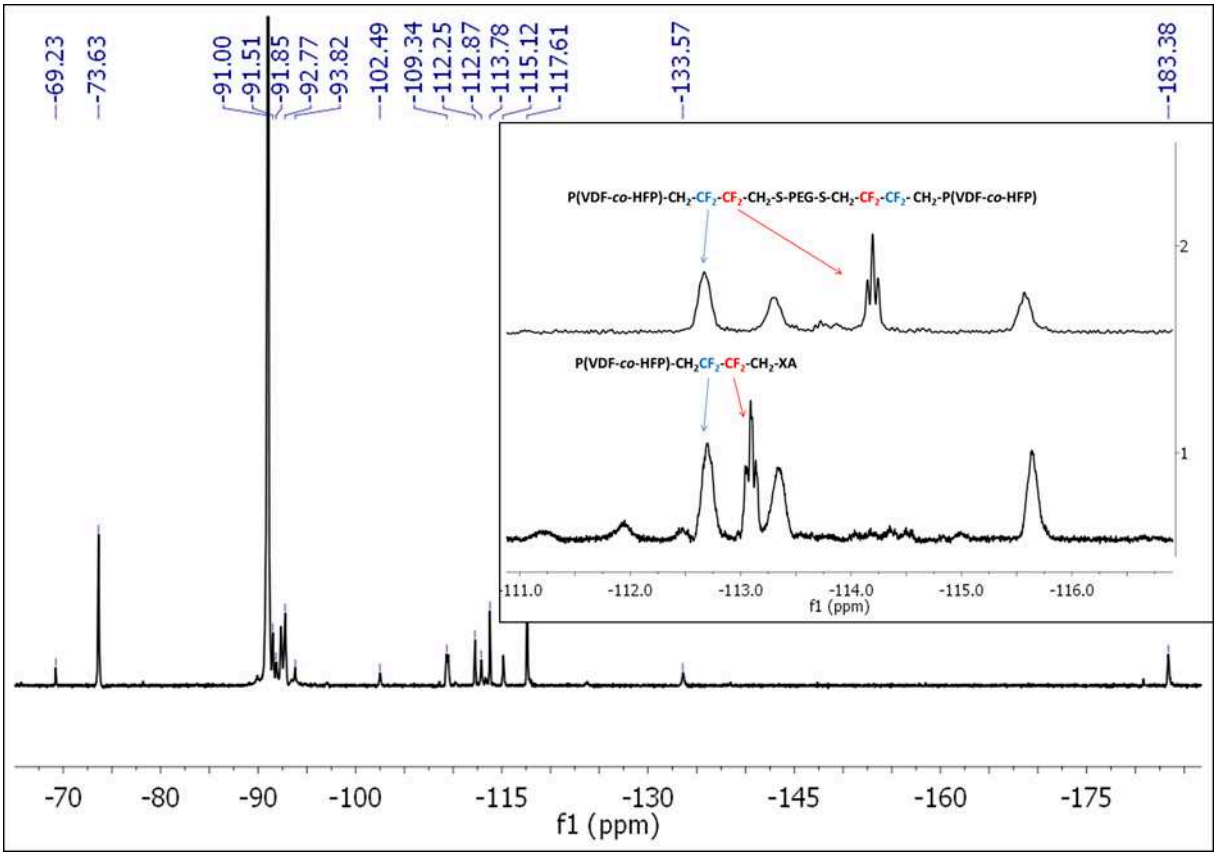

Figure S7. ^{19}F NMR spectrum ($(CD_3)_2SO$, 376 MHz) of P(VDF_{51}-*co*-HFP_4)-*b*-PEG_{136}-*b*- P(VDF_{51}-*co*-HFP_4). Inset: Shift of signals after the "one-pot" (aminolysis and thia-Michael) coupling reaction.

S8 Determination of –CH_2-CF_2H end group proportion from ^{1}H NMR.

$$(\%) - CH_2 - CF_2H = \frac{\int_{6.05}^{6.50}(-CH_2 - CF_2H + -CF_2 - CFH(CF_3) + -CF(CF_3)CF_2H)}{\frac{1}{3}\int_{1.71}^{1.87} -CF_2 - CH_3 + \int_{6.05}^{6.50}(-CH_2 - CF_2H + -CF_2 - CFH(CF_3) + -CF(CF_3)CF_2H) + \frac{1}{2}\int_{4.02}^{4.20} -CF_2 - CH_2 - XA}$$

*Data extracted from Figure S1.

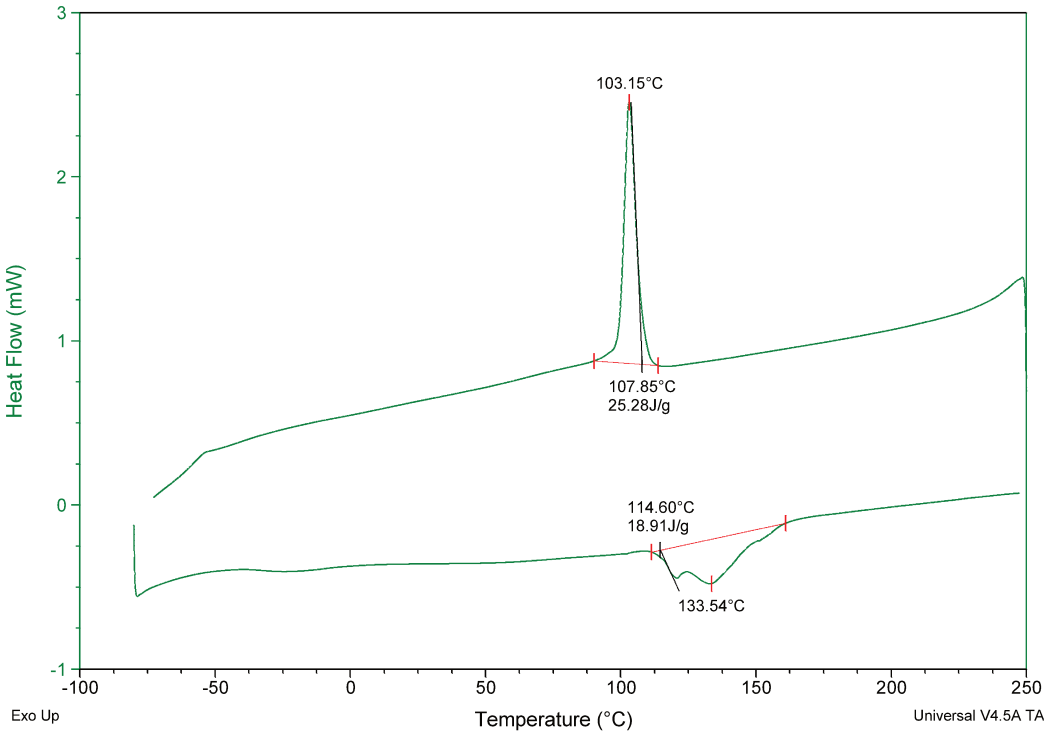

Figure S9. P(VDF-*co*-HFP) DSC thermograms. Second heating and cooling ramps.

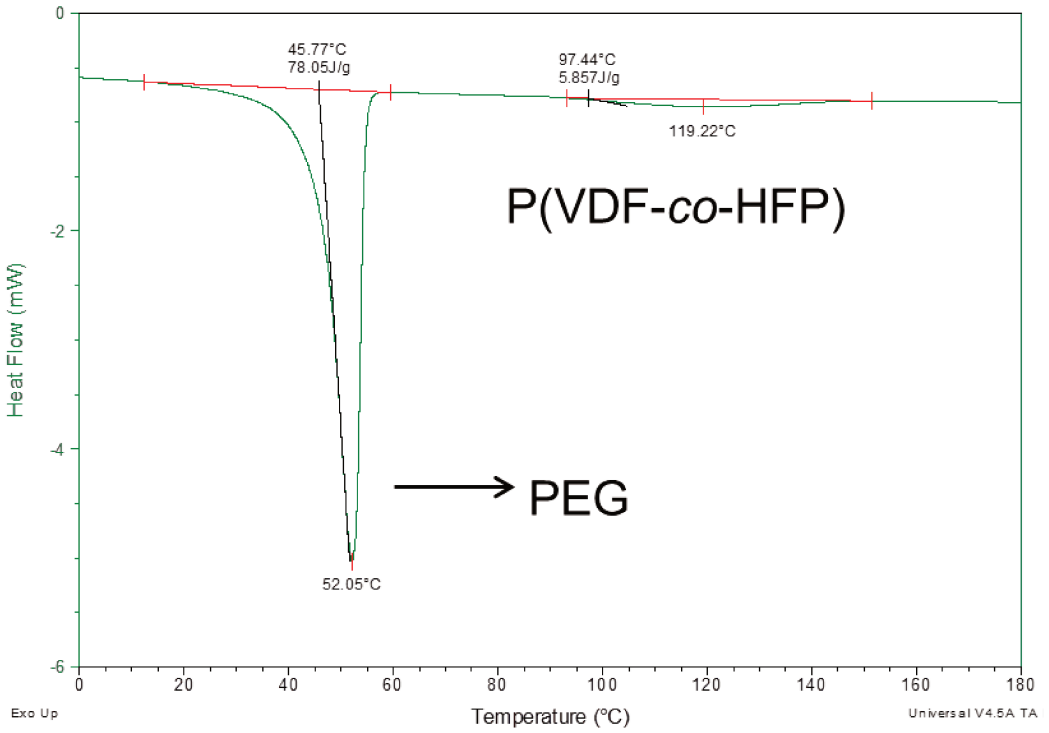

Figure S10. P(VDF-*co*-HFP)-*b*-PEG-*b*-P(VDF-*co*-HFP) DSC thermogram. Second heating ramp.

S11. Calculation of the degrees of crystallinity.

$$\chi_c(\%) = \frac{\Delta H_f}{\Delta H_{f^\circ}\, \Phi_m} \times 100$$

Where ΔH_f is heat of melting (extracted from the DSC trace) and ΔH_{f° is a reference value and represents the heat of melting if the polymer were 100% crystalline (both in J/g). Φ_m is the weight fraction of the different polymer forming the triblock copolymer.

ΔH_{f° of PVDF and PEG were extracted from the literature as 104.7 $J \cdot g^{-1}$ and 196.8 $J \cdot g^{-1}$ respectively.[46,47]

The molar mass of the triblock copolymer is estimated to be 14100 $g \cdot mol^{-1}$ and the Weight fraction of the PVDF and PEG blocks (Φ_m) are 0.56 and 0.44 respectively.

χ_c PVDF = (5.857/(104.7·0.56))x100= 9.90%

χ_c PEG = (78.05/(196.8·0.44))x100=90.10%

46. Hietala, S. et al. Structural investigation of radiation grafted and sulfonated poly(vinylidene fluoride), PVDF , membranes. J. Mater. Chem. 7, 721–726 (1997).

47. Pielichowska, K., Bieda, J. & Szatkowski, P. Polyurethane / graphite nano-platelet composites for thermal energy storage. Renew. Energy 91, 456–465 (2016).

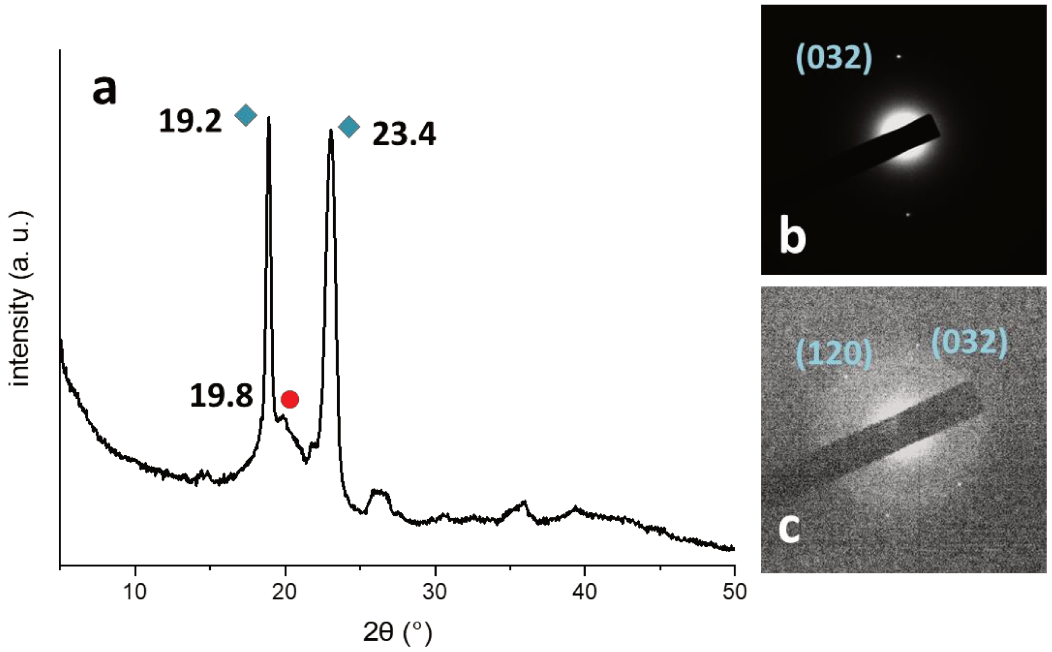

Figure S12. (a) XRD pattern of P(VDF-*co*-HFP)-*b*-PEG-*b*-P(VDF-*co*-HFP). Blue Rhombus and red dots correspond to PEG and PVDF characteristic diffraction signals respectively. (b, c) SAED patterns recorded during TEM analysis of ovoids and squares presented in figures 5a 6e and 6f respectively.

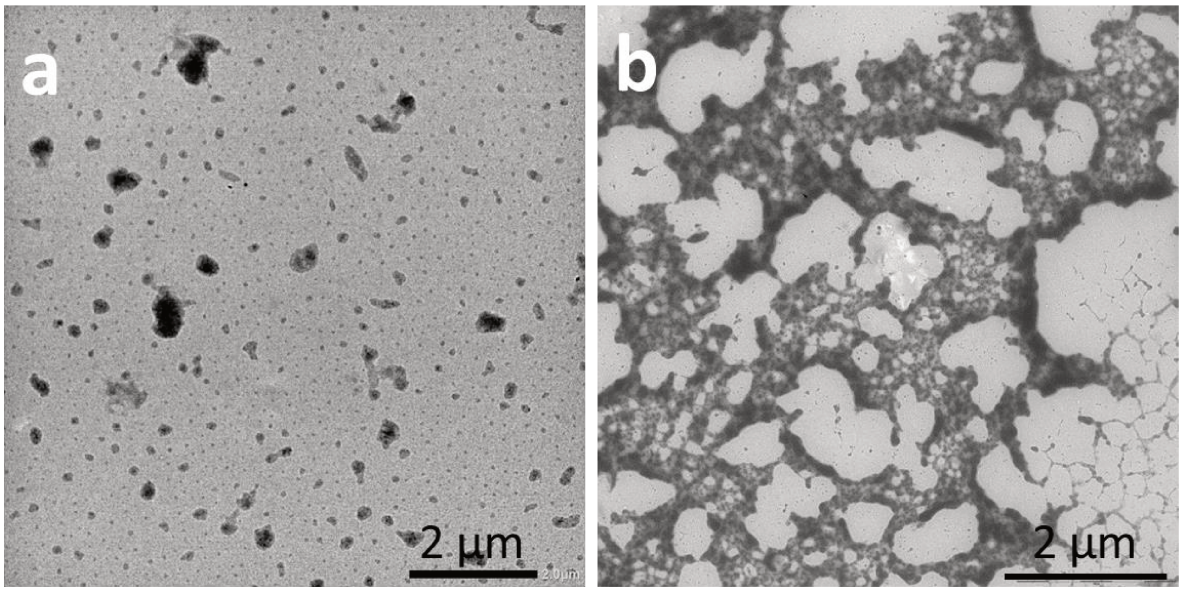

Figure S13. TEM images of self-assembled structures obtained by micellization of 1 mg mL^{-1} solutions of the P(VDF-*co*-HFP)-*b*-PEG-*b*-P(VDF-*co*-HFP) triblock copolymer in THF employing: (a) ethanol, (b) water, as selective solvent for PEG. Final concentration of all samples = 0.14 mg mL^{-1}, solvent: selective solvent final ratio=1:6.

Chapter 4

PNIPAM-*b*-PVDF amphiphilic diblock copolymer synthesis and self-assembly

In chapters two and three SAED analysis during TEM was employed in order to determine the crystallinity of the assemblies. The crystallinity of PEG block was evidenced in both cases. In the case of the triblock copolymer presented in chapter three the crystallinity of PEG was much higher than that of P(VDF-co-HFP) making difficult to determine the impact of the core forming block crystallinity on the self-assembly. In order to determine how PVDF crystallinity affects the self-assembly, a new triblock where the hydrophilic block was not crystalline was considered. For the preparation of new PVDF amphiphilic block copolymers we could either use a PVDF macroCTA and chain extend with a hydrophilic polymer or use a hydrophilic macroCTA and chain extend with VDF. The second strategy had been studied before, and it was shown that, from the monomers studied, only VAc radicals where able to reactivate PVDF chains. We decided then, to chain extend from a hydrophilic macroCTA. This approach is limited by the solubility of the macroCTA in DMC, the solvent of choice for VDF polymerization and, by the limited ability of xanthates to control the polymerization of more activated monomers (MAMs). From the macro CTAs proposed (PEG-XA, PAA-XA and PNIPAM-XA) only PNIPAM-XA was soluble in DMC. PNIPAM-*b*-PVDF BCPs synthesis, self-assembly and, decoration of the assemblies with Au NPs is described in this chapter.

PNIPAM-*b*-PVDF amphiphilic diblock copolymer synthesis and self-assembly.

Enrique Folgado,[a,b] Matthias Mayor,[b] Didier Cot,[b] Michel Ramonda,[c] Franck Godiard,[d] Vincent Ladmiral,[b*] Mona Semsarilar[a*]

[a]Institut Charles Gerhardt de Montpellier, ICGM UMR5253, Univ Montpellier, CNRS, ENSCM, Montpellier, France.

[b]Institut Européen des Membranes, IEM, UMR5635, Univ Montpellier, CNRS, ENSCM, Montpellier, France.

[c]Centre de technologie de Montpellier, CTM, Université de Montpellier, Bât. 5, cc007 Campus Saint Priest - France

[d]Service de Microscopie Electronique, Université Montpellier 2, Place Eugene Bataillon, 34095 Montpellier Cedex 5, France.

1. Abstract

PNIPAM-*b*-PVDF block copolymers (BCPs) were synthesized using PNIPAM macromolecular chain transfer agents (macro-CTAs). The polymerizations were conducted at 73 °C in DMC using two PNIPAM macro-CTAs of different molar masses and targeting various DPs of the PVDF block. The VDF RAFT polymerization experiments resulted in relatively well-defined BCPs (Đ $\leqslant$ 1.50). The obtained amphiphilic BCPs have the ability to self-assemble into varied morphologies such as spherical, crumped, lamellar and lenticular 2D aggregates by changing the common solvent or the self-assembly protocol. Size of the aggregates can be controlled by varying the DP of the PVDF block. The polymers were characterized by ^{1}H and ^{19}F NMR, SEC, TGA, DSC, and the assembled structures were studied by TEM, SEM and AFM. The thermosensitive behavior and the ability of the lenticular aggregates to immobilize Au NPs and their use for *in situ* preparation of Au NPs were also examined.

2. Introduction

Poly(vinylidenefluoride) (PVDF), despite its remarkable properties such as piezoelectricity, ferroelectricity, chemical inertness, and biocompatibility[1,2] has not received as much attention as other polymers in fields such as nanotechnology and polymer self-assembly. This is likely due to the synthesis constraints for the preparation of block copolymers that

can self-assemble into nano- or microstructures of interest for such applications (i.e. micelles, vesicles, structured thin films, etc.).

The RAFT/MADIX and Iodine-mediated polymerizations of VDF leads to the accumulation of VDF tail-terminated chains (-$CF_2CF_2CH_2$-X, X = xanthate or iodine).[3] These chains are not easily reactivated which hinders the preparation of PVDF-based block copolymers. For example, so far, only PVDF-*b*-PVAc block copolymers have been obtained by chain extension of CF_2-CH_2-XA-terminated-PVDF (XA = xanthate) made by MADIX.[4] Although, coupling strategies using click chemistry (CuAAC, or thia Michael addition for example)[5–8] are efficient, they may require the preparation of functional RAFT agents and often lead to mixtures of block copolymers and homopolymers which are not easily purified. An alternative solution is the chain extension of other MADIX polymers with PVDF.

To date, only four reports describe the preparation of PVDF-based block copolymers from RAFT macro-CTAs using sequential addition of VDF monomer. Kostov *et al.* described the synthesis of PVAc-*b*-P(VDF-*co*-TFP) block copolymers.[9] Girard *et al.* reported the preparation of either PDMA-*b*-PVDF or PDMA-*b*-P(VDF-*co*-PMVE) by chain extension of a PDMA macro-CTA.[10] Guerre *et al.* reported the preparation of PEVE-*b*-PVDF block copolymers via the sequential combination of cationic RAFT polymerization of vinyl ethers and radical RAFT polymerization of VDF.[11] Guerre *et al.* also reported the polymerization-induced self-assembly (PISA) of PVAc-*b*-PVDF block copolymers.[12] VAc units can be hydrolyzed to vinyl alcohol groups to access to poly(vinyl alcohol) (PVA) hydrophilic blocks.[13] To sum up, only PDMA- and PVA-based PVDF-containing amphiphilic block copolymers have been prepared by sequential addition of VDF.

It is now well-established that xanthates and dithiocarbamates[11] are RAFT agents of choice for controlling the polymerization of LAM monomers such as vinyl acetate,[14] *N*-vinylpyrrolidone (NVP), or *N*-vinyl caprolactam.[14,15] Xanthates were also recently successfully used for the polymerization of MAMs such as acrylamides[16,17] and acrylic acid.[18–20]

One limitation of the chain extension by PVDF approach to prepare amphiphilic PVDF-based block copolymers is the rather low solubility of hydrophilic macro-CTAs in dimethyl carbonate (DMC) (the solvent) leading to low amount of transfer reactions while maintaining a high rate of polymerization.[21,22]

Poly(*N*-isopropyl acrylamide) (PNIPAM) is hydrophilic and soluble in DMC at the required temperature for VDF polymerization (ca. 70 ° C). Nowadays, PNIPAM and its copolymers receive a lot of attention from the polymer community.[23–27] PNIPAM with a near body lower critical solution temperature value (LCST = 32 °C), and biocompatibility makes it very appealing for biomedical applications. Nevertheless, references including both PVDF and PNIPAM only describe blends of those polymers for the preparation of electrospun fibers or flat membranes, or the grafting of PNIPAM on PVDF membranes.[28] To date, no references are dealing with the preparation of PNIPAM-*b*-PVDF block copolymers (BCPs) and the study of their self-assembly in selective solvents.

This study presents the RAFT sequential monomer addition of VDF using PNIPAM macro-CTAs to afford amphiphilic diblock copolymers. The BCPs were characterized by ^{1}H and ^{19}F nuclear magnetic resonance (NMR) spectroscopies and gel permeation chromatography (GPC). The morphologies obtained by the self-assembly of the BCPs in mixed solvents were analyzed using dynamic light scattering (DLS), transmission electron microscope (TEM), scanning electron microscopy (SEM), and atomic force microscopy (AFM). Moreover, the capability of the self-assembled structures to immobilize gold nanoparticles (Au NPs) was also studied.

3. Experimental section

3.1. Materials

All reagents were used as received unless otherwise stated. 1,1-Difluoroethylene (vinylidene fluoride, VDF) was supplied by Arkema (Pierre-Bénite, France). *O*-Ethyl-*S*-(1-methoxycarbonyl) ethyldithiocarbonate (CTA_{XA}) was prepared according to the method described by Liu *et al*.[29] *tert*-Amyl peroxy-2-ethylhexanoate (Trigonox

121, purity 95%) was purchased from AkzoNobel (Chalons-sur-Marne, France). PBS stabilized gold nanoparticles (10 and 50 nm), sodium tetrachloroaurate(III) dihydrate ($NaAuCl_4 \cdot 2H_2O$), ethanol (EtOH), dimethyl carbonate (DMC), diethyl ether, toluene, laboratory reagent grade hexane (purity >95%), *N*-isopropylacrylamide (NIPAM, purity 97%) were purchased from Sigma Aldrich. All deuterated solvents were purchased from Eurisotop. NIPAM was recrystallized twice from hexane/toluene (10/1, v/v).

3.2. Measurements

Nuclear Magnetic Resonance (NMR). The NMR spectra were recorded on a Bruker AV III HD Spectrometer (400 MHz for ^{1}H and 376 MHz for ^{19}F).

Coupling constants and chemical shifts are given in hertz (Hz) and parts per million (ppm), respectively. The experimental conditions for recording ^{1}H and ^{19}F NMR spectra were as follows: flip angle, 30°; acquisition time, 4s (2s for ^{19}F NMR); pulse delay, 1 s (2s for ^{19}F NMR); number of scans, 16; and pulse widths of 9.25 and 11.4 µs for ^{1}H and ^{19}F NMR, respectively.

Size-Exclusion Chromatography (SEC). Size exclusion chromatograms were recorded using a Triple detection GPC system from Agilent Technologies with its corresponding Agilent software, dedicated to multi-detector GPC calculation. The system used two ResiPore 3µm 300 x 7.5 mm columns with DMF as the eluent with a flow rate of 1 mL/min and toluene as flow rate marker. The detectors were a PL0390-06034 capillary viscometer and a 390-LC PL0390-0601 refractive index detector. The entire SEC-HPLC system was thermostated at 35°C. Low dispersity PMMA standards were used for the calibration. Typical sample concentration was 10 mg/mL.

Differential Scanning Calorimetry (DSC). DSC measurements were performed on 2–3 mg samples on a TA Instruments DSC Q20 equipped with an RCS90 cooling system. For all measurements, the following heating / cooling cycle was employed: cooling from 40 °C to −73°C, isotherm at - 73 °C for 5 min, first heating ramp from −73 °C to 200 °C at 10 °C/min, isotherm at 200 °C for 5 min, cooling stage from 200 °C to −73 °C at 10 °C/min, isotherm plateau at −73 °C for 1 min, second heating ramp from −73 °C

to 200 °C at 10 °C/min, isotherm at 200 °C for 1 min, and last cooling stage from 200 °C to 40 °C. Calibration of the instrument was performed with noble metals and checked before analysis with an indium sample. Melting points were determined at the maximum of the enthalpy peaks.

Thermogravimetric analysis (TGA). TGA analyses were carried out with a TA Instruments TGA G500 from 20 °C to 800 °C. A heating rate of 10 °C min^{-1} was used under air atmosphere with a flow rate of 60 mL min^{-1}. Dry sample weight of 3 mg was used.

Dynamic light scattering (DLS). DLS measurements of polymer solutions were carried out in a Malvern ZEN1600 using a quartz cuvette. Refractive indices of solvent mixtures were determined using the following equation:

$$\frac{{n_m}^2 - 1}{{n_m}^2 + 2} = y_1 \frac{{n_1}^2 - 1}{{n_1}^2 + 2} + y_2 \frac{{n_2}^2 - 1}{{n_2}^2 + 2}$$

(Equation X1)

Where n_1, n_2, n_m are the solvent 1, solvent 2 and, mixture refractive indices at a certain temperature, and y_1, y_2 are solvent 1 and solvent 2 volume fractions. Viscosities of solvent mixtures where extracted from scientific publications[30,31] and online resource.[32]

Transmission electron microscopy (TEM). TEM studies were conducted using a JEOL 1400+ instrument equipped with a numerical camera, operating with a 120 kV acceleration voltage at 25 °C. To prepare TEM samples, a drop (10.0 µL) of micellar solution was placed onto a Formvar/carbon coated copper grid for 60 s, blotted with filter paper and dried under ambient conditions. All TEM grids were prepared from self-assembly solutions without further dilution.

Scanning electron microscopy (SEM). SEM analyses were conducted using a Hitachi S-4500 instrument operating at spatial resolution of 1.50 nm at 15 kV energy. The samples were folded on a 45° SEM Mount after being coated with an ultrathin layer of electrically conducting Platinum deposited by high-vacuum evaporation.

Atomic force microscopy (AFM). AFM images were obtained using a Nanoman V from Bruker Instrument employing repulsive-Tapping mode , and a tip Nanosensors PPP NCL freq = 158kHz Q factor = 350, k ~14N/m, R_{tip} ~5nm

3.3. Synthesis

PNIPAM-XA synthesis.

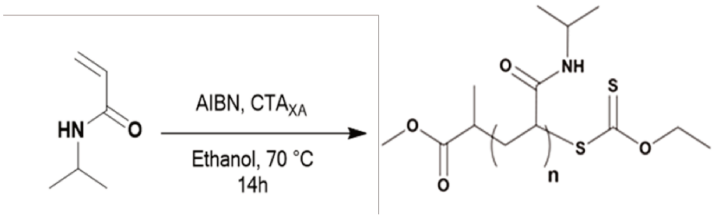

Scheme 1. RAFT/MADIX synthesis of PNIPAM macro CTA.

NIPAM (6 g), AIBN (25 mg) and CTA_{XA} (315 mg) were dissolved in ethanol (9 mL) in a round bottom flask, under magnetic stirring at 20 °C. The solution was degassed by N_2 bubbling for 20 min. Then, the flask was placed in an oil bath at 70 °C for 14h. The reaction was followed by ^{1}H NMR and was stopped at NIPAM conversion > 99 %. The polymer was isolated by precipitation in chilled ether and centrifugation and was dried overnight under vacuum at 30°C.

^{1}H NMR (400 MHz, $(CD_3)_2CO$, δ (ppm), Figure S1): 0.9 – 1.28 (m, -NH-CH(C**H$_3$**)$_2$), 1.28 - 1.90 (m, -C**H$_2$**-CH-(C=O)), 1.90 – 2.50 (m, -CH$_2$-C**H**-(C=O)), 3.64 (-O-C**H$_3$**, (R CTA)) 3.95 – 4.25 (m, -NH-C**H**(CH$_3$)$_2$), 4.50 – 4.76 (O-C**H$_2$**-CH$_3$ (Z CTA)), 6.50 – 8.00 (m, -N**H**-CH(CH$_3$)$_2$).

PNIPAM-*b*-PVDF synthesis.

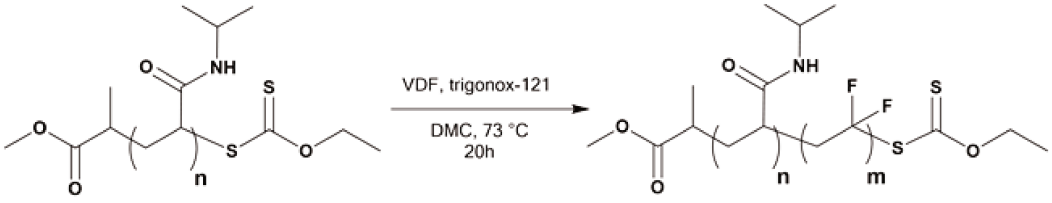

Scheme 2. RAFT/MADIX synthesis of PNIPAM-*b*-PVDF block copolymers using PNIPAM macro CTA.

Thick 8 mL Carius tubes containing PNIPAM-XA, DMC and the initiator (Trigonox-121) were sonicated for 5 min or until complete dissolution of PNIPAM-XA. Then, the tube was degassed with three freeze-pump-thaw cycles to remove oxygen. The gaseous VDF monomer (1 g) was transferred into the Carius tube and condensed in the tube using a liquid nitrogen bath. The tubes were then sealed, before being placed horizontally in a shaking water bath thermostated at 73 °C (see Scheme S1). After 20 hours, the tube was placed into a liquid nitrogen bath and the opened. After return to room temperature, the crude sample was precipitated twice in a tenfold excess of chilled pentane. The PNIPAM-*b*-PVDF block copolymers were recovered by centrifugation at 4000 rpm for 5 min in 50 mL conical centrifuge tubes. The polymers were dried overnight under vacuum at 25 °C. Polymerization yields were determined gravimetrically (mass of dried precipitated polymers / mass of monomer introduced in the Carius tube).

^{1}H NMR (400 MHz, $(CD_3)_2CO$, δ (ppm), Figure S2): 0.90 - 1.26 (m, -NH-CH(C**H$_3$**)$_2$-), 1.28 - 1.90 (m, -C**H$_2$**-CH-NIPAM), 1.90 - 2.50 (m, -CH$_2$-C**H**-NIPAM), 2.16 - 2.37 (t, -CF$_2$-C**H$_2$**-C**H$_2$**-CF$_2$-, VDF-VDF HH reverse addition), 2.66 - 3.01 (t, -CF$_2$-C**H$_2$**-CF$_2$-, VDF-VDF HT regular addition), 3.8 (s, C**H$_3$**-O-(C=O)-(CH$_3$)CH-), 3.95 - 4.25 (m, -NH-C**H**(CH$_3$)$_2$), 4.30 - 4.39 (t, CH$_2$-CF$_2$-CF$_2$-C**H$_2$**-S-, $^{3}J_{HF}$ = 6.5 Hz), 4.60 - 4.78 (q, -S(C=S)OC**H$_2$**-CH$_3$, $^{3}J_{HH}$ = 7.1 Hz), 6.09 - 6.50 (tt, -CH$_2$-CF$_2$-**H**, $^{2}J_{HF}$ = 55.6 Hz , $^{3}J_{HH}$ = 4.7 Hz), 6.50 – 8.00 (m, -N**H**-CH(CH$_3$)$_2$).

^{19}F NMR (376 MHz, $(CD_3)_2CO$, δ (ppm), Figure S3): -115.64 (-CH$_2$-CF$_2$-C**F$_2$**-CH$_2$-CH$_2$-, VDF-VDF HH reverse addition), -114.45- (-CH$_2$-C**F$_2$**-H), -113.36 (-CH$_2$-C**F$_2$**-CF$_2$-CH$_2$-CH$_2$-, HH reverse addition), -113.09 (CH$_2$-CF$_2$-C**F$_2$**-CH$_2$-S-), -112.69 (-CH$_2$-C**F$_2$**-CF$_2$-CH$_2$-S-), -107.40 (-C**F$_2$**-CH$_3$) -94.81 (-CH$_2$-CH$_2$-C**F$_2$**-CH$_2$-, TT reverse addition), -93.00 (CH$_3$-O-(C=O)-O-CH$_2$-CH$_2$-C**F$_2$**-, DMC-initiated PVDF), -92.50 (PNIPAM-CH$_2$-C**F$_2$**-), 92.06 (-CH$_2$-C**F$_2$**-CH$_2$-CF$_2$H), -91.43 (-CH$_2$-CH$_2$-CF$_2$-CH$_2$-C**F$_2$**-CH$_2$-CF$_2$-, regular VDF-VDF HT addition), -91.00 (-CH$_2$-C**F$_2$**-CH$_2$-, regular VDF-VDF HT addition).

DP and M_n calculations using NMR.

The calculation of the degrees of polymerization of the PNIPAM macro-CTA was done using the following equation:

$$DP_{PNIPAM-XA} = \frac{\frac{1}{6}\int_{0.9}^{1.28}\text{-}NH\text{-}CH(\boldsymbol{CH_3})_2 + \frac{1}{2}\int_{1.28}^{1.90}\boldsymbol{CH_2}\text{-}CH(C\text{-}O) + \int_{1.90}^{2.50}\text{-}CH_2\text{-}\boldsymbol{CH}(C\text{-}O) + \int_{3.95}^{4.25}\text{-}NH\text{-}\boldsymbol{CH}(CH_3)_2 + \int_{6.50}^{8.00}\text{-}\boldsymbol{NH}\text{-}CH(CH_3)_2}{\frac{5}{2}\int_{4.5}^{4.76}\text{-}\boldsymbol{CH_2}\text{-}CH_3(CTA)} \quad (2)$$

$$M_{n,theo} = \frac{[NIPAM]_0}{[CTA]_0} \times Yield \times M_{n,NIPAM} + M_{n,CTA-XA} \quad (3)$$

$$M_{n,PNIPAM-XA} = M_{n,CTA-XA} + DP_{PNIPAM-XA} \times M_{n,NIPAM} \quad (4)$$

With $M_{n,NIPAM-XA}$= 113.16 g.mol^{-1}, and $M_{n,CTA-XA}$= 208.29 g.mol^{-1}.

The degree of polymerization of the PVDF block can be calculated from the ^{1}H NMR spectrum of the purified BCP using the integrals of the signals (at 0.9 – 1.28 ppm) corresponding to the methyl groups (-C**H$_3$**) of the NIPAM units, as reference, and the integral of the signals of the -C**H$_2$**- group of the normal (HT) VDF additions (at 2.70–3.19 ppm). The signal of the -CH_3 of the NIPAM unit is the only signal visible for BCP with a DP higher than 150. Regarding the reverse (TT) VDF additions, the average number of monomer additions occurring per chain between two degenerative transfers increases with increasing $[VDF]_0/[CTA]_0$ initial ratio. However, the total amount of HH VDF additions (intra-chain + chain-end) stabilizes to identical proportion (ca. 4.1%) for PVDF homopolymerization as previously reported by our group.[3] As the signals assigned to those inversions overlap with signals of the PNIPAM macro-CTA, a 1.041 multiplying factor was employed for the determination of the DP of PVDF.

$$DP_{PVDF} = \frac{\frac{1}{2}\int_{2.70}^{3.19}\text{-}\boldsymbol{CH_2}(\text{HT VDF additions})}{\frac{1}{6}\int_{0.9}^{1.28}\text{-}NH\text{-}CH(\boldsymbol{CH_3})_2} \times 1.041 \quad (5)$$

Molar masses were then calculated using equation (6) (with $M_{n,PNIPAM–XA}$ calculated using eqn (4) and (2)):

$$M_{n,NMR} = M_{n,PNIPAM-XA} + DP_{PVDF} \times M_{n,VDF} \quad (6)$$

Theoretical molar masses were calculated using equation (6) with yield = conversion and the $[VDF]_0/[PNIPAM–XA]_0$ ratios listed in Table 1.

$$M_{n,theo} = \frac{[VDF]_0}{[PNIPAM-XA]_0} \times Yield \times M_{n,VDF} + M_{n,PNIPAM-XA} \quad (7)$$

With Mn_{VDF} = 64.03 g mol^{-1}.

3.4. Self-assembly

Preparation of block copolymer solutions

Stock solutions of 2 mg mL^{-1} of block copolymer were prepared in DMF, acetone or THF at room temperature using magnetic stirring until full solubilisation.

Nanoprecipitation

Glass vials containing 2 mL of non-solvent and a magnetic bar were placed on a stirring plate. To each vial 0.1 mL of block copolymer solution (2 mg mL^{-1}) in DMF were added dropwise. After 1h of stirring, samples were analysed by DLS and TEM. Final concentration of 0.1 mg mL^{-1} in DMF: water (1:20).

Micellization

Vials containing 0.5 mL of the stock solutions (2 mg mL^{-1}) in different solvents (THF, DMF and acetone) were placed on a stirring plate. Water (2, 3 or 4 mL) was added dropwise using a syringe pump at a fixed rate of (4 mL h^{-1}). 10 µL were taken to prepare TEM samples at 1:4, 1:6 and 1:8 solvent / non-solvent ratios.

3.5. Immobilisation of Au NPs

Immobilisation of Au NPs on BCP nanoaggregates.

A solution of $PNIPAM_{35}$-*b*-$PVDF_{450}$ self-assembled from a 2 mg mL^{-1} acetone solution was prepared (using water as non-solvent) with final concentration of 0.4 mg mL^{-1} in acetone: water (1:4) solvent mixture (non-solvent addition rate of 4 mL h^{-1}). Acetone was removed under vacuum using a rotary evaporator at room temperature. To 1 mL of this solution, 200 µL of Au NPs (10 nm diameter) in 0.1 mM PBS was added and the mixture was stirred for 30 min at room temperature.

In-situ synthesis of Au NPs using UV reduction of $NaAuCl_4$ in the presence of BCP nanoaggregates.

A solution of 0.05 mg mL^{-1} of $NaAuCl_4$ in water was used in the self-assembly procedure using the protocol described above. Once the 1:4 solvent: non-solvent ratio was reached, the solution containing the gold salt and BCP nanoaggregates were placed in UV light chamber (6 U36W-411 lamps; UV-C, λ = 254 nm) for 30 minutes. At the end of this period the reaction mixture had turned purple indicating the formation of gold nanoparticles.

4. Results and discussion

PNIPAM-XA macro CTAs were synthesized by RAFT polymerization using CTA_{XA} following protocols described previously by Sistach *et al.*[33] The reactions were stopped when the NIPAM conversion reached at least 99%. After purification by precipitation, ^{1}H NMR spectroscopy of the resulting PNIPAM-XA macroCTAs was employed to determine their molar masses and degrees of polymerization. Amphiphilic PVDF-based block copolymers with different PVDF degrees of polymerization were prepared from these PNIPAM macro-CTAs (see Table 1) by chain extension with VDF in DMC (a common solvent for PNIPAM and PVDF allowing relatively high rate of VDF polymerization) using Trigonox 121 as the radical initiator.

Table 1. Synthesis and characterization of PNIPAM macro-CTA, and PNIPAM-*b*-PVDF block copolymers prepared by RAFT polymerization of VDF in DMC at 73 °C.

Entry	CTA	M	$[M]_0$ / $[CTA]_0$	Reaction time (h), Solvent	yield(%)	$DP_{(NMR)(R)}$	$M_{n(theo)}$[d] (g/mol)	$M_{n(NMR)(R)}$[e] (g/mol)	M_{nSEC}[f] (g/mol)	Đ[f]
1	CTA_{XA}	NIPAM	25	14, EtOH	>99	25[a]	3000	3000	3200	1.30
2	$PNIPAM_{25}$-XA	VDF	50	20, DMC	60[b]	35[c]	4900	5300	6700	1.38
3	CTA_{XA}	NIPAM	35	14, EtOH	>99	35[a]	4100	4200	4400	1.19
4	$PNIPAM_{35}$-XA	VDF	100	20, DMC	60[b]	60[c]	8000	8000	7500	1.29
5	$PNIPAM_{35}$-XA	VDF	150	20, DMC	61[b]	100[c]	10000	10600	9200	1.36
6	$PNIPAM_{35}$-XA	VDF	200	20, DMC	62[b]	150[c]	12100	13800	9800	1.43
7	$PNIPAM_{35}$-XA	VDF	600	20, DMC	61[b]	450[c]	27600	33000	25500	1.50

Reactions conditions: *(i)* (entry 1 and 3) NIPAM homopolymerization: $[I]/[CTA_{XA}]$ = 0.1 with I = AIBN and CTA_{XA} = *O*-ethyl-*S*-(1-methoxycarbonyl)ethyldithiocarbonate, T = 70 °C; *(ii)* (entries 2 and 4-7) chain extension of $PNIPAM_{35}$-XA : $[I]/[CTA_{XA}]$ = 0.2 with I = Trigonox 121, T = 73 °C. [a]Determined by ^{1}H NMR using equation (2). [b]Determined gravimetrically. [c]Determined by ^{1}H NMR using equation (5). [d]Calculated using yield as conversion and equations (3) for PNIPAM and (7) for the BCP. [e]Calculated from DP_{NMR} using equations (4) for PNIPAM and (6) for PVDF. [f]Determined by SEC (RI detector).

^{19}F NMR spectroscopy of the resulting polymers showed the successful chain extension of PVDF from the PNIPAM macro-CTAs. The presence of the –C**F$_2$**-C**F$_2$**-CH$_2$-XA signals at δ = -113.09 ppm and -112.69 ppm (see Figure S3) indicates the formation of the diblock copolymers.

As expected, the polymerization of VDF was accompanied by a non-negligible amount of transfer to DMC. The characteristic signals of these transfer reactions can be observed in the ^{1}H NMR spectrum (Figure S2a) as a triplet of triplets at 6.3 ppm corresponding to the $-CF_2\mathbf{H}$ chain-end, and in the ^{19}F NMR (Figure S3) spectrum as a multiplet at -107.3 ppm corresponding to the C**F$_2$**CH$_3$ chain end. The ^{1}H NMR spectrum also shows a singlet at 5.77 ppm assigned to the $CH_3O(C=O)O-C\mathbf{H_2}-XA$ (DMC – xanthate adduct), a well-defined triplet at 4.35 ppm and a singlet at 3.73 ppm assigned to the $-CH_2-$ and $-CH_3$ groups of the DMC moieties of the DMC-initiated-PVDF chains, respectively. The RAFT polymerization of VDF is accompanied by a progressive loss of chain-end functionality (loss of xanthate group). This phenomenon has been reported for the synthesis of PVAc-*b*-PVDF BCPs.[12] The short DMC–xanthate adducts are removed from the final polymer upon purification by precipitation (Figure S2b).

Despite these transfer reactions and loss of functionality, the chain extension of PNIPAM macro-CTAs with PVDF produced relatively well-defined BCP with dispersity below 1.50 and monomodal SEC traces without shoulders or significant tailing (Figure 1). These SEC traces also show a clear shift towards higher molar masses with the increasing DP of PVDF.

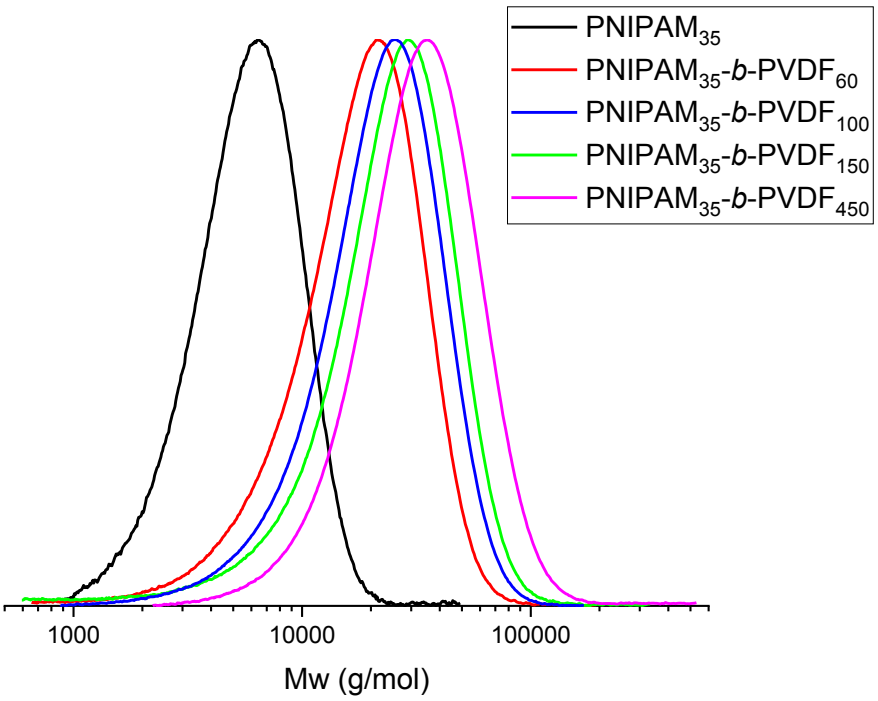

Figure 1. Normalized SEC traces (viscometric detector) of: $PNIPAM_{35}$-XA (black trace), $PNIPAM_{35}$-*b*-$PVDF_{60}$ (red trace), $PNIPAM_{35}$-*b*-$PVDF_{100}$ (blue trace), $PNIPAM_{35}$-*b*-$PVDF_{150}$ (green trace) and $PNIPAM_{35}$-*b*-$PVDF_{450}$ (pink trace) after purification by precipitation in chilled ether (for PNIPAM) and cold pentane (for BCPs).

These amphiphilic block copolymers were then used to prepare self-assembled morphologies in different of solvents.

Self-assembly of amphiphilic BCP using rapid solvent exchange usually lead to the formation of colloidal objects via micro phase separation. The final structure of these block copolymer colloids is primarily dictated by the volume fraction of the blocks and by the interfacial surface tensions. A feature of the nanoprecipitation process is the ability to access kinetically trapped morphologies in nonequilibrium states due to its significantly faster mixing times. This kinetic trapping is even more pronounced in the case of semicrystalline polymer such as PVDF. In such case, the PVDF segments often crystallize before the polymer chains can reach the equilibrium morphology during phase separation.

The self-assembly of the PNIPAM-*b*-PVDF block copolymers was achieved via nanoprecipitation in water of a DMF BCP solution. After 1h of stirring, samples were analyzed by DLS and TEM. This approach led to the formation of spherical aggregates of roughly 20 to 60 nm in diameter (Figure 2).

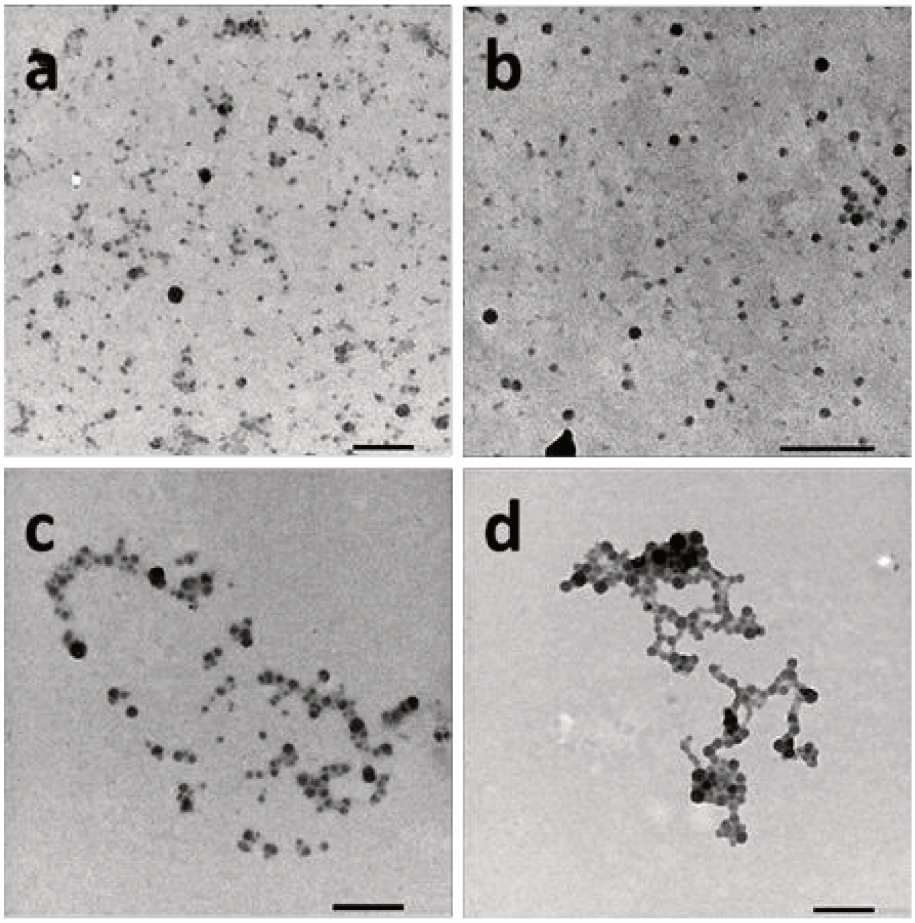

Figure 2. TEM images of spherical aggregates prepared from (a) $PNIPAM_{35}$-*b*-$PVDF_{60}$, (b) $PNIPAM_{35}$-*b*-$PVDF_{100}$, (c) $PNIPAM_{35}$-*b*-$PVDF_{150}$ and (d) $PNIPAM_{35}$-*b*-$PVDF_{450}$. All samples were prepared by nanoprecipitation in water from BCP solutions in DMF at 2 mg mL^{-1} (final concentration = 0.1 mg mL^{-1} in DMF: water (1:20). Scale bars correspond to 200 nm.

The particle sizes measured by TEM were in good agreement with the average hydrodynamic diameters measured by DLS (Figure S4) ranging between 30 and 80 nm and increasing with the DP of the core-forming block (PVDF).

Micellization experiments (slow addition of water into a solution of $PNIPAM_{35}$-*b*-$PVDF_X$ in DMF, THF or acetone) were also performed using three (1:4, 1:6 and 1:8) solvent: non-solvent ratios.

When DMF was employed as common solvent and water as selective solvent for the PNIPAM block, irregular crumpled spherical aggregates were obtained at all of the solvent: non-solvent ratios (Figure 3).

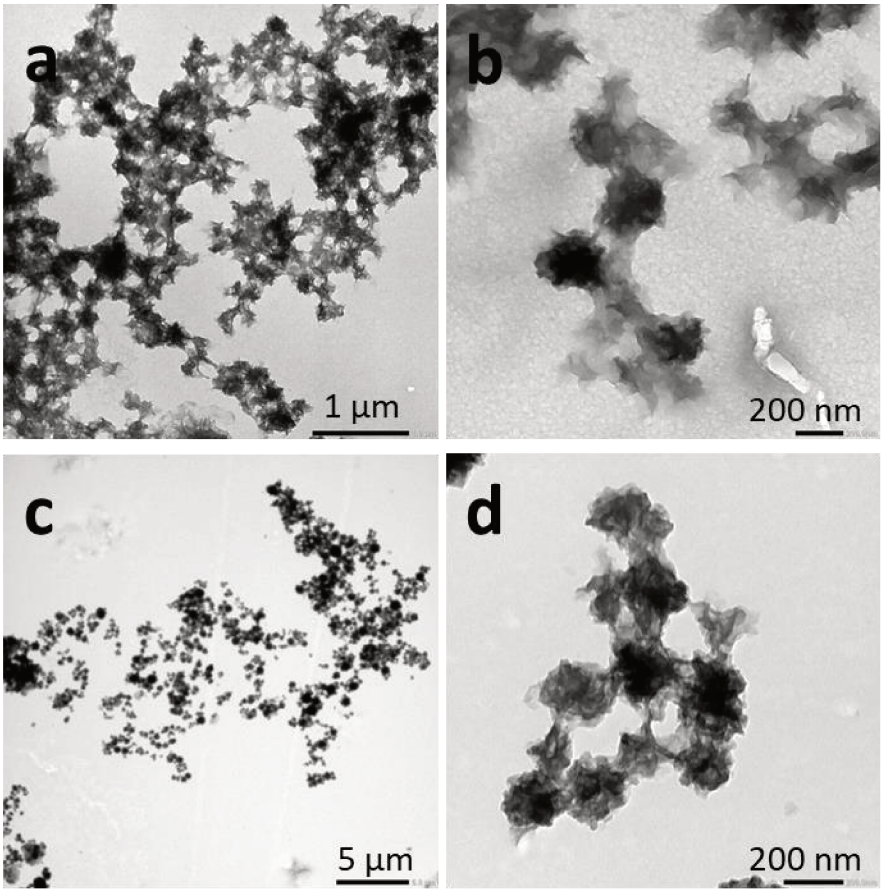

Figure 3. TEM images of crumpled aggregates obtained from micellization of (a and b) $PNIPAM_{25}$-*b*-$PVDF_{35}$, and (b and c) $PNIPAM_{35}$-*b*-$PVDF_{450}$ in DMF at 2 mg mL^{-1}. Final concentration = 0.4 mg mL^{-1} in DMF: water (1:4) mixture.

When the rate of addition of water (the selective solvent for PNIPAM) was increased tenfold (40 mL h^{-1}) spherical aggregates were formed along with the crumpled morphologies (Figure 4). These results suggest that the crumpled spherical morphologies maybe equilibrium morphologies since they form at relatively slow solvent exchange rate. These

crumpled morphologies are, also formed at very slow rate (0.5 mL h^{-1}) of non-solvent addition.

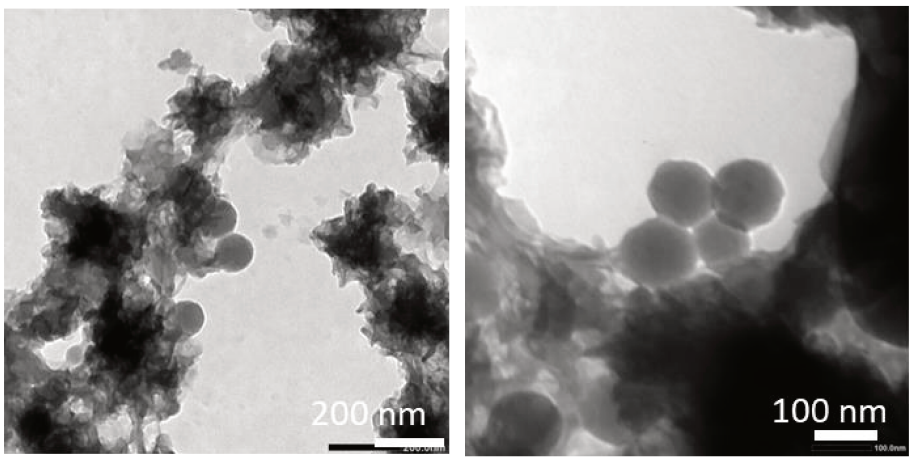

Figure 4. TEM images of a mixture of spherical and crumpled aggregates obtained by micellization protocol of $PNIPAM_{35}$-*b*-$PVDF_{450}$ in DMF at 2 mg mL^{-1}. Final concentration = 0.4 mg.mL^{-1} in DMF:water (1:4) mixture. Water addition rate was 40 mL h^{-1}.

When THF was used as the good solvent for both blocks, micellization protocols led to formation of flat sheet morphologies, presumably 2D bilayer aggregates (Figure 5).

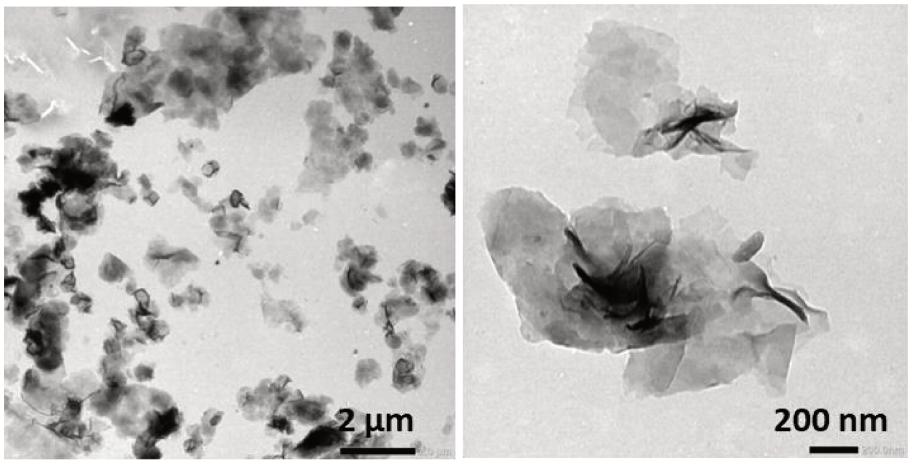

Figure 5. TEM images of the bilayer aggregates obtained by micellization of $PNIPAM_{35}$-*b*-$PVDF_{450}$. Initial polymer concentration in THF = 2 mg mL^{-1}. Final concentration = 0.4 mg mL-1 in THF:water (1:4) mixture. Water addition rate was 4 mL h^{-1}.

When acetone was used as the good solvent, well-defined flat 2D lenticular morphologies with relatively low dispersities and good dimensional control were obtained (Figures 6-8).

In the case of PNIPAM$_{25}$-*b*-PVDF$_{35}$ these lenticular objects had an average length of 600 nm and width of 250 nm, with sharp edges that seemed to be formed by aggregation of smaller 1D rod-like aggregates (Figure 6b and S5). These short 1D micelles have an average length and width of 98 and 19 nm, respectively.

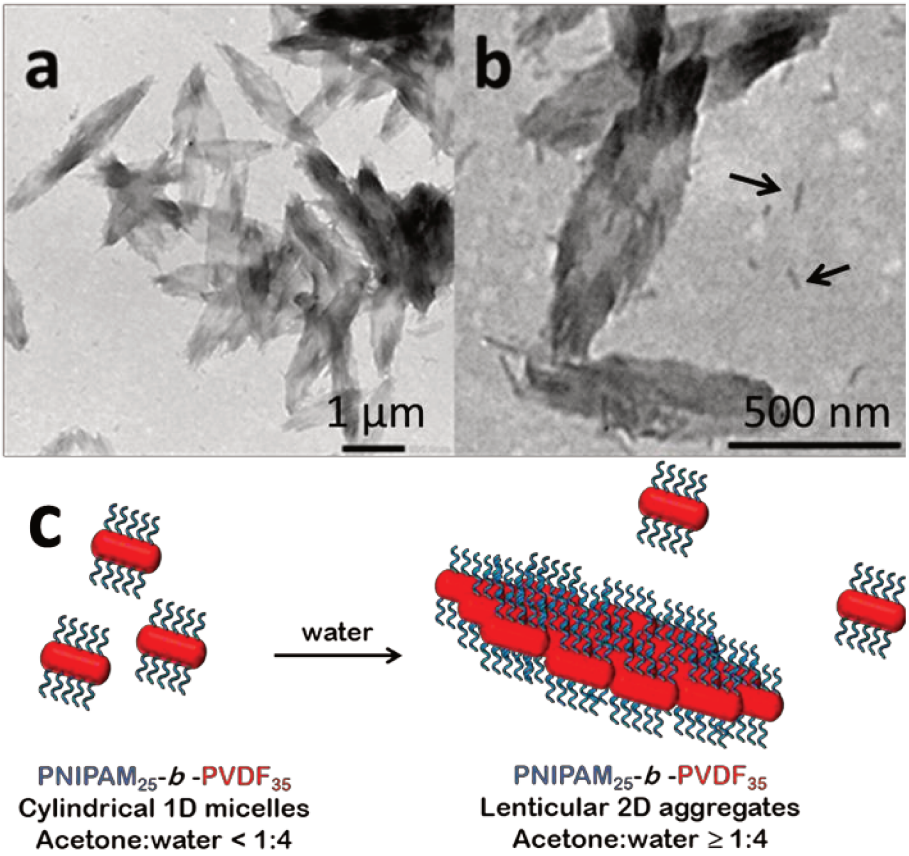

Figure 6. a and b. TEM images of 2D lenticular micelles obtained by self-assembly via micellization protocol of PNIPAM$_{25}$-*b*-PVDF$_{35}$. Initial BCP concentration in acetone = 2 mg mL^{-1}. Final concentration = 0.4 mg mL^{-1} in acetone:water (1:4) mixture. Non-solvent addition rate was 4 mL.h^{-1}. Arrows indicate the isolated 1D micelles. c. Schematic representation of the proposed mechanism of formation of PNIPAM$_{25}$-*b*-PVDF$_{35}$ lenticular aggregates from short 1D rod-like micelles.

In contrast, the PNIPAM-*b*-PVDF BCP prepared from the PNIPAM$_{35}$ macroCTA self-assembled into lenticular objects with much smoother-looking edges with average lengths of 200, 600, 1000 and 2300 nm and widths of 90, 250, 400 and 850 nm for PVDF DPs of 60, 100, 150 and 450, respectively (Figure 7).

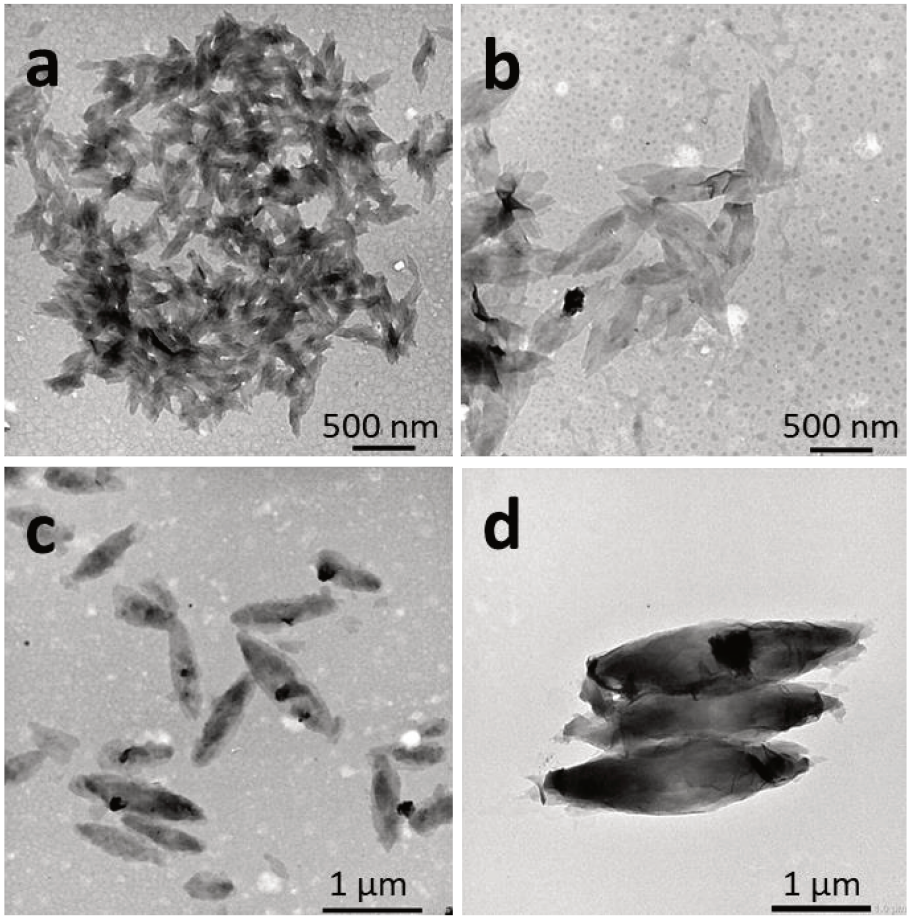

Figure 7. TEM images of representative self-assembled 2D lenticular morphologies prepared from (a) $PNIPAM_{35}$-*b*-$PVDF_{60}$, (b) $PNIPAM_{35}$-*b*-$PVDF_{100}$, (c) $PNIPAM_{35}$-*b*-$PVDF_{150}$ and (d) $PNIPAM_{35}$-b-$PVDF_{450}$. All samples were prepared via micellization in acetone:water mixtures. Initial polymer concentration in acetone = 2 mg mL^{-1}. Final concentration = 0.4 mg mL^{-1} in acetone: water (1:4) mixture. Water addition rate = 4 mL h^{-1}.

The length and width of the lenticular 2D micelles showed a linear dependence to the PVDF degree of polymerization up to 150 (Figure S6). The fact that the BCP with a PVDF DP of 450 does not follow the trend may be due to the fact that the accuracy of DP calculation from NMR is reduced, and the real DP of the PVDF might be closer to 300 than the calculated 450.

Due to their relatively large size (in the micrometric range), these morphologies were not colloidally stable and sedimented over time (ca. 14h). However, they were easily redispersed by simple shaking of the solutions.

The shape and size of these morphologies were not affected by the concentration of the initial BCP solutions over the concentration range studied (Figure S7). In addition, once the

self-assembled structures were formed in acetone:water mixture (1:4) they did not evolve within the time of the observations (2 weeks), they thus seemed to be kinetically trapped. Increasing the water content of the self-assembly media or decreasing (by evaporation) the acetone content of the solvent mixture only affected the aggregation rate. The lenticular shape of the assemblies is however strongly affected by the ratio of the hydrophobic and hydrophilic blocks. The morphologies are rather patchy with sharp edges for the $PNIPAM_{25}$-*b*-$PVDF_{35}$, while better-defined objects are found for $PNIPAM_{35}$-*b*-$PVDF_n$ BCPs for n > 60. Better defined lenticular objects were obtained as higher DPs of the PVDF were targeted.

The crystallinity of PVDF (Figure S8) was not observed on these self-assembled structures by electron diffraction during TEM analysis. This is likely caused by the thinness of these lenticular objects, which promotes fast amorphisation under the electron beam.

SEM images of these objects (Figure 8) suggest that they can fold and twist to an extent, and are often stacked on top of each other, making their characterization quite difficult even by AFM. These AFM images (Figure 9) also show that the thickness of the objects increases with the DP of the PVDF block.

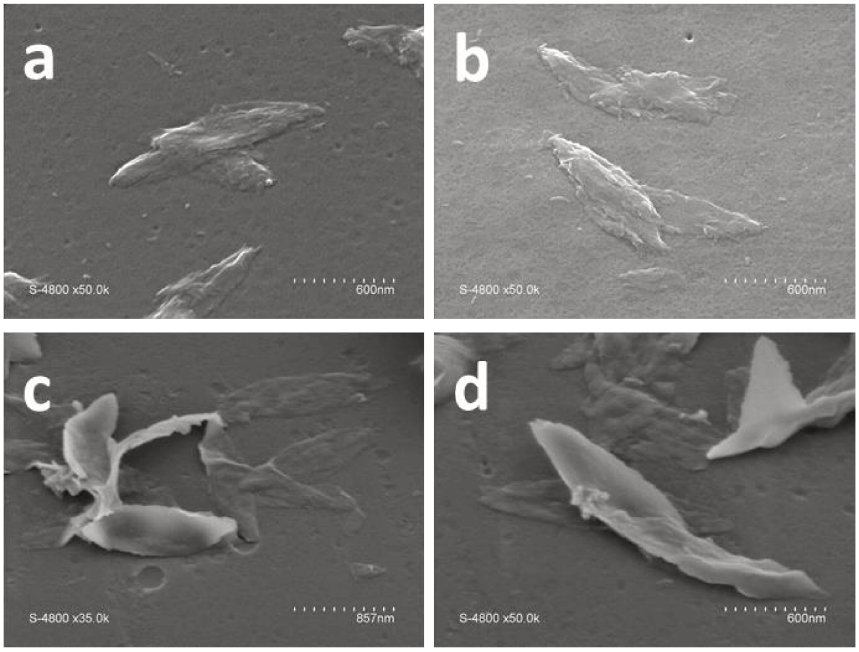

Figure 8. SEM images of 2D lenticular objects prepared from: $PNIPAM_{25}$-*b*-$PVDF_{35}$ (a, b), $PNIPAM_{35}$-*b*-$PVDF_{450}$ (c, d).

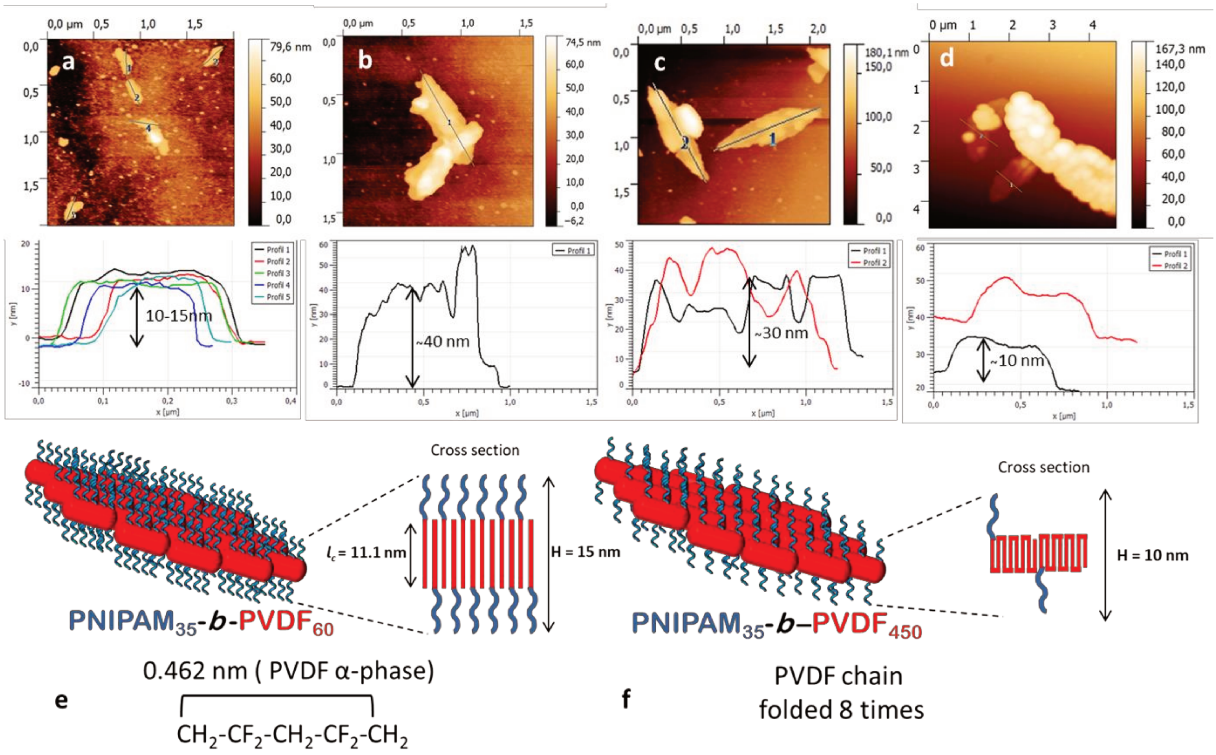

Figure 9. Probable conformation of 2D lenticular micelles. AFM images of 2D lenticular aggregates prepared from: (a) PNIPAM$_{35}$-*b*-PVDF$_{60}$, (b) PNIPAM$_{35}$-*b*-PVDF$_{100}$, (c) PNIPAM$_{35}$-*b*-PVDF$_{150}$, and (d) PNIPAM$_{35}$-*b*-PVDF$_{450}$. (e and f) Schematic representation and proposed molecular arrangement of the 2D lenticular aggregates formed by assembly of PNIPAM$_{35}$-*b*-PVDF$_{60}$ and PNIPAM$_{35}$-*b*-PVDF$_{450}$ respectively.

The lenticular morphologies are likely formed by aggregation of smaller 1D micelles upon addition of non-solvent. The thickness of these lenticular aggregates seems to be closely related to the length and folding of the PVDF segments. As the degree of polymerization of the PVDF core forming block increases, the thickness of the aggregates increases. Although it was not possible here to determine the crystalline form of the PVDF in these aggregates, PVDF crystallized in the α-form in self-assembled structures formed by PVDF-*b*-PEG-*b*-PVDF BCP.[8] α-form is the most common and spontaneously forming crystalline form of PVDF.[34,35] With the hypothesis that PVDF in these aggregates crystallizes in the α-form it is possible to estimate the number of folding of the PVDF chains. In this α-form crystal, 0.462 nm is the size taken by 2.5 VDF units.[36] Crystallized PVDF chains of DP 60, 100, 150 and 450 would thus extend over 11.1, 18.5, 27.7 and 83.2 nm, respectively. The thicknesses of the lenticular objects derived from the AFM topographic images shown in Figure 9 are in agreement with these calculations for PVDF$_{60}$, PVDF$_{100}$ and PVDF$_{150}$. Figure 9a, corresponding to PNIPAM$_{35}$-*b*-

$PVDF_{60}$, shows a thickness of 10-15 nm. Figure 9 and Figure S9, corresponding to $PNIPAM_{35}$-*b*-$PVDF_{100}$ give a thickness of 40 nm. This value is roughly twice the calculated length of the $PVDF_{100}$ (18.5 nm). This is because the AFM images show two aggregates stacked on to each other. The thickness measured for the $PNIPAM_{35}$-*b*-$PVDF_{150}$ in Figure 9c is 30 nm which also is agrees with the corresponding calculated value (27.7 nm). In the case of $PNIPAM_{35}$-*b*-$PVDF_{450}$, the calculated thickness of 83.2 nm does not match the thickness of 10 nm measured on Figure 9d. This discrepancy may be explained by considering, that; in this case, crystallized PVDF chains are likely in folded conformation rather than fully extended. Indeed, the calculated and measured values can be reconciled if the $PVDF_{450}$ chains were folded 8 times. This explanation is also consistent with the observation of larger aggregates with increasing PVDF degree of polymerization. The more the PVDF chains are folded the smaller the repulsion of the PNIPAM hydrophilic chains, allowing the formation of larger but thinner 2D aggregates.

Since the degree of crystallinity can be modified by temperature annealing, a heating and cooling treatment was applied to the crumpled structures obtained by self-assembly from DMF solution. In addition, higher temperature could also partially redissolve the PVDF segments in DMF/water. A 5 mg mL^{-1} $PNIPAM_{25}$-*b*-$PVDF_{35}$ solution in DMF was self-assembled by adding water to a 1:1 solvent: non-solvent ratio, and this solution was then heated at 90°C for 30 min and slowly cooled down to room temperature. Figure S10 shows that this annealing led to a mixture of ill-defined aggregates and spindle shaped morphologies with length ranging from 300 nm to 1 µm. The formation of these straight spindle shaped structures is thought to proceed via temperature-induced crystallization-driven self-assembly (TI-CDSA).

To sum up, five different morphologies were obtained as depicted in Table 2.

Table 2. Self-assembled aggregates shapes for the different polymer systems and protocols. **NP**, **M** and **TI-CDSA** stands for Nanoprecipitation and Micellization and Temperature-induced crystallization-driven self-assembly protocols respectively. *(sharp edges). In all $PNIPAM_{35}$-*b*-$PVDF_m$ systems examined, the size of the nanoaggregates increased with increasing DP of PVDF block.

Polymer	NP DMF:H_2O	M DMF: H_2O	M THF: H_2O	M Acetone: H_2O	M + TI-CDSA
$PNIPAM_{25}$-*b*-$PVDF_{35}$	spherical	Crumpled spherical	flat sheet	lenticular*	spindle
$PNIPAM_{35}$-*b*-$PVDF_{60}$	spherical	-	-	lenticular	-
$PNIPAM_{35}$-*b*-$PVDF_{100}$	spherical	-	-	lenticular	-
$PNIPAM_{35}$-*b*-$PVDF_{150}$	spherical	-	-	lenticular	-
$PNIPAM_{35}$-*b*-$PVDF_{450}$	spherical	Crumpled spherical	flat sheet	lenticular	-

Without surprise, the nature of the solvents and of the self-assembly protocol played a crucial role in the resulting BCP structures. The same BCP afforded different morphologies depending on the solvent system and if the micellization technique was used.

Thermoresponse of PNIPAM-*b*-PVDF lenticular nanoparticles

The thermoresponsiveness of the PNIPAM-*b*-PVDF lenticular aggregates were also investigated. In this work the usual turbidity test could not be used due to the poor colloidal stability of the BCP aggregates even at room temperature. Since the LCST of PNIPAM is affected by the presence of organic solvents, acetone was completely removed from the PNIPAM-*b*-PVDF BCP suspensions by evaporation under vacuum at room temperature to prepare an aqueous suspension of the self-assembled morphologies. TEM analysis of this suspension (Figure S11) showed that the size and shape of the assemblies were not affected by the removal of acetone.

Figure 10 shows the effect of temperature on the PNIPAM-*b*-PVDF BCP morphologies. The lenticular objects partly lose their well-defined shape, crumpled to an extent and also broken into smaller flat sheet pieces. This irreversible effect is likely caused by the decrease of the PNIPAM solubility in water at $T > LCST_{PNIPAM}$.

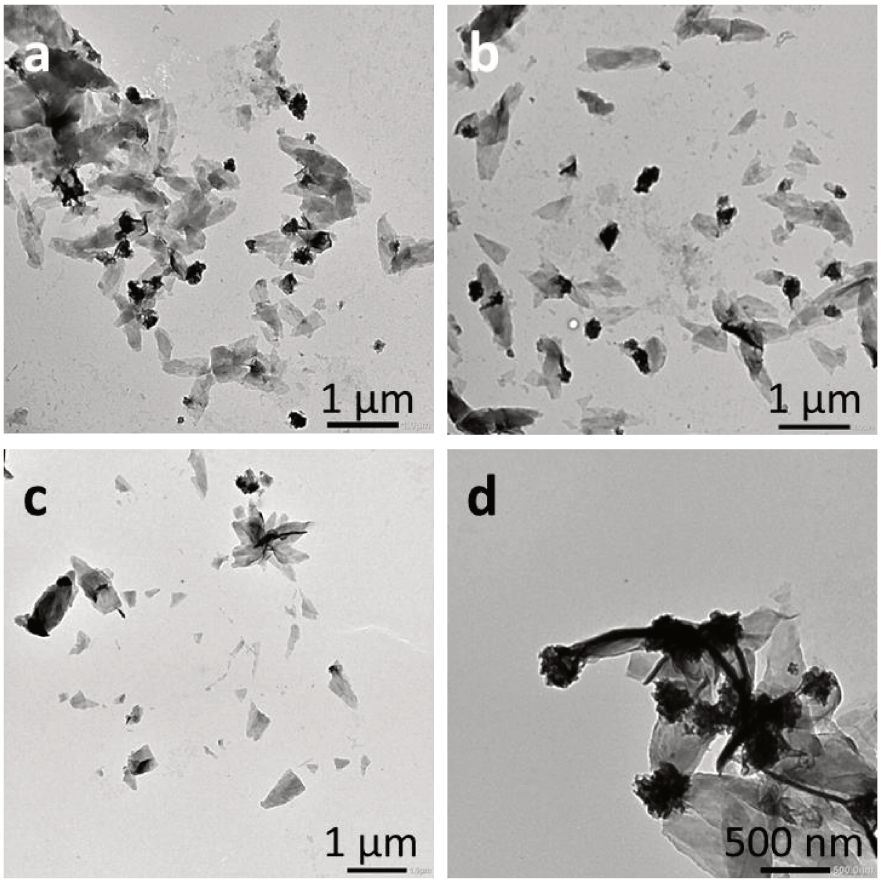

Figure 10. TEM images of representative samples of 2D lenticular aggregates prepared from: (a, b) $PNIPAM_{35}$-b-$PVDF_{150}$, (c, d) PNIPAM35-b-PVDF450 in pure water after being heated at 45°C for 30 min.

Immobilization of Gold Nanoparticles (Au NPs) in PNIPAM-*b*-PVDF aggregates.

Trithiocarbonates and dithiobenzoates have been reported to directly bind to gold nanoparticles.[37] To explore the accessibility of the xanthate moieties present at the end of the core-forming block in the lenticular 2D aggregates, they were put in contact with small Au NPs (diameter~ 10 nm).

To do this 50µL of Au NPs aqueous solution (~$6.0 \cdot 10^{12}$ particles mL^{-1}) were added to a suspension of the aggregates (0.4 mg mL^{-1}), and the resulting suspension was stirred for 30 minutes. When the stirring was stopped (after 14h) both the micelles and the Au NPs sedimented (Figure S12). The solution containing the sedimented aggregates and Au NPs was clear and DLS studies showed no evidence of presence of Au NPs in the supernatant. It should be noted that these Au NPs are colloidally stable in pure water. TEM pictures of the BCP morphologies + Au NPs (Figure 11) clearly show interaction between the lenticular aggregates and the Au NPs. The Au NPs were

indeed clearly attached to the lenticular aggregates. This result suggests that the xanthate moieties are available to interact with the gold surface. Especially since Destarac and co-workers have previously showed that PNIPAM moieties cannot bind to Au NPs.[38]

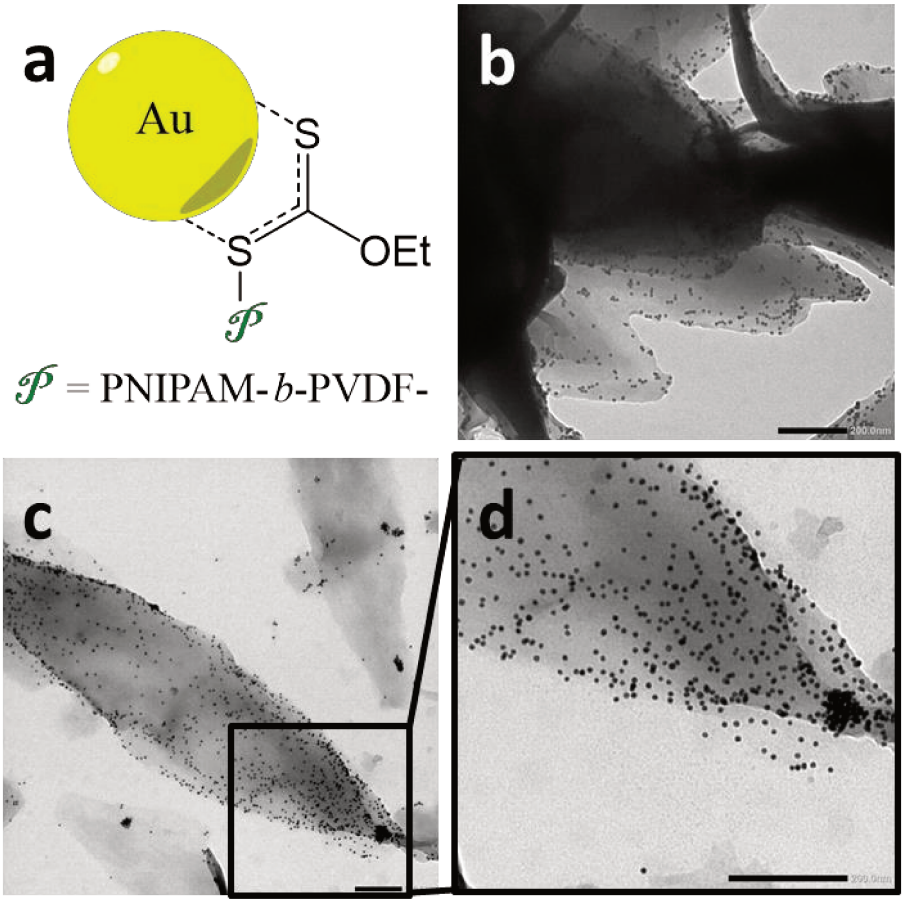

Figure 11. (a) Schematic representation of the interaction of xanthate moieties of BCPs and Au NPs, (b,c) TEM images of Au NPs immobilised on PNIPAM$_{35}$-*b*-PVDF$_{150}$ BCP lenticular aggregates, (d) higher magnification of TEM image (c). All scale bars correspond to 200 nm.

In-situ synthesis of Au NPs by UV reduction of $NaAuCl_4$ in the presence of PNIPAM-*b*-PVDF BCP nanoaggregates.

Au NPs were also prepared directly in the presence of the PNIPAM-*b*-PVDF BCP morphologies. Gold salt ($NaAuCl_4$) was dissolved in a suspension of PNIPAM$_{35}$-*b*-PVDF$_{100}$ lenticular aggregates and the resulting liquid was placed under UV irradiation following the technique described by Shang et al.[38] The more typical Au NPs synthesis method by reduction of gold precursors using $NaBH_4$ was used as such reducing

agents are known to also reduce the xanthate moieties. After 30 minutes exposure to UV, the suspension of the BCP aggregates became purple, indicating the presence of small gold nanoparticles.

The presence of Au NPs was further confirmed by the TEM images (Figure 12) which showed small gold nanoparticles located on the surface of the lenticular aggregates. In addition to lenticular aggregates, spherical objects (also decorated with Au NPs) were also observed (Figure 12b). These spherical structures were likely formed during the UV irradiation which also heated the reaction medium to about 50 °C, above the LCST of PNIPAM.

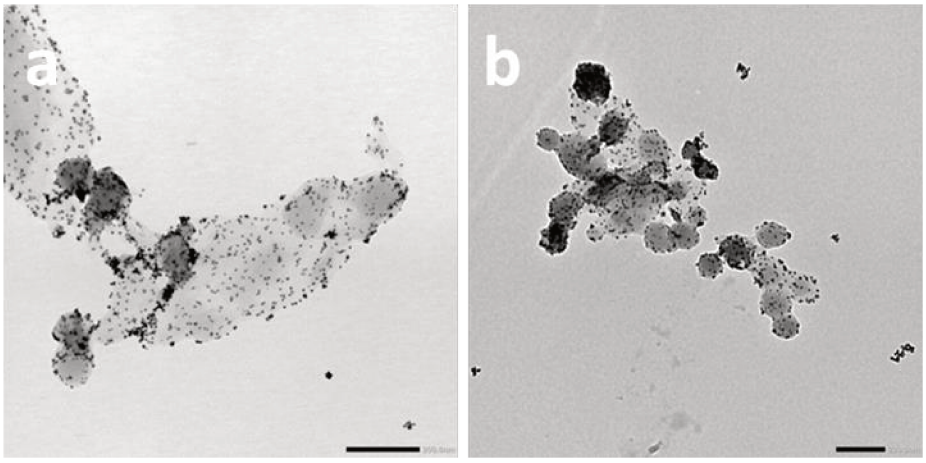

Figure 12. images of gold nanoparticles prepared in the presence of $PNIPAM_{35}$-*b*-$PVDF_{100}$ lenticular objects. (a) Au NPs in the surface of a lenticular micelle, (b) spherical aggregates decorated of Au NPs potentially due to the temperature increase caused by the UV lamps.

5. Conclusions

A series of relatively well-defined PNIPAM-*b*-PVDF amphiphilic diblock copolymers has been successfully prepared by RAFT employing PNIPAM macroCTAs. The diblock copolymers were fully characterized by ^{1}H and ^{19}F NMR spectroscopy, TGA, DSC and SEC. Thanks to their amphiphilic nature the BCPs have the ability to self-assemble into different morphologies. The self-assembled structures were characterized by TEM, SEM and AFM microscopies. The final structures were strongly affected by the common solvent employed in the self-assembly experiments. Surprisingly self-assembly from acetone initial solutions lead to the

formation of 2D lenticular aggregates with sizes increasing with the degree of polymerization of PVDF reaching lengths of 2.3 µm for the higher PVDF DP. These 2D lenticular objects offer a versatile 2D platform for the fabrication of functional materials. For a proof of-concept demonstration, commercial Au NPs were immobilized onto the surface of those aggregates. The xanthate moieties, which have strong affinity for gold, likely located on the surface of the PVDF core were accessible to the Au NPs. The decoration of these lenticular aggregates with Au NPS was also achieved by *in situ* preparation of Au NPs via UV reduction of Au salt in the presence of the self-assembled structures. To date most of reported controllable-size 2D self-assembled aggregates are made by Crystallization-Driven Self-Assembly (CDSA) and require heating and aging times to be formed. In addition, most of these examples are based on polycaprolactone (PCL)[39–41] or poly(ferrocene-dimethylsilane) (PFS)[42,43] as the semi-crystalline core-forming blocks. No reference describes the preparation of 2D aggregates from fluorinated block copolymers.

6. References

1. Soulestin, T., Ladmiral, V., Domingues, F., Santos, D. & Améduri, B. Progress in Polymer Science Vinylidene fluoride- and trifluoroethylene-containing fluorinated electroactive copolymers . How does chemistry impact properties ? *Prog. Polym. Sci.* **72**, 16–60 (2017).

2. Yu, Y. *et al.* Biocompatibility and in vivo operation of implantable mesoporous PVDF-based nanogenerators. *Nano Energy* **27**, 275–281 (2016).

3. Guerre, M. *et al.* Limits of Vinylidene Fluoride RAFT Polymerization. *Macromolecules* **49**, 5386–5396 (2016).

4. Guerre, Marc; Wahidur Rahaman, S. M.; Améduri, Bruno; Poli, R. & Ladmiral, V. Polymer Chemistry. *Polym. Chem.* **7**, 6918–6933 (2016).

5. Guerre, M. *et al.* Self-assembly of poly(vinylidene fluoride)-block-poly(2-(dimethylamino)ethylmethacrylate) block copolymers prepared by CuAAC click coupling. *Polym. Chem.* 5203–5211 (2017).

6. Guerre, M., Ameduri, B. & Ladmiral, V. One-pot synthesis of poly(vinylidene fluoride)

methacrylate macromonomers via thia-Michael addition. *Polym. Chem.* **7**, 441–450 (2016).

7. Lopez, G. *et al.* An amphiphilic PEG-b-PFPE-b-PEG triblock copolymer: synthesis by CuAAC click chemistry and self-assembly in water. *Polym. Chem.* **7**, 402–409 (2016).

8. Folgado, E. *et al.* "One-Pot" Aminolysis/Thiol-ene preparation of well-defined amphiphilic PVDF-b-PEG-b-PVDF triblock copolymers: Self-assembly behaviour in mixed solvents. *Polym. Chem.* (2019).

9. Kostov, G. *et al.* First amphiphilic poly(vinylidene fluoride-co-3,3,3-trifluoropropene)-b- oligo(vinyl alcohol) block copolymers as potential nonpersistent fluorosurfactants from radical polymerization controlled by xanthate. *Macromolecules* **44**, 1841–1855 (2011).

10. Girard, E., Marty, J. D., Ameduri, B. & Destarac, M. Direct synthesis of vinylidene fluoride-based amphiphilic diblock copolymers by RAFT/MADIX polymerization. *ACS Macro Lett.* **1**, 270–274 (2012).

11. Guerre, M. *et al.* Combination of Cationic and Radical RAFT Polymerizations: A Versatile Route to Well-Defined Poly(ethyl vinyl ether)-block-poly(vinylidene fluoride) Block Copolymers. *ACS Macro Lett.* **6**, 393–398 (2017).

12. Guerre, M., Semsarilar, M., Godiard, F., Améduri, B. & Ladmiral, V. Polymerization-induced self-assembly of PVAc-b-PVDF block copolymers via RAFT dispersion polymerization of vinylidene fluoride in dimethyl carbonate. *Polym. Chem.* **8**, 1477–1487 (2017).

13. Guerre, M., Schmidt, J., Talmon, Y., Améduri, B. & Ladmiral, V. An amphiphilic poly(vinylidene fluoride)-b-poly(vinyl alcohol) block copolymer: synthesis and self-assembly in water. *Polym. Chem.* **8**, 1125–1128 (2017).

14. Cortez-Lemus, N. A. & Licea-Claverie, A. Preparation of a mini-library of thermo-responsive star (NVCL/NVP-VAc) polymers with tailored properties using a hexafunctional xanthate RAFT agent. *Polymers (Basel).* **10**, 1–25 (2017).

15. Jia, F. *et al.* Amino-functionalized poly(N-vinylcaprolactam) derived from lysine: A

sustainable polymer with thermo and pH dual stimuli response. *Polym. Chem.* **7**, 7101–7107 (2016).

16. Barthet, C. *et al.* Influence of sodium dodecyl sulfate on the kinetics and control of RAFT/MADIX polymerization of acrylamide. *J. Polym. Sci. Part A Polym. Chem.* **56**, 760–765 (2018).

17. Read, E. *et al.* Low temperature RAFT/MADIX gel polymerisation: Access to controlled ultra-high molar mass polyacrylamides. *Polym. Chem.* **5**, 2202–2207 (2014).

18. Sütekin, S. D. & Güven, O. Radiation-induced controlled polymerization of acrylic acid by RAFT and RAFT-MADIX methods in protic solvents. *Radiat. Phys. Chem.* **142**, 82–87 (2018).

19. Taton, D., Wilczewska, A. Z. & Destarac, M. Direct synthesis of double hydrophilic statistical di- and triblock copolymers comprised of acrylamide and acrylic acid units via the MADIX process. *Macromol. Rapid Commun.* **22**, 1497–1503 (2001).

20. Maniego, A. R. *et al.* Degree of branching in poly(acrylic acid) prepared by controlled and conventional radical polymerization. *Polym. Chem.* **10**, 2469–2476 (2019).

21. Guerre, M. *et al.* Deeper Insight into the MADIX Polymerization of Vinylidene Fluoride. *Macromolecules* **48**, 7810–7822 (2015).

22. Asandei, A. D., Adebolu, O. I. & Simpson, C. P. Mild-temperature Mn 2(CO) 10-photomediated controlled radical polymerization of vinylidene fluoride and synthesis of well-defined poly(vinylidene fluoride) block copolymers. *J. Am. Chem. Soc.* **134**, 6080–6083 (2012).

23. Lv, C. *et al.* Self-Assembly of Thermosensitive Amphiphilic Pentablock Terpolymer PNIPAMx-b-PtBA90-b-PPO36-b-PtBA90-b-PNIPAMx in Dilute Aqueous Solution. *Macromolecules* **51**, 10136–10149 (2018).

24. Zeng, T., Yang, D., Li, H. & Gao, Y. Polymer Chemistry The fabrication of amphiphilic double dynamers for responsive Pickering emulsi fi ers †. *Polym. Chem.* **9**, 627–636 (2018).

25. Korolovych, V. F. *et al.* Thermally Responsive Hyperbranched Poly(ionic liquid)s: Assembly and Phase Transformations. *Macromolecules* **51**, 4923–4937 (2018).

26. Cao, M., Nie, H., Hou, Y., Han, G. & Zhang, W. Polymer Chemistry block copolymer nano-assemblies and the e ff ect. *Polym. Chem.* **10**, 403–411 (2019).

27. Zhao, P. *et al.* Stimuli-enabled switch-like paracetamol electrochemical sensor based on thermosensitive polymer and MWCNTs-GQDs composite nanomaterial. *Nanoscale* **11**, 7394–7403 (2019).

28. Porous, P. N. *et al.* Thermoresponsive Gating Characteristics of fluoride) Membranes. *Ind. Eng. Chem. Res.* **43**, 2643–2649 (2004).

29. Liu, X. *et al.* Enhanced Solubility of Polyvinyl Esters in scCO 2 by Means of Vinyl Tri fl uorobutyrate Monomer. *ACS Macro Lett.* **4**, 89–93 (2015).

30. Bernal-garcía, J. M. *et al.* Densities and Viscosities of (N , N -Dimethylformamide + Water) at Atmospheric Pressure from (283 . 15 to 353 . 15) K. *J. Chem. Eng. Data* **53**, 1024–1027 (2008).

31. Yang, C., Sun, Y., He, Y. & Ma, P. Volumetric Properties and Viscosities of Binary Mixtures of N , N -Dimethylformamide with Methanol and Ethanol in the Temperature Range (293 . 15 to 333 . 15) K. *J. Chem. Eng. Data* **53**, 293–297 (2008).

32. Acetone-Water Mixture Viscosity: Datasheet from ``Dortmund Data Bank (DDB) -- Thermophysical Properties Edition 2014'' in SpringerMaterials Available at: https://materials.springer.com/thermophysical/docs/vism_c4c174.

33. Sistach, S. *et al.* Thermoresponsive amphiphilic diblock copolymers synthesized by MADIX/RAFT: Properties in aqueous solutions and use for the preparation and stabilization of gold nanoparticles. *Chem. Mater.* **22**, 3712–3724 (2010).

34. Martins, P., Lopes, A. C. & Lanceros-Mendez, S. Electroactive phases of poly(vinylidene fluoride): Determination, processing and applications. *Prog. Polym. Sci.* **39**, 683–706 (2014).

35. El Mohajir, B. E. & Heymans, N. Changes in structural and mechanical behaviour of

PVDF with processing or thermal treatment. 2. Evolution of mechanical behaviour. *Polymer.* **42**, 7017–7023 (2001).

36. Mirfakhrai, T., Madden, J. D. W. & Baughman, R. H. Polymer artificial muscles. *Mater. Today* **10**, 30–38 (2007).

37. Duwez, A.-S., Guillet, P., Colard, C., Gohy, J.-F. & Fustin, C.-A. Dithioesters and Trithiocarbonates as Anchoring Groups for the "Grafting-To" Approach. *Macromolecules* **39**, 2729–2731 (2006).

38. Shang, Y. *et al.* Synthesis of gold nanoparticles by reduction of HAuCl4 under UV irradiation. *Solid State Sci.* **15**, 17–23 (2013).

39. Wang, J., Lu, Y. & Chen, Y. Fabrication of 2D surface-functional polymer platelets via crystallization- driven self-assembly of poly (ε -caprolactone) -contained block copolymers. *Polymer.* **160**, 196–203 (2019).

40. Cha, Y. *et al.* Crystallization-Driven Self-Assembly of Metallo-Polyelectrolyte Block Copolymers with a Polycaprolactone Core-Forming Segment. *ACS Macro Lett.* 835–840 (2019).

41. Rizis, G., Van De Ven, T. G. M. & Eisenberg, A. "Raft" Formation By Two-Dimensional Self-Assembly of Block Copolymer Rod Micelles in Aqueous Solution. *Angew. Chemie - Int. Ed.* **53**, 9000–9003 (2014).

42. Hudson, Z. M. *et al.* Tailored hierarchical micelle architectures using living crystallization-driven self-assembly in two dimensions. *Nat. Chem.* **6**, 893–898 (2014).

43. Qiu, H. *et al.* implement a channel closure scheme by assuming U. *Science* **352**, 697–702 (2016).

7. Supporting information

Scheme S1. PNIPAM$_m$-*b*-PVDF$_n$ Synthesis Scheme

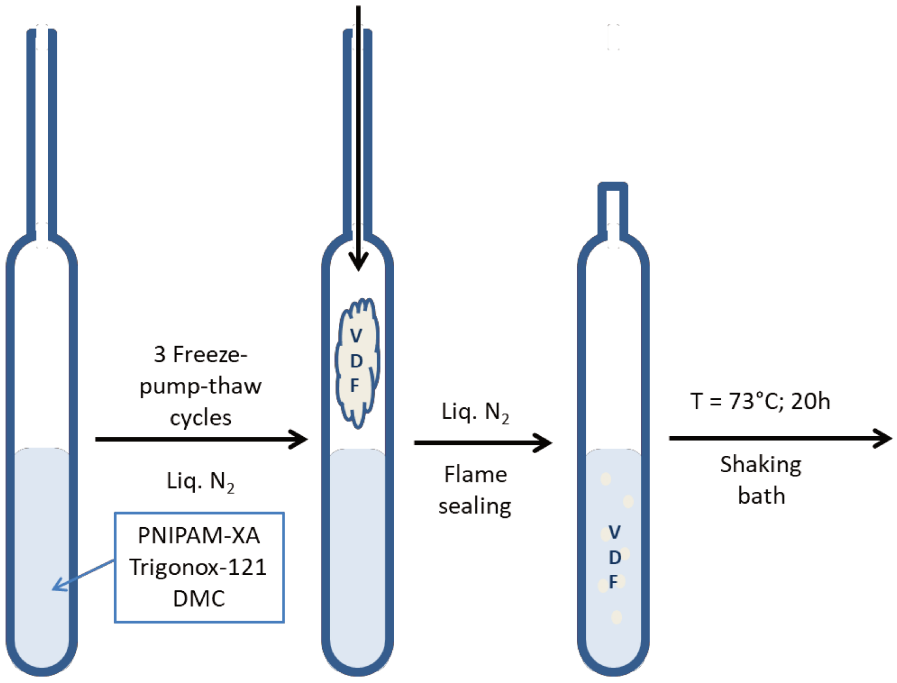

Scheme S1. Synthesis pathway of PVDF BCPs in carius tubes using PNIPAM macroCTAs.

Figure S1. PNIPAM$_{35}$-XA ^{1}H NMR spectrum

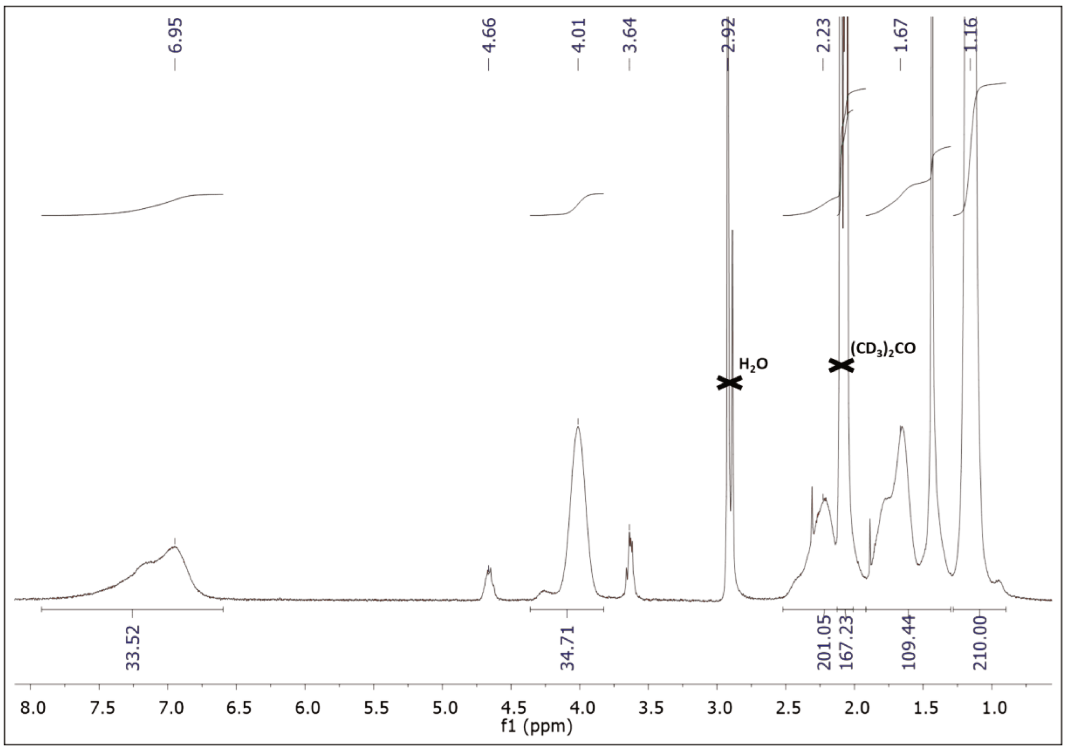

Figure S1. ^{1}H NMR (400 MHz) spectrum PNIPAM$_{35}$-XA in $(CD_3)_2CO$.

Figure S2. PNIPAM$_{35}$-*b*-PVDF$_{150}$ ^{1}H NMR spectra of crude and purified product

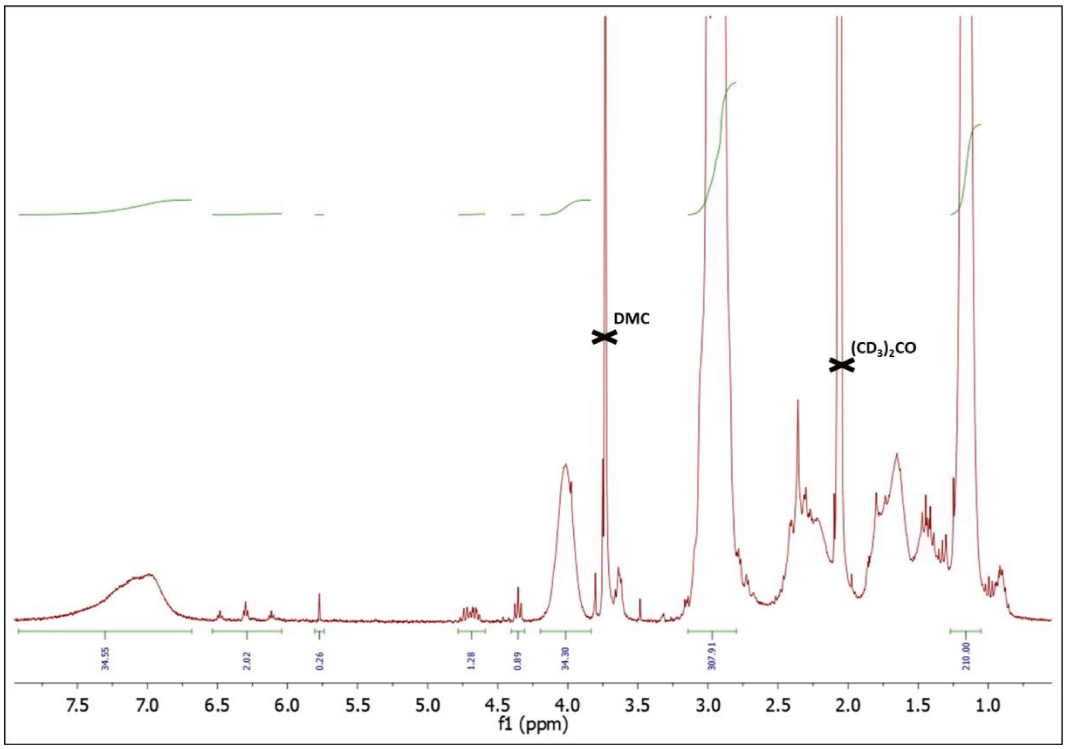

Figure S2a. ^{1}H NMR (400 MHz) spectrum of the crude PNIPAM$_{35}$-*b*-PVDF$_{150}$ in $(CD_3)_2CO$.

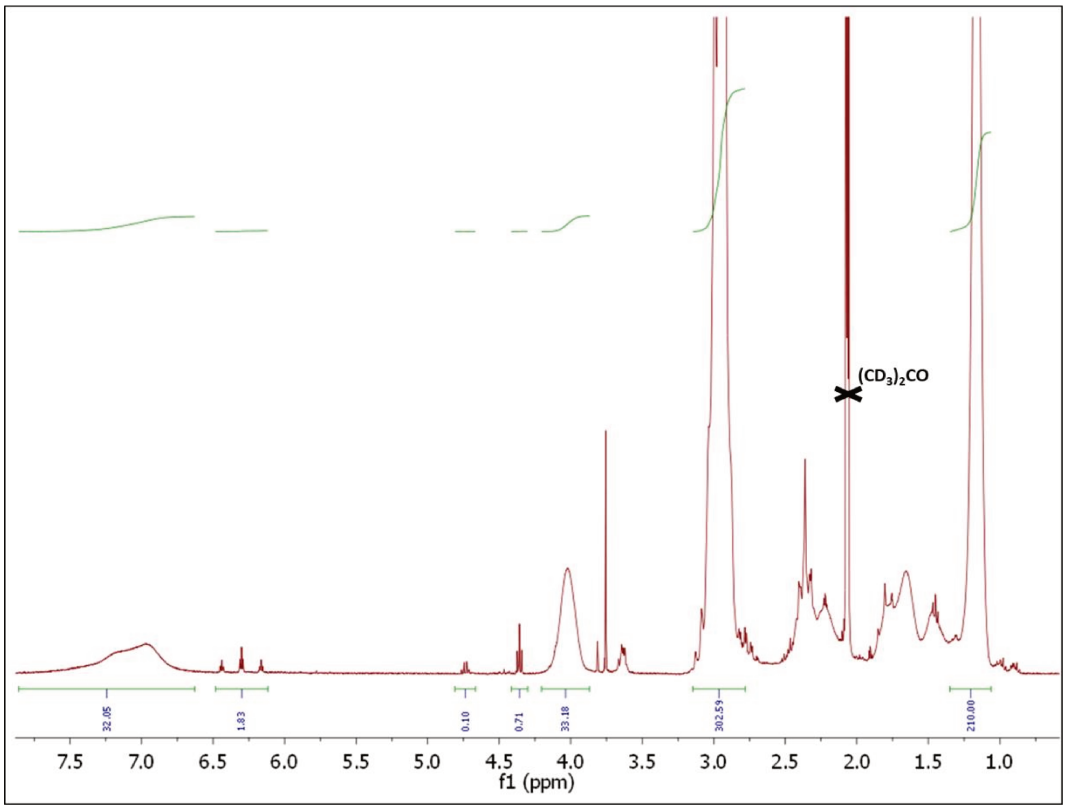

Figure S2b. ^{1}H NMR (400 MHz) spectrum of the purified PNIPAM$_{35}$-*b*-PVDF$_{150}$ in $(CD_3)_2CO$.

Figure S3. PNIPAM-*b*-PVDF ^{19}F NMR spectra

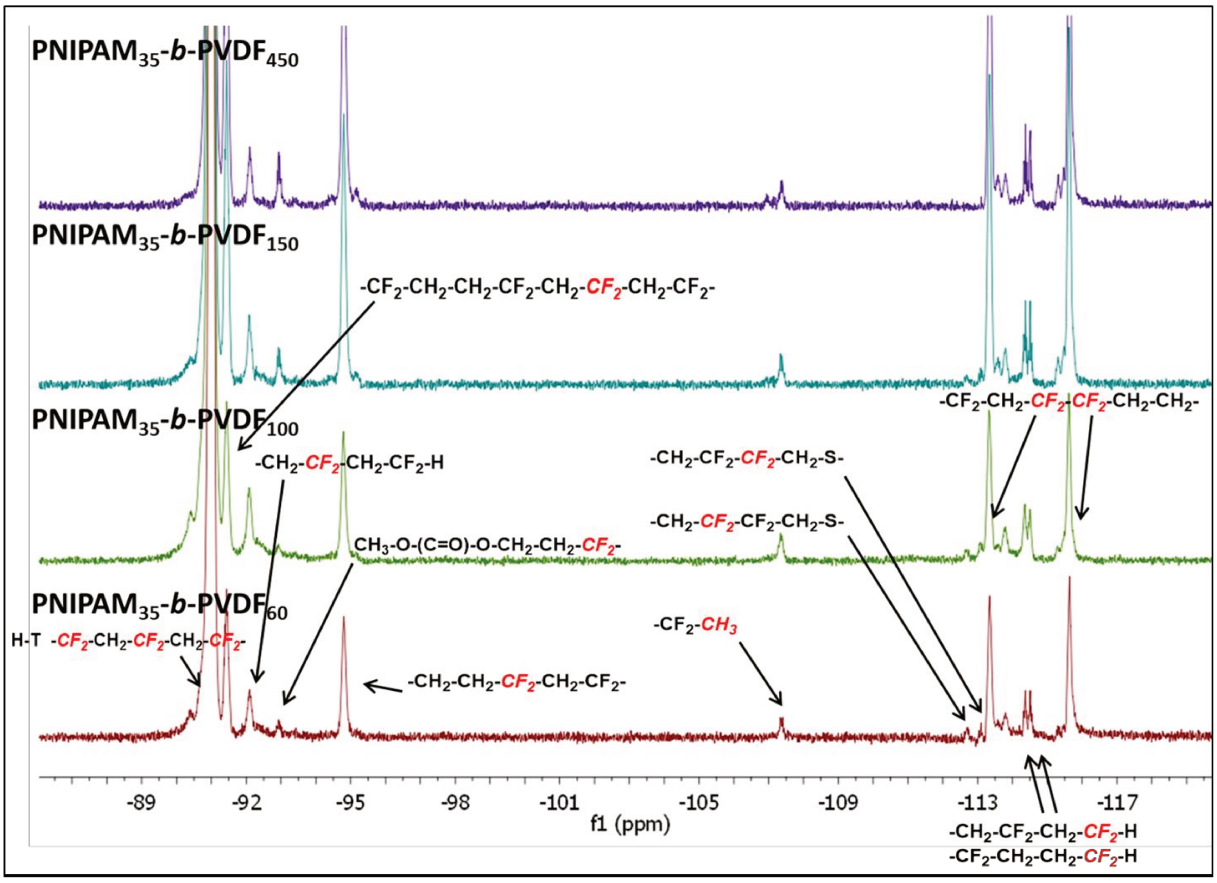

Figure S3. PNIPAM$_m$-*b*-PVDF$_n$ ^{19}F NMR spectra in $(CD_3)_2CO$

Figure S4. TEM and DLS measurements of spherical BCP aggregates.

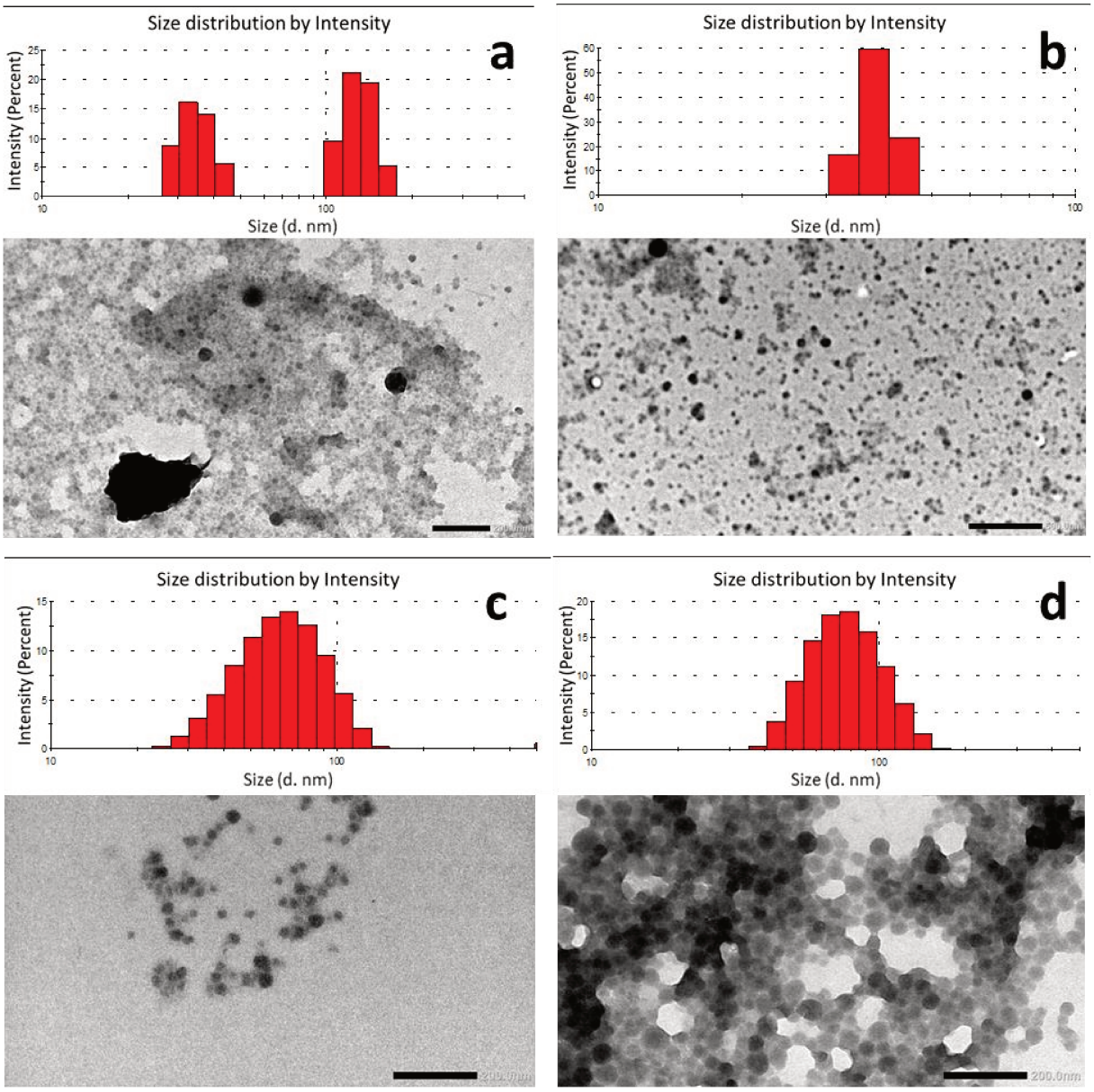

Figure S4. TEM images of spherical micelles prepared from (a) $PNIPAM_{35}$-*b*-$PVDF_{60}$, (b) $PNIPAM_{35}$-*b*-$PVDF_{100}$, (c) $PNIPAM_{35}$-*b*-$PVDF_{150}$ and (d) $PNIPAM_{35}$-*b*-$PVDF_{450}$. All samples were prepared by nanoprecipitation in water from polymer solutions in DMF at 2 mg mL^{-1} (final concentration = 0.1 mg mL^{-1} in DMF: water (1:20). Scale bars correspond to 200 nm. Insets correspond to the intensity DLS data for each sample.

Figure S5. 1D aggregates observed around PNIPAM$_{25}$-*b*-PVDF$_{35}$ lenticular aggregates.

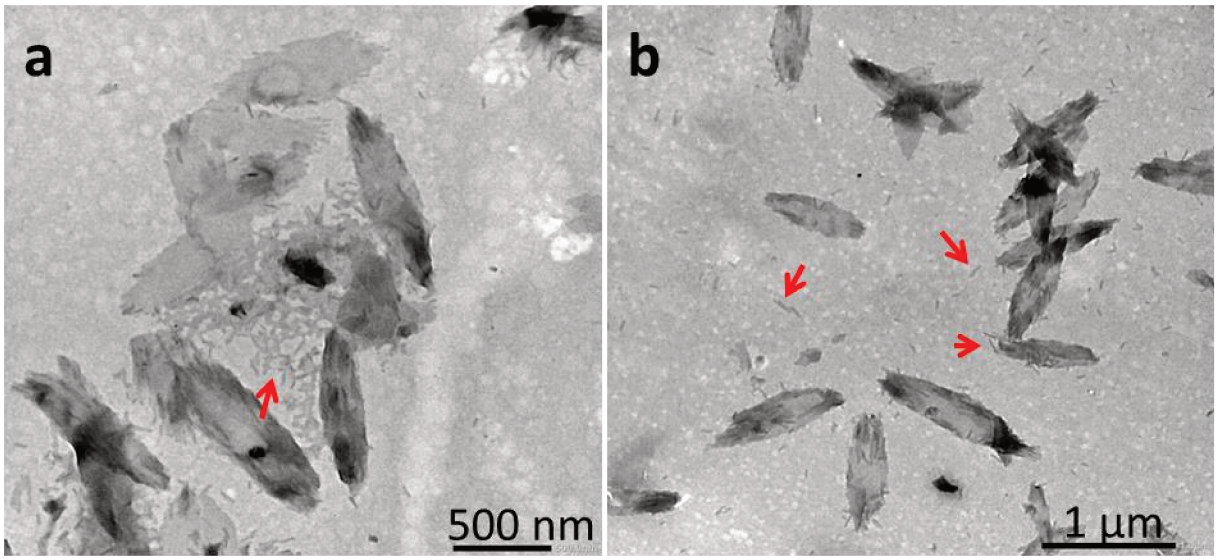

Figure S5. TEM images of 2D lenticular aggregates obtained by micellization protocol of PNIPAM$_{25}$-*b*-PVDF$_{35}$ (a and b). Initial polymer concentration in acetone = 2 mg mL^{-1}. Final concentration = 0.5 mg mL^{-1} in acetone:water (1:3) mixture (for a) and 0.4 mg mL^{-1} in acetone:water (1:4) mixture (for b). water addition rate = 4 mL h^{-1}. Red arrows indicate some of the observed short 1D aggregates.

Figure S6. Dependence of the lenticular aggregates size with the DP of PVDF

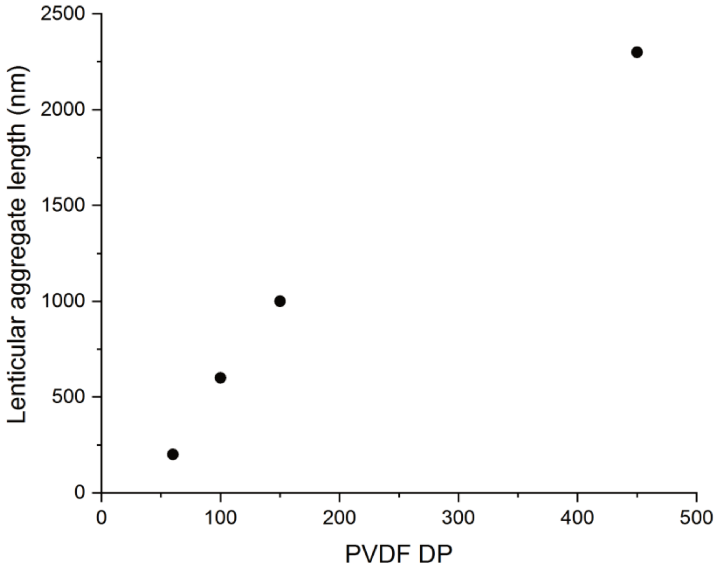

Figure S6. Plot of PVDF degree of polymerization *vs.* length of lenticular aggregates.

Figure S7. Effect of BCP initial concentration on the self-assembly.

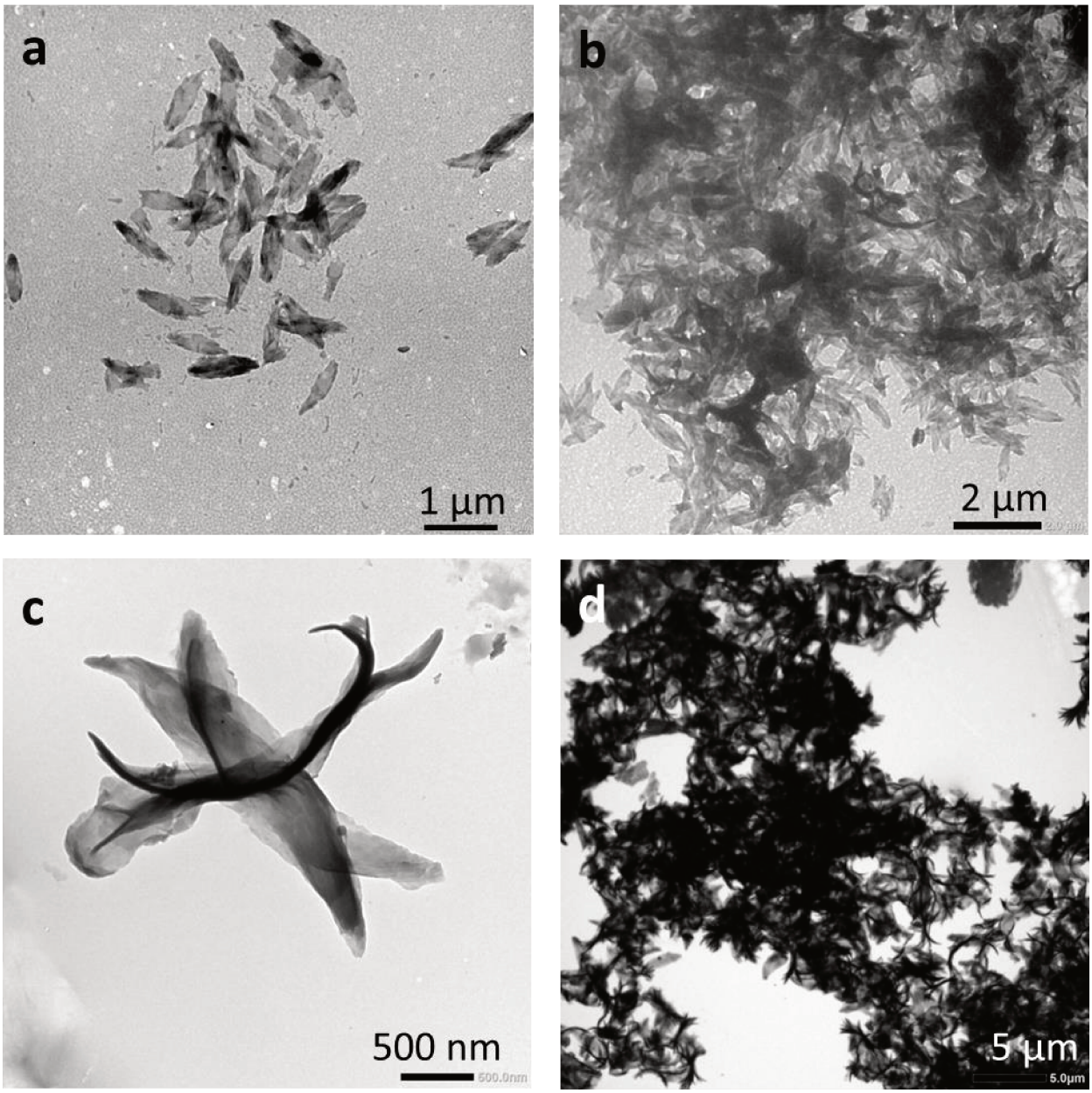

Figure S7. Self-assembled structures prepared by micellization using water as selective solvent and: a) 1 mg mL^{-1} acetone stock solutions of $PNIPAM_{25}$-*b*-$PVDF_{35}$, b) 4 mg mL^{-1} acetone stock solutions of $PNIPAM_{25}$-*b*-$PVDF_{35}$, c) 1 mg mL^{-1} acetone stock solutions of $PNIPAM_{35}$-*b*-$PVDF_{450}$, and d) 4 mg mL^{-1} acetone stock solutions of $PNIPAM_{35}$-*b*-$PVDF_{450}$. Final 1:4 acetone:water ratio. Water addition rate = 4 mL h^{-1}.

Figure S8. DSC thermograms of PNIPAM$_m$-*b*-PVDF$_n$ and crystallinity estimation.

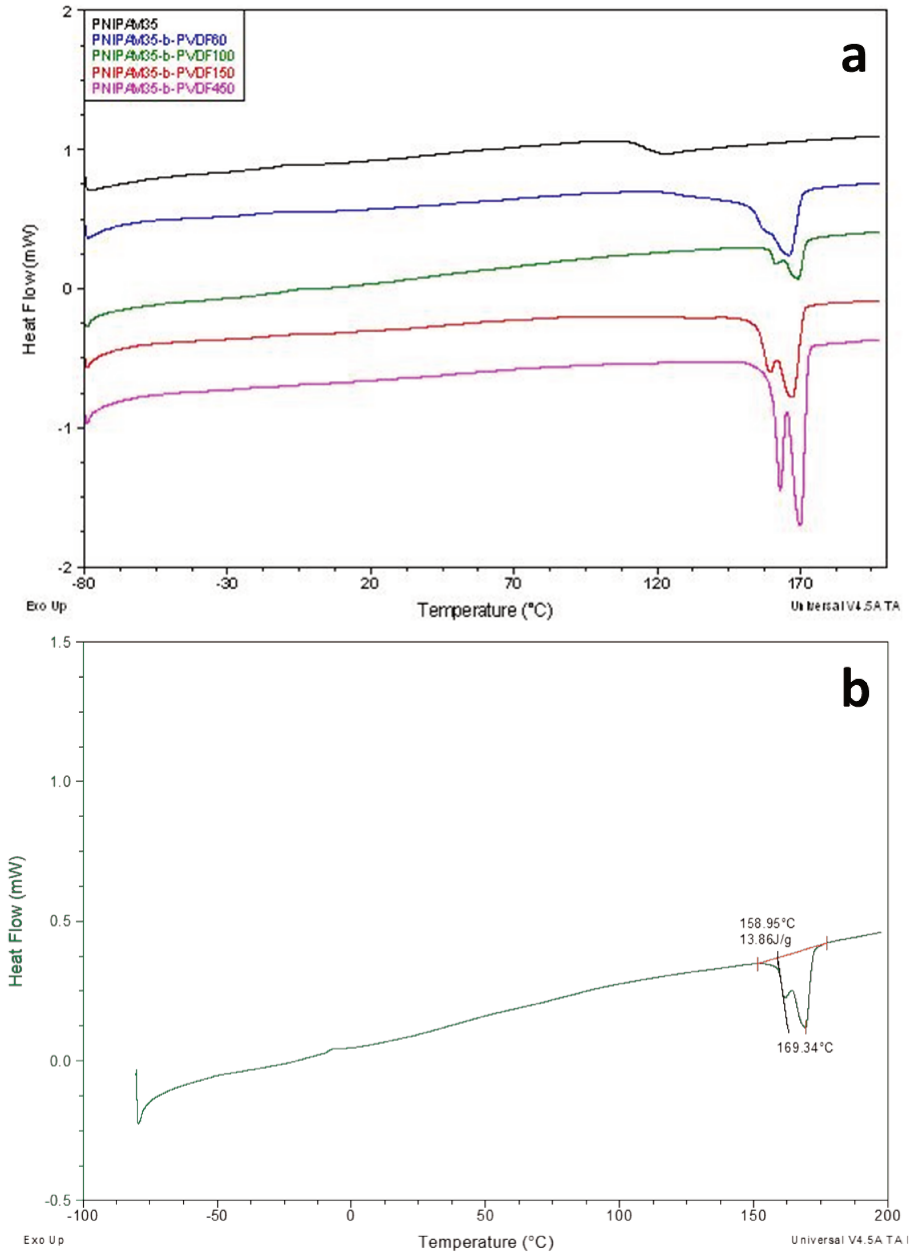

Figure S8. DSC thermograms of PNIPAM$_m$-*b*-PVDF$_n$ (a). DSC thermogram of PNIPAM$_{35}$-*b*-PVDF$_{150}$ and determination of ΔH_f for the PVDF block.

$$\chi_c(\%) = \frac{\Delta H_f}{\Delta H_f^\circ \, \phi_m} \times 100$$

Where ΔH_f is heat of melting (extracted from the DSC trace) and ΔH_f° is a reference value and represents the heat of melting if the polymer were 100% crystalline (both in J/g). ϕ_m is the weight fraction of the different block forming the diblock copolymer.

ΔH_f° of PVDF is 104.7 J·g^{-1}.

The molar mass of the block copolymer PNIPAM$_{35}$-*b*-PVDF$_{150}$ (deduced from NMR) is 13,700 g·mol^{-1} and the weight fraction of the PVDF and PNIPAM blocks (ϕ_m) are 0.68 and 0.32 respectively.

$\chi_{c\,PVDF}$= (13.86/(104.7·0.68))x100= 19.5%

Figure S9. AFM amplitude image of PNIPAM$_{35}$-*b*-PVDF$_{100}$ lenticular aggregates.

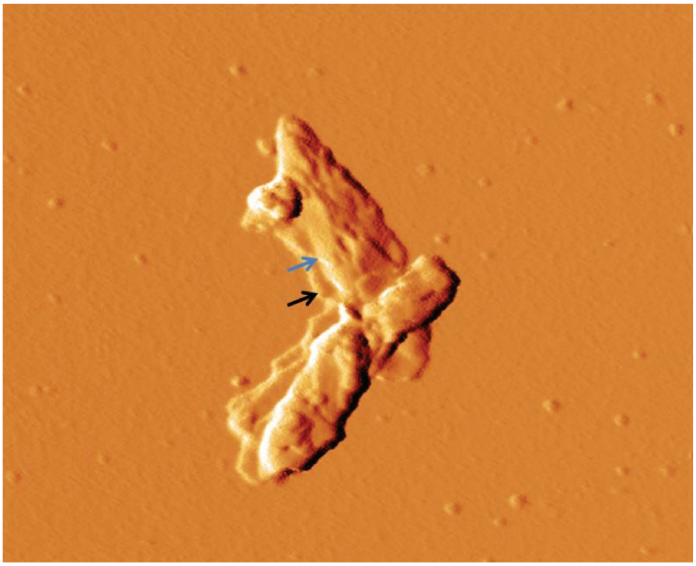

Figure S9. AFM amplitude image of PNIPAM$_{35}$-*b*-PVDF$_{100}$ lenticular aggregates. Arrows indicate two stacked lenticular aggregates.

Figure S10. TEM images of PNIPAM$_{25}$-*b*-PVDF$_{35}$ crystalline aggregates.

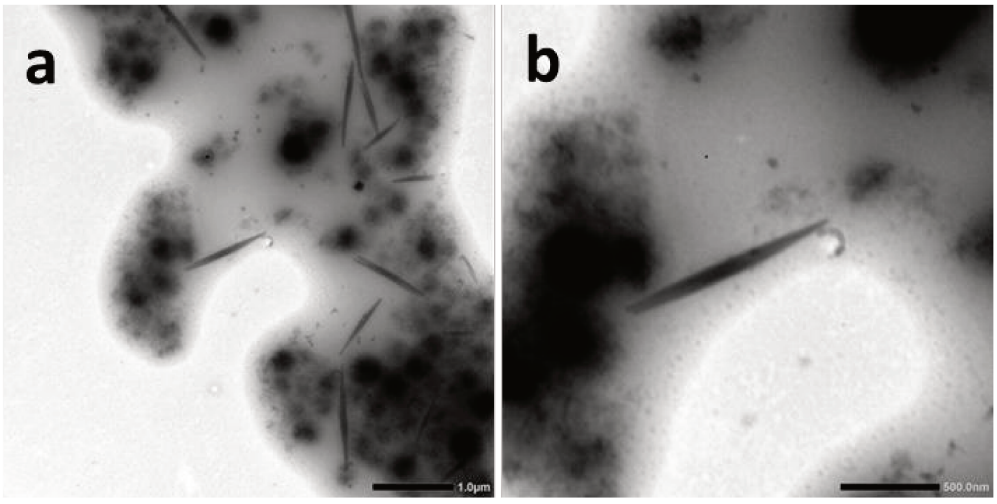

Figure S10. TEM images of crystalline structures prepared from a 5 mg mL^{-1} PNIPAM$_{25}$-*b*-PVDF$_{35}$ solution in DMF by micellization. DMF:water (1:1) solvent mixture. Water addition rate = 4 mL h^{-1}. Solution heated at 90°C for 30 min then cooled down to room temperature. Scale bars are 1 µm (a) and 500 nm (b).

Figure S11. Lenticular aggregates after acetone removal

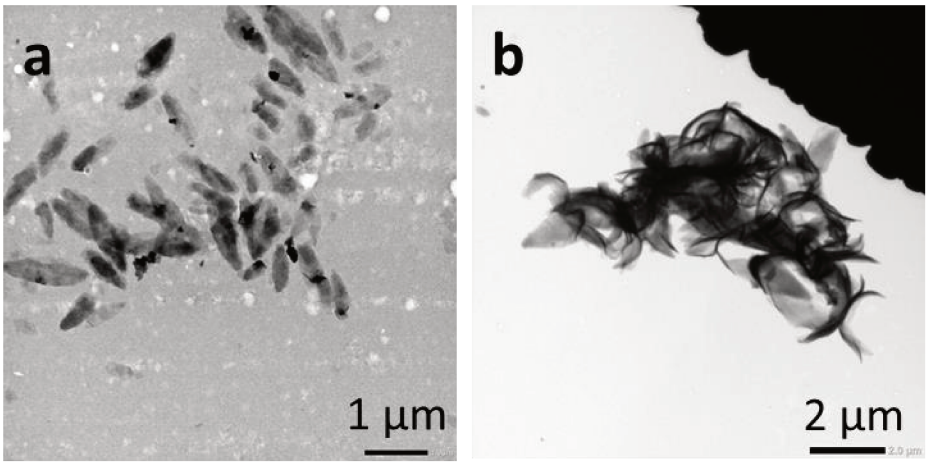

Figure S11. TEM images of self-assembled 2D lenticular morphologies prepared from (a) $PNIPAM_{35}$-*b*-$PVDF_{150}$ and (b) $PNIPAM_{35}$-b-$PVDF_{450}$ via micellization in acetone : water mixture after acetone removal by rotary evaporation at room temperature.

Figure S12. Au NPs in the presence of $PNIPAM_{35}$-*b*-$PVDF_{150}$ lenticular aggregates

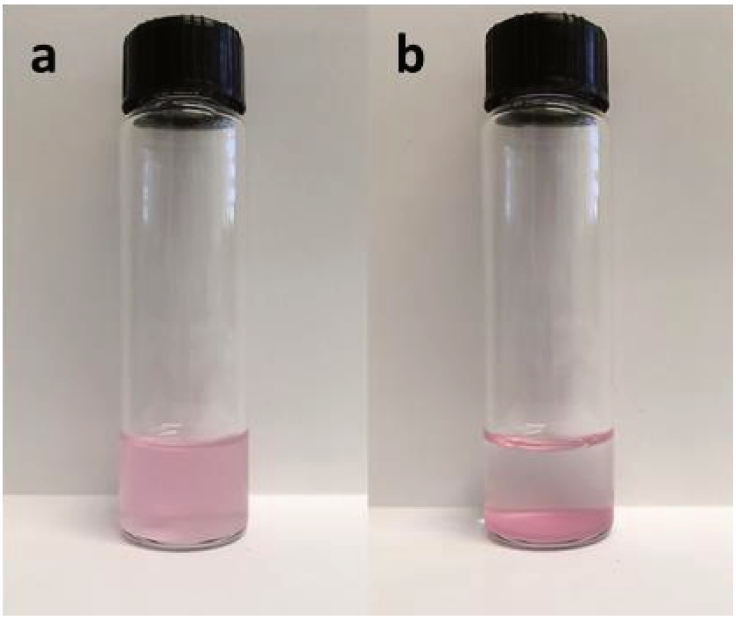

Figure S12. Au NPs in the presence of $PNIPAM_{35}$-*b*-$PVDF_{150}$ lenticular aggregates at t=0 h (a) and t = 24 h (b).

Chapter 5

"Grafting-from" RAFT polymerization of VDF from preassembled cyclic peptide macro CTAs. Synthesis and self-assembly of PVDF-CP conjugates

This work was performed in collaboration with Sebastien Perrier's team in the University of Warwick. They have experience on the conjugation of polymers to cyclic peptides. The conjugates size and functionality can be controlled at some extent and found application in different fields such as transmembrane channels, porous membranes and drug delivery vectors. Since PVDF is a material of choice for the preparation of water filtration membranes, the combination of CP and PVDF could result in an interesting material for a membrane application. The aim was to study the impact of PVDF on the self-assembly and investigate their potential for a membrane application.

"Grafting-from" RAFT polymerization of VDF from preassembled cyclic peptide macro CTAs: Synthesis and Self-assembly of PVDF-CP conjugates

Enrique Folgado,[a,b] Qiao Song,[c] Sebastien Perrier,[c,d,e*], Vincent Ladmiral,[a*] Mona Semsarilar[b*]

[a]Institut Charles Gerhardt Montpellier, ICGM UMR5253, Univ Montpellier, CNRS, ENSCM, Montpellier, France.

[b]Institut Européen des Membranes, IEM, UMR5635, Univ Montpellier, CNRS, ENSCM, Montpellier, France.

[c]Department of Chemistry, University of Warwick, Gibbet Hill Road, Coventry CV4 7AL, UK.

[d]Faculty of Pharmacy, Monash University, 381 Royal Parade, Parkville, VIC 3052, Australia

[e]Warwick Medical School, The University of Warwick, Coventry CV4 7AL, UK.

1. Abstract

The synthesis of cyclic peptide-poly(vinylidene fluoride) (CP-PVDF) conjugates comprising (D-alt-L)-cyclopeptides as aggregator domains and their self-assembly into tube-like structures is described. By growing two poly(vinylidene fluoride) blocks to opposite sides of a preassembled cyclic-peptide macro-CTA, a PVDF-CP-PVDF bioconjugate was prepared. The "grafting-from" strategy, allowed the synthesis of the conjugate with high purity and no time-consuming purification steps. The controlled self-assembly of the conjugate from DMF or DMSO solutions was carried out by addition of THF. This triggers the aggregation process that led to formation of uniform tube-like structures. The length and the width of the conjugated tubes were measured using Atomic force microscopy (AFM) and transmission electron microscopy (TEM). Surprisingly, the self-assembly of the CP-PVDF conjugates in DMF allowed the preparation of long (up to 25 μm) tube-like structures. The formation of such long tubular peptide-polymer aggregates via stacking of the cyclopeptides is most probably due to the presence of the PVDF arms since the cyclic peptides alone do not form such long tubes.

2. Introduction

Recently, peptide–polymer conjugates have attracted special attention for their application in a wide range of fields, including therapeutics and separation technologies.[1–5] A fascinating class of peptides that are known to self-assemble into supramolecular nanotubes (NTs) are cyclic peptides (CPs) comprising 4, 6, 8, 10 or 12 alternating D- and L-amino acids.[6,7] The pioneering work on cyclic peptide nanotubular structures was carried out by Ghadiri and co-workers.[6] The alternating chirality of the amino acids in the macrocycle leads to amide bonds that alternate in orientation perpendicular to the plane of the CP rings.[8] As a result, a contiguous intermolecular hydrogen-bonded network arises, resulting in the formation of hollow and extended cylinder structures.

In these structures, all of the amino acid side chains are directed towards the outside of the cycle. Because of this side chain arrangement, the interior of the formed assemblies remain empty, thus creating an orifice along the axis of the cyclic-peptide nanotubes. In addition, both the functional groups and the diameter of the nanotube can be precisely controlled by changing the sequence and the number of amino acids in the cyclic peptide.[5,9]

Despite the great progress that has been made with CP NTs in applications such as ion sensing,[10] transmembrane ion channels[2,11] and drug delivery systems,[12] limitations with respect to NT solubility, functionality and lack of control over NT length restrict the expansion of applications. Polymer conjugation allows some degree of control over the tube length, and the nature of the grafted polymer influences the solubility of the CP–polymer NTs.[13,14] To a great extent, CP–polymer conjugates, whereby the CP has been used as a supramolecular template, have addressed these issues.[13,15–18]

Typically, CP-polymer conjugates are synthesized via grafting-from (divergent) or grafting-to (convergent) approach.[9,19,20] In the grafting-from approach,[3,20] the polymer chains are grown from the peptide using a variety of polymerization techniques[21,22] while in the grafting-to approach the polymers are synthesized separately and then grafted to the peptide using highly efficient coupling reactions.[18,23] However, despite the use of these highly efficient reactions, such as

copper(I)-catalyzed alkyne-azide cycloaddition (CuAAC),[13] or activated ester-mediated ligations,[20] the grafting-to approach often requires an excess of polymer and additional often time- and labor-consuming purification steps to remove the unreacted polymer.[24] The grafting-from synthetic strategy is not limited by monomer side chain functionalities orthogonal to the chain end group used for the conjugation, as in the grafting-to route.[13,24]

In 2016, Perrier *et al.* reported the functionalization of such cyclic peptides using a trithiocarbonate RAFT agent bearing a NHS moiety and synthesized CP-polymer conjugates.[20] They also compared the "grafting-from" and "grafting-to" approaches. They concluded that the grafting-to strategy is more flexible in terms of choice of solvent and polymer to be grafted. However, the grafting-from approach affords purer conjugate in shorter time. This approach is, however dependent on the availability of a solvent that can solubilize the peptide, the monomer and resulting conjugate.

Poly(vinylidene fluoride) (PVDF), a semi-crystalline polymer presenting excellent physicochemical properties as well as electroactive properties (piezoelectricity, pyroelectricity and ferroelectricity) is used in very diverse fields.[25–30] Supramolecular PVDF made of hollow tubes could find application in membrane science or in other fields of nanotechnology.

Conjugates of such cyclic peptides with polymers, have recently gain lots of attention,[1,5,11,24,31] and to the best of our knowledge, PVDF-CP conjugates have not been studied to date.

We report herein the fabrication of the first CP–PVDF NTs, as illustrated in Scheme 1, constructed via a divergent synthetic approach using a CP(-Xanthate)$_2$ building block and the first RAFT polymerization of VDF in acetone, including also the first NHS-functionalized PVDF. The use of a CP containing eight alternating D- and L-amino acids permits a facile templated approach for the formation of well-defined PVDF NTs featuring sub nanometre channels within their cores.

In appropriate solvents, self-assembly is possible, resulting in well-defined PVDF nanotubular structures.

3. Experimental section

3.1. Materials

N-hydroxysuccinimide (98 %), triethylamine (TEA) (>99.5%), 2-bromopropionyl bromide (97%), magnesium sulfate anhydrous (>99.5%), potassium ethyl xanthogenate (96%), 4-dimethylaminopyridine (DMAP, 99 %), 2-chloro-4,6-dimethoxy-1,3,5-triazine (97 %), triisopropylsilane (TIPS, 99 %), and aluminum oxide were purchased from Sigma-Aldrich. 1,1,1,3,3,3-Hexafluoroisopropanol (HFIP, 99 %) and iodine were purchased from Acros Organics. *N*-methylmorpholine (NMM, 99 %) and piperidine were purchased from Alfa Aesar. Sodium hydroxide pellets, sodium thiosulfate pentahydrate and anhydrous magnesium sulfate ($MgSO_4$) were purchased from Fisher. *N,N*-diisopropylethylamine (DIPEA, 99 %), was purchased from Merck. Fmoc-D-Leu-OH, Fmoc-L-Lys-OH, Fmoc-L-Trp(Boc)-OH, O-(benzotriazole-1-yl)-*N,N,N',N'*-tetramethyluronium hexafluorophosphate (HBTU), 2-chlorotrityl chloride resin (100-200 mesh) and 1-ethyl-3-(3- dimethylaminopropyl)carbodiimide (EDC) were purchased from Iris Biotech and used as received. Tert-amyl peroxy-2-ethylhexanoate (Trigonox 121, purity 95%) was purchased from AkzoNobel (Chalons-sur-Marne, France). Deuterated solvents for NMR were purchased from Euristop. All solvents were bought from commercial sources and used as received. VDF was kindly supplied by ARKEMA. The cyclization coupling agent 4-(4,6-dimethoxy-1,3,5-triazin-2-yl)-4-methylmorpholinium tetrafluoroborate (DMTMM·BF4) was synthesized according to an established literature method.[8]

3.2. Measurements

Nuclear Magnetic Resonance (NMR).

The NMR spectra were recorded on a Bruker AV III HD Spectrometer (400 MHz for ^{1}H and 376 MHz for ^{19}F).

Coupling constants and chemical shifts are given in hertz (Hz) and parts per million (ppm), respectively. The experimental conditions for recording ^{1}H and ^{19}F NMR spectra were as follows: flip angle, 30°; acquisition time, 4s ; pulse delay, 1 s; number of scans, 16 (or 32 for ^{19}F); and pulse widths of 9.25 and 11.4 µs for ^{1}H and ^{19}F NMR respectively.

Dynamic light scattering (DLS).

DLS measurements of polymer solutions were carried out in a Litesizer^{TM} 500 de Anton Paar using a quartz cuvette at 25°C.

Transmission electron microscopy (TEM).

TEM studies were conducted using a JEOL 1400+ instrument equipped with a numerical camera, operating with a 120 kV acceleration voltage at 25 °C. To prepare TEM samples, a drop (10.0 µL) of micellar solution was placed onto a Formvar/Carbon or Lacey/Carbon coated copper grid for 30 s, blotted with filter paper and dried under ambient conditions.

Scanning electron microscopy (SEM).

SEM analyses were conducted using a Hitachi S-4500 instrument operating at spatial resolution of 1.50 nm at 15 kV energy. The samples were prepared by spin coating of 50 µL of the solution on a silicon wafer. The samples were then placed on a flat mount after being coated with an ultrathin layer of electrically conducting Platinum deposited by high-vacuum evaporation.

Atomic force microscopy (AFM).

AFM samples were prepared by spin coating of 50 µL (diluted 10 times in acetone in the case of PVDF-CP crude of polymerization reaction) of the solution in a freshly cleaved mica wafer. AFM images were obtained with a Pico SPM II provided by Molecular Imaging. The imagery was controlled by the PicoView 1.10 software. The experiments were all carried out in tapping mode. The types of tips used were PPS-FMR purchased from Nanosensors with a frequency resonance between 45 and 115 kHz and a force constant between 0.5 and 9.5 N/m. Gwyddion 2.25 software was used to treat the images.

Samples were prepared by spin coating 50 µL of the solution on the surface of freshly cleaved mica wafers (sample concentration 0.1 mg mL^{-1} in DMF: THF (1:9)).

Mass spectrometry.

Measurements were performed on a Bruker MicroToF for ESI ToF and on an Agilent 6130B Single Quad for ESI.

3.3. Synthesis

Synthesis of *N*-succinimidyl bromoacetate

N-hydrosuccinimide (NHS) (6.33 g; 55 mmol) was placed in a 250 mL round bottom flask and dissolved in 80 mL of DCM under magnetic stirring. The flask was placed in an ice bath and TEA (8.1 mL, 58 mmol) in 16 mL of DCM was added dropwise. After stirring for 30 min, 2-bromopropionyl bromide (6.08 mL; 58mmol) in 16 mL of DCM was added dropwise over a period of 1 h. The reaction was left for 24 h at room temperature (25°C). The mixture was then washed with brine and the organic phase was collected and dried over anhydrous magnesium sulfate. The solvent was removed by rotary evaporation. The brownish solid was dissolved in isopropanol at 75°C and a few drops of DCM were added. The product was left to crystallize in the fridge and was filtered to yield 92%.

^{1}H NMR (400 MHz, $CDCl_3$, ppm, Figure S1) δ = 4.65 (q, J = 7.4 Hz, 1H), 2.88 (s, 4H), 2.00 (d, J = 7.4 Hz, 3H)

Synthesis of NHS-CTA-XA

N-succinimidyl bromoacetate (6 g; 24 mmol) was placed in a 100 mL round bottom flask and dissolved in 45 mL of absolute ethanol. The flask was placed in an ice bath and potassium ethyl xanthogenate (4.8 g; 29 mmol) was added with a spatula over a period of 45 min. The heterogeneous solution was stirred 3 h at room temperature, then filtered over Celite and the solvent removed by rotary evaporation. The product was dissolved in 90 mL of DCM and washed with pure water (4 x 150 mL) and dried over magnesium sulphate then solvent was removed by rotary evaporation yielding a crystalline yellow powder (65 %).

^{1}H NMR (400 MHz, $CDCl_3$, ppm, Figure S2) δ = 4.70 (dq, J = 7.1, 2.3 Hz, 1H), 4.64 (q, J = 7.4 Hz, 2H), 2.86 (s, 4H), 1.73 (d, J = 7.4 Hz, 3H), 1.44 (t, J = 7.1 Hz, 3H).

^{13}C {^{1}H} DEPT135 NMR (101 MHz, $CDCl_3$, Figure S3) δ = 13.52 (-O-CH_2-**C**H_3), 16.50 (-CH(**C**H_3), 25.60 (-**C**H_2-**C**H_2-), 44.19 (-**C**H(CH_3), 70.91 (-O-**C**H_2-CH_3).

Synthesis of the Cyclic Peptide CP-$(NH_2)_2$

Standard Fmoc-deprotection solid-phase peptide synthesis was used to first synthesize the protected linear peptide. Using a coupling agent, the cyclization was completed in dilute conditions to avoid intermolecular reactions. The insolubility of the stacked cyclic peptides in methanol was used to isolate the pure cyclic peptide. The cyclic peptide was then deprotected using TFA to reveal the amines of the lysines and azoles on the tryptophans.[20]

Synthesis of the Linear Peptide

H_2N-L-Lys(Boc)-D-Leu-L-Trp(Boc)- D-Leu-L-Lys(Boc)- D-Leu-L-Trp(Boc)- D-Leu-COOH

Fully protected linear octapeptide was prepared via solid phase peptide synthesis (SPPS) on a Prelude Automated Peptide SynthesizerTM (Protein Technologies Inc.) using 2-chlorotrityl chloride resin as the solid support. The first Fmoc protected amino acid was coupled to the resin using DIPEA (4 eq.) in DCM, followed by capping of unreacted resin sites using a solution of MeOH:DIPEA:DCM (7:1:2, v/v/v). Deprotection of the Fmoc group of the amino acids was done using 20% piperidine in DMF. Subsequent amino acids were coupled using Fmoc-amino acids (5 eq.), HCTU (5 eq.) and NMM (10 eq.) in DMF. In the last step, the linear octapeptide was cleaved from the resin (while keeping protecting groups on) by a solution of 20 vol % 1,1,1,3,3,3-hexafluoro-2-propanol (HFIP) in DCM.

^{1}H-NMR (400 MHz, TFA-d, ppm, Figure S4): δ = 8.07 (m, 2H, Trp), 7.54-7.22 (m, 8H, Trp), 5.11 (m, 2H, Hα Trp), 4.68-4.48 (m, 5H, Hα Leu and Hα Lys), 4.21 (m, 1H, Hα Lys Nend), 3.32-3.03 (m, 8H, CH_2 Trp and CH_2-NH Lys), 2.07-0.86 (m, 60H, CH_2-CH_2-CH_2 Lys, CH_2-CH Leu, C(CH_3)$_3$ Boc), 0.85-0.58 (m, 24H, CH_3 Leu), NH signals not observed

MS (ESI): $[M+H]^+$ calculated: 1498.9, found 1498.8.

Protected cyclic peptide

Cyclo(-L-Lys(Boc)-D-Leu-L-Trp(Boc)-D-Leu-L-Lys(Boc)-D-Leu-L-Trp(Boc)-D-Leu-)

Linear peptide (200 mg, 0.127 mmol) was dissolved in DMF (20 mL) and N_2 was bubbled through the solution for 20 min. DMTMM·BF_4 (1.2 eq., 51 mg, 0.152 mmol) was dissolved in DMF (5 mL), N_2 bubbled through the solution for 20 min, then this solution was added dropwise to the linear peptide solution. The mixture was stirred under an atmosphere of N_2 for 5 days. The DMF solution was reduced to a volume of ~ 1 mL under reduced pressure, and methanol (20 mL) was added. Aliquots of the suspension were distributed into 2 mL eppendorf tubes and centrifuged at 10000 rpm for 4 minutes using a benchtop centrifuge. After removal of the supernatant, the pellets were redispersed in methanol. The eppendorf tubes were centrifuged once more and the supernatant discarded. The pellets were redispersed in methanol and the solvent was evaporated under reduced pressure to yield the Boc-protected cyclic peptide in the form of a white powder.

Yield 73 % (138 mg, 0.093 mmol).

^{1}H-NMR (400 MHz, TFA-d, ppm, Figure S5): δ = 8.07 (m, 2H, Trp), 7.54-7.22 (m, 8H, Trp), 5.15 (m, 2H, Hα Trp), 4.79-4.52 (m, 6H, Hα Leu and Hα Lys), 3.29-2.96 (m, 8H, CH_2 Trp and CH_2-NH Lys), 2.07-0.86 (m, 60H, CH_2-CH_2-CH_2 Lys, CH2-CH Leu, $C(CH_3)_3$ Boc), 0.85- 0.58 (m, 24H, CH_3 Leu), NH signals not observed (Figure S5).

MS (ESI) $[M+Na]^+$ calculated: 1503.89, found: 1503.8.

Deprotected Cyclic Peptide

Cyclo(-L-Lys-D-Leu-L-Trp-D-Leu-L-Lys-D-Leu-L-Trp-D-Leu-)

Boc groups were removed in using a deprotection solution of TFA/TIPS/H_2O (18:1:1 vol, 5 mL). The protected cyclic peptide was stirred for 2 hours in the deprotection solution, then precipitated using chilled diethyl ether and washed twice more with chilled diethyl ether. The off-white powder was collected and dried under vacuum.

Yield: quantitative

^{1}H-NMR (400 MHz, TFA-d, ppm, Figure S6): δ = 7.64-6.60 (m, 10H, Trp), 5.16 (m, 2H, Hα Trp), 4.73 (m, 6H, Hα Leu and Hα Lys), 3.29-2.96 (m, 8H, CH_2 Trp and CH_2-NH Lys), 2.07-0.86 (m, 24H, CH_2-CH_2-CH_2 Lys, CH_2-CH Leu,), 0.85-0.58 (m, 24H, CH_3 Leu), NH signals not observed.

MS (ESI) $[M+Na]^+$ calculated: 1103.67, found: 1103.7.

Synthesis of the Cyclic Peptide Chain Transfer Agent

The desired cyclic peptide chain transfer agent CP-$(XA)_2$ was obtained by coupling the chain transfer agent (NHS-CTA-XA) to the lysine residues of CP (Scheme 1). The CP (120 mg; 0.11 mmol; 1 eq.) was dissolved in 6 mL DMSO. Complete dissolution was reached after 10 min in ultrasound bath. Then NHS-CTA-XA (64.68 mg; 0.222 mmol, 2 eq.) and NMM (0.074 mL; 0.666 mmol, 3eq.) were added and the solution was stirred at room temperature for 3 days. Mass spectrometry monitoring indicated that the coupling reaction was quantitative, as no residual CP or mono-functionalized product was detected, affording CP-$(XA)_2$ in high yield. The product was precipitated twice in chilled diethyl ether and dried under vacuum.

MS (ESI)(Figure S7) $[M+Na]^+$ calculated: 1433.91, found: 1433.95.

VDF RAFT/MADIX polymerization using NHS-CTA-XA in acetone

RAFT polymerization was carried out in a thick Carius tube containing NHS-CTA-XA (38 mg, 13.01 10^{-5} mmol), acetone (7 ml) and the initiator (Tigonox-121)(3.3 mg, 1.30 10^{-5} mmol) were mixed and the tube was degassed with three freeze-pump-thaw cycles to remove any trace of oxygen. The gaseous VDF monomer (0.5 g, 7.81 10^{-3} mmol) was transferred into the Carius tube and cooled in liquid nitrogen. The tube was then sealed, before being placed horizontally in a shaking water bath thermostated at 73 °C. After 24 hours, the tube was frozen in liquid nitrogen and opened. After reaching room temperature the crude sample was precipitated twice in a tenfold excess of chilled pentane. The NHS-PVDF polymer was recovered by centrifugation at 4000 rpm for 15 min in 10 mL conical centrifuge tubes. The polymer was dried overnight under vacuum at 25 °C. (Yield 60 %) **Yield was used as conversion** since conversion is very difficult to calculate accurately for gaseous monomers.

^{1}H NMR (400 MHz, $(CD_3)_2CO$, ppm, Figure S8) : δ = 1.39-1.49 (m, -CH(C**H$_3$**)(C=O)-O-NHS and –S-(C=S)-O-CH_2-C**H$_3$**), 1.65-1.85 (m, -CF_2-C**H$_3$**), $^3J_{HH}$= 7.2 Hz), 2.21-2.43 (m,-CF_2-C**H$_2$**-C**H$_2$**-CF_2-, VDF-VDF TT (tail-to-tail) reverse addition), 2.70-3.23 (t, -CF_2-C**H$_2$**-CF_2-, VDF-VDF HT (head-to-tail) regular addition), 3.60-3.69 (s, -(C=O)-O-C**H$_3$**), 4.05-4.18 (t, -CF_2-C**H$_2$**-S(C=S)OEt, $^3J_{HF}$= 18 Hz), 4.70-4.78 (q, (-S(C=S)O-C**H$_2$**-CH_3, $^3J_{HH}$= 7.1 Hz), 6.10-6.50 (tt, $^2J_{HF}$= 55 Hz , $^3J_{HH}$= 4.5 Hz -CH_2-CF_2-**H**).

^{19}F NMR (376 MHz $(CD_3)_2CO$, ppm, Figure S9) : δ = -115.63 (-CH_2-CF_2-C**F$_2$**-CH_2-CH_2-, VDF-VDF HH reverse addition), -114.29 ($^2J_{HF}$= 55 Hz, -CH_2-C**F$_2$**-H), -113.34 (-CH_2-C**F$_2$**-CF_2-CH_2-CH_2-, HH reverse addition), -113.09 (CH_2-CF_2-**CF_2**-CH_2-S-), -112.69 (-CH_2-**CF_2**-CF_2-CH_2-S-), -94.79 (-CH_2-CH_2-C**F$_2$**-CH_2-, TT reverse addition), -107.7 (-CF_2-C**H$_3$**), -93.50 (-CH_2-C**F$_2$**-CH_2-CH(CH_3)(C=O)-), -92.12 (-CH_2-C**F$_2$**-CH_2-CF_2H), -91.44 (-CH_2-CH_2-CF_2-CH_2-**CF_2**-CH_2-CF_2-, regular VDF-VDFHT addition), -91.00 (-CH_2-C**F$_2$**-CH_2-, regular VDF-VDF HT addition).

VDF RAFT/MADIX grafting-from polymerization using CP-$(XA)_2$

RAFT polymerization was carried following the same protocol described above. CP-$(XA)_2$ (93 mg, 6.51 10^{-5} mmol), acetone (7 ml) and the initiator (Trigonox-121)(3 mg, 1.30 10^{-5} mmol) were sonicated for 10 min or until complete CP-$(XA)_2$ dispersion before degassing and introducing the gaseous VDF monomer (0.5 g, 7.81 10^{-3} mmol). *Conversion was not estimated since the study of the aggregates in solution required no further purification. However, by weighting the carious tube before and after polymerization (after breaking the glass tube to allow unreacted VDF to evaporate) 50% yield was estimated.

^{1}H NMR (400 MHz, C_3D_7NO, ppm, Figure S10): δ = 9.00-8.50 (m, -NH), 7.80-7.10 (m, **H** Trp), 5.55 (m, **Hα** Trp), 5.00 (m, C**H$_2$** Z CTA), 4.85-4.50 (m, **Hα** Leu and **Hα** Lys), 4.40-4.20 (m, CF_2C**H$_2$**S-), 4.10-3.80 (m, C**H$_2$**CF_2S-), 3.40-3.30 (m, -CH_2- Trp), 3.25 (t, C**H$_2$**CF_2 PVDF), 2.00-1.30 (m, C**H$_2$**-C**H$_2$**-C**H$_2$** Lys, CH_2- C**H** Leu), 1.35-0.85 (m, C**H$_3$** Leu, -CH-C**H$_3$** R CTA, -CH_2-C**H$_3$**).

^{19}F NMR (376 MHz, C_3D_7NO, ppm, Figure S11): δ = -115.39 (-CH_2-CF_2-C**F$_2$**-CH_2-CH_2-, VDF-VDF HH reverse addition), -113.92 (-CH_2-C**F$_2$**-H), -112.97 (-CH_2-C**F$_2$**-CF_2-CH_2-CH_2-, HH reverse addition), -112.80 (-C**F$_2$**-CH_2-S-), -106.98 (-C**F$_2$**-CH_3), -94.14 (-CH_2-CH_2-C**F$_2$**-CH_2-, TT reverse addition), -93.53 (CP-NH-(C=O)-(CH_3)CH-CH_2-C**F$_2$**-), 91.85 (-CH_2-C**F$_2$**-

CH_2-CF_2H), -91.45 (CH_2-C**F_2**-CH_2-CF_2-S-), -91.25 (-CF_2-CH_2-C**F_2**-CH_2-CF_2-CF_2), -91.00 (C**F_2**-CH_2-C**F_2**- CH_2-C**F_2**, regular VDF-VDF HT addition).

DP estimation:

$$DP_{theo} = \frac{\frac{1}{2}[VDF]_0}{[CP(XA)_2]_0} = \frac{\frac{1}{2}7.81\ 10^{-3}\ \text{mmol}}{6.51\ 10^{-5}\ \text{mmol}} = 60 \quad (1)$$

DP estimated from ^{19}F NMR spectrum of CP-$(PVDF)_2$ (Figure S11) using equation 2:

$$DP = \frac{(\int_{-70.0}^{-70.1} + \int_{-74.0}^{-74.1} + \int_{-112.7}^{-112.9} CF_2(Z\ end\ group)) + (\int_{-90.9}^{-94.0} + \int_{-112.8}^{-115.5} CF_2((HT),(HH),(R\ end\ group)\ and\ (H\ termination)))}{(\int_{-70.0}^{-70.1} + \int_{-74.0}^{-74.1} + CF_2(Z\ end\ group))} \quad (2)$$

3.4. Self-assembly

Preparation of CP-$(PVDF)_2$ solutions

Stock solutions of 1 mg mL^{-1} of CP-$(PVDF)_2$ were prepared in DMF or DMSO, using ultrasounds and heating at 60°C until full solubilisation.

Preparation of the self-assembled nanotubes

0.1 mL of the solutions described above were placed in stirring plates with magnetic stirring bars. Then, 0.9 or 9.9 mL of THF were added dropwise using a syringe pump at a fixed rate of (4 mL h^{-1}) (final conjugate concentration and solvent ratios of 0.1 or 0.01 mg mL^{-1} and 1:9 or 1:99, respectively). The solutions were let stirred slowly for 24h. 10 µL and 50 µL were taken to prepare TEM and AFM samples respectively.

4. Results and discussion

As mentioned in the introduction two approaches are commonly employed for the preparation of polymer-CP conjugates (i.e., grafting-to and grafting-from). Grafting-to appeared to be more suitable for the preparation of well-defined PVDF-CP

conjugates, as it allows the synthesis and characterization of the polymer before conjugation, and is less restrictive (i.e., necessity of a common solvent to solubilize the CP and suitable for VDF MADIX polymerization). A grafting-to strategy was then designed (see Fig. S12). It included the synthesis of an azide-functionalized PVDF (N_3-PVDF), following a protocol previously described.[32] The lysine moieties of the CP were first modified with an activated alkyne group in order to carry a copper-free "click-reaction" involving the N_3-PVDF and the activated alkyne-CP. Such reactions are commonly carried out in the presence of an excess of polymer and the conjugate is purified by selective precipitation in a selective-solvent or solvent mixture that allows the precipitation of the conjugate or excess of unreacted polymer.[20] However, in our case this purification step was not successful and only led to mixtures of CP-PVDF and N_3-PVDF. Therefore, a grafting-from synthetic route was designed (see Scheme 1).

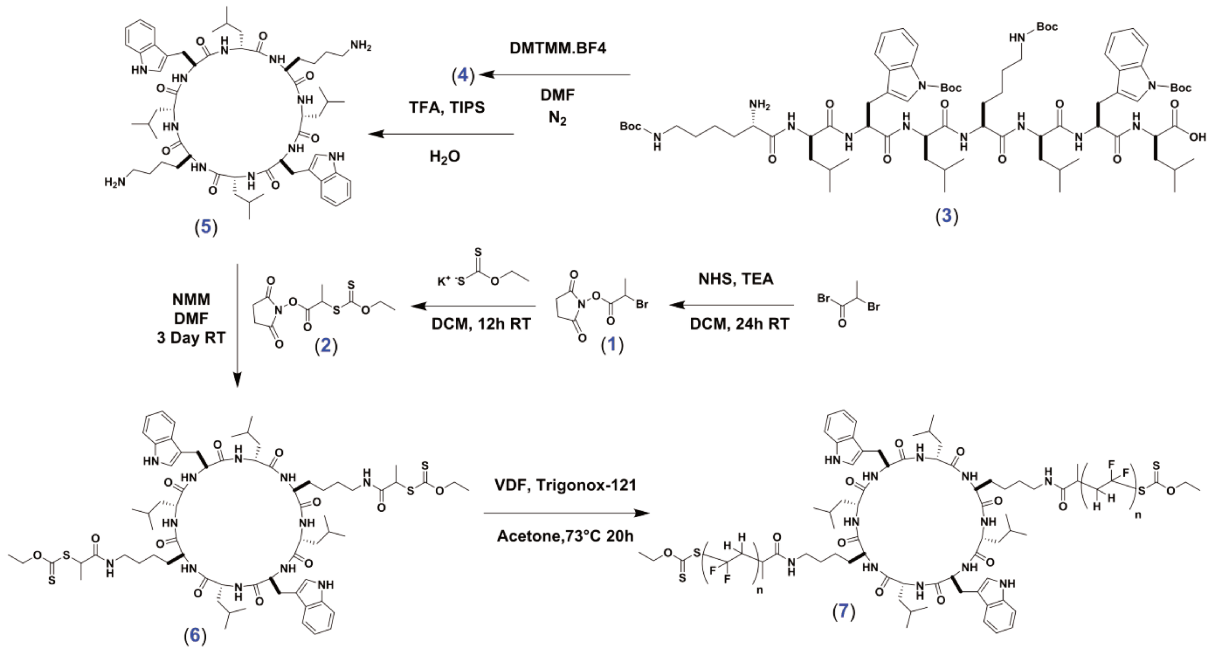

Scheme 1. Synthetic route to the cyclic peptide-PVDF conjugate employing a "grafting-from" approach.

Synthesis of the Cyclic Peptide Chain Transfer Agent

The initial cyclic peptide (CP) (sequence of amino acids: L-Lys(Boc)-D-Leu-L-Trp(Boc)-D-Leu-L-Lys(Boc)-D-Leu-L-Trp(Boc)-D-Leu) (see Scheme 1) was synthesized according to previously reported procedures.[20] The desired cyclic peptide chain transfer agent CP-$(XA)_2$ was then obtained by coupling the chain transfer agent (NHS-CTA-XA) to the

lysine residues of the CP. Mass spectrometry indicated that the reaction proceeded quantitatively in 72 hours. Although aminolysis of the xanthate moiety by the lysine residues is a potential side reaction, no evidence of such corresponding *O*-thiocarbamate formation was found.

Study of the Suitable Polymerization Conditions

Recent studies show that xanthate RAFT agents, peroxide initiators and DMC as solvent are good conditions for VDF RAFT/MADIX polymerization.[33] VDF polymerization using DMC proceeds faster than in numerous other organic solvents, affording high yields, and also leads to relatively small quantities of $-CH_2-CF_2-H$ terminated dead chains (mainly formed by radical transfer from $-CF_2^{\bullet}$ radicals to DMC).[33,34] However, in this case the prepared $CP(-XA)_2$ was not soluble in DMC. DMF and DMSO are both suitable solvents for the CP and PVDF as well as being solvent of choice for most polymerizations initiated from CP macroCTA[20,22]. Unfortunately, these 2 solvents are not suitable for the polymerization of VDF, as they act as strong chain transfer agents leading to poor conversion.[34] Acetone was however identified as a suitable solvent for the polymerization of VDF, although more prone to H-abstraction than DMC. The unmodified CP was insoluble in acetone, but the modified CP macro CTA ($CP(-XA)_2$) was found to form a stable milky solution in acetone. This milky appearance could presumably be due to the strong tendency of the CP to self-assemble into nanotubes (see S17). Having no better choice than acetone as solvent and a test polymerization of VDF using NHS-CTA-XA as the RAFT agent and acetone as solvent was carried out. ^{1}H NMR results confirmed that PVDF is formed albeit at the cost of loss of end-group functionality due to an increased amount of transfer to the solvent (i.e., higher amount of dead chains ($-CH_2-CF_2-H$) (Figure S8, signals at -92.00 and -114.5 ppm)). The molar fractions of the different end-groups were determined using equations S13 to S16 and data from the ^{19}F NMR spectrum (Figure S9), and estimated to be: $-CF_2$-XA (0%), $-CH_2$-XA (40.4 %), $-CF_2-CH_3$ (6.2 %) and $-CF_2H$ (49.4 %). A typical VDF polymerization in DMC usually leads to up to 15 % of $-CF_2H$ and 85 % of $-CH_2$-XA for a polymer of DP=50.[33] Higher DP with high functionality can only be obtained at low conversions due to a progressive disappearance of the chain-ends (loss of xanthate group) of the PVDF-XA chains.[35]

"Grafting-from" VDF RAFT Polymerization

The polymerization of VDF was carried out in the milky suspension of $CP(XA)_2$ in acetone. This system is presumably more akin to a grafting-from system due to the suboptimal solubility of the macroCTA in acetone. Visually no changes were observed in terms of solubility and colloidal stability at the end of the polymerization.

The PVDF segments polymerized from the CP had an average DP of 64 (the DP was calculated using Eqn 2). As the CP macroCTA carries two propagating radicals per CTA, the obtained polymer had slightly higher molecular weight than the estimated theoretical DP of 60 (calculated from Eqn 1). However, the results suggest that in spite of partial solubility of the $CP(XA)_2$ macroCTA in acetone, the xanthate sites were available for VDF polymerization. They might be exposed at the outer surface of the self-assembled structures or VDF is able to diffuse to the polymerization sites of the self-assembled CPs.

Interestingly, this polymerization led to PVDF segments possessing major amounts of regular functional end groups ($-CH_2CF_2$-XA). The molar fraction of the different end-groups determined from the ^{19}F NMR spectrum (Figure S11) are: $–CF_2$-XA (36.0%), $-CH_2$-XA (9.7 %), $-CF_2-CH_3$ (8.2 %) and $–CF_2H$ (46.1 %). These values are surprising as previous studies had shown that the RAFT polymerization of VDF in DMC quickly leads to the accumulation of the reversely terminated functional end-groups ($-CF_2-CH_2$-XA) due to their inferior reactivity towards the majority radicals $–CF_2^{\bullet}$.[33,34,36] This usually leads to polymers composed of 85 % of $–CF_2-CH_2$-XA (due to reverse additions) and a minimal amount of H-ended dead chains (15%). In any case, $-CF_2$-XA chains are not present at that stage of the polymerization.[33,35] The use of acetone as solvent does not seem to be related, since the polymerization of PVDF in acetone using the NHS-CTA-XA only leads to more $-CF_2$-H end group (due to solvent transfer) but no presence of $-CF_2$-XA is observed at the end of the polymerization. This could be related to the big size of the R substituent (the CP) of the macroCTA. Larnaudie and co-workers observed that the apparent propagation constant $k_{p,app}$ appeared lower in the case of polymerizations mediated by a CP macroCTA when compared to a polymerization mediated by the CTA.[20] Here, the milky solution is likely to be formed of pre-

assembled CP macroCTAs, thus, each preassembled aggregate would present more than two CTA-XA moieties, leading to a slower polymerization.

Self-Assembly

The alternating D- and L-amino acid conformation of the peptide leads to the formation of a flat disk-like structure. Perpendicular to the plane of the cyclic peptide ring, the amide bonds participate in hydrogen bonding to form a nanotubular assembly.[6,37,38] The L-lysines positioned on the opposite sides of the peptide ring provide anchor functionalities for attachment of the polymer segments, where PVDF polymer chains have been grown via a grafting-from approach.

First, the crude product obtained after VDF polymerization was examined to observe the structures present in the acetone suspension shown in Figure 1a.

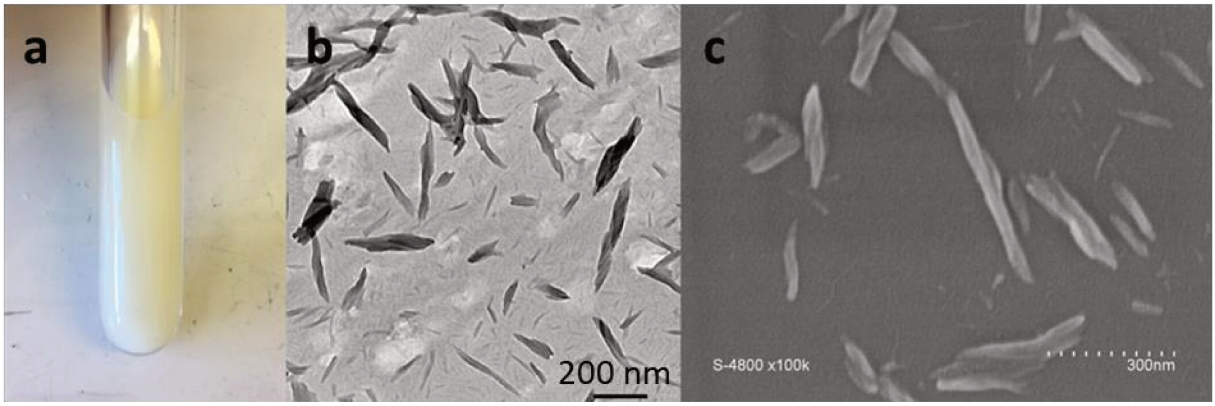

Figure 1. a) Photograph of the Carius tube containing the acetone suspension after polymerization of VDF in the presence of CP-$(XA)_2$, b) and c) TEM and SEM images of the diluted suspension shown in a) respectively.

TEM and SEM images (Figure 1b and 1c respectively) show that the CP-$(PVDF)_2$ spontaneously self-assembled in acetone into aggregates of various sizes which look like short rods and twisted ribbon (see Figure 1 b, c and Figure S18). The width of these objects was not homogeneous (30 to 100 nm) and exceeded, in most cases, the diameter of the CP-$(PVDF)_2$.

The disassembly of the CP-$(PVDF)_2$ structures in various solvents was investigated by dynamic light scattering (DLS). A very limited range of solvents lead to macroscopically clear solutions of the unconjugated CP: trifluoroaceticacid (TFA), dimethyl-sulfoxide (DMSO) and *N*,*N*-dimethylformamide (DMF).[2,13,16,38] However,

solution of CP-$(PVDF)_2$ in TFA turned black after 1h (PVDF is not attacked by strong acids so it must the result of degradation of CP moieties). DMF and DMSO were thus preferred. Nevertheless, DLS analyses of DMF or DMSO (also good solvents for PVDF) solutions of the CP-$(PVDF)_2$ conjugates at room temperature showed the presence of big aggregates. This may be caused by the crystallinity of PVDF which prevents complete dissolution of the conjugates. These results evidenced that stable aggregates are formed and that usually strong competitive solvents, such as trifluoroethanol (TFE), that effectively disaggregate pure cyclic peptides are not able to efficiently disassemble the CP(-$PVDF)_2$ aggregates. This observation highlights the huge potential of these cyclic peptides for the organization of PVDF chains due to the H-bond directed assembly of the CPs (Figure S19). PVDF itself cannot assemble into either tubular or twisted ribbon structures.

In order to study the self-assembly behavior of these CP-PVDF conjugates, complete dissociation of the aggregates is necessary. This was achieved by using hot DMF or DMSO (60 or 80 °C respectively) and sonication (2h). The efficiency of this procedure to completely dissolve the CP-$(PVDF)_2$ was confirmed by DLS (Figure S20). Then addition of THF to these solutions decreased the H-bonding acceptor properties of the solvent and triggered the aggregation process.[18]

First the objects formed from the CP(-$PVDF)_2$ DMF solution were studied. The formation of tubular aggregates was first confirmed by SEM (Figure 2).

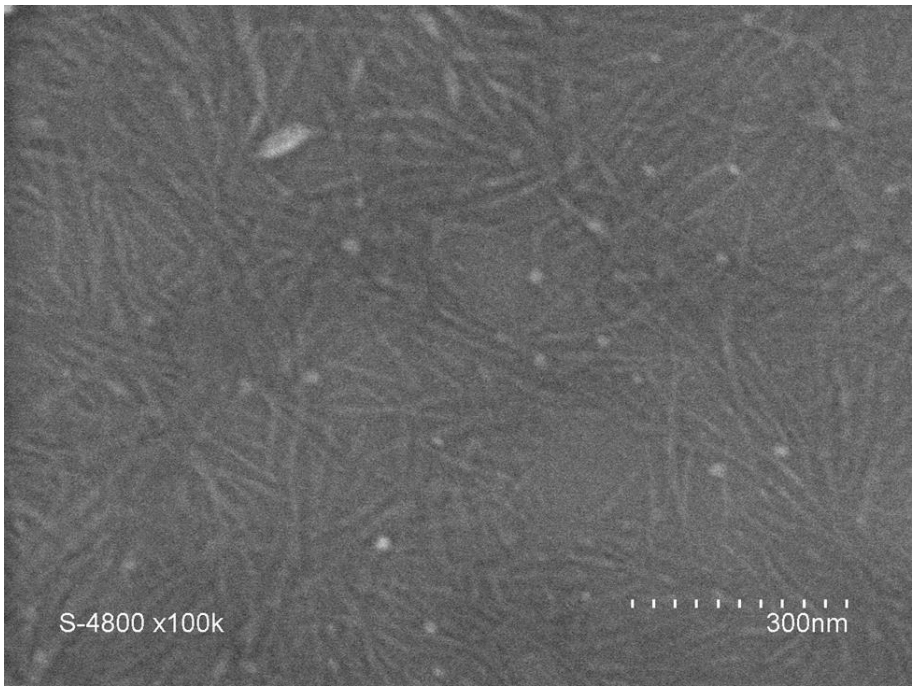

Figure 2. SEM image of CP(-PVDF)$_2$ prepared from a 1 mg mL^{-1} DMF solution by adding THF (addition rate was 4 mL h^{-1}). Final concentration 0.1 mg mL^{-1} (DMF 10% v/v in the final solution).

Tubular structures with lengths up to 200 nm seemed to have formed (Figure 2). TEM observations were also carried out (Figure 3). The images obtained from a sample prepared on a Formvar/carbon TEM grid (Figure 3a and 3b) show an extended area of tubular aggregates. However, it seemed to be too concentrated and lacked good contrast. The same sampled was diluted ten times with pure THF (note that the dilution in pure THF can affect the aggregation (reducing DMF concentration)) and deposited on a Lacey/Carbon TEM grid (Figure 3b and 3c) exhibited better contrast and easier imaging. The self-assembled structures appeared to be tubes with length ranging from 200 to 300 nm and width/diameter of around 40 nm.

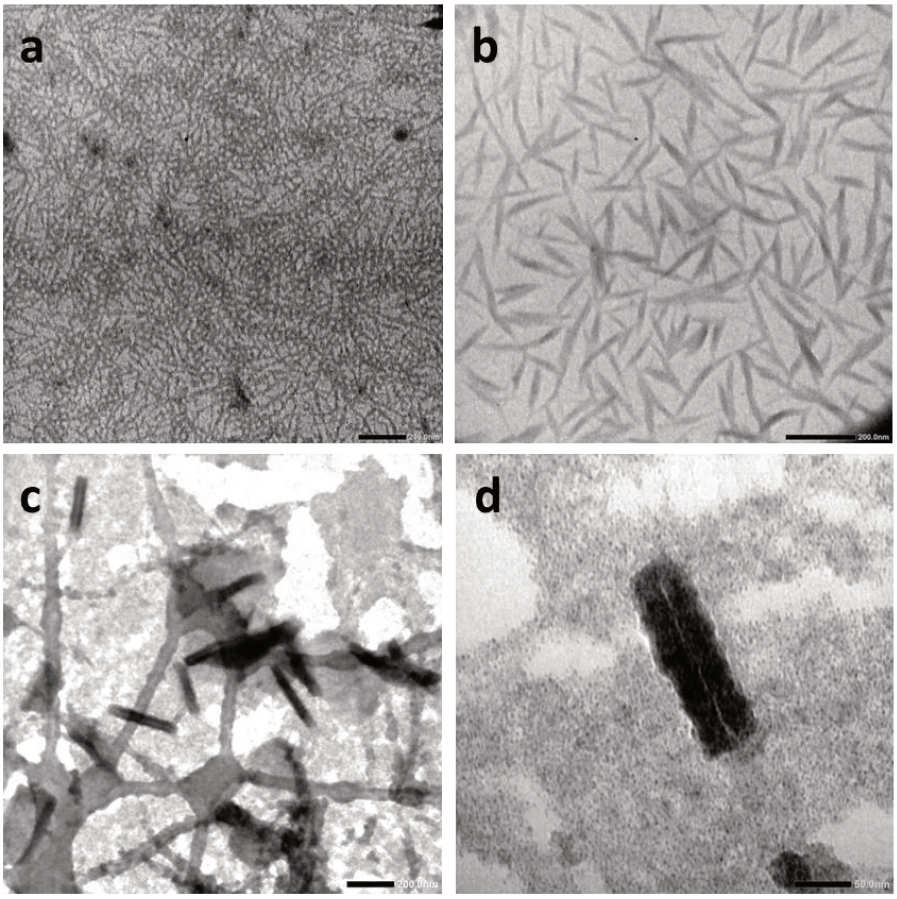

Figure 3. TEM image of CP(-PVDF)$_2$ prepared from a 1 mg mL^{-1} DMF solution by adding THF (addition rate was 4 mL h^{-1}). Final concentration (a, b) 0.1 mg mL^{-1} and (c, d) 0.01 mg mL^{-1} (DMF 10 and 1% v/v respectively in the final solutions). Sample prepared in Formvar/Carbon coated copper TEM grid (a and b). Sample prepared in Lacey/Carbon coated copper TEM grid (c and d) scales bars are 200 nm (a, b, and c) and 50 nm (d).

Further study of the self-assembled objects was performed using AFM. (see Fig. 4).

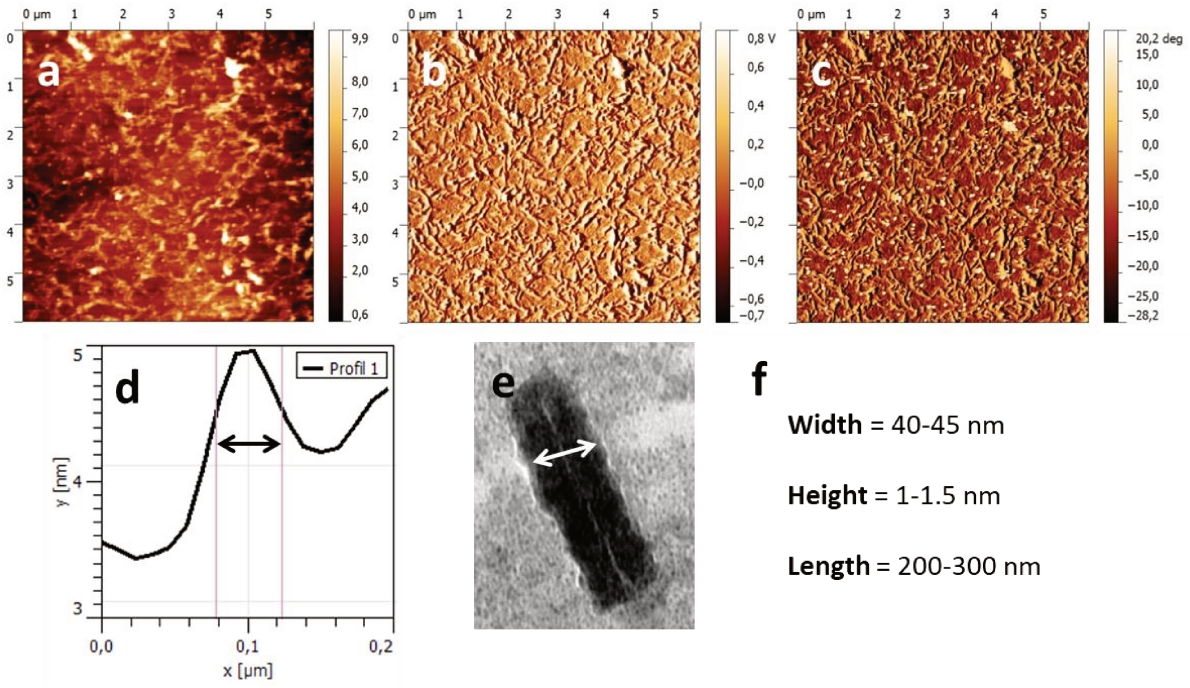

Figure 4. AFM images of the nanotubes formed by CP(-PVDF)$_2$ deposited onto mica substrate. The sample was prepared from a 1:9 DMF:THF solution (conjugate concentration 0.1 mg mL^{-1}). (a) Topography, (b) Amplitude, (c) Phase, (d) Height profile and width measurement, (e) width from TEM image, (f) values extracted from the analysis TEM and AFM images.

AFM micrographs obtained from spin-coating of the CP containing solutions onto a mica substrate show an extended area of fiber like aggregates (Fig. 4a-c). The length and diameter of the fiber-like assemblies was extracted from the topographic image (Fig. 4a) and compared to data obtained from TEM (Fig. 3 and Fig 4e) and the obtained average results (Fig. 4f) were employed to determine the aggregation number (N_{agg}).

Considering that the distance between each cyclic peptide, reported to be 0.47 nm,[31] and the data extracted from the TEM and AFM (length = 200-300 nm) we found that the aggregation number (N_{agg} ,number of stacked CPs) is between 425 and 638 for this system. The width of such aggregates is dictated by the CP diameter and the DP of PVDF. Considering PVDF in its α crystalline phase, PVDF arms of 64 units are estimated to have an approximated length of 12 nm. The CP has an approximate diameter of 10 nm (having an internal diameter of 7-8 nm). This makes a CP(-PVDF)$_2$ conjugate of 34 nm, not far from the widths observed under TEM (40-45 nm).

The objects formed from the CP(-PVDF)$_2$ solution in DMSO were quite different. As in the previous case, the samples prepared on Formvar/carbon TEM grids did not afford high quality images at high magnification, while samples prepared on

Lacey/Carbon TEM grids did. These images (Figure 5) revealed the presence of long tubular aggregates.

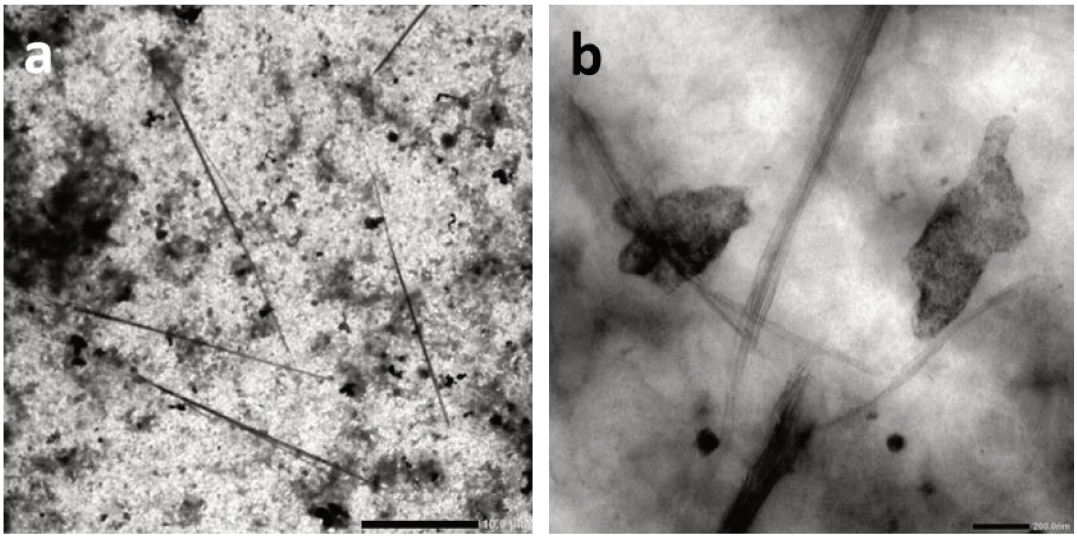

Figure 5. SEM image of CP(-PVDF)$_2$ prepared from a 1 mg mL^{-1} DMF solution by adding THF (addition rate was 4 mL h^{-1}). Final concentration 0.1 mg mL^{-1} (DMF 10% v/v in the final solution).

These tubular aggregates of up to 25 µm in length (Figure 5a) seemed to be composed by laterally stacked peptide-polymer long tubes (Figure 5b). Bundles of laterally stacked peptides in deuterated DMSO has already been reported.[14] Koh *et al.* observed the presence of unconjugated CP small aggregates in deuterated DMSO.[14] They interpreted their results as bundles of short tubes laterally stacked. This behavior was also observed in the case of partially conjugated CP-polymer (i.e., some CP bearing only one polymer arm) with polybutylacrylate (pBA) as the polymer, due to imperfect conjugation when a "grafting-to" approach in DMSO was used (due to poor compatibility of pBA and DMSO the conjugation was not complete).[14] Two hypotheses can be proposed to explain the formation of these aggregates. If some of the CP(-PVDF)$_2$ aggregates were not completely dissociated in DMSO, the addition of THF may have triggered the aggregation of the dissolved unimers on the laterally stacked conjugates. It is assumed that not all polymerization sites were accessed during the polymerization in the milky suspension of CP(XA)$_2$.

With the lengths obtained from TEM analysis (25 µm) we can conclude that the N_{agg} is of up to 53,191 which is greater than any value reported for similar cyclic peptides. Such

long assemblies have not been reported for other CP-polymer conjugates, suggesting that PVDF polymer chains have an important impact on the assembly of these conjugates. More analysis such as small angle neutron scattering (SANS) are necessary to elucidate the structure of these aggregates in solution.

5. Conclusions

The synthesis of a cyclic peptide macroCTA bearing two xanthate moieties (CP(-XA)$_2$) was successfully achieved by the coupling of a NHS-functionalized RAFT agent onto the lysine residues of the cyclic peptide. The RAFT/MADIX polymerisation of VDF in the presence of this CP(-XA)$_2$ difunctional macroCTAs was carried out in acetone, although CP(-XA)$_2$ form a stable suspension in this solvent. The success of the polymerisation was confirmed by ^{19}F NMR. The presence of the signal of the first VDF unit directly connected to the R-group of the macro CTA, and of that of CF$_2$-XA moiety confirmed that the PVDF grew from the macroCTA and that the polymerisation was controlled by the RAFT mechanism, despite a high extent of transfer (three times more than a VDF RAFT polymerization carried in DMC) leading to a major loss of polymer functionality. PVDF-based tubular structures of different lengths were prepared by self-assembly of the CP(-PVDF)$_2$ polymer-conjugate using DMSO or DMF as good solvent and THF as the PVDF-selective solvent. These PVDF-based tubular aggregates might find an application in the preparation of thin-film membranes (Figure S21) thanks to its ability to form porous nanostructured surfaces in the absence of pore forming additives.

6. References

1. Shu, J. Y., Panganiban, B. & Xu, T. Peptide-Polymer Conjugates: From Fundamental Science to Application. *Annu. Rev. Phys. Chem.* **64**, 631–657 (2013).
2. Kim, H. S., Hartgerink, J. D. & Ghadiri, M. R. Oriented self-assembly of cyclic peptide nanotubes in lipid membranes. *J. Am. Chem. Soc.* **120**, 4417–4424 (1998).
3. Ruiz, L., Wu, Y. & Keten, S. Tailoring the water structure and transport in nanotubes with tunable interiors. *Nanoscale* **7**, 121–132 (2015).
4. Hartlieb, M. *et al.* Stimuli-responsive membrane activity of cyclic-peptide–polymer

conjugates. *Chem. Sci.* 5476–5483 (2019).

5. Rodriguez-Vazquez, N. *et al.* Membrane-Targeted Self-Assembling Cyclic Peptide Nanotubes. *Curr. Top. Med. Chem.* **14**, 2647–2661 (2015).

6. Granja, J. R., McRee, D. E., Khazanovich, N., Milligan, R. A. & Ghadiri, M. R. Self-assembling organic nanotubes based on a cyclic peptide architecture. *Nature* **366**, 324–327 (1993).

7. Chapman, R., Danial, M., Koh, M. L., Jolliffe, K. A. & Perrier, S. Design and properties of functional nanotubes from the self-assembly of cyclic peptide templates. *Chem. Soc. Rev.* **41**, 6023–6041 (2012).

8. De Santis, P., Morosetti, S. & Rizzo, R. Conformational Analysis of Regular Enantiomeric Sequences. *Macromolecules* **7**, 52–58 (1973).

9. Dehn, S., Chapman, R., Jolliffe, K. A. & Perrier, S. Synthetic strategies for the design of peptide/polymer conjugates. *Polym. Rev.* **51**, 214–234 (2011).

10. Motesharei, K. & Reza Ghadiri, M. Diffusion-Limited Size-Selective Ion Sensing Based on SAM-Supported Peptide Nanotubes. *J. Am. Chem. Soc.* **119**, 11306–11312 (1997).

11. Binfield, J. G., Brendel, J. C., Cameron, N. R., Eissa, A. M. & Perrier, S. Imaging Proton Transport in Giant Vesicles through Cyclic Peptide–Polymer Conjugate Nanotube Transmembrane Ion Channels. *Macromol. Rapid Commun.* **39**, 1–6 (2018).

12. Larnaudie, S. C. *et al.* Cyclic Peptide-Polymer Nanotubes as Efficient and Highly Potent Drug Delivery Systems for Organometallic Anticancer Complexes. *Biomacromolecules* **19**, 239–247 (2018).

13. Chapman, R., Jolliffe, K. A. & Perrier, S. Modular design for the controlled production of polymeric nanotubes from polymer/peptide conjugates. *Polym. Chem.* **2**, 1956–1963 (2011).

14. Koh, M. L., FitzGerald, P. A., Warr, G. G., Jolliffe, K. A. & Perrier, S. Study of (Cyclic Peptide)–Polymer Conjugate Assemblies by Small-Angle Neutron Scattering. *Chem. - A Eur. J.* **22**, 18419–18428 (2016).

15. Couet, J. & Biesalski, M. Polymer-wrapped peptide nanotubes: Peptide-grafted polymer mass impacts length and diameter. *Small* **4**, 1008–1016 (2008).

16. Poon, C. K., Chapman, R., Jolliffe, K. A. & Perrier, S. Pushing the limits of copper mediated azide-alkyne cycloaddition (CuAAC) to conjugate polymeric chains to cyclic peptides. *Polym. Chem.* **3**, 1820–1826 (2012).

17. Chapman, R., Koh, M. L., Warr, G. G., Jolliffe, K. A. & Perrier, S. Structure elucidation and control of cyclic peptide-derived nanotube assemblies in solution. *Chem. Sci.* **4**, 2581–2589 (2013).

18. Ten Cate, M. G. J., Severin, N. & Börner, H. G. Self-assembling peptide-polymer conjugates comprising (D-alt-L)- cyclopeptides as aggregator domains. *Macromolecules* **39**, 7831–7838 (2006).

19. Gauthier, M. A. & Klok, H. A. Peptide/protein-polymer conjugates: Synthetic strategies and design concepts. *Chem. Commun.* 2591–2611 (2008).

20. Larnaudie, S. C., Brendel, J. C., Jolliffe, K. A. & Perrier, S. Cyclic peptide-polymer conjugates: Grafting-to vs grafting-from. *J. Polym. Sci. Part A Polym. Chem.* **54**, 1003–1011 (2016).

21. Couet, J. & Biesalski, M. Surface-initiated ATRP of N-isopropylacrylamide from initiator-modified self-assembled peptide nanotubes. *Macromolecules* **39**, 7258–7268 (2006).

22. Larnaudie, S. C., Brendel, J. C., Jolliffe, K. A. & Perrier, S. PH-Responsive, Amphiphilic Core-Shell Supramolecular Polymer Brushes from Cyclic Peptide-Polymer Conjugates. *ACS Macro Lett.* **6**, 1347–1351 (2017).

23. Danial, M., My-Nhi Tran, C., Young, P. G., Perrier, S. & Jolliffe, K. A. Janus cyclic peptide-polymer nanotubes. *Nat. Commun.* **4**, (2013).

24. Rho, J. Y. *et al.* Probing the Dynamic Nature of Self-Assembling Cyclic Peptide–Polymer Nanotubes in Solution and in Mammalian Cells. *Adv. Funct. Mater.* **28**, 1–11 (2018).

25. Ameduri, B. M. *et al.* Organometallic Mediated Radical Polymerization of Vinylidene Fluoride. *Angew. Chemie Int. Ed.* **57**, 2934–2937 (2018).

26. Ribeiro, C. *et al.* Electroactive poly(vinylidene fluoride)-based structures for advanced applications. *Nat. Protoc.* **13**, 681–704 (2018).

27. Wu, Y., Qu, J., Daoud, W. A., Wang, L. & Qi, T. Flexible composite-nanofiber based piezo-triboelectric nanogenerators for wearable electronics. *J. Mater. Chem. A* **7**, 13347–13355 (2019).

28. Najjar, R. *et al.* Biocompatible silk/polymer energy harvesters using stretched poly (vinylidene fluoride-cohexafluoropropylene) (PVDF-HFP) Nanofibers. *Polymers (Basel).* **9**, (2017).

29. Marino, T., Russo, F., Figoli, A. & May, H. The Formation of Polyvinylidene Fluoride Membranes with Tailored Properties via Vapour / Non-Solvent Induced Phase Separation. 1–17 (2018).

30. Wang, Y. *et al.* A silane-based interfacial crosslinking strategy to design PVDF membranes with versatile surface functions. *J. Memb. Sci.* **520**, 769–778 (2016).

31. Song, Q., Yang, J., Rho, J. Y. & Perrier, S. Supramolecular switching of the self-assembly of cyclic peptide-polymer conjugates: Via host-guest chemistry. *Chem. Commun.* **55**, 5291–5294 (2019).

32. Folgado, E. *et al.* Well-defined poly(vinylidene fluoride) (PVDF) based-dendrimers synthesized by click chemistry: Enhanced crystallinity of PVDF and increased hydrophobicity of PVDF films. *Polym. Chem.* **7**, 5625–5629 (2016).

33. Guerre, M. *et al.* Deeper Insight into the MADIX Polymerization of Vinylidene Fluoride. *Macromolecules* **48**, 7810–7822 (2015).

34. Asandei, A. D., Adebolu, O. I. & Simpson, C. P. Mild-temperature Mn 2(CO) 10-photomediated controlled radical polymerization of vinylidene fluoride and synthesis of well-defined poly(vinylidene fluoride) block copolymers. *J. Am. Chem. Soc.* **134**, 6080–6083 (2012).

35. Guerre, M. *et al.* Limits of Vinylidene Fluoride RAFT Polymerization. *Macromolecules* **49**, 5386–5396 (2016).

36. Boyer, C., Valade, D., Sauguet, L., Ameduri, B. & Boutevin, B. Iodine Transfer Polymerization (ITP) of Vinylidene Fluoride (VDF). influence of the defect of VDF chaining on the control of ITP. *Macromolecules* **38**, 10353–10362 (2005).

37. Reza Ghadiri, M. Self-assembled nanoscale tubular ensembles. *Adv. Mater.* **7**, 675 (1995).

38. Scanlon, S. & Aggeli, A. Self-assembling peptide nanotubes. *Nano Today* **3**, 22–30 (2008).

7. Supporting information

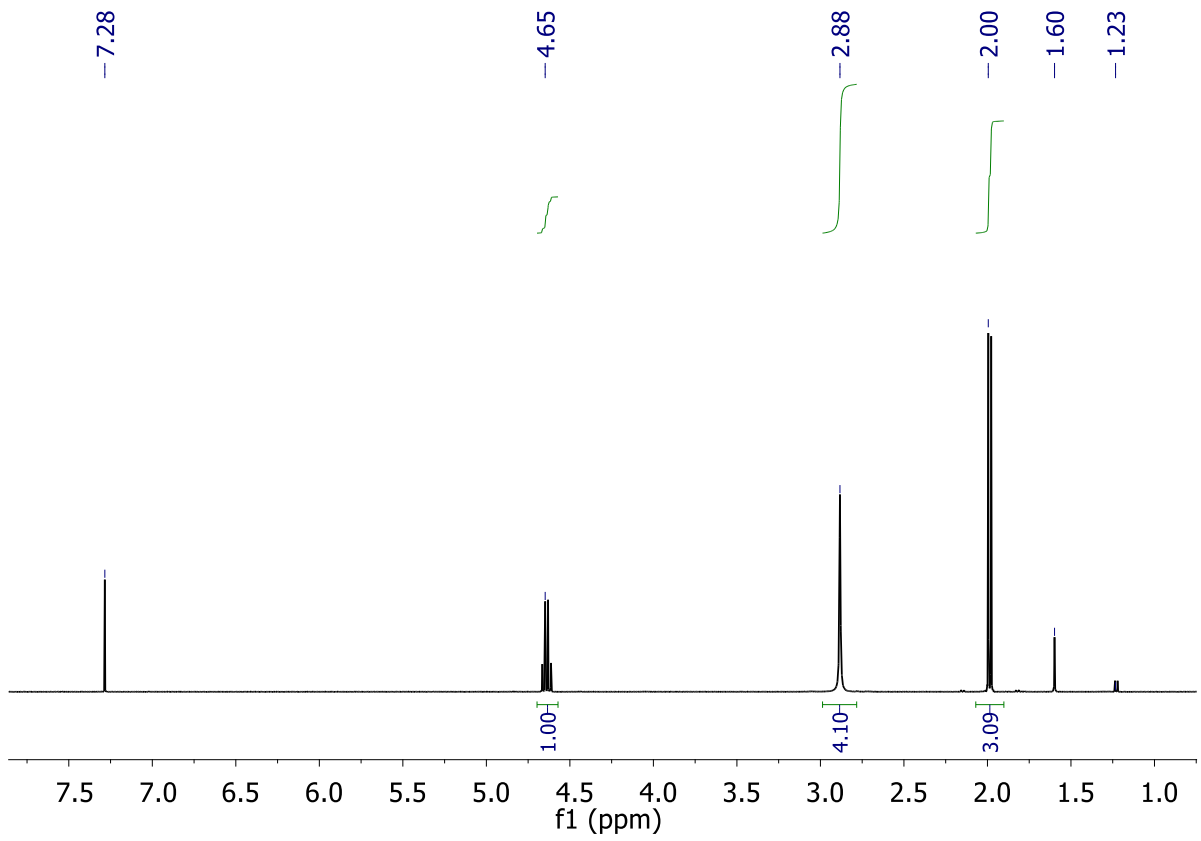

Figure S1. ^{1}H NMR spectrum ($CDCl_3$, 400 MHz) of *N*-succinimidyl bromoacetate.

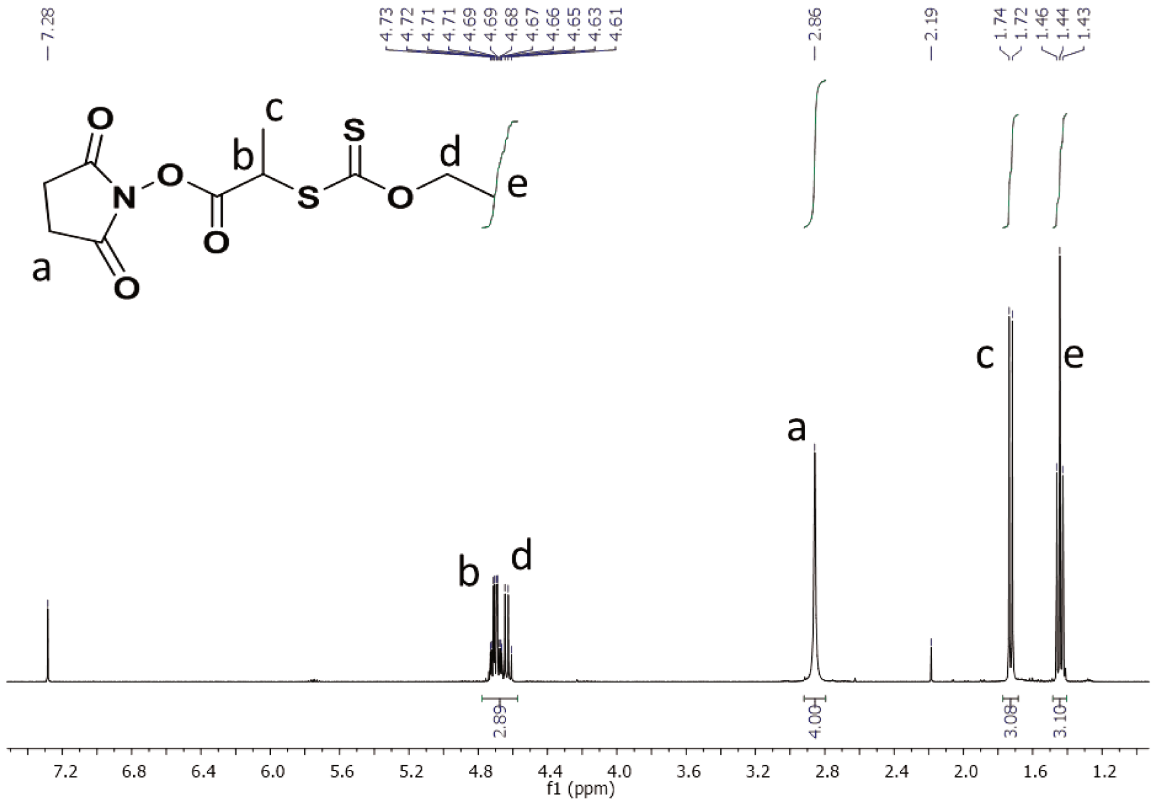

Figure S2. ^{1}H NMR spectrum ($CDCl_3$, 400 MHz) of NHS-CTA-XA.

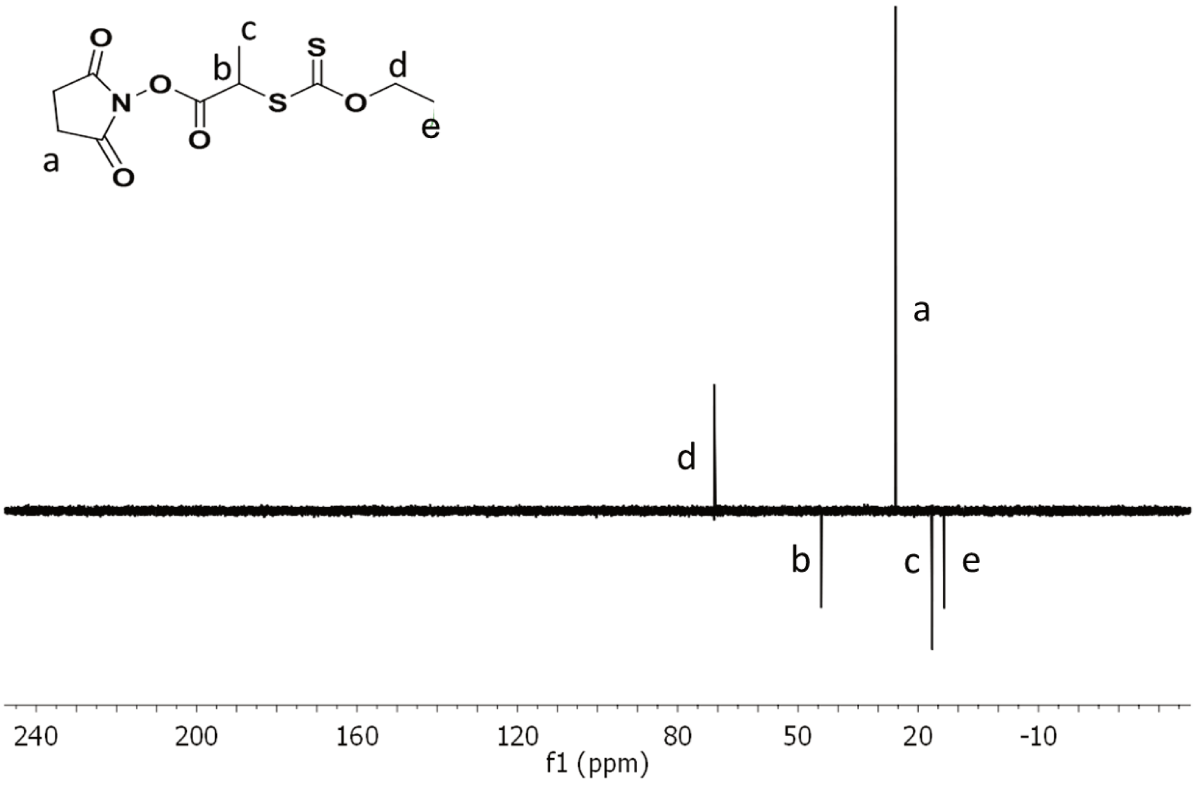

Figure S3. ^{13}C DEPT 135 NMR spectrum ($CDCl_3$, 101 MHz) of NHS-CTA-XA.

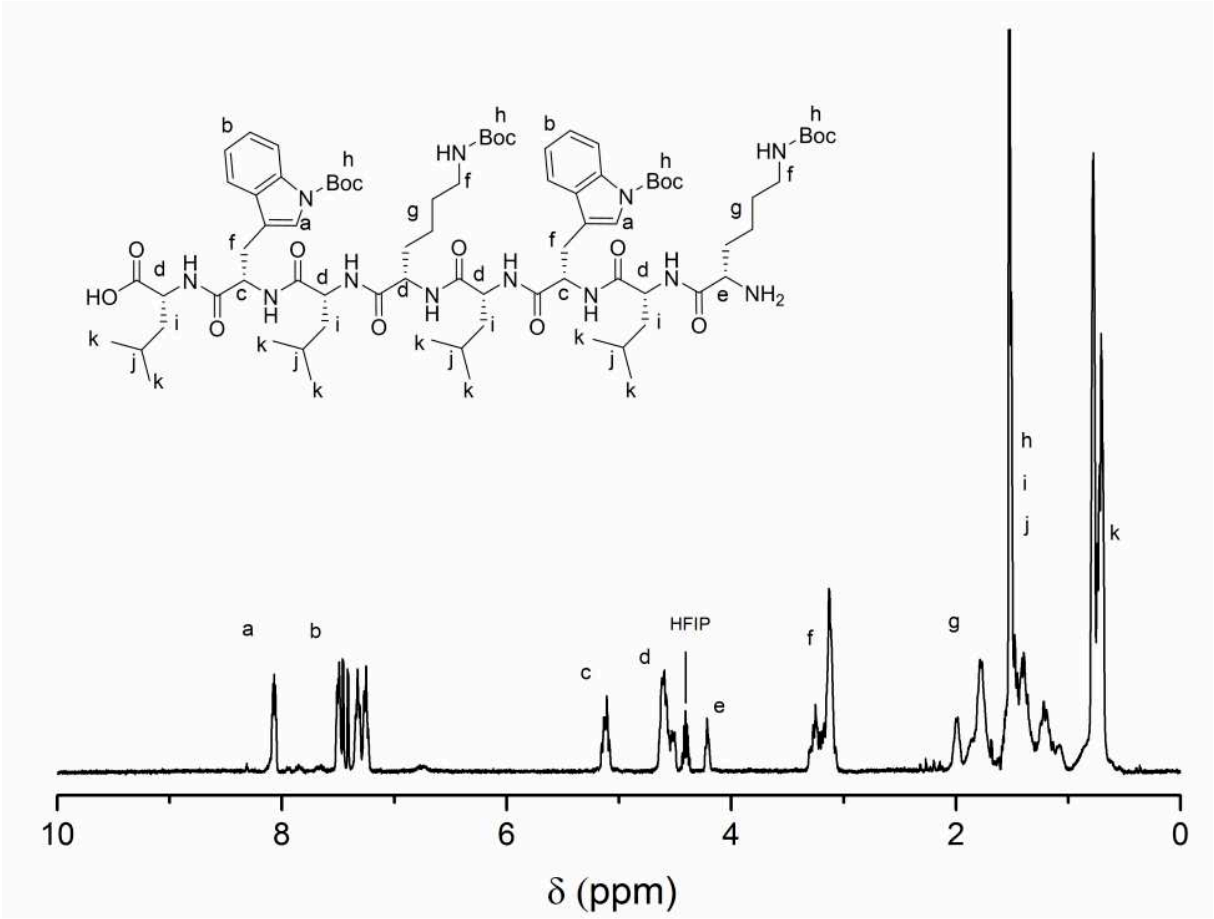

Figure S4. ^{1}H NMR spectrum (TFA-d, 400 MHz) of linear peptide H_2N-L-Lys(Boc)-D-Leu-L-Trp(Boc)-D-Leu-L-Lys(Boc)-D-Leu- L-Trp(Boc)-D-Leu-COOH

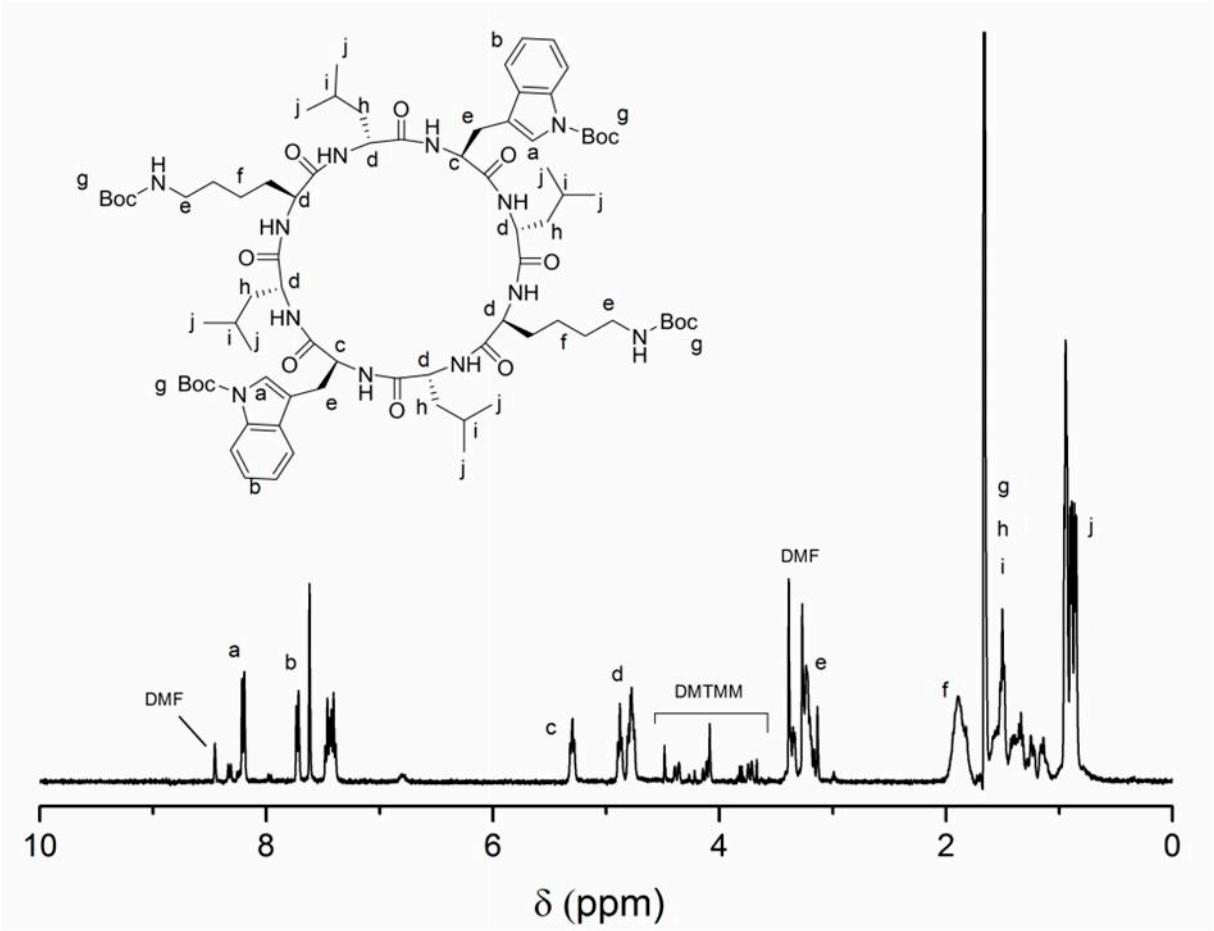

Figure S5. ^{1}H NMR spectrum (TFA-d, 400 MHz) of cyclic peptide (L-Lys(Boc)-D-Leu-L-Trp(Boc)-D-Leu)$_2$

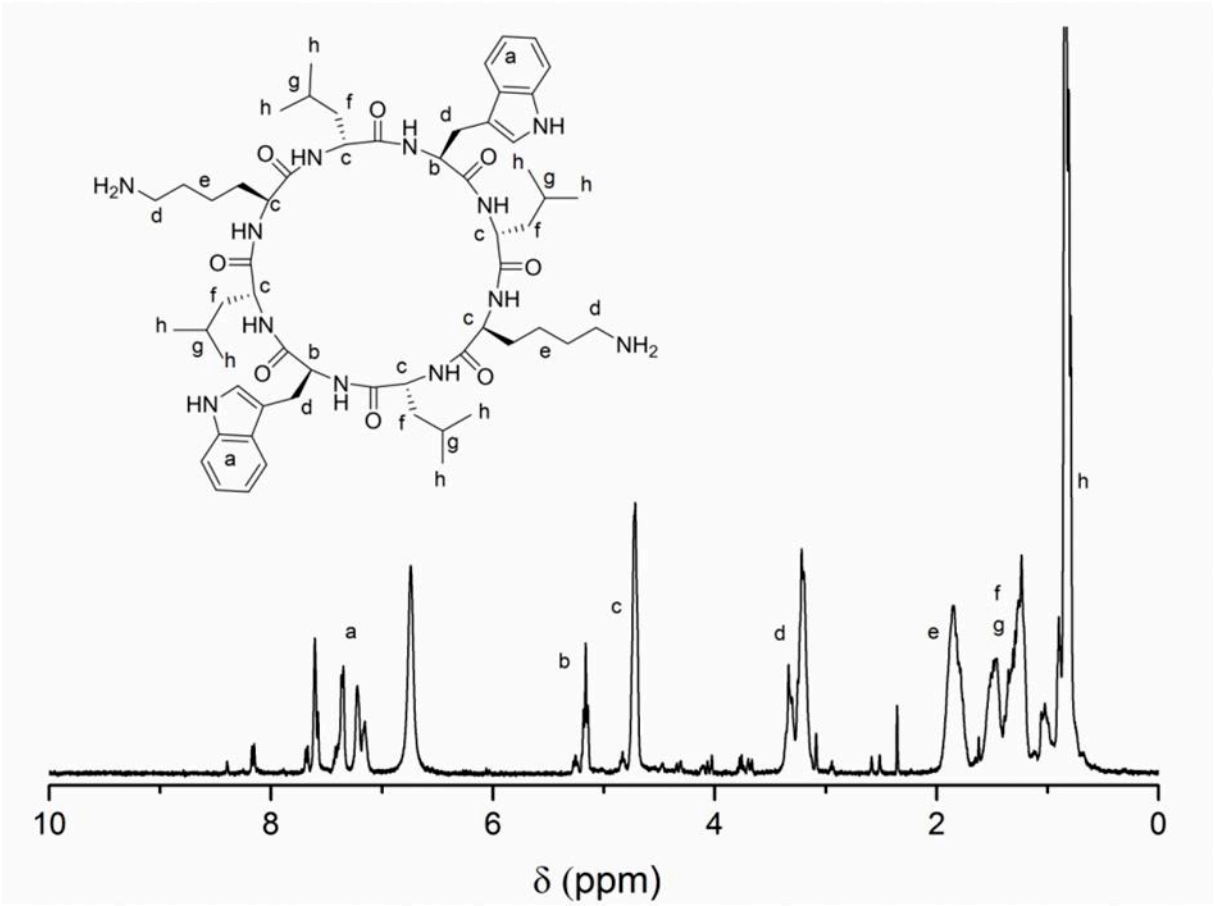

Figure S6. ^{1}H NMR spectrum (TFA-d, 400 MHz) of cyclic peptide (L-Lys-D-Leu-L-Trp-D-Leu)$_2$

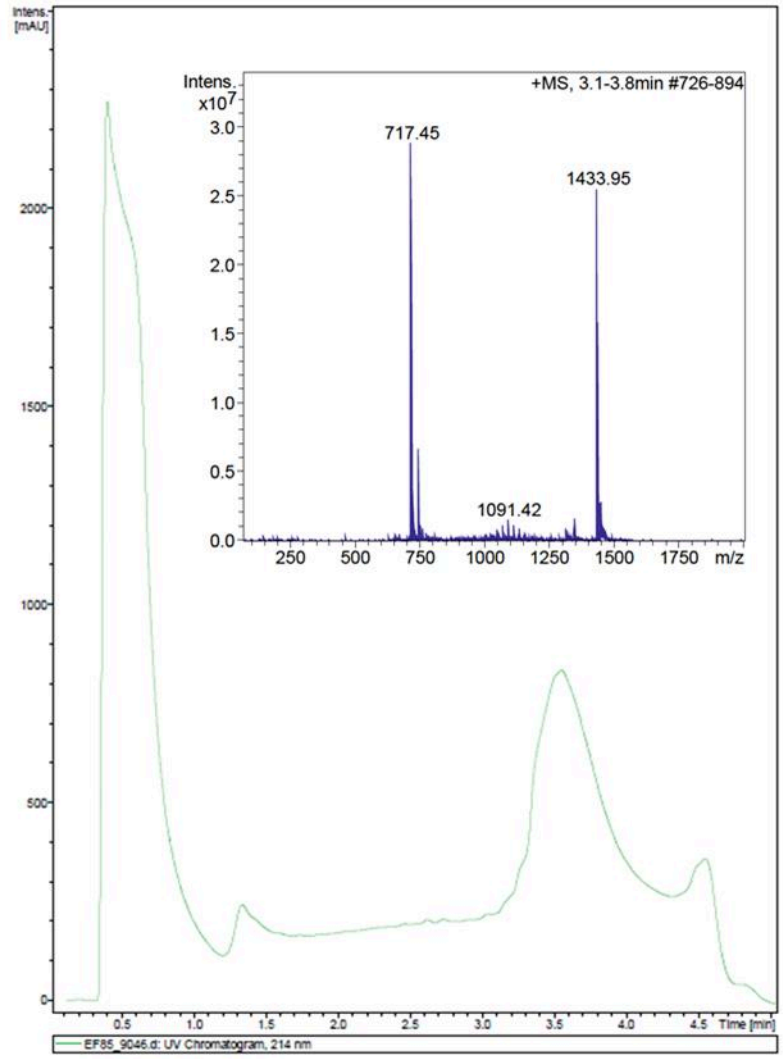

Figure S7. Mass spectrometry of the purified CP-$(XA)_2$.

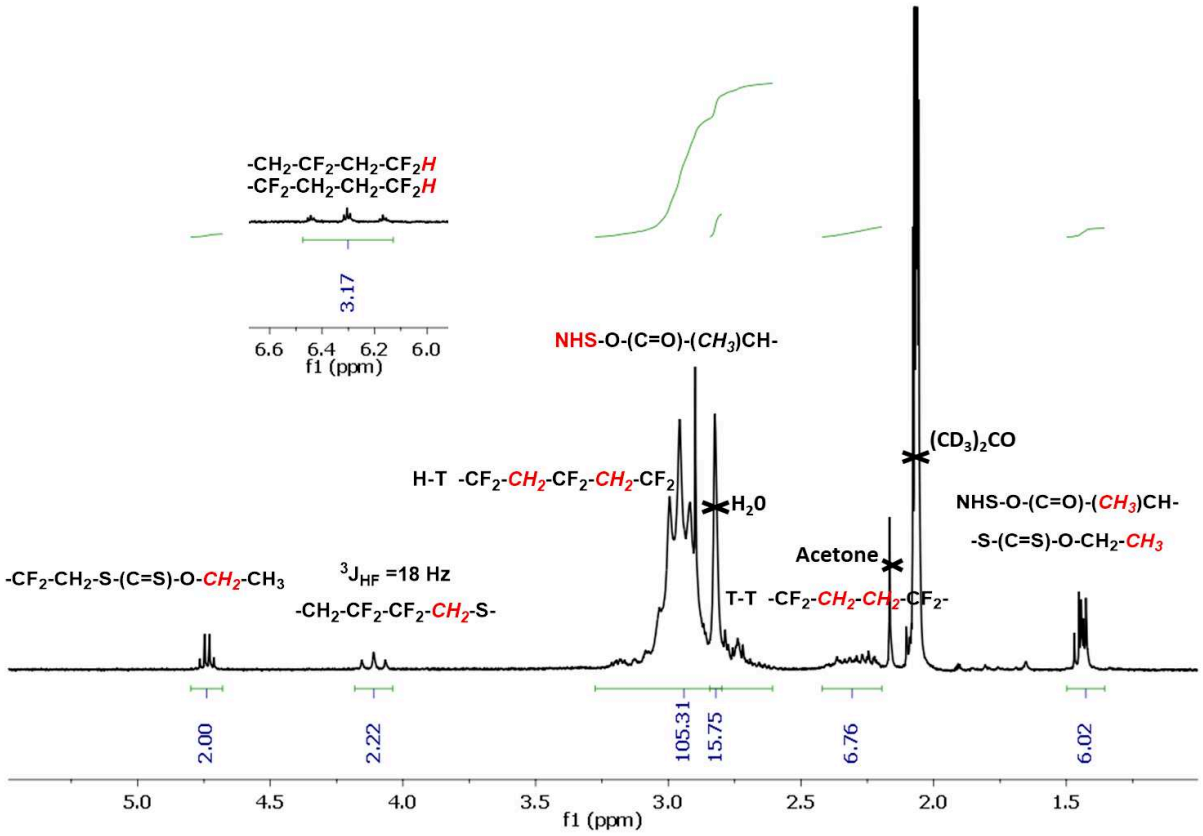

Figure S8. ^{1}H NMR spectrum in $(CD_3)_2CO$ of a PVDF homopolymer synthesized by RAFT polymerization with NHS-CTA-XA.

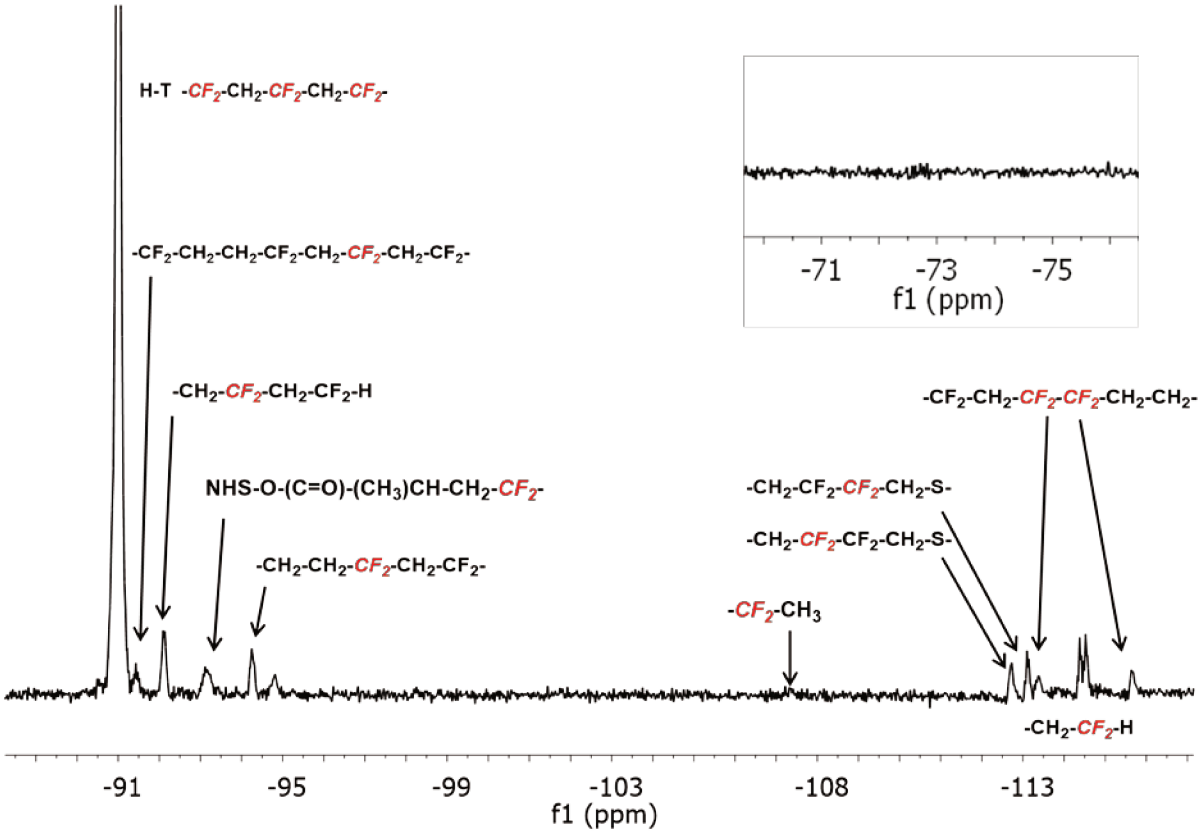

Figure S9. ^{19}F NMR spectrum in $(CD_3)_2CO$ of a PVDF homopolymer synthesized by RAFT polymerization with NHS-CTA-XA.

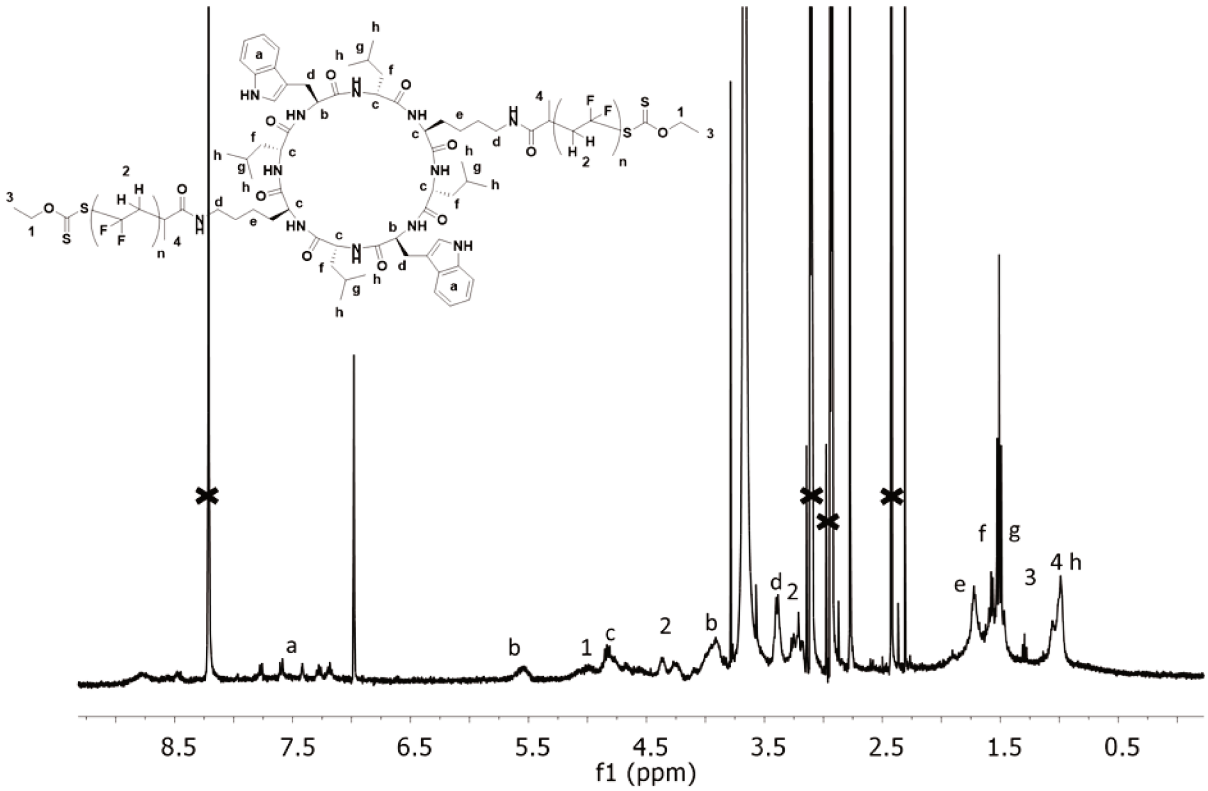

Figure S10. ^{1}H NMR spectrum in C_3D_7NO of a CP-$(PVDF)_2$ conjugate synthesized by surface initiated RAFT polymerization with CP$(-XA)_2$.

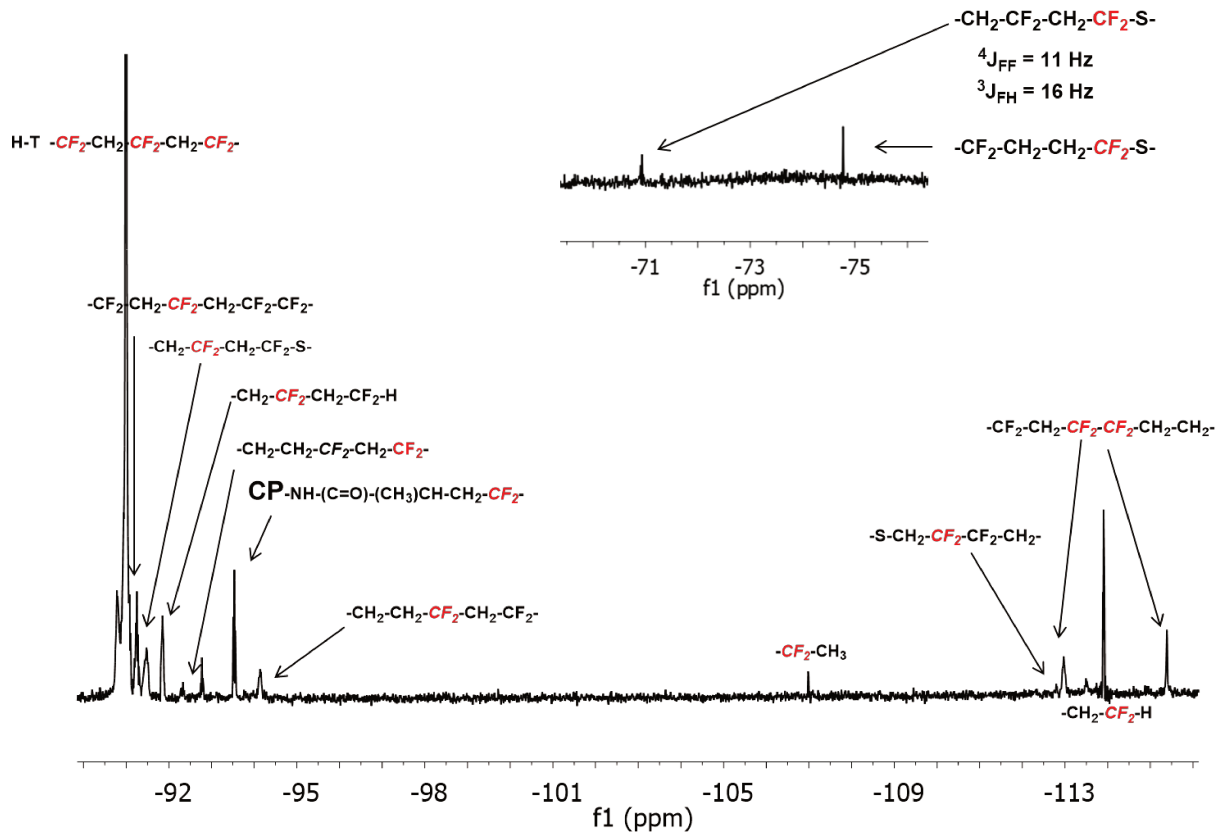

Figure S11. ^{19}F {^{1}H} NMR spectrum in C_3D_7NO of a CP-$(PVDF)_2$ conjugate synthesized by surface initiated RAFT polymerization with CP$(-XA)_2$.

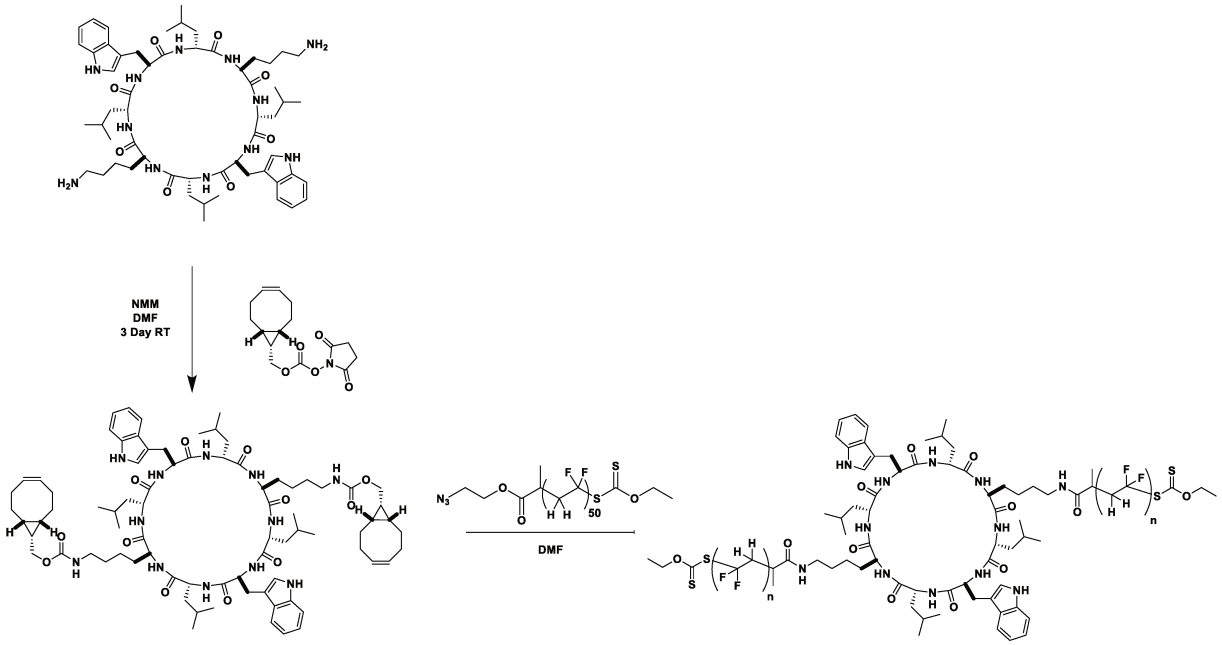

Figure S12. Synthetic route to the cyclic peptide-PVDF conjugate employing a »grafting-to » approach.

$$(\boldsymbol{S13})\ (\%) - CF_2 - CH_2 - XA = \frac{\int_{-112.85}^{-112.72} -CF_2 - CH_2 - XA}{\int_{-107.02}^{-106.95} -CF_2 - CH_3 + \int_{-74.82}^{-74.70} CH_2 - CH_2 - CF_2 - XA + \int_{-113.95}^{-113.85} -CH_2 - CF_2H + \int_{-112.85}^{-112.72} -CF_2 - CH_2 - XA}$$

$$(\boldsymbol{S14})\ (\%) - CH_2 - CF_2H = \frac{\int_{-113.95}^{-113.85} -CH_2 - CF_2H}{\int_{-107.02}^{-106.95} -CF_2 - CH_3 + \int_{-74.82}^{-74.70} CH_2 - CH_2 - CF_2 - XA + \int_{-113.95}^{-113.85} -CH_2 - CF_2H + \int_{-112.85}^{-112.72} -CF_2 - CH_2 - XA}$$

$$(\boldsymbol{S15})\ (\%) - CH_2 - CF_2 - XA = \frac{\int_{-74.82}^{-74.70} CH_2 - CH_2 - CF_2 - XA}{\int_{-107.02}^{-106.95} -CF_2 - CH_3 + \int_{-74.82}^{-74.70} CH_2 - CH_2 - CF_2 - XA + \int_{-113.95}^{-113.85} -CH_2 - CF_2H + \int_{-112.85}^{-112.72} -CF_2 - CH_2 - XA}$$

$$(\boldsymbol{S16})\ (\%) - CF_2 - CH_3 = \frac{\int_{-107.02}^{-106.95} -CF_2 - CH_3}{\int_{-107.02}^{-106.95} -CF_2 - CH_3 + \int_{-74.82}^{-74.70} CH_2 - CH_2 - CF_2 - XA + \int_{-113.95}^{-113.85} -CH_2 - CF_2H + \int_{-112.85}^{-112.72} -CF_2 - CH_2 - XA}$$

Equations used to calculate the proportions of chain-ends. Chain-end proportions were calculated using data from ^{19}F NMR of CP(PVDF)$_2$ (Fig S11).[1]

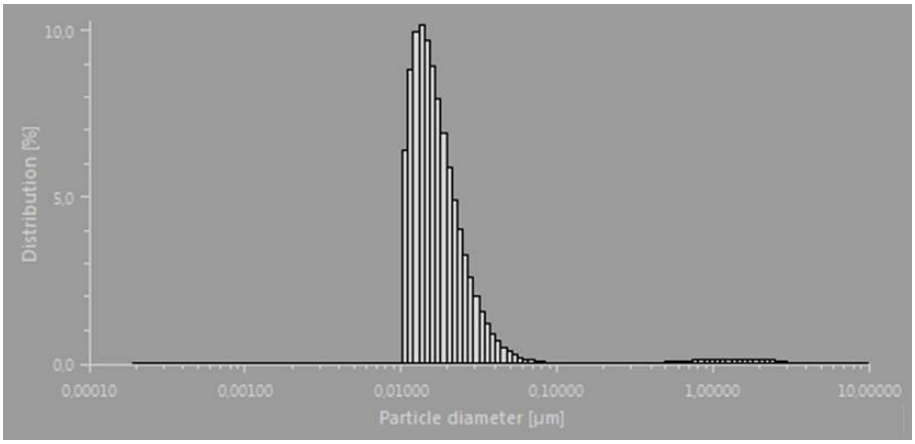

Figure S17. DLS number-average hydrodynamic diameter distribution of CP(XA)$_2$ conjugates (13.3 mg mL^{-1}) in acetone after heating at 50 °C (20 min) and sonication (20 min).

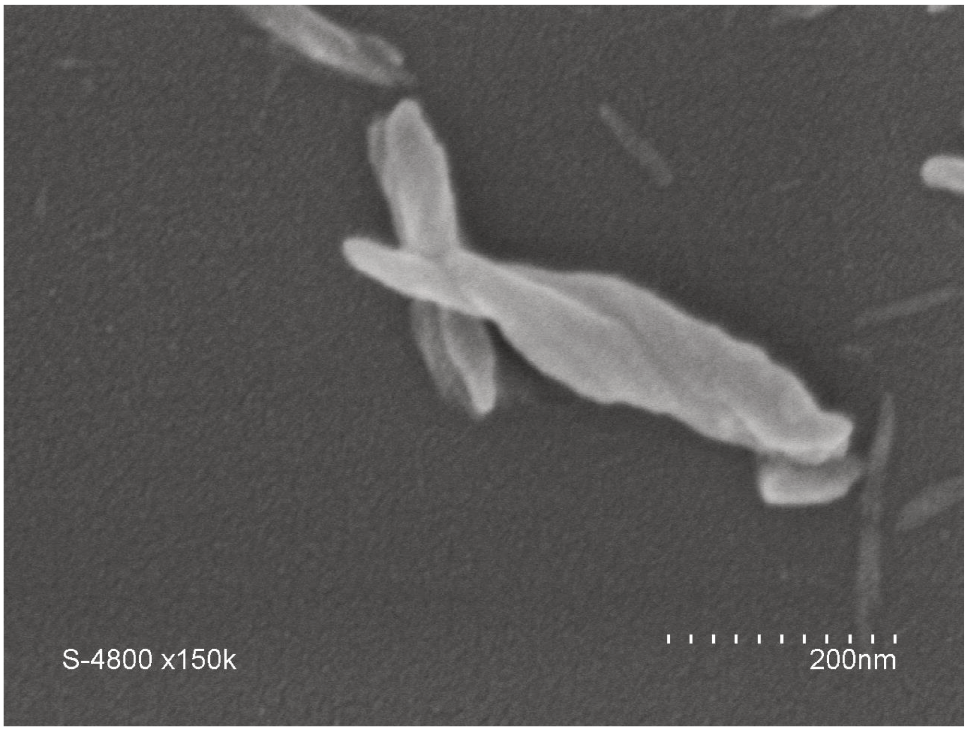

Figure S18. SEM images of twisted ribbon structures observed in the diluted suspension shown in Figure 1a.

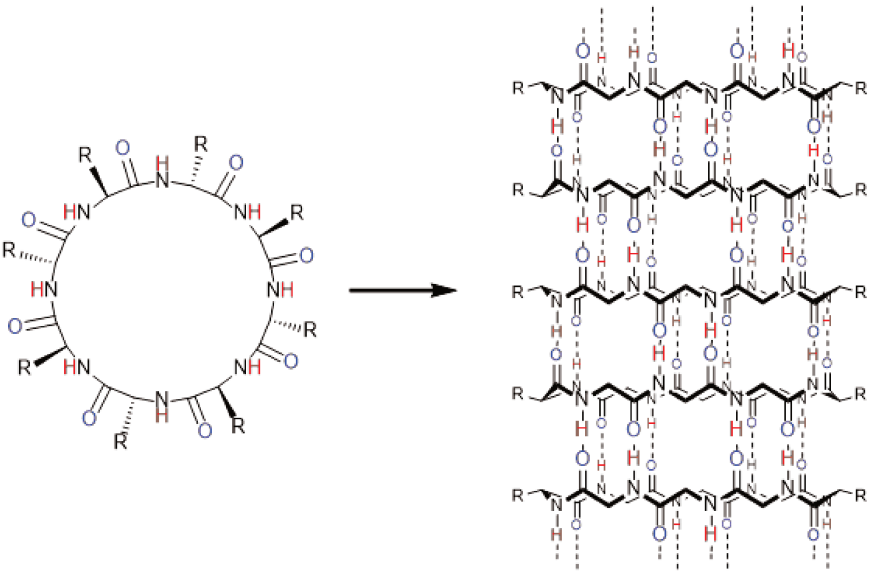

Figure S19. Schematic representation of the cyclic peptide assembly. Antiparallel sheet-like cylindrical structure formed by the cyclic peptide subunits. Most of the side chains have been omitted for clarity.

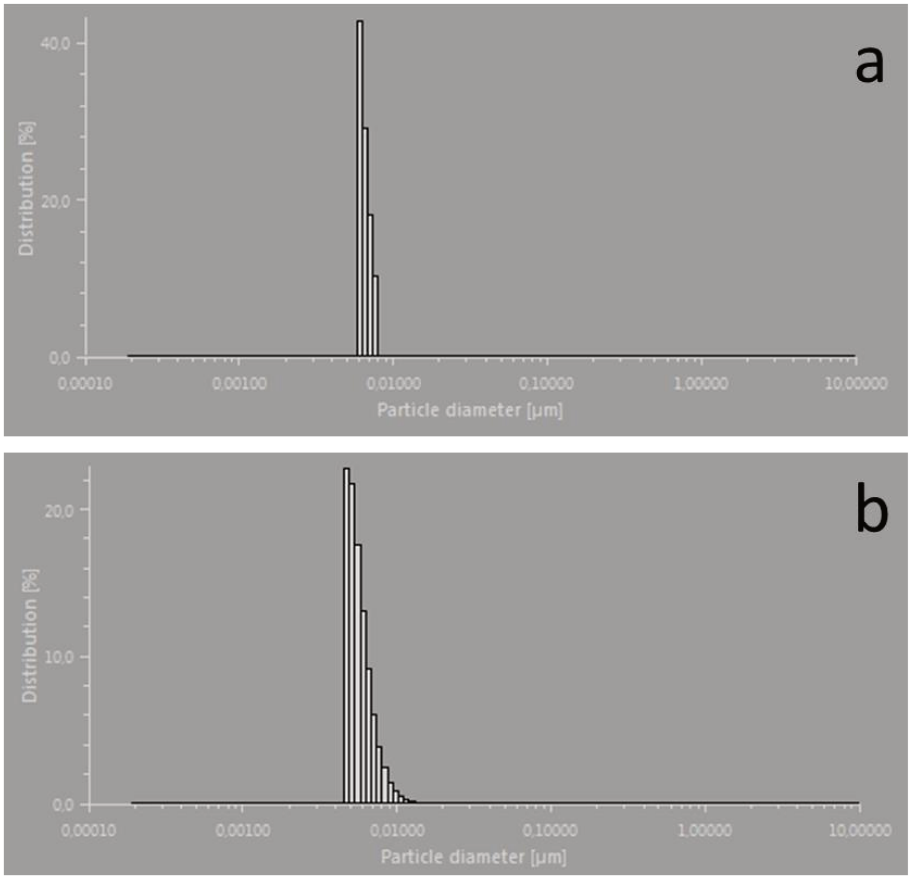

Figure S20. DLS intensity-average hydrodynamic diameter distribution of CP(PVDF)$_2$ conjugates (1 mg mL^{-1}) in (a) DMF after heating at 60 °C (1h) and sonication (20 min) and (b) DMSO after heating at 80 °C (1h) and sonication (20 min).

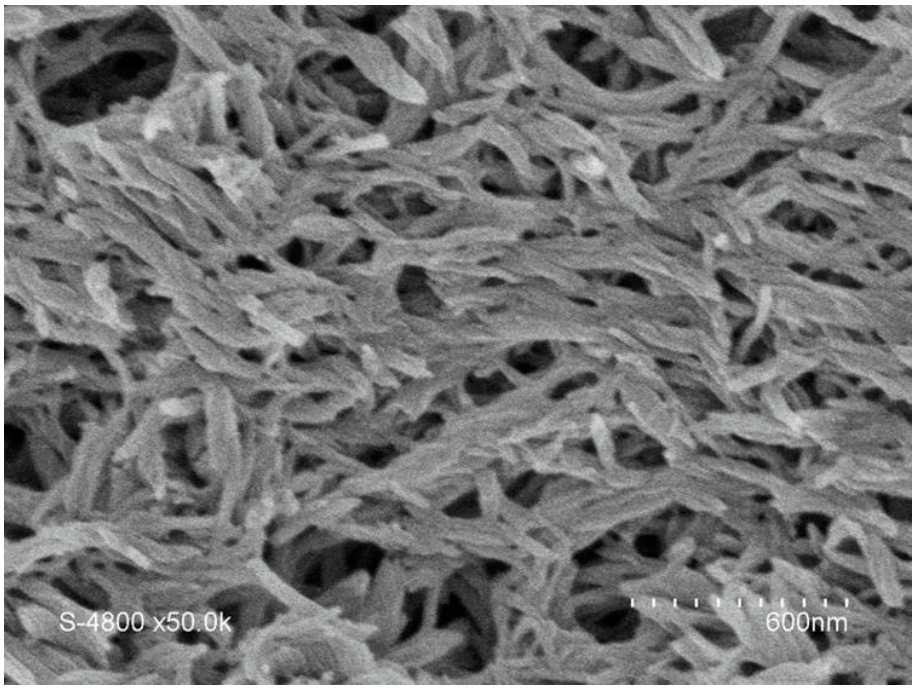

Figure S21. SEM image of thin films prepared from the crude CP-$(PVDF)_2$ conjugate (without further purification or dilution) by spin coating of 50 µL of suspension on a silicon wafer.

Chapter 6

Towards permanent hydrophilic PVDF membranes. Amphiphilic PVDF-*b*-PEG-*b*-PVDF block copolymer as membrane additive

Hydrophobicity is the major drawback of PVDF based polymers for application in filtration membranes. PVDF membrane efficiency is considerably limited due to their highly hydrophobic nature. The PVDF-*b*-PEG-*b*-PVDF amphiphilic block copolymer presented in chapter two was designed to create specific strong interactions between the hydrophilic additive and the bulk PVDF forming the membrane to reduce / eliminate the possibility of the additive leaching out of membrane during the preparation and filtration stages. Here the specific interaction between the bulk PVDF and the additive comes from the amphiphilic nature of the block copolymer where its short PVDF block can co-crystalize with the bulk PVDF during phase inversion step. Subsequent characterizations and permeability tests were conducted for PVDF membranes containing this new additive.

Towards permanent hydrophilic PVDF membranes. Amphiphilic PVDF-*b*-PEG-*b*-PVDF block copolymer as membrane additive

Enrique Folgado,[1,2] Mona Semsarilar,[2*] and Vincent Ladmiral[1*]

[1]Institut Charles Gerhardt Montpellier, Team: Ingénierie et Architectures Macromoléculaires, UMR5253, CNRS-UM-ENSCM, 8 rue de l'école Normale, 34296, Montpellier Cedex 5, France.
[2]Institut Européen des Membranes, IEM, UMR5635, UM-ENSCM-CNRS, Place Eugène Bataillon, 34095 Montpellier cedex 5, France.

1. Abstract

Poly(vinylidene fluoride) (PVDF) ultrafiltration membranes were prepared by NIPS using a blend of a new amphiphilic PVDF based triblock copolymer (PVDF-*b*-PEG-*b*-PVDF) and high molecular weight PVDF. During the phase inversion step, the new additive acts both as pore forming and surface modifying agent. However, thanks to the presence of the short PVDF blocks present in the triblock copolymer (additive), leaching out was reduced. PVDF-*b*-PEG-*b*-PVDF improved the surface hydrophilicity and significantly increased the PVDF membrane's pure water flux and permeability. The blend composition was optimized in terms of additive concentration and compared to membranes containing an equivalent amount of commercial PEG of similar molecular weight. Pure water filtration tests and contact angle measurements suggested that addition of small amounts of the additive (2-5 w/w %) has a strong impact on the performance and hydrophilic characteristic of the prepared PVDF membranes. The control tests showed that less than 21-27 % w/w of the additive is lost after 9 months, while most commercial PEG (59 % w/w) leached out of the membrane matrix after only two months.

2. Introduction

Membrane technology plays a crucial role in water and energy sustainability.[1] Access to water is one of the keys for economic, social and cultural development. The main reason why membrane technology has become an important separation technology over the past years is the fact that membranes work with relatively low energy use, [1,2] they are atom efficient and are nowadays economically viable for conventional techniques.[3]

Ultrafiltration (UF) and microfiltration (MF) membranes are employed when high separation efficiency is required.[4–7] Use of these filtration membranes in water treatment is susceptible to their low fouling resistance.[8] Membrane fouling affects productivity, additional operating costs, and the need for regular chemical cleaning that shortens the membrane lifetime. Membrane surface hydrophilicity is generally accepted as the main factor affecting fouling. A hydrophilic membrane surface generally has higher fouling resistance compared to hydrophobic membranes.[9–12] To help solve these problems, materials scientists and chemical engineers are working to develop inexpensive, scalable, and sustainable methods to produce and purify water, for example with new polymer membranes that can filter contaminants from water.[13]

Polymer membranes lead the membrane separation industry market because they are very competitive in performance, cheap and easy to handle and functionalize. Many polymers are available, but the choice of the material is the most important as it dictates the chemical properties and the final performance of the membrane. A polymer must have appropriate characteristics for their use in micro (MF) and ultrafiltration (UF) membrane formulations. The polymer has to tolerate the cleaning conditions (i.e., high pressure backwash, sodium hypochlorite solution wash), the driving forces (i.e., pressure) and has to be compatible with chosen membrane fabrication method (i.e., phase inversion, stretching of semi-crystalline polymer foils or hollow fibers, interfacial polymerization), Temperature induced phase separation (TIPS), non-solvent induced phase separation (NIPS)). Significant effort has been put into enhancing the permeation flux,[3,14–17] fouling resistance,[4,5,13,16,18,19] operation stability,[20] and the service life of membranes.[3,8,21]

The most common commercial polymers used for fabrication of MF and UF membranes are poly(ether sulfone) (PES),[22] polyethylene (PE),[23] polypropylene (PP),[8] polytetrafluoroethylene (PTFE)[24,25] and poly(vinylidene fluoride) (PVDF).[7,13,26–28] All mentioned polymers are hydrophobic in nature with the exception of hydrophilic PES.

Among all the methods that can be employed for the fabrication of polymer membranes, the phase inversion method is the most popular technique. The non-solvent-induced phase separation (NIPS) method is the method of choice for the industry. In this method, the polymer is dissolved in a suitable solvent, casted into the desired shape (i.e., flat, hollow fiber) and is then immersed into a non-solvent bath (coagulation bath) where the phase inversion process takes place. For this method to work, the polymers (membrane forming polymer and the additives) should be insoluble in the non-solvent and, solvent and non-solvent should be miscible. Apart from the NIPS method, the phase inversion can proceed via thermally induced phase separation (TIPS),[28,29] vapor induced phase separation (VIPS)[30] and evaporation-induced phase separation.[31]

PVDF is one of the most widely used polymers in membrane formulations due to its remarkable properties such as wide chemical compatibility, excellent mechanical properties, easy processing and high temperature resistance. [2,13,19] In defiance of PVDF attractiveness as a high-performance polymer for water filtration membranes, membrane efficiency is considerably limited due to its high hydrophobicity.[6,7,11] Ultrafiltration and/or microfiltration PVDF membranes need high operating pressures resulting in high energy consumption to provide acceptable flux values.

There are several studies describing the hydrophilic modification of PVDF membranes via introducing hydrophilic modifiers in form of polymers[3,26] and copolymers[5,32,33] aiming to improve the hydrophobicity of membranes for water filtration. However, these additives (mainly hydrophilic polymers or nanoparticles[6,8,10,21]) leak out during the membrane formation process, as well as during the filtration process. This is because they are often simply blended into the polymer matrix and are not covalently linked/ attached to the main membrane-forming material.

Post-fabrication treatment via physical surface modification (e.g., coating with a hydrophilic polymer layer)[5,7,16] or chemical treatment (e.g., plasma grafting of polar groups)[11,12,17] are the common techniques used to confer hydrophilicity to PVDF membranes. Until now, finding the correct formulation and preparation method that would be cost-effective, facile and efficient, remains a challenge. Among the existing methods to obtain hydrophilic PVDF membranes blending PVDF with hydrophilic polymers (e.g. poly(vinyl alcohol) (PVA), poly(ethylene glycol) (PEG), polyvinylpyrrolidone (PVP)) through phase separation process is the most used method in the industry. Preparation of membrane from a mixture of polymers is relatively easy, convenient and adaptable with the classical membrane fabrication set-up. Although this doesn't result in long homogeneous and lasting hydrophilicity as the hydrophilic polymers tend not to form miscible blends and leach out of the membrane matrix during fabrication and filtration steps.

Several studies have been performed with conventional additives such as PVP[3,9,26] and PEG[32,34] in the past. These polymers act as both pore formers (increasing porosity and hence membrane permeability) and hydrophilic conferrers. However, it is difficult to predict the real and final impact of these polymer additives, since it is very difficult to establish a relationship between the amounts of additive added in the casting solution and their final concentration in the membrane matrix after coagulation bath. Therefore, a systematic study is required each time a new formulation is tested. Likewise, establishing the rate of the additive migration within the polymer matrix and their resting time in the membrane is very difficult.[35,36] For example, when PEG is blended with PVDF, a large part of it gets washed out during the phase inversion step (coagulation bath). The non-solvent is often water, which dissolves the majority of the PEG chains, promoting the pore formation. In such cases very small amount of the PEG is remained in the membrane matrix.[32,36] To confer higher hydrophilicity, more additive should be added which also increases the porosity of the membrane. As a result it is difficult to find the right balance between hydrophilicity and porosity.

On this basis, we have designed a triblock copolymer containing PVDF and PEG blocks. Aiming to increase hydrophilicity (by increasing wettability) and reduce fouling due to the

increased wettability we have used PVDF-*b*-PEG-*b*-PVDF amphiphilic triblock copolymer as an additive for PVDF membranes.

As PEG and the PVDF segments are connected via covalent bond and the PVDF block will co-crystallize with high molecular weight PVDF forming the matrix of the membrane, the chance of the additive leaching during both preparation and filtration steps is reduced. In this study, different percentages of the synthesized triblock copolymer are used in the casting solution. Membranes are prepared by NIPS process and compared with similar membranes prepared from casting solutions containing an equivalent amount of commercial PEG with similar molecular weight to the PEG block present in the triblock copolymer. This study shows how the presence of short PVDF segments covalently attached to the PEG fixes the additive in the membrane matrix and makes it less likely to leach out during the phase inversion process. This almost permanent hydrophilicity, results in higher flux values and permeability when compared to membranes prepared using conventional additives (i.e. Free PEG chains).

3. Experimental section

3.1. Materials

All reagents were purchased from Sigma-Aldrich and were used as received unless otherwise stated. High molecular weight PVDF (Kynar 761; M_w: 441,000 g/mol) was kindly donated by ARKEMA. Deuterated water (D_2O) and dimethylsulfoxide ($(CD_3)_2SO$) were purchased from Eurisotop. PVDF-*b*-PEG-*b*-PVDF block copolymer was synthesized as reported previously.[37]

3.2. Methods

Preparation of dope solutions containing the triblock copolymer

The dope solutions were prepared by blending a 15 % w/w high molecular weight PVDF in NMP with different amounts of PVDF-*b*-PEG-*b*-PVDF triblock copolymer (2 to 20% w/w)

dissolved in NMP. The mixture was stirring at 80 °C for 24h to assure homogeneous blending.

Preparation of control dope solutions

A 15 % w/w high molecular weight PVDF solution in NMP was blended with two different concentrations of PEG136 (2 and 5 % w/w) at 80 °C for 24h.

Blade casting

In the case of NIPS, block copolymers solutions at 80 °C in NMP were casted on a glass plate substrate at 25 °C using a blade with a 250 µm thickness to obtain membrane sheets of 20 cm x 20 cm. After 60 s evaporation the substrate was transferred to a water coagulation bath at 25°C for 24 h, then dried at room temperature for another 24h (see Scheme 1).

Contact angle (CA)

The CAs were measured using a monochrome camera B-CAM-21-BW (CCCIR) and a Led R60 lamp purchased from CONRAD. For each sample, 10.0 µL of ultra-pure water was deposited on a polymer coated silica wafer using a micro needle. The images were recorded using One Touch Graber software and treated using Image J software.

NMR spectroscopy

NMR spectra were acquired in either D_2O or a mixture of D_2O and $(CD_3)_2SO$ using a Bruker 300 MHz spectrometer. All chemical shifts are reported in ppm (δ).

Scanning electron microscopy (SEM)

The porous structure of virgin PVDF membrane and modified PVDF membranes were characterized using microscopy techniques. SEM analyses were conducted using a Hitachi S-4500 instrument operating at a spatial resolution of 1.50 nm at 15 kV energy. The samples were dried and coated with an ultrathin layer of electrically conducting platinum deposited by high vacuum evaporation.

Water filtration experiments

For filtration tests, the prepared membrane (d = 2.5 cm) was fitted with a 10 mL filtration cell (Amicon 8010 stirred cell). Then filtration cell was connected to a water reservoir and compressed air line. The measurements were then performed at pressures between 0.1 and 2.0 bar. The mass of the water passing through the membrane (permeate) was recorded by the Sarto Connect software at regular time intervals. All filtration experiments were performed at room temperature with dust free ultrapure water (filtered through a 400-µm filter). Before recording the water flux, the membranes were conditioned for 2h at 2 bar. According to Darcy's law the volumetric flux and permeability could be calculated from equations (1) and (2):

$$Flux\ (J_v) = V_p/(t * S)\ (\text{L h}^{-1}\ \text{m}^{-2}) \quad (1)$$

$$Permeability\ (L_p) = J_v/\Delta P\ (\text{L h}^{-1}\ \text{m}^{-2}\ \text{bar}^{-1}) \quad (2)$$

Where V_p = Permeate volume, t = Time, S = Surface area and ΔP = pressure difference.

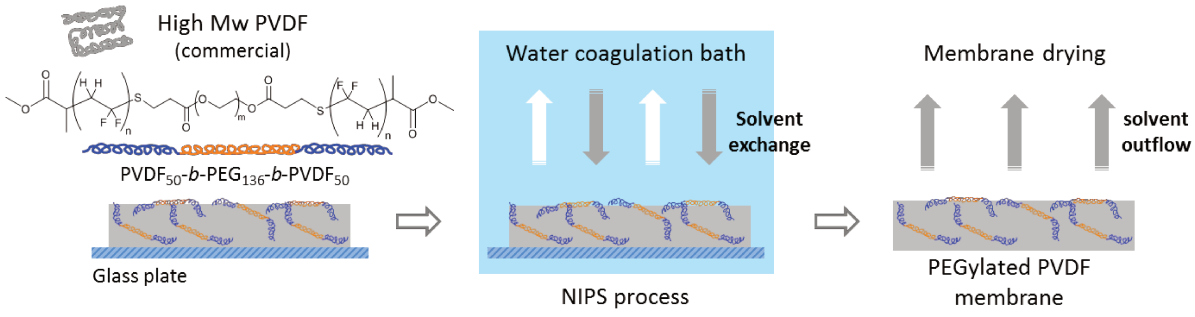

Scheme 1. Membrane preparation via NIPS process from casting solutions containing high M_w PVDF (15 % w/w in NMP) and different concentrations of added $PVDF_{50}$-*b*-PEG_{136}-*b*-$PVDF_{50}$.

Porosity and Pore Size Determination

The porosity of the membrane was determined through its dry-wet weight. The membrane was immersed in water for 24 h. After that, the weight of the wet membrane was measured after wiping of excess water using filter paper. Then, the wet membranes were dried in an oven for 10 h at 25°C and the weight of the dried membrane was measured. The porosity was calculated using the following equation[38]:

$$\varepsilon(\%) = \frac{w_w - w_d}{w_w - \frac{w_d}{d_w} + \frac{w_d}{d_p}} \times 100 \quad (3)$$

Where ε is the membrane porosity, w_w is the wet membrane weight (g), w_d is the dry membrane weight (g), d_w is the pure water density while d_p is polymer density. The density of the polymer blends was estimated considering the weight fractions of PEG and PVDF. Being $d_{PVDF} =$ 1.78 g·cm^{-3} and d_{PEG} = 1.20 g·cm^{-3}. Thus, the density of the blend containing 2 % w/w of triblock (or 0.81 % w/w of PEG) was estimated to be 1.775 g·cm^{-3} while the density of the blend containing 5% w/w of triblock (or 1.95 % w/w of PEG) was 1.769 g·cm^{-3}.

The mean pore radius size (r_m) was calculated based of the pure water flux (PWF) and porosity data obtained previously using the Guereout-Elford-Ferry equation as follows[39]:

$$r_m = \sqrt{\frac{(2.9 - 1.75 \cdot \varepsilon) \cdot 8 \cdot \eta \cdot l \cdot Q}{\varepsilon \cdot A \cdot \Delta P}} \quad (4)$$

Where η is water viscosity (mPa·s) (1.002 at 20°C), l is membrane thickness (m) (150-200μm), Q is the pure water flux (m^3·s^{-1}), A is area of membrane (m^2) (d = 2.5cm) and ΔP is the operating pressure (mPa) (2 bar = 2·10^8 mPa).

4. Results and discussion

The well-defined triblock copolymer $PVDF_{50}$-*b*-PEG_{136}-*b*-$PVDF_{50}$ was synthesized according to our previously published work.[37] This triblock copolymer was then used as the hydrophilic-conferring additive in the preparation of PVDF membranes. A series of dope solutions (high molecular weight PVDF and the triblock copolymer) containing different amounts of this triblock copolymer was prepared by varying the percentage of the added triblock copolymer between 0 and 20 % w/w. The concentration of the commercial high molecular weight PVDF in NMP was fixed at 15 % w/w. To ensure complete dissolution of PVDF the sample was heated at 80 °C under stirring for 24h. Different amounts of the triblock copolymer $PVDF_{50}$-*b*-PEG_{136}-*b*-$PVDF_{50}$ (1, 2, 5, 10, 15 and 20 % w/w) were then added to the homogeneous PVDF solution. These mixtures were stirred at 25°C until homogeneous. A series of membranes via NIPS process were prepared using the different dope solutions containing different amounts of the triblock copolymer (see Table 1). Additionally, control membranes were made from dope solutions containing commercially available PEG. The amounts of PEG added was carefully calculated to match with the equivalent amount of PEG present in the triblock copolymer.

Effect of $PVDF_{50}$-*b*-PEG_{136}-*b*-$PVDF_{50}$ on PVDF membrane formation.

The membranes were prepared using NIPS process using water coagulation bath. As mentioned before different amounts of the triblock copolymer (1, 2, 5, 10, 15, 20 % w/w) were added to the membrane casting solutions (Table 1.). Membranes with triblock copolymer content above 5 % w/w became very soft (like swollen hydrogel) after immersion in the coagulation bath. They seem to retain large amounts of water that caused the membranes to become unstable and fall apart (see Figure S4). For this reason only the membranes prepared with 1, 2 and 5 % w/w of triblock copolymer were used in the rest of the study.

SEM images of these membranes (Fig. 1) show the expected finger-like structures with porous skin top-layer and macro voids known for the NIPS process. The surface and cross-section images of the membranes show that as the PVDF-*b*-PEG-*b*-PVDF content in the dope solution increases more porous membranes are obtained. This observation is logical and

matches the reports in the literature[34,40–42] as the PEG segment of the triblock copolymer retains water and facilitates the formation of the pores. In the NIPS process the phase separation happens very fast (as soon as the casted layer is put into the coagulation bath). This causes the PVDF blocks of the copolymer to precipitate along with the high molecular weight PVDF forming the matrix of the membrane. This co-precipitation of the entangled PVDF segments from the additive and the high molecular weight PVDF chains results in fixing the triblock copolymer in the membranes matrix, reducing the possibility of the additive leaching out.

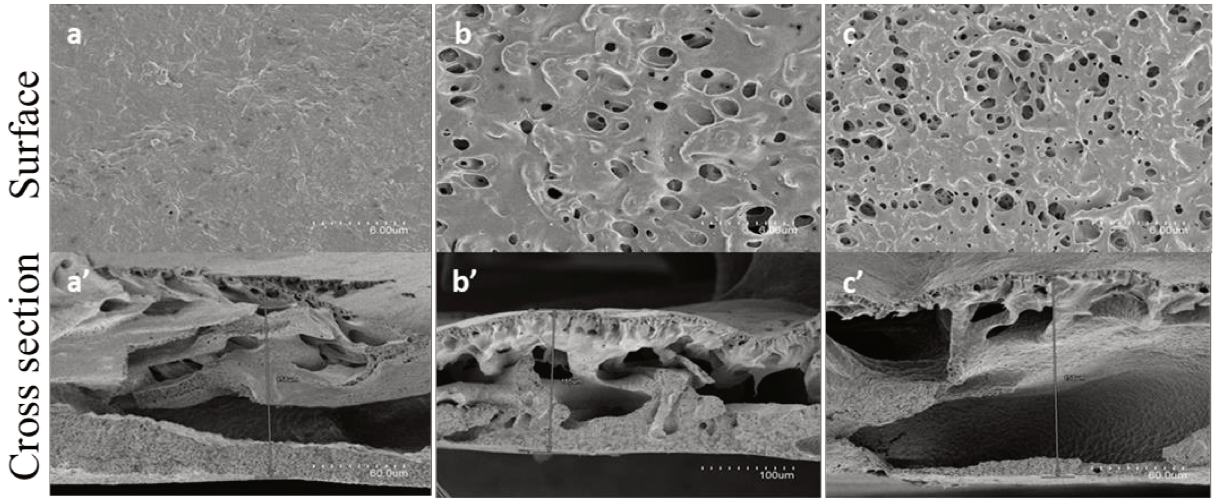

Figure 1. SEM images of membrane surface and cross section containing (a, a') 0 % w/w, (b, b') 2 % w/w and (c, c') 5 % w/w.

The relevant changes in the number and size of the macro voids with increasing amount of the additive could not be calculated using the SEM cross-section images. All analyzed membranes presented large macro voids. We believe that this is due to the presence of the PEG segments in the triblock copolymer that retains water molecules, enhancing the in-flow/out-flow of solvent and non-solvent molecules in the coagulation bath resulting in high porosity.

Effect of $PVDF_{50}$-*b*-PEG_{136}-*b*-$PVDF_{50}$ on the surface hydrophilicity of PVDF membranes.

As explained above the addition of triblock copolymer containing PEG resulted in increased membrane porosity in general and surface porosity in specific. As expected membranes

containing block copolymer were more porous than the pure PVDF membranes. As observed by SEM (Fig. 1), as more block copolymer is incorporated the surface porosity increases. This porosity is rather irregular which results in large porosity distribution as well as increased roughness on the membrane surface. Nonetheless the hydrophilicity of the surface of the membranes increased with increasing additive concentration due to the higher wettability as the result of presence of the triblock copolymer.

Contact angle measurements (Table 1 and Fig. 2) were also performed to evaluate the membrane surface hydrophilicity.

Table 1. Dope solution formulations for the preparation of the hydrophilic PVDF membranes.

Membrane ID	The composition of the casting solution				Copolymer % w/w	$W_{copolymer}/W_{PVDF}$ (%)[a]	CA (deg)
	PVDF (g)	Copolymer (g)	PEG_{136} (g)	NMP (g)			
Triblock0	0.750	-	-	4.85	0	0	95±18
Triblock1	0.750	0.057	-	4.79	1.00	7.6	74±6
Triblock2	0.750	0.114	-	4.74	2.00	15.2	54±5
Triblock5	0.750	0.295	-	4.55	5.00	39.3	39±6
Triblock10	0.750	0.622	-	4.23	10.00	82.9	10±10
Triblock15	0.750	0.988	-	3.86	15.00	131.7	0
Triblock20	0.750	1.4	-	3.45	20.00	186.7	0
PEGeq2	0.818	-	0.046	4.74	-	-	61±7
PEGeq5	0.930	-	0.115	4.55	-	-	47±5

Water contact angle of the pure PVDF membrane (Triblock0) was (95 ± 18°). A value expected for a hydrophobic surface. When the membrane contained only 1% w/w of the triblock copolymer the contact angle decreased drastically (74 ± 6°). This value decreased to 54°, 39° and 10° as the triblock content was increased to 2, 5 and 10% w/w. In samples with more triblock copolymer content (> 5% w/w) the water droplet only lasted few seconds (10s or less) before full adsorption on the membrane surface. Figure 2 shows the rate of water droplet adsorption during the first 25 seconds. The water droplet on the hydrophobic pure PVDF membrane surface retained its initial contact angle while droplets on the membranes containing the triblock copolymer (both 2 and 5% w/w) were adsorbed completely by the 25th second.

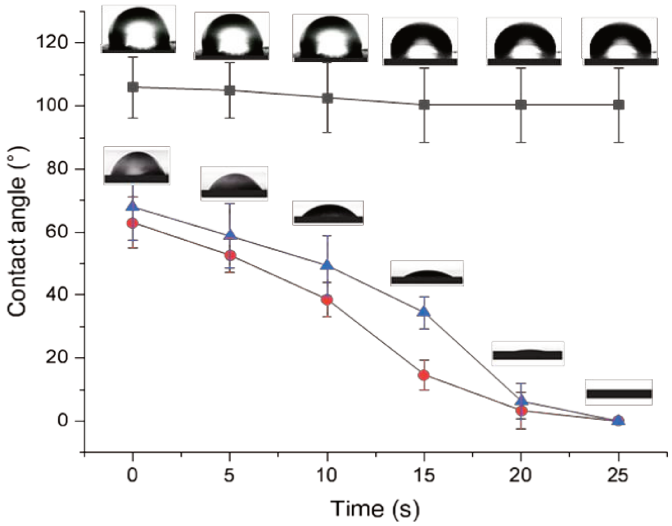

Figure 2. Contact angles of PVDF membranes. Pure PVDF membrane (black squares), and membranes containing 2% w/w and 5% w/w of the copolymer (blue triangles and red dots respectively).

These results show that incorporation of the triblock copolymer even at very low concentrations (1-5% w/w) enhances the hydrophilicity of PVDF membranes hugely. This is probably due the fact that most of the added triblock copolymer stays in the membrane matrix since the two short PVDF block of the triblock copolymer act as an anchor attaching the triblock to the high molecular weight PVDF chains forming the membrane. Also, the presence of this short PVDF block enhances the homogeneous distribution of the triblock in the membrane matrix as it helps the compatibility of the triblock chains with the PVDF chains. It should be noted that PEG chains added to the PVDF dope solutions in the classical method of hydrophilic PVDF membrane preparation leads to inhomogeneous distribution of the PEG chains and phase separation as PEG and PVDF are not compatible.

Membrane Aging– effect on CAs, flux, and permeability.

In order to check our hypothesis that the presence of the short PVDF block in the triblock copolymer would lead to strong interaction of the triblock copolymer with the high molecular weight PVDF and fix the PEG segments in the membrane matrix, aging experiments were carried out over 9 months. For aging experiments two membranes with dimensions of 10 cm x 10 cm were prepared using dope solutions containing 2 and 5% w/w

triblock copolymer (**Triblock2** and **Triblock5**). Also, two membranes (10 cm x 10 cm) were prepared from dope solutions containing equivalent amount of commercial PEG (as compared to the amount of PEG in the triblock copolymers). The latter membranes (**PEGeq2** and **PEGeq5** in Table 2) were used as reference to establish the leaching out profile. The prepared membranes were stored in pure water after removal from the coagulation bath. Circles of 2.5 cm in diameter were cut from each membrane and were placed in sealed petri dishes filled with distilled water. This water was replaced weekly with fresh distilled water during the study period of 9 months.

The contact angle measurements (see Table 2) indicate that there is a small change in the hydrophilicity of the membranes containing the triblock copolymer during the study period. In the case of membranes with 2% w/w triblock copolymer (**Triblock2**), the CA increases by 13°. This increase for the membrane with 5% w/w (**Triblock5**) is about 14° where most loss happened during the first two months. The CA of the membranes prepared with commercial PEG after 9 months is almost the same as the CA of the membranes prepared from pure PVDF (90° and 95° respectively). This suggests that the triblock copolymer is well anchored to the matrix of the membranes while almost the entire amount of the commercial PEG additive is lost (loss of 29° for **PEGeq2** and 41° for **PEGeq5**) during the 9 months period. When comparing the 2 additives, it is clear that the presence of the short PVDF block is sufficient to lock the additive in the membrane.

Table 2. Membrane CAs during the aging process.

Membrane ID	Mean Contact Angles at 10 s.		
	0 month	2 month	9 month
Triblock2	54	63	67
Triblock5	39	47	53
PEGeq2	61	78	90
PEGeq5	47	73	88

To quantify the amount of the additive (triblock and commercial PEG) loss, proton NMR studies were carried out. Integrals of the PVDF and PEG (3.5 ppm) signals were used to determine the percentage of additive loss (see Table 3 and S6). The CH_2 signal of the PVDF ($\int_{2.66}^{3.01} \mathrm{CH_2(PVDF)}$) was taken as reference. Unfortunately there is no way of differentiating

the signals of high molecular weight PVDF and that of the triblock copolymer. However the error caused by this would not be too much as the ratio of PVDF from the triblock to the high molecular weight PVDF is very low (0.056 – 0.124 for **Triblock2** and **Triblock5**, respectively). To estimate the additive loss the following equation was employed:

$$Additive\ loss(\%) = 100 - \frac{\int_{3.47}^{3.55} CH_2(PEG) aged\ membrane}{\int_{3.47}^{3.55} CH_2(PEG) reference\ membrane} x\ 100 \quad (5)$$

Table 3. Additive loss *vs.* aging.

Membrane ID	additive content	Additive loss after 2 months (%)	Additive loss after 9 months (%)
Triblock2	2% w/w	9.1	21.4
PEGeq2	0.81% w/w	41.2	58.8
Triblock5	5% w/w	21.4	27.3
PEGeq5	1.95% w/w	41.7	70.8

The data summarized in Table 3 implies that the loss of the triblock copolymer compared to the commercial PEG is much less. When only 2% w/w of the triblock copolymer is used (membrane **Triblock2**) about 21% of the additive leached out during 9 months while during the same time period about 59% of the commercial PEG had leached out (membrane **PEGeq2**). These values increase to 27 and 71% for membranes containing 5% w/w of triblock copolymer and equivalent commercial PEG (membranes **Triblock5** and **PEGeq5**). These data also indicates that addition of only 2% w/w of the triblock copolymer is largely sufficient to confer hydrophilicity to the PVDF membranes as when more of the additive is added more material loss is observed.

The flux and permeability of these 4 types of membranes were evaluated via three cycles of pure water filtration (Fig. 3). Membrane specimens were mounted in a 10 mL Amicon filtration cell connected to a 1L water reservoir. The membranes were conditioned at 2 bar for 2 hours at room temperature. For membranes containing 2% w/w triblock copolymer, flux reached up to 1400 L/h·m^2 at 2 bar right after preparation (T_0). After 2 and 9 months the flux values almost halved to around 600 L/h·m^2. This decrease would be mainly due to the loss of hydrophilicity (see Table 2 and 3) and water retaining ability and to a lower extent to fouling (bacteria growth) as shown in Figure S5. Membranes with 5% w/w triblock copolymer follow a similar trend although the decrease in the flux value during the aging period was not as much (only drops by 200 L/h·m^2). However both membranes presented an improvement in terms of flux when compared with membranes prepared with commercial PEG as additive. The highest flux values obtained for membranes containing commercial PEG were 100 and 200 L/h·m^2 (for membranes with 2 and 5% w/w equivalent amount of PEG during the first filtration experiments) while the membranes containing the triblock copolymer reach flux values of 650 and 1400 L/h·m^2.

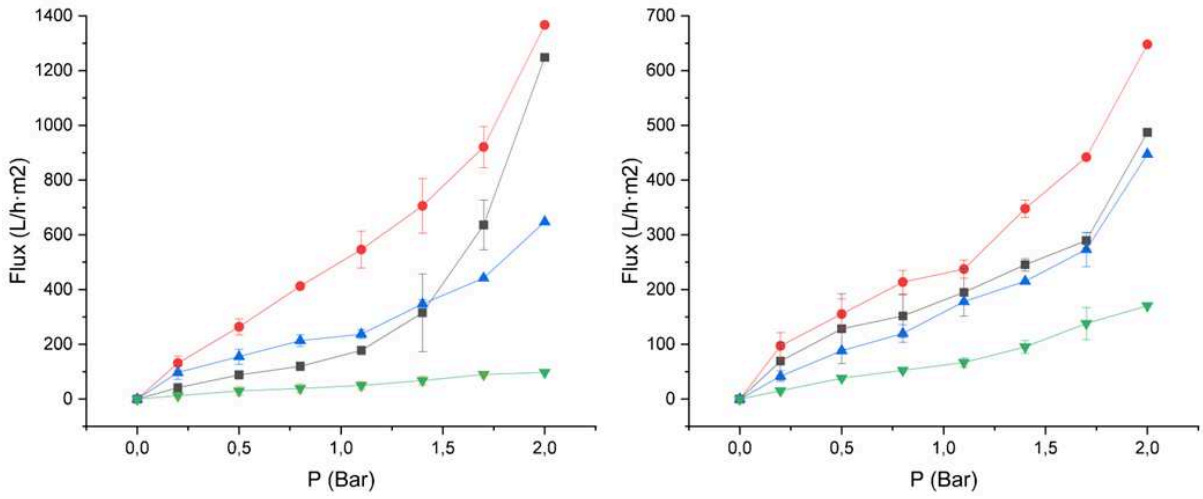

Figure 3. Flux vs. pressure of membranes containing 2% (left) and 5% w/w (right) of PVDF-*b*-PEG-*b*-PVDF block copolymer in a matrix of high molecular weight PVDF were tested right after their formulation (black traces, squares), after 2 months (red traces, dots), after 9 months (blue traces, triangles) and compared to flux values obtained from membranes loaded with an equivalent amount of PEG at t=0 (green traces, inversed triangle).

The permeability graphs (Figure S7) show that membranes containing commercial PEG show that these membranes are relatively stable with a low permeability (110-150 L h^{-1} m^{-2} Bar). The permeability profile of the membranes containing 2% w/w triblock copolymer show moderate fluctuations. This is most probably due to the pore size and pore density of the membrane rather than their degree of hydrophilicity. In the case of membrane containing 5% w/w of the triblock copolymer, permeability values stay almost constant between 0 and 2 bar, suggesting good structural stability under tested conditions. The stability of the membranes with commercial PEG additive is much more than the membranes containing the triblock copolymer. This is due to the fact that membrane made with commercial PEG doesn't retain much PEG in their structure hence their pores do not swell as much when in contact with water as compared to the membranes containing triblock copolymer.

Since the SEM images of the membranes containing different amounts of added triblock copolymer did not show major change in structure and porosity, water uptake was used as an indirect method to estimate pore size and porosity (see Table 3). Membranes containing 5% w/w of triblock copolymer are more porous when compared to the membranes with 2% w/w of triblock copolymer (61% and 76%). However, membranes with 2% w/w of triblock copolymer has larger pore size (62 - 73 nm) while the membranes containing 5% w/w has smaller pore size (43 - 50 nm). These data are in agreement with flux values obtained for each membrane. Membranes containing 5% w/w triblock copolymer had lower flux at all 3 time intervals (T0, 2 and 9 months). Membranes containing commercial PEG (at both concentrations) presented the smallest pore size (~17 and 23 nm) hence the very low flux and permeability values. The presence of the hydrophilicity conferring polymer leads to formation of pores lined with PEG chains. Due to the hydrophilic nature of the PEG, water is retained in the membranes structure leading to membranes swelling. This swelling leads to pore tightening and eventually pore blockage.

Table 4. Membrane porosity (ε) and mean pore size (r_m).

PVDF Membrane (additive or PEG content)	Porosity (%)	Mean pore radii (nm)*
Triblock as additive (2% w/w)	60.5	62.2-73.0
PEG as additive (0.81% w/w)	41.3	16.8-19.4
Triblock as additive (5% w/w)	75.7	43.1-49.7
PEG as additive (1.95% w/w)	48.3	22.8-26.3

**Pore size estimated using two thicknesses (150 and 200μm)*

5. Conclusions

In summary, a well-defined ABA triblock copolymer is synthesized using RAFT and click chemistry. This triblock copolymer was then blended with the high molecular weight PVDF. Membranes were cast from this mixture following the NIPS process. The resulting porous membranes were fully characterized using ^{1}H NMR, CA and filtration tests. The tests show that the hydrophilicity of the membrane increases linearly with the increasing PEG content. As PEG chains retain water, the membrane pores become smaller leading to lower flux values. The control tests showed that most of the commercial PEG leaches out during the 1 month after membrane preparation. It was also demonstrate that a very small amount of the triblock copolymer (2-5% w/w) is required to confer hydrophilicity to the PVDF membranes. Higher amounts of the added triblock copolymer lead to membrane swelling and instability. Our study suggests that migration of the copolymer additive towards the top layer of the membrane could be possible however leaching out is heavily suppressed as the short PVDF block in the triblock copolymer anchors the PEG segment to the high molecular weight PVDF forming the membrane.

Acknowledgments

The authors thank Arkema (Pierre-Bénite, France) for providing VDF.

6. References

1. Le, N. L. & Nunes, S. P. Materials and membrane technologies for water and energy sustainability. *SUSMAT* **7**, 1–28 (2016).
2. Cui, Z., Drioli, E. & Lee, Y. M. Recent progress in fluoropolymers for membranes. *Prog. Polym. Sci.* **39**, 164–198 (2014).
3. Bi, Q., Li, Q., Tian, Y., Lin, Y. & Wang, X. Hydrophilic modification of poly(vinylidene fluoride) membrane with poly(vinyl pyrrolidone) via a cross-linking reaction. *J. Appl. Polym. Sci.* **127**, 394–401 (2013).
4. Li, H. J. *et al.* Development and characterization of anti-fouling cellulose hollow fiber UF membranes for oil-water separation. *J. Memb. Sci.* **279**, 328–335 (2006).
5. Revanur, R., McCloskey, B., Breitenkamp, K., Freeman, B. D. & Emrick, T. Reactive amphiphilic graft copolymer coatings applied to poly(vinylidene fluoride) ultrafiltration membranes. *Macromolecules* **40**, 3624–3630 (2007).
6. Benhabiles, O., Galiano, F., Marino, T. & Mahmoudi, H. Preparation and characterization of TiO 2 - PVDF / PMMA blend membranes using an alternative non-toxic solvent for UF / MF and photocatalytic application. 1–20 (2018).
7. Wang, X., Chen, C., Liu, H. & Ma, J. Preparation and characterization of PAA/PVDF membrane-immobilized Pd/Fe nanoparticles for dechlorination of trichloroacetic acid. *Water Res.* **42**, 4656–4664 (2008).
8. Saffar, A., Carreau, P. J., Kamal, M. R. & Ajji, A. Hydrophilic modi fi cation of polypropylene microporous membranes by grafting TiO 2 nanoparticles with acrylic acid groups on the surface. *Polymer (Guildf).* **55**, 6069–6075 (2014).
9. Higuchi, A. *et al.* Chemically modified polysulfone hollow fibers with vinylpyrrolidone having improved blood compatibility. *Biomaterials* **23**, 2659–2666 (2002).
10. Ghaemi, N., Daraei, P. & Palani, S. Surface Modification of Polysulfone Membranes Using Poly (Acrylic Acid) - Decorated Alumina Nanoparticles. 261–269 (2018).
11. Liu, F., Zhu, B. K. & Xu, Y. Y. Improving the hydrophilicity of poly(vinylidene fluoride) porous membranes by electron beam initiated surface grafting of AA/SSS binary monomers. *Appl. Surf. Sci.* **253**, 2096–2101 (2006).
12. Wang, P., Tan, K. L., Kang, E. T. & Neoh, K. G. Plasma-induced immobilization of poly (ethylene glycol) onto poly (vinylidene fluoride) microporous membrane. *J. Memb. Sci.* **195**, 103–114 (2002).
13. Kang, G. dong & Cao, Y. ming. Application and modification of poly(vinylidene fluoride) (PVDF) membranes - A review. *J. Memb. Sci.* **463**, 145–165 (2014).
14. Wang, Y. Q. *et al.* Remarkable reduction of irreversible fouling and improvement of the permeation properties of poly(ether sulfone) ultrafiltration membranes by blending with pluronic F127. *Langmuir* **21**, 11856–11862 (2005).

15. Kuila, A., Chatterjee, D. P., Maity, N. & Nandi, A. K. Multi-functional poly(vinylidene fluoride) graft copolymers. *J. Polym. Sci. Part A Polym. Chem.* **55**, 2569–2584 (2017).

16. Du, J. R., Peldszus, S., Huck, P. M. & Feng, X. Modification of poly(vinylidene fluoride) ultrafiltration membranes with poly(vinyl alcohol) for fouling control in drinking water treatment. *Water Res.* **43**, 4559–4568 (2009).

17. Han, M. J., Baroña, G. N. B. & Jung, B. Effect of surface charge on hydrophilically modified poly(vinylidene fluoride) membrane for microfiltration. *Desalination* **270**, 76–83 (2011).

18. Liu, J., Shen, X., Zhao, Y. & Chen, L. Acryloylmorpholine-grafted PVDF membrane with improved protein fouling resistance. *Ind. Eng. Chem. Res.* **52**, 18392–18400 (2013).

19. Liu, F., Hashim, N. A., Liu, Y., Abed, M. R. M. & Li, K. Progress in the production and modification of PVDF membranes. *J. Memb. Sci.* **375**, 1–27 (2011).

20. Li, N., Xiao, C., An, S. & Hu, X. Preparation and properties of PVDF/PVA hollow fiber membranes. *Desalination* **250**, 530–537 (2010).

21. Liang, S., Xiao, K., Mo, Y. & Huang, X. A novel ZnO nanoparticle blended polyvinylidene fluoride membrane for anti-irreversible fouling. *J. Memb. Sci.* **394**–**395**, 184–192 (2012).

22. Zhao, W. *et al.* Fabrication of antifouling polyethersulfone ultrafiltration membranes using Pluronic F127 as both surface modifier and pore-forming agent. *J. Memb. Sci.* **318**, 405–412 (2008).

23. Akbari, A., Yegani, R., Pourabbas, B. & Behboudi, A. Analysis of antifouling behavior of high dispersible hydrophilic poly (ethylene glycol)/ vinyl functionalized SiO 2 nanoparticles embedded polyethylene membrane. **76**, 20652 (2017).

24. Membranes, P., Dow, N., Milne, N. & Zhang, J. Membrane Distillation Trial on Textile Wastewater Containing Surfactants Using Hydrophobic and Hydrophilic-Coated Polytetrafluoroethylene.

25. Khumalo, N., Nthunya, L., Derese, S., Motsa, M. & Verliefde, A. Separation and Puri fi cation Technology Water recovery from hydrolysed human urine samples via direct contact membrane distillation using PVDF / PTFE membrane. *Sep. Purif. Technol.* **211**, 610–617 (2019).

26. Cha, B. J. & Yang, J. M. Effect of high-temperature spinning and PVP additive on the properties of PVDF hollow fiber membranes for microfiltration. *Macromol. Res.* **14**, 596–602 (2006).

27. Sun, D., Yue, D., Li, B., Zheng, Z. & Meng, X. Preparation and Performance of the Novel PVDF Ultra fi ltration Membranes Blending With PVA Modi fi ed SiO 2 Hydrophilic Nanoparticles. (2019).

28. Zhao, J., Yi, J., Shi, L. & Wang, R. Explorations of combined nonsolvent and thermally induced phase separation (N-TIPS) method for fabricating novel PVDF hollow fi ber membranes using mixed diluents. *J. Memb. Sci.* **572**, 210–222 (2019).

29. Zhang, H. *et al.* Study of the dual role mechanism of water-soluble additive in low

temperature thermally-induced phase separation. *J. Memb. Sci.* **543**, 1–9 (2017).

30. Marino, T., Russo, F., Figoli, A. & May, H. The Formation of Polyvinylidene Fluoride Membranes with Tailored Properties via Vapour / Non-Solvent Induced Phase Separation. 1–17 (2018).

31. Pervin, R., Ghosh, P. & Basavaraj, M. G. Tailoring pore distribution in polymer films via evaporation induced phase separation . *RSC Adv.* **9**, 15593–15605 (2019).

32. Venault, A. *et al.* Low-biofouling membranes prepared by liquid-induced phase separation of the PVDF/polystyrene-b-poly (ethylene glycol) methacrylate blend. *J. Memb. Sci.* **450**, 340–350 (2014).

33. Park, S., Ahn, Y., Jang, M., Kim, H. & Yong, K. Separation and Puri fi cation Technology E ff ects of methacrylate based amphiphilic block copolymer additives on ultra fi ltration PVDF membrane formation. *Sep. Purif. Technol.* **202**, 34–44 (2018).

34. Kim, J. H. & Lee, K. H. Effect of PEG Addative on Membrane Formation by Phase Inversion. *J. Memb. Sci.* **138**, 153–163 (1998).

35. Yun, Y. *et al.* Formation kinetics and characterization of polyphthalazinone ether ketone hollow fiber ultrafiltration membranes. *J. Memb. Sci.* **389**, 416–423 (2012).

36. Liu, J., Zhong, Z., Ma, R., Zhang, W. & Li, J. Development of high-antifouling PPSU ultrafiltration membrane by using compound additives: Preparation, morphologies, and filtration resistant properties. *Membranes (Basel).* **6**, (2016).

37. Folgado, E. *et al.* "One-Pot" Aminolysis/Thiol-ene preparation of well-defined amphiphilic PVDF-b-PEG-b-PVDF triblock copolymers: Self-assembly behaviour in mixed solvents. *Polym. Chem.* (2019).

38. Li, X., Wang, Y., Lu, X. & Xiao, C. Morphology changes of polyvinylidene fluoride membrane under different phase separation mechanisms. **320**, 477–482 (2008).

39. Feng, C., Shi, B., Li, G. & Wu, Y. Preparation and properties of microporous membrane from for membrane distillation. **237**, 15–24 (2004).

40. Wang, D.-M. & Lai, J.-Y. Recent advances in preparation and morphology control of polymeric membranes formed by nonsolvent induced phase separation. *Curr. Opin. Chem. Eng.* **2**, 229–237 (2013).

41. Matsen, M. W. Effect of Architecture on the Phase Behavior of AB-Type Block Copolymer Melts. *Macromolecules* 2161–2165 (2012).

42. Heng Loh, C. & Wang, R. Effects of Additives and Coagulant Temperature on Fabrication of High Performenace PVDF/Pluronic F127 Blend Hollow Fiber Membranes via Nonsolvent Induced Phase Separation. *Chinese J. Chem. Eng.* **1**, 71–79 (2012).

7. Supporting information

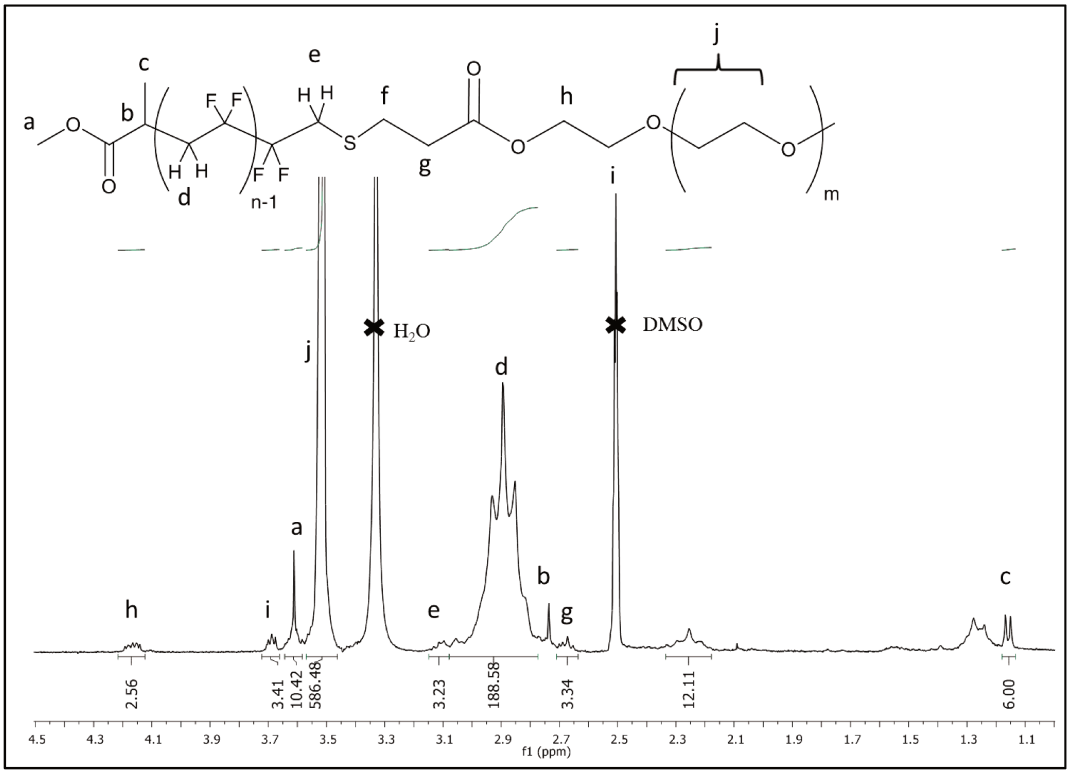

Figure S1. PVDF-*b*-PEG-*b*-PVDF ^{1}H NMR (400 MHz, $(CD_3)_2SO$), recorded at 60 °C).

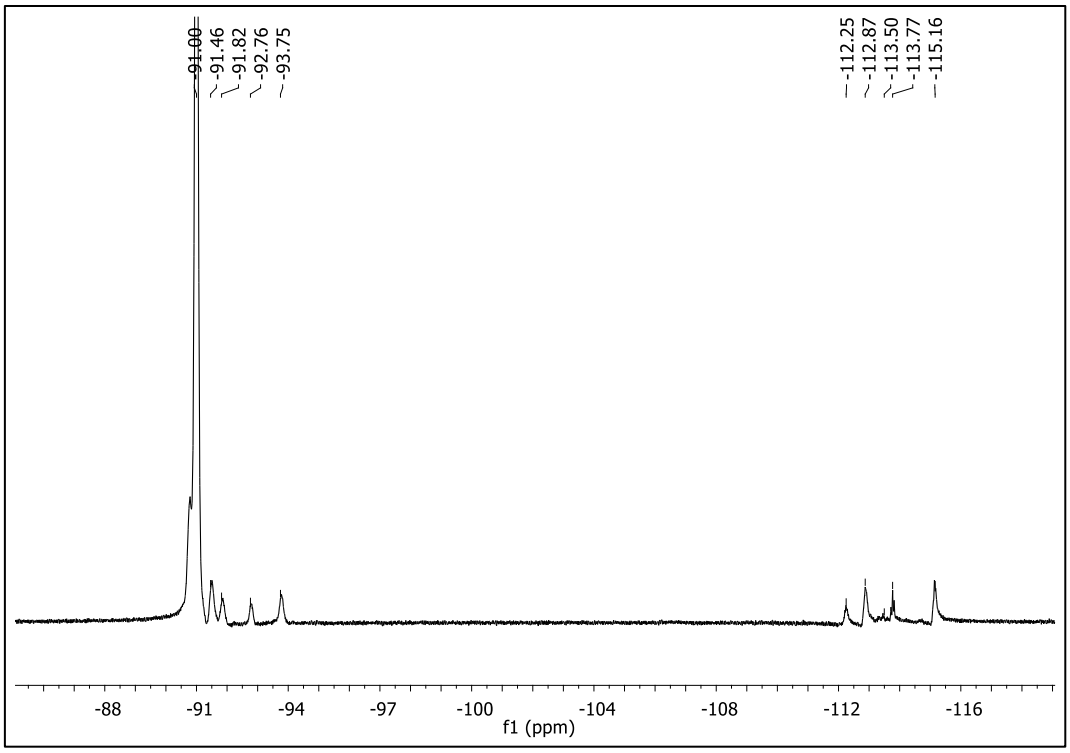

Figure S2. PVDF-*b*-PEG-*b*-PVDF ^{19}F NMR (376 MHz, (CD3)2SO).

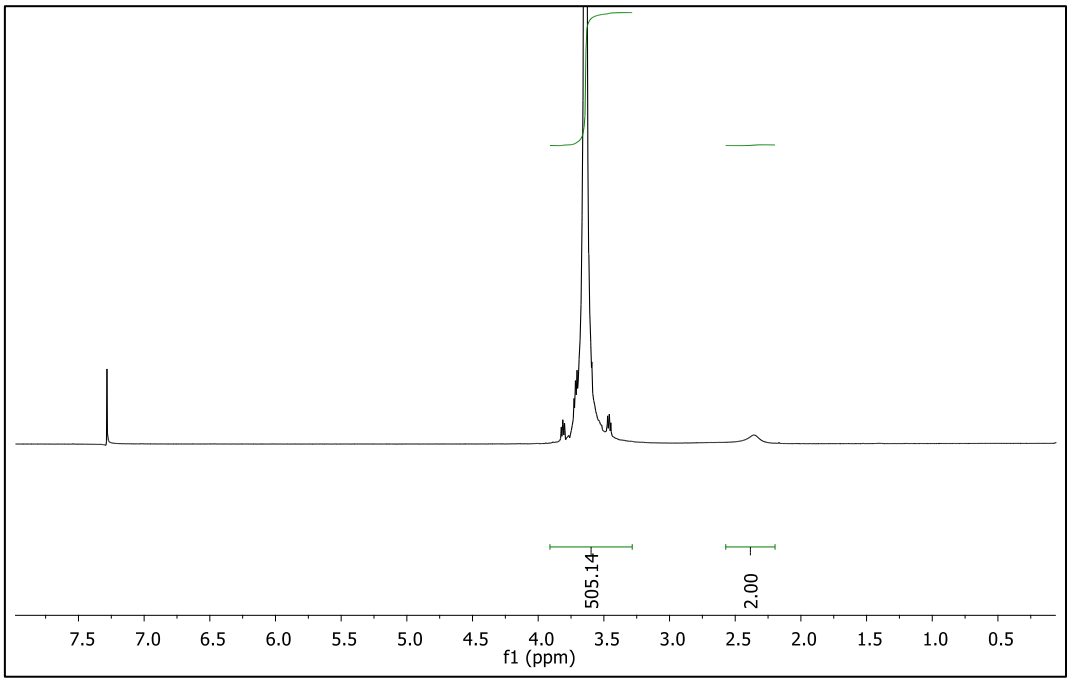

Figure S3. PEG6000 commercial polymer ^{1}H NMR (400 MHz, $CDCl_3$).

S4. SEM image of membrane prepared from dope solution containing 10 % w/w triblock copolymer after conditioning in pure water at 2 bar.

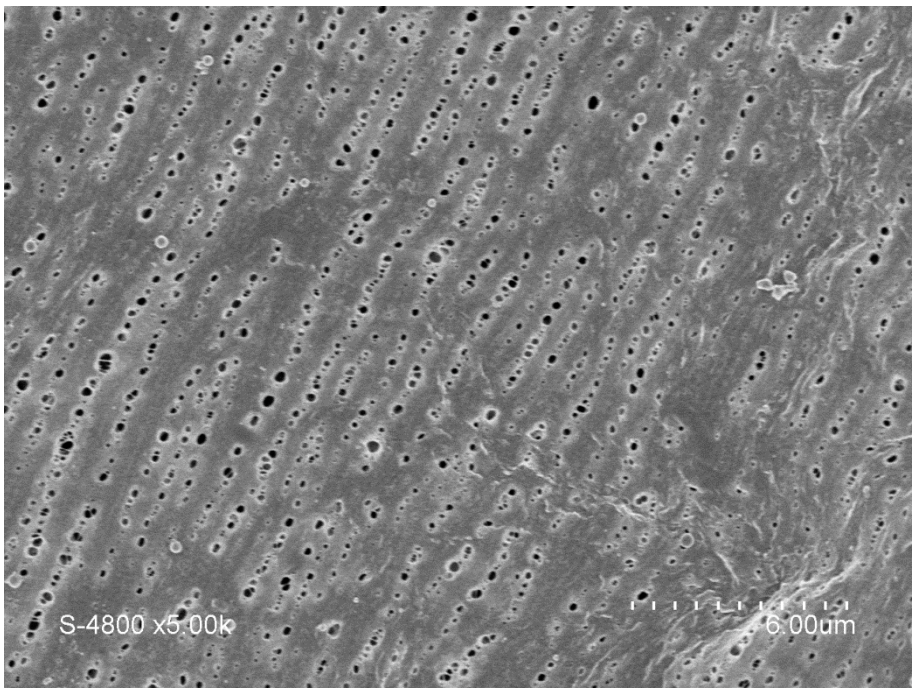

Figure S4. Pore formation/distribution induced by stretching due to pressure during the membrane conditioning in membranes with additive load higher than 5 % w/w. These membranes crack during the conditioning step.

S5. SEM images of membrane prepared from dope solutions containing (a, b) 2 and (c, d) 5 % w/w of triblock copolymer after (a, c) 2 and (b, d) 9 months of aging.

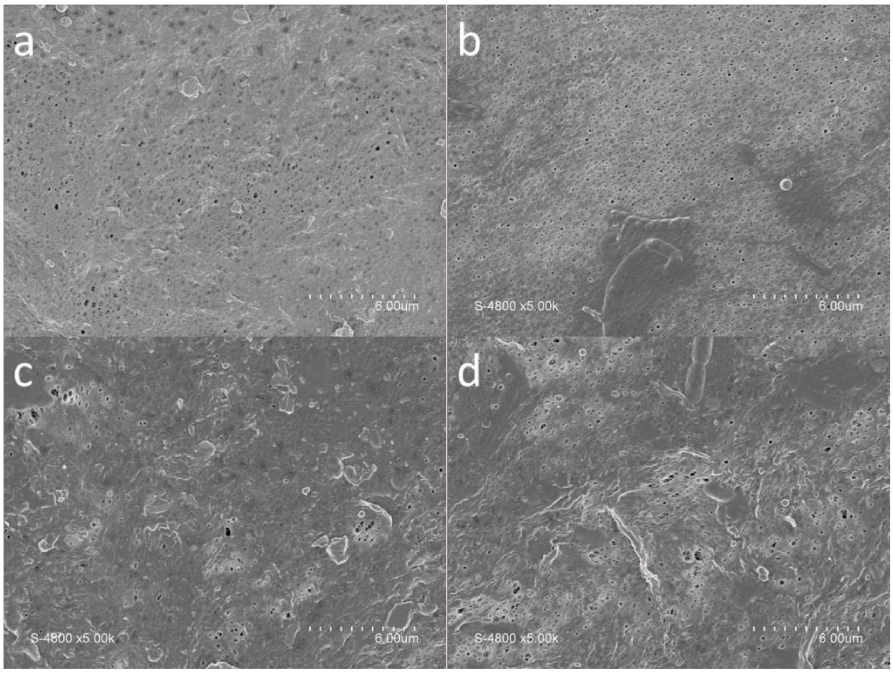

Figure S5. Membrane loaded with 2 % w/w of additive after (a) 2 months (b) and 9 months (b) of aging. Membrane loaded with 5 % w/w of additive after (c) 2 months (d) and 9 months of aging. Bacteria are visible in figures b and d. Membranes were kept in pure water, no additive was used to prevent bacteria growth.

S6. PEG loss estimation using 1H NMR.

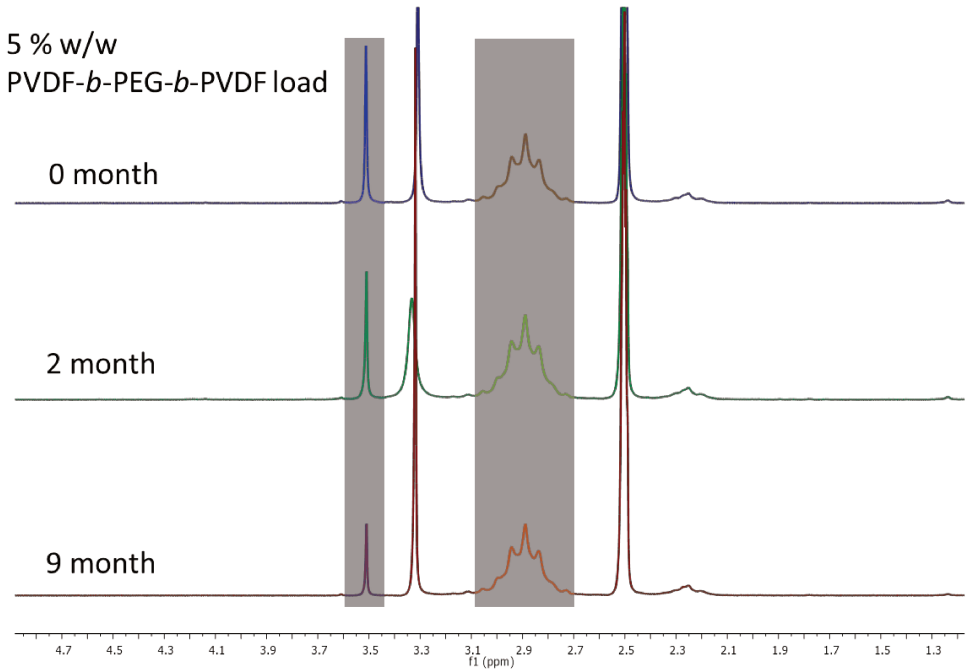

Figure S6. . Signals inside de blue zone (around 3.5 ppm) correspond to CH_2-CH_2-O protons of PEG and Signals inside the yellowish area (between 2.7 and 3.1 ppm) correspond to CH_2 resonances of PVDF backbone protons.

S7. Permeability vs. pressure

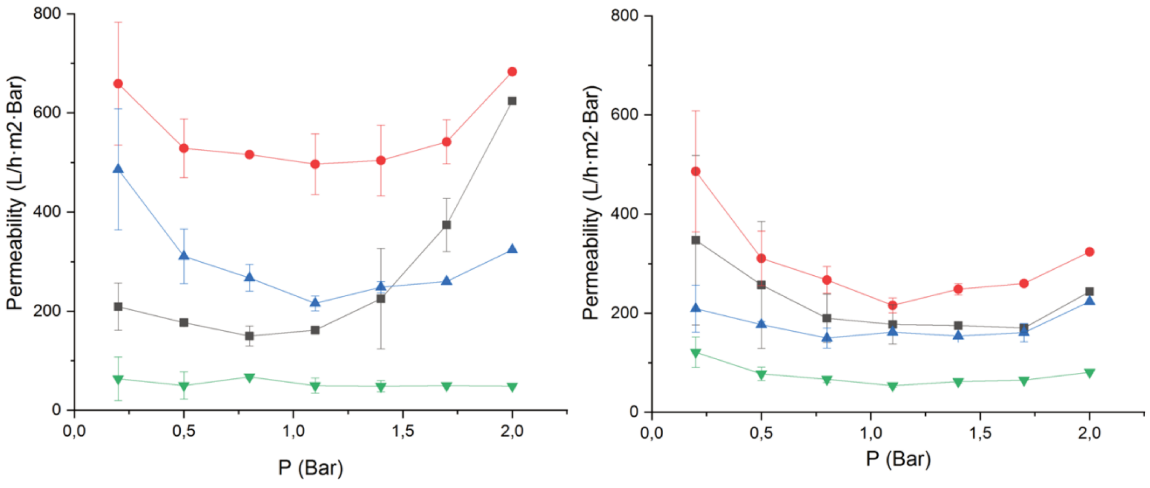

Figure S7. Permeability vs. pressure of membranes containing 2% (left) and 5% w/w (right) of PVDF-*b*-PEG-*b*-PVDF block copolymer in a matrix of high molecular weight PVDF were tested right after preparation (black traces, squares), after 2 months (red traces, dots), after 9 months (blue traces, triangles) and compared to flux values obtained from membranes loaded with an equivalent amount of PEG (green traces, inversed triangles).

GENERAL CONCLUSION & FUTURE PERSPECTIVES

In this thesis, different approaches were reported to synthesize PVDF-based block copolymers (BCPs) and CP-PVDF conjugates. All the BCPs and conjugates had the ability to self-assemble in solution leading to a wide range of PVDF nano- and microstructures.

RAFT/MADIX polymerization of VDF was used to synthesize all the BCP and the CP-PVDF conjugates.

In Chapters 2 and 3, the synthesis and self-assembly of two amphiphilic triblock copolymers (PVDF-*b*-PEG-*b*-PVDF and P(VDF-*co*-HFP)-*b*-PEG-*b*-P(VDF-*co*-HFP)) was described. Using an efficient one-pot aminolysis / thia-Michael addition of PVDF-XA or P(VDF-*co*-HFP) and PEG diacrylate, ABA amphiphilic block copolymers were synthesized. These novel PVDF- and P(VDF-*co*-HFP) ABA triblock copolymers were thoroughly characterised by NMR spectroscopies, GPC, TGA, DSC and XRD.

The self-assembly experiments led to spherical aggregates, vesicles and micrometric crystalline oval morphologies in the case of the triblock with pure PVDF as the hydrophobic block. The crystallinity of these structures was confirmed by SAED patterns recorded during TEM analysis and confirmed by XRD measurement.

Secondly, the self-assembly of P(VDF-*co*-HFP)-*b*-PEG-*b*-P(VDF-*co*-HFP) was studied by TEM. The self-assembly of both triblock copolymers described in chapters 2 and 3 demonstrated the strong impact of the self-assembly conditions on the morphologies obtained. The results suggested that the Temperature-Induced Crystallization-Driven Self-Assembly (CDSA) conditions allow for some control over the preparation of different morphologies.

In Chapter 4 relatively well-defined PNIPAM-*b*-PVDF amphiphilic diblock copolymers were prepared by RAFT using PNIPAM macro-CTAs. Thanks to their amphiphilic nature the resulting BCPs self-assembled into different morphologies in aqueous solutions. The final structures were also strongly affected by the self-assembly conditions. Surprisingly self-assembly from initial acetone solutions lead to the

formation of 2D lenticular aggregates with sizes increasing with the DP of PVDF, reaching lengths of 2.3 µm for the highest PVDF DP. To the best of our knowledge, these are the first reported 2D fluorinated lenticular assembles and these objects offer a versatile 2D platform for the fabrication of functional materials. As a proof of-concept, it was demonstrated, that commercial or in situ prepared Au NPs could be adsorbed onto the surface of these flat aggregates thanks to the strong affinity for gold to the xanthate moieties present at the end of the PVDF chains (likely located on the surface of the PVDF core).

Thanks to collaboration with Prof. Perrier's lab in University of Warwick (UK), funded by Royal Society cyclic peptide-PVDF conjugates (CP-PVDF) were also synthesized. Cyclic peptides bearing two lysine moieties (CP(-NH_2)) were synthesized and modified with xanthate moieties (CP(-$XA)_2$) via the coupling of a NHS-functionalized RAFT agent onto the lysine residues. The RAFT/MADIX polymerization of VDF in the presence of these difunctional macroCTAs was carried out in acetone. NMR spectroscopy (^{1}H and ^{13}F) was used to confirm that the PVDF grew from the CTA attached to the surface of the cyclic peptide and that the polymerization was controlled by RAFT mechanism, despite a high extent of transfer (due to the choice of acetone as polymerization solvent) leading to a major loss of polymer end-group functionality. PVDF-based tubular structures of different lengths were prepared by self-assembly of the CP(-$PVDF)_2$ polymer-conjugates. These PVDF-based tubular aggregates might find an application in the preparation of thin-film membranes thanks to their ability to form porous nanostructured surfaces (an example was given in the supporting information) in the absence of other additives.

The last chapter described the preparation of blend membranes using the BCP described in chapter 2 (PVDF-*b*-PEG-*b*-PVDF) as an additive. Membranes were prepared following NIPS process. The resulting porous membranes were fully characterized using ^{1}H NMR, CA and filtration tests. The tests showed that the hydrophilicity of the membrane increased linearly with the increasing PEG content. It was demonstrated that a very small amount of the triblock copolymer (2-5% w/w) was required to confer hydrophilicity to the PVDF membranes. Our study suggested that additive leaching out was heavily subsidized thanks to the presence of the short

PVDF block in the triblock copolymer that allows the anchoring of the PEG segment to the high molecular weight PVDF forming the membrane.

In an overview, in the course of these PhD studies different synthetic routes were used to prepare a range of well-defined PVDF-based block copolymers and CP-conjugates. There are no precedent reports on such PVDF-containing structures. The self-assembly study of these structures lead to preparation of novel semi-crystalline structures that could have potential use in different fields of science and advanced technology such as wearable electronics, sensors, biomedical applications as well as membrane science.

Regarding the future perspectives, there are some things that could be done to improve this work. The following perspectives were identified:

These studies suggested that different CDSA protocols can be employed to get some control over the formation of different morphologies when one block of the block copolymer is crystalline. It could be applied to study the PVDF-*b*-PEG-*b*-PVDF and PNIPAM-*b*-PVDF systems, in such BCPs the crystallinity of PVDF is higher than the studied BCP where the semi-crystalline block is P(VDF-*co*-HFP). SAXS could also be employed to better understand the formation of the formed nanostructures in solution and solid state.

Also, the self-assembly of the CP-PVDF conjugates can be studied by scattering techniques such as SAXS or SANS. The availability of the pore inside the nanotubes as well as the CP-PVDF conjugates alignment for membrane application could be explored.

Regarding membrane applications, concentrated solutions of PVDF-based spherical aggregates could be casted on a porous support membrane as a hydrophilic nanostructured active layer and examine their performance for water filtration.

Thanks to PVDF electroactive properties, some of the nanostructures obtained could be examined for their application in nanosensors for example.

SCIENTIFIC CONTRIBUTIONS

Publications:

- Guerre, M., Uchiyama, M., Folgado, E., Semsarilar, M., Ameduri, B., Satoh, K., Kamigaito, M., Ladmiral, V. Combination of Cationic and Radical RAFT Polymerizations: A Versatile Route to Well-Defined Poly(ethyl vinyl ether)-block-poly(vinylidene fluoride) Block Copolymers. ACS Macro Lett. 6, 393–398 (2017). In ***ANNEXES***
- Folgado, E., Guerre, M., Mimouni, N., Collière, V., Bijani, C., Moineau-Chane Ching, K., Caminade, A.-M., Ladmiral, V., Ameduri, B., Ouali, A. π-Stacking Interactions of Graphene-Coated Cobalt Magnetic Nanoparticles with Pyrene-Tagged Dendritic Poly (Vinylidene Fluoride). Chempluschem 84, 78–84 (2019). In ***ANNEXES***
- Folgado, E., Guerre, M., Da Costa, A., Ferri, A., Addad, A., Ladmiral, V., Semsarilar, M. "One-Pot" Aminolysis/Thiol-ene preparation of well-defined amphiphilic PVDF-b-PEG-b-PVDF triblock copolymers: Self-assembly behaviour in mixed solvents. Polym. Chem. (2019), *Just Accepted,* DOI: 10.1039/C9PY00970A. ***CHAPTER 2***

Communications:

- Oral presentation at **MACRO 2018**, Cairns, Australia
- Oral presentation at **Journées GFP Mediterranée 2018**, Montpellier, France
- Oral presentation at **JEPO 2017**, Gravelines, France
- Poster at **ICOM 2017**, San Francisco, CA USA

ANNEXES

ACS Macro Letters

Letter

pubs.acs.org/macroletters

Combination of Cationic and Radical RAFT Polymerizations: A Versatile Route to Well-Defined Poly(ethyl vinyl ether)-*block*-poly(vinylidene fluoride) Block Copolymers

Marc Guerre,[†] Mineto Uchiyama,[‡] Enrique Folgado,[†,§] Mona Semsarilar,[§] Bruno Améduri,[†] Kotaro Satoh,[‡,∥] Masami Kamigaito,*[,‡] and Vincent Ladmiral*[,†]

[†]Institut Charles Gerhardt Montpellier, Team: Ingénierie et Architectures Macromoléculaires, UMR5253, CNRS-UM-ENSCM, 8 rue de l'école Normale, 34296 Cedex 5 Montpellier, France

[‡]Department of Applied Chemistry, Graduate School of Engineering, Nagoya University, Furo-cho, Chikusa-ku, Nagoya 464-8606, Japan

[§]Institut Européen des Membranes, IEM, UMR5635, UM-ENSCM-CNRS, Place Eugène Bataillon, 34095 Cedex 5 Montpellier, France

[∥]Precursory Research for Embryonic Science and Technology, Japan Science and Technology Agency, 4-1-8 Honcho, Kawaguchi, Saitama 332-0012, Japan

Supporting Information

ABSTRACT: Poly(vinylidene fluoride)-containing block copolymers are difficult to prepare and still very rare in spite of their potential use in high added value applications. This communication describes in detail the synthesis of unprecedented poly(ethyl vinyl ether)-*block*-poly(vinylidene fluoride) (PEVE-*b*-PVDF) block copolymers (BCP) via the sequential combination of cationic RAFT polymerization of vinyl ethers and radical RAFT polymerization of vinylidene fluoride (VDF). Dithiocarbamate chain transfer agents were found to efficiently control the radical RAFT polymerization of VDF and to be suitable for the preparation of PEVE-*b*-PVDF BCP. These new block copolymers composed of incompatible polymer segments may find applications owing to their phase segregation and self-assembly behavior.

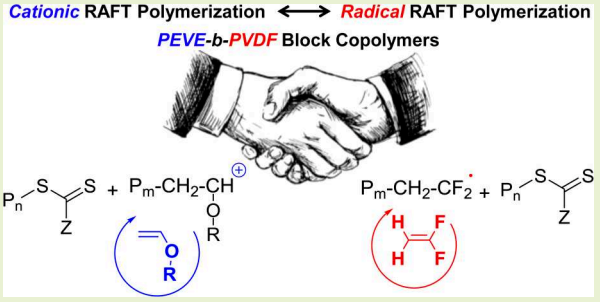

Fluoropolymers are an intriguing class of materials which attract much curiosity in the field of materials science, owing to their chemical inertness, thermal stability, and low surface energy.[1,2] Poly(vinylidene fluoride) (PVDF) is a fluorinated semicrystalline polymer endowed with exceptional electroactive properties with potential uses in many high value-added electronic devices.[3] PVDF is usually prepared by conventional radical polymerization in aqueous dispersed medium (in suspension or emulsion).[4] The preparation of PVDF block copolymers[5,6] has so far been achieved via three main strategies: using functional PVDF telomers,[7−12] functional initiators,[13−16] or reversible deactivation radical polymerization (RDRP) techniques such as iodine transfer polymerization (ITP)[17] for example.[18−20] However, these methods are somewhat limited as they often only achieve low molar masses, high dispersities, or bimodal SEC traces.

Recently, the reversible addition−fragmentation chain transfer (RAFT) polymerization of VDF in dimethyl carbonate has been thoroughly investigated and has been shown to be an efficient method to prepare PVDF with predictable molar mass, narrow molar mass distribution, and high end-group fidelity.[21−23] However, the RAFT of VDF suffers from the accumulation of less reactive end groups (−CF_2−CH_2−$SC(S)OCH_2CH_3$ termini) resulting from VDF head-to-head addition and transfer to the RAFT chain transfer agent (CTA). These less reactive chain ends are responsible for a slowdown of the degenerative chain transfer process which leads to a broadening of the molar mass distribution[21,23] and to a reduced reactivity toward radicals which impairs the synthesis of a wide range of block copolymers. So far, PVDF RAFT macromolecular chain transfer agents (macro-CTAs) could only be efficiently chain extended with vinyl acetate (VAc) to form PVDF-*b*-PVAc[24] (and its poly(vinyl alcohol) derivative[25]). Similarly, few RAFT macro-CTAs are able to produce well-defined PVDF-containing block copolymers. VDF RAFT dispersion polymerization protocols in the presence of PVAc macro-CTAs allowed the polymerization-induced self-assembly (PISA) of PVAc-*b*-PVDF block copolymers and resulted in original crystalline block copolymer morphologies.[26] Moreover, VDF behaves as a less activated monomer (LAM), and its polymerization is only adequately controlled by xanthate RAFT

Received: February 27, 2017
Accepted: March 21, 2017
Published: March 23, 2017

DOI: 10.1021/acsmacrolett.7b00150
ACS Macro Lett. 2017, 6, 393−398

agents. Therefore, the synthesis of well-defined PVDF-based block copolymers is still very challenging.

In 2015, Kamigaito's group reported the cationic RAFT polymerization of vinyl ether (which does not homopolymerize under radical polymerization conditions), using thiocarbonylthio compounds as CTAs and a small amount of a strong Brønsted acid acting as the initiator.[27,28] This cationic polymerization proceeds through the degenerative chain transfer of growing carbocationic species to dormant thiocarbonylthio species. Very efficient control of the polymerization of vinyl ethers was demonstrated using trithiocarbonate and dithiocarbamate RAFT agents, which remain at the chain ends even after isolation of the resulting poly(vinyl ether)s (PVEs).

This communication reports the development of a facile strategy for the synthesis of unprecedented PVDF-containing block copolymers. This strategy, which relies on the combination of cationic RAFT polymerization and radical RAFT polymerization, produces well-defined PVE-*b*-PVDF block copolymers (BCPs). Xanthate CTAs, which are well-suited for the radical RAFT polymerization of VDF, are not very efficient in controlling the cationic polymerization of vinyl ethers[27] and lead to poorly defined PVE with relatively high dispersity (Đ = 1.50). Dithiocarbamate CTAs thus appeared as a better choice, provided that they also control the radical polymerization of VDF, since they offer efficient control over the cationic polymerization of VEs. In consequence, the still unreported RAFT of VDF using dithiocarbamates was carefully examined using ^{1}H and ^{19}F NMR spectroscopy and size exclusion chromatography (SEC). RAFT polymerization of VDF in the presence of *N*,*N*-diethyldithiocarbamate (CTA_1) was performed according to Scheme 1 (Table S1, runs 1−7).

Scheme 1. Schematic Representation of the Vinylidene Fluoride (VDF) Radical RAFT Homopolymerization Using Methyl 2-((*N*,*N*-Diethylcarbamothioyl)thio)propanoate (CTA_1) and the Synthesis of PEVE-*b*-PVDF Block Copolymers via Sequential Cationic RAFT Polymerization of EVE (Ethyl Vinyl Ether) and Radical RAFT Polymerization of VDF

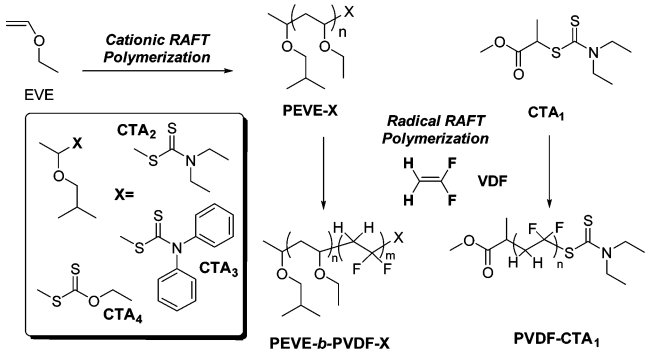

The first-order kinetic plot and the evolution of the molar mass and of the dispersity of the resulting PVDF versus VDF conversion for this radical RAFT polymerization of VDF (Table S1) are displayed in Figure 1b and Figure 1a, respectively. The first-order kinetic plot (Figure 1b) exhibited the three different regimes of polymerization already observed by Guerre et al. in the case of the xanthate RAFT polymerization of VDF.[21,23]

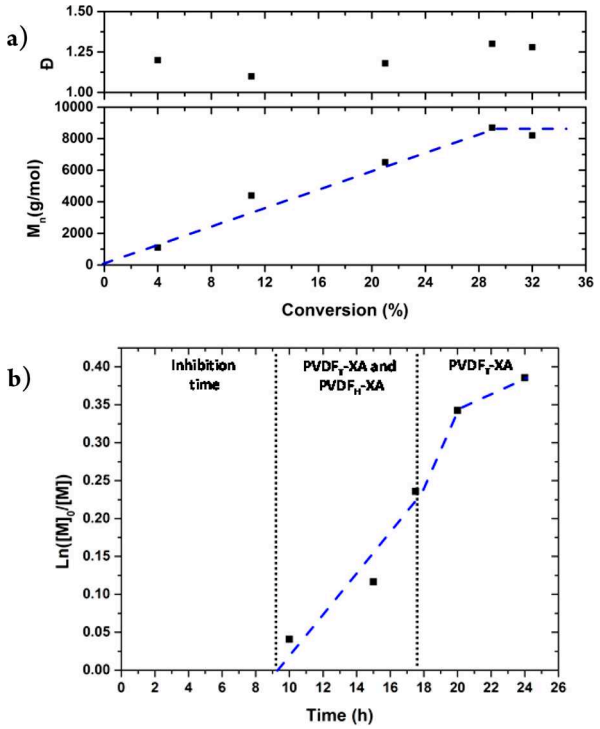

Figure 1. (a) Evolutions of molar mass and dispersity with VDF conversion and (b) first-order kinetic plot of the radical RAFT polymerization of VDF using methyl 2-((*N*,*N*-diethylcarbamothioyl)-thio)propanoate as chain transfer agent (CTA_1) (Table S1). Reaction conditions: $[VDF]_0/[CTA_1]_0/[I]_0$ = 100/1/0.1, I = Trigonox 121, T = 73 °C, solvent, DMC.

However, this RAFT polymerization proceeded at a surprisingly slower rate (initial molar ratio $[M]_0/[CTA]_0$ = 100, inhibition time = 8 h, and first-order kinetic slope = 0.029) compared to the RAFT polymerization of VDF using xanthate CTA ($[M]_0/[CTA]_0$ = 50, inhibition time = 5 h, and first-order kinetic slope = 0.041[21]). This slowdown of the polymerization is thought to arise from the presence of the nitrogen atom which causes the strong stabilization of the intermediate radical (compared to the *O*-ethyl moiety).

The apparent transfer constant $C_{Tr(app)}$ of the PVDF$^{\bullet}$ radicals toward CTA_1 was determined using the O'Brien and Gornick method (Figure S3). This method gave $C_{Tr(app)}$ = 32 at 73 °C, a slightly inferior value to that determined with a xanthate CTA ($C_{Tr(app)}$ = 49 at 73 °C)[23] but high enough to ensure fast transfer to the CTA and efficient control. As in the xanthate-CTA-mediated polymerization of VDF, the molar mass of the resulting PVDF increased linearly with conversion up to 28% conversion, and the dispersity remained below 1.3 throughout the polymerization (Figure 1a and S4) suggesting that the dithiocarbamate CTA_1 efficiently controls the polymerization of VDF. As in the VDF RAFT polymerization controlled by xanthate, the slope of the "M_n vs conversion" plot changed abruptly in the later stage of the polymerization.[23] This is likely caused by the disappearance of the last $PVDF_H$-CTA end-group (where $PVDF_H$-CTA designates PVDF chains terminated with a head-to-tail (regular) addition: $-CH_2CF_2-CH_2CF_2-S-C(S)NEt_2$) which leads to a slowdown of the degenerative chain transfer and marks the onset of a less efficient control of the polymerization.[23] Here, this slowdown of the DT mechanism did not significantly affect Đ because the target DP was rather small (DP_{target} = 100), and the conversion

DOI: 10.1021/acsmacrolett.7b00150
ACS Macro Lett. 2017, 6, 393−398

increased after the onset of the DT slowdown was limited (11%). This analogy with the xanthate-mediated RAFT polymerization of VDF was further confirmed by NMR. A typical ^{1}H NMR spectrum recorded after 10 h of polymerization (run 1, Table S1) is displayed in Figure 2. This spectrum shows the typical doublet at 1.22 ppm and singlet at 3.65 ppm assigned, respectively, to the $-O-\mathbf{CH}_3$ and $\mathbf{CH}_3-$CH of the CTA R-group at the PVDF α-chain end.

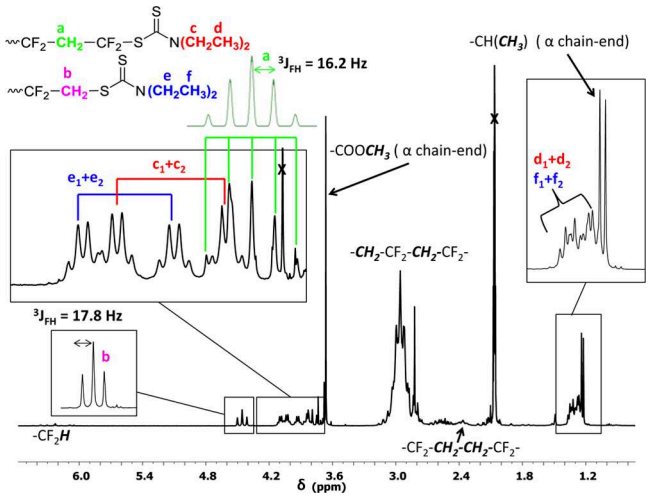

Figure 2. ^{1}H NMR spectrum of $PVDF_{17}$-CTA_1 (run 1, Table S1) synthesized by radical RAFT polymerization using CTA_1. Reaction conditions: $[VDF]_0/[CTA_1]_0/[I]_0 = 100/1/0.1$, I = Trigonox 121, T = 73 °C, solvent, DMC, t = 10 h.

The complex signal (two doublets of quartets) between 3.76 and 4.17 ppm was assigned to the $-N(\mathbf{CH}_2CH_3)_2$ protons of the Z-group of the CTA at the PVDF ω-chain-end. This signal splitting also observed in the ^{1}H NMR spectrum of CTA_1 (Figure S1) is likely caused by the slow configuration inversion of the nitrogen atom in the dithiocarbamate functional group and also by the presence of two different chain-ends consisting of $-CH_2-CF_2-S(C{=}S)N(CH_2CH_3)_2$ ($PVDF_H$-CTA_1) and $CF_2-CH_2-S(C{=}S)N(CH_2CH_3)_2$ ($PVDF_T$-CTA_1). The CH_2 of the VDF terminal unit in the $PVDF_T$-CTA chains (PVDF chains terminated with a (inverse) head-to-head addition: $-CH_2CF_2-CF_2CH_2-S-C(S)N(CH_2CH_3)_2$) was clearly identified at 4.44 ppm with a typical triplet ($^3J_{HF}$ = 17.8 Hz), while the CH_2 of the terminal VDF unit in the $PVDF_H$-CTA chains at 3.77 ppm overlapped with the protons c of the CTA Z-group ($-N(\mathbf{CH}_2CH_3)_2$). A simulation of this multiplet is provided in Figure 2, for clarity. The presence of these two types of end-groups confirms that the RAFT polymerization of VDF in the presence of CTA_1 proceeds, just like the RAFT polymerization mediated by xanthate,[21−23] with the progressive accumulation of $PVDF_T$-CTA.

In addition, the usual signals corresponding to the head-to-tail (HT) and tail-to-tail (TT) additions of PVDF were observed at 2.94 ppm (broad signal) and 2.35 ppm, respectively. The ^{19}F NMR spectrum of this PVDF-CTA_1 (Figure S5) displayed the expected signals previously reported for the xanthate-mediated RAFT VDF polymerization:[21] signal at −93.51 ppm of the CF_2 of the first-added VDF unit (connected to the R-group of CTA_1) and signals of the CF_2 of the ultimate and penultimate VDF units at the ω-end of the PVDF (−69.1 and −91.65 ppm, respectively, for $PVDF_H$-CTA_1 and −112.3 and −112.7 ppm, respectively, for $PVDF_T$-CTA_1).

Since well-defined PVDF can be successfully synthesized using dithiocarbamate CTA, a series of poly(ethyl vinyl ether) (PEVE) macro-CTAs were prepared via cationic RAFT polymerization using different CTAs: CTA_2 (Z-group = diethylcarbamate), CTA_3 (Z-group = diphenylcarbamate), and CTA_4 (Z-group = xanthate) (Scheme 1 and Table S2).

The narrowest dispersities ($Đ$ < 1.1) were obtained for the diethylcarbamate and diphenylcarbamate CTAs ($Đ_{CTA2}$= 1.08 and $Đ_{CTA3}$ = 1.09, Table S2), whereas the xanthate CTA_4 led to broader dispersity ($Đ_{CTA4}$ = 1.52). Indeed, dithiocarbamate CTAs with electron-donating nitrogen atoms are most effective at controlling the molar masses, most likely through the formation of a more stabilized cationic intermediate, in contrast to the oxygen atom of an ester group.[27] The structures of the resulting PEVE macro-CTAs were further characterized by ^{1}H and ^{13}C NMR spectroscopy (Figures 3 and S7−S11).

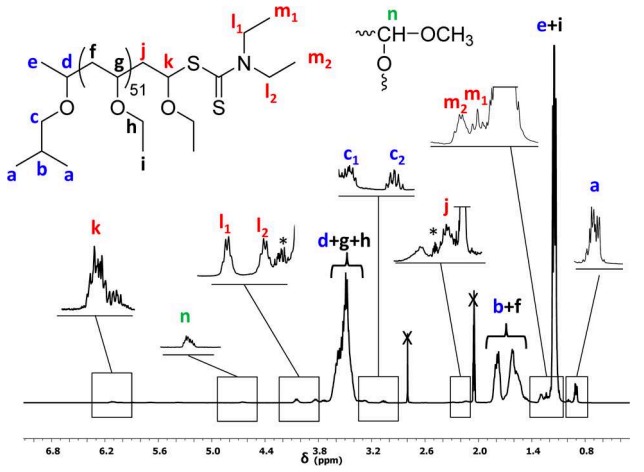

Figure 3. ^{1}H NMR spectrum of $PEVE_{52}$-CTA_2 (run 1, Table S2) synthesized by cationic RAFT polymerization. Crossed-out peaks correspond to residual acetone and water. *Spinning side bands. Reaction conditions: $[EVE]_0/[CTA_2]_0/[I]_0 = 50/1/0.05$, T = −40 °C, solvent, hexane/dichloromethane/diethyl ether (80/10/10).

The ^{1}H NMR spectrum of $PEVE_{52}$-CTA_2 (Figure 3) shows typical signals corresponding to the CH_2 (l_1 and l_2) and CH_3 (m_1 and m_2) of the $-N(CH_2CH_3)_2$ CTA Z-group at 3.78−4.13 ppm and 1.21−1.33 ppm, respectively. The signal assigned to the ultimate EVE unit adjacent to the diethylcarbamate end-group was easily identified at 6.11 ppm. Signals corresponding to the CH_3 and CH_2 of the isobutyl vinyl ether moiety were also identified at 0.9 ppm and 3.28/3.06 ppm, respectively (two peaks were observed for the CH_2 due to their diastereotopicity). As reported by Kamigaito et al.,[27] the small peak (signal n) at 4.6 ppm was assigned to the $-C\mathbf{H}(OEt)OCH_3$ ω-chain-end originating from quenching of the polymerization by methanol. The functionality of $PEVE_{52}$-CTA_2 was calculated to be 83% (while those of $PEVE_{50}$-CTA_3 and $PEVE_{52}$-CTA_4 were estimated at 95 and 91%, respectively; Table S2, eq S8).

These PEVE macroCTAs were then used in the radical RAFT polymerization of VDF (Scheme 1). Figure S11 shows the ^{1}H NMR spectrum of the resulting $PEVE_{50}$-*b*-$PVDF_{454}$−CTA_2 BCP. The expected chain-end signals already observed for the PVDF synthesized by RAFT polymerization using

DOI: 10.1021/acsmacrolett.7b00150
ACS Macro Lett. 2017, 6, 393−398

CTA_1 (Figure 2) were clearly identified in the ^1H NMR spectrum of this BCP.

This suggests that the PVDF chains formed were efficiently end-capped by the dithiocarbamate group and that the RAFT polymerization of VDF proceeded with a degree of control. However, a large quantity of dead chains (58 mol % of $-CF_2H$ ω-chain-ends) likely caused by transfer to DMC and often observed during VDF polymerization in DMC for high target DP[23] can be seen as a triplet of triplets at 6.3 ppm. The important signal to ascertain the formation of block copolymer and corresponding to the connection between the PEVE and PVDF blocks was only observed in the ^{19}F NMR spectrum of the BCP at −93.4 ppm (Figure 4). These ^{19}F NMR signals are

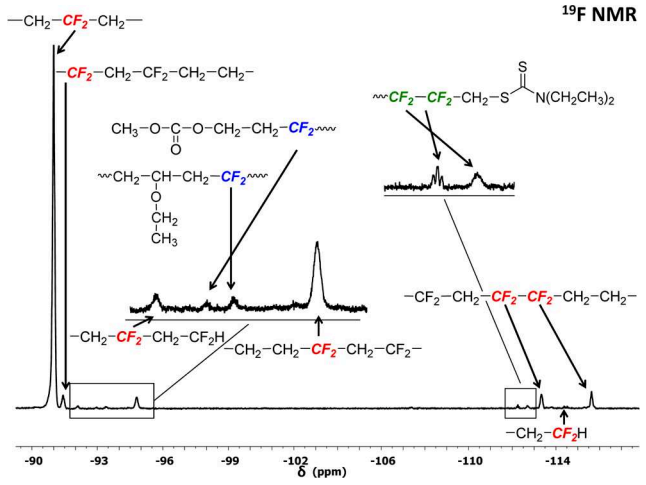

Figure 4. Expansion of the −90 to −118 ppm region of the ^{19}F NMR spectrum in $(CD_3)_2CO$ of the purified $PEVE_{52}$-*b*-$PVDF_{454}$−CTA_2 block copolymer (run 1, Table S3) synthesized by RAFT polymerization of VDF using $PEVE_{52}$-CTA_2 as the CTA.

also visible in the ^{19}F NMR spectra of the PEVE-*b*-PVDF block copolymers synthesized using $PEVE_{50}$-CTA_3 and $PEVE_{52}$-CTA_4 as macro-CTAs (Figure S12). The efficient chain extension was also confirmed by SEC (Figure 5).

The SEC trace of the crude $PEVE_{52}$-*b*-$PVDF_{454}$−CTA_2 BCP (Figure 5b, left) shows the presence of a large amount of

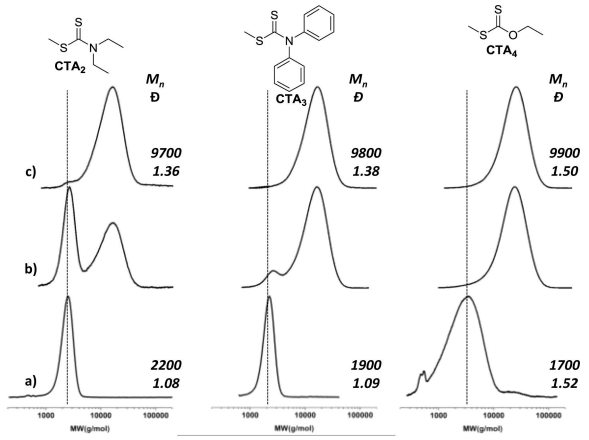

Figure 5. SEC traces of polymers synthesized using different CTAs (from left to right: CTA_2, CTA_3, CTA_4): (a) PEVE-CTA, (b) crude PEVE-*b*-PVDF−CTA, and (c) PEVE-*b*-PVDF−CTA after precipitation in hexane (good solvent for PEVE and bad solvent for PVDF).

unreacted PEVE (at 2000 $g{\cdot}mol^{-1}$) and indicates the relatively poor reactivation of $PEVE_{52}$-CTA_2 macro-CTA by $PVDF^\bullet$ radicals. In contrast, $PEVE_{50}$-CTA_3 macro-CTA was better reactivated by $PVDF^\bullet$ radicals. The SEC trace of the crude $PEVE_{50}$-*b*-$PVDF_{431}$−CTA_3 (Figure 5b, middle) only showed a small $PEVE_{50}$-CTA_3 macro-CTA residual peak. Finally $PEVE_{52}$-CTA_4, although of higher dispersity than its dithiocarbamate analogues, was entirely reactivated by $PVDF^\bullet$ radicals (Figure 5b, right). To further investigate this contamination caused by the suboptimal reactivation of the PEVE-CTA, the ^1H NMR spectra of the crude and purified BCP (precipitated in hexane, good solvent for PEVE, and bad solvent for PVDF) were compared (Figures S16−18). The residual fraction of $PEVE_{52}$-CTA_2 (peak at 6.1 ppm in Figure S15), which was not reactivated by $PVDF^\bullet$ radicals, was eliminated by this precipitation (Figures S15−17). This observation strongly supports the hypothesis of a slow reactivation of $PEVE_{52}$-CTA_2 macroCTA by $PVDF^\bullet$ radicals compared to $PEVE_{50}$-CTA_3 and $PEVE_{52}$-CTA_4 and is in agreement with the slowdown of the polymerization observed for the VDF RAFT polymerization mediated by CTA_1. In addition, the PEVE-O−CH_3 dead chains (peak at 4.6 ppm in Figures S15−17), formed by quenching by methanol and which did not take part in the RAFT polymerization of VDF, were also removed in the precipitation process.

It is also important to note the absence of the characteristic signal of the xanthate end group in the ^1H NMR spectrum of the purified $PEVE_{52}$-*b*-$PVDF_{920}$−CTA_4 BCP (Figure S17). The *O*-ethyl signals observed at 1.39 and 4.65 ppm in the ^1H NMR of the crude BCP disappeared after precipitation. This means that side reactions occurred on the *O*-ethyl xanthate end-group during the VDF polymerization. These reactions also affect the dithiocarbamate-functionalized polymers, but at a much slower rate. DMC radicals produced by proton abstraction by $-CF_2^\bullet$ radicals were shown to either initiate new PVDF chains (as observed on all BCPs ^1H NMR spectra: peaks at 3.71 and 4.31 ppm corresponding to the CH_3 and CH_2 of the DMC moiety, respectively) or transfer to the PVDF xanthate ω-end-group.[21,23] In the present case, these transfer reactions likely consume entirely the remaining xanthate end-group to form $(CH_3O(C{=}O)OCH_2{-}S(C{=}S){-}OCH_2CH_3)$ adducts which are eliminated by precipitation.[21] In comparison, the functionalities of $PEVE_{50}$-*b*-$PVDF_{454}$−CTA_2 (58%) and $PEVE_{52}$-*b*-$PVDF_{431}$−CTA_3 (80%) are much higher.

The PEVE-*b*-PVDF block copolymers were analyzed by differential scanning calorimetry (DSC) to investigate the miscibility of PEVE and PVDF. The DSC thermograms of all BCPs display a melting temperature at ca. 160−170 °C corresponding to the melting point of PVDF (Figure S18). In addition, the glass transition (T_g) of PEVE at −35 °C was also observed on all thermograms. Note that the T_g of PVDF around −40 °C is difficult to observe[21,24] but may overlap with that of PEVE in Figure S18. These results strongly suggest the immiscibility of the PVDF and of the PEVE segments.

This communication describes the successful use of sequential cationic RAFT polymerization and radical RAFT polymerization to prepare novel well-defined PEVE-*b*-PVDF block copolymers. Dithiocarbamate RAFT agents are particularly well-suited for this synthesis which leads to block copolymers containing incompatible blocks. These new block copolymers could be very useful as compatibilizers, for example for electronic devices. The study of the self-assembly of these

DOI: 10.1021/acsmacrolett.7b00150
ACS Macro Lett. 2017, 6, 393−398

block copolymers in selective solvents[29] and in the bulk[5] is underway and will be published in due course.

■ ASSOCIATED CONTENT

Supporting Information

The Supporting Information is available free of charge on the ACS Publications website at DOI: 10.1021/acsmacrolett.7b00150.

Experimental procedures, additional ^{1}H and ^{19}F NMR spectra, equations used for calculation of DP and M_n, plots of $\ln([CTA]_0/[CTA])$ versus $\ln([VDF]_0/[VDF])$, SEC traces of VDF polymerization with CTA_1, DSC thermograms of the BCPs (PDF). (PDF)

■ AUTHOR INFORMATION

Corresponding Authors

*E-mail: kamigait@apchem.nagoya-u.ac.jp.
*E-mail: vincent.ladmiral@enscm.fr.

ORCID

Bruno Améduri: 0000-0003-4217-6664
Vincent Ladmiral: 0000-0002-7590-4800

Author Contributions

The manuscript was written through contributions of all authors, and all authors have given approval to the final version of the manuscript.

Notes

The authors declare no competing financial interest.

■ ACKNOWLEDGMENTS

This work was supported by the Japan Society for the Promotion of Science (JSPS) Summer program fellowship granted to MG; by a PhD grant awarded to MG by the Ministère de l'Education Nationale et de l'Enseignement Supérieur et de la Recherche; and by the PhD grant awarded to EF by the Institut Carnot Chimie Balard and the LABEX CheMISyst (ANR-10-LABX-05−01). The authors thank Arkema (Pierre-Bénite, France) for providing VDF.

■ REFERENCES

(1) Smith, D. W.; Iacono, S. T.; Suresh, S. I. In *Handbook of Fluoropolymers Science and Technology*; John Wiley & Sons, Inc.: New York, 2004.
(2) Gardiner, J. Fluoropolymers: Origin, Production, and Industrial and Commercial Applications. *Aust. J. Chem.* **2015**, *68*, 13−22.
(3) Améduri, B.; Boutevin, B. In *Well-Architectured Fluoropolymers: Synthesis, Properties and Applications*; Elsevier: Amsterdam, 2004.
(4) Ameduri, B. From Vinylidene Fuoride (VDF) to the Applications of VDF-Containing Polymers and Copolymers: Recent Developments and Future trends. *Chem. Rev.* **2009**, *109*, 6632−6686.
(5) Voet, V. S. D.; ten Brinke, G.; Loos, K. Well-defined copolymers based on poly(vinylidene fluoride): From preparation and phase separation to application. *J. Polym. Sci., Part A: Polym. Chem.* **2014**, *52*, 2861−2877.
(6) Asandei, A. D. Photomediated Controlled Radical Polymerization and Block Copolymerization of Vinylidene Fluoride. *Chem. Rev.* **2016**, *116*, 2244−2274.
(7) Zhang, Z. B.; Ying, S. K.; Shi, Z. Q. Synthesis of fluorine-containing block copolymers via ATRP 1. Synthesis and characterization of PSt-PVDF-PSt triblock copolymers. *Polymer* **1999**, *40*, 1341−1345.
(8) Jo, S. M.; Lee, W. S.; Ahn, B. S.; Park, K. Y.; Kim, K. A.; Rhee Paeng, I. S. New AB or ABA type block copolymers: atom transfer radical polymerization (ATRP) of methyl methacrylate using iodine-terminated PVDFs as (macro)initiators. *Polym. Bull.* **2000**, *44*, 1−8.
(9) Destarac, M.; Matyjaszewski, K.; Silverman, E.; Améduri, B.; Boutevin, B. Atom Transfer Radical Polymerization Initiated with Vinylidene Fluoride Telomers. *Macromolecules* **2000**, *33*, 4613−4615.
(10) Shi, Z. Q.; Holdcroft, S. Synthesis of Block Copolymer Possessing Fluoropolymer and Non-Fluoropolymer Segments by Radical Polymerization. *Macromolecules* **2004**, *37*, 2084−2089.
(11) Shi, Z. Q.; Holdcroft, S. Synthesis and Proton Conductivity of Partially Sulfonated Poly([vinylidene difluoride-*co*-hexafluoropropylene]-*b*-styrene) Block Copolymers. *Macromolecules* **2005**, *38*, 4193−4201.
(12) Laruelle, G.; Nicol, E.; Améduri, B.; Tassin, J. F.; Ajellal, N. J. Synthesis of poly(vinylidene fluoride)-b-poly(styrene sulfonate) block copolymers by controlled radical polymerizations. *J. Polym. Sci., Part A: Polym. Chem.* **2011**, *49*, 3960−3969.
(13) Xu, K.; Li, K.; Khanchaitit, P.; Wang, Q. Synthesis and Characterization of Self-Assembled Sulfonated Poly(styrene-*b*-vinylidene fluoride-*b*-styrene) Triblock Copolymers for Proton Conductive Membranes. *Chem. Mater.* **2007**, *19*, 5937−5945.
(14) Chanthad, C.; Masser, K. A.; Xu, K.; Runt, J.; Wang, Q. J. Synthesis of triblock copolymers composed of poly(vinylidene fluoride-co-hexafluoropropylene) and ionic liquid segments. *J. Mater. Chem.* **2012**, *22*, 341−344.
(15) Voet, V. S. D.; Tichelaar, M.; Tanase, S.; Mittelmeijer-Hazeleger, M. C.; ten Brinke, G.; Loos, K. Poly(vinylidene fluoride)/nickel nanocomposites from semicrystalline block copolymers precursors. *Nanoscale* **2013**, *5*, 184−192.
(16) Voet, V. S. D.; Hermida-Merino, D.; ten Brinke, G.; Loos, K. Block copolymer route towards poly(vinylidene fluoride)/poly(methacrylic acid)/nickel nanocomposites. *RSC Adv.* **2013**, *3*, 7938−7946.
(17) David, G.; Boyer, C.; Tonnar, J.; Ameduri, B.; Lacroix-Desmazes, P.; Boutevin, B. Use of iodo-compounds in Radical Polymerization. *Chem. Rev.* **2006**, *106*, 3936−3981.
(18) Tatemoto, M. In *The First Regular Meeting of Soviet Japanese Fluorine Chemists*, Tokyo, 1979.
(19) Valade, D.; Boyer, C.; Ameduri, B.; Boutevin, B. Poly(vinylidene fluoride)-b-poly(styrene) Block Copolymers by Iodine Transfer Polymerization (ITP): Synthesis, Characterization, and Kinetics of ITP. *Macromolecules* **2006**, *39*, 8639−8651.
(20) Asandei, A. D.; Adebolu, O. I.; Simpson, C. P. Mild-Temperature Mn2(CO)10-Photomediated Controlled Radical Polymerization of Vinylidene Fluoride and Synthesis of Well-defined Poly(vinylidene fluoride) Block Copolymers. *J. Am. Chem. Soc.* **2012**, *134*, 6080−6083.
(21) Guerre, M.; Campagne, B.; Gimello, O.; Parra, K.; Ameduri, B.; Ladmiral, V. Deeper Insight into the MADIX Polymerization of Vinylidene Fluoride. *Macromolecules* **2015**, *48*, 7810−2799.
(22) Guerre, M.; Soulestin, T.; Lopez, G.; Totée, C.; Améduri, B.; Silly, G.; Ladmiral, V. A journey into the Microstructure of PVDF Made by RAFT. *Macromol. Chem. Phys.* **2016**, *217*, 2275−2285.
(23) Guerre, M.; Rahaman, S. M. W.; Améduri, B.; Poli, R.; Ladmiral, V. Limits of Vinylidene Fluoride RAFT Polymerization. *Macromolecules* **2016**, *49*, 5386−5396.
(24) Guerre, M.; Rahaman, S. M. W.; Améduri, B.; Poli, R.; Ladmiral, V. RAFT Synthesis of well-defined PVDF-*b*-PVAc block copolymers. *Polym. Chem.* **2016**, *7*, 6918−6933.
(25) Guerre, M.; Schmidt, J.; Talmon, Y.; Ameduri, B.; Ladmiral, V. An amphiphilic poly(vinylidene fluoride)-*b*-poly(vinyl alcohol) block copolymer: synthesis and self-assembly in water. *Polym. Chem.* **2017**, *8*, 1125−1128.
(26) Guerre, M.; Semsarilar, M.; Godiard, F.; Ameduri, B.; Ladmiral, V. Polymerization-induced self-assembly of PVAc-*b*-PVDF block copolymers *via* RAFT dispertion polymerization of vinylidene fluoride in dimethyl carbonate. *Polym. Chem.* **2017**, *8*, 1477−1487.
(27) Uchiyama, M.; Satoh, K.; Kamigaito, M. Cationic RAFT Polymerization Using ppm Concentrations of Organic Acid. *Angew. Chem., Int. Ed.* **2015**, *54*, 1924−1928.

DOI: 10.1021/acsmacrolett.7b00150
ACS Macro Lett. 2017, 6, 393−398

(28) McKenzie, T. G.; Fu, Q.; Uchiyama, M.; Satoh, K.; Xu, J.; Boyer, C.; Kamigaito, M.; Qiao, G. G. Controlled Polymerization: Beyond Traditional RAFT: Alternative Activation of Thiocarbonylthio compounds for Controlled Polymerization. *Adv. Sci.* **2016**, *3*, 1500394.
(29) Mai, Y.; Eisenberg, A. Self-assembly of block copolymers. *Chem. Soc. Rev.* **2012**, *41*, 5969−5985.

DOI: 10.1021/acsmacrolett.7b00150
ACS Macro Lett. 2017, 6, 393−398

Supporting Information

Combination of cationic and radical RAFT polymerizations: A versatile route to well-defined poly(ethyl vinyl ether)-block-poly(vinylidene fluoride) block copolymers

Marc Guerre,[†] Mineto Uchiyama,[‡] Enrique Folgado,[†∥] Mona Semsarilar,[∥] Bruno Ameduri,[†] Kotaro Satoh,[‡§] Masami Kamigaito,[‡*] and Vincent Ladmiral[†*]

[†]Institut Charles Gerhardt Montpellier, Team: Ingénierie et Architectures Macromoléculaires, UMR5253, CNRS-UM-ENSCM, 8 rue de l'école Normale, 34296, Montpellier Cedex 5, France.

[‡]Department of Applied Chemistry, Graduate School of Engineering, Nagoya University, Furo-cho, Chikusa-ku, Nagoya 464-8606, Japan.

[∥]Institut Européen des Membranes, IEM, UMR5635, UM-ENSCM-CNRS, Place Eugène Bataillon, 34095 Montpellier cedex 5, France.

[§]Precursory Research for Embryonic Science and Technology, Japan Science and Technology Agency, 4-1-8 Honcho, Kawaguchi, Saitama 332-0012, Japan.

RAFT, Poly(vinylidene fluoride), Block copolymer, Poly(vinyl ether), PVDF, PVE

Table of Content

Experimental Procedures

Materials and Method

Radical RAFT

All reagents were used as received unless stated otherwise. 1,1-Difluoroethylene (vinylidene fluoride, VDF) was kindly supplied by Arkema (Pierre-Bénite, France). tert-Amyl peroxy-2- ethylhexanoate (Trigonox® 121, purity 95%) was purchased from AkzoNobel (Chalons-sur-Marne, France). Methyl 2-((diethylcarbamothioyl)thio)propanoate **(CTA_1)** was synthesized according to the method described by Liu et al.[1] slightly modified (The potassium ethyl xanthogenate salt was replaced by sodium diethyldithiocarbamate trihydrate salt).
Ethyl vinyl ether (EVE), methyl 2-bromopropionate, dimethyl carbonate (DMC), methanol (MeOH), acetone ($(CH_3)_2CO$), ethanol (EtOH) and n-hexane (Hex) (>99 %) were purchased from Sigma Aldrich and used as received.

Cationic RAFT

Ethyl vinyl ether (EVE) (TCI, 98%) was distilled over calcium hydride under reduced pressure before use. Trifluoromethanesulfonic (Triflic) acid (TfOH) (TCI,>98.0%) was used as received. *S-1*-Isobutoxyethyl *N,N*-diethyl dithiocarbamate[1] **(CTA_2)**, *S-1*-Isobutoxyethyl *N,N*-diphenyl dithiocarbamate[2] **(CTA_3)** and *S-1*-isobutoxyethyl *O*-ethyl xanthate[2] **(CTA_4)** were synthesized according to previously published protocols.
Toluene (KANTO, >99.5%; H_2O <10 ppm), *n*-hexane (KANTO, >96%; H_2O <10 ppm), diethyl ether (KANTO, >99.5%; H_2O <50 ppm), and dichloromethane (KANTO, >99.5%; H_2O <0.005%) were dried and deoxygenized by passage through column of Glass Contour Systems before use.

Nuclear magnetic resonance (NMR)

The Nuclear Magnetic Resonance (NMR) spectra were recorded on a Bruker AC 400 instrument. Deuterated acetone was used as the solvent. Coupling constants and chemical shifts are given in hertz (Hz) and part per million (ppm), respectively. The experimental conditions for recording ^{1}H, ^{19}F, spectra were as follows: flip angle 90° (or 30°), acquisition time 4.5 s (or 0.7 s), pulse delay 2 s (or 2 s), number of scans 128 (or 512), and a pulse width of 5 μs for ^{19}F NMR.

Size Exclusion Chromatography (SEC)

Size exclusion chromatograms were recorded using a Triple detection GPC from Agilent Technologies with its corresponding Agilent software, dedicated to multi-detector GPC calculation. The system used two PL1113-6300 ResiPore 300 x 7.5 mm columns (all range of Mw) with DMF as the eluent with a flow rate of 0.8 mL/min and toluene as flow rate marker. The detector suite comprised a PL0390-0605390 LC light scattering detector with 2 diffusion angles (15° and 90°), a PL0390-06034 capillary viscometer, and a 390-LC PL0390-0601 refractive index detector. The entire SEC-HPLC system was thermostated at 35°C. PMMA narrow standards were used for the calibration. Typical sample concentration was 10 mg/mL.

Differential scanning calorimetry (DSC)

DSC measurements were performed on 10–15 mg samples on a Netzsch DSC 200 F3 instrument using the following heating/ cooling cycle: cooling from room temperature (ca. 20 °C) to −50 °C at 20 °C min^{-1}, isotherm plateau at −50 °C for 5 min, first heating ramp from −50 to 200 °C at 10 °C min^{-1}, cooling stage from 200 to −50 °C at 10 °C min^{-1}, isotherm plateau at −50 °C for 3 min, second heating ramp from −50 °C to 200 °C at 10 °C min-1 and last cooling stage from 200 °C to room temperature (ca. 20 °C). The instrument was calibrated with noble metals and checked before analysis with an indium sample. Melting points were determined at the maximum of the enthalpy peaks. T_g were assessed from the inflexion point in the heat capacity jump.

Autoclave

The radical polymerizations of VDF were performed in a 100 mL Hastelloy Parr autoclave systems (HC 276), equipped with a mechanical Hastelloy stirring system, a rupture disk (3000 PSI), inlet and outlet valves, and a Parr electronic controller to regulate the stirring speed and the heating. Prior to reaction, the autoclave was pressurized with 30 bars of nitrogen to check for leaks. The autoclave was then put under vacuum (20.10^{-3} mbar) for 30 minutes to remove any trace of oxygen. A degassed solution of solvent, initiator and CTA was introduced via a funnel. The reactor was then cooled down in liquid nitrogen to about -80°C, and the desired

quantity of VDF was transferred by double weighing (i.e. the difference of weight before and after filling the autoclave with VDF). After warming up to ambient temperature (*ca.* 20 °C), the autoclave was heated to the target temperature under mechanical stirring.

Syntheses

Methyl 2-((diethylcarbamothioyl)thio)propanoate (CTA_1)
^{1}H NMR (400 MHz $(CD_3)_2CO$, (δ ppm), Fig S1): 1.18 – 1.34 (-N(CH_2**CH_3**)$_2$), 1.49-1.58 (d, (**CH_3**)CH-(C=O)), 3.65-3.72 (s, -(C=O)O**CH_3**), 3.73-3.86 (q, (-N(**CH_2**CH_3)$_2$), 3.96-4.10 (q, (-N(**CH_2**CH_3)$_2$), 4.66-4.79 (q, (CH_3)**CH**-(C=O)).
^{13}C NMR (100 MHz $(CD_3)_2CO$, (δ ppm), Fig S2): 11.63 (-N(CH_2**CH_3**)$_2$), 12.75 (-N(CH_2**CH_3**)$_2$), 17.85 ((**CH_3**)CH-(C=O)), 47.53 (-N(**CH_2**CH_3)$_2$), 49.41 ((CH_3)**CH**-(C=O)), 50.16 (-N(**CH_2**CH_3)$_2$), 52.68 (-(C=O)O**CH_3**), 172.70 (-(**C=S**)S-), 193.43 (**C=O**).

RAFT Homopolymerization of Vinylidene Fluoride (VDF) with CTA_1
Using the experimental setup described above, a typical polymerization of VDF was performed as follows: A solution of Trigonox® 121 (158 mg, 6.87×10^{-4} mol) and **CTA_1** (1.47 g, 6.25×10^{-3} mol) in DMC (60 mL) was degassed by N_2 bubbling for 30 min. This homogeneous solution was introduced into the autoclave using a funnel, VDF gas (19.0 g, 0.297 mol) was transferred in the autoclave at low temperature, and the reactor was gradually heated to 73 °C. The reaction was stopped after 20 h. During the reaction, the pressure increased to a maximum of 25 bar and then decreased to 10 bar after 20 h. The autoclave was cooled to room temperature (ca. 20 °C), purged from the residual monomers, and the dimethylcarbonate solvent was removed under vacuum. The crude product was dissolved in 30 mL of warm THF (ca. 40 °C) and left under vigorous stirring for 30 min. This polymer solution was then precipitated from 400 mL of chilled hexane. The precipitated polymer (white powder) was filtered through a filter funnel and dried under vacuum (15×10^{-3} mbar) for 2 h at 50 °C. The polymerization yield (24%) was determined gravimetrically (mass of dried precipitated polymers/mass of monomer introduced in the pressure reactor). Yields were used as conversion, since conversion is very difficult to measure accurately for VDF and other gaseous monomers.

Typical Cationic RAFT Polymerization of EVE
The cationic RAFT polymerization of EVE was carried out by the syringe technique under dry nitrogen in baked glass tubes equipped with a three-way stopcock. A typical example for the polymerization procedure is given below. The reaction was initiated by addition of TfOH (4.3 mL of 0.65 mM in Et_2O) via dry syringe into monomer solution (43.17 mL) containing EVE (27.7 mM), *S-1*-Isobutoxyethyl *N,N*-diethyl dithiocarbamate (0.55 mM), and toluene (0.97 mL) in *n*-hexane/CH_2Cl_2 mixture (8/1 vol) at –40 ºC. At predetermined intervals, the polymerization was terminated with methanol (15.0 mL) containing small amount of triethylamine. The monomer conversion was determined from the concentration of residual monomer measured by ^{1}H NMR with toluene as an internal standard (e.g., for 25 sec, 90% conversion). The quenched reaction mixture was washed with distilled water to remove initiator residues, evaporated to dryness under reduced pressure, and vacuum-dried to yield a viscous oil (Yield = 99%).

Typical Block copolymers synthesis (PEVE-*b*-PVDF) via RAFT radical polymerization
Radical RAFT chain extension reactions were carried out in thick 8 mL Carius tubes in which a solution of the initiator (Trigonox® 121, 2.7 mg, 1.17 10^{-5} mol) and the macro-CTA (PEVE)-CTA_2, 0.225 mg, 5.85 10^{-5} mol) in DMC (5 mL), was added and then degassed by performing at least three freeze–pump–thaw cycles. The gaseous monomer was introduced into the Carius tube at the liquid nitrogen temperature (VDF, 1.5 g, 2.34 10^{-2}, mol, 1 ΔP) using a custom-made manifold that enables accurate measurement of quantities of gas (using “pressure drop *vs* mass of monomer” calibration curves). The tube was then sealed under dynamic vacuum at the temperature of liquid nitrogen, before being placed horizontally in a shaking water bath thermostated at 73 °C. After 24 h, the tube was placed into liquid nitrogen, opened, and then the solvent was evaporated at 50 °C under reduced pressure. Conversion was determined gravimetrically after drying under vacuum for 16 hours until constant weight. The unreacted PEVE macro-CTA was then eliminated by dissolving the powder in 2 mL of acetone and precipitation in 50 mL of chilled pentane (good solvent for PEVE, bad solvent for PVDF). The PVDF was then isolated as a white powder by centrifugation, and dried at 40 °C and 8 mbar for 2h in a vacuum.

Results and Discussion

(CTA_1) : Methyl 2-((*N*,*N*-diethylcarbamothioyl)thio)propanoate

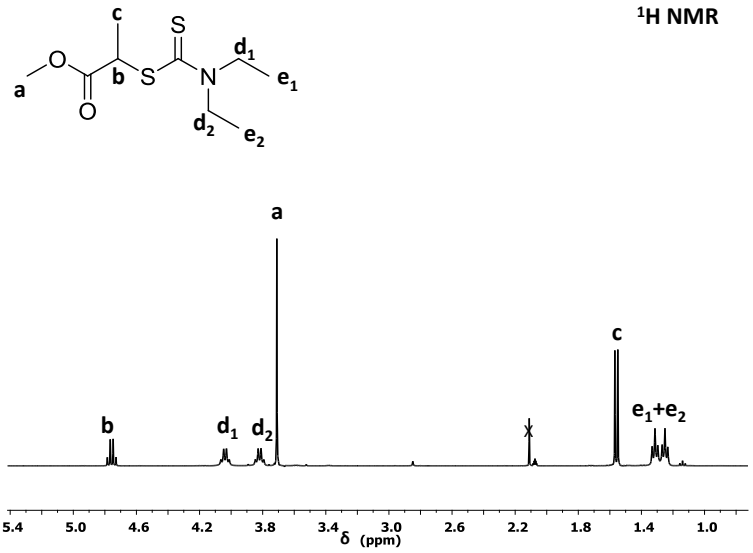

Figure S1. Expansion of the 0.7 to 5.4 ppm region of ^{1}H NMR of Methyl 2-((*N*, *N*-diethylcarbamothioyl)thio)propanoate (CTA_1) in $(CD_3)_2CO$. The crossed-out peak is assigned to residual solvent (acetone).

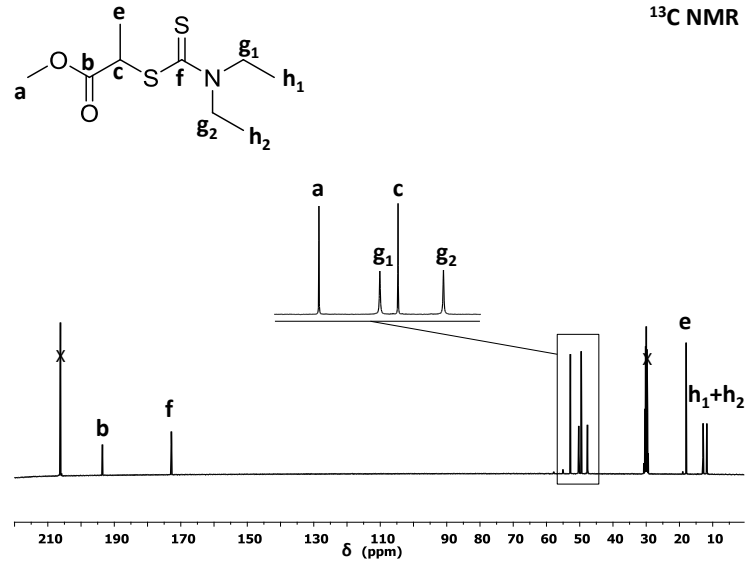

Figure S2. Expansion of the 0 to 220 ppm region of the ^{13}C NMR of Methyl 2-((*N*, *N*-diethylcarbamothioyl)thio)propanoate (CTA_1) in $(CD_3)_2CO$. The crossed-out peak is assigned to residual solvent (acetone).

Radical RAFT polymerization of VDF with CTA_1:

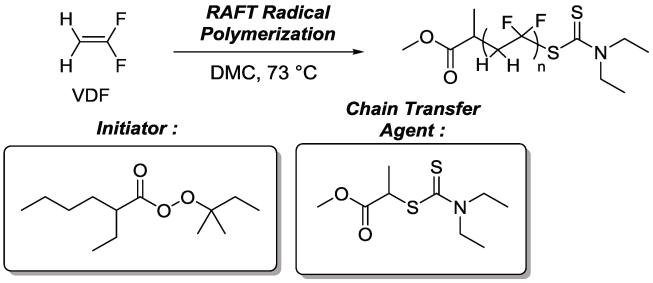

Scheme S1. Schematic Representation of VDF RAFT VDF polymerization with CTA_1.

Table S1. Experimental conditions and results for the radical RAFT polymerization of VDF using CTA_1[a]

Entry	M	$[M]_0/[CTA]_0/[I]_0$	Time (h)	Yield[b] (%)	$M_{n(theo)}$ [c] (g/mol)	DP[d]	$M_{n(NMR)}$ [e] (g/mol)	$M_{n(SEC)}$ [f] (g/mol)	$Đ$[f]
1	VDF	100/1/0.11	10	4	370	17	1300	1100	1.20
2	VDF	100/1/0.11	15	11	600	22	1600	4400	1.10
3	VDF	100/1/0.11	17.5	21	900	39	2700	6500	1.18
3	VDF	100/1/0.11	20	29	1200	59	4000	8700	1.30
5	VDF	100/1/0.11	24	32	1300	67	4500	8200	1.28
6	VDF	50/1/0.1	24	24	1000	23	1700	4600	1.08
7	VDF	200/1/0.1	24	32	4300	82	5500	11100	1.31

[a] Reactions conditions: Initiator (I) = Trigonox® 121, T= 73 °C, solvent = DMC. [b] Determined gravimetrically. [c] Calculated using yield as conversion and equation S1. [d] Calculated using equations S2 [e] Calculated using equations S3. [f] Determined by SEC calibrated using with PMMA narrow standards.

$$(S1) \quad M_{n(theo)} = \frac{[M]_0}{[CTA]_0} \times Yield \times M_{n,VDF} + M_n CTA$$

$$(S2) \quad DP = \frac{\int_{2.70}^{3.19} \mathrm{CH_2\,(HT)} + \int_{2.28}^{2.43} \mathrm{CH_2(TT)} + \int_{4.37}^{4.52} \mathrm{CH_2(End-group)}}{2/3 \times \int_{1.19}^{1.24} \mathrm{CH_3\,(R-CTA)}}$$

$$(S3) \quad M_{nNMR} = M_n CTA + DP \times M_n VDF$$

With $M_{n\ CTA}$ = 235.07 g.mol^{-1} and $M_{n,VDF}$ = 64.04 g.mol^{-1}

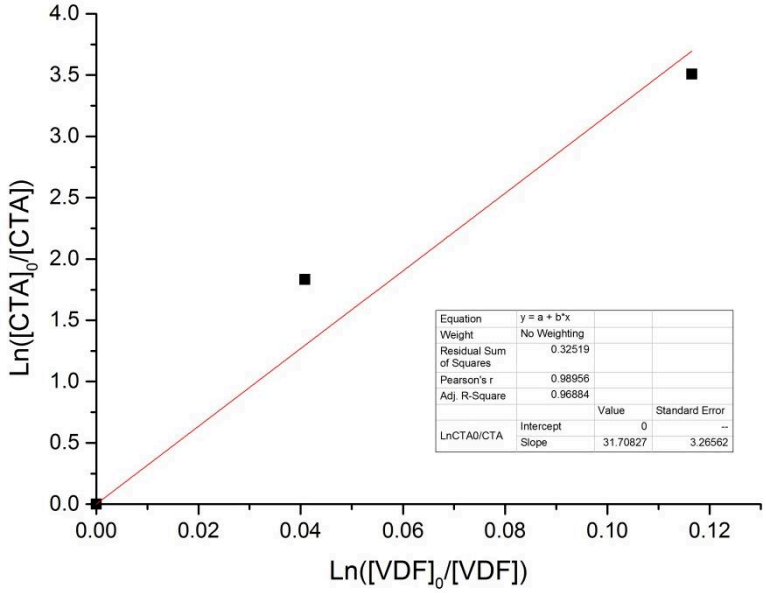

Figure S3. Determination of the transfer constant of Methyl 2-((*N*,*N*-diethylcarbamothioyl)thio)propanoate (CTA_1) with VDF using O'Brien and Gornick's method.[3] Figure displays the plots of $Ln([CTA]_0/[CTA])$ versus $Ln([VDF]_0/[VDF])$. The slope of the linear fit of this plot provide the $C_{Tr(app)}$ value using equation S4:

$$(S4) \quad Ln\left(\frac{[CTA]_0}{[CTA]}\right) = C_{Tr(app)} Ln\left(\frac{[VDF]_0}{[VDF]}\right)$$

$C_{Tr(app)}$ = 32 at 73 °C

O'Brien and Gornick's method is a simple method to assess the apparent transfer constant of a RAFT agent at a desired temperature. This C_{Tr}(app) value is determined by plotting Ln ($[CTA]_0/[CTA]$) representing the consumption of RAFT agent by activation during the reinitiation step (calculated by NMR), versus Ln ($[VDF]_0/[VDF]$), representing the conversion of VDF (calculated by gravimetry). The slope of the linear fitting corresponds to the apparent transfer constant. This transfer constant is only apparent since it does not take into account the reversible transfers that may occur. In consequence, the resulting value is underestimated.

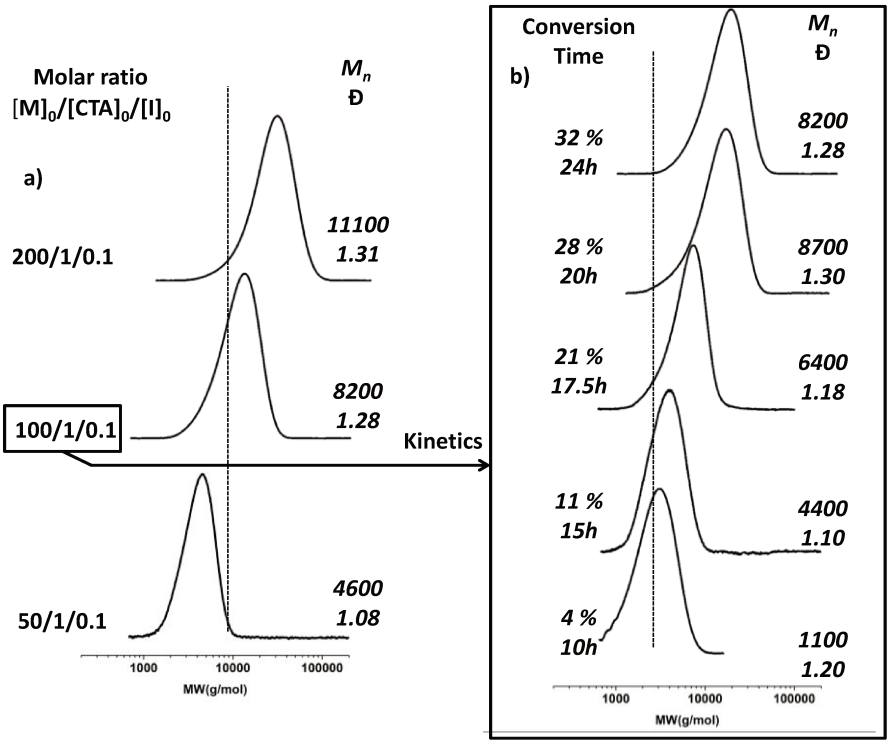

Figure S4. a) SEC traces of the PVDF synthesized by RAFT polymerization in the presence of CTA_1 and using 3 different initial molar ratio $[M]_0/[CTA]_0/[I]_0$ = 50/1/0.1; 100/1/0.1; 200/1/0.1. b) Evolution of the SEC trace of the PVDF formed during the RAFT polymerization of VDF carried out in the presence of CTA_1. *Reaction conditions:* $[VDF]_0/[CTA_1]_0/[I]_0$ =100/1/0.1.

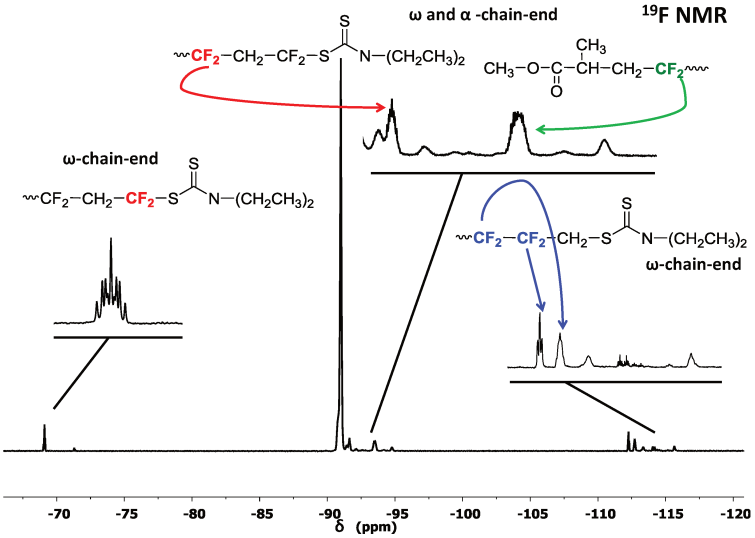

Figure S5. Expansion of the -66 to -120 ppm region of the ^{19}F NMR spectrum in $(CD_3)_2CO$ of PVDF-CTA_1 homopolymer (run 1, Table S1) synthesized by RAFT polymerization using CTA_1.

Cationic RAFT polymerization of Ethyl Vinyl Ether (EVE) with CTA_2, CTA_3, CTA_4

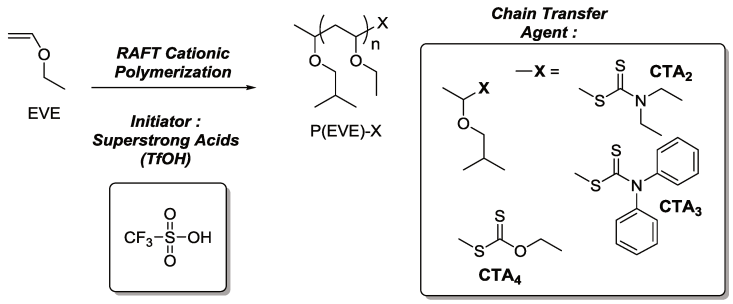

Scheme S2. Schematic representation of the EVE cationic RAFT polymerization using CTA_2, CTA_3 or CTA_4.

Table S2. Experimental conditions and results for the RAFT cationic polymerization of EVE homopolymers[a]

Entry	CTA	$[M]_0/[CTA]_0/[I]_0$	Time (h)	Conversion[b] (%)	$M_{n(theo)}$ [c] (g/mol)	DP[d]	$M_{n(NMR)}$ [e] (g/mol)	$M_{n(SEC)}$ [f] (g/mol)	$Đ$[g]	Functionality[g]
1	CTA_2	50/1/0.005	1	99	3870	52	3970	2200	1.08	83
2	CTA_3	50/1/0.005	1	99	3970	50	4000	1900	1.09	95
3	CTA_4	50/1/0.005	45	85	3300	52	3950	1700	1.52	91

[a] Reactions conditions: Initiator (I) = TfOH, T = -40 °C for entry 1 and 2, -78 °C for entry 3, solvent : Hexane/CH_2Cl_2/Et_2O (80:10:10). [b] Determined from the residual monomer concentration measured by ^1H NMR with toluene as an internal standard. [c] Calculated using equation S5. [d] Calculated using equation S6. [e] Calculated using eq S7 [f] Determined by SEC calibrated using PMMA narrow standards. [g] Determined using equation S8.

$$(S5) \quad M_{n(theo)} = \frac{[M]_0}{[CTA]_0} \times Conv. \times M_{n,EVE} + M_n CTA$$

$$(S6) \quad DP = \frac{[\int_{1.38}^{1.91} \mathrm{CH_2}\ PEVE(backbone) - 1H(CH\ R - CTA)] + \int_{5.94}^{6.21} CH - CTA\ (end\ group)}{1/3 \times \int_{0.87}^{0.94} (CH_3)_2\ (\mathrm{R-CTA})}$$

$$(S7) \quad M_{nNMR} = M_n CTA + DP\ \times\ M_n EVE$$

$$(S8) \quad Functionality\ (\%) = \frac{\int_{5.93}^{6.24} \mathrm{CH} - CTA\ (k)}{\int_{5.93}^{6.24} \mathrm{CH} - CTA\ (k) + \int_{4.56}^{4.71} \mathrm{CH} - OCH_3\ (n)} \times 100$$

With $M_{n,CTA2}$ = 249.43 g.mol^{-1}, $M_{n,CTA3}$ = 345.52 g.mol^{-1}, $M_{n,CTA4}$ = 222.36 g.mol^{-1} and $M_{n,EVE}$ = 72.11 g.mol^{-1}

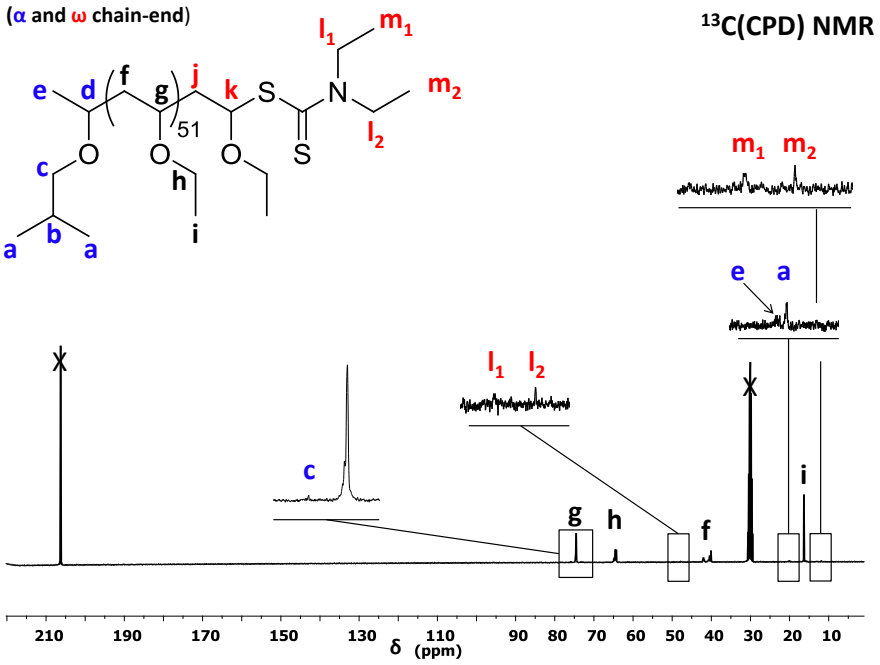

Figure S6. Expansion of the 0 to 220 ppm region of the ^{1}H decoupled ^{13}C NMR spectrum of $PEVE_{52}$-diethylcarbamate homopolymer (run 1, Table S2) synthesized by RAFT polymerization using CTA_2 in $(CD_3)_2CO$. Highlighted signals were assigned to PEVE α- and ω-CTA end-groups.

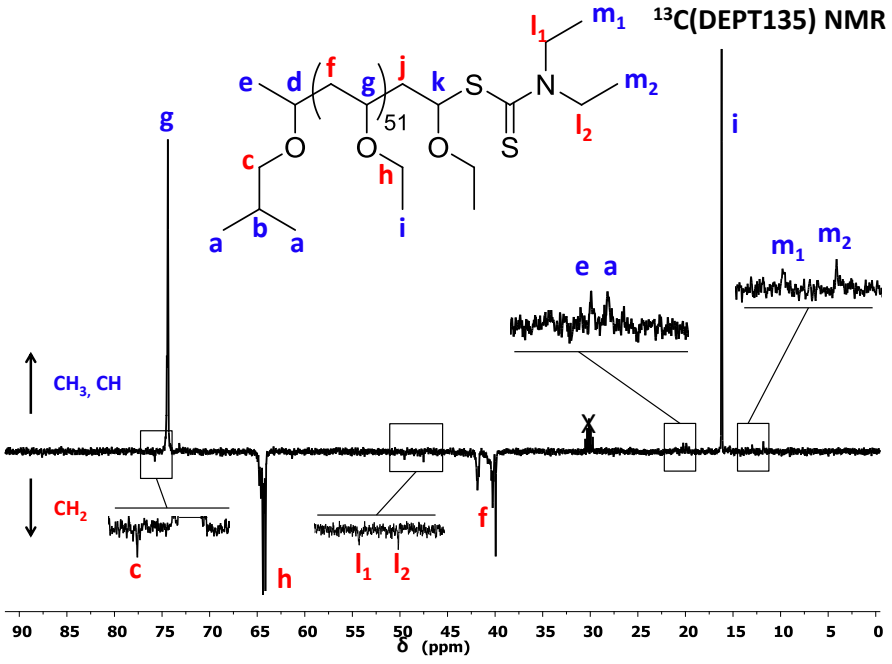

Figure S7. Expansion of the 0 to 90 ppm region of the DEPT135 ^{13}C NMR spectrum of $PEVE_{52}$-diethylcarbamate homopolymer (run 1, Table S2) synthesized by RAFT polymerization using CTA_2 in $(CD_3)_2CO$. Highlighted signals were assigned to PEVE α- and ω-CTA end-groups.

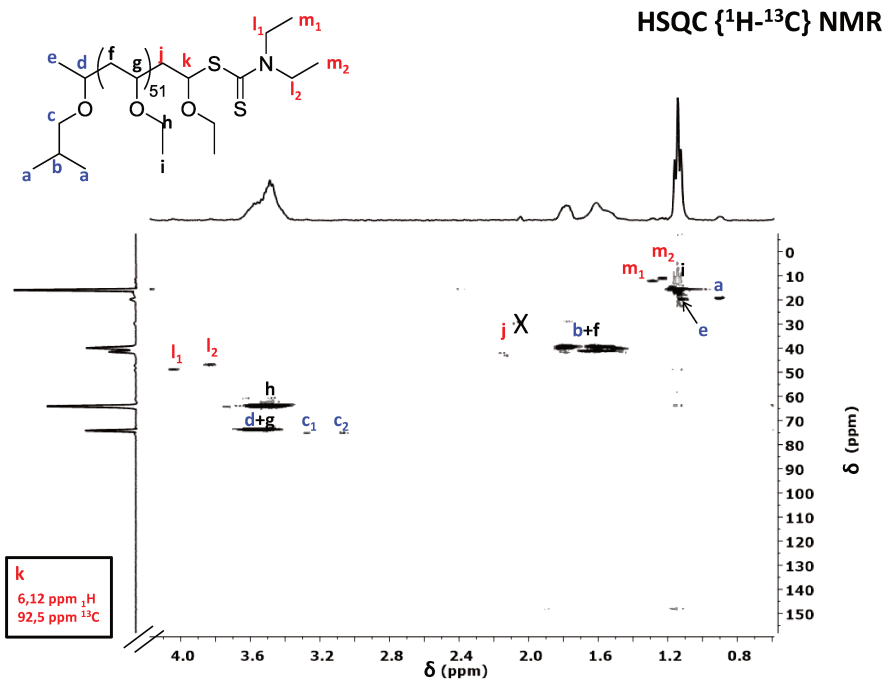

Figure S8. HSQC ^{1}H-^{13}C NMR correlation spectrum of $PEVE_{52}$-diethylcarbamate homopolymer (run 1, Table S2) synthesized by RAFT polymerization using CTA_2 in $(CD_3)_2CO$.

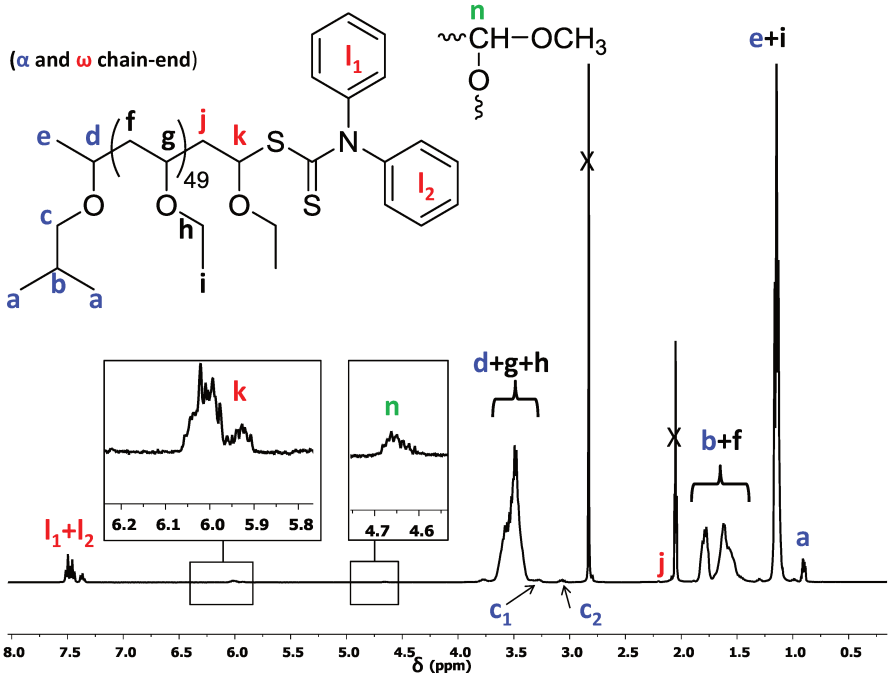

Figure S9. Expansion of the 0 to 8 ppm region of the ^{1}H NMR spectrum of $PEVE_{50}$-diphenylcarbamate homopolymer (run 2, Table S2) synthesized by RAFT polymerization using CTA_3 in $(CD_3)_2CO$. Highlighted signals were assigned to PEVE α- and ω-CTA end-groups.

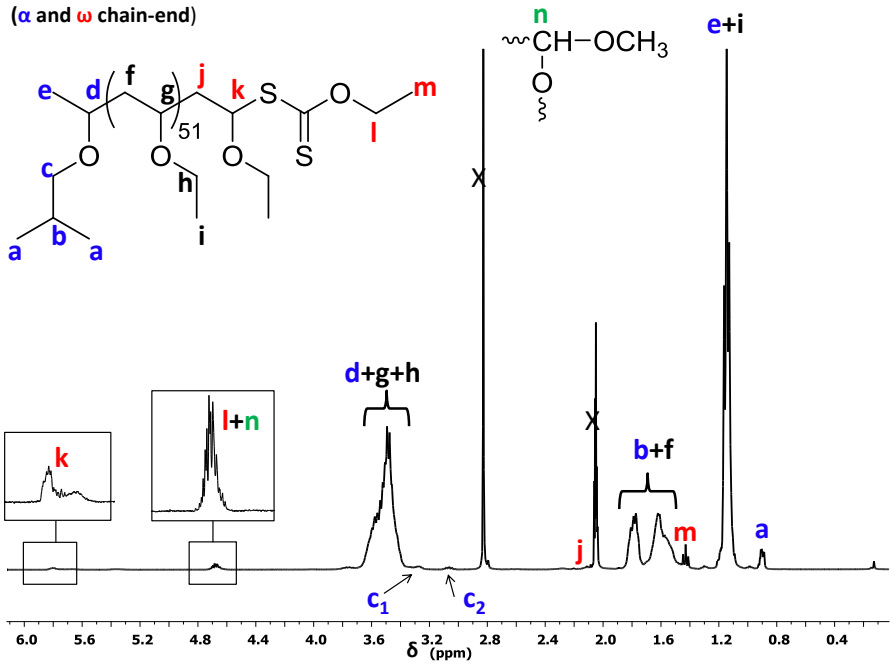

Figure S10. Expansion of the 0 to 6 ppm region of the ^{1}H NMR spectrum of $PEVE_{51}$-xanthate homopolymer (run 3, Table S2) synthesized by RAFT polymerization using CTA_4 in $(CD_3)_2CO$. Highlighted signals were assigned to PEVE α- and ω-CTA end-groups.

Radical RAFT polymerization of VDF with PEVE-CTA$_{2,3,4}$:

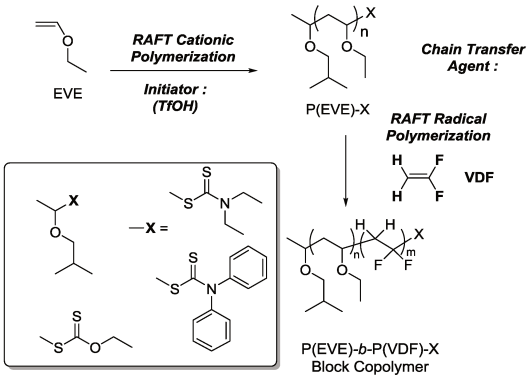

Scheme S2. Schematic representation of VDF radical RAFT polymerization using PEVE-CTA$_2$, CTA$_3$ or CTA$_4$.

Table S3. Experimental conditions and results for the chain extension of PEVE-CTA by RAFT radical polymerization of VDF[a]

Entry	Macro-CTA	M	$[M]_0/[CTA]_0/[I]_0$	Yield[b] (%)	$M_{n(theo)}$ [c] (g/mol)	DP[d]	$M_{n(NMR)}$ [e] (g/mol)	$M_{n(SEC)}$ [f] (g/mol)	$Đ$[f]
1	PEVE$_{52}$-CTA$_2$	VDF	400/1/0.1	33	12500	454	33100	9700	1.36
2	PEVE$_{50}$-CTA$_3$	VDF	400/1/0.1	57	16600	431	31600	9800	1.38
3	PEVE$_{52}$-CTA$_4$	VDF	400/1/0.1	60	19400	920	63000	9900	1.50

[a] Reactions conditions: Initiator (I) = Trigonox® 121, T= 73 °C, solvent = DMC. [b] Determined gravimetrically. [c] Calculated using yields as conversion following equation S9. [d] Calculated using equation S10. [e] Calculated using equation S11[f] Determined by SEC with PMMA standard.

$$(S9) \quad M_{n(theo)} = \frac{[M]_0}{[PEVE-CTA]_0} \times Yield \times M_{n,VDF} + M_n PEVE - CTA$$

$$(S10) \quad DP = \frac{\int_{2.70}^{3.19} \mathrm{CH_2\,(HT)} + \int_{2.28}^{2.43} \mathrm{CH_2(TT)} + \int_{4.02}^{4.17} \mathrm{CH_2(End-group)}}{1/3 \times \int_{0.87}^{0.94} (CH_3)_2\,(\mathrm{R-CTA\ PEVE\ block})}$$

$$(S11) \quad M_{nNMR} = M_n PEVE - CTA + DP \times M_n VDF$$

With $M_{n,PEVE\text{-}CTA2}$ = 3970 g.mol^{-1}, $M_{n,PEVE\text{-}CTA3}$ = 4000 g.mol^{-1}, $M_{n,PEVE\text{-}CTA4}$ = 3950 g.mol^{-1} and $M_{n,VDF}$ = 64.04 g.mol^{-1}.

The $M_{n(SEC)}$ values are not accurate. Entries 1 and 2 have similar values because the DP of their constituting blocks are similar. Entry 3 has a similar $M_{n(SEC)}$ value to entries 1 and 2 because of the effect of dispersity on the Mn values calculated by SEC. In addition, these $M_{n(SEC)}$ values are calculated on the RI traces although PEVE and PVDF have positive and negative responses in the GPC eluent used (DMF), respectively. These response differences probably also contribute to the similarity in the $M_{n(SEC)}$ values.

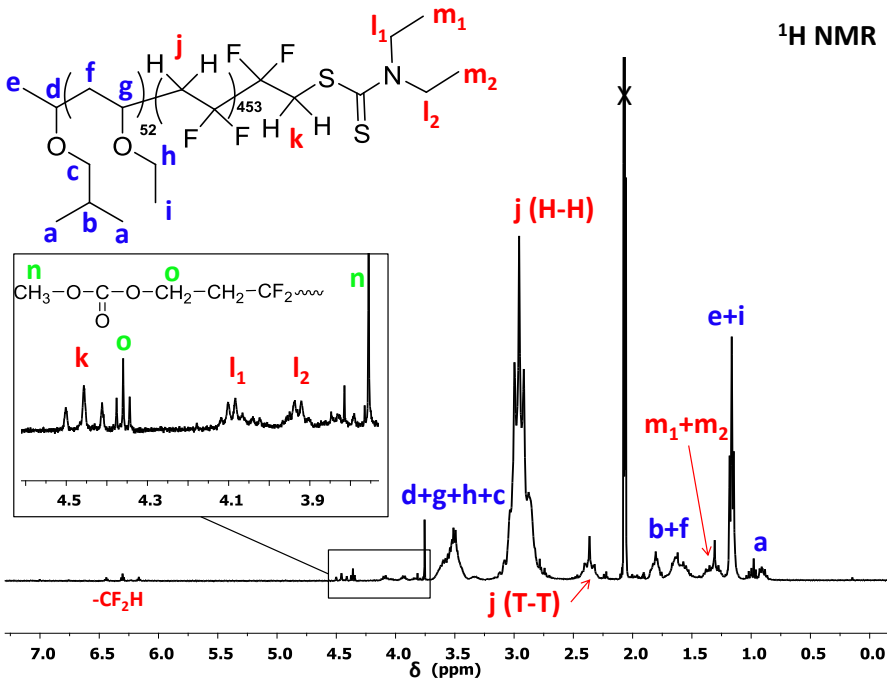

Figure S11. Expansion of the 0 to 7.5 ppm region of the ^{1}H NMR spectrum in $(CD_3)_2CO$ of the purified $PEVE_{52}$-*b*-$PVDF_{454}$-CTA_2 block copolymer (run 1, Table S3) synthesized by RAFT polymerization using $PEVE_{52}$-CTA_2. H-H and T-T stand for head-to-head and tail-to-tail, respectively.

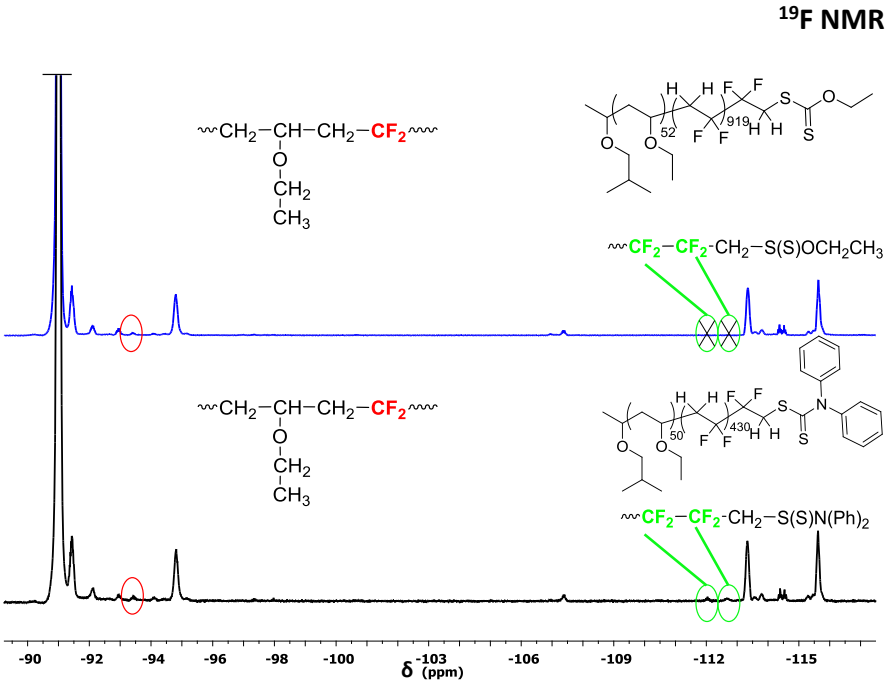

Figure S12. Expansion of the -89 to -117 ppm region of the ^{19}F NMR spectra in $(CD_3)_2CO$ of the purified $PEVE_{50}$-*b*-$PVDF_{431}$-CTA_3 (bottom) and of $PEVE_{52}$-*b*-$PVDF_{920}$-CTA_4 (top) block copolymer (run 2 and 3, Table S3) synthesized by RAFT polymerization using $PEVE_{50}$-CTA_3 and $PEVE_{52}$-CTA_4, respectively.

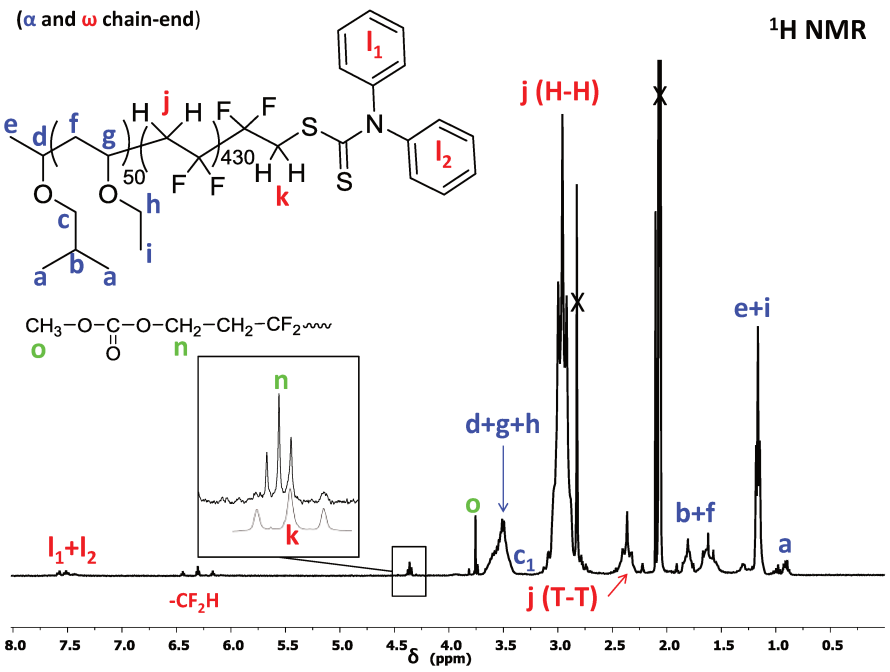

Figure S13. Expansion of the 0 to 8 ppm region of the ^{1}H NMR spectrum in $(CD_3)_2CO$ of the purified $PEVE_{50}$-*b*-$PVDF_{431}$-CTA_3 (run 2, Table S3) synthesized by RAFT polymerization using $PEVE_{50}$-CTA_3.

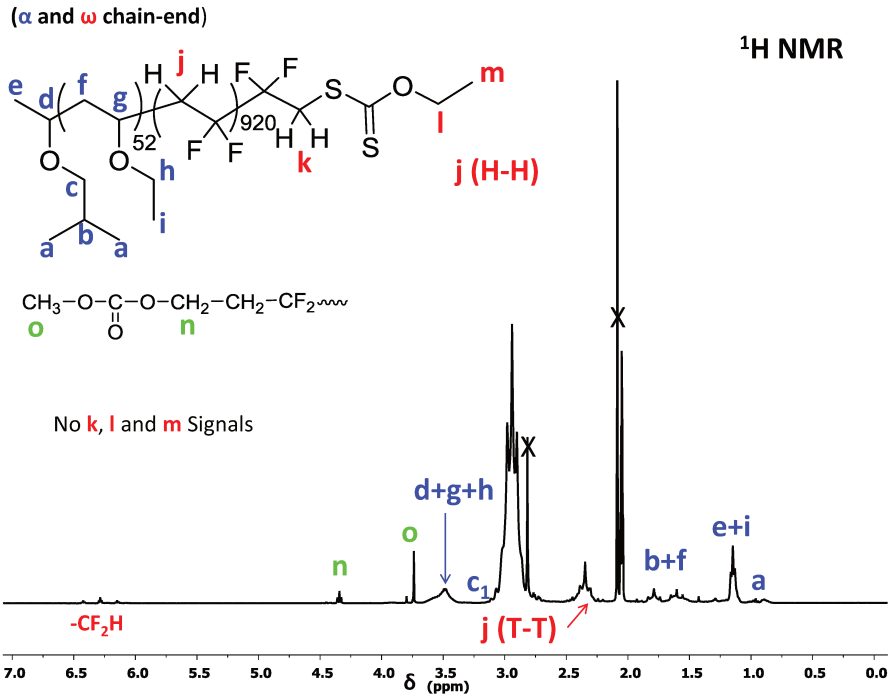

Figure S14. Expansion of the 0 to 7 ppm region of the ^{1}H NMR spectrum in $(CD_3)_2CO$ of the purified $PEVE_{52}$-*b*-$PVDF_{920}$-CTA_4 (run 3, Table S3) synthesized by RAFT polymerization using $PEVE_{52}$-CTA_4.

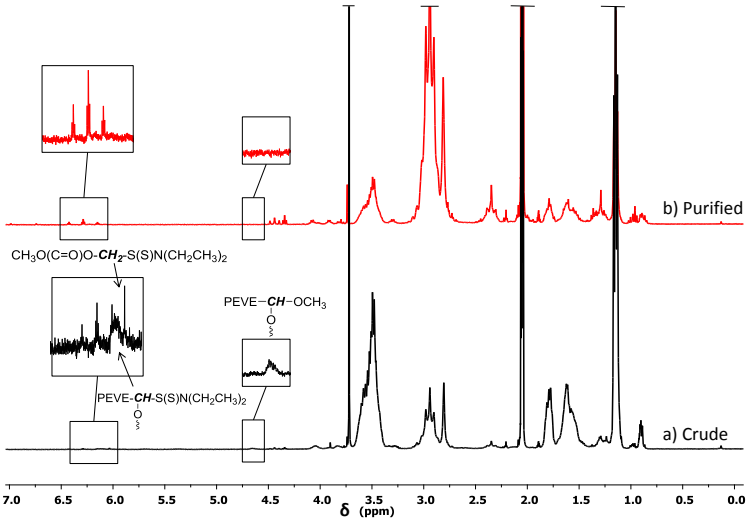

Figure S15. Expansion of the 0 to 7 ppm region of the ^{1}H NMR spectrum in $(CD_3)_2CO$ of a) crude and b) purified $PEVE_{52}$-*b*-$PVDF_{454}$-CTA_2 block copolymer (run 1, Table S3) synthesized by RAFT polymerization using $PEVE_{52}$-CTA_2.

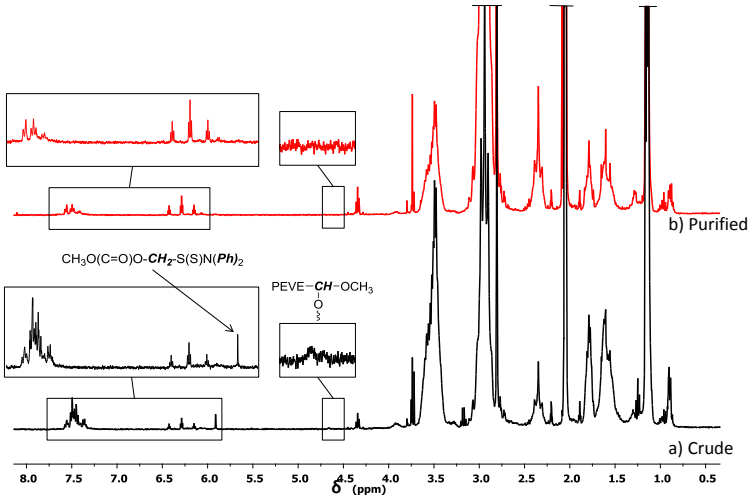

Figure S16. Expansion of the 0 to 8 ppm region of the ^{1}H NMR spectrum in $(CD_3)_2CO$ of a) crude and b) purified $PEVE_{50}$-*b*-$PVDF_{431}$-CTA_3 block copolymer (run 2, Table S3) synthesized by RAFT polymerization using $PEVE_{50}$-CTA_3.

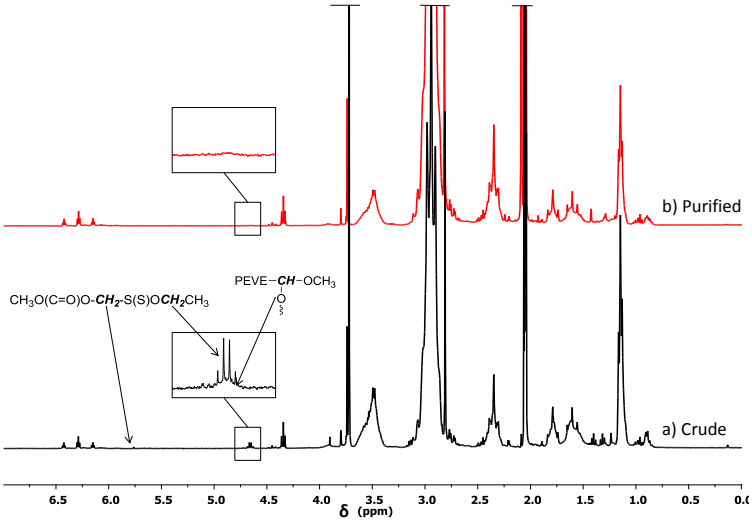

Figure S17. Expansion of the 0 to 7 ppm region of the ^{1}H NMR spectrum in $(CD_3)_2CO$ of a) crude and b) purified $PEVE_{52}$-*b*-$PVDF_{920}$-CTA_4 block copolymer (run 3, Table S3) synthesized by RAFT polymerization using $PEVE_{52}$-CTA_4.

Differential Scanning Calorimetry:

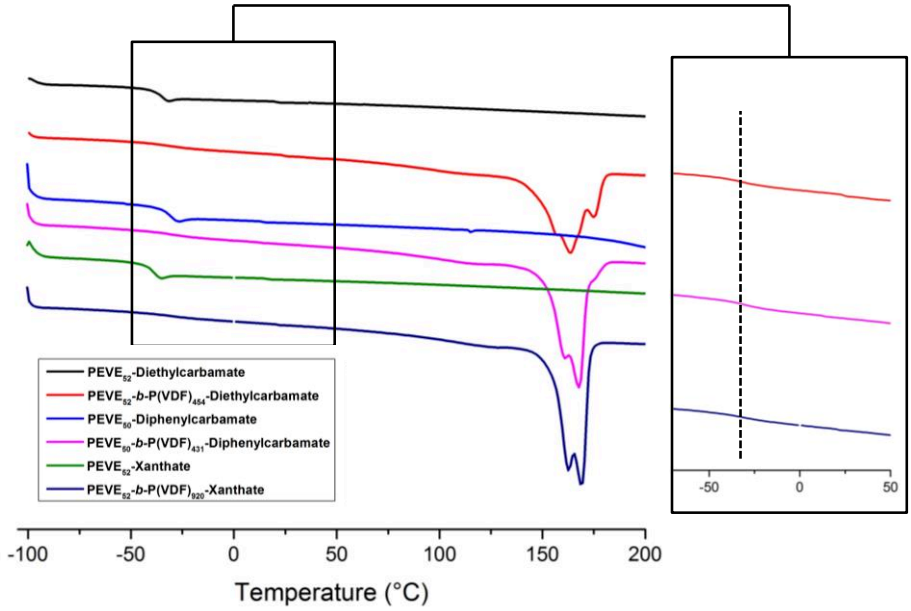

Figure S18. DSC thermograms (second heating) of PEVE-$CTA_{2,3,4,}$ PEVE-*b*-PVDF-CTA_2, PEVE-*b*-PVDF-CTA_3 and PEVE-*b*-PVDF-CTA_4.

References

[1] X. Liu, O. Coutelier, S. Harrisson, T. Tassaing, J-D. Marty, M. Destarac, *ACS Macro Lett*., **2015**, *4*, 89–93.
[2] M. Uchiyama, K. Satoh, M. Kamigaito, *Angew. Chem*., **2015,** *127*, 1944-1948.
[3] J. L., O'Brien, F. Gornick, *J. Am. Chem. Soc.,* **1955**, *77*, 4757.

ChemPubSoc Europe

DOI: 10.1002/cplu.201800471

CHEMPLUSCHEM Full Papers

π-Stacking Interactions of Graphene-Coated Cobalt Magnetic Nanoparticles with Pyrene-Tagged Dendritic Poly (Vinylidene Fluoride)

Enrique Folgado,[a] Marc Guerre,[a] Nidhal Mimouni,[b, c] Vincent Collière,[b, c] Christian Bijani,[b, c] Kathleen Moineau-Chane Ching,[b, c] Anne-Marie Caminade,[b, c] Vincent Ladmiral,[a] Bruno Améduri,[a] and Armelle Ouali*[a]

This study investigates the non-covalent coating of cobalt magnetic nanoparticles (MNPs) involving a graphene surface with pyrene-tagged dendritic poly(vinylidene fluoride) (PVDF). Dendrimers bearing a pyrene moiety were selected to play the role of spacers between the graphene surface of the MNPs and the PVDF chains, the pyrene unit being expected to interact with the surface of the MNPs. The pyrene-tagged dendritic spacer **11** decorated with ten acetylenic units was prepared and fully characterized. Azido-functionalized PVDF chains were then grafted onto each branch of the dendrimer using Huisgen's [3 + 2] cycloaddition reaction. Next, the association of the resulting pyrene-tagged dendritic PVDF **13** with commercially available Co/C MNPs by π-stacking interactions was studied by fluorescence spectroscopy. Evaluated were the stability of the π-stacking interactions when the temperature increased and the reversibility of the process when the temperature decreased. Also, hybrid MNPs were prepared from pyrene-tagged dendrimers decorated either with acetylenic functions (**11**) or with PVDF branches (**13**), and they were characterized by transmission electron microscopy and comparative elemental analysis was carried out with naked MNPs.

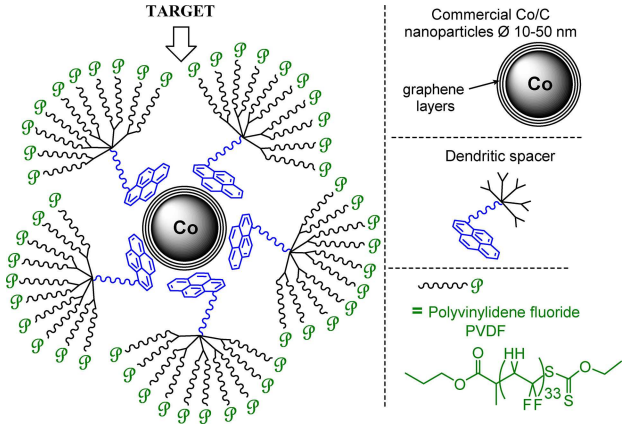

Figure 1. Targeted multifunctional materials: study of the non-covalent coating of Co/C magnetic nanoparticles (MNPs) by pyrene-tagged PVDF-dendrons.

[a] *E. Folgado, Dr. M. Guerre, Dr. V. Ladmiral, Dr. B. Améduri, Dr. A. Ouali*
Institut Charles Gerhardt – UMR 5253 – CNRS, UM, ENSCM
8 Rue de l'Ecole Normale, 34296 Montpellier Cedex 5 (France)
E-mail: armelle.ouali@enscm.fr
[b] *N. Mimouni, V. Collière, Dr. C. Bijani, Dr. K. Moineau-Chane Ching, Dr. A.-M. Caminade*
Laboratoire de Chimie de Coordination du CNRS
205 Route de Narbonne, BP 44099, 31077 Toulouse Cedex 4 (France)
[c] *N. Mimouni, V. Collière, Dr. C. Bijani, Dr. K. Moineau-Chane Ching, Dr. A.-M. Caminade*
LCC-CNRS
Université de Toulouse, CNRS
Toulouse (France)

Supporting information for this article is available on the WWW under https://doi.org/10.1002/cplu.201800471

Introduction

Polymer-coated nanoparticles are of great interest for both industry and academic research laboratories for various applications in materials science or in biosciences.[1] Besides, nanoparticles (NPs) display a high surface-to-volume ratio creating large interfacial areas at the origin of unique properties compared to their micro- or macro-scale counterparts. Therefore, dispersing nanoparticles in polymer matrices allows the design of novel polymer nanocomposites materials that combine the properties and functions of both the NP and the polymer.[1] However, this task is intrinsically difficult and challenging since attractions between NPs prevent their homogeneous dispersions. This is particularly true for magnetic nanoparticles (MNPs).[1]

The present work aims at studying the non-covalent coating of MNPs with dendritic[2] poly(vinylidene fluoride) (PVDF)[3,4] (Figure 1). PVDF is an interesting fluoropolymer with remarkable properties such as thermal stability, barrier properties, chemical inertness to solvents and acids as well as piezo-, pyro- and ferroelectric properties.[3] Targeting materials combining such advantages together with magnetic properties thus appears as a challenging and valuable objective. The hybrid MNPs targeted here may constitute key building blocks for the dispersion of MNPs in the PVDF matrix and lead to highly attractive nanocomposites. Such functional nanocomposites could find applications in the growing fields of printed and flexible electronics, binders for lithium ion batteries, and additives for coatings. The MNPs chosen as models are cobalt nanoparticles coated with graphene layers (Co/C MNPs).[5] First described by Grass et al.[5] and now commercially available,[6] these NPs are prepared by

reducing flame synthesis while the core-shell arrangement is achieved by the addition of acetylene to the cobalt-nanoparticle-forming process, resulting in the controlled deposition of carbon sheet onto the particles. To date, these MNPs have been widely employed as supports for homogeneous catalysts or adsorbents and the main interest of the resulting magnetic constructs is their recovery by magnetic decantation and possible reuse.[7–12]

Interestingly, the graphene surface of the MNPs makes their functionalization possible using either covalent chemistry or by resorting to a non-covalent strategy. Only a few reports describe the grafting of pyrene-tagged functional species (e.g. boradiazaindacene fluorescent dye[8] or palladium catalyst[9]) onto the graphene surface of MNPs through π-stacking interactions.[7] The present work focuses on this by far less studied non-covalent strategy to coat MNPs with polymers. Although π-stacking interactions were used to graft pyrene-tagged polymers onto carbon nanotubes,[10] it has never been reported for the grafting of polymers onto the surface of such Co/C MNPs. Indeed, usual strategies mainly involve the covalent grafting to graphene surface via a phenyl or a biphenyl linker.[12]

Besides, whatever the grafting strategy used (either covalent or by π-stacking), only low density of functionalization of the surface can be reached for these MNPs. Along these lines, polymers (mainly polystyrene and polypropyleneimine) and dendrimers have been successfully used in the past as multivalent spacers to increase loadings of catalysts, adsorbents or dyes on the surface of such MNPs.[7,8,9b,12] Dendrimers are synthesized by a step-by-step method which affords perfect control of their size and structure, as well as the incorporation of a great number of functions.[2] In this project, they were thus preferred as multivalent spacers between the surface of the MNP and the PVDF chain to reach a fine-tuning of the number of polymer chains grafted. Among the possible dendritic spacers available, the zeroth generation of phosphorous dendrimers was chosen because it was previously shown to allow a significant loading enhancement in the case of Pd catalysts.[9b]

Therefore, this article reports the preparation and characterization of new dissymmetric dendrimers bearing ten PVDF branches and one flexible arm ended by a pyrene moiety able to interact with the graphene surface (Figure 1). The association of these dendrimers with MNPs was studied by fluorescence spectroscopy, and the thermal stability of these interactions was also evaluated. Hybrid MNPs were prepared and characterized by High-Resolution Transmission Electron Microscopy (HRTEM) and comparative elemental analysis with naked MNPs to evaluate the loading of dendritic PVDF.

Results and Discussion

Pyrene tagged spacer **5** (Scheme 1), consisting in a tetraethylene glycol moiety bearing one pyrene tag at one chain end and a phenol function at the other end, was prepared in two steps from the corresponding tetraethylene glycol dimesylate **1** (see section S2 in the Supporting Information). The first

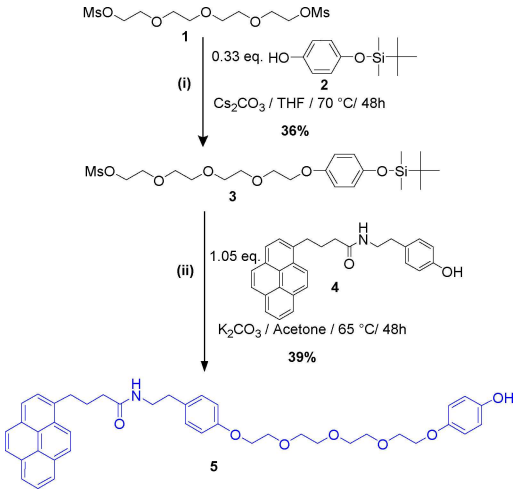

Scheme 1. Preparation of the pyrene-tagged arm to be linked to the dendritic core.

step (Scheme 1 **(i)**) consisted in the substitution of one of the mesylate groups of 1 with 4-([tert-butyl(dimethyl)silyl]oxy) phenol **2**. The second step (Scheme 1 **(ii)**) involved the nucleophilic substitution of pyrene-containing phenol **4** onto the remaining mesylate of compound **3** in the presence of a base (K_2CO_3) in refluxing acetone. To our delight, under these reaction conditions, the deprotection of the protecting trialkylsilyl group ($SiMe_2tBu$) also occurred. Due to this simultaneous substitution and deprotection, the synthesis of **5** from **3** was possible in one step. Afterward, a nucleophilic substitution reaction allowed the coupling of spacer **5** containing the pyrene moiety with unsymmetrical core **6** prepared according to previously reported methods[13] (Scheme 2 **(i)**). The reaction was monitored by ^{31}P-NMR spectroscopy by following the disappearance of the initial signals at 20.72 ppm. Compound **7** was

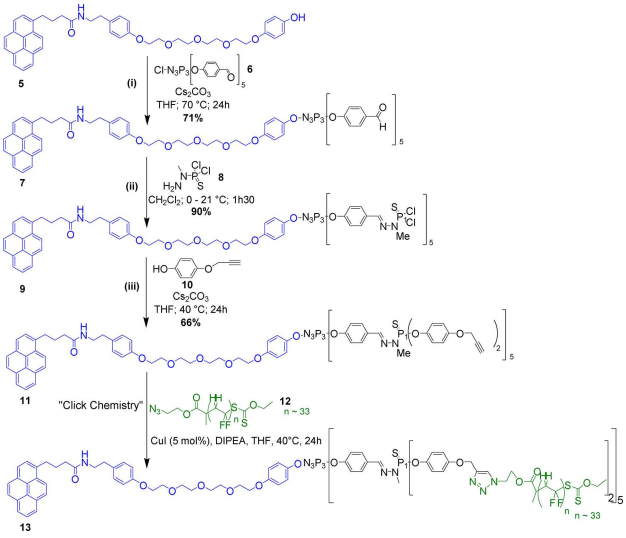

Scheme 2. Attachment of the pyrene-tagged arm to the dendritic cyclotriphosphazene core, dendritic growth, and grafting of the PVDF chains on the dendrimer surface (DIPEA = *N*,*N*-diisopropylethylamine).

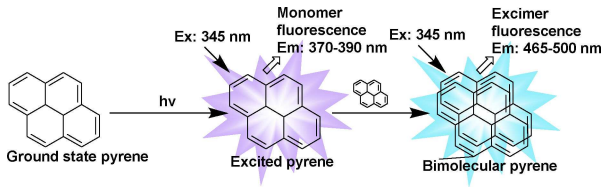

Figure 2. Pyrene Excimer formation, λ Ex: Excitation, λ Em: Emission Monomer λ Em. of pyrene within 370–390 nm. Excimer emission within 465–500 nm-

obtained in good yield (71%) after purification by flash chromatography and characterized by ^{1}H, ^{31}P, and ^{13}C NMR. The $^{31}P\{^{1}H\}$ NMR spectrum obtained was relatively complex due to second-order effects (see Figure S5.5 in the Supporting Information). The grafting of the flexible pyrene-tagged arm was indeed found to induce a slightly different environment for the two phosphorus atoms bearing the same substituents (two –O–C_6H_4–CHO groups) leading to their magnetic non-equivalence (see Figure S2.1 in the Supporting Information). The signals were exhaustively analyzed, and an NMR signal line shape fitting analysis allowed the calculations of the chemical shifts and coupling constants of the three phosphorous atoms. This non-equivalence of the phosphorous atoms as well as the large differences between coupling constants have already been reported for hexasubstituted cyclotriphosphazenes involving five identical substituents.[14] Hence, the condensation of the aldehyde functions of **7** with dichlorothiophosphorhydrazide **8** yielded compound **9** bearing five new phosphorous atoms as divergence points in high yield (90%). Besides the complex signals corresponding to the core (Figure S5.8 in the Supporting Information), the ^{31}P NMR spectrum of compound **9** displays three signals in a 2/1/2 ratio, corresponding to the five $P(S)Cl_2$ functions (Figure S5.9 in the Supporting Information). The small signal can be assigned to the $P(S)Cl_2$ group linked to the phosphorus of N_3P_3 that bears the pyrene, whereas one of the other signals corresponds to two $P(S)Cl_2$ functions on the same side as the pyrene, while the other to the two $P(S)Cl_2$ functions on the opposite side, relative to the N_3P_3 plane. Such an observation has already been reported.[15] Next, the growth of dendron **9** was achieved by performing nucleophilic substitution of the ten terminal chlorine atoms ($P(S)Cl_2$ functions) by phenol **10** using previously reported experimental conditions.[4] Peripheral acetylenic functions of dendron **11** were then allowed to react with azide-functionalized PVDF[4,16] **12** to lead to the targeted dendron **13** (yield 95%) possessing a pyrene core and 10 PVDF chains.

The reaction was monitored by FT-IR spectroscopy (disappearance of the characteristic frequency of the azido group of **12** at 2111 cm^{-1}) and ^{1}H, and ^{31}P NMR spectra confirmed the completion of the reaction. It is worth noting that the structures of compounds **9** and **11** were confirmed by matrix-assisted laser desorption/ionization coupled time-of-flight mass spectroscopy (MALDI-TOF) (see Figures S5.11 and S5.15, respectively, in the Supporting Information).

To gain further insights into the interactions existing between the pyrene-tagged dendrimers and the surface of the MNPs, fluorescence spectrometry was employed. This technique can quantify the amounts of pyrene moieties present in solution. Monomer emission of pyrene occurs within 370–390 nm whereas that of the excimer is observed within 465–500 nm.[10] An excimer is a bimolecular complex where one molecule exists in an excited state while the other one is in the ground state. When two pyrene molecules are in close proximity, they form an excimer that fluoresces prominently at a longer wavelength compared to monomeric pyrene (Figure 2).

To assess the existence of interactions between the graphene surface and the pyrene moiety, the methodology previously reported to get insight into the π-stacking interactions between pyrene-tagged polymers, and carbon nanotubes was employed.[10] A preliminary UV spectroscopy study allowed the determination of the wavelength of maximum absorption (λ_{max}) for **11** and **13** (340 nm and 320 nm, respectively, for solutions at 9.25 10^{-6} mol L^{-1} of each compound in THF/water (2:5 vol/vol) for an absorbance below 0.1 a.u.). Afterward, the emission spectra of both compounds were recorded by irradiation at their respective λ_{max} (340 nm for **11** and 320 nm for **13**, Figure 3. A THF/water (2:5) mixture was chosen for these studies since it was demonstrated to be optimal to achieve π-stacking of phosphorous pyrene-tagged dendrons decorated with related aldehyde and phosphine moieties onto Co/C MNPs.[9b] Less polar solvents (e.g. THF/water mixtures with THF/water > 2:5) were indeed shown to disfavor π-stacking interactions while more polar solvents did not sufficiently solubilize the pyrene-tagged organic molecules.

The emission spectra of dendrimers **11** and **13** displayed three sharp bands around 350–450 nm assigned to the pyrene monomer. Only compound **11** exhibited one extra broadband at 460 nm corresponding to the excimer emission (Figure 3, black line). It is worth noting that the formation of excimers is not visible in the case of PVDF-functionalized molecule **13**. This observation might be rationalized by the steric hindrance induced by the PVDF chains in compound **13** preventing interactions between two pyrene units. Aliquots of Co/C MNPs were then successively added to these homogeneous solutions (Figures 3, Experimental Section and sections S1 and S3 in the Supporting Information). After each addition, the suspension was sonicated for 30 min, the MNPs removed by magnetic decantation and the supernatant analyzed by fluorescence spectroscopy. Each addition was found to induce a decrease of the emission intensity (Figure 3 a,b). The observed extinction of the emission corresponded to a decrease of the concentration of pyrene-tagged dendrimers **11** or **13** in the supernatant. This strongly suggested that **11** and **13** interacted with the MNPs (Figure 3 a,b). These results thus support the existence of interactions between the graphene surface of the MNPs and the pyrene moieties of dendrimers **11** and **13**.

Next, the reversibility of the π-stacking interactions was evaluated. Indeed, as previously reported, the efficiency of the interactions between the pyrene moiety and the graphene surface may depend on the temperature.[9] π-stacking interactions were found to be inefficient at temperatures exceeding 60 °C but to be reversible since the π-stacking interactions were

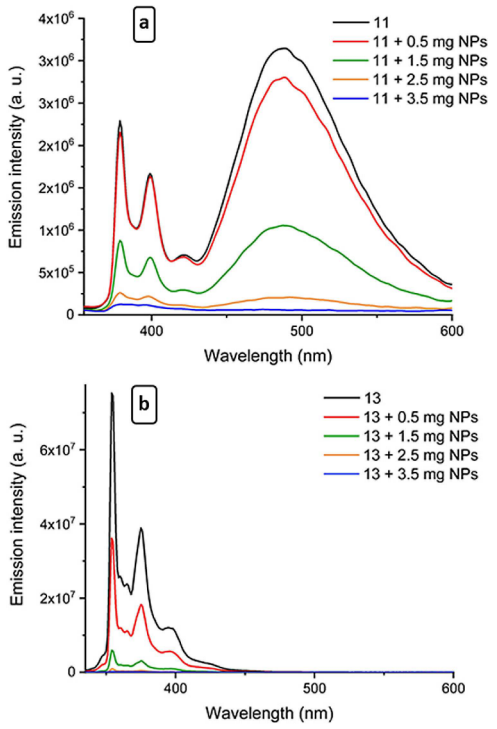

Figure 3. Fluorescence emission spectra of pyrene-acetylenic dendrimer **11** (a) and pyrene-PVDF dendrimer **13** (b) in the absence of Co/C-MNPs in THF/water (2:5) (black curve). After each addition of MNPs, the suspension was sonicated, then magnetically decanted with a magnet and the emission spectra of the supernatant were recorded and reported in these graphics (see detailed conditions in sections S1 and S3 in the Supporting Information).

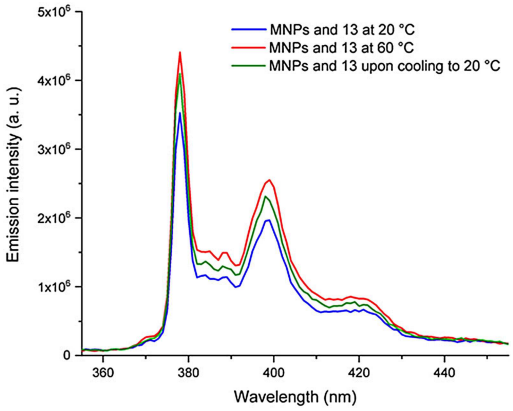

Figure 4. Reversibility test: a suspension of **13** and MNPs was sonicated for 30 minutes at 20 °C, magnetically decanted and the fluorescence spectrum of the supernatant recorded (blue curve). The mixture (supernatant and MNPs) was then heated to 60 °C for 10 h, and the spectrum of the resulting supernatant analyzed (red curve). Upon cooling to 20 °C, the concentration of 13 in the solution decreased (green curve). (see details in Experimental Section and section S3 in the Supporting Information).

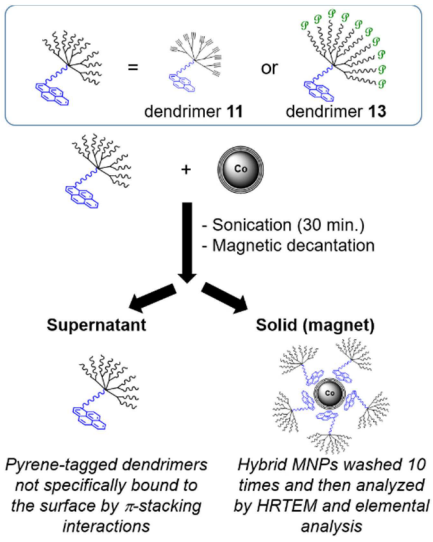

Figure 5. The procedure used for the preparation of hybrid NPs composed of Co/C MNPs coated with pyrene-tagged dendrimers **11** or **13** (dendrimers are used in large excess compared to dendrimers-to-MNPs ratios used for fluorescence studies, see section S3 in the Supporting Informationyes >).

restored upon cooling. For this study, pyrene-tagged dendrimer **13** was used.

Therefore, a suspension of **13** and MNPs was sonicated for 30 minutes at 20 °C first, then magnetically decanted with a magnet and the fluorescence spectrum of the supernatant further recorded (Figure 4, blue curve). The mixture (supernatant and MNPs) was then heated up to 60 °C for 10 h, and the spectrum of the resulting supernatant analyzed (Figure 4, red curve). The latter experiment indicated that the concentration of pyrene-tagged dendritic PVDF **13** significantly increased in accordance with a partial release of **13** from the surface of the MNPs at 60 °C. Upon cooling to 20 °C, the concentration of **13** in the solution decreased (Figure 4, green curve) suggesting partial reversibility of the π-stacking interactions. Importantly, the fluorescence spectra recorded after 1 h or 12 h after cooling to ambient temperature were identical. Contrary to pyrene-tagged dendritic phosphines previously reported,[9b] the reversibility is not complete.

After having studied the interactions of pyrene-tagged dendrimers **11** and **13** with the graphene surface of MNPs by fluorescence spectroscopy and assessed the existence and partial reversibility (case of **13**) of π-stacking interactions, preliminary tests for the preparation of hybrid MNPs were performed according to the protocol depicted in Figure 5: **(i)** a homogeneous suspension of pyrene-tagged dendrimers **11** or **13** in large excess and MNPs in a THF/water (2:5) solution was prepared and sonicated for 30 min; **(ii)** the nanoparticles were then magnetically decanted and rinsed ten times with hot THF/water mixtures to remove ungrafted pyrene-tagged dendrimers **11** or **13** from the medium; **(iii)** the MNPs were recovered using a magnet, then dried and analyzed by HRTEM to evaluate the grafting of the MNPs with PVDF, and by elemental analysis to determine the amount of polymers incorporated in these hybrid constructs. To optimize the grafting process and according to previously reported protocols,[9b] dendrimers, **11** or **13** were introduced in large excess in these experiments (dendrimer/MNPs ratio roughly 90 times higher than those used for fluorescence studies, see S3 in SI). The excess of pyrene-tagged dendrimers not specifically bound through π-stacking interac-

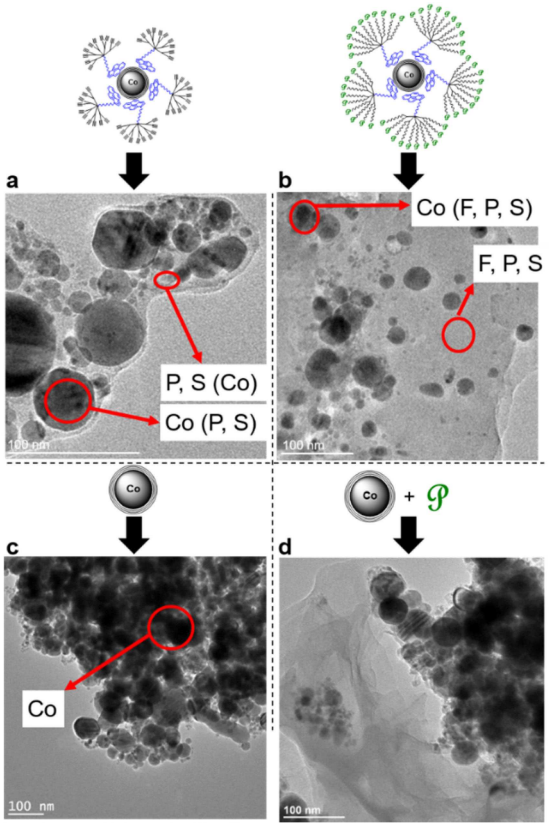

Figure 6. HRTEM images of **a**) MNPs grafted with acetylenic dendrimer **11. b**) MNPs grafted with dendritic PVDF **13. c**) naked Co/C MNPs. **d**) attempts of grafting using MNPs and PVDF without pyrene unit. In cases, **a**, **b** and **d**, the procedure detailed in Figure 5 was employed.

tions to the graphene surface was expected to be removed by washing.[9b] TEM images showed the presence of MNPs surrounded by pyrene-tagged dendrons **11** (Figure 6a) or **13** (Figure 6b). EDX analyses confirmed the presence of Co in the dark areas, while the lighter grey shells around the Co core mainly displayed the presence of heteroelements in high amount (for dendrimer **11**: P and S, characteristic elements of dendritic skeleton; for dendrimer **13**: P, S and F, characteristic elements of PVDF chains and dendritic spacers, see Section S4 in the Supporting Information).

It is, however, worth noting that Figure 6b shows the presence of large areas containing only dendritic PVDF (light grey areas on the images) sometimes reaching several tens of nanometers in size. This suggests that the washing procedure used to remove ungrafted dendritic PVDF **13** was not completely efficient. The high crystallinity and poor solubility of PVDF is likely responsible for the incomplete removal of dendritic PVDF **13** in excess and additional washing steps with solvents including DMF, and fluorinated solvents did not improve the results. The magnetic decantation did not isolate only the functionalized MNPs, but it also trapped non-negligible amounts of free (not bound to the MNPs by π-stacking) dendritic PVDF **13**. Interestingly, when performing the procedure depicted in Figure 5 using **11** instead of **13**, the pyrene-tagged dendrimers in excess that were not specifically associated with MNPs through π-stacking interactions were efficiently removed. Therefore, the resulting MNPs were found to be surrounded by thin light grey shells containing the phosphorous dendrons **11** according to EDX experiments (Figure 6a). The significantly lower efficiency of the washing procedures in the case of dendrimer **13** was confirmed by elemental analysis which showed that up to 7 mmol of pyrene-tagged dendrons were associated with one gram of MNPs. Such a loading is much higher than (and therefore not consistent with) those calculated for pyrene-tagged dendrimer **11** (0.04 mmol of pyrene tag per gram of MNPs) and those previously reported for pyrene-tagged dendritic phosphines (0.03 mmol of pyrene tag per gram of MNPs).[7] Interestingly, compared to the "naked" Co/C MNPs (Figure 6c), the MNPs functionalized by pyrene-tagged dendrimers (Figure 6a,b) were found to be less aggregated. In addition, when non-functional PVDF chains (i.e., not bearing pyrene moieties) were used, a complete segregation between dendritic PVDF and the MNPs was observed (Figure 6d). This result was consistent with fluorescence studies and highlighted the crucial role of the pyrene moiety in the grafting process.

Conclusion

The objective of this work was to study the non-covalent coating of MNPs with pyrene-tagged poly(vinylidene fluoride). Phosphorous dendrimers bearing a pyrene moiety were selected as spacers between the surface of the MNP and the polymer chains. Indeed, the pyrene unit was expected to interact with the graphene surface. The dendritic spacer decorated with acetylenic functions was successfully prepared and fully characterized (compound **11**). Azido-functionalized PVDF chains were next successfully grafted onto each branch of dendrimer **11** by using Huisgen [3+2] cycloadditions ("click chemistry"). Afterwards, the association of pyrene-tagged dendrimers **11** and **13** (decorated with PVDF chains) with commercially available Co/C MNPs was studied. Fluorescence studies confirmed the existence of interactions between pyrene-tagged dendrimers and the MNPs as well as the crucial role played by the pyrene moiety. Moreover, dendritic PVDF **13** was found to be released upon temperature increase and interestingly, the partial reversibility of the π-stacking interactions between **13** and the graphene-functionalized surface of the MNPs was observed upon temperature decrease. Afterward, the syntheses of hybrid MNPs obtained from pyrene-tagged dendrimers **11** and **13** were achieved according to previously reported protocols (i. sonication of a mixture of MNPs and pyrene-tagged dendrimers; ii. magnetic decantation. iii. washings of the resulting hybrid MNPs). The hybrid MNPs syntheses were performed in the presence of large excess of pyrene-tagged dendrimers to optimize the grafting process and the excess of pyrene-tagged dendrimers not specifically bound through π-stacking interactions to the graphene surface can be removed by washing. TEM images and related EDX experiments revealed in both cases the presence of pyrene-tagged dendrimers surrounding the MNPs. On the contrary and interest-

ingly, complete phase segregation occurred when associating "naked Co/C MNPs" and pyrene-free PVDF which highlighted the crucial role of the pyrene moiety in the grafting process and was thus consistent with fluorescence studies. As expected, in the case of **11**, thin shells containing the characteristic P and S heteroatoms were observed. For **13**, the organic shells containing P, S and F atoms were found to be larger (up to several tens of nm). This showed that some free dendritic PVDF **13** was also trapped despite careful washing in contrast to the case of the more soluble and less crystalline compound **11** which excess could be completely removed by washings. These MNP-dendrimer constructs were also shown by fluorescence studies to display a thermo-responsive behavior whereby the non-covalent interactions (and thus the grafting) were partially reversible upon heating. This interesting property might allow the future use of such hybrid MNPs in thermo-responsive materials combining magnetic properties together with the well-known and outstanding features of PVDF for high-tech applications. More generally, the first coating of MNPs with polymers through π-stacking interactions reported here opens the way to more modular and tunable nanocomposites.

Experimental Section

The preparation and characterization (including NMR and mass spectra) of compounds **3**, **5**, **7**, **9**, **11** and **13** are detailed in the Electronic Supporting Information. The π-stacking procedures are summarized below (for more details and EDX spectra, see Supporting Information section).

Fluorescence Studies with 11 and 13 (Figure 3)

Solutions of dendrimers **11** or **13** ($9.25\ 10^{-6}$ mol L^{-1} in a THF-water (2:5)) were prepared and their fluorescence recorded. Aliquots of Co/C MNPs were then successively added to these homogeneous solutions (0.5 mg for the first addition and 1 mg for each further addition, Figure 3). After each addition, the suspension was sonicated for 30 min, the MNPs removed by magnetic decantation and the supernatant analyzed by fluorescence spectroscopy.

Fluorescence Studies to Perform Reversibility Test with 13 (Figure 4)

A suspension of **13** (solution in a THF-water (2:5); $9.25\ 10^{-6}$ mol L^{-1}) and MNPs was sonicated for 30 minutes at 20 °C, magnetically decanted with a magnet and the fluorescence spectrum of the supernatant recorded (blue curve). The mixture (supernatant and MNPs) was then heated to 60 °C for 10 h, and the spectrum of the resulting supernatant analyzed (red curve). Upon cooling to 20 °C, the concentration of 13 in the solution decreased (green curve). Importantly, the fluorescence spectra recorded after 1 hour or 12 hours after return to ambient temperature were found to be identical.

Grafting Measurements with 13

A mixture of THF-water 2:5 (15 mL) was added to Co/C nanoparticles (15 mg) and pyrene-tagged dendrimer **13** (194 mg, 7.10^{-3} mmol) and were sonicated for 30 minutes at 20 °C. The nanoparticles were then magnetically decanted and rinsed ten times with the same hot solvent mixture (THF-water 2:5) to try to remove ungrafted pyrene-tagged dendrimer from the medium. The recovered MNPs were dried and analyzed by TEM (see Figure 6b) and by elemental analysis. By comparison with the result obtained for free nanoparticles, the loading of the pyrene-tag was calculated.

Acknowledgements

We thank Arkema S. A. (Pierre Bénite, France) for providing VDF and the Ministère de l'Education Nationale et de l'Enseignement Supérieur et de la Recherche for a PhD grant to M.G.

Conflict of Interest

The authors declare no conflict of interest.

Keywords: dendrimers · magnetic nanoparticles · π-stacking · poly(vinylidene fluoride) · pyrenes

[1] For some reviews, see: a) J. Gonzalez-Benito, D. Olmos, *Society of Plastics Engineers* **2010**, *31*, 946–955; b) M. Supova, G. S. Martynkova, K. Barabaszova, *Sci. Adv. Mater.* **2011**, *3*, 1–25; c) G. D. Smith, D. Bedrov, *Langmuir* **2009**, *25*, 11239–11243; d) P. Ajayan, L. S. Schadler, P. V. Braun, *Nanocomposite Science and Technology*; Wiley-VCH: Weinheim, **2003**; e) P. Gomez-Romero, C. Sanchez, *Functional Hybrid Materials*; Wiley-VCH: Weinheim, **2004**; f) H. Zou, S. Wu, J. Shen, *Chem. Rev.* **2008**, *108*, 3893–3957; g) C. M. Lukehart, R. A. Scott, *Nanomaterials: Inorganic and Bioinorganic Perspectives*; Wiley: New York, **2008**; h) S. D. Achilleos, M. Vamvakaki, *Materials* **2010**, *3*, 1981–2026; i) M. Krishnamoorthy, S. Hakobyan, M. Ramstedt, J. E. Gautrot, *Chem. Rev.* **2014**, *114*, 10976–11026; j) S. Xia, L. Song, V. Körstgens, M. Opel, M. Schwartzkopf, S. V. Roth, P. Müller-Buschbaum, *Nanoscale* **2018**, *25*, 11930–11941; k) D. Kim, K. Shin, S. G. Kwon, T. Hyeon, *Adv. Mater.* **2018**, 1802309.

[2] Dendrimers are perfectly defined globular macromolecules with a regular hyperbranched structure and tunable multivalent surfaces. They find applications in many scientific fields including catalysis, nanomedicine and material science. For some examples: a) D. A. Tomalia, J. B. Christensen, U. Boas, *Dendrimers, Dendrons, and Dendritic Polymers*; Cambridge University Press: New York, **2012**; b) A. M. Caminade, C. O. Turrin, R. Laurent, A. Ouali, B. Delavaux-Nicot, *Dendrimers. Towards Catalytic, Material, and Biomedical Uses*; Wiley & Sons Ltd: Chichester, **2011**; c) F. Vögtle, G. Richardt, N. Werner, *Dendrimer Chemistry*, Wiley VCH: Weinheim, **2009**; d) D. Astruc, E. Boisselier, C. Ornelas, *Chem. Rev.* **2010**, *110*, 1857–1959.

[3] a) B. Ameduri, *Chem. Rev.* **2009**, *109*, 6632–6686; b) J. S. Humphrey, R. Amin-Sanayei, *Vinylidene Fluoride Polymers.* Encyclopedia of Polymer Science and Technology, 3rd ed.; H. F. Mark, Ed.; Wiley; New York, **2004**; Vol. 4, pp 510–533. For original properties of PVDF-based nanocomposites, see also for recent examples: c) Z. Li, L. Zhang, R. Qi, F. Xie, S. Qi, *J. Appl. Polym. Sci.* **2016**, *133*, 43554; d) K. Ke, P. Pötschke, N. Wiegand, B. Krause, B. Voit, *ACS Appl. Mater. Interfaces* **2016**, *8*, 14190–14199; e) J. T. Goldbach, R. Amin-Sanayei, W. He, J. Henry, W. Kosar, A. Lefebvre, G. O'Brien, D. Vaessen, K. Wood and S. Zerafati, *Commercial synthesis and applications of poly(vinylidene fluoride)*, in Fluorinated

Polymers Vol. 2: Applications, Chapter 6, pp 126–157, ed. B. Ameduri and H. Sawada, Royal Society of Chemistry, Cambridge, **2016**.

[4] Noteworthy, some of us recently reported the preparation of PVDF-decorated dendrimers constituting promising candidates for applications in coatings, as processing aids or as additives for nanocomposites. E. Folgado, M. Guerre, C. Bijani, V. Ladmiral, A.-M. Caminade, B. Ameduri, A. Ouali, *Polym. Chem.* **2016**, *7*, 6632–6686.

[5] R. N. Grass, E. K. Athanassiou, W. J. Stark, *Angew. Chem. Int. Ed.* **2007**, *46*, 4909–4912; *Angew. Chem.* **2007**, *119*, 4996–4999.

[6] Purchased from Aldrich. CAS 7440–48-4. Reference 697745.

[7] Q. M. Kainz, O. Reiser, *Acc. Chem. Res.* **2014**, *47*, 667–677.

[8] Q. M. Kainz, A. Schätz, A. Zöpfl, W. J. Stark, O. Reiser, *Chem. Mater.* **2011**, *23*, 3606–3613.

[9] a) S. Wittmann, A. Schätz, R. N. Grass, W. J. Wendelin, O. Reiser, *Angew. Chem. Int. Ed.* **2010**, *49*, 1867–1870; *Angew. Chem.* **2010**, *122*, 1911–1914; b) M. Keller, V. Collière, O. Reiser, A. M. Caminade, J. P. Majoral, A. Ouali, *Angew. Chem. Int. Ed.* **2013**, *52*, 3626–3629; *Angew. Chem.* **2013**, *125*, 3714–3717.

[10] Z. Guo, H. Yin, Y. Feng, S. He, *RSC Adv.* **2016**, *6*, 37953–37964.

[11] in some examples, polymers are physisorbed onto the Fe/C or Co/C NPMs and these materials were shown to be less stable (leaching of MNP). e.g. R. Fuhrer, C. M. Schumacher, M. Zeltner, W. J. Stark, *Adv. Funct. Mater.* **2013**, *23*, 3845–3849.

[12] a) C. J. Hofer, V. Zlateski, P. R. Stoessel, D. Paunescu, E. M. Schneider, R. N. Grass, M. Zeltner, W. J. Stark, *Chem. Commun.* **2015**, *51*, 1826; b) M. Zeltner, A. Schätz, M. L. Hefti, W. J. Stark, *J. Mater. Chem.* **2011**, *21*, 299; c) M. Zeltner, R. N. Grass, A. Schaetz, S. B. Bubenhofer, N. A. Luechinger, W. J. Stark, *J. Mater. Chem.* **2012**, *22*, 12064–12071; d) R. Fuhrer, E. K. Athanassiou, N. A. Luechinger, W. J. Stark, *Small*, **2009**, *5*, 383; e) X. Zhang, O. Alloul, J. Zhu, Q. He, Z. Luo, H. A. Colorado, N. Haldolaarachchige, D. P. Young, T. D. Shen, S. Wei, Z. Guo, *RSC Adv.* **2013**, *3*, 9453; f) M. Keller, A. Perrier, R. Linhardt, L. Travers, S. Wittmann, A. M. Caminade, J. P. Majoral, O. Reiser, A. Ouali, *Adv. Synth. Catal.* **2013**, *355*, 1748–1754.

[13] a) G. Franc, S. Mazères, C.-O. Turrin, L. Vendier, C. Duhayon, A.-M. Caminade, J.-P. Majoral, *J. Org. Chem.* **2007**, *72*, 8707–8715; b) O. Rolland, L. Griffe, M. Poupot, A. Maraval, A. Ouali, Y. Coppel, J.-J. Fournié, G. Bacquet, C.-O. Turrin, A.-M. Caminade, J.-P. Majoral, R. Poupot, *Chem. Eur. J.* **2008**, *14*, 4836–4850.

[14] V. Vicente, A. Fruchier, H.-J. Cristau, *Magn. Reson. Chem.* **2003**, *41*, 183–192.

[15] D. Riegert, A. Pla-Quintana, S. Fuchs, R. Laurent, C. O. Turrin, C. Duhayon, J. P. Majoral, A. Chaumonnot, A. M. Caminade, *Eur. J. Org. Chem.* **2013**, 5414–5422.

[16] Copper-catalyzed azide-alkyne [3 + 2]-cycloaddition (CuAAC)CuAAC is an attractive ligation method in terms of atom-economy, high yield, reaction rate and for the robustness of the triazole ring it generates. It has been widely exploited to design and prepare functional dendritic and polymeric architectures, including fluorinated ones. For reviews, see: a) M. Arsenault, C. Wafer, J.-F. Morin, *Molecules* **2015**, *20*, 9263–9294; b) W. Xi, T. F. Scott, C. J. Kloxin, C. N. Bowman, *Adv. Funct. Mater.*, **2014**, *24*, 2572–2590; c) J. A. Johnson, M. G. Finn, J. T. Koberstein, N. J. Turro, *Macromol. Rapid Commun.*, **2008**, *29*, 1052–1072. For some examples: d) S. A. McNelles, A. Adronov, *Macromolecules* **2017**, *50*, 7993–8001; e) G. Tillet, G. Lopez, M.-H. Hung, B. Ameduri, *J. Polym. Sci. Part A* **2015**, *53*, 1171–1173; f) D. Lu, M. D. Hossain, Z. Jia, M. J. Monteiro, *Macromolecules* **2015**, *48*, 1688–1702; g) X. Feng, D. Taton, E. Ibarboure, E. L. Chaikof, Y. Gnanou, *J. Am. Chem. Soc.* **2014**, *130*, 11662–11676; h) F. Yao, L.-Q. Xu, G.-D. Fu, B.-P. Lin, *Polym. Int.* **2012**, *61*, 749–759; i) G. Tillet, P. De Leonardis, A. Alaaeddine, M. Umeda, S. Mori, N. Shibata, S. M. Aly, D. Fortin, P. D. Harvey, B. Ameduri, *Macromol. Chem. Phys.* **2012**, *213*, 1559–1568; j) A. Soules, B. Ameduri, B. Boutevin, G. Callega, *Macromolecules* **2010**, *43*, 4489–4499; k) A. Carlmark, C. J. Hawker, H. Anders, M. Malkoch, *Chem. Soc. Rev.* **2009**, *38*, 352–362; l) V. Ladmiral, G. Mantovani, G. J. Clarkson, S. Cauet, J. L. Irwin, D. M. Haddleton, *J. Am. Chem. Soc.* **2006**, *128*, 4823–4830; m) E. Arnaiz, E. Vacas-Cordoba, M. Galan, M. Pion, R. Gomez, M. A. Angeles Munoz-Fernandez, J. Javier de la Mata, *J. Polym. Science, Part A.* **2014**, *52*, 1099–1112.

Manuscript received: September 12, 2018
Revised manuscript received: November 9, 2018
Accepted manuscript online: November 16, 2018
Version of record online: December 18, 2018

CHEMPLUSCHEM

Supporting Information

π-Stacking Interactions of Graphene-Coated Cobalt Magnetic Nanoparticles with Pyrene-Tagged Dendritic Poly (Vinylidene Fluoride)

Enrique Folgado, Marc Guerre, Nidhal Mimouni, Vincent Collière, Christian Bijani, Kathleen Moineau-Chane Ching, Anne-Marie Caminade, Vincent Ladmiral, Bruno Améduri, and Armelle Ouali*

Supporting information

S1. Materials and methods

● Chemicals and purification methods.

Chemicals were purchased from Aldrich, Acros, Fluka, Alfa Aesar and Strem, and were used without further purification, except for $P_3N_3Cl_6$ and 4-hydroxybenzaldehyde, which were recrystallized from hexane and diethyl ether, respectively. Organic solvents were dried and distilled according to usual procedures.[1] Dendrimers were synthesized according to published procedures.[2] Compounds **4**[3] and **6**[4] were also synthesized according to published procedures.

Purifications by column chromatography were performed on silica gel (60 Å, 53-250 μm) or on automatic Flash chromatography system, SPOT™ II Ultimate. TLCs were performed on silica gel 60 F254 plates and detection was carried out under UV light.

● NMR

NMR spectra were recorded with Bruker AV 300, AV 400 and Avance 500 (equipped with a 5 mm triple resonance inverse Z-gradient probe (TBI ^{1}H, ^{31}P, BB)) spectrometers. All spectra were measured at 25 °C in the indicated deuterated solvents. All chemical shifts for ^{1}H and ^{13}C are relative to TMS using ^{1}H (residual) or ^{13}C chemical shifts of the solvent as a secondary standard. The ^{19}F NMR chemical shifts are relative to $CFCl_3$. ^{1}H, ^{19}F, ^{13}C and ^{31}P chemical shifts (δ) are reported in ppm and coupling constants (J) are reported in Hertz (Hz). The signals in the spectra are described as s (singlet), d (doublet), t (triplet), m (multiplet) and br (broad resonances). All the ^{1}H and ^{13}C NMR signals were assigned on the basis of chemical shifts, spin-spin coupling constants, splitting patterns and signal intensities, and by using ^{1}H-^{1}H COSY45, ^{1}H-^{13}C HSQC and ^{1}H-^{13}C HMBC experiments.

Line shape fitting analysis was performed using the DNMR module of Topspin 3.2 software of Bruker. This program is able to simulate the experimental spectra by setting up and refining some parameters in order to adjust them to the experimental NMR spectra obtained.

● Mass spectrometry

Mass spectrometry was carried out with a Thermo Fisher DS QII (DCI/NH_3), GTC Premier Waters (DCI/CH_4) or with Maldi Micro MX Waters (Maldi/DCTB).

● HR Transmission electron microscopy

High resolution transmission electron microscopy (HRTEM), scanning transmission electron spectroscopy (STEM) and energy dispersive X-ray (EDX) were performed at the UMS 3623 - Centre de microcaractérisation Raimond Castaing, Toulouse, France and recorded on a JEOL JEM 2100 F electron microscope working at 200 kV with a resolution point of 2.5 Å and equipped with X-ray analysis PGT (light elements detection, resolution 135 eV). Samples for HRTEM analyses were prepared by slow evaporation of a drop of crude colloidal solution deposited onto carbon-covered copper grids. On the EDX spectra, Cu signals are due to the grids on which the samples were deposited and Si signals were found to come from the preparation of samples.

● UV-visible and fluorimetry

UV-VIS-NIR absorption spectra were recorded on a Perkin Elmer Lambda 35 spectrometer, using spectrometric grade solvent. The solutions used for the electronic absorption analyses were typically about 10^{-5} mol.L^{-1} in molecule. Steadystate fluorescence spectroscopic studies were performed on a HORIBA Jobin Yvon FluoroMax-4 spectrofluorometer, the solutions used for emission analyses were typically

---

[1] D. D. Perrin et W. L. F. Almerego, *Purification of Laboratory Chemicals 3rd Ed.*, Pergamon Press. Oxford, **1998**.

[2] N. Launay, A.-M. Caminade, J.-P. Majoral, *J. Organomet. Chem.* **1997**, *529*, 51.

[3] M. Keller, V. Collière, O. Reiser, A. M. Caminade, J. P. Majoral, A. Ouali, *Angew. Chem. Int. Ed.* 2013, **52**, 3626-3629.

[4] G. Franc, S. Mazere, C.O. Turrin, L. Vendier, C. Duhayon, A.M. Caminade, J.P. Majoral, J. Org. Chem. 2007, 72, 8707-8715.

around 1.6 10^{-6} mol.L^{-1} in molecule (i.e. exhibiting an absorbance ≤ 0.1). The slit width was 1 nm. Fluorescence spectra were corrected.

S2. Characterization of compounds

Only the characterizations of the new products are listed below.

Compound 3: $C_{21}H_{38}O_8SiS$, Mw: 478.67 g.mol^{-1}

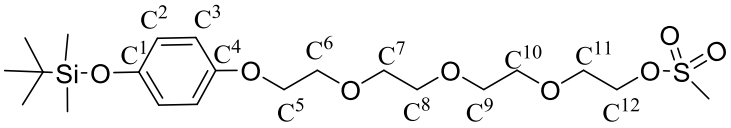

In a 25 mL Schlenk tube equipped with a Teflon magnetic stirring bar were combined molecule **1** (1.854 g, 5.29 mmol), 4-(t-Butyldimethylsilyloxy)Phenol (0.406 g, 1.81 mmol), cesium carbonate (0.575 g, 1.77 mmol), and THF (5 mL). The mixture was heated to 70 °C for 48 h. The mixture was cooled to room temperature and filtered to remove any solids. The residual solvent was evaporated under reduced pressure and the resulting oily product was purified by silica gel flash chromatography eluting with 6:4 to 3:7 hexane/ethyl acetate. Fractions containing product were combined and concentrated under reduced pressure and dried in vacuo. The product was obtained as a yellowish oil (0.30 g, 35 % yield).

^{1}H NMR (300 MHz, $CDCl_3$): δ = 0.18 (s, 6H, Si-Me), 0.99 (s, 9H, Si-tBu), 3.08 (s, 3H, S-Me), 3.66 – 3.86 (m, 12H, C^6-C^{11}), 4.06 – 4.11 (m, 2H, C^5), 4.35 – 4.42 (m, 2H, C^{12}), 6.78 (d, *J* = 3.0 Hz, 4H, C^2-C^3) ppm.
^{13}C {^{1}H} NMR (75 MHz, $CDCl_3$): δ = 4.49 (s, Si-Me), 18.18 (s, Si-C), 25.71 (s, tBu), 37.71 (S-Me), 67.90-70.50 (C^5-C^{12}), 115.35 (s, C^3), 120.61 (s, C^2), 149.53 (s, C^4), 153.23 (s, C^1) ppm.

Compound 5: $C_{42}H_{45}NO_7$, Mw: 675.82 g.mol^{-1}

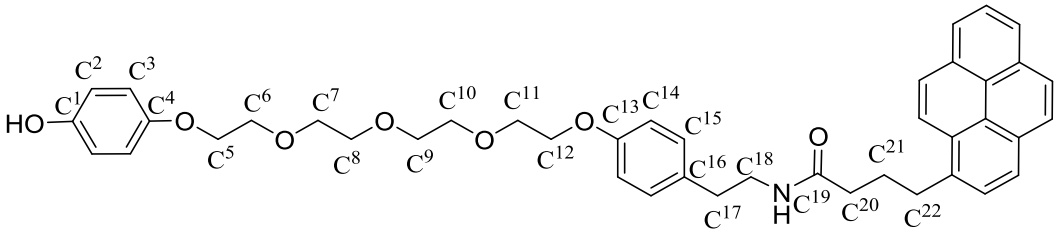

In a round flask, the pyrene derivative **4** (234.31 mg, 0.575 mmol) and K_2CO_3 (199 mg, 1.44 mmol) were dissolved in acetone (3mL) and the reaction mixture was refluxed at 65 °C for 8h for the deprotonation of the phenol group. After 8 h, molecule **3** (250 mg, 0.522 mmol) dissolved in acetone (1 mL) was added and the reaction mixture was refluxed at 65 °C for 48 h. The reaction mixture was cooled to RT and filtered through a celite pad to remove solids. The solvent was evaporated under reduced pressure and the product was purified by silica gel flash chromatography eluting with 8:2 pentane/ethyl acetate to 7:3 pentane/ethyl acetate. The product was obtained as a slightly yellow solid (136 mg, 38.5 % yield).

^{1}H NMR (300 MHz, $CDCl_3$) δ = 2.23 (m, 4H, C^{20}, C^{21}), 2.72 (t, 2H, C^{17}), 3.37 (m, 6H, C^{22}), 3.48 (m, 2H, C^{18}), 3.74 (m, J = 33.6 Hz, 12H, C^6-C^{11}), 4.00 (m, 4H, C^5,C^{12}), 5.52 (s, 1H, -NH) , 6.77 (d, 6H, C^{14}, C^2, C^3), 7.04 (d, 2H, C^{15}), 8.30 (d, 1H, pyr), 8.19 (m, 2H, pyr), 8.09 (m, 2H, pyr), 8.04 (m, 3H, pyr), 7.81 (d, 1H, pyr) ppm
^{13}C {^{1}H} NMR (75 MHz, $CDCl_3$) δ = 27.33 (s, C^{21}), 32.64 (s, C^{22}), 34.76 (s, C^{17}), 36.05 (s, C^{20}), 40.72 (s, C^{18}), 67.40 (s, C^5), 68.15 (s, C^{12}), 69.66 (s, C^6), 69.85 (s, C^{11}), 70.68 – 70.74 (m, 4C, C^7-C^{10}), 114.74 (s, C^{14}), 115.74 (s, C^3), 116.09 (s, C^2), 123.35 (s, C^{III} pyr), 124.78 (s, 2C^{III} pyr), 124.91 (s, C^{III} pyr), 124.96 (s, C^{IV} pyr), 125.06 (s, C^{IV} pyr), 125.86 (s, C^{III} pyr), 126.71 (s, C^{III} pyr), 127.32 (s, C^{III} pyr), 127.39 (s, C^{III} pyr), 127.48 (s, C^{III} pyr), 128.75 (s, C^{IV} pyr), 129.58 (s, C^{15}), 129.92 (s, C^{16}), 130.76 (s, C^{IV} pyr), 130.89 (s, C^{IV} pyr), 131.39 (s, C^{IV} pyr), 135.74 (s, C^{IV} pyr), 150.36 (C^1), 152.55 (s, C^4), 157.44 (s, C^{13}), 172.96 (s, C^{19}) ppm.
MALDI TOF-MS: m/z: 676 $[M+H]^+$ (spectrum below, Figure S5.3).

Compound 7: $C_{77}H_{69}O_{17}N_4P_3$, Mw: 1415.36 g.mol^{-1}

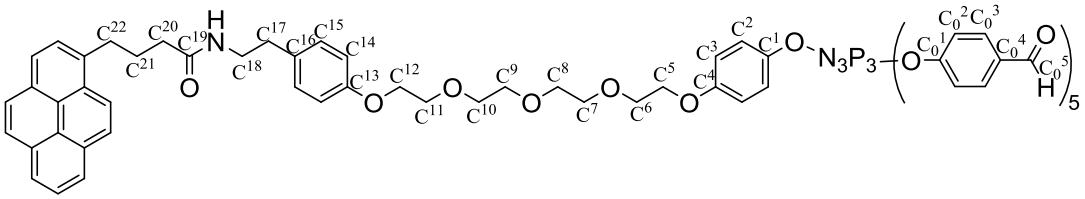

In a Schlenk tube equipped with a Teflon magnetic stirring bar, were combined molecule **5** (100 mg, 0.148 mmol), cesium carbonate (96.5 mg, 0.296 mmol), and THF (5 mL). The mixture was heated to 70 °C for 8 h. After 8 h, the mixture was cooled to room temperature and phosphorous pentasubstitued core AB_5 (molecule **6**) (122 mg, 0.141 mmol) was added to the reaction mixture. The mixture was heated to 70 °C for 24 h. The mixture was cooled to room temperature and filtered to remove any solids. The residual solvent was evaporated under reduced pressure and the resulting product was purified by silica gel flash chromatography eluting with 8:2 DCM/acetone to 99:1 acetone/triethylamine. Fractions containing the product were combined and concentrated under reduced pressure and dried *in vacuo*. The product was obtained as a yellow foam (45.30 mg, 71 % yield).

^{1}H NMR (500 MHz, $CDCl_3$) δ = 2.23 (m, 4H, C^{20}, C^{21}), 2.73 (t, 2H, C^{17}), 3.36 (m, 2H, C^{22}) 3.50 (m, 2H, C^{18}), 3.76 (m, 12H, C^6-C^{11}), 4.02 (m, 4H, C^5, C^{12}), 5.45 (s, 1H, -NH) , 6.70-6.83 (m, 6H, C^{14}, C^2, C^3), 7.06 (m, 10H, C_0^2), 7.19 (m, 2H, C^{15}), 7.73 (m, 10H, C_0^3), 7.84-8.27 (m, 9H, pyr), 9.94 (m, 5H, C_0^5) ppm.
^{31}P-{^{1}H} NMR (166.7 MHz, $CDCl_3$): δ = 8.06 ($^2J_{1\text{-}2}$ = 58 Hz, P_0^1), 7.51 ($^2J_{2\text{-}3}$ = -48 Hz, P_0^2), 7.40 ($^2J_{1\text{-}3}$ = 113 Hz, P_0^3) ppm.
^{13}C {^{1}H} NMR (125 MHz, $CDCl_3$) δ = 27.41 (s, C^{21}), 32.70 (s, C^{22}), 34.77 (s, C^{17}), 36.05 (s, C^{20}), 40.66 (s, C^{18}), 67.41 (s, C^{12}), 67.87 (s, C^5), 69.69 (s, C^6, C^{11}), 70.63 – 70.74 (m, 4C, C^7-C^{10}), 114.06 (s, C^2), 114.78 (s, C^{14}), 115.26 (s, C^3), 121.20 (s, C_0^2), 123.40 (s, C^{III} pyr), 124.79 (s, 2C^{III} pyr), 124.90 (s, C^{III} pyr), 124.95 (s, C^{IV} pyr), 125.04 (s, C^{IV} pyr), 125.88 (s, C^{III} pyr), 126.70 (s, C^{III} pyr), 127.35 (s, 2 C^{III} pyr), 127.48 (s, C^{III} pyr), 128.76 (s, C^{IV} pyr), 129.64 (s, C^{15}), 129.88 (s,C^{16}), 130.89 (s, C^{IV} pyr), 131.35 (s, C_0^3), 131.37 (s, C^{IV} pyr), 133.52-133.66 (s, C_0^4), 135.88 (s, C^{IV} pyr), 154.59 (s, C_0^1), 156.44 (C^1), 157.42 (s, C^4), 157.5 (s, C^{13}), 172.61 (s, C^{19}), 190.5 (s, C_0^5) ppm.

The magnetic non-equivalence of P_0^2 and P_0^3 is only observed after having grafted the pyrene-tagged chain. The latter was indeed found to induce a slightly different environment for the two phosphorus atoms bearing the same substituents (two -O-C_6H_4-CHO groups) leading to their magnetic inequivalence. The signals were exhaustively analyzed and a NMR signal simulation allowed the calculations of the chemical shifts of the three phosphorous atoms and of their coupling constants (see above). Noteworthy, such non-equivalence of the phosphorous atoms as well as the high differences between coupling constants have already been reported for hexasubstituted cyclotriphosphazenes involving five identical substituents.[5]

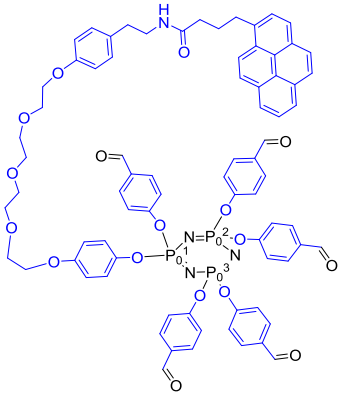

Figure S2.1

[5] V. Vicente, A. Fruchier, H.-J. Cristau, *Magn. Reson. Chem.*. **2003**, *41*, 183-192.

Compound 9: $C_{82}H_{84}O_{12}N_{14}P_8S_5Cl_{10}$, Mw = 2220.27 g.mol^{-1}

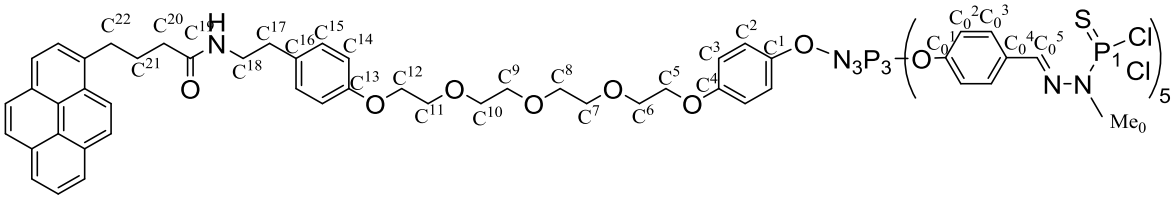

In a flame dried Schlenk flask equipped with a Teflon magnetic stirring bar, Na_2SO_4 (182 mg, 1.28 mmol) and pyrene-functionalised-G_0 dendrimer (molecule **7**) (45.3 mg, 0.032 mmol) were dissolved in 1.3 mL of dry DCM in an Argon atmosphere. The mixture was cooled at 0 °C for 15 min. Dichlorothiophosphoromethylhydrazide (molecule **8**) (0.24 M solution in $CHCl_3$, 0.74 mL, 0.177 mmol) was added to the reaction mixture. The mixture was stirred for 1.5 h at room temperature. The mixture was then filtered through a Celite pad to remove any solids and residual solvents were evaporated under reduced pressure. The resulting product was purified by silica gel flash chromatography eluting with DCM to 8:2 DCM/acetones. The product was obtained as a yellow foam-like solid (64 mg, 90 % yield).

^{1}H NMR (500 MHz, $CDCl_3$) δ = 2.20 (m, 2H, C^{21}), 2.24 (m, 2H, C^{20}), 2.73 (t, 2H, C^{17}), 3.35 (m, 2H, C^{22}), 3.43 (m, 2H, C^{18}), 3.48-3.50 (m, 15H, Me^0), 3.67- 3.71 (m, 8H, C^7-C^{10}), 3.76 (m, 2H, C^{11}), 3.82 (m, 2H, C^6) 4.00 (m, 2H, C^{12}), 4.02 (m, 2H, C^5), 5.41 (s, 1H, -NH), 6.67 (m, 2H, C^3), 6.80 (m, 2H, C^{14}), 6.85 (m, 2H, C^2), 7.05 (m, 10H, C_0^2), 7.06 (m, 2H, C^{15}), 7.60 (m, 10H, C_0^3) 7.83-8.29 (m, 9H, pyr) ppm.
^{31}P-{^{1}H} NMR (203 MHz, $CDCl_3$): δ = 8.38 ($^2J_{1\text{-}2}$ = 37 Hz, P_0^1), 8.41 ($^2J_{2\text{-}3}$ = 43 Hz, P_0^2), 8.69 ($^2J_{1\text{-}3}$ = 127 Hz, P_0^3), 62.40 (s, P_1), 62.44 (s, P_1), 62.62 (s, P_1) ppm.
^{31}P NMR (203 MHz, $CDCl_3$) δ = 62.62 (s), 62.42 (d, *J* = 8.4 Hz), 8.70 (s), 8.58 – 8.38 (m), 8.28 (s), 7.89 (s).
^{13}C {^{1}H} NMR (125 MHz, $CDCl_3$) δ = 27.42 (s, C^{21}), 31.94 (s, C_0^6), 32.68 (s, C^{22}), 34.77 (s, C^{17}), 36.02 (s, C^{20}), 40.65 (s, C^{18}), 67.4 (s, C^{12}), 67.89 (s, C^5), 69.72 (s, C^6, C^{11}), 70.67 – 70.89 (m, 4C, C^7-C^{10}), 114.78 (s, C^{14}), 115.21 (s, C^3), 121.41 (s, C_0^2), 121.76 (s, C^2), 123.40 (s, C^{III} pyr), 124.78 (s, 2C^{III} pyr), 124.90 (s, C^{III} pyr), 124.94 (s, C^{IV} pyr), 125.04 (s, C^{IV} pyr), 125.86 (s, C^{III} pyr), 126.69 (s, C^{III} pyr), 127.34 (s, C^{III} pyr), 127.36 (s, C^{III} pyr), 127.42 (s, C^{III} pyr), 128.66-128,68 (s, C_0^3), 128.74 (s, C^{IV} pyr), 129.64 (s, C^{15}), 130.87 (s, C^{IV} pyr), 130.96 (s, C^{IV} pyr), 131.38 (s, C^{IV} pyr), 131.0 (m, C_0^4, C^{16}), 135.84 (s, C^{IV} pyr), 140.70-140.84(m, C_0^5), 143.90 (s, C^1), 152.0 (C_0^1), 156.0 (s, C^4), 157.50 (s,C^{13}), 172.52 (s, C^{19}) ppm.
MALDI TOF-MS: m/z: 2221 $[M+H]^+$ (spectrum below, Figure S5.11).

Compound 11: $C_{172}H_{154}O_{32}N_{14}P_8S_5$, Mw: 3337.25 g.mol^{-1}

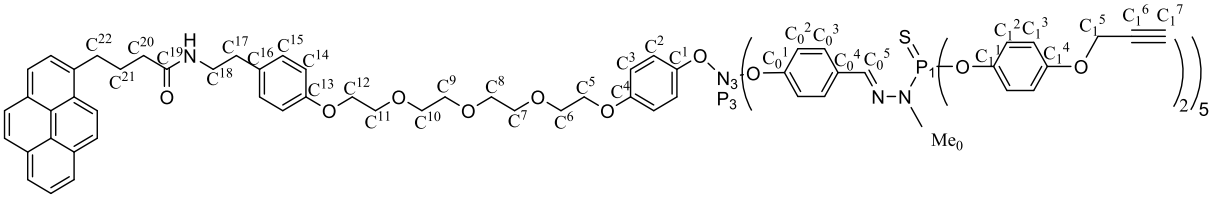

Cs_2CO_3 (152.5 mg, 0.468 mmol) was added to a THF (4 mL) solution of molecule **9** (52 mg, 0.023 mmol) and propargyloxyphenol (38.1 mg, 0.257 mmol), and the reaction mixture was stirred at 40 °C until the reaction was complete (24 h, monitored by 31P{1H} NMR spectroscopy). Inorganic salts were filtered through a Celite® pad and the residual solvent was evaporated under reduced pressure. The crude product was purified by silica gel flash chromatography eluting with pentane/ethyl acetate (7:3 to 1:1). The product was obtained as a white solid (52 mg, 66%).

^{1}H NMR (500 MHz, $CDCl_3$) δ = 2.20 (m, 2H, C^{21}), 2.23 (m, 2H, C^{20}), 2.50 (m, 10H, C_0^7), 2.73 (t, 2H, C^{17}), 3.23-3.31 (m, 15H, Me_0), 3.35 (m, 2H, C^{22}), 3.48 (m, 2H, C^{18}), 3.63-3.65 (m, 8H, C^7-C^{10}), 3.74 (m, 4H, C^6, C^{11}), 3.98 (m, 4H, C^{12}, C^5) 4.60 (m, 2H, C_1^5), 5.41 (s, 1H, -NH), 6.71 (m, 2H, C^5), 6.79 (m, 2H, C^{14}), 6.92 (m, 2H, C^2), 7.03 (m, 10H, C_0^2), 7.05 (m, 2H, C^{15}), 7.58 (m, 5H, C_0^5), 7.61 (m, 10H, C_0^3), 7.84-8.27 (m, 9H, pyr) ppm.
^{31}P-{^{1}H} NMR (203 MHz, $CDCl_3$): δ = 8.38 ($^2J_{1\text{-}2}$ = 37 Hz, P_0^1), 8.41 ($^2J_{2\text{-}3}$ = 43 Hz, P_0^2), 8.69 ($^2J_{1\text{-}3}$ = 127 Hz, P_0^3), 63.91 (s, P_1), 63.93 (s, P_1) ppm.
^{13}C {^{1}H} NMR (125 MHz, $CDCl_3$) δ = 27.39 (s, C^{21}), 32.6 (s, C_0^6), 32.71 (s, C^{22}), 34.76 (s, C^{17}), 36.03 (s, C^{20}), 40.65 (s, C^{18}), 56,15 (s, C_1^5), 67.38 (s, C^5, C^{12}), 69.63 (s, C^6, C^{11}), 70.68 (m, 4C, C^7-C^{10}), 75.8 (s, C_1^7), 78.38 (s, C_1^6), 114.78

(s, C^{14}), 115.23 (s, C^3), 121.37 (s, C_0^2), 121.76 (s, C^2), 123.40 (s, C^{III} pyr), 124.78 (s, 2C^{III} pyr), 124.90 (s, C^{III} pyr), 124.94 (s, C^{IV} pyr), 125.04 (s, C^{IV} pyr), 125.86 (s, C^{III} pyr), 126.69 (s, C^{III} pyr), 127.34 (s, C^{III} pyr), 127.36 (s, C^{III} pyr), 127.48 (s, C^{III} pyr), 128.2 (s, C_0^3), 128.74 (s, C^{IV} pyr), 129.65 (s, C^{15}), 129.88 (s, C^{16}), 130.87 (s, C^{IV} pyr), 130.96 (s, C^{IV} pyr), 131.38 (s, C^{IV} pyr), 132.0 (s, C_0^4), 135.84 (s, C^{IV} pyr), 138.51 (s, C_0^5), 144.21 (s, C^1), 144.39 (s, C_1^1), 151.3 (s, C_0^1), 154.9 (s, C_1^4), 156.13 (s, C^4), 157.46 (s, C^{13}), 172.53 (s, C^{19}) ppm.
MALDI TOF-MS (matrice): m/z: 3338 $[M+H]^+$ (spectrum below, Figure S5.15).

Compound 13: $C_{912}H_{874}F_{660}N_{44}O_{42}S_{25}P_8$ **Mw:** 26711.29 g.mol^{-1}

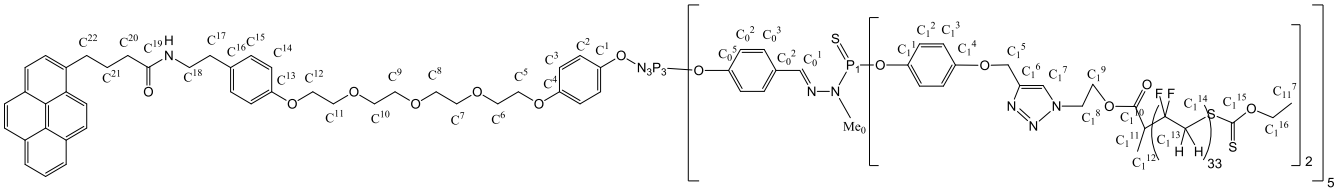

To a solution of CuI (1.37 mg, 7.18 µmol) and N,N-diisopropylethylamine (25 µl, 143.6 %mol) in THF (5 ml), were added the polymer (170 mg, 71,8 µmol) and the molecule **11** (24 mg, 7.18 µmol). The reaction mixture was stirred at 40°C for 24 h. The reaction was monitored by FT-IR spectroscopy (vanishing of the characteristic band of the azido group of **12** at 2111 cm^{-1}) and ^{31}P {^{1}H} and ^{1}H NMR confirmed the completion of the reaction. As previously described for the dendritic PVDF,[6] inorganic salts were hot filtered through a Celite® pad and the residual solvent was evaporated under reduced pressure. The crude product was washed several times with cold THF to remove the excess of **12**. Yield: 95%.

^{1}H NMR (300 MHz, DMSO-d6) δ = 1.04 (m, 30H, C_1^{12}), 2.18 (s, 1H, C^{20}), 2.24 (s, 1H, C^{21}), 2.44 (s, 1H, C^{22}), 2.62 (s, 1H, C^{17}), 2.66 (m, 10H, C_1^{11}), 2.89 (m, ~660H, CF_2-CH_2), 3.25 (m, 150H, Me_0), 3.42 (m, 8H, C^7-C^{10}), 3.53 (m, 4H, C^6 ,C^{11}), 3.85 (m, 4H, C^5 ,C^{12}), 4.36 - 4.47 (m, 10H, C_1^9) ,C^{12}(m, 4H, C^5 ,C^{12}),4.62 (m, 20H, C_1^8), 5.04 (m, 20H, C_1^5), 6,74 (m, 2H, C^{14}), 6.96 (m, 20H, C_1^3), 6.97 (m, 20H, C_1^2), 7.05 (m, 2H, C^{15}), 7.06 (m, 40H, C_0^2, C_1^3), 7.86 (s, C^{III} pyr),8.02 (s, C^{III} pyr),8.10 (m, 2C^{III} pyr), 8.17(m, 3C^{III} pyr), 8.18 (m, 11H, C^{III} pyr, C_1^7), 8.31 (s, C^{III} pyr) ppm.
^{31}P-{^{1}H} NMR (203 MHz, DMSO-d6) : δ = 8.59 (br s, $N_3\underline{P}_3$), 63.34 (br s, P_1) ppm.
^{13}C {^{1}H} NMR (75 MHz, DMSO-d6) δ = 18.23 (m, C_1^{12}), 22.86 (s, C^{22}), 28.67 (s, C^{21}) 33.49 (m, Me_0) 33.50 (m, C_1^{11}), 35.42 (s, C^{20}), 40.22 (s, C^{18}), (m, C_1^{12}), 43.27 (m, *CH_2-CF_2), 49.0 (m, C_1^8), 61.84 (m, C_1^5), 62.90 (m, C_1^9), 67.36 (m, C^5 , C^{12}), 69.09 (m, C^7, C^{10}), 70.10 (m, C^9-C^{12}), 114.44 (s, C^{14}), 115.0 (s, C^2),115.89 (m, C_1^2), 120.5 (m, CH_2-*CF_2), 122.35 (s, C^3), 122.44 (m, C_1^3),123.94 (s, C^{III} pyr), 124.8 (m, 3C^{III} pyr), 125.2 (s, C^{III} pyr), 126.45 (s, C^{III} pyr), 126.9 (s, C^{III} pyr), 127.8 (s, C^{III} pyr), 127.9 (s, C^{III} pyr), 125.32 (m, C_1^7), 129.91 (m, C^{15}) 143.09 (m, C_1^6), 144.27 (m, C_1^1), 144.4 (s, C^1), 155.83 (m, C_1^4), 156.0 (s, C^4), 172.27 (s, C^{19}), 174.9 (m, C_1^{10}) ppm.
^{19}F{1H} NMR (376 MHz, DMSO-d6): δ **(ppm)** see below.

[6] E. Folgado, M. Guerre, C. Bijani, V. Ladmiral, A.-M. Caminade, B. Ameduri, A. Ouali, *Polym. Chem.,* 2016, **7**, 6632-6686.

S3. π-stacking procedures:

- Fluorescence studies with 11 and 13 (main text, Figure 3)
Solutions of dendrimers **11** or **13** ($9.25\ 10^{-6}$ mol L^{-1} in a THF-water (2:5)) were prepared and their fluorescence recorded. Quantities of Co/C MNPs were then successively added to these homogeneous solutions (0.5 mg for the first addition and 1 mg for each further addition, cf Figure 3 Main text). After each addition, the suspension was sonicated for 30 min, the MNPs removed by magnetic decantation and the supernatant analyzed by fluorescence spectroscopy.

- Fluorescence studies to perform reversibility test with 13 (main text, Figure 4)
A suspension of **13** (solution in a THF-water (2:5); $9.25\ 10^{-6}$ mol.L^{-1}) and MNPs was sonicated for 30 minutes at 20 °C, magnetically decanted with a magnet and the fluorescence spectrum of the supernatant recorded (blue curve). The mixture (supernatant and MNPs) was then heated to 60 °C for 10 h and the spectrum of the resulting supernatant analyzed (red curve). Upon cooling to 20 °C, the concentration of **13** in the solution decreased (green curve). Importantly, the fluorescence spectra recorded after 1 hour or 12 hours after return to ambient temperature were found to be identical.

Note: the fluorescence experiments were performed in highly diluted conditions (typically 0.5 mg of dendrons for 1 to 3.5 mg of naked MNPs). However, to prepare the MNPs decorated by pyrene-tagged dendrons (Figure 4, main article) and to get hybrid MNPs observed in Figure 5a, a large excess of pyrene-tagged dendron was used (typically about 194 mg of pyrene-tagged dendrons for 15 mg of MNPs ; pyrene-to-MNPs mass ratio-90th higher than when performing fluorescence studies). Such an excess has been typically used for π-stacking studies in previous works involving those MNPs (cf ref 9 of the main article). Such excess aims at optimizing the grafting process and the excess of pyrene-tagged dendrons not specifically bound through π-stacking interactions to the graphene surface is generally removed by washing except when dealing with very crystalline dendrons (typically PVDF dendrons).

- Grafting measurements with 11 (main text, Figure 6a)
A mixture of THF/H_2O 2:5 (15 mL) was added to Co/C nanoparticles (15 mg) and pyrene-tagged dendrimer **13** (25 mg, 7.10^{-3} mmol) and were sonicated for 30 minutes at 20 °C. The nanoparticles were then magnetically decanted and rinsed ten times with the same hot solvent mixture (THF/H_2O 2:5) to remove ungrafted pyrene-tagged dendrimer from the medium. The recovered MNPs were dried and analysed by TEM (see Figure 6a, main article) and by elemental analysis. By comparison with the result obtained for free nanoparticles, the loading of the pyrene-tag was calculated. Starting from dendron **11**, the pyrene-tagged dendrons in excess that were not specifically associated to MNPs through π-stacking interactions were efficiently removed. Therefore, the resulting MNPs were found to be surrounded by thin shells (between 2 and 4 nm approximatively) containing the phosphorous dendrons (according to EDX experiments that highlighted the presence of Phosphorous and Sulfur, characteristics elements from dendrimers).

- Grafting measurements with 13 (main text, Figure 6b)
A mixture of THF/H_2O 2:5 (15 mL) was added to Co/C nanoparticles (15 mg) and pyrene-tagged dendrimer **13** (194 mg, 7.10^{-3} mmol) and were sonicated for 30 minutes at 20 °C. The nanoparticles were then magnetically decanted and rinsed ten times with the same hot solvent mixture (THF/H_2O 2:5) to try to remove ungrafted pyrene-tagged dendrimer from the medium. The recovered MNPs were dried and analysed by TEM (see Figure 6b, main article) and by elemental analysis. By comparison with the result obtained for free nanoparticles, the loading of the pyrene-tag was calculated.

S4. EDX spectra of the MNPs embedded in pyrene-tagged dendrimer 13 (TEM image Fig. 5, a)

Cu signals are due to the grids on which the samples were deposited and Si signals were found to come from the preparation of samples.

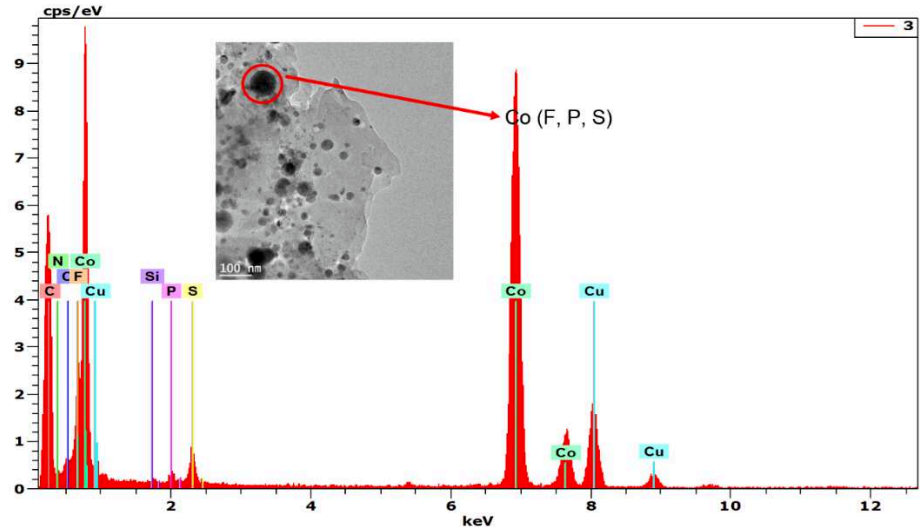

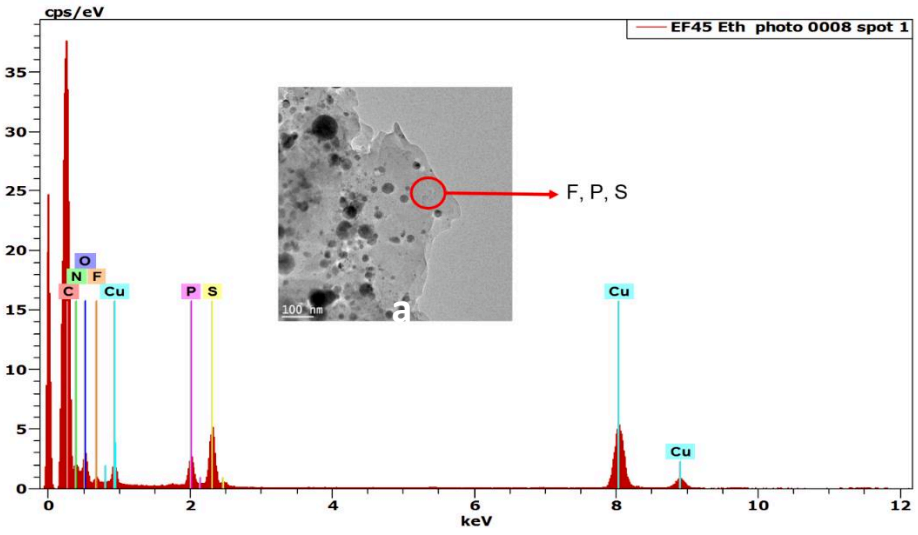

S5. Some NMR and mass spectra

Figure S5.1: ^{1}H NMR spectrum ($CDCl_3$, 300 MHz) of compound 3

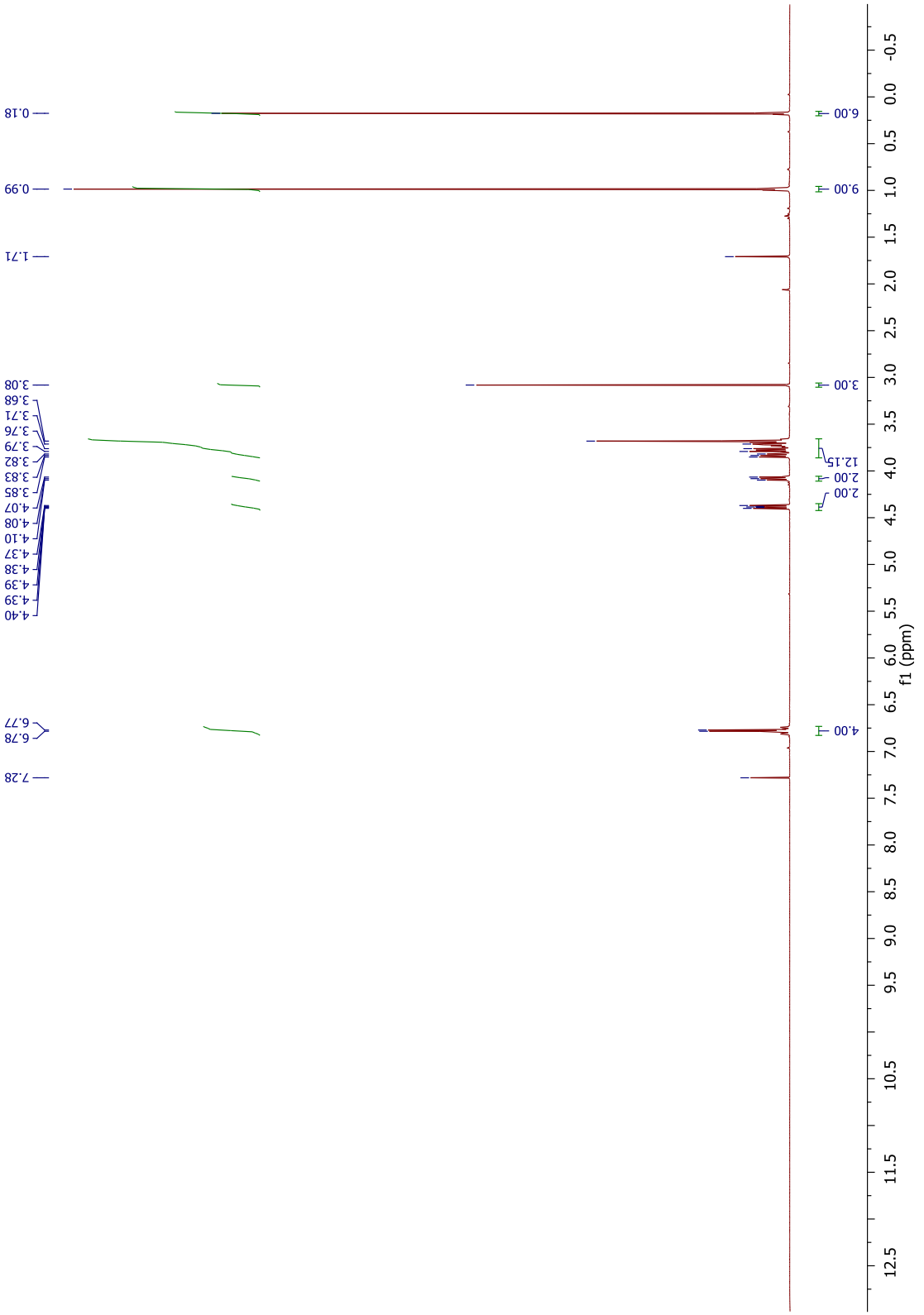

Figure S5.2: ^{1}H NMR spectrum ($CDCl_3$, 300 MHz) of compound 5

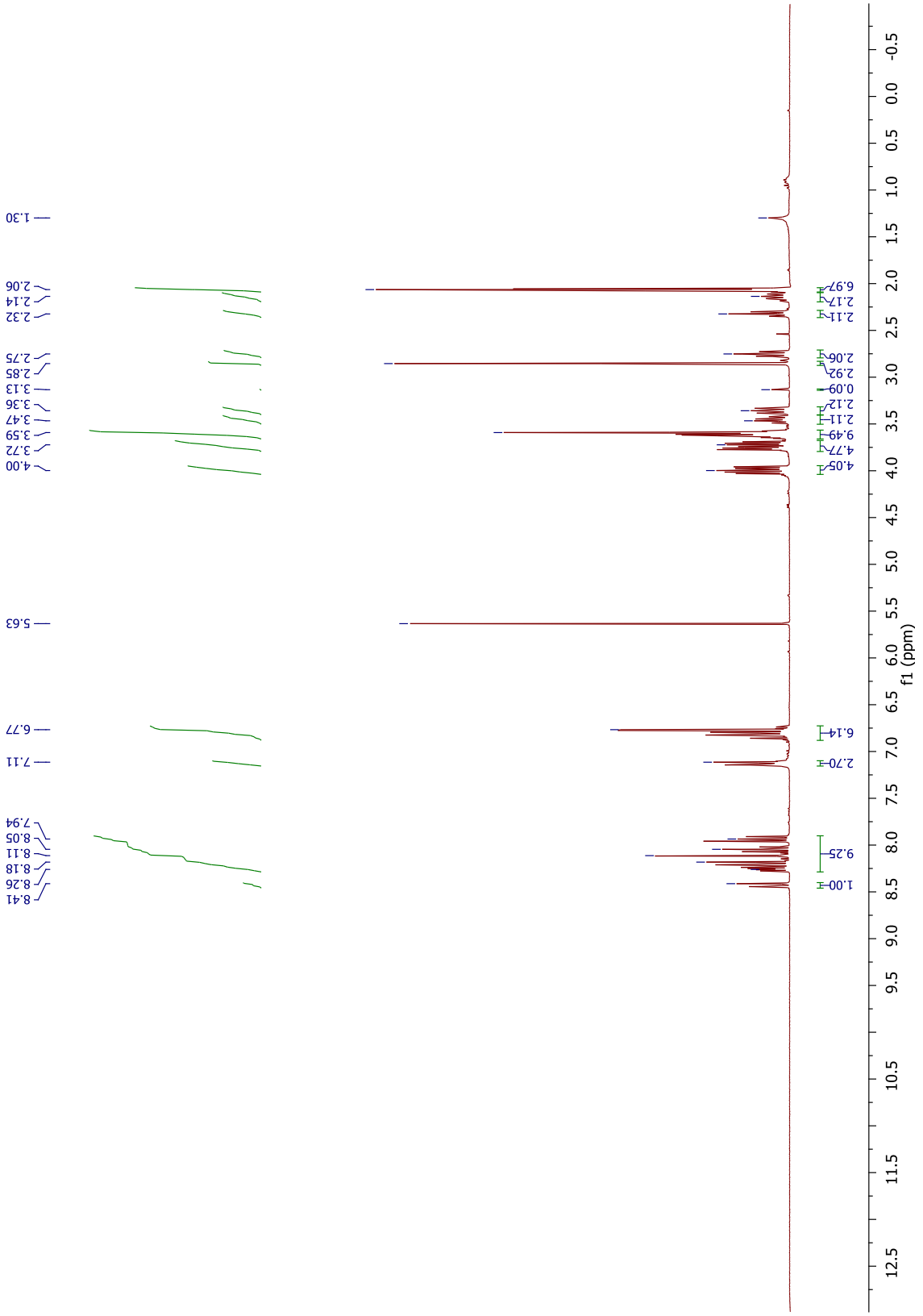

Figure S5.3: Maldi-TOF Mass Spectrum of compound 5

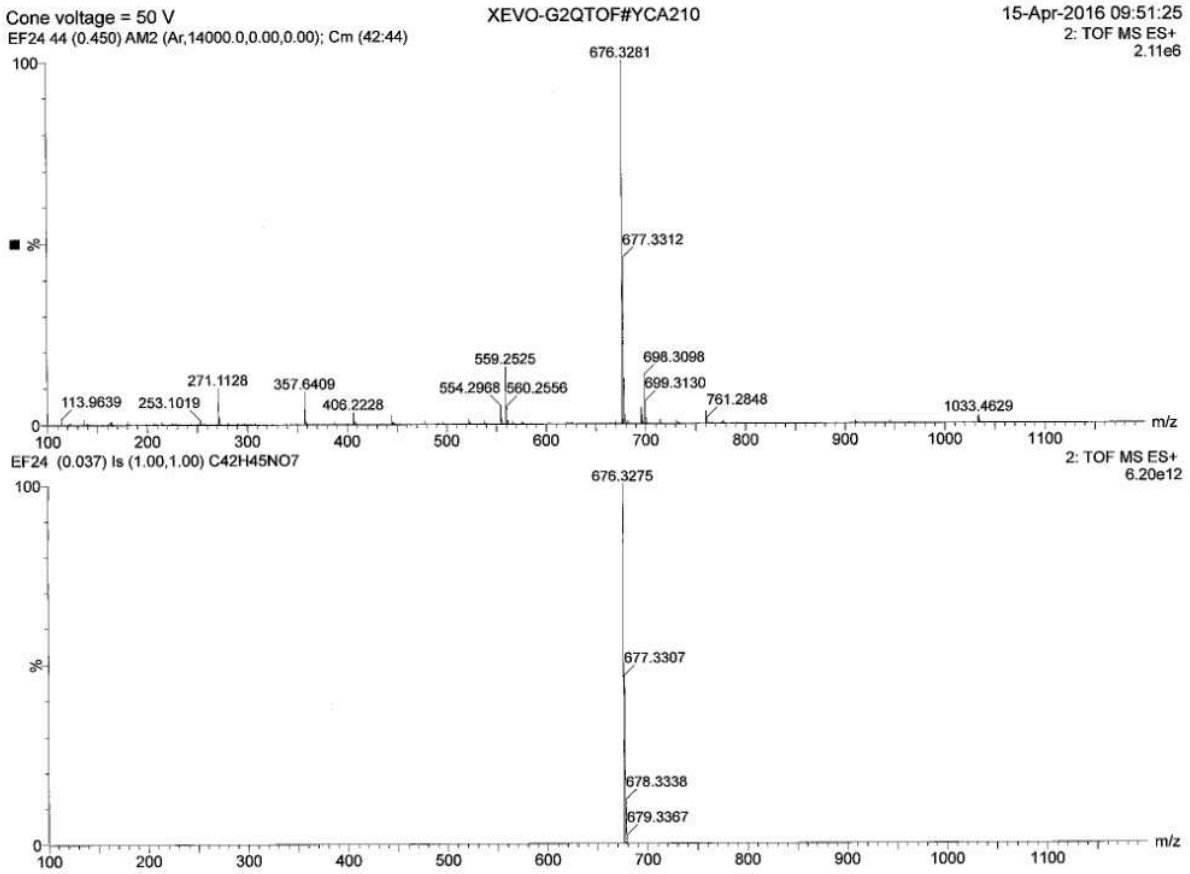

Figure S5.4: ^{1}H NMR spectrum ($CDCl_3$, 300 MHz) of compound 7

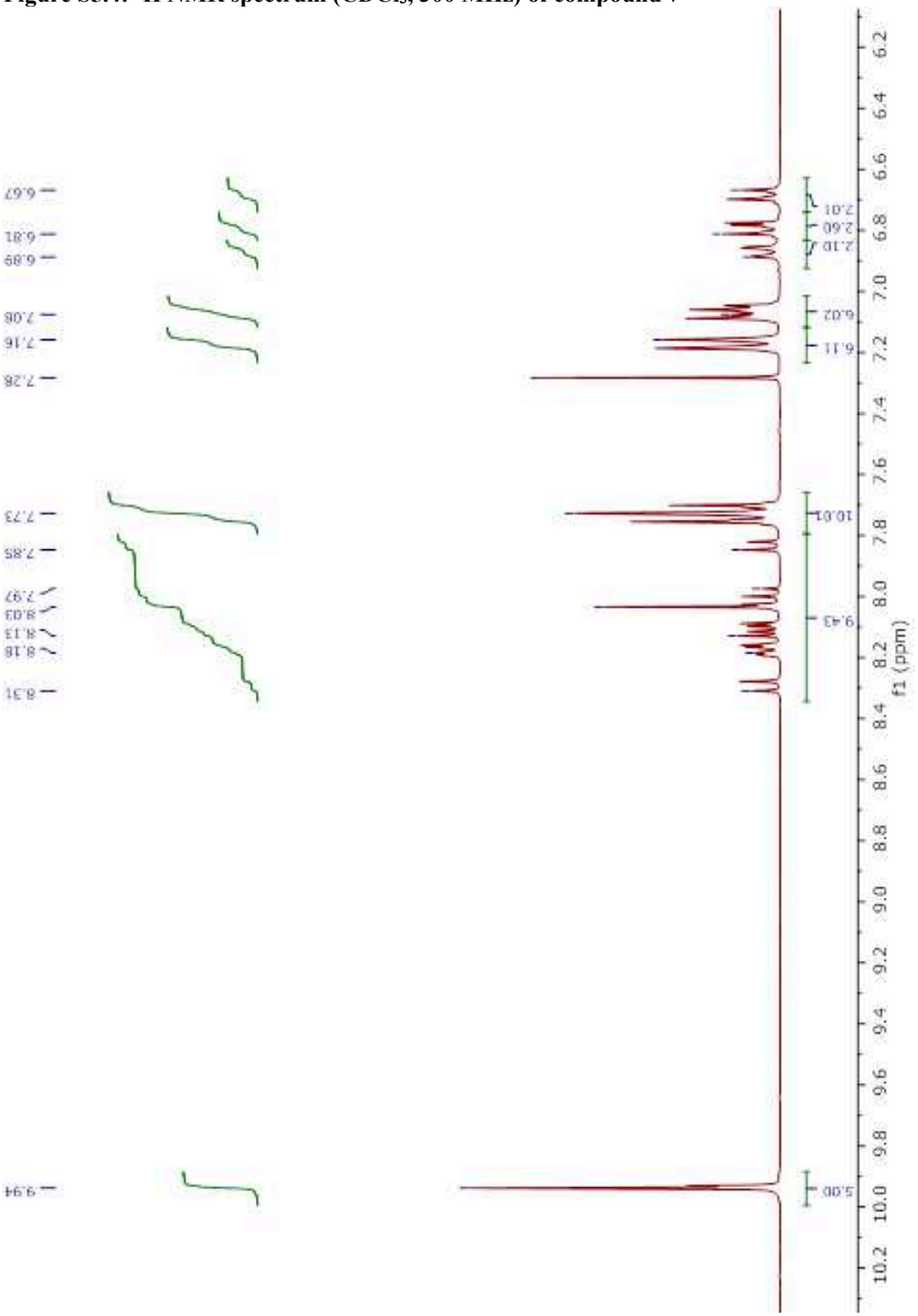

Figure S5.5: ^{31}P-{^{1}H} NMR spectrum ($CDCl_3$, 203 MHz) of compound 7

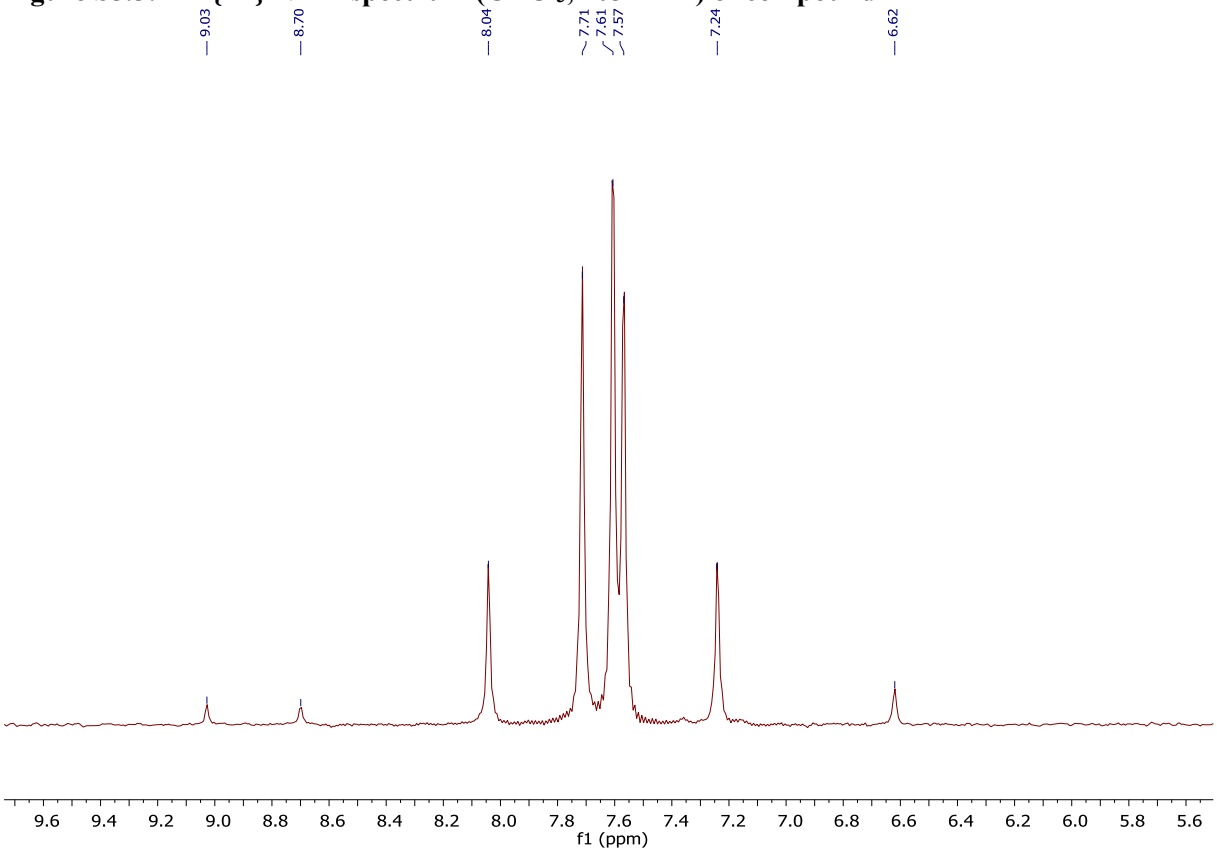

Figure S5.6: ^{13}C NMR and DEPT spectra ($CDCl_3$, 125 MHz) of compound 7

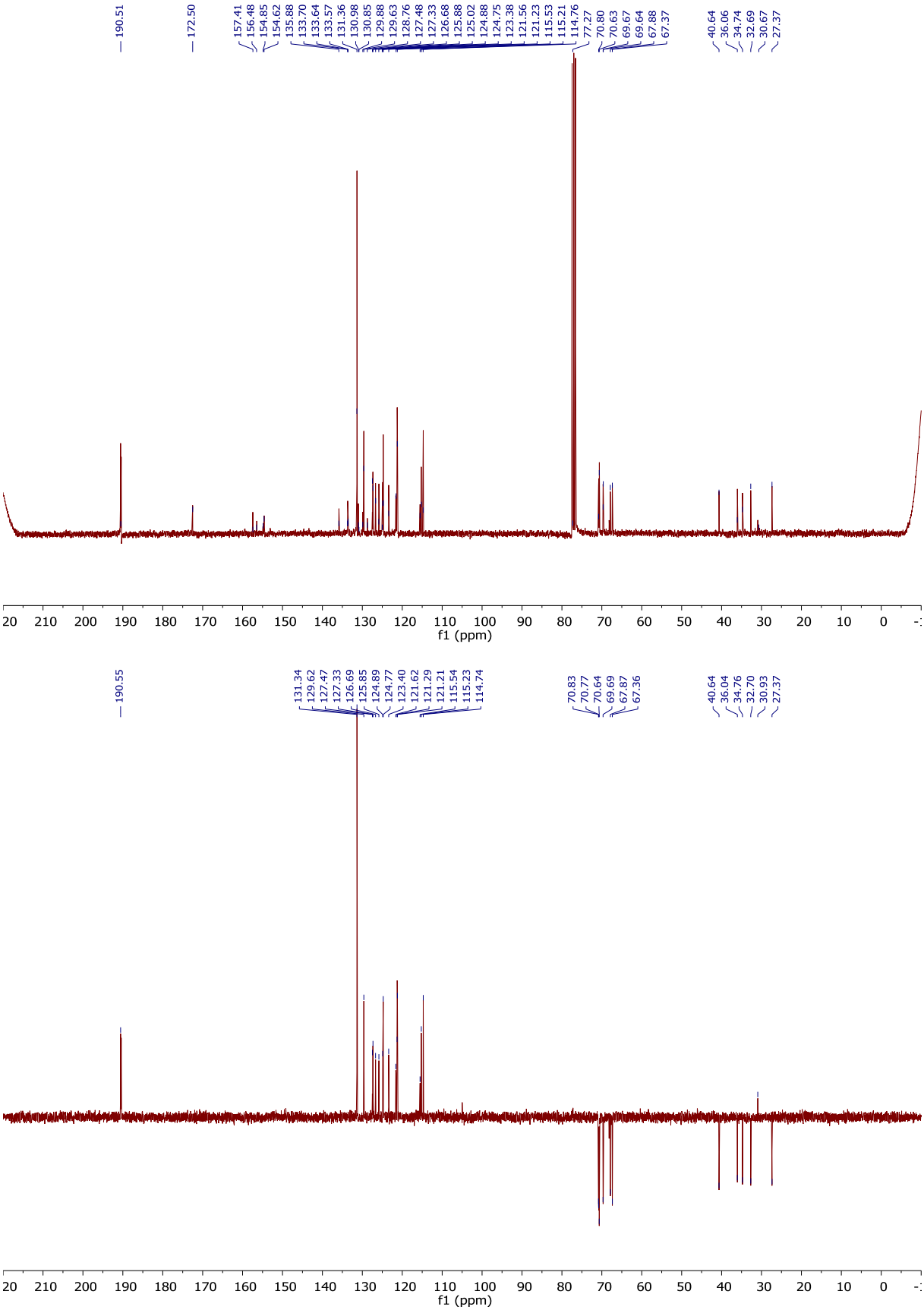

Figure S5.7: Spectrum ^{1}H NMR ($CDCl_3$, 500 MHz) of compound 9

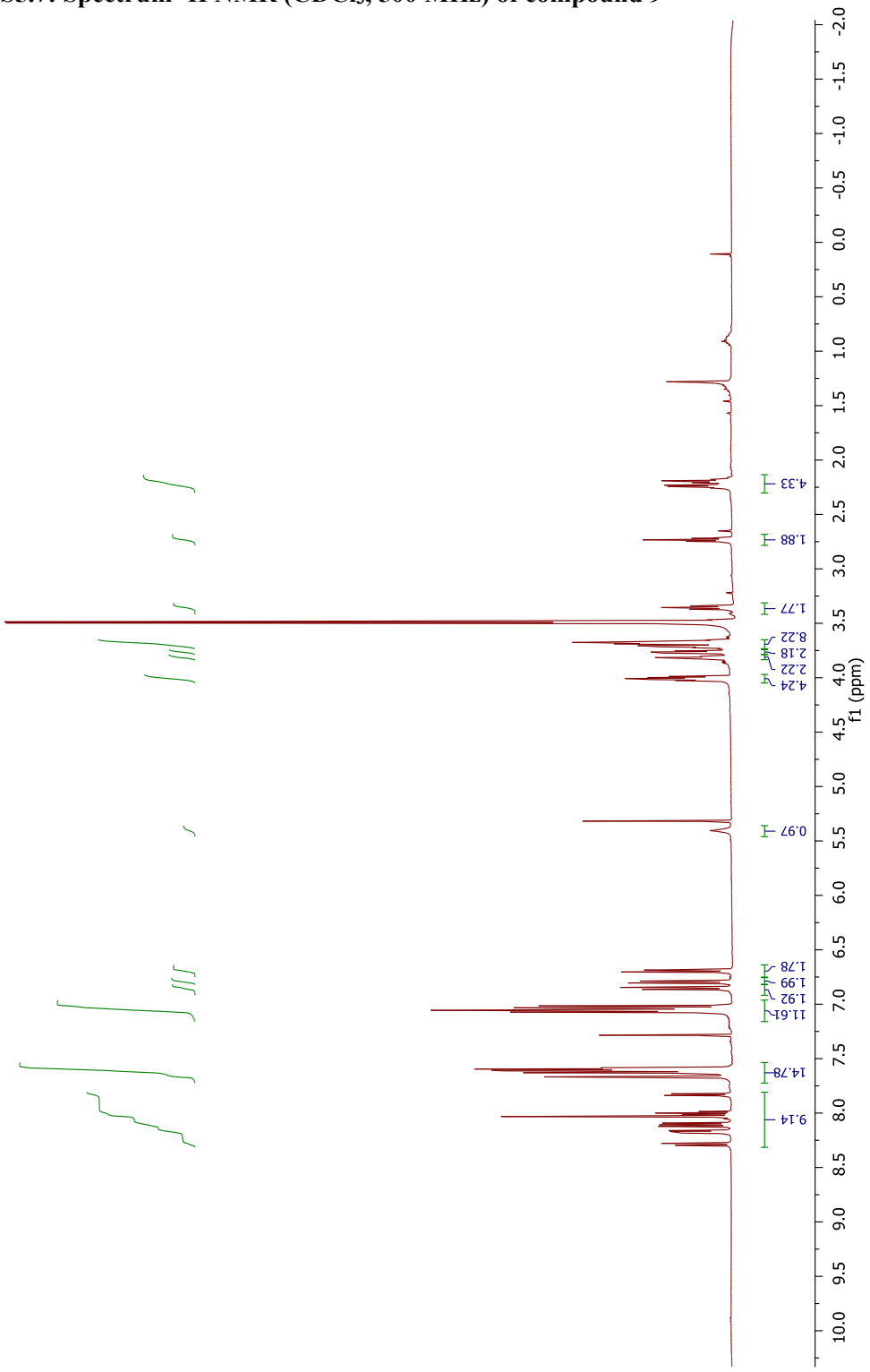

Figure S5.8: ^{31}P-{^{1}H} NMR spectrum simulation of compound 9

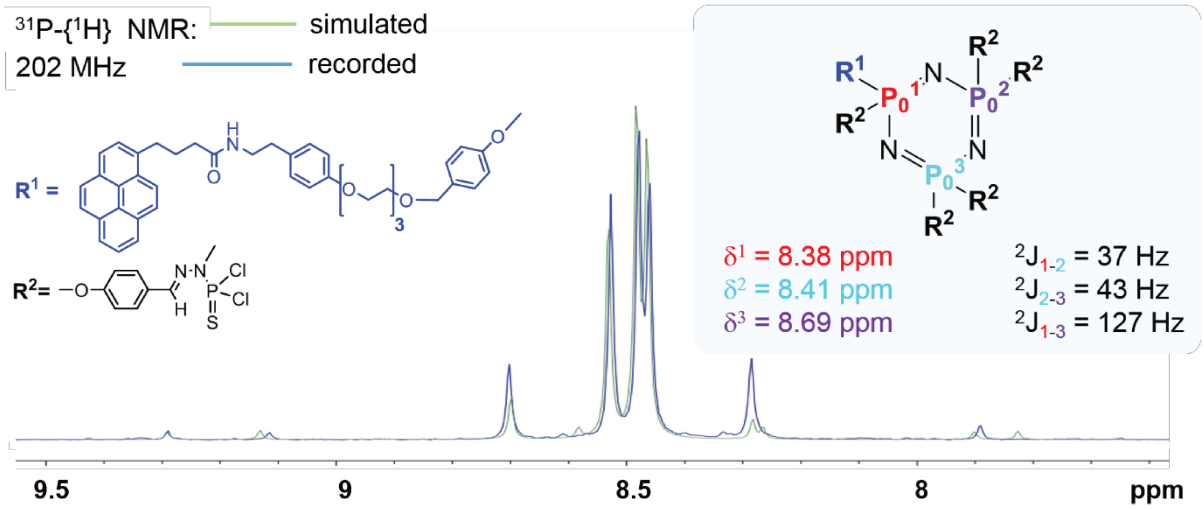

Figure S5.9: ^{31}P-{^{1}H} NMR spectrum ($CDCl_3$, 203 MHz) of compound 9 and zooms of P_0 and P_1 areas

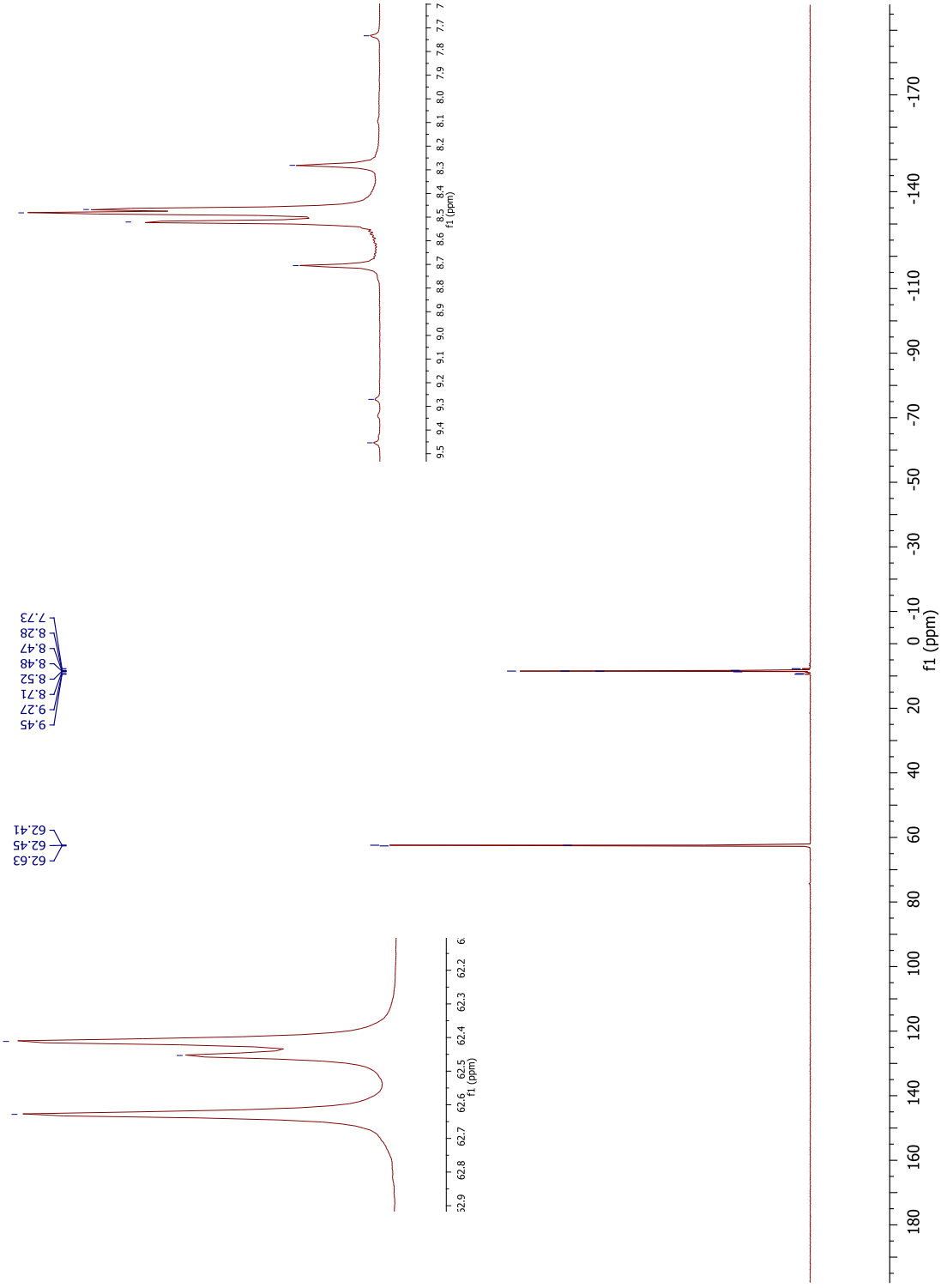

Figure S5.10: Spectrum ^{13}C NMR ($CDCl_3$, 125 MHz) of compound 9

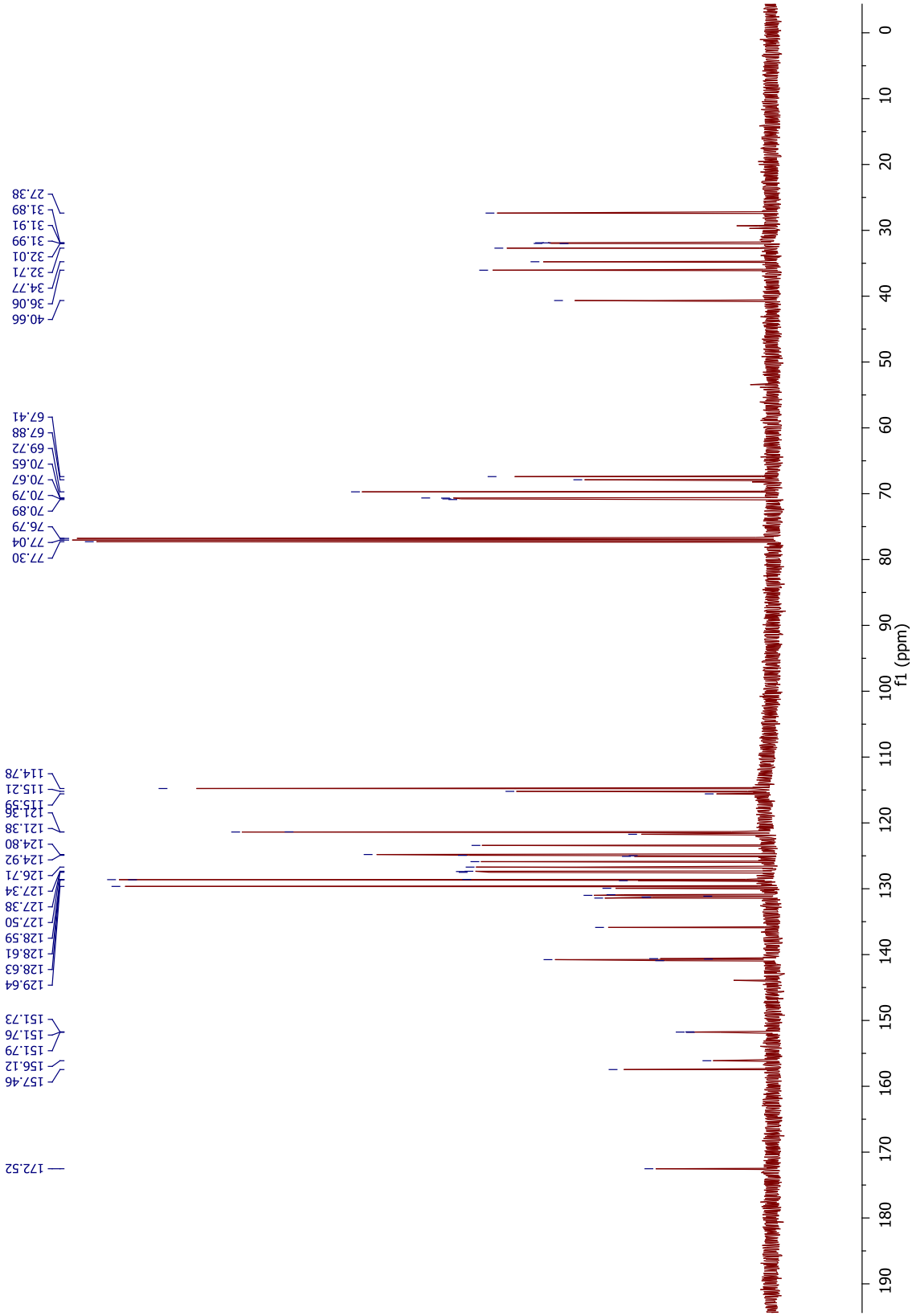

Figure S5.11: MS spectrum (MALDI-TOF-MS) of compound 9

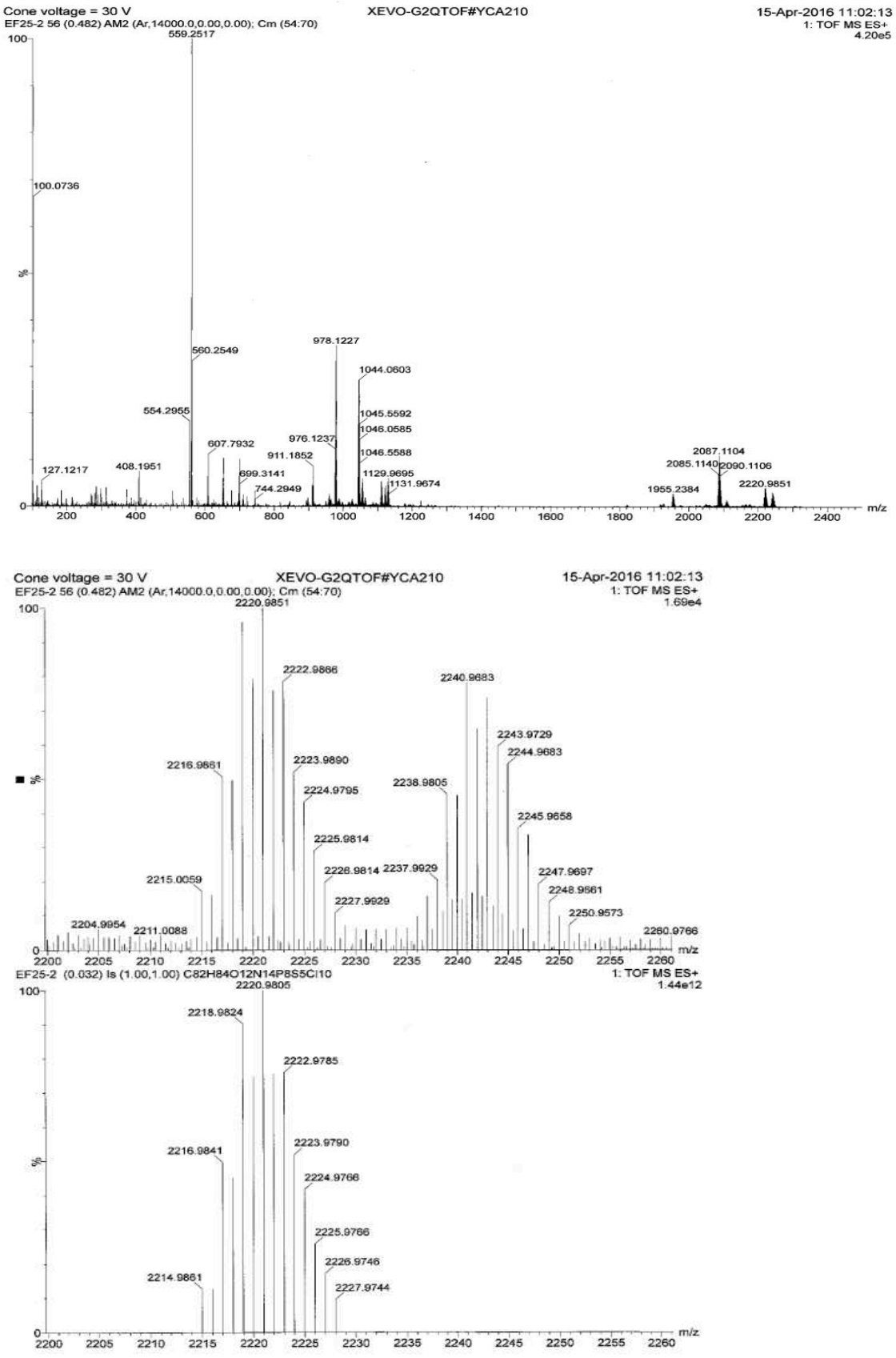

Figure S5.12: Spectrum ^{1}H NMR ($CDCl_3$, 500 MHz) of compound 11

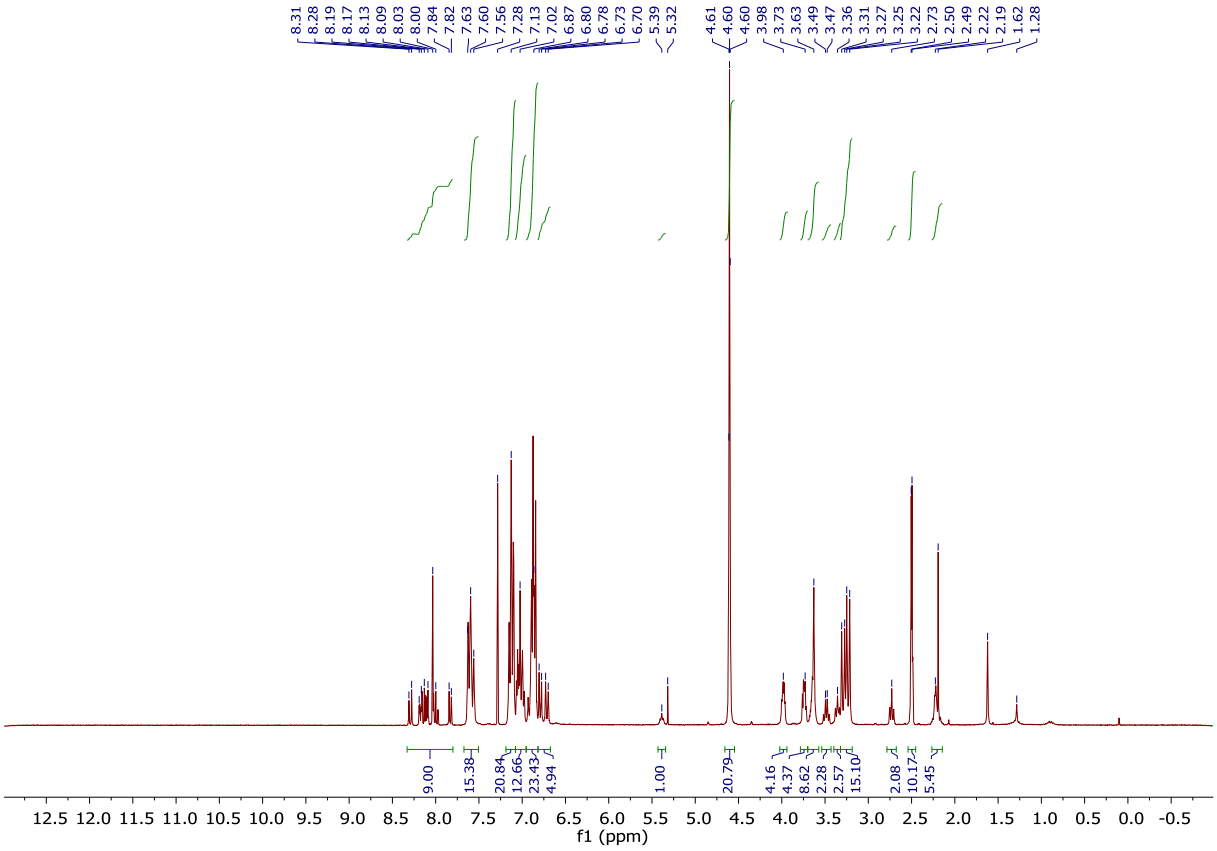

Figure S5.13: zooms of P_0 and P_1 areas of spectrum ^{31}P-{^1H} NMR ($CDCl_3$, 203 MHz) of compound 11

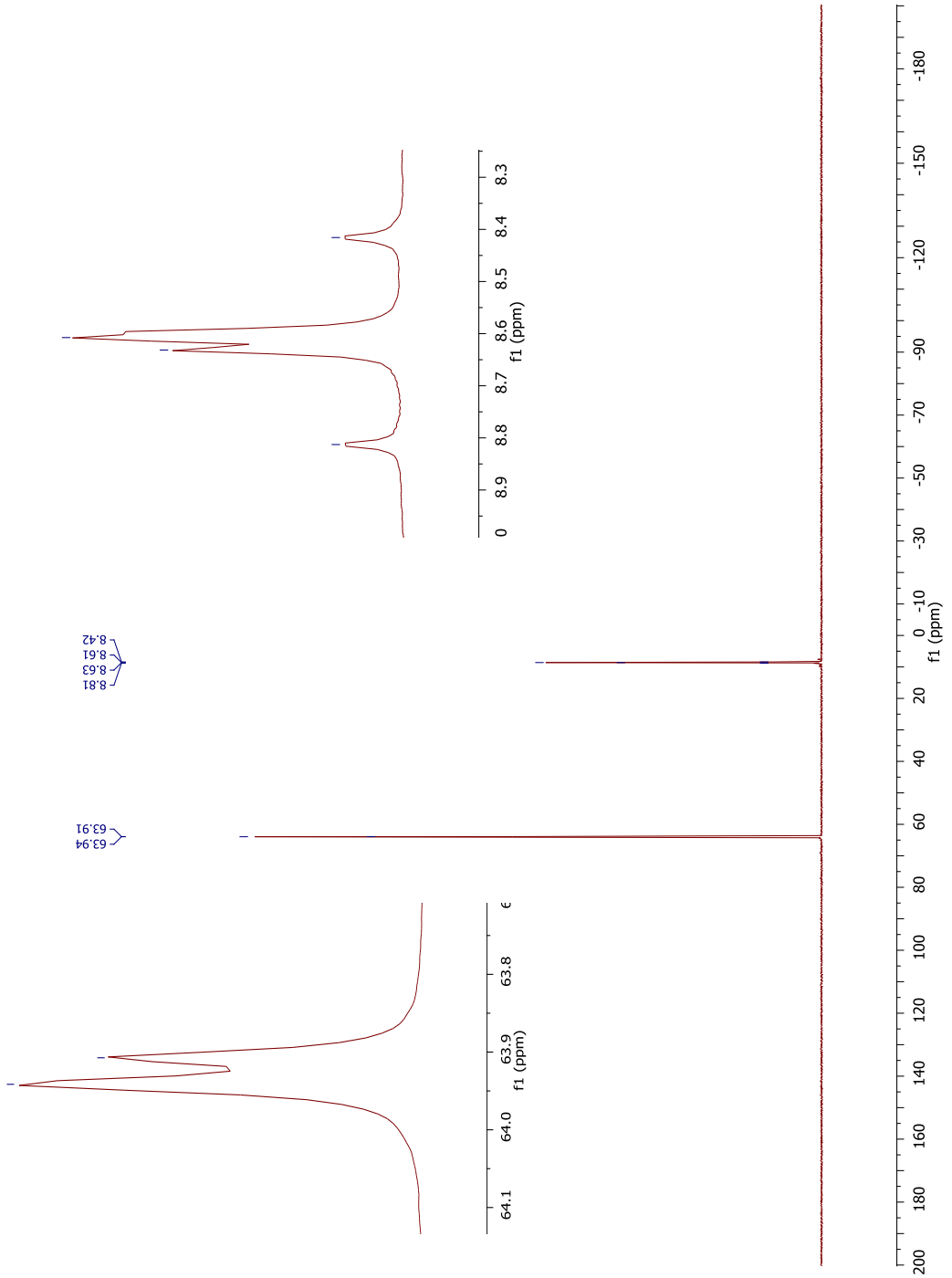

Figure S5.14: Spectrum ^{13}C NMR ($CDCl_3$, 125 MHz) of compound 11

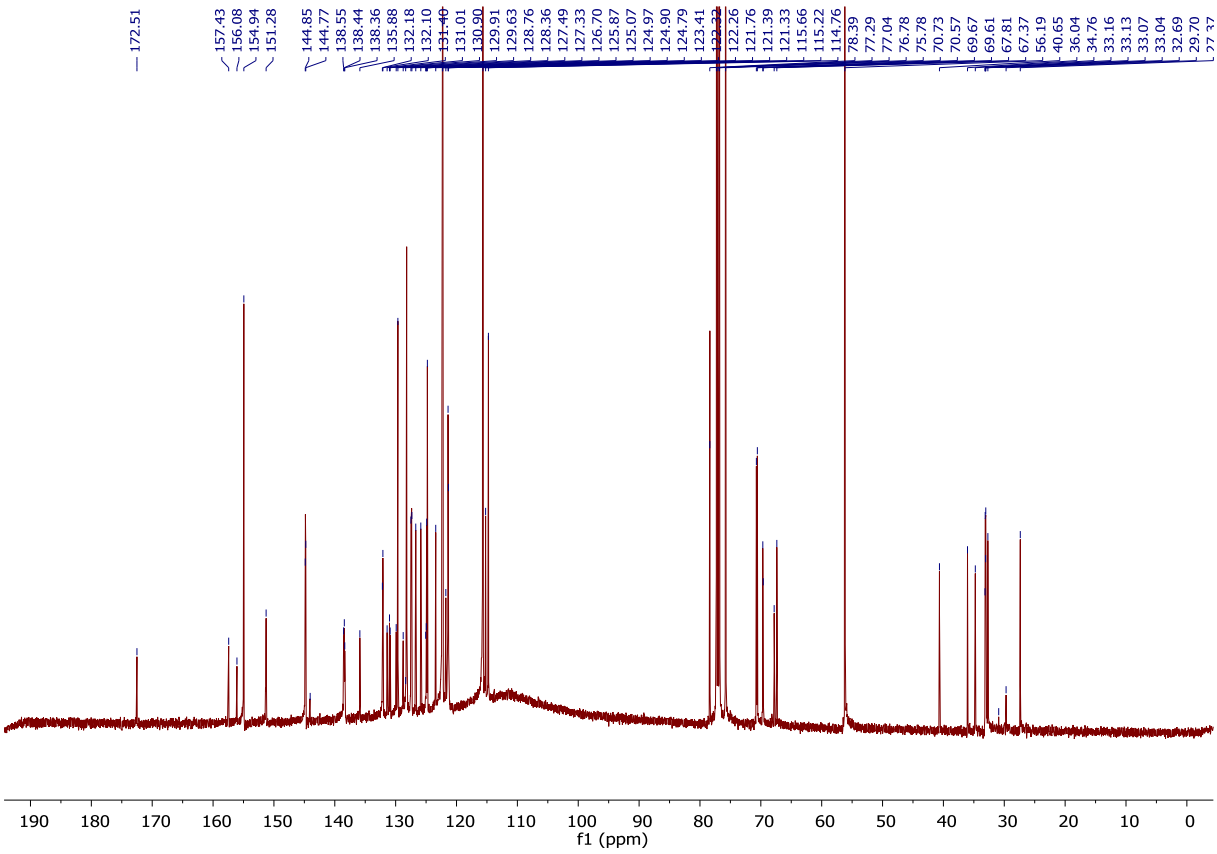

Figure S5.15: MS spectrum (MALDI-TOF-MS) of compound 11

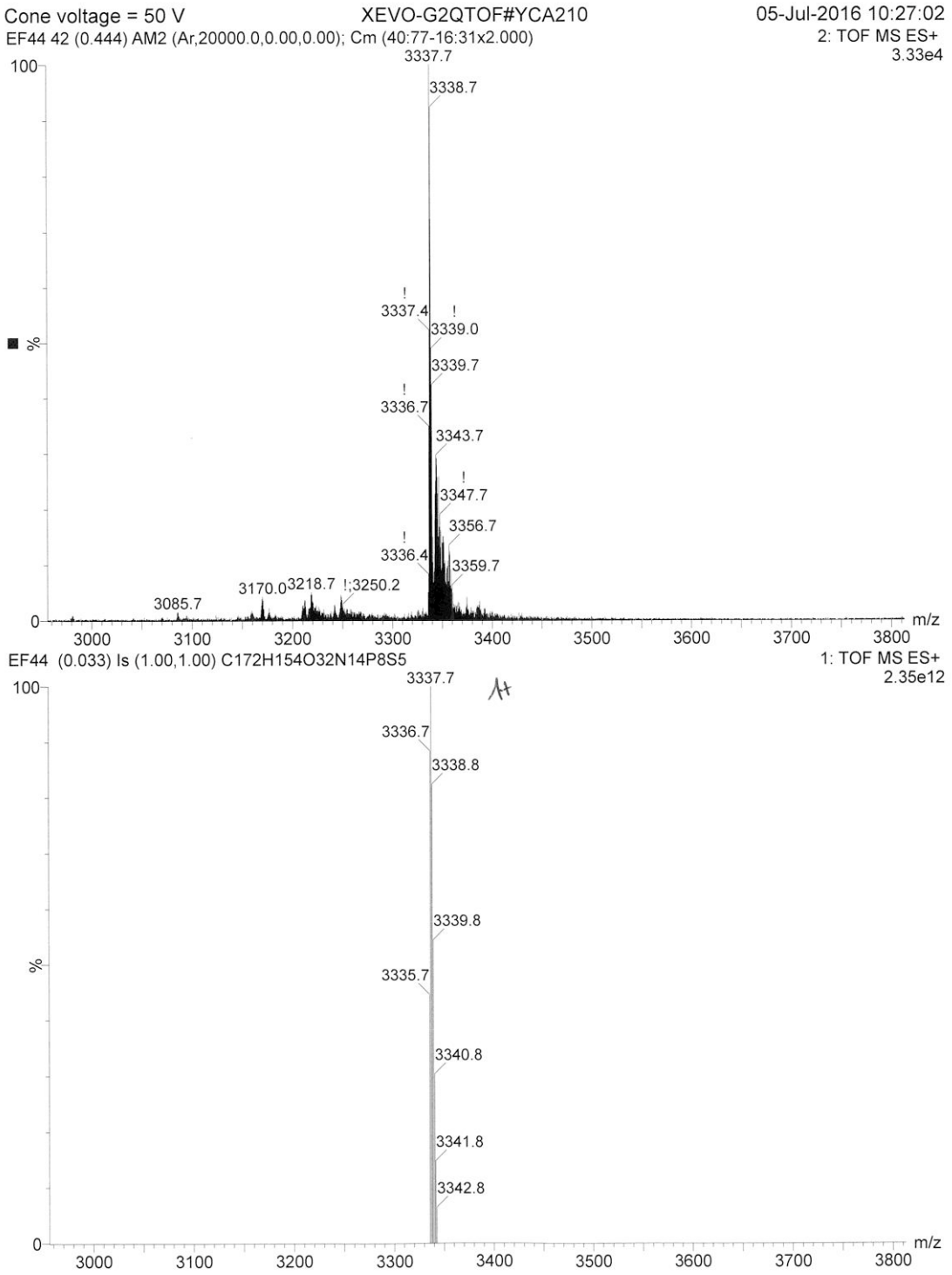

Figure S5.16: ^{31}P-{^{1}H} spectrum (DMSO, 203 MHz) of compound 11

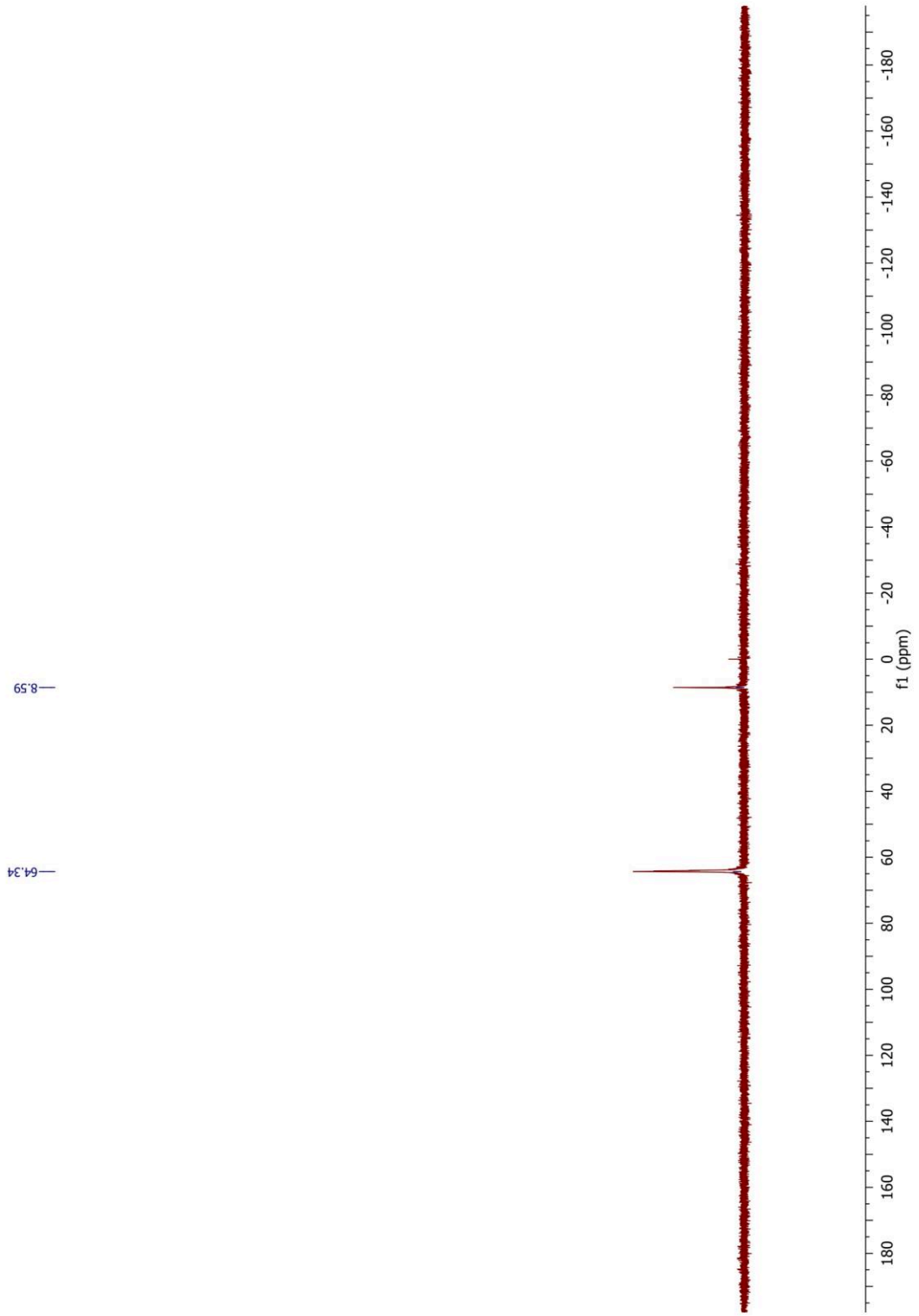

Figure S5.17: ^{19}F spectrum (DMSO, 500 MHz) of compound 13